THE
PHYSICAL REVIEW

A journal of experimental and theoretical physics established by E. L. Nichols in 1893

SECOND SERIES, VOL. 80, NO. 5 DECEMBER 1, 1950

Proton Groups from the $N^{14}(d, p)N^{15}$ and $N^{15}(d, p)^{16}$ Reactions*

ROBERT MALM† AND W. W. BUECHNER
Physics Department and Laboratory for Nuclear Science and Engineering, Massachusetts Institute of Technology, Cambridge, Massachusetts

(Received July 26, 1950)

The proton groups from nitrogen targets bombarded with deuterons have been investigated with a magnetic spectrometer. Seven groups have been identified as arising from the $N^{14}(d,p)N^{15}$ reaction with Q-values of 8.615±0.010; 3.339±0.005; 3.310±0.005; 2.287±0.005; 1.451±0.005; 1.306±0.005; and 0.300±0.005. One group has been found which is assigned to $N^{15}(d,p)N^{16}$ with $Q=-0.034\pm0.005$ Mev.

I. INTRODUCTION

THE proton groups from the $N^{14}(d,p)N^{15}$ reaction have been the subject of numerous investigations, the most complete being those of Guggenheimer, Heitler, and Powell[1] and of Wyly.[2] Guggenheimer and his co-workers bombarded gaseous nitrogen targets with 6.5-Mev deuterons. They observed proton groups with Q-values of 8.55, 3.5, 2.5, 1.3, and 0.3 Mev, indicating energy levels in N^{15} at 5.0, 6.0, 7.2, and 8.2 Mev. The 7.2 and 8.2 levels were believed to be doublets from evidence provided by the variation with angle of the intensities of the groups. Since the photographic-detection technique used in these experiments allowed an energy resolution of somewhat less than 0.3 Mev for proton groups in the range from 2 to 13 Mev, it is probable that the spacing of these doublets is of the order of 100 kev. The work of Wyly has confirmed the existence of the lower-energy groups. Wyly obtained Q-values of 8.61, 3.29, 2.30, and 1.40 Mev, indicating levels in N^{15} at 5.32, 6.31, and 7.21 Mev. He also found indications that the 7.21 level is a doublet.

Recently, Kinsey, Bartholomew, and Walker[3] have used a pair spectrometer to investigate the gamma-rays from the $N^{14}(n,\gamma)N^{15}$ reaction. Their results lead to the following values for energy levels in N^{15}: 5.287±0.010; 6.318±0.010; 7.164±0.010; 7.356±0.012; 8.278±0.16; 9.156±0.30. The 7.356- and 7.164-Mev levels probably correspond to the 7.2-Mev doublet reported by Guggenheimer *et al.* and by Wyly.

There is considerable variation among the values for the Q of the $N^{15}(d,p)N^{16}$ reaction which can be calculated from published measurements. Wyly investigated this reaction directly, using normal and enriched ammonia targets. By normalizing his data, and subtracting the normal-target data from the enriched-target data, he obtained a proton group corresponding to a Q-value of 0.23±0.15 Mev for this reaction. Measurements of the Q-value of the $F^{19}(n,\alpha)N^{16}$ reaction by Bleuler and Rossel[4] and by Jelley and Paul[5] indicate ground-state values for the $N^{15}(d,p)N^{16}$ reaction of 1.1±0.3 Mev and 0.7±0.9 Mev, respectively. Measurements on the maximum energy of the beta-particles from N^{16} by Sommers and Scherr[6] and by Bleuler, Sherrer, Walter, and Zunti[7] give 0.6±0.5 Mev and 0.3±0.8 Mev, respectively, for the $N^{15}(d,p)N^{16}$ reaction. In addition, Szelenyi[8] has calculated the mass of N^{16} using interpolation in a plot of mass-defect differences, and the value obtained indicates a Q-value for this reaction of 1.1±0.7 Mev.

With a view toward obtaining further information regarding the $N^{14}(d,p)N^{15}$ and $N^{15}(d,p)N^{16}$ reactions, we have used a high-resolution magnetic spectrometer to study the protons emitted from nitrogen targets bombarded with deuterons.

* This work has been assisted by the joint program of the ONR and AEC.

† AEC Predoctoral Fellow, now at the Argonne National Laboratory, Chicago, Illinois.

[1] Guggenheimer, Heitler, and Powell, Proc. Roy. Soc. **A190**, 196 (1947).

[2] L. D. Wyly, Phys. Rev. **76**, 316 (1949).

[3] Kinsey, Bartholomew, and Walker, Phys. Rev. **77**, 723 (1950).

[4] E. Bleuler and J. Rossel, Helv. Phys. Acta **20**, 445 (1947).

[5] J. V. Jelley and E. B. Paul, Proc. Roy. Soc. **63A**, 122 (1950).

[6] H. S. Sommers, Jr., and R. Scherr, Phys. Rev. **69**, 21 (1946).

[7] Bleuler, Sherrer, Walter, and Zunti, Helv. Phys. Acta **20**, 96 (1947).

[8] T. Z. Szelenyi, Phys. Rev. **75**, 1105 (1950).

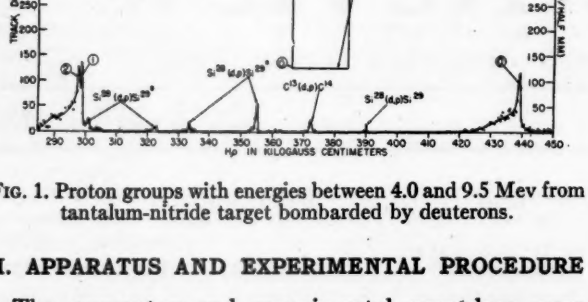

FIG. 1. Proton groups with energies between 4.0 and 9.5 Mev from tantalum-nitride target bombarded by deuterons.

II. APPARATUS AND EXPERIMENTAL PROCEDURE

The apparatus and experimental procedure were essentially the same as those described in a previous paper.[9] The deuteron beam from an electrostatic generator was sharply defined in space, direction, and momentum by means of a slit arrangement and magnetic analysis. The target was located in the annular gap of a large annular magnet, in which the magnetic field was parallel to the direction of the incident beam. A fraction of those particles emitted in the plane normal to the incident beam was focused by the 180-degree focusing action of the uniform magnetic field in the annular gap and were detected with Eastman *NTA* nuclear-track plates. These plates were also located in the annular gap in a position diametrically opposite to that of the target and were inclined at an angle of 20 degrees with respect to the direction of the observed particles. From measurements of the magnetic field and the radii of curvature, the momentum of the particles could be computed.

The magnetic field in the annular region was measured with a fluxmeter consisting of a small current-carrying coil rigidly attached at the center of an analytical balance. When the small coil was placed in a magnetic field it experienced a torque which was proportional to the product of the field intensity and the current through the coil. In practice, by the adjustment of the current through the coil, a balance was achieved between this torque and a constant mechanically applied torque. The calibration constant for the fluxmeter was determined from measurements of the radius of curvature of polonium alpha-particles in the magnetic field of the annular magnet and the current through the small coil, together with Brigg's value[10] for the $H\rho$ of RaC′ alpha-particles, and Lewis and Bowden's value[11] for the ratio of the velocities of RaC′ alpha-particles and polonium alpha-particles. These values determine the velocity of the polonium alphas with a precision of 1 part in 5000.

The incident deuteron energy was determined from energy measurements of deuterons elastically scattered by carbon and oxygen nuclei in thin Formvar films.

After exposure the nuclear-track plates were processed and examined under microscopes, and the track-density distribution as a function of the radius of curvature was determined. For this purpose, it was necessary to correlate the positions of the nuclear-track plates during exposure with the position of the target. This correlation was made possible by means of a narrow slit which was located permanently with respect to the target position and which could be optically imaged on each plate during exposure. Since for each plate the range of radii covered is small and constant, the actual calculations involve in a sensitive way only the distance between the calibrating polonium source and the position of the beam on the target.

The track-density distribution functions were corrected for background-track density in those cases where it was necessary. This background-track density was determined from the leading edge of the distribution function at points sufficiently removed from the peak itself so that the contribution from the reaction concerned was negligible.

Because the photographic plates record particles that are emitted from the target within a small range of angles around 90 degrees with respect to the beam (± 0.2 degree), the peaks obtained from measurements made across the full width of the plates are slightly broadened. A similar effect occurs because the particles are emitted from a line rather than a point source on the target. These small effects were corrected for analytically for each of the observed peaks.

Most of the targets used in this work consisted of thin surface layers of tantalum nitride on tantalum. Tantalum was selected because of its availability and the stability of its nitride. These targets were prepared in the following way. Ammonium nitrate was treated with an aqueous solution of sodium hydroxide, and the ammonia released was passed through barium oxide (a basic drying agent) and collected in a small evacuated quartz vessel containing small squares of sheet tantalum. The tantalum was then maintained at a temperature of approximately 1000°C for several minutes through the use of an induction heater. This procedure resulted in the formation of thin surface layers of tantalum nitride on the pieces of tantalum.

In addition to nitrogen, there was the possibility of the presence of other elements in the targets. The simplest and most effective means of identifying the nitrogen groups was by the variation of peak heights with targets of different isotopic concentrations. For this purpose, ammonium nitrate with the NH_3 radical enriched in N^{15} was obtained from the Eastman Kodak Company and was used in the preparation of enriched tantalum-nitride targets. A further check on the iden-

[9] Buechner, Strait, Stergiopoulos, and Sperduto, Phys. Rev. 74, 1569 (1948).
[10] G. H. Briggs, Proc. Roy. Soc. 157A, 183 (1936).
[11] W. B. Lewis and B. V. Bowden, Proc. Roy. Soc. 145A, 250 (1934).

tification of certain groups was obtained by comparisons of the changes in energy of the groups with the changes in energy of the incident deuterons.

The presence of surface contaminants on the targets could lead to appreciable errors in the calculated values of reaction energies. In the present work a tantalum-nitride target essentially free of volatile contaminants was obtained by the use of a flat, mica-insulated heating element wound with 5-mil wolfram wire. The heating element was placed between the target and a metallic backing which was supported by a 40-mil wolfram wire. This target was maintained at a temperature corresponding to a dull red color during exposures. Since hot tantalum combines readily with both nitrogen and oxygen and in general absorbs gases, there was a strong possibility that nonvolatile surface contaminants remained even at high temperatures. The existence of such contaminants was determined from a comparison of the energies of one of the alpha-particle groups from the $N^{14}(d,\alpha)C^{12}$ reaction from a heated tantalum-nitride target and from a freshly prepared target consisting of a thin layer of ammonium nitrate deposited on a platinum backing. It was found that a small amount of such contamination was indeed present, and all of the measured Q-values obtained with the heated tantalum-nitride targets were corrected accordingly.

In order to investigate the proton groups having values of $H\rho$ less than those for the elastically scattered deuterons, it was necessary to discriminate between the two types of particles in the detection process. Since the solid-target yield of elastically scattered deuterons was much greater than the yield of reaction protons, it was not possible to make this discrimination by track-length comparisons under a microscope. Instead, the nuclear-track plates were shielded with aluminum foils of sufficient thickness to absorb the deuterons but not the protons. In this way, only the protons were allowed to register on the plates.

The Q-equation ordinarily used in the calculation of reaction energies has been derived on the basis of the non-relativistic relation between energy and momentum and errors comparable to the experimental errors would have been introduced by its use. Consequently, a relativistically correct Q-equation was derived and used in the calculation of the reaction energies.

III. EXPERIMENTAL RESULTS

As the analyzing magnet is employed in these experiments, each photographic plate is exposed at a fixed field strength and, hence, records an interval in the momentum spectrum of the particles emitted from the target. In Figs. 1 and 2 are plotted the results obtained from a number of plates exposed at various magnetic fields so as to cover the region of proton energy from 1.5 to 9.5 Mev. The field strengths for each plate were adjusted so that the regions covered by each overlapped slightly. The data shown in the figures were taken with an incident deuteron energy of 1.420 Mev and an unheated tantalum-nitride target. Only the observed proton groups are shown. In addition, a number of alpha-particle groups were observed, most of which corresponded to reactions in which C^{12} and C^{13} were formed as residual nuclei. For the reasons mentioned in the preceding section, those plates exposed at field strengths less than those corresponding to an $H\rho$ of 240 kgauss-cm were shielded with thin aluminum foils so as to prevent the recording of deuterons elastically scattered from the targets.

Of the proton groups observed, seven, numbered from 0 through 6 in the figures, were identified as arising from the $N^{14}(d,p)N^{15}$ reaction. Of the other peaks, four are due to the well-known groups from carbon and oxygen, and complete data for these peaks have not been plotted. The group at $H\rho = 371$ kgauss-cm was identified by an independent measurement on an enriched C^{13} target as arising from the small concentration of C^{13} in the carbon contamination on the target. That the remaining groups were probably due to silicon was indicated by measurements on the shift in position of these groups as a function of the energy of the incident deuteron beam. That this assignment was correct was checked by a series of measurements on a thin silicon target. The presence of silicon contamination on the target is probably due to the fact that a quartz tube was used in the preparation of the tantalum-nitride layers.

As can be seen, the groups due to C^{12} and O^{16} are of very considerable intensity. The possibility that other proton groups due to nitrogen might be obscured by the presence of these intense groups was to a large extent eliminated by observations in these regions made with a heated target. Group 3 in Fig. 2 is plotted from data taken in this way, and its intensity relative to the other groups has been adjusted from measurements taken with the heated and unheated targets.

From the figures, it can be seen that the groups from nitrogen show a considerable tail on the low energy side. This is presumably due to the difficulty of preparing nitrogen targets. In the present case it is probable that

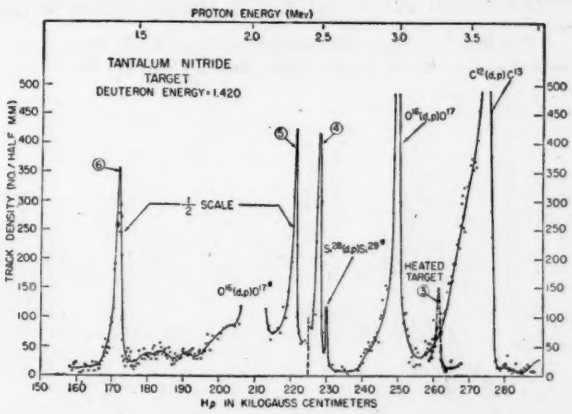

FIG. 2. Proton groups with energies between 1.2 and 4.0 Mev from tantalum-nitride target bombarded by deuterons.

TABLE I. Q-values for $N^{14}(d,p)N^{15}$.

Present work		Kinsey *et al.*[a]
Q-value in Mev	Level in N^{15} in Mev	Level in N^{15} in Mev
8.615±0.010	0	0
3.339±0.005	5.276±0.006	5.287±0.010
3.310±0.005	5.305±0.006	
2.287±0.005	6.328±0.006	6.318±0.010
1.451±0.005	7.164±0.006	7.164±0.010
1.306±0.005	7.309±0.006	7.356±0.012
0.300±0.005	8.315±0.006	8.278±0.016

[a] See reference 3.

there is considerable diffusion of the nitrogen into the tantalum supports.

The measured half-widths of the proton groups were compared with the half-widths which would be expected if the broadening were due entirely to target thickness and to geometrical factors, such as the width of the entrance slit to the analyzing magnet. As can be seen from the figure, the peaks tend to broaden at the lower energies, as would be expected from the first of these factors. The only serious discrepancy in the measured and computed values occurred for the group corresponding to the 8.3-Mev level. The half-width of this group was considerably larger than the expected value, and it is possible that it is actually composed of two groups with a separation of about 10 to 20 kev.

Particular attention was paid to the particles having an $H\rho$ in the region of 300 kgauss-cm (groups 1 and 2). The track distribution in this region was accurately reproducible and varied with target thickness in the manner to be expected if the distribution were due to two closely spaced groups. These groups are of particular interest because they indicate the presence of two energy levels in N^{15} with the unusually small separation[12] of 29 kev.

The Q-values for the groups assigned to the $N^{14}(d,p)N^{15}$ reaction are listed in Table I.

In each case the values have been corrected for the effects of a surface layer of contamination, the thickness of which was estimated from the results of measurements carried out as outlined in the preceding section. In no case did these corrections amount to more than 4 kev. Also listed in Table I are the levels in N^{15} corresponding to these groups. These are compared in the table with the results of Kinsey, Bartholomew, and Walker which were obtained from measurements of the gamma-rays from the $N^{14}(n,\gamma)N^{15}$ reaction. The two sets of values for the energy levels agree in most cases within the probable errors, and in all cases within the limits of error; that is, three times the probable error.

An energy-level diagram for N^{15} showing the levels found in the present work is included in Fig. 1.

Kinsey and his collaborators[3] have also measured the Q-value for the $N^{14}(n,\gamma)N^{15}$ reaction. If the binding energy of the deuteron is subtracted from this value, 8.593±0.014 Mev is obtained for the Q of the $N^{14}(d,p)N^{15}$ reaction. This value is in fair agreement with the figure of 8.615±0.010 Mev obtained in the present work. It is to be noted that, in the present work, possible errors due to calibration, surface contaminants, and so forth tend to affect the energies of the group in the same direction so that the values obtained for the energy levels are somewhat more reliable than the Q-values for the individual groups.

Since N^{15} is present only to the extent of about 0.4 percent in ordinary nitrogen compounds, it is unlikely that groups from this isotope would be observed from unenriched nitrogen targets. In connection with the identification of the groups, however, targets with both normal and enriched concentrations of N^{15} were used in the investigation of the energy region covered in these experiments. Only one proton group was found that could be attributed to the $N^{15}(d,p)N^{16}$ reaction. For this group, a Q-value of -0.034 ± 0.005 Mev was obtained. While no higher energy group from this reaction was found at the bombarding energy used in these experiments, it is probable that the one observed does not correspond to the ground-state transition but is associated with the formation of N^{16} in the excited state at about 0.3 Mev indicated in the work of Wyly.[2]

We are indebted to the staff of the High Voltage Laboratory for much helpful discussion and assistance. We are particularly grateful to Miss C. O'Brien and Mr. W. A. Tripp for their careful measurements on the photographic plates.

[12] Possible interpretations regarding these levels have recently been discussed by D. Inglis, Phys. Rev. **78**, 616 (1950).

On the Bombardment of Li_2O and C by Alpha-Particles and Deuterons*

ISADORE B. BERLMAN**
Physics Department, Washington University, St. Louis, Missouri
(Received June 9, 1950)

Photographic nuclear emulsions were used to record the scattered and recoiling particles when Li_2O and C targets were each independently bombarded by 10-Mev deuterons and 20-Mev alpha-particles. The 1.0-Mev level in C^{13} has been confirmed and a new level at 6.8 Mev in C^{13} has been determined. The relative scattering of deuterons and alpha-particles from nuclei in the ground state and in their various nuclear energy levels are illustrated. Finally the alpha-particle range-energy curve, as applied to Ilford E-1 nuclear emulsions, has been modified at higher energies.

I. INTRODUCTION

THE Washington University cyclotron was used as a source of 10-Mev deuterons, and 20-Mev alpha-particles. These particles were independently made to impinge on a thin Li_2O target or on a thin carbon target. In each case the recoiling and scattered particles were recorded in Ilford E-1 nuclear emulsion plates which were set at predetermined angles to the cyclotron beam. From an analysis of the track lengths certain conclusions were drawn as to energy levels and transmutation products.

II. APPARATUS

The beam from the cyclotron enters the scattering chamber[1] through a collimator and impinges on a target held in the center of the chamber. A large annular ring contains slits which define the various directions of the scattered particles. Around the periphery of the ring are steel blocks the upper surfaces of which are inclined at 5° to the horizontal. Photographic plates are cut to size and placed on these blocks to detect the scattered and recoiling particles. The undeflected beam enters the collector cup directly opposite the inlet. *O* rings are used to seal various joints in the system so that the experiment can be run under vacuum conditions. The apparatus meets Bethe's[2] requirements for good geometry.

Gold leaf, 0.88 mg/cm², served as a target backing on which the carbon and the lithium oxide were deposited. The carbon target was prepared by burning camphor and letting the resulting smoke deposit on a target holder. Approximately 0.14 mg/cm², corresponding to a thickness of 4×10^{-4} cm, was deposited. The energy lost by alpha-particles on penetrating the complete target amounted to 44 kev for the carbon and 50 kev for two layers of gold leaf. For deuterons, the energy loss was approximately one-fourth of this amount.

The lithium-oxide target was prepared by burning metallic lithium in an iron crucible. Traces of carbon impurity were unavoidable. The energy loss of alpha-particles on passing through the lithium-oxide coating

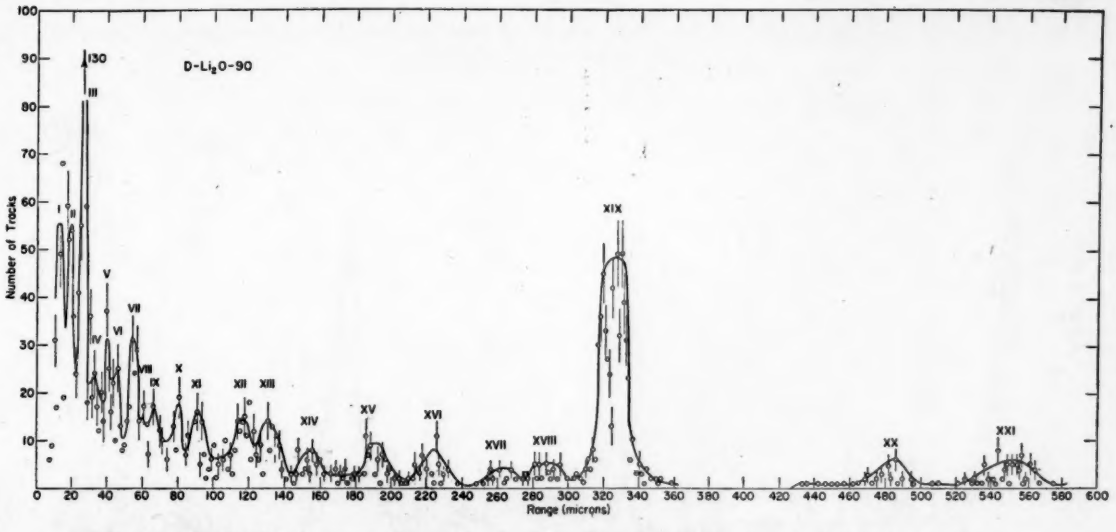

FIG. 1. Distribution in range of particles resulting from the bombardment of Li_2O by deuterons. The angle of recoil is 90° to the cyclotron beam.

* Assisted by the joint program of the ONR and AEC.
** Present Address: Argonne National Laboratory, Chicago, Illinois.
[1] Originally constructed by K. B. Mather, subsequently modified by this author.
[2] M. S. Livingston and H. A. Bethe, Rev. Mod. Phys. 9, 278 (1937).

TABLE I. $D-Li_2O-90$.

Peak number	Reaction	Level (Mev)	Q (Mev)	E (Mev)	Range (microns)	Observed range (microns)
XXI	$O^{16}(d,p)O^{17}$	0	1.94	10.08	565	555
	$C^{12}(d,p)C^{13}$	0	2.7	10.3	586	
XX	$O^{16}(d,p)O^{17*}$	0.88	1.06	9.25	491	485
XIX	$Au^{179}(d,d)Au^{179}$	0	0	9.7	328	326
XVIII	$C^{12}(d,p)C^{13*}$	3.95	−1.25	6.64	288	288
XVII	$Li^{7}(d,p)Li^{8}$	0	−0.22	6.4	270	265
XVI	$O^{16}(d,d)O^{16}$	0	0	7.7	226	224
XV	$C^{12}(d,d)C^{12}$	0	0	7.07	196	192
XIV	$C^{12}(d,p)C^{13*}$	6.0	−3.3	4.73	158	156
XIII	$Li^{7}(d,d)Li^{7}$	0	0	5.5	131	131
XII	$Li^{7}(d,d)Li^{7*}$	0.477	−0.477	5.13	117	116
	$Li^{6}(d,d)Li^{6}$	0	0	4.95	111	
XI	$C^{12}(d,d)C^{12*}$	3.1	−3.1	4.4	95	92
	$Li^{6}(d,d)He^{4}$	0	22.2	13.6	92	
X	$C^{12}(d,d)C^{12*}$	3.58	−3.58	4.0	·80	80
IX	$Li^{7}(d,\alpha)He^{5}$	0	14.3	11.24	67.5	66
VIII	$Li^{7}(d,t)Li^{6}$	0	0.98	3.75	60	60
VII	$C^{12}(d,d)C^{12*}$	4.5	−4.5	3.2	57	55.5
VI	$O^{16}(d,\alpha)N^{14}$	0	3.06	8.98	49	46
Va	$Li^{7}(d,He^{5})He^{4}$	0	14.3	8.57	40.5	40
Vb	$C^{13}(d,p)C^{13*}$	8.9	6.2	2.04	41	
IV	$O^{16}(d,d)O^{16*}$	6.15	−6.15	2.24	34	33.5
	$O^{16}(d,\alpha)N^{14*}$	2.3	0.76	7.2	35	
III	$O^{16}(d,\alpha)N^{14*}$	4.0	−0.94	5.87	25.5	26
II	$O^{16}(d,\alpha)N^{14*}$	5.0	−1.94	5.1	21	19.5
	$O^{16}(d,d)O^{16*}$	7.0	−7.0	1.48	18	
	$C^{13}(d,\alpha)B^{10}$	0	−1.44	4.6	18	
I	$O^{16}(d,\alpha)N^{14*}$	6.6	−3.54	3.85	14	13
	$C^{13}(d,\alpha)B^{10*}$	0.71	−7.15	4.07	15.3	

was 62.5 and 18.5 kev for deuterons. Since these target losses were less than the uncertainty in the cyclotron beam energy they were neglected.

Ilford E-1 nuclear emulsion plates of 200 microns thickness were used. Since thick emulsions have a tendency to peel under prolonged vacuum conditions it was found advisable to daub the edges of each plate with Polystyrene Q Dope. The procedure of development of these plates was similar to that recommended by Wilson and Vanselow.[3] A Spencer microscope of 900× magnification and a Wetzlar microscope of 720× magnification were used to measure the tracks on the processed plates.

III. METHOD

Figure 1 shows the number of tracks *vs.* range resulting from the bombardment of Li_2O by deuterons. The interpretation of the title, $D-Li_2O-90$, is as follows; the first letter indicates the bombarding particle, the second letter or group of letters indicate the type of target bombarded, and the third set (numbers) indicates the angle at which the scattered and recoil particles were recorded. Thus in the present example Li_2O was bombarded by deuterons and the particles were recorded at 90° to the cyclotron beam.

The following equation[4] may be described as the energy-balance equation for a nuclear reaction.

$$(E_c)^{\frac{1}{2}}=\frac{(m_a m_c E_a)^{\frac{1}{2}}}{m_c+m_d}\cos\theta+\left\{\left[\frac{m_d-m_a}{m_c+m_d}+\frac{m_a m_c}{(m_c+m_d)^2}\cos^2\theta\right]E_a+\frac{m_d Q}{m_c+m_d}\right\}^{\frac{1}{2}}. \quad (1)$$

The subscript a refers to the incident particle, and c and d to the recoil particles. E_c is the energy of the recoil or scattered particle when the energy of the reaction,

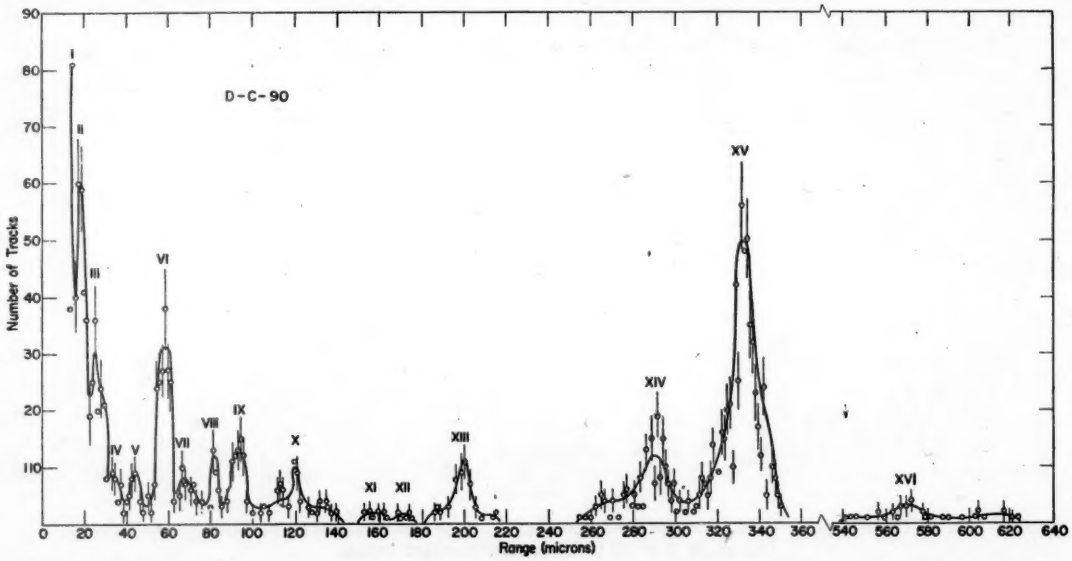

FIG. 2. Distribution in range of particles resulting from the bombardment of a carbon target by deuterons. The angle of recoil is 90° to the cyclotron beam. There are no tracks in the section from 360 to 540 microns. This section was therefore omitted for reasons of space economy.

[3] M. J. Wilson and W. Vanselow, Phys. Rev. **75**, 1144 (1949).
[4] J. Mattauch, *Nuclear Physics Tables* (Interscience Publishers, Inc., New York, 1946), p. 59.

Q, the angle of recoil in the laboratory system, θ, and the energy of the incident particle, E_a, are known. From the recoil energy and the use of the proper range-energy curve, the range of the particle in the emulsion can be computed.

The problem involved in analyzing an experimental curve showing the number of recoils with any given range, is to determine, largely by a method of trial and error, the nuclear reaction which is responsible for each set of recoils. The choice of the proper reaction is quite tedious at times because of the numerous possibilities. Thus if a 10-Mev deuteron is the bombarding particle, the recorded particle may be a proton, a deuteron, a triton, or an alpha-particle, and any one of these recoil particles may have several recoil energies associated with it depending on the number and prominence of the energy levels in the resultant nucleus. Finally these permutations must be calculated not only for all the known elements in the target but also for the suspected impurities. By the use of Eq. (1) the recoil energy or energies of each possible recoil particle for each possible nuclear reaction are determined for a given angle. This angle is the angle with respect to the cyclotron beam in the laboratory system at which the nuclear plate is set to receive the recoil particles. Finally, the recoil energy must be converted to range by use of the proper

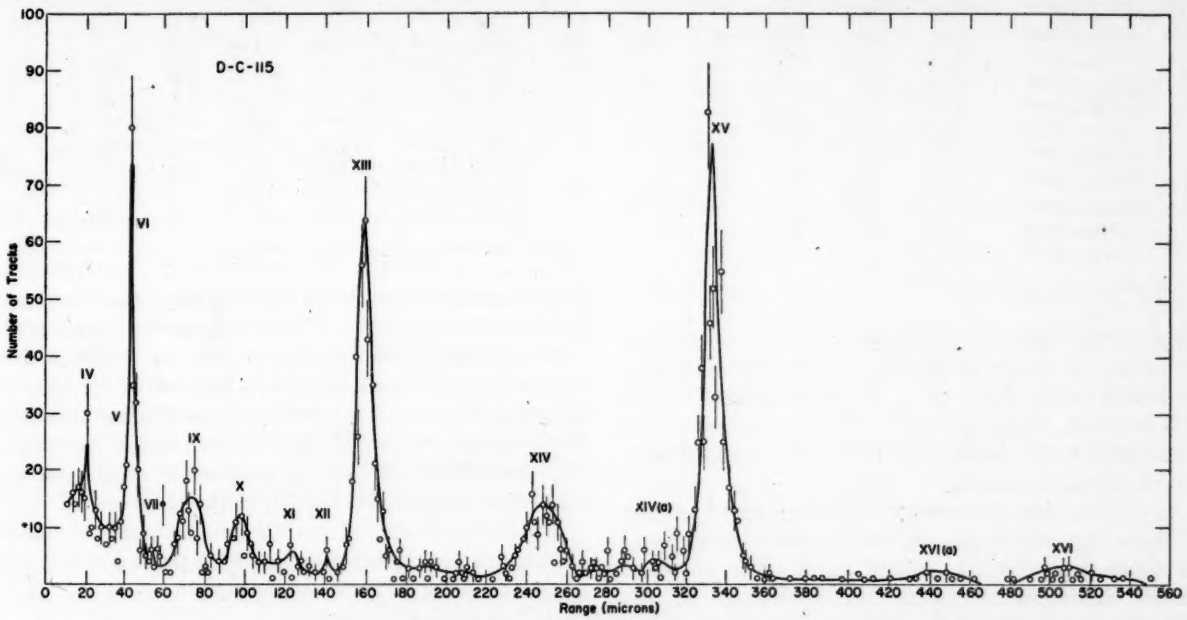

FIG. 3. Distribution in range of particles resulting from the bombardment of a carbon target by deuterons. The angle of recoil is 115° to the cyclotron beam.

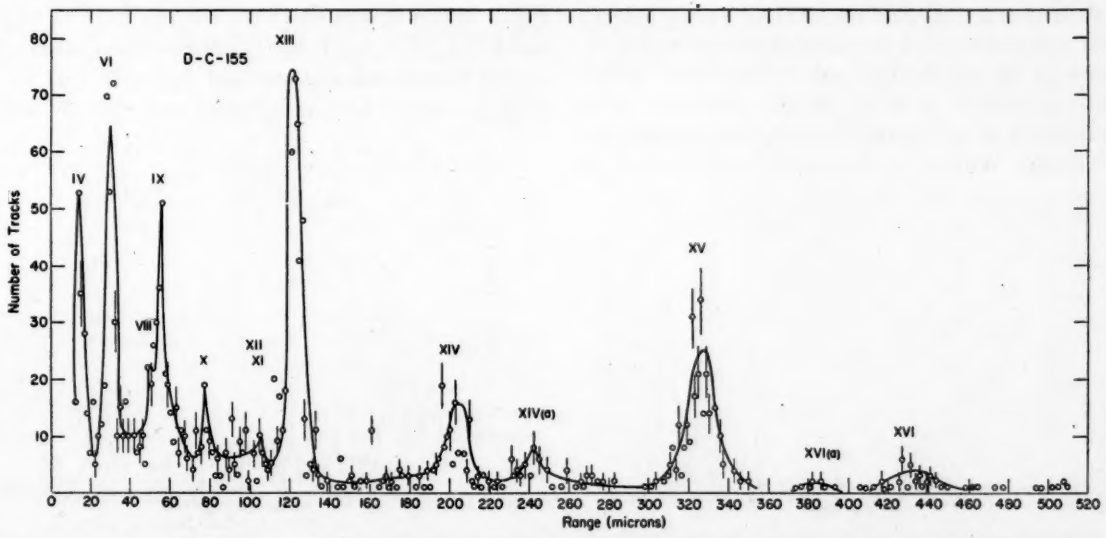

FIG. 4. Distribution in range of particles resulting from the bombardment of a carbon target by deuterons. The angle of recoil is 155° to the cyclotron beam.

TABLE II. $D-C-90$.

Peak number	Reaction	Level (Mev)	Q (Mev)	E (Mev)	Range (microns)	Observed range (microns)
XVI	$C^{12}(d,p)C^{13}$	0	2.70	10.4	591	570
XV	$Au^{179}(d,d)Au^{179}$	0	0	9.78	332	331
XIV	$C^{12}(d,p)C^{13*}$	3.95	−1.25	6.68	290	290
XIII	$C^{13}(d,d)C^{12}$	0	0	7.14	200	200
XII	$C^{13}(d,t)C^{12}$	0	1.3	7.7	176	170
XI	$C^{12}(d,p)C^{13*}$	6.0	−3.3	4.78	160	159
X	$C^{12}(d,p)C^{13*}$	6.84	−4.14	4.0	120	120
IX	$C^{12}(d,d)C^{12*}$	3.1	−3.1	4.48	95	92
VIII	$C^{12}(d,d)C^{12*}$	3.58	−3.58	4.0	80	81
VII	$C^{13}(d,p)C^{13*}$	8.25	−5.55	2.7	64	66
VI	$C^{12}(d,d)C^{12*}$	4.5	−4.5	3.28	59	60
	$C^{13}(d,\alpha)B^{11}$	0	5.12	9.76	56	
V	$C^{12}(d,p)C^{13*}$	8.9	−6.2	2.1	44.0	43.5
	$C^{13}(d,\alpha)B^{11*}$	2.1	3.0	8.36	44	
IV	$C^{13}(d,\alpha)B^{11*}$	4.4	0.72	6.53	30	33
	$C^{12}(d,d)C^{12*}$	5.5	−5.5	2.4	37	
III	$C^{13}(d,\alpha)B^{11*}$	5.8	−0.68	5.5	23.5	25
II	$C^{13}(d,\alpha)B^{10}$	0	−1.44	4.68	18.6	18.5
	$C^{12}(d,\alpha)B^{10*}$	0.41	−1.85	4.39	17	
I	$C^{12}(d,\alpha)B^{10*}$	0.71	−2.15	4.13	15.5	

TABLE III. $D-C-115$.

Peak number	Reaction	Level (Mev)	Q (Mev)	E (Mev)	Range (microns)	Observed range (microns)
XVI	$C^{12}(d,p)C^{13}$	0	2.7	9.5	510	508
XVIa	$C^{12}(d,p)C^{13*}$	1.0	1.7	8.6	440	442
XV	$Au^{179}(d,d)Au^{179}$	0	0	9.7	329	330
XIVa	$C^{12}(d,p)C^{13*}$	3.1	−0.4	6.77	300	304
XIV	$C^{12}(d,p)C^{13*}$	3.95	−1.25	6.0	240	246
XIII	$C^{12}(d,d)C^{12}$	0	0	6.2	158	158
XII	$C^{13}(d,t)C^{12}$	0	1.31	6.55	138	141
XI	$C^{12}(d,p)C^{13*}$	6.0	−3.3	4.2	131	124
X	$C^{12}(d,p)C^{13*}$	6.84	−4.14	3.5	97	98
IX	$C^{12}(d,d)C^{12*}$	3.1	−3.1	3.71	72	73
VIII	$C^{12}(d,d)C^{12*}$	3.58	−3.58	3.4	62	
VII	$C^{12}(d,p)C^{13*}$	8.25	−5.55	2.26	48.5	53
VI	$C^{12}(d,d)C^{12*}$	4.5	−4.5	2.7	44	
	$C^{13}(d,\alpha)B^{11}$	0	5.12	8.35	44	
V	$C^{12}(d,p)C^{13*}$	8.9	−6.25	1.75	32	not ob-
	$C^{13}(d,\alpha)B^{11*}$	2.1	3.0	6.38	26	served
IV	$C^{13}(d,\alpha)B^{11*}$	4.4	0.72	5.32	22	20
	$C^{12}(d,d)C^{12*}$	5.5	−5.5	1.9	26	

range-energy curve. It then becomes possible to compare the predicted ranges arising from these reactions with the actual peaks observed in the experimental curves. This has been done and Table I shows the correlation of each observed peak in Fig. 1 with the assumed reaction or reactions causing it.

An examination of the experimental curves of number of tracks *vs.* track length shows that while some peaks are sharp and distinct, others are so low as to be scarcely distinguishable from the background. In connection with the low peaks, two comments are made. First, when scattering experiments were conducted using the gold foil alone, a careful examination of the plates showed practically no tracks at all having lengths that did not correspond to scattering from the gold. This absence of "accidentals" or "background" under the same conditions used in regular scattering runs lends assurance to the significance of peaks having only 8 or 10 tracks. While 8 or 10 tracks do not constitute good statistical data, their importance grows when it is known that no tracks at all are the normal expectancy.

The second point concerning the low peaks is that some of them have frankly been located on the basis of known energy levels, where the small number of counts in the present work left the exact location uncertain. This has been done for the purpose of exhibiting the relative heights of the various peaks observed.

The use of Ilford E-1 nuclear emulsions allows one to distinguish clearly between an alpha-particle track and a proton track. The same cannot be said for short proton and deuteron tracks.

Table I correlates each peak of Fig. 1 with the assumed reaction causing it. Thus peak number XXI in Fig. 1 is due to protons from the reactions $O^{16}(d,p)O^{17}$ and $C^{12}(d,p)C^{13}$, see Table I, column two. Column three of this table is marked *level* and indicates that for this peak no energy level is involved and that O^{17} was left

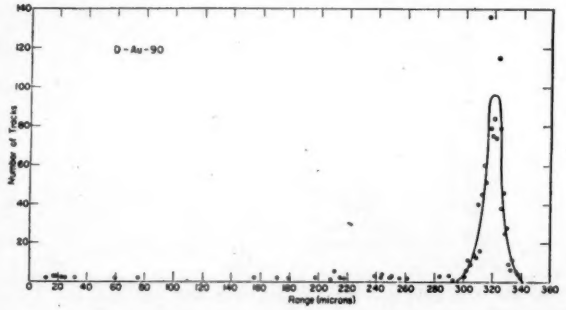

FIG. 5. Distribution in range of particles resulting from the bombardment of a gold target by deuterons. The angle of recoil is 90° to the cyclotron beam.

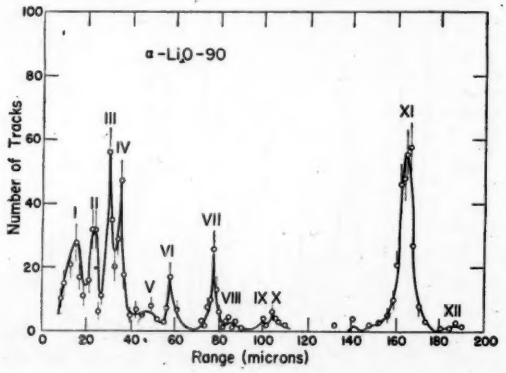

FIG. 6. Distribution in range of particles resulting from the bombardment of a Li_2O target by alpha-particles. The angle of recoil is 90° to the cyclotron beam.

TABLE IV. $D-C-155$.

Peak number	Reaction	Level (Mev)	Q (Mev)	E (Mev)	Range (microns)	Observed range (microns)
XVI	$C^{12}(d,p)C^{13}$	0	2.7	8.7	447	450
	$O^{16}(d,p)O^{17}$	0	1.9	8.78	450	
XVIa	$C^{12}(d,p)C^{13*}$	1.0	1.7	7.85	380	382
XV	$Au^{179}(d,d)Au^{179}$	0	0	9.6	323	328
XIVa	$C^{12}(d,p)C^{13*}$	3.1	−0.4	6.07	238	241
XIV	$C^{12}(d,p)C^{13}$	3.95	−1.25	5.35	194	202
XIII	$C^{12}(d,d)C^{12}$	0	0	5.3	124	121
XII	$C^{13}(d,t)C^{12}$	0	1.31	5.51	105	105
XI	$C^{12}(d,p)C^{13*}$	6.0	−3.3	3.69	105	105
X	$C^{12}(d,p)C^{13*}$	6.84	−4.14	3.04	76	77
IX	$C^{12}(d,d)C^{12*}$	3.1	−3.1	3.1	55	56
VIII	$C^{12}(d,d)C^{12*}$	3.58	−3.58	2.7	45	49
VII	$C^{12}(d,p)C^{13*}$	8.25	−5.55	1.9	37	
VI	$C^{12}(d,d)C^{12*}$	4.5	−4.5	2.1	31	29
	$C^{13}(d,\alpha)B^{11}$	0	5.12	6.9	33	
V	$C^{13}(d,p)C^{13*}$	8.9	−6.25	1.42	24	
	$C^{13}(d,\alpha)B^{11*}$	2.1	3.02	5.7	24.5	

TABLE V. $\alpha-Li_2O-90$.

Peak number	Reaction	Level (Mev)	Q (Mev)	E (Mev)	Range (microns)	Observed range (microns)
XII	$Li^6(\alpha,d)Be^8$	0	−1.6	6.7	180.0	186
XI	$Au^{179}(\alpha,\alpha)Au^{179}$	0	0	19.6	168.0	164
X	$Li^7(\alpha,p)Be^{10*}$	3.36	−5.94	3.69	106.0	104
II	$Li^7(\alpha,t)Be^8$	0	−2.56	5.42	102.0	100
VIII	$Li^6(\alpha,d)Be^{8*}$	3.1	−4.7	4.2	86.0	84.5
VII	$O^{16}(\alpha,\alpha)O^{16}$	0	0	12.0	78.0	77.5
VI	$C^{12}(\alpha,\alpha)C^{12}$	0	0	10	0.58	57.5
	$Li^7(\alpha,d)Be^9$	0	−7.1	3.38	61.0	
V	$Li^7(\alpha,t)Be^{8*}$	3.1	−5.66	3.16	48.0	49
	$Li^6(\alpha,d)Be^{8*}$	4.8	−6.4	2.86	56.0	
IV	$O^{16}(\alpha,\alpha)O^{16*}$	6.0	−6.0	7.2	35.0	35
	$O^{16}(\alpha,\alpha)O^{16*}$	6.15	−6.15	7.1	34.0	
III	$O^{16}(\alpha,\alpha)O^{16*}$	7.0	−7.0	6.75	32.0	29.5
	$C^{12}(\alpha,\alpha)C^{12*}$	4.5	−4.5	6.6	30.5	
II	$Li^7(\alpha,\alpha)Li^7$	0	0	5.46	23	
	$Li^7(\alpha,\alpha)Li^{7*}$	0.477	−0.477	5.16	21.5	
I	$Li^6(\alpha,\alpha)Li^6$	0	0	4.0	15.0	15.5

in the ground state. The energy of reaction, Q, is given in column four as 1.94 Mev. Q is usually obtained either from Lauritsen[5] or, if not given there, is computed from the masses involved.[6,7] Column five gives the recoil energy, E, of the light particle as 10.08 Mev. This value is obtained from Eq. (1) assuming that the bombarding energy of the deuteron is 9.9 Mev. The range is computed from the range-energy curve for protons and appears in column six. The observed range appears in column seven.

IV. RESULTS

(a) Reactions caused by 9.9-Mev deuteron bombardment of a thin Li_2O target. See Fig. 1.

1. $O^{16}(d,p)O^{17}$

Peak	Energy levels in O^{17}	Comments
XXI	Ground state	XXI and XX may contain some protons from $C^{12}(d,p)C^{13}$ (from carbon contaminant).
XX	0.88 Mev	

2. $O^{16}(d,d)O^{16}$

Peak	Energy levels in O^{16}	Comments
XVI	Ground state	Evidence for an O^{16} level at 6.0 Mev as listed by Lauritsen[5] is obscured by the background of tracks.
IV	6.15 Mev	
II	7.0 Mev	

3. $O^{16}(d,\alpha)N^{14}$

Peak	Energy levels in N^{14}	Comments
VI	Ground state	II and I are somewhat obscured by alpha-particles from $C^{12}(d,\alpha)B^{10}$. Evidence for N^{14} levels at 5.5 or 6.1 Mev as listed by Lauritsen[5] is obscured by the background tracks.
IV	2.3 Mev	
III	4.0 Mev	
II	5.0 Mev	
I	6.6 Mev	

4. $C^{12}(d,p)C^{13}$

Peak	Energy levels in C^{13}	Comments
XXI	Ground state	No evidence for levels in C^{13} at 5.0 and 8.25 Mev as listed by Lauritsen.[5]
XVIII	3.95 Mev	
XIV	6.0 Mev	
V	8.9 Mev	

5. $C^{12}(d,d)C^{12}$

Peak	Energy levels in C^{12}	Comments
XV	Ground state	See below.
XI	3.1 Mev	
X	3.58 Mev	
VII	4.5 Mev	

Further discussion of this section will be found in paragraph (b).

6. $Li^7(d,p)Li^8$

Peak	Energy levels in Li^8	Comments
XVII	Ground state	Further decay of Li^8 is not considered since the half-life is relatively long in comparison to the collision process.

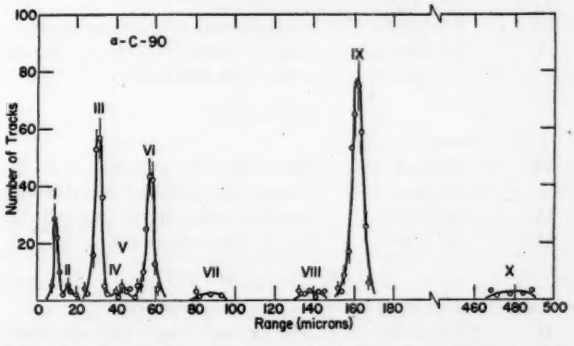

FIG. 7. Distribution in range of particles resulting from the bombardment of a carbon target by alpha-particles. The angle of recoil is 90° to the cyclotron beam.

[5] T. Lauritsen, Preliminary Report No. 5, National Research Council, Nuclear Science Series (1949).

[6] *Handbook of Chemistry and Physics* (1949), thirty-first edition.

[7] K. T. Bainbridge, Preliminary Report No. 1, National Research Council, Nuclear Science Series (1948).

TABLE VI. $\alpha-C-90$.

Peak number	Reaction	Level (Mev)	Q (Mev)	E (Mev)	Range (microns)	Observed range (microns)
X	$C^{12}(\alpha,p)N^{15}$	0	−4.92	9.14	480	480
IX	$Au^{179}(\alpha,\alpha)Au^{179}$	0	0	19.13	161.5	161
VIII	$C^{12}(\alpha,p)N^{15*}$	5.4	−10.12	4.26	134	138
VII	$C^{12}(\alpha,p)N^{15*}$	6.2	11.1	3.33	90	85
VI	$C^{12}(\alpha,\alpha)C^{12}$	0	0	10	58	58
V	$C^{12}(\alpha,p)N^{15*}$	7.5	12.4	2.1	43.5	44
IV	$C^{12}(\alpha,\alpha)C^{12*}$	3.1	−3.1	7.68	39	39
III	$C^{12}(\alpha,\alpha)C^{12*}$	4.5	−4.5	6.7	31	30
II	$C^{12}(\alpha,\alpha)C^{12*}$	7.3	−7.3	4.5	18	15.5
I	$C^{12}(\alpha,\alpha)C^{12*}$	9.5	−9.5	2.88	10	8.5

7. $Li^7(d,d)Li^7$

Peak	Energy levels in Li^7	Comments
XIII	Ground state	Elastically scattered deuterons from Li^6 will also contribute to XII.
XII	0.48 Mev	

The number of observed tracks was too small to permit any conclusions about additional excited states in Li^7 in the region from 0.5 Mev to 1 Mev.

8. $Li^7(d,\alpha)He^5$

By using the corrected range-energy curve the Q of this reaction is 14.3 Mev as given by Lauritsen.[5]

(b) Reactions caused by 10-Mev deuteron bombardment of a thin C target. See Figs. 2 to 4, also Tables II to IV.

1. $C^{12}(d,p)C^{13}$

Peak	Energy levels in C^{13}	Comments
XVI	Ground state	XVIa does not appear at 90° to the cyclotron beam. X is a new level in C^{13} that appears with about the same intensity as XIVa does.
XVIa	1.0 Mev	
XIVa	3.1 Mev	
XIV	3.95 Mev	
XI	6.0 Mev	
X	6.84 Mev	
VII	8.25 Mev	
V	8.9 Mev	

It is of interest to compare the relative intensities of these peaks and how they change as one goes to larger angles as shown in the successive figures.

2. $C^{12}(d,d)C^{12}$

Peak	Energy levels in C^{12}	Comments
XIII	Ground state	The VIII is somewhat doubtful as it appears only at 90° and not at 115° and 155°. VI and IV contain some alpha-particles from the reaction $C^{13}(d,\alpha)B^{11}$. There is 1.1 percent C^{13} in the target.
IX	3.1 Mev	
VIII	3.85 Mev	
VI	4.5 Mev	
IV	5.5 Mev	

3. $C^{12}(d,\alpha)B^{11}$

Peak	Energy levels in B^{11}	Comments
VI	Ground state	Since there is so little C^{13} in the target it is doubtful whether this reaction contributes appreciably to the observed peaks.
V	2.1 Mev	
IV	4.4 Mev	
III	5.8 Mev	

4. $C^{12}(d,\alpha)B^{10}$

Peak	Energy levels in B^{10}	Comments
II	0 and 0.41 Mev	The ground state and the 0.41-Mev level fall close enough together to be represented by one peak, II.
I	0.71 Mev	

(c) Figure 5 is a background run to demonstrate that there is only one peak resulting from the bombardment of gold by deuterons, and that it is due to elastically scattered deuterons.

(d) Reactions caused by 20-Mev alpha-particle bombardment of a thin Li_2O target. See Fig. 6 and Table V.

1. $O^{16}(\alpha,\alpha)O^{16}$

Peak	Energy levels in O^{16}	Comments
VII	Ground state	The 0.88-Mev level does not appear. The resolution of the instrument does not allow for the separation of the 6.0- and 6.15-Mev levels. III contains some alpha-particles elastically scattered from carbon.
IV	6.0 and 6.15 Mev	
III	7.0 Mev	

2. $C^{12}(\alpha,\alpha)C^{12}$

Peak	Energy levels in C^{12}	Comments
VI	Ground state	That VI and III are correctly identified is readily shown by superimposing Fig. 7 on Fig. 6.
III	4.5 Mev	

3. $Li^7(\alpha,p)Be^{10}$

Peak	Energy levels in Be^{10}	Comments
X	3.36 Mev	There are a few tracks from the ground level but too few to be shown by a peak. These tracks are easily recognized since they are produced by singly charged particles.

4. $Li^7(\alpha,d)Be^9$

Peak	Energy levels in Be^9	Comments
VI	Ground state	

5. $Li^7(\alpha,t)Be^8$

Peak	Energy levels in Be^8	Comments
IX	Ground state	In V there are probably a few deuterons due to the reaction $Li^6(\alpha,d)Be^{8*}$ where Be^{8*} is in the 4.8-Mev level. The further decay of Be^8 into two alpha-particles is not considered since no broad peak as would result from such a three-body process has been observed.
V	3.1 Mev	

6. $Li^7(\alpha,\alpha)Li^7$

Peak	Energy levels in Li^7	Comments
II	Ground state and 0.48-Mev level	The instrument is incapable of distinguishing between these two states at low energies.

7. $Li^6(\alpha,\alpha)Li^6$

Peak	Energy levels in Li^6	Comments
I	Ground state	To obtain greater recoil energies a smaller scattering angle will be necessary.

(e) Reactions caused by 20-Mev alpha-particle bombardment of a thin carbon target. See Fig. 7 and Table VI.

1. $C^{12}(\alpha,p)N^{15}$

Peak	Energy levels in N^{15}	Comments
X	Ground state	
VIII	5.4 Mev	
VII	6.2 Mev	
V	7.5 Mev	

2. $C^{12}(\alpha,\alpha)C^{12}$

Peak	Energy levels of C^{12}	Comments
VI	Ground state	If IV exists, it is a very weak peak. Lauritsen[5] lists IV as a doubtful level. Other doubtful levels at 3.58 and 5.5 Mev do not appear.
IV	3.1 Mev	
III	4.5 Mev	
II	7.3 Mev	
I	9.5 Mev	

From peak XI in Fig. 6 and IX in Fig. 7, which are due to the elastic scattering of alpha-particles from gold, it was found necessary to modify the range-energy curve of Lattes[8] at higher energies. Other evidence as to a need for modification came from an alpha-alpha-bombardment when the recoiling and scattered particles were recorded at small angles. The observed ranges fell short of the predicted ranges when Lattes' curve was used. This was true for the three aforementioned cases even after all possible corrections were made. If the beam energy were lower than 20 Mev, i.e., 17.5 Mev, then XI in Fig. 6 and IX in Fig. 7 would be correctly identified but then the other peaks in Figs. 6 and 7 would be displaced too far to the right. Therefore it was assumed that the bombarding energy was 20 Mev, that the lower portion of the alpha-energy range curve, below 10 Mev, was correct, but that above 10 Mev a modification was necessary. This modification was made from the proton range-energy curve by assuming that an alpha-particle and a proton of the same velocity have the same range. The corrected curve has already been published.

[8] Lattes, Fowler, and Cuer, Proc. Phys. Soc. London **59**, 883 (1947).

V. CONCLUSION

The 1.0-Mev level in C^{13} has been confirmed, and a new level at 6.8 Mev has been determined. The proton group giving rise to the 1.0-Mev level is small statistically, consisting of only approximately 11 tracks at 115°, yet this number is large compared to the expected background at this range and is an appreciable fraction of the 33 proton tracks observed which resulted from C^{13} in the ground state. A level in C^{12} at 3.58 Mev has been found at 90° but the results are doubtful because of non-appearance at 115° and 155° or under alpha-particle bombardment. The relative scattering of deuterons and alpha-particles from nuclei in the ground state and in the various nuclear energy levels are illustrated. The results indicate that 10-Mev deuterons are more effective in studying energy levels than are 20-Mev alpha-particles. Finally the alpha-particle range-energy curve, as applied to Ilford E-1 nuclear emulsions, has been modified at higher energies for alpha-particles.

This author wishes to thank Messrs. Chia-Hua Chang and Wen-Jsao Yang for their careful reading of the plates, and Dr. Robert N. Varney for his constructive criticism.

PHYSICAL REVIEW VOLUME 80, NUMBER 5 DECEMBER 1, 1950

The New Element Berkelium (Atomic Number 97)*

S. G. THOMPSON, A. GHIORSO, AND G. T. SEABORG
Radiation Laboratory and Department of Chemistry, University of California, Berkeley, California

(Received July 24, 1950)

An isotope of the element with atomic number 97 has been discovered as a product of the helium ion bombardment of americium. This isotope decays with the emission of alpha-particles of maximum energy 6.72 Mev (30 percent) and it emits lower energy alpha-particles of energies 6.55 Mev (53 percent) and 6.20 Mev (17 percent). The half-life of this isotope is 4.6±0.2 hr. and it decays primarily by electron capture with about 0.1 percent branching decay by alpha-particle emission. The mass number is probably 243 as indicated by chemical separation of the alpha-particle and electron-capture daughters. The name berkelium, symbol Bk, is proposed for element 97.

The chemical separation of element 97 from the target material and other reaction products was made by combinations of precipitation and ion exchange adsorption methods making use of its anticipated (III) and (IV) oxidation states and its position as a member of the actinide transition series. The distinctive chemical properties made use of in its separation and the equally distinctive decay properties of the particular isotope constitute the principal evidence for the new element.

The isotope Cm^{243} is identified experimentally as a result of its production as a decay product of Bk^{243}. The Cm^{243} decays by the emission of alpha-particles of maximum energy 5.89 Mev (15 percent) and lower energy alpha-particles of energy 5.79 Mev (85 percent); the half-life for alpha-particle emission is estimated to be roughly 100 yr.

I. INTRODUCTION

THE transuranium elements numbers 96, curium, and 95, americium, were discovered in 1944, the first by Seaborg, James, and Ghiorso,[1] the second by Seaborg, James, and Morgan.[2] The search for transcurium elements was begun by us in the fall of 1945. It was anticipated[3] that element 97 as eka-terbium in the actinide transition series would possess oxidation states (III) and (IV) with properties similar to curium in the (III) oxidation state and to plutonium (IV) in

* This work was performed under the auspices of the AEC.

[1] Seaborg, James, and Ghiorso, *The Transuranium Elements: Research Papers* (McGraw-Hill Book Company, Inc., New York, 1949), Paper No. 22.2, National Nuclear Energy Series, Plutonium Project Record, Vol. 14B.

[2] Seaborg, James, and Morgan, National Nuclear Energy Series, see reference 1, Paper No. 22.1.

[3] G. T. Seaborg, Nucleonics **5**, No. 5, 16 (1949).

its (IV) oxidation state. It was more difficult to estimate the oxidation potential of the (III)→(IV) couple but it was expected that element 97 would be somewhat easier to oxidize than terbium (III) which is not oxidizable to higher states in aqueous solution at all. The salient point is that if element 97 could not be converted to an oxidation state higher than (III) in solutions it would be extremely difficult to separate in a short period of time from rare earth elements and from the actinide elements from which it would be produced. Americium is very difficult and curium probably impossible to oxidize above the (III) state in aqueous solution.[3] In other words, it appeared that it might be necessary to use tedious rare earth separations in order to separate and identify the new element, the isotopes of which do not exist in nature and whose neutron-deficient isotopes as produced by alpha-particle and deuteron bombardments would have short half-lives as a result of considerable instability toward alpha-particle emission and electron-capture decay.

In view of the fact that sufficiently intense beams of energetic particles of nuclear charge greater than two were not available at the time of this research, it is obvious that there were only two methods of approach to the production of element 97. The first approach was through the bombardment of americium with helium ions or the bombardment of curium with deuterons or helium ions. The second (not yet successful) was through intensive neutron irradiations of curium in order to produce eventually through successive (n, γ) reactions a curium isotope of mass sufficient to be unstable toward negative beta-particle decay and so to produce an isotope of element 97.

Both methods were employed in attempting to observe element 97 and for each, different chemical procedures were used. Some of these procedures were designed to separate the new element in oxidation states greater than (III) and others were used on the assumption that element 97 existed in solution under most conditions in the tripositive oxidation state.

Although the broad assumptions made when the work was started were all correct, the experiments done prior to December, 1949, were unsuccessful for many reasons which may be grouped into three classes. First, the methods of predicting the properties of the new isotopes were relatively undeveloped and the experiments were never done with sufficient speed. The further development of the alpha-decay systematics[4] made it possible to estimate energies and half-lives for alpha-particle decay. The resulting estimated alpha-particle decay energies could be used in calculating by closed decay cycles the total energies for electron-capture decay or beta-particle decay. An empirical method of estimating electron-capture half-lives from disintegration energies was also developed[5] which, although very rough due to uncertainties in the degree of prohibition of this mode of decay in any given case, was very useful in making half-life estimates.

The second major difficulty was that of obtaining sufficiently large amounts of americium and curium as sources for the production of element 97. Eventually americium became available in milligram amounts through neutron irradiation of plutonium.[6] The isolation of the americium from the plutonium required tedious chemical procedures. The curium was produced in smaller amounts by the irradiation of americium with neutrons.[2, 6]

The intense radioactivity of the americium and curium source materials presented the third major difficulty. This radioactivity necessitated not only the design and development of advanced techniques and equipment[7] for its safe handling, but also made it necessary to attain enormous separation factors in the isolation of the new element from the target material in order to be able to detect the small amounts of radioactivity due to it. Furthermore, this high degree of separation had to be carried out in good yield in a short length of time.

Essentially three chemical steps were developed to solve these chemical problems. The conversion of the americium to a hexapositive oxidation state[8] was used in the rapid removal of the bulk of the bombarded americium. An ion exchange method involving the separation of the actinide elements as a group from the rare earth fission products by elution with concentrated HCl from a cation exchange column[9] was exploited for the rapid separation of the tripositive actinide elements. An ion exchange method involving elution from a cation exchange resin at elevated temperature with ammonium citrate solution was used in the rapid separation of the tripositive actinide elements from each other. These steps had been worked out adequately by December, 1949, and the first successful experiment

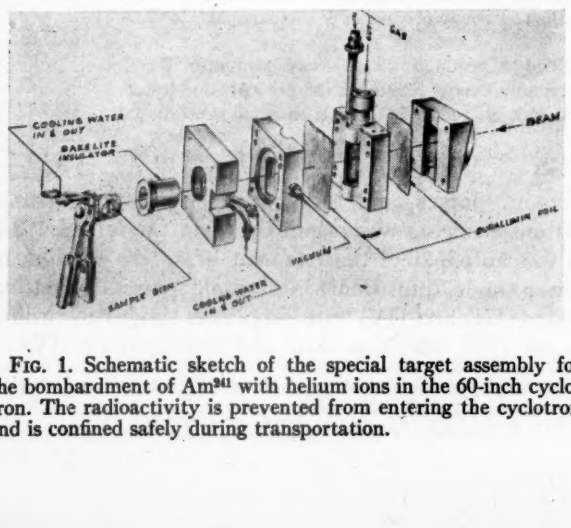

FIG. 1. Schematic sketch of the special target assembly for the bombardment of Am^{241} with helium ions in the 60-inch cyclotron. The radioactivity is prevented from entering the cyclotron and is confined safely during transportation.

[4] Perlman, Ghiorso, and Seaborg, Phys. Rev. 77, 26 (1950).
[5] S. G. Thompson, Phys. Rev. 76, 319 (1949).
[6] Ghiorso, James, Morgan, and Seaborg, Phys. Rev. 78, 472 (1950).
[7] Nelson Garden and co-workers (unpublished work).
[8] Asprey, Stephanou, and Penneman, J. Am. Chem. Soc. 72, 1425 (1950).
[9] K. Street, Jr. and G. T. Seaborg, J. Am. Chem. Soc. 72, 2790 (1950).

was done on December 19, 1949, as recently reported in a preliminary fashion.[10] Three successful confirmatory experiments were completed by February 15, 1950. For convenience of expression the name berkelium, symbol Bk, will be employed in the following discussion. The reasons for suggesting this name will be presented at the end of the paper.

II. EXPERIMENTAL METHODS

Extraction of Americium

The Am^{241} used as target material for the production of element 97 was separated from strongly neutron-irradiated plutonium into which it grew as the daughter of the beta-particle decay of ~10-yr. Pu^{241}. The isotope Pu^{241} is produced[6] by the reactions $Pu^{239}(n,\gamma)Pu^{240}$ $(n,\gamma)Pu^{241}$ and the americium was separated and purified by combinations of precipitation and ion exchange methods.

Preparation and Bombardment of Targets

The americium targets were prepared for bombardment in the Crocker Laboratory 60-inch cyclotron by the evaporation of americium nitrate solutions in small platinum dishes of ~0.5-cm^2 area followed by ignition to form black americium oxide. The americium used was of about 96 percent chemical purity as determined by spectrographic analysis. The major impurities were sodium (about 1.5 percent), zinc (about 1 percent), calcium (0.2 percent), aluminum (0.5 percent), and titanium (0.2 percent). These targets were placed inside a special target assembly, indicated schematically in Fig. 1, which was designed to prevent alpha-radioactivity from entering the cyclotron and to eliminate its spread to the surroundings during transportation. In this assembly the particle beam from the cyclotron was passed through two thin duralumin foils (each 1.5 mil in thickness) before entering the evacuated compartment containing the sample, and the compartment was isolated from the surroundings. The beam was also passed through a thin platinum foil placed directly in contact with and over the target dish. The thickness of this foil was changed to vary the energy of the particles (initial energy about 40 Mev). The duralumin foils reduced the energy to about 37 Mev and the 0.5-mil platinum foil further reduced it to about 35 Mev. This platinum foil also served to reduce the spread of radioactivity through the evacuated compartment. The back of the platinum dish containing the sample was cooled directly with a water jet. The intensity of the beam of helium ions striking the sample was determined by measuring the charge accumulated on the insulated target dish and foil. The energies of the helium ions were calculated as ranging from 30 to 35 Mev in various bombardments. (The intensity of the bombardments averaged about 2 $\mu a/cm^2$ and the time of bombardment was usually about 6 hr.)

[10] Thompson, Ghiorso, and Seaborg, Phys. Rev. 77, 838 (1950).

Chemical Procedure

Following the bombardments, the platinum dish containing the sample was removed to a gloved box and the americium oxide dissolved in 6*M* nitric acid with heating (about 75°C). Americium hydroxide was precipitated with the addition of excess ammonium hydroxide and separated by centrifugation. The hydroxide was dissolved in dilute (0.1*M*) HNO_3, the solution was made 0.2*M* in ammonium persulfate and 0.2*M* in ammonium sulfate and the americium converted to the hexapositive (fluoride-soluble) oxidation state by heating (in the case of the best results) for about 1½ hr. at 75°C. The major part of the americium was separated early in this manner in order to reduce the bulk of material with the berkelium and make possible the use of resin columns of smaller diameter. Although not absolutely necessary, this improves the sharpness and speed of the chemical separations. Unoxidized americium was precipitated by the addition of hydrofluoric acid (3*M*), the insoluble americium (III) fluoride carrying with it curium, element 97, and some—mostly rare earth—fission products. The fluoride precipitate was converted to a hydroxide by treatment with 6*M* KOH followed by centrifuging and washing. The hydroxide precipitate was dissolved in dilute perchloric acid (0.5*M*) and the mixture of radioactivities was adsorbed on a small amount of ammonium form Dowex-50 resin[10a] (spherical fines) which was then transferred to a 20-cm length, 2-mm diameter column packed with the same resin. The column was surrounded by a vapor jacket through which passed trichloroethylene vapor to maintain the temperature at about 87°C. The elution was performed by passing ammonium citrate (buffered with citric acid to *p*H 3.5—total citrate concentration 0.25*M*) through the column at a rate of 1 drop (~0.030 cm^3) about every two minutes and the drops were collected separately. (The element 97 fractions were usually collected in drops 40–45, and for comparison curium was collected in drops 65–70. The element 97 position is between terbium and gadolinium on these columns.) In order to separate the element 97 which was being sought from residual rare earth fission products, the citrate fractions in which it was present were combined and made acidic by the addition of hydrochloric acid. The activity was adsorbed on Dowex-50 resin and transferred to an approximately 7-cm length column packed with Dowex-50 resin (hydrogen form). Berkelium was then removed from the column more rapidly than the lanthanide elements by elution with 13*M* HCl, which forms stronger complex ions with tripositive actinide elements than it does with rare earth elements.[9] In the first successful search for element 97, the column employing hydrochloric acid for elution was used first for separation of the actinide elements as a group from the rare earth elements before using the column in which elution is performed with citrate to separate the in-

[10a] Dow Chemical Company, Midland, Michigan.

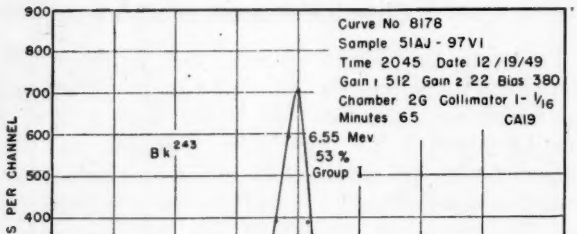

FIG. 2. Typical alpha-particle pulse analysis curve of the 4.6-hr. radioactivity obtained from the chemical separations of an element 97 fraction. The three alpha-particle groups, their energies and abundances are shown.

dividual actinide elements, thus making it possible to observe electron and electromagnetic radiations as well as alpha-radioactivity during the latter step. In this case the excess hydrochloric acid was removed from the actinide fraction elutriant solution by rapid evaporation of the solution in the presence of an air jet. The berkelium separated in either manner was carrier-free and could be evaporated directly on platinum plates for counting purposes. Ignition of the plates to red heat removed the citric acid. In some cases where extremely thin samples of the radioactivity were desirable for alpha-pulse analysis, berkelium was volatilized in a vacuum from a hot filament and collected on a platinum disk.

In those experiments directed toward the determination of the mass number of the berkelium isotope, a radiochemically pure element 97 fraction was obtained and after its decay the residual daughter activities were separated in another high temperature column employing Dowex-50 resin and ammonium citrate as the eluting agent as described above. Traces of Am^{241} and Cm^{242} were present and served to mark the positions of these elements in the fractions from the column. The thin plates made of these fractions were examined in the differential pulse analyzer and in the windowless proportional counter mentioned below.

Experimental Methods Used in Radioactivity Measurements

The thin deposits of the radiochemically pure element 97 fractions on platinum plates were examined in the differential alpha-particle pulse analyzer.[11] In this instrument individual pulses from an ionization chamber are sorted electronically and recorded on 48 fast mechanical registers in such a manner as to separate the individual alpha-particle energies from a mixture of alpha-emitters. In establishing values for the alpha-particle energies of the new isotope, direct comparison was made with pulse analyses of thin samples of isotopes whose alpha-energies are well known, using the same instrumental conditions.

The thin deposits containing the element 97 fraction were also examined for any electron, x-ray, or gamma-ray radiations which might accompany decay by electron capture. In some instances high efficiency was obtained by using a windowless proportional counter to detect Auger electrons. The samples obtained in the precipitation chemistry experiments (to be mentioned) were counted close to the thin window (3 mg/cm² mica) of a bell-jar-type Geiger counter filled with a mixture of 0.8 cm pressure of amyl acetate plus 11 cm pressure of xenon instead of the usual alcohol-argon mixture. The use of xenon enhances the efficiency for counting L x-rays. Hereafter in this paper this type of tube will be referred to as a xenon-filled Geiger tube. In the case of these relatively thick samples an aluminum

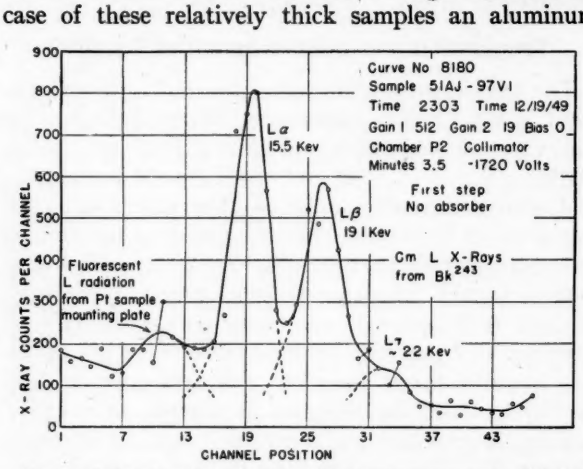

FIG. 3. L x-ray pulse analysis of the electron-capture radiations of Bk^{243} using a xenon gas proportional counter connected to the differential pulse analyzer. The energies of these x-rays agree well with the values expected for curium.

absorber of thickness ~20 mg/cm² was used between the sample and counter window to reduce errors due to variable absorption of soft components as a function of differences in sample thickness. In some of the experiments samples were counted with various thicknesses of absorber (usually beryllium and beryllium together with lead) between the sample and the counter window in order to estimate energies and distinguish between electrons and electromagnetic radiations.

The L x-rays as counted in the xenon-filled Geiger counter were used as the basis for calculation of disintegration rates and total numbers of atoms. The L x-ray counting yield for the electron-capture isotope U^{231} had been determined previously by Crane, Ghiorso, and Perlman[12] using the same counter and conditions of measurement as were used by us. They compared the number of L x-ray counts of their U^{231} samples with the number of Pa^{231} daughter alpha-particles observed after complete decay. Defining counting yield as the

[11] Ghiorso, Jaffey, Robinson, and Weissbourd, National Nuclear Energy Series, see reference 1, Paper No. 16.7.

[12] Crane, Ghiorso, and Perlman (unpublished work).

total number of L x-ray counts at approximately 10 percent geometry observed with a xenon-filled Geiger tube corrected to the number of counts at no absorber divided by the corresponding total number of electron-capture daughter atoms produced, Crane *et al.* obtain a counting yield of 0.0025. The same factor was used in the present work to calculate the disintegration rate after making suitable corrections for the differences in absorption and in counting efficiency in the counter used resulting from differences in energies of the x-rays of curium and protactinium. The use of this method tacitly assumes that the number of L x-rays emitted per disintegration is the same for the two isotopes U^{231} and Bk^{243}. There was some experimental justification for this as evidenced by the ratios of counting rates in the xenon-filled counter and in the windowless proportional counter where the Auger electrons are counted. (These measurements made under as nearly identical conditions as possible gave ratios for the two isotopes which agreed within five percent.) Further justification was found in the observation that there are no significant numbers of soft gamma-rays of energies close to those of the L x-rays emitted in the decay of either isotope. This observation was made by pulse analysis of the pulses produced in a xenon gas-filled proportional counter using the same 48-channel instrument as was used in measuring alpha-particle energies. This method of x-ray energy determination is similar to one reported previously.[13] The energies of the L x-rays were established to be approximately those of curium and no extraneous soft gamma-rays were observed.

III. EXPERIMENTAL RESULTS

Results of Radioactivity Measurements

Applying the procedures described above to helium ion bombarded targets of Am^{241} and examining the radioactivity in the separated fractions expected to contain element 97, distinctive high energy alpha-radioactivity and radiations typical of the electron-capture process were revealed. All of the radioactivity decayed with a 4.6-hr. half-life.

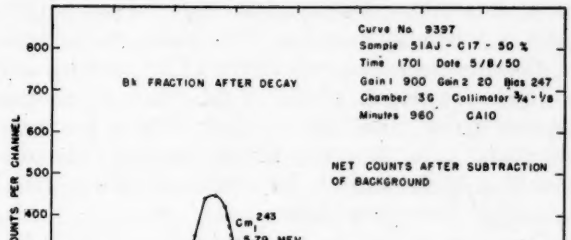
Curve No. 9397
Sample 51AJ - C17 - 50 %
Time 1701 Date 5/8/50
Gain 1 900 Gain 2 20 Bias 247
Chamber 3G Collimator ¾ - ⅛
Minutes 960 CA10
Bk FRACTION AFTER DECAY
NET COUNTS AFTER SUBTRACTION OF BACKGROUND
ALPHA-COUNTS PER CHANNEL
CHANNEL POSITION
Cm1 243 5.79 MEV
Cm0 243 5.89 MEV
Cm 242 6.08 MEV

FIG. 4. Alpha-pulse analysis of alpha-radioactivity remaining after complete decay of the 4.6-hr. radioactivity. A new alpha-radioactivity of energy 5.89 Mev (15 percent) and 5.79 Mev (85 percent) is observed which was proved by chemical separations to be a curium isotope (probable mass 243). The isotope Cm^{242} is present as a trace not completely removed in the chemical separations.

[13] Kirkwood, Pontecorvo, and Hanna, Phys. Rev. 74, 497 (1948).

The results of a typical experiment in which alpha-particle energies and group abundances were measured by differential pulse analysis are shown in Fig. 2. The rate of decay of each energy group was measured by plotting the area under each peak *versus* the time of decay of the radioactivity. All three peaks were observed to decay with a half-life of 4.6±0.2 hr. through a decay factor of more than 100. Furthermore, it was observed in examining berkelium fractions from separate bombardments that the ratio of the numbers of alpha-particles corresponding to the three different energy groups of the 4.6-hr. activity remained constant regardless of the energy of the helium ions used for bombardment.

The radiations associated with the electron-capture decay were characterized in a qualitative manner by differential absorption in beryllium and lead absorbers using the xenon-filled Geiger counter previously mentioned. Present were electromagnetic quanta of energy 10 to 20 kev and harder electromagnetic quanta of energy greater than about 70 kev, some of which were probably K x-rays. No attempt was made to measure more energetic gamma-rays. Present also were conversion electrons of maximum energy of about 0.5 Mev, and the number of these electrons appeared to be about five percent of the total number of disintegrations based on the assumptions as to counting yield given in the previous section.

The half-life for the decay of the new berkelium isotope was also determined by observing the variation of its counting rate with time both in the windowless proportional counter and in the xenon-filled Geiger counter. In the latter case three determinations, each with different absorbers placed between the sample and the counter window, were made. The absorbers used were 6.9 mg/cm² aluminum, 1.46 g/cm² beryllium, and 1.46 g/cm² beryllium together with 93 mg/cm² lead above the beryllium, respectively. In all cases the counting rate was followed through a decay factor varying between 100 and 1000 giving a value for the half-life of 4.6±0.2 hr.

The energies of the L x-rays associated with the decay of the new isotope were determined using the xenon-filled proportional counter as mentioned previously. The data are best shown by reference to the typical pulse analysis curve of Fig. 3.

Daughters of the Alpha-Particle and Electron-Capture Decay

Following the complete decay of the berkelium radioactivity, differential alpha-pulse analysis of the residual activity indicated the peaks shown in Fig. 4. The alpha-particle groups of 5.89 Mev (15 percent)

and 5.79 Mev (85 percent) are taken to be due to the orbital electron-capture daughter of berkelium. The other peak represents a small amount of Cm^{242}, incompletely separated in the original column runs. In this connection it should be noted that all of the alpha-radioactivity in the sample amounts to only a few disintegrations per minute.

No decay of the previously unknown 5.89- and 5.79-Mev alpha-particle groups occurred over a period of a few weeks. The chemical separations to be mentioned below showed that this new group belongs to a new curium isotope, probably Cm^{243}, and that it was produced by the electron-capture decay of the 4.6-hr. berkelium activity. The amount of the new curium alpha-radioactivity observed, together with the initial electron-capture disintegration rate of the 4.6-hr. activity in the same sample, made it possible to calculate a partial alpha-particle decay half-life of about 100 yr. for the curium isotope. In this calculation the method described in the section on experimental work was used in which the disintegration rate of the 4.6-hr. activity was calculated from its L x-ray counting rate in the xenon-filled Geiger counter at the time the berkelium was first isolated from other radioactivities. From this value, the total number of curium atoms produced by the complete decay of the berkelium was calculated and this, together with the disintegration rate of the curium thus produced, were used to calculate the half-life. Other considerations[14] show that Cm^{243} may be either very slightly unstable toward decay by electron capture or perhaps beta-stable.

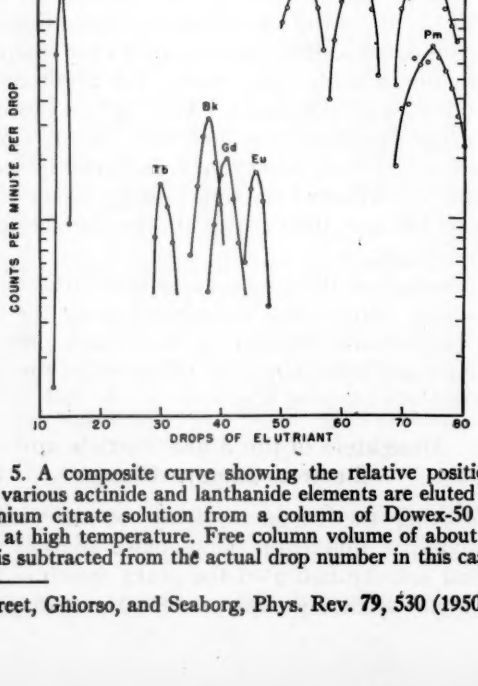

FIG. 5. A composite curve showing the relative positions at which various actinide and lanthanide elements are eluted by an ammonium citrate solution from a column of Dowex-50 maintained at high temperature. Free column volume of about seven drops is subtracted from the actual drop number in this case.

[14] Street, Ghiorso, and Seaborg, Phys. Rev. **79**, 530 (1950).

The americium and curium daughters produced by the electron capture and alpha-particle decay of the new 4.6-hr. activity were separated chemically using a Dowex-50 resin column according to the method previously described. This separation was made approximately 27 hr. after the berkelium fraction had been isolated from other radioactivities. At this time all except about two percent of the berkelium had undergone decay so that the daughters were present as the result of essentially complete decay, but there was still enough berkelium present to indicate its position in the column elution sequence. Present also was a trace of Am^{241} to mark the position of americium isotopes. The elutriant fractions from the column showed the presence in the proper fractions of the curium isotope with the alpha-particles of 5.89 and 5.79 Mev energy of abundance 15 and 85 percent, respectively, shown in Fig. 4, and a very small amount of an americium isotope of about 15-hr. half-life as shown by counting Auger electrons in the windowless proportional counter (previously described).

It was only possible to follow the 15-hr. activity through a very small decay factor (about 2) so the probable error in half-life determination is about 40 percent. The background resulting from the presence of Am^{241} was approximately one-half the total counting rate. The amount of this short-lived activity formed was very nearly the amount expected if it is due to the 12-hr. electron-capturing Am^{239} produced[14] by the alpha-particle decay branching of Bk^{243} and if it is also assumed that the counting efficiencies in the windowless proportional counter for these two isotopes are the same.

Branching Ratio and the Cross Section for Formation of Bk^{243}

The disintegration rates corresponding to measured fractions of the total berkelium produced in the bombardments were calculated from the L x-ray counting rates as previously described. The corresponding alpha-particle disintegration rates of the 4.6-hr. activity allow a direct calculation of the alpha-decay to electron-capture decay ratio. The alpha-branching percentage was found to be approximately 0.1 percent. The corresponding partial half-life for alpha-particle emission is calculated directly as about a year.

The cross section for the production of the 4.6-hr. activity in the bombardment of Am^{241} with 35-Mev helium ions is calculated as about 10^{-26} cm^2. The corresponding cross section for the reaction at 30 Mev appears to be lower possibly by as much as a factor of two, although the latter value is less reliable. These calculations are based on the assumptions mentioned previously in regard to counting yields for the L x-rays.

Chemical Results—Ion Exchange Behavior

The behavior of the new 4.6-hr. activity in the ion exchange separations used in its isolation are highly significant for the assignment of the atomic number 97.

The results of the column separations involving ammonium citrate elution from a Dowex-50 resin column are best shown by the elution curves given in Fig. 5. This curve is a composite taken from several typical experiments. In some of the experiments the rare earth fission products were not removed until after the 4.6-hr. activity had been separated from curium and residual americium; in such cases a direct comparison of the elution position of element 97 with the elution positions of some rare earth elements was obtained and these results are included in the composite curves of Fig. 5. The relative positions of the other rare earths were obtained from separate experiments performed under as nearly identical conditions as possible. In all cases radioactive isotopes of the elements were present at tracer concentrations without added inactive isotopes. The activities were counted with a Geiger counter except for americium and curium whose alpha-particles were counted. The ordinate is given as counts per minute per drop; in some cases the counting rates are normalized to allow plotting on a scale suitable for comparison.

These results might be summarized thus: element 97 elutes in a position well ahead of curium as would be expected, and it is found between the rare earths terbium and gadolinium.

A region of particular importance is illustrated in Fig. 6 which compares the elution positions of the group berkelium-curium-americium of the actinides with those of the homologous lanthanide group terbium-gadolinium-europium. Here the ordinates are normalized to show equal amounts. These results might also be summarized thus: the difference in rates of elution between berkelium and curium as compared with the difference between curium and americium is remarkably similar to the spacing terbium-gadolinium and gadolinium-europium.

With regard to the group separation of actinides from rare earths using the Dowex-50 resin column with 13*M* HCl, the new 4.6-hr. activity was always separated in the fraction containing curium and americium. These fractions were free of rare earth fission products which were removed from the column much more slowly because of the lesser extent of rare earth complexing with hydrochloric acid.

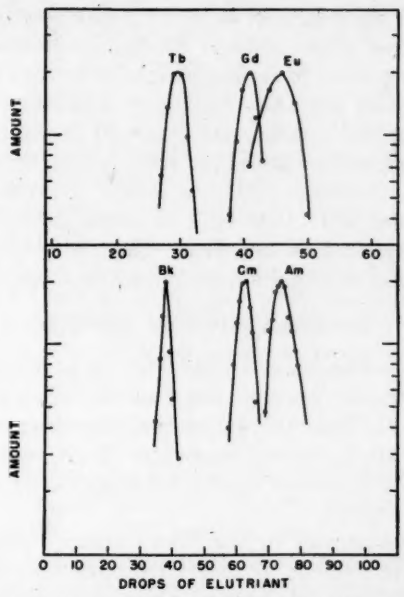

FIG. 6. Relative spacing of berkelium-curium-americium and their rare earth homologues, terbium-gadolinium-europium, in their elution from a high temperature Dowex-50 resin column with ammonium citrate solution. Free column volume of about seven drops is subtracted from the actual drop numbers in this comparison.

Chemical Results—Tracer Experiments

Using pure solutions of the 4.6-hr. activity prepared by the ion exchange separations method a number of separate tracer experiments were performed to extend the knowledge of the chemical properties of the new element. Carriers such as lanthanum fluoride, lanthanum hydroxide, copper sulfide, zirconium phosphate, and ceric iodate were employed under conditions in which the behavior of other actinide elements is well known. The oxidation-reduction properties of berkelium were studied with such agents as bromine, chlorine, dichromate ion, bromate ion, cerium (IV) ion, permanganate ion, and sodium bismuthate. In these experiments the distribution of the berkelium into the various fractions was determined by counting the radiation with a Geiger counter. A complete report of these experiments is published elsewhere[15] but the salient results will be summarized here.

It was found that the 4.6-hr. activity was not carried by zirconium phosphate unless powerful oxidizing agents such as bromate ion or sodium bismuthate were present; in the presence of these oxidizing agents it was well carried. It was well carried by the carriers lanthanum fluoride or lanthanum hydroxide in solutions ranging from strongly reducing to strongly oxidizing.

In the case of lanthanum hydroxide, excellent carrying was obtained regardless of whether potassium hydroxide or ammonium hydroxide was used for precipitation of the carrier. In the absence of oxidizing agents, the 4.6-hr. radioactivity was not carried by the insoluble sulfides of copper and bismuth precipitated in 0.3*M* HCl; and in strong hydrochloric acid, it was not adsorbed by the anion exchange resin Dowex A-1. By means of the use of various oxidizing agents including mixtures of cerium (III) and cerium (IV), the 4.6-hr. activity was found to have behavior so near to that of cerium as indicated by carrying or non-carrying with zirconium phosphate and ceric iodate that the oxidation potential for the couple Bk (III)$\rightarrow$Bk (IV)$+\epsilon^-$ must be about -1.6 volt on the scale where the hydrogen-

[15] Thompson, Cunningham, and Seaborg, J. Am. Chem. Soc. 72, 2798 (1950).

hydrogen ion potential is zero.[16] These results may be summarized thus: element 97 has properties closely resembling those of cerium, particularly with regard to its oxidation potential. However, differences between berkelium and cerium were observed in the properties of the tripositive oxidation state where berkelium is more like terbium (III), as shown by resin column separations. With 13*M* HCl, of course, relatively large differences between berkelium (III) and all rare earths with respect to formation of complex ions were observed.

IV. DISCUSSION OF RESULTS

The experiments and results which have been given provide the evidence for the discovery of an isotope of element 97. That the 4.6-hr. activity observed in the experiments is, beyond reasonable doubt, an isotope of element 97 is proved by the following essentially independent means:

(1) It separates in the "eka-terbium" position expected for element 97 in elutriant fractions from the Dowex-50 resin column with ammonium citrate as the eluting agent. The relative spacing between berkelium and its actinide neighbors is remarkably similar to the relative spacings between the homologous lanthanides.

(2) Its behavior with various carriers and oxidizing agents shows it to have (III) and (IV) oxidation states as expected. Although very similar to cerium in this respect, the cerium and all rare earth fission products were separated from it by means of the Dowex-50 resin column employing hydrochloric acid as the eluting agent.

(3) Its radioactive properties, particularly the high alpha-particle energies, are distinctive for a very heavy element. This may be illustrated by referring to the various figures of reference 4 which show the mass number and alpha-half-life *versus* energy relationships of various nuclides as a function of atomic number. That the atomic number is clearly greater than 94 is also proved by measurement of the energy spectrum of the *L* x-rays in the xenon proportional counter connected to the pulse analyzer. It may be noted there are no known plutonium, americium, or curium isotopes of 4.6-hr. half-life.

(4) The identification of curium and americium daughters which are produced by electron capture and alpha-particle decay place the atomic number as 97.

The best evidence in regard to the mass assignment is the growth of the americium daughter activity of half-life about 15 hrs. which must have been produced by the alpha-particle decay of the 4.6-hr. activity. The small observed amount of this approximately 15-hr. activity made it difficult to determine a precise value of the half-life or to characterize the radiations. However, the only known americium isotope of similar half-life characteristics is the 12-hr. electron-capture isotope Am^{239} whose assignment is practically certain.[14] The activities were sufficiently similar and the amount of the 15-hr. activity sufficiently near expectations as to make the identification probable. Therefore, the mass number of the 4.6-hr. berkelium activity is probably 243.

The growth of the curium isotope which emits alpha-particles of about 5.89 and 5.79 Mev energy also suggests the assignment to mass 243 for the following reasons. Other experiments performed in this laboratory have indicated that Cm^{244} emits alpha-particles of about 5.79 Mev energy and that its alpha-half-life is of the order of 10 yr.[17] The amount of curium daughter alpha-radioactivity which was formed by the electron-capture decay of the berkelium isotope indicates that the alpha-decay half-life of the new heavy curium isotope is of the order of 100 yr. This energy and half-life would agree best with the alpha-decay systematics[4] if assigned to Cm^{243}. In this connection it should be pointed out that the 30-Mev helium ions used in the lowest energy bombardment of the americium are below the threshold for the production of observable yields of the $(\alpha, 4n)$ reaction in this region so that berkelium isotopes of mass number less than 242 should not have been produced. The observed cross section ($\sim 10^{-26}$ cm^2) is of the same order of magnitude as cross sections for the $(\alpha, 2n)$ reaction with helium ions of 30 to 35 Mev energy in the production of other heavy isotopes.

When the three alpha-particle groups of the 4.6-hr. activity were first observed, the possibility was indicated that more than one isotope of element 97 might be present. This possibility was probably eliminated as follows: All three groups decayed with a 4.6-hr. half-life as did the electron-capture radiations. There was no difference in the ratios of the three groups when the energies of the helium ions used in the bombardments were varied. If another isotope had been present in significant amounts, its daughters would have been detected.

It is interesting to consider the explanation of the three groups of alpha-particles. Reference to the half-life *versus* energy relationships for the odd atomic number nuclides as given in Fig. 8 of reference 4 shows that an alpha-decay half-life of the order of a day or less might be expected for an isotope of element 97 with an unforbidden transition having a maximum alpha-particle energy of 6.72 Mev. Therefore, alpha-particle decay in the isotope 97^{243} is highly forbidden, perhaps by a factor of 10^2 or 10^3. Since the transition between ground states is highly forbidden, the transition to excited states of the product nucleus becomes probable even though the total difference in energy involved is less, so it is reasonable to have low energy alpha-groups of intensity comparable to the ground state transition. This is not unreasonable for a nucleus with an odd nucleon (proton) like Bk^{243}.

It is also interesting to consider the relationship between energy and the half-life for electron capture. The disintegration energy of Bk^{243} may be calculated by

[16] W. M. Latimer, *Oxidation Potentials* (Prentice-Hall, Inc., New York, 1938).

[17] Street, Ghiorso, and Thompson (unpublished work).

means of closed cycles and used to estimate a half-life for electron capture by the method of Thompson.[5] The disintegration energy so obtained corresponds to a half-life considerably less than one hour if applied to the curve[5] which includes most of the data. The new isotope appears to represent a case whose electron-capture decay is more forbidden than most of the other heavy odd-even type nuclei. This situation is, of course, fortunate insofar as the identification of the new element is concerned. If the isotope Bk^{243} had not been forbidden with respect to decay by electron capture, the identification of the new element might have been delayed until even more rapid chemical separations and techniques could be developed. The other isotopes of berkelium formed in the present bombardments are presumably all shorter-lived than Bk^{243}.

V. SUMMARY

An isotope of element 97 (berkelium, symbol Bk) has been produced and identified. This isotope probably the mass number 243 as produced in the reaction $Am^{241}(\alpha, 2n)Bk^{243}$. It decays predominantly by electron capture with a half-life of 4.6 ± 0.2 hr. and exhibits about 0.1 percent alpha-particle decay branching. The alpha-particles are of three groups, the maximum energy being 6.72 Mev (30 percent). The other two energy groups are 6.55 Mev (53 percent) and 6.20 Mev (17 percent). The bombardments were made with 30- to 35-Mev helium ions in the Berkeley Crocker Laboratory 60-inch cyclotron. The chemical separations were made using a combination of precipitation methods and high temperature ion exchange columns with Dowex-50 resin. The growth of a curium isotope decaying by the emission of alpha-particles of energy 5.89 Mev (15 percent) and 5.79 Mev (85 percent) was observed in a radiochemically pure berkelium fraction. This curium isotope is probably Cm^{243} produced by the electron-capture decay of Bk^{243} and has a half-life estimated from yield of some 100 yr. Chemical separations on the decay products of the Bk^{243} also revealed an americium isotope of about 15-hr. half-life, which appears to be identical within the limits of error of the experiment with the known 12-hr. electron-capturing Am^{239}. The cross section for the formation of Bk^{243} by the $(\alpha, 2n)$ reaction is approximately 10^{-26} cm^2. The chemical properties of the berkelium are typical of those of the actinide elements. Its tripositive oxidation state bears the same relationship to curium as does terbium to gadolinium as shown by the separations on ion exchange resin columns. The analogy between these two groups of elements is apparent, indicating the same kind of break in ionic radius at the point of half-filling of the $5f$ electron shell (curium) for the actinide elements as has been known to exist for the analogous point of half-filling of the $4f$ electron shell (gadolinium) for the lanthanide elements. The oxidation potential for the (III)→(IV) couple of berkelium is close to that of the corresponding couple for cerium (about -1.6 volt).

VI. NAME

It is suggested that element 97 be given the name berkelium (symbol Bk) after the city of Berkeley in a manner similar to that used in naming its chemical homologue terbium (atomic number 65) whose name was derived from the town of Ytterby, Sweden, where the rare earth minerals were first found.

VII. ACKNOWLEDGMENTS

We wish to acknowledge the assistance in the early phases of the problem and the continuous advice of Professor B. B. Cunningham, whose help contributed greatly to the success of the work. It is also a pleasure to acknowledge the continued support and interest of Professor E. O. Lawrence.

It is a pleasure to acknowledge the special help in the bombardment of the americium samples of Professor J. G. Hamilton, G. B. Rossi, T. M. Putnam, Jr., M. T. Webb, and the operating crew of the 60-inch cyclotron in the Crocker Laboratory. The successful handing in a safe manner of the radioactivity involved was made possible through the use of the excellent protective equipment provided by Nelson Garden and the members of his Health Chemistry Group, particularly C. M. Gordon, W. G. Ruehle, and J. M. Davis. We wish also to thank E. K. Hulet and G. H. Higgins for their assistance in some of the experiments and to express our appreciation to Dr. Kenneth Street, Jr., for valuable suggestions and for the development of methods which were useful in the chemical separations.

The New Element Californium (Atomic Number 98)*

S. G. THOMPSON, K. STREET, JR., A. GHIORSO, AND G. T. SEABORG
Radiation Laboratory and Department of Chemistry, University of California, Berkeley, California
(Received August 7, 1950)

Definite identification has been made of an isotope of the element with atomic number 98 through the irradiation of Cm^{242} with about 35-Mev helium ions in the Berkeley Crocker Laboratory 60-inch cyclotron. The isotope which has been identified has an observed half-life of about 45 min. and is thought to have the mass number 244. The observed mode of decay of 98^{244} is through the emission of alpha-particles, with energy of about 7.1 Mev, which agrees with predictions. Other considerations involving the systematics of radioactivity in this region indicate that it should also be unstable toward decay by electron capture.

The chemical separation and identification of the new element was accomplished through the use of ion exchange adsorption methods employing the resin Dowex-50. The element 98 isotope appears in the eka-dysprosium position on elution curves containing berkelium and curium as reference points—that is, it precedes berkelium and curium off the column in like manner that dysprosium precedes terbium and gadolinium. The experiments so far have revealed only the tripositive oxidation state of eka-dysprosium character and suggest either that higher oxidation states are not stable in aqueous solutions or that the rates of oxidation are slow.

The successful identification of so small an amount of an isotope of element 98 was possible only through having made accurate predictions of the chemical and radioactive properties.

I. INTRODUCTION

THE discovery[1] of element 97 in December, 1949, was immediately followed by a concentration of effort on the search[2] for element 98. The methods used in the search for these two transuranium elements were similar and the solutions to the most difficult problems in the work on element 97 were directly applicable toward element 98.

All of the experiments completed prior to February, 1950, were unsuccessful for reasons which are now clearly apparent and the present success in this work has been due to relatively recent advances of several types. A very important contribution has been the further development of the systematics of radioactivity,[3] particularly in the region of heavy isotopes. The use of these systematics enables fairly reliable predictions of the half-lives and radiation energies of heavy radioactive nuclides to be made. Advances in the knowledge and understanding of the chemical properties[4] of the heavy elements with improvements in the methods of separation[5,6] were likewise of great importance in making a solution of the problem possible. Important contributions were made through the improvement of the methods for the handling and measurement of radioactivity.[7]

In view of the fact that sufficiently intense beams of energetic particles with nuclear charge greater than two were not available at the time of this work, it was clear from the beginning that there were only two methods of approach to the production of synthetic element 98. The first approach, which proved successful, was through the bombardment of curium with helium ions. This approach provided an advantage in that the yields of the (α,xn) reactions were more or less predictable. At the same time it possessed a disadvantage in that the isotopes of element 98 so produced should be neutron deficient and of relatively short half-life as the result of considerable instability toward electron-capture and alpha-particle decay. The second approach was through intensive neutron irradiations of curium in order to eventually produce, through successive (n,γ) reactions, curium and berkelium isotopes of masses sufficient to be unstable toward negative beta-particle decay and so produce isotopes of element 98.

This second approach was subject to great handicap in that it involved great uncertainty in the prediction of the mass numbers of the desired curium and berkelium isotopes which decay by beta-particle emission. The first isotope of element 98 so produced might be of mass 248 or 250. Not only is the order of the reaction in which these isotopes are produced very large, but also the cross sections for the (n,γ) reactions cannot be reliably estimated. Thus, in this second approach, the intense irradiation of curium samples with neutrons bears a time scale uncertain within several years. So far this method has been employed without success.

One of the important problems which had to be solved was that of obtaining sufficiently large amounts of curium as sources for the production of element 98. Americium, the source for the production of curium, became available in milligram amounts through the neutron irradiation of plutonium.[8] The curium was

* This work was performed under the auspices of the AEC.
[1] Thompson, Ghiorso, and Seaborg, Phys. Rev. 77, 838 (1950).
[2] Thompson, Street, Ghiorso, and Seaborg, Phys. Rev. 78, 298 (1950).
[3] Perlman, Ghiorso, and Seaborg, Phys. Rev. 77, 26 (1950).
[4] G. T. Seaborg, Nucleonics 5, No. 5, 16 (1949).
[5] K. Street, Jr. and G. T. Seaborg, J. Am. Chem. Soc. 72, 2790 (1950).
[6] Thompson, Cunningham, and Seaborg, J. Am. Chem. Soc. 72, 2798 (1950).
[7] N. B. Garden and co-workers (unpublished work).
[8] Ghiorso, James, Morgan, and Seaborg, Phys. Rev. 78, 472 (1950).

produced in smaller amounts by the irradiation of americium with neutrons.[8,9] Each step required the use of tedious chemical separations.

Since the isotope Cm^{242} has an alpha-decay half-life of about 160 days, its intense radioactivity presented a major difficulty. The microgram amounts of curium available for the alpha-particle bombardments emit alpha-particles at the rate of approximately 10^{11} disintegrations per minute. This high level of radioactivity necessitated not only the design and development of advanced techniques and equipment for its safe handling[7] but also made it necessary to attain enormous separation factors of the order of 10^6 in the isolation of an expected 10^3 to 10^4 atoms of the new element from the target material in order to permit the detection of its expected radioactivity, amounting to less than 10^3 disintegrations per minute. Furthermore, this high degree of separation had to be carried out in good yield in a short length of time. In order to provide the greatest sensitivity of detection and thus a possibility of observing the radioactivity of the new element, it was clearly necessary to predict accurately the nuclear properties, including the half-life and radiation characteristics of the isotopes of element 98, so that the experiments could be properly designed. Only then could the optimum period of the bombardment, time of chemical separations and optimum adjustments for the measurement of the radioactivity be established. Likewise, it was necessary to predict the chemical properties of the new element so that its rapid separation from the target material, Cm^{242}, and other isotopes produced by bombardment could be made. An erroneous prediction of any of these properties would have meant unsuccessful experiments.

The discovery[1,10] of element 97 was of primary importance in making possible better predictions of the chemical properties of element 98. In such predictions it was first necessary to consider its normal oxidation state in aqueous solution. Since the oxidation potential of the change Bk(III)→Bk(IV) was found to be quite negative[6,11] (−1.6 volt), it seemed likely that the tripositive state of element 98 would be the state normally existing in aqueous solutions. Since the tripositive oxidation state appeared to be the one on which the chemical separations would have to depend, it was necessary to use the ion exchange methods as they were used in the search for element 97 and to estimate precisely the position of element 98 relative to berkelium and curium in the separations.

Since berkelium had taken its place as the eighth member of the actinide transition series, there was every reason to believe that element 98 should be an "eka-dysprosium." The properties of berkelium made clear the existence of the same sort of break in ionic radius at the point of half-filling of the 5*f* electron shell, as occurs in rare earth elements at the point of half-filling of the 4*f* shell. Knowing, then, the relation between gadolinium, terbium, and dysprosium on the one hand, and the homologues curium and berkelium on the other, one could estimate with confidence the fractions from the adsorption columns in which tripositive eka-dysprosium (element 98) would be present. Using this information it was predicted that element 98 should be eluted at about 1.4 times the rate of elution of berkelium. Needless to say, element 98 could also be expected to exhibit normal chemical behavior similar to the rare earths—namely, it should carry well with rare earth or actinide fluoride and hydroxide precipitates.

The identification[1,6,10] of the isotope Bk^{243} and measurement of the energies of its alpha-particles also provided the key to better predictions of the nuclear properties of the isotopes of element 98. By making use of these data to extend the systematics of alpha-radioactivity,[3] it was possible to make improved estimates of the alpha-particle energies of the isotopes of element 98 and of other isotopes of element 97. These estimated alpha-particle energies could in turn be used to estimate the alpha-decay half-lives of the transcurium isotopes[3] and also to calculate by closed decay cycles the total energies for electron capture or beta-decay. The electron-capture disintegration energies then led to the estimation of half-lives for this mode of decay, using an empirical energy *versus* half-life relationship,[12] which, although very rough due to uncertainties in the degree of prohibition, was nevertheless successful in attaining useful half-life estimates. By means of these methods, it was estimated that the longest-lived isotope of element 98 that could be produced by the bombardment of the isotope Cm^{242} with helium ions should be the isotope 98^{244} by the $(\alpha,2n)$ reaction, with an anticipated half-life between 30 min. and several hours and emitting alpha-particles with energy in the range 7.0 to 7.3 Mev.

The high energies of the alpha-particles emitted in the decay of the isotopes of the new element were expected to make possible a sensitive means for their detection. Such high energy alpha-particles are conveniently observed with great sensitivity and their energies measured by means of a differential alpha-energy pulse analyzer.[13] In using our instrument in the most sensitive manner, it is necessary to limit the total amount of alpha-radioactivity in the sample examined to less than about 10^4 disintegrations per minute. Thus the enormous amount of curium radioactivity in the target material used for producing element 98 had to

[9] Seaborg, James, and Morgan, *The Transuranium Elements: Research Papers* (McGraw-Hill Book Company, Inc., New York, 1949), Paper No. 22.1, National Nuclear Energy Series, Plutonium Project Record, Vol. 14B.

[10] Thompson, Ghiorso, and Seaborg, Phys. Rev. **80**, 781 (1950), preceding paper.

[11] W. M. Latimer, *Oxidation Potentials* (Prentice-Hall, Inc., New York, 1938).

[12] S. G. Thompson, Phys. Rev. **76**, 319 (1949).

[13] Ghiorso, Jaffey, Robinson, and Weissbourd, National Nuclear Energy Series, Paper No. 16.7, see reference 9.

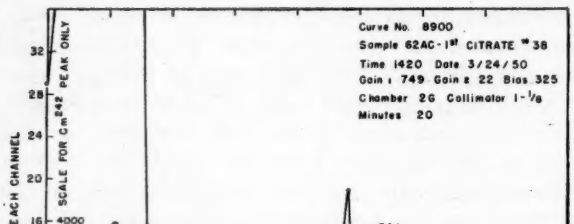

FIG. 1. Alpha-particle pulse analysis on element 98 fraction from first resin column showing 7.1-Mev alpha-particle radioactivity in presence of large amount of Cm^{242} alpha-radioactivity.

be separated from the isotopes of the new element by a factor of some 10^6 to 10^7, as mentioned previously, before the alpha-energy pulse analyzer could be used.

The observation of alpha-particles of energy 7.0 to 7.3 Mev is of particular significance in itself. Radiations of such energy have been observed previously only in the decay of the isotopes of elements just above lead as members of distinctive chains of alpha-emitters.[14] These isotopes are of so much lower mass that they cannot be produced in bombardments with helium ions of less than 40 Mev energy.

For these reasons the observation of distinctive alpha-particle radiations should be expected to provide good evidence for the existence of element 98. Furthermore, evidence based on the alpha-particle radiations, together with the observation of the chemical properties expected for the element by means of which all of the other elements above and including lead are separated, should constitute proof of the existence of the new element.

The first successful experiment[2] in which an isotope of element 98 was observed was completed February 9, 1950. This experiment was designed to allow the detection of the long-range alpha-particles of an isotope decaying with a half-life as short as 20 min.

II. EXPERIMENTAL WORK

Extraction of Curium

The Cm^{242} used as target material for the production of element 98 was separated from strongly neutron-irradiated americium in which it was produced as a daughter of the beta-particle decay of the 16-hr. Am^{242m}. The curium was separated from americium and purified by combinations of precipitation and ion exchange methods.

[14] G. T. Seaborg and I. Perlman, Revs. Mod. Phys. **20**, 585 (1948).

Preparation and Bombardment of Targets

The curium targets were prepared for bombardment in the Crocker Laboratory 60-inch cyclotron by the evaporation of solutions containing microgram amounts of curium nitrate in small platinum dishes of about 0.5 cm^2 area followed by ignition to form curium oxide. In some of the experiments Am^{241} was present to facilitate handling of the smaller amounts of curium and to produce Bk^{243} for purposes of comparison. These targets were bombarded in the same target assembly and in the same manner as has been described previously in a paper on berkelium.[10] The energies of the helium ions used in the bombardments were about 35 Mev (actually more nearly 33 Mev). The intensity of the bombardments averaged about 3 $\mu a/cm^2$ of target area and the time of bombardment was usually 2 to 3 hr. The helium ion beam also contained some deuterons of energies approximately one-half the energy of the helium ions. [The presence of the isotope Bk^{243} observed in the experiments where Am^{241} was absent was due to the reaction $Cm^{242}(d,n)Bk^{243}$.]

Chemical Procedure

Following the bombardment, the platinum dish containing the sample was removed to a gloved box and the curium oxide dissolved in $6M$ HNO_3 with heating (about 75°C). Curium hydroxide was precipitated with added lanthanum carrier by the addition of excess ammonium hydroxide and was separated by centrifugation. The hydroxide precipitate was dissolved in dilute perchloric acid ($0.5M$) and the mixture of radioactivities was adsorbed on a small amount of ammonium form Dowex-50 resin (spherical fines) which was then transferred to an approximately 17-cm length, 2-mm diameter column packed with the same resin. The column was surrounded by a vapor jacket through which passed trichloroethylene vapor to maintain the temperature at about 87°C. The elution was performed by passing ammonium citrate (buffered with citric acid to pH 3.5—total citrate concentration $0.25M$) through the column at a rate of one drop (about 0.030 cm^3) about every two minutes and the drops were collected separately or in groups of two in the region where the actinide elements were expected. Element 98 was collected in drops of elutriant from the columns just preceding those containing berkelium.

Each drop or a suitable fraction of each drop collected from the column was evaporated on a platinum plate using a heat lamp. Ignition of the plates to red heat removed the citric acid. Each of these samples which preceded the curium peak was examined for high energy alpha-radioactivity using the differential alpha-energy pulse analyzer.

The fractions which should contain elements 97 and 98 were submitted in some experiments to further separation from remaining radioactive contaminants (mainly approximately 10^4 alpha-disintegrations per

minute of Cm^{242}) by means of a second Dowex-50 resin column operated in a manner similar to the first column run. In this case, the appropriate elutriant fractions from the first column containing the ammonium citrate were acidified with hydrochloric acid to make the hydrogen ion concentration about $0.1M$. Then the mixture of radioactivities was adsorbed on Dowex-50 resin and the column separation made as described previously. (The separation of curium from element 97 and element 98 in one column run as described above is limited to a factor of approximately 10^6 to 10^7. After the second column run the curium present in element 98 fractions is reduced to a few alpha-disintegrations per minute.) In some of the experiments the lengths of the resin columns were shortened to about 15-cm length in order to increase the speed of separation. Each drop of elutriant preceding the curium peak was again examined for high energy alpha-particles in the same manner as described above in connection with the first column separation. In addition to differential alpha-energy pulse analysis, certain fractions obtained in some of the experiments were also counted in a windowless proportional counter in order to look for soft electrons with high efficiency. In this case it was possible to observe the electrons emitted by some of the radioactive fission products such as yttrium, which were produced in the bombardments.

Some of the fractions containing element 98 were used for independent investigation of the chemical properties of the new element. These investigations included separations in a Dowex-50 resin column with concentrated ($13M$) HCl for elution and experiments employing powerful oxidizing agents with carriers such as zirconium phosphate and lanthanum fluoride.

Experimental Methods Used in Radioactivity Measurements

The thin deposits on platinum of the fractions expected to contain element 98 were examined in the differential alpha-particle pulse analyzer. In this instrument individual pulses from an ionization chamber are sorted electronically and recorded on 48 fast mechanical registers in such a way as to separate the individual alpha-particle energies from a mixture of alpha-emitters. In establishing a value for the alpha-particle energy of the new isotope, direct comparison was made with pulse analyses of thin samples of nuclides whose alpha-energies are well known, using the same instrumental conditions.

No attempt was made to observe electrons and electromagnetic radiations in the element 98 fractions because of the possible presence of unseparated fission product isotopes in larger abundances which emit similar radiations.

Results of Radioactivity Measurements

The application of the procedures described above to helium ion bombarded targets of Cm^{242} and the examination in the pulse analyzer of the separated fractions expected to contain element 98 revealed a small amount of 7.1 ± 0.1-Mev alpha-particle radioactivity together with the expected amount of residual 6.08-Mev Cm^{242} alpha-particle activity.

The results of a typical experiment in which the alpha-particle energies and rate of decay were measured by differential pulse analysis are shown in Fig. 1. The rate of decay was measured by plotting the area under the 7.1-Mev energy peak *versus* the time of decay of the radioactivity. This peak was observed to decay with a half-life of approximately 45 min. through a decay factor of more than 10, as shown in Fig. 2. The tailing out of this curve is caused by a relatively high "electronic" background from the "piling up" effects in the amplifier of the intense Cm^{242} activity.

The presence of the 45-min. radioactivity was observed in four separate experiments. It was observed in the presence of a relatively large amount of unseparated Cm^{242} (approximately 10^4 alpha-disintegrations per minute), upon completion of the operation of the first resin column as shown in Fig. 1. The presence of the isotope Bk^{243} produced either by (d,n) or $(\alpha,2n)$ reactions in the separate bombardments was not observed after only one column separation because of the closer proximity of the berkelium elution peak to that of curium and the consequent larger amount of curium activity in the berkelium samples. However, after the second column run in which the residual Cm^{242} radioactivity was separated, it was possible to observe the presence of the separate elution peaks due to the 45-min. activity, Bk^{243} and Cm^{242} with the help of the alpha-

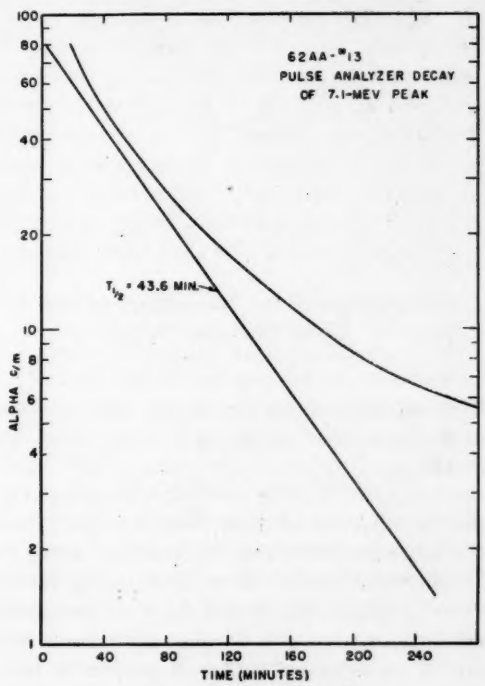

FIG. 2. Decay curve obtained by plotting area under 7.1-Mev peak from pulse analyzer data *versus* time.

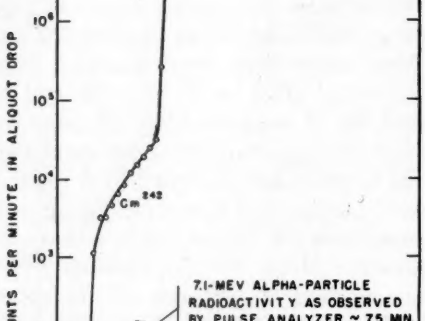

FIG. 3. Results of separation in first Dowex-50 resin column showing small amount of new 7.1-Mev alpha-radioactivity separated ahead of large amount of Cm^{242} alpha-radioactivity.

particle pulse analyzer. The electron and electromagnetic radiations of the 4.6-hr. Bk^{243} were also observed by the methods described in reference 10. The best values for the alpha-particle energies and half-life of the 45-min. activity were obtained on the larger samples resulting from the operation of the first resin column. Although samples from the second column run were essentially free of Cm^{242} contamination, the 45-min. radioactivity had decayed during this additional time interval by a factor of approximately six so that no advantage was gained by the second separation insofar as the radioactivity measurements were concerned. However, important information was obtained concerning the chemical identity, since the isotope Bk^{243} was observed to separate from the 45-min. radioactivity.

The Search for Daughters of the Alpha-Particle Decay

The fractions containing the 45-min. activity resulting from separations on the second resin column were examined for possible daughter radioactivities. In these fractions alpha-radioactivity from Cm^{242} had been reduced to approximately one disintegration per minute. Careful examination of these fractions using the alpha-particle pulse analyzer failed to show any alpha-particle peak other than that of the residual unseparated Cm^{242} after the 45-min. activity had decayed completely. On the assumption that the 45-min. activity is 98^{244}, the amount of its alpha-radioactivity present in the initial fractions should have produced approximately 0.1 disintegration per minute of alpha-radioactivity due to the alpha-decay daughter Cm^{240}. The level of the background radioactivity in the pulse analyzer chamber was too high to show a definite identification of this amount of daughter isotope.

Cross Section for Formation of Element 98 Isotope

The cross section for the production of the 45-min. activity in the bombardment of Cm^{242} with approximately 33-Mev helium ions was calculated as roughly 3×10^{-27} cm^2. In this calculation, decay is assumed to be entirely by the emission of the alpha-particles which were observed. A comparable rate of decay by electron capture is entirely possible and this would of course lead to a proportionately higher cross section. The chemical yield of the 45-min. radioactivity was estimated as approximately 90 percent, based on measured values for separations of the same type. Measured values of the effective weight of target material, the cyclotron beam and time intervals were used in the calculations.

Results of the Chemical Separations

The behavior of the new 45-min. activity in the ion exchange procedures used in its separation are highly significant for the assignment of the atomic number 98. Figure 3 shows the results of one of the separations in the first resin column after which the Cm^{242} present in the element-98-containing fractions was reduced to approximately 10^5 alpha-disintegrations per minute. The results of one of the separations in the second resin column are shown in Fig. 4. In this case the position of the 45-min. radioactivity is shown relative to berkelium, curium, and yttrium. The alpha-radioactivity was measured for curium and element 98 and the windowless proportional counter was used for the

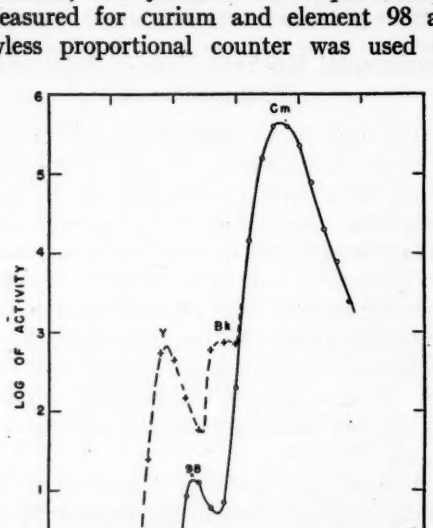

FIG. 4. Results of separation in second Dowex-50 resin column showing 7.1-Mev, 45-min. radioactivity in eka-dysprosium position as compared with isotopes Bk^{243} and Cm^{242}. Solid curve indicates alpha-particle counts/min.; dashed curve, Auger and conversion electrons and beta-particles (and alpha-particles).

radiations from 4.6-hr. Bk^{243} and the fission product yttrium. These results might be summarized in the statement that element 98 is eluted in the expected eka-dysprosium position preceding berkelium from the resin column.

A region of particular importance is illustrated in Fig. 5, which compares the elution positions of the actinide group element 98-berkelium-curium-americium with the homologous lanthanide group dysprosium-terbium-gadolinium-europium. The comparison is based in part on a number of separate experiments performed under as nearly identical conditions as possible. The ordinates are normalized to show equal amounts. These particular results might be summarized as follows: the difference in rates of elution between element 98 and berkelium as compared with the difference between berkelium and curium is remarkably similar to the spacing dysprosium-terbium and terbium-gadolinium. There is a remarkable similarity in the spacing of the four members of each group, with breaks at the points of half-filling of the *f* electron shells, gadolinium and curium; the spacings here reflect the relative changes in ionic radii which determine the relative separations in the ion exchange adsorption method.

With regard to the group separation of actinides from rare earths using the Dowex-50 resin column with 13*M* hydrochloric acid,[5] the new 45-min. activity was separated in the fractions containing curium and americium. These fractions were free of rare earth fission products, which were removed from the column much more slowly because of the lesser degree of rare earth complexing with hydrochloric acid.

Additional Chemical Experiments

In some of the later experiments small amounts (approximately 50 counts/min.) of the new alpha-emitter were isolated and further chemical experiments performed in order to characterize somewhat more closely its chemical properties. In these experiments the activity was first separated by carrying on LaF_3 and $La(OH)_3$ and by the use of ion exchange columns as described above. Because of the small amount of activity produced and the short half-life only a few chemical experiments could be done after each bombardment. The results of these tracer experiments are given below. In all cases the distribution of the 45-min. activity into the various fractions was followed by pulse analysis of the 7.1-Mev alpha-particles.

Several attempts were made to oxidize the 45-min. activity to a higher oxidation state. Carrying with zirconium phosphate was used as a test for oxidation to the (IV) state and lack of carrying on LaF_3 as a test for the (VI) state on the basis of analogy with the behavior of other actinide elements in tracer experiments.

Experiments following oxidation with 0.2*M* ammonium persulfate for 10 min. at 70°C in a solution 1*M* in HNO_3 and 0.2*M* in sulfate showed less than 10 percent carrying with zirconium phosphate and greater than 80 percent carrying with LaF_3 precipitated by adding La^{+++} and making the supernatant 1*M* in HF.

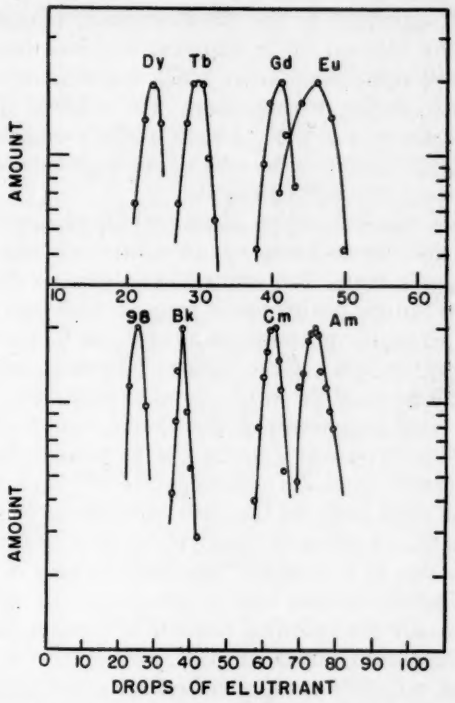

FIG. 5. Summary of relative spacings between actinides and homologous rare earth elements in elution from high temperature Dowex-50 resin columns. The remarkable similarity between homologous actinides and rare earths may be seen.

Experiments following oxidation with sodium bismuthate for 5 min. at 60°C in 5*M* HNO_3 also showed less than 10 percent carrying with zirconium phosphate and greater than 80 percent carrying with LaF_3 from the supernatant made 3*M* in HCl and 1*M* in HF.

Although there are uncertainties in the tracer experiments, due largely to the small amount of element 98 available, it can be concluded that the oxidation of the 45-min. isotope to the (IV) or (VI) states in aqueous solution even with these strong oxidizing agents is not possible or that the oxidation is slow. In connection with the rapid chemical separations used in this type of work, it is indicated that the introduction of steps to prevent oxidation during the separations are unnecessary.

The chemical properties of element 98 are discussed in somewhat greater detail in another publication.[15]

III. DISCUSSION OF RESULTS

The experiments and results which have been presented provide the evidence for the discovery of an isotope of element 98. That the 45-min. activity observed in the experiments is, beyond reasonable doubt, an isotope of element 98 has been proved by the following essentially independent means:

[15] Street, Thompson, and Seaborg, J. Am. Chem. Soc. 72, 4832 (1950).

(1) It separated in the eka-dysprosium position expected for element 98 in elutriant fractions from the Dowex-50 resin columns in which ammonium citrate was used as the eluting agent. The relative spacing between the new activity and its actinide neighbors is remarkably similar to the relative spacings between the homologous rare earth elements.

(2) Its distinctive high alpha-particle energy proves that it must be an isotope of an element above lead in the periodic table. The chemical experiments done on the new isotope distinguish it from all such previously known elements of atomic number 82 to 97 inclusive. Therefore, in view of the method of preparation, the new activity must be an isotope of element 98.

The mass assignment of the 45-min. isotope of element 98 must remain tentative for the present, pending experimental proof. Its assignment as 98^{244} is suggested as being most likely on the basis of estimates using the systematics of alpha-radioactivity as described in the introduction to this paper. The bombardment of Cm^{242} with 33-Mev helium ions is considered to produce directly only the following possible isotopes of element 98 in significant yield—namely, 98^{243}, 98^{244}, and 98^{245}. Of these, only 98^{244} is expected to have a half-life longer than one-half hour unless the electron-capture decay is unusually highly forbidden. The observed alpha-particle energy and half-life fit the alpha decay systematics[8] very well for an even-even type nucleus (unforbidden decay) of the element with atomic number 98.

The cross section for the production of the new isotope is about 3×10^{-27} cm^2, based on the observation of the alpha particles alone. This value is typical of those obtained in the production of other transuranium elements by bombardment with helium ions of energy 30 to 40 Mev. This cross section is sufficiently large to indicate in itself that alpha-particle emission is the principal mode of decay. For example, an electron-capture-to-alpha-decay branching ratio of 10 would require a cross section higher by a factor of 10 than the above and thus a much higher reaction cross section for the (α,xn) reactions than has been observed previously for the production of transplutonium isotopes. It is believed, however, based on estimates using the systematics of radioactivity, that the isotope 98^{244} is unstable toward electron-capture decay. Estimates based on the electron capture disintegration energy as determined from closed decay cycles involving estimated energies and on the very rough empirical relationship between half-life and disintegration energy[12] indicate that the half-life of 98^{244} for decay by electron capture should be somewhat longer than that for decay by alpha-emission and hence that the branching ratio toward electron-capture decay is less than unity.

It is interesting to note that the amount of element 98 which has been isolated has never exceeded a few thousand atoms in any of the bombardments to date.

IV. NAME

It is suggested that element 98 be given the name californium (symbol Cf) after the university and state where the work was done. This name, chosen for the reason given, does not reflect the observed chemical homology of element 98 to dysprosium (No. 66) as the names americium (No. 95), curium (No. 96), and berkelium (No. 97) signify that these elements are the chemical homologues of europium (No. 63), gadolinium (No. 64), and terbium (No. 65), respectively.

V. ACKNOWLEDGMENTS

It is a pleasure to acknowledge the special help in the bombardment of the curium samples of Professor J. G. Hamilton, G. B. Rossi, T. M. Putnam, Jr., M. T. Webb, and the operating crew of the 60-inch cyclotron in the Crocker Laboratory. The successful handling in a safe manner of the radioactivity involved was made possible through the use of the excellent protective equipment provided by Nelson Garden, the members of his Health Chemistry Group, and C. M. Gordon. We wish also to thank E. K. Hulet and G. H. Higgins for their assistance in the experiments. We are happy to acknowledge the continued support and interest of Professor E. O. Lawrence in this work.

PHYSICAL REVIEW VOLUME 80, NUMBER 5 DECEMBER 1, 1950

Singular Potentials*

K. M. CASE
Institute for Advanced Study, Princeton, New Jersey
(Received May 15, 1950)

The difficulties arising in quantum mechanics when the potential is highly singular are considered. It is found that the Hamiltonian needs further specification in such cases. This may be done conveniently by requiring a fixed phase for the wave functions at the origin. A proof that all the well-known singular examples are amenable to this treatment is given. For illustration the spectra for spin zero and one-half particles in the fields of highly charged nuclei are found. It is also shown that a complete set of eigenfunctions for a vector particle in a Coulomb field can be found.

I. INTRODUCTION

SINCE the advent of quantum mechanics, a number of problems have been found which seemingly do not fall into the formal structure of the Schrödinger equation and its conventional interpretation. Thus, with sufficiently singular potentials, the customary methods of finding energy eigenvalues and eigenfunctions fail. When these examples have been encountered in the literature, they have been rather summarily dismissed. In this paper an attempt will be made to show how the exceptional cases may be dealt with and what physical interpretations are necessary.

Historically, the first[1] place where these difficulties showed up was probably the strongly attractive $1/r^2$ potential. Other non-relativistic examples are potentials which behave as $1/r^n$ near the origin with $n>2$ and the tensor force problem with a $1/r^3$ singularity. With relativistic wave equations, even a Coulomb potential is highly singular. Thus, for spin 0 or $\frac{1}{2}$ particles, "singular" cases arise if the nucleus is sufficiently highly charged. For spin 1, difficulties arise in any Coulomb field.[2] It will be shown that the difficulties in these diverse problems can all be resolved by the same technique.

II. THE $1/r^2$ POTENTIAL

Consider the non-relativistic Schrödinger equation with a potential

$$V(r)=[-V_0 f(r/r_0)/(r/r_0)^n]. \tag{1}$$

On separation of the angular dependence, the radial wave equation is:

$$\frac{d^2u}{dx^2}+\left[\frac{\lambda f(x)}{x^n}-\frac{l(l+1)}{x^2}-\eta^2\right]u=0, \quad 0\leq x<\infty, \tag{2}$$

where

$$x=r/r_0;\ \lambda=MV_0r_0^2/\hbar^2;\ \eta=r_0(-ME/\hbar^2)^{\frac{1}{2}},\ \psi=u/r. \tag{3}$$

Hence, $\lambda>0$ implies an attractive potential. It is assumed that

$$f(0)=1. \tag{4}$$

Since for the general arguments that follow, the exact functional form of $f(x)$ and the value of l are unimportant, we shall consider the case $f(x)=1$ and S states only. Then for the $1/r^2$ potential the radial Schrödinger equation is:

$$\frac{d^2u}{dx^2}+\left[\frac{\lambda}{x^2}-\eta^2\right]u=0. \tag{5}$$

Assuming u to be expressible as a power series in the neighborhood of the origin beginning with x^ρ, the indicial equation for (5) is:

$$\rho(\rho-1)+\lambda=0, \tag{6}$$

or

$$\rho=\tfrac{1}{2}\pm(\tfrac{1}{4}-\lambda)^{\frac{1}{2}}. \tag{7}$$

For $\lambda<\frac{1}{4}$ the treatment is conventional and can be found in reference 1. For $\lambda>\frac{1}{4}$, that is if the potential is sufficiently attractive, (7) shows that both solutions of (5) behave in essentially the same way. An elegant means of deciding between the solutions of (5) has been given by Von Neumann[3] using the general principles of quantum mechanics. These tell us that a complete, quadratically integrable, orthonormal set of solutions of (5) is needed. Since

$$\int\psi^*\psi d\tau\sim\int_0^\infty u^2(x)dx, \tag{8}$$

Eq. (7) shows that all solutions are quadratically integrable in the neighborhood of the origin. Usually this integrability condition suffices to distinguish between the two independent solutions (7). Here the orthogonality condition must be used. Take the general solution of (5) to be real. Then for small x

$$u\sim Ax^{\frac{1}{2}}\cos(\lambda'\ln x+B), \tag{9}$$

where

$$\lambda'=(\lambda-\tfrac{1}{4})^{\frac{1}{2}}.$$

Suppose further that the solutions are chosen so as to fall off exponentially with large x. Then for small x

* This work was supported by a grant-in-aid from the Institute for Advanced Study, supported by the AEC.

[1] Mott and Massey, *Theory of Atomic Collisions* (Clarendon Press, Oxford, 1949), p. 30.

[2] H. C. Corben and J. Schwinger, Phys. Rev. 58, 953 (1940); I. Tamm, Phys. Rev. 58, 952 (1940).

[3] Private communication from W. Pauli.

the corresponding solutions will [from Eq. (9)] behave as:

$$u_1 \sim A_1 x^{\frac{1}{2}} \cos(\lambda' \ln x + B_1), \quad u_2 \sim A_2 x^{\frac{1}{2}} \cos(\lambda' \ln x + B_2), \tag{9a}$$

and A and B are arbitrary constants.

Consider solutions of (5), u_1 and u_2, corresponding to two different η_1 and η_2. These satisfy

$$d^2u_1/dx^2 + [(\lambda/x^2) - \eta_1^2]u_1 = 0, \tag{10a}$$

$$d^2u_2/dx^2 + [(\lambda/x^2) - \eta_2^2]u_2 = 0. \tag{10b}$$

Multiplying (10a) by u_1, (10b) by u_2, subtracting, and integrating yields:

$$(\eta_1^2 - \eta_2^2)\int_0^\infty u_2 u_1 dx = \left[u_2 \frac{du_1}{dx} - u_1 \frac{du_2}{dx}\right]_0^\infty. \tag{11a}$$

Usually the orthogonality relations are deduced from the vanishing of the right-hand side of (11a). However, here one obtains on inserting (9a) and remembering that u_1 and u_2 vanish at infinity:

$$(\eta_1^2 - \eta_2^2)\int_0^\infty u_2 u_1 dx = A_1 A_2 \lambda' \sin(B_2 - B_1). \tag{11b}$$

Hence, in general, solutions corresponding to two different energies are not orthogonal. However, if it is required of the solutions that

$$B_1 = B_2 = B, \tag{12}$$

then orthogonality is achieved. (It is to be noted that choosing

$$B_i = B + n\pi, \tag{13}$$

where n is a positive or negative integer will also insure orthogonality. It is shown below that no greater generality is so obtained.) The significance of B will be discussed later.

The eigenvalue problem for (5) can now be stated. We require those values of η for which u vanishes exponentially for large x and behaves as

$$u \sim x^{\frac{1}{2}} \cos(\lambda' \ln x + B), \tag{9b}$$

for x small.

The eigenvalues and eigenfunctions can now be computed. Two linearly independent solutions of (5) are:

$$u = x^{\frac{1}{2}} I_{\pm i\lambda'}(\eta x), \tag{14}$$

where I is the Bessel function defined by Watson.[4] Taking as solution the linear combination

$$u = x^{\frac{1}{2}}[e^{i\alpha} I_{i\lambda'}(\eta x) + e^{-i\alpha} I_{-i\lambda'}(\eta x)], \tag{15}$$

one finds for small x that

$$u \approx 2x^{\frac{1}{2}} \cos(\lambda' \ln \eta x + \alpha). \tag{16}$$

Hence, if

$$\alpha = B - \lambda' \ln \eta, \tag{17}$$

then u is of the requisite form (9b). Using the asymptotic forms of the Bessel functions, one finds for large x

$$u \approx \frac{1}{(2\pi\eta)^{\frac{1}{2}}}\{[e^{i\alpha} + e^{-i\alpha}]e^{\eta x} + (\text{constant})e^{-\eta x}\}. \tag{18}$$

Hence, if

$$\cos\alpha = 0, \tag{19}$$

or

$$\alpha = (n + \tfrac{1}{2})\pi, \tag{20}$$

where n is any positive or negative integer, u decays exponentially.

Inserting (17) into (20) and solving for η gives the eigenvalues:

$$\eta_n = \exp[(B - (n + \tfrac{1}{2})\pi)/\lambda']. \tag{21}$$

From (3) it can be seen that the bound states then form a point spectrum extending from minus infinity to zero. At zero there is a point of accumulation. From (21) it is seen that a displacement of B by a multiple of π has no effect on the spectrum.

III. THE $1/r^n$ POTENTIAL: $n > 2$

The Schrödinger equation is:

$$d^2u/dx^2 + [(\lambda/x^n) - \eta^2]u = 0. \tag{22}$$

Since the singular behavior is different for each n in this form, it is convenient to introduce the new variable

$$y = x^{1 - \frac{1}{2}n}, \tag{23}$$

in terms of which (22) becomes:

$$\frac{d^2u}{dy^2} + \frac{n}{n-2}\frac{1}{y}\frac{du}{dy} + \frac{4}{(n-2)^2}\left[\lambda - \frac{\eta^2}{y^{2n/n-2}}\right]u = 0. \tag{24}$$

Here we are interested in the behavior of the solution for large y. It is obvious that a series of descending powers of y will not satisfy (24) since the occurrence of the λ term will always require the vanishing of the highest power in the series, and hence of the entire series. The correct treatment at such essential singularities is well known.[5] Let

$$u = e^{\alpha y} v. \tag{25}$$

Then:

$$v'' + \left[2\alpha + \frac{n}{n-2y}\right]v' + \left[\frac{4\lambda}{(n-2)^2} + \alpha^2 + \frac{\alpha n}{(n-2)y} - \frac{4\eta^2}{(n-2)^2}\cdot\frac{n-2}{2ny}\right]v = 0. \tag{26}$$

If we choose

$$\alpha^2 = -4\lambda/(n-2)^2, \tag{27}$$

[4] G. N. Watson, *Theory of Bessel Functions* (The Macmillan Company, New York, 1944), p. 77.

[5] See E. L. Ince, *Ordinary Differential Equations* (Dover Publications, New York, 1944), p. 425.

it is possible to obtain a descending power series for v. The highest power is y^ρ where

$$\rho=-n/2(n-2). \tag{28}$$

Restricting ourselves to real solutions the behavior of the general solution of (22) for small x is:

$$u\sim Ax^{n/4}\cos\left[\frac{2}{n-2}\left(\frac{\lambda}{x^{n-2}}\right)^{\frac{1}{2}}+B\right]. \tag{29}$$

As in Section II, consider the solutions u_1 and u_2 of

$$d^2u_1/dx^2+[(\lambda/x^n)-\eta_1^2]u_1=0, \tag{30a}$$

$$d^2u_2/dx^2+[(\lambda/x^n)-\eta_2^2]u_2=0, \tag{30b}$$

where η_1 and η_2 are two different values. In particular it is required that u_1 and u_2 vanish at infinity. Then for small x

$$\begin{aligned} u_1&\sim A_1x^{n/4}\cos\left[\frac{2}{n-2}\left(\frac{\lambda}{x^{n-2}}\right)^{\frac{1}{2}}+B_1\right],\\ u_2&\sim A_2x^{n/4}\cos\left[\frac{2}{n-2}\left(\frac{\lambda}{x^{n-2}}\right)^{\frac{1}{2}}+B_2\right]. \end{aligned} \tag{31}$$

As usual one finds:

$$(\eta_1^2-\eta_2^2)\int_0^\infty u_2u_1dx=\left[u_2\frac{du_1}{dx}-u_1\frac{du_2}{dx}\right]_0^\infty. \tag{32}$$

Insertion of the asymptotic forms for small and large x gives:

$$(\eta_1^2-\eta_2^2)\int_0^\infty u_2u_1dx=A_1A_2\lambda^{\frac{1}{2}}\sin(B_1-B_2). \tag{33}$$

Hence, if all eigenfunctions are required to behave as

$$u\sim x^{n/4}\cos\left[\frac{2}{n-2}\left(\frac{\lambda}{x^{n-2}}\right)^{\frac{1}{2}}+B\right], \tag{34}$$

where now B is a fixed phase factor common to *all* eigenfunctions, we will have orthogonality. Conversely, it can be said that the requirement of vanishing at infinity and having the designated behavior for small x makes the eigenvalue problem uniquely soluble.

IV. DISCUSSION OF THE NON-RELATIVISTIC CASE

The principal difference between "singular" and "non-singular" potentials is seen to be that in the latter case the solutions of the Schrödinger equation subject to the condition of quadratic integrability form a complete orthonormal set. In the singular case the solutions are too numerous and hence, over complete. Some other parameter in addition to the functional form of the potential is needed to specify completely the potential. This is conveniently taken as the phase, B.

This distinction may be expressed in physical terms somewhat differently. In any physical problem in which we express the interaction between two systems by means of a potential which becomes infinite when the distance between them becomes zero, we are dealing with an idealization. Thus, the Coulomb interaction between an electron and a nucleus is not strictly proportional to $1/r$ down to $r=0$. The finite size of the nucleus sets one limit. Even for a single proton there is the probable finite radius of the proton. The important point is, however, that if the $1/r$ law holds down to sufficiently small distances the eigenvalues and eigenfunctions are essentially independent of exactly when or how the power law breaks down. For potentials as singular as $1/r^2$ or greater, this is no longer true. The eigenvalues and eigenfunctions do depend on the nature of the cut-off. The main conclusion from the above work is, though, that only a single parameter is needed to describe the situation for small distances. Thus it is not necessary to know exactly at what distance the power law breaks down and what functional form replaces it. All one would need to know from experiment is the value of B for the given system.

From this it is seen that B describes the breakdown of the power law at small r. For a simple model one might consider the true potential to be $1/r^n$ down to $r=\epsilon$ and then to be an infinitely high repulsive square well. Then B is directly related to the "cut-off radius," ϵ.

For the non-relativistic cases, this discussion is rather academic, since the spectrum of energy values is a point spectrum extending from minus infinity to zero, plus the usual positive energy continuum. That the negative energies are discrete follows from the quadratic integrability of the wave functions. That the spectrum extends to minus infinity is obvious, since the Hamiltonian operator is not bounded below. Now no physical system has an infinite binding energy. Therefore such singular potentials have no application as an approximation in the calculation of term values of real systems. One possible remaining application is to describe some scattering processes. Resonance, for example, is well exemplified by scattering by such potentials.

If only the non-relativistic Schrödinger equation were to be considered, these highly singular potentials might well be forgotten.

V. RELATIVISTIC WAVE EQUATIONS WITH SINGULAR POTENTIALS—SPIN 1/2

Here the situation is altered considerably. Firstly, much weaker infinities in the potential are "highly singular." Even the Coulomb field gives rise to difficulties of the form considered above. Secondly, the discrete energy levels of a relativistic system are restricted to the region between $\pm mc^2$. Thus, it certainly will not be possible to ignore singular potentials because they lead to infinite binding energies.

The most famous singular example is that of the Dirac equation for an electron in the Coulomb field of a fictitious nucleus of charge such that $\alpha Z>137$. Sepa-

rating out the angular dependence the equations for the radial wave functions may be written in the form given by Bethe.[6]

$$\frac{du}{dr}-\chi\frac{u}{r}=\left(1-E-\frac{\alpha Z}{r}\right)w,$$
$$\frac{dw}{dr}+\chi\frac{w}{r}=\left(1+E+\frac{\alpha Z}{r}\right)u. \tag{35}$$

(Here Bethe's notation has been altered slightly and units such that $\hbar=c=m=1$ have been chosen.) χ is the angular momentum quantum number of Dirac such that

$$\chi=-(j+\tfrac{1}{2}) \quad \text{for} \quad j=l+\tfrac{1}{2},$$
$$\chi=+(j+\tfrac{1}{2}) \quad \text{for} \quad j=l-\tfrac{1}{2}. \tag{36}$$

The normalization is such that the scalar product of two different eigenfunctions

$$\begin{pmatrix}u_1\\w_1\end{pmatrix} \quad \text{and} \quad \begin{pmatrix}u_2\\w_2\end{pmatrix}$$

is defined by

$$\int_0^\infty (u_1u_2+w_1w_2)dr. \tag{37}$$

Consider solutions of (35), in the neighborhood of the origin, of the form:

$$u=r^\rho[a_0+a_1r+\cdots],$$
$$w=r^\rho[b_0+b_1r+\cdots]. \tag{38}$$

Inserting into (35) and equating to zero the coefficient of the lowest power of $r(r^{\rho-1})$ gives as the indicial equations:

$$a_0\rho-\chi a_0=-\alpha Zb_0,$$
$$b_0\rho-\chi b_0=\alpha Za_0, \tag{39}$$

or solving for b_0/a_0 and ρ:

$$\rho=\pm[\chi^2-(\alpha Z)^2]^{\frac{1}{2}}, \tag{40}$$
$$b_0/a_0=\alpha Z/(\rho+\chi). \tag{41}$$

Since the smallest possible value of j is $\frac{1}{2}$ one sees from (36) that

$$\chi^2\geq 1. \tag{42}$$

Hence, if $\alpha Z>1$, at least for $j=\frac{1}{2}$ the two possible solutions (40) are equally good. In fact, from (37) one sees that both solutions of (35) are quadratically integrable in this case.

For convenience, limiting ourselves to real solutions when $(\alpha Z)^2>\chi^2$ one sees that the general solution of (35) can be written as:

$$\begin{pmatrix}u\\w\end{pmatrix}\approx C\begin{pmatrix}\cos(\lambda\ln r+B)\\a\cos(\lambda\ln r+B+\gamma)\end{pmatrix} \quad \text{for } r \text{ small} \tag{43}$$

where

$$\lambda=+[\alpha^2Z^2-\chi^2]^{\frac{1}{2}}, \tag{44}$$
$$(\chi-i\lambda)/\alpha Z=ae^{i\gamma},$$

and C and B are two unknown constants.

Consider Eqs. (35) corresponding to two different energies E_1 and E_2. These are:

$$\frac{du_1}{dr}-\chi\frac{u_1}{r}=\left(1-E_1-\frac{\alpha Z}{r}\right)w_1, \tag{45a}$$
$$\frac{dw_1}{dr}+\chi\frac{w_1}{r}=\left(1+E_1+\frac{\alpha Z}{r}\right)u_1, \tag{45b}$$
$$\frac{du_2}{dr}-\chi\frac{u_2}{r}=\left(1-E_2-\frac{\alpha Z}{r}\right)w_2, \tag{46a}$$
$$\frac{dw_2}{dr}+\chi\frac{w_2}{r}=\left(1+E_2+\frac{\alpha Z}{r}\right)u_2. \tag{46b}$$

Multiplying (45a) by w_2, (46a) by w_1, (45b) by $(-u_2)$, (46b) by $(-u_1)$, adding and integrating yields:

$$(E_1-E_2)\int_0^\infty (u_2u_1+w_2w_1)dr=[u_2w_1-u_1w_2]_0^\infty. \tag{47}$$

Suppose the solutions 1 and 2 are adjusted to vanish exponentially at infinity. Inserting the asymptotic behavior (43) into (47) yields:

$$(E_1-E_2)\int_0^\infty (u_2u_1+w_2w_1)dr = aC_1C_2\sin(B_1-B_2)\sin\gamma, \tag{48}$$

where the B_i, C_i are the constants describing the respective solutions. From (48) one sees that if all

$$B_i=B, \tag{49}$$

where B is a *fixed* constant all eigensolutions will be orthogonal. It is also possible to prove completeness in this case.

To solve this eigenvalue problem we make the substitution given by Bethe:[6]

$$u=(1-E)^{\frac{1}{2}}e^{-\rho/2}(\varphi-\psi),$$
$$w=(1+E)^{\frac{1}{2}}e^{-\rho/2}(\varphi+\psi), \tag{50}$$
$$\rho=2(1-E^2)^{\frac{1}{2}}r,$$

one finds:

$$d\varphi/d\rho=[1-(E\delta/\rho)]\varphi-(\chi+\delta)\psi/\rho, \tag{51}$$
$$d\psi/d\rho=(E\delta/\rho)\psi-(\chi-\delta)\varphi/\rho,$$

where

$$\delta=\alpha Z/(1-E^2)^{\frac{1}{2}}. \tag{52}$$

Elimination of φ from (51) gives:

$$\frac{d^2\psi}{d\rho^2}+\left(\frac{1}{\rho}-1\right)\frac{d\psi}{d\rho}+\left(\frac{E\delta}{\rho}+\frac{\alpha^2Z^2-\chi^2}{\rho^2}\right)\psi=0. \tag{53}$$

[6] H. A. Bethe, *Handbuch der Physik* XXIV, 1, p. 313 (1933).

Let

$$\psi=[e^{\rho/2}\rho^{-\frac{1}{2}}]w. \tag{54}$$

Then:

$$\frac{d^2w}{d\rho^2}+\left(-\frac{1}{4}+\frac{k}{\rho}+\frac{\frac{1}{4}-m^2}{\rho^2}\right)w=0, \tag{55}$$

where

$$k=E\delta+\tfrac{1}{2};\quad m=+i\lambda. \tag{56}$$

(55) is just the canonical form of the confluent hypergeometric equation.[7] Two linearly independent solutions are: $M_{k,\pm m}(\rho)$. For small r the corresponding φ and ψ are:

$$\begin{aligned}&\psi\sim\rho^{\pm m},\\ &\varphi\sim\pm[(m-E\delta)/(\delta-\chi)]\rho^{\pm m},\end{aligned} \tag{57}$$

which gives

$$u\sim(\text{constant})\left[\pm\frac{m-E\delta}{\delta-\chi}-1\right]\rho^{\pm m}. \tag{58}$$

Let

$$w=e^{i\alpha}M_{k,+m}(\rho)+e^{-i\alpha}M_{k,-m}(\rho). \tag{59}$$

Then if

$$\Pi e^{i\theta}=\frac{i\lambda-E\delta}{\delta-\chi}-1, \tag{60}$$

one finds for small r:

$$u\approx 2\cos[\chi\ln r+\alpha+\theta+\lambda\ln 2(1-E^2)^{\frac{1}{2}}]. \tag{61}$$

Comparing with (43) we see:

$$\alpha=B-\theta-\lambda\ln 2(1-E^2)^{\frac{1}{2}}. \tag{62}$$

With this solution:

$$\psi=\rho^{-\frac{1}{2}}e^{\rho/2}[e^{i\alpha}M_{k,m}(\rho)+e^{-i\alpha}M_{k,-m}(\rho)]. \tag{63}$$

The condition of exponential decrease at infinity yields:

$$e^{i\alpha}\frac{\Gamma(2m+1)}{\Gamma(\frac{1}{2}+m-k)}+e^{-i\alpha}\frac{\Gamma(-2m+1)}{\Gamma(\frac{1}{2}-m-k)}=0. \tag{64}$$

Let

$$\frac{\Gamma(2m+1)}{\Gamma(\frac{1}{2}+m-k)}=be^{i\sigma}. \tag{65}$$

Then condition (64) is:

$$b\cos(\alpha+\sigma)=0, \tag{66}$$

or

$$\alpha+\sigma=(n+\tfrac{1}{2})\pi, \tag{67}$$

where n is a positive or negative integer. Using (62) and (60) one has with

$$B'=B-\lambda\ln 2-arg[\Gamma(2i\lambda+1)]-\pi/2, \tag{68}$$

$$\frac{B'-n\pi}{\lambda}-\frac{1}{\lambda}\tan^{-1}\frac{\lambda}{\chi-\delta(1+E)}-\frac{1}{\lambda}arg\left[\Gamma\left(\frac{-E\alpha Z}{(1-E^2)^{\frac{1}{2}}}+i\lambda\right)\right]=\ln(1-E^2)^{\frac{1}{2}}. \tag{69}$$

[7] E. T. Whittaker and G. N. Watson, *Modern Analysis* (MacMillan Company, 1943), American Edition, p. 337.

Let us consider this equation for small λ. The right-hand side as a function of E goes from $-\infty$ at $E=-1$ to 0 at $E=0$ to $-\infty$ at $E=+1$.

$$\frac{B'-n\pi}{\lambda}\text{ is constant. }\frac{1}{\lambda}arg\left[\Gamma\left(\frac{-E\alpha Z}{(1-E^2)^{\frac{1}{2}}}+i\lambda\right)\right]$$

suffers jumps of $-\pi/\lambda$ at the poles of the Γ function; i.e., at

$$-E\alpha Z/(1-E^2)^{\frac{1}{2}}=n', \tag{70}$$

where $n'=0$ or a positive integer. $\tan^{-1}[\lambda/(\chi-\delta(1+E))]$ is approximately constant if $\chi=-|\chi|$. If $\chi=+|\chi|$ this quantity suffers a jump of $+\pi$ if E passes from -0 to $+0$. Hence, if λ is small the discrete spectrum consists of levels near $-E\alpha Z/(1-E^2)^{\frac{1}{2}}=n'$ where $n'=1,2,3,\cdots$ if $\chi=+|\chi|$ and $n'=0,1,2,3,\cdots$ if $\chi=-|\chi|$. Comparison[6] with the conventional results for $\alpha Z<1$ but αZ near 1 shows that the levels found for $\alpha Z<1$ go over into ones close by.

Of particular interest is the behavior of the lowest energy level. As $\alpha Z\to 1$ from below the lowest Dirac level tends to $E=0$. What happens for αZ slightly larger? For the case λ is small it is possible to solve (69) for the energy level near zero. One finds:

$$E_0=\lambda/\tan B'. \tag{71}$$

Thus, if B' is chosen between zero and $\pi/2$ the energy level is positive, while it is negative if $\frac{1}{2}\pi<B'<\pi$. The difficulties of interpretation would be so great if the lowest level passed from positive to negative values as αZ passes through 1 that one is inclined to require that B' lie in the first-named range. Then we have the following picture of the behavior of the levels as Z increases. Approaching 137 all the ordinary levels go to well-defined limiting values, the lowest going to zero. Increasing Z further, all except the lowest of these levels move to nearby positions. The lowest level starts up again from zero. One interesting point to be gleaned from (69) is that the famous degeneracy of the Dirac equation is removed for $Z>137$. Here the energies of levels for $\chi=|\chi|$ and $\chi=-|\chi|$ are slightly different.

VI. SPIN ZERO AND ONE

For integral spin particles a certain amount of care must be used in formulating the problems. An appropriate "particle form" of the equations must be used. The following equations for integral spin particles given by several authors[8] are most convenient for our purposes (again units of $\hbar=c=m=1$ are chosen):

$$i(\partial\psi/\partial t)=\mathfrak{H}\psi, \tag{72a}$$

$$\mathfrak{H}=eV+\tau_3[1+\tfrac{1}{2}P^2-\tfrac{1}{2}e\mathbf{S}\cdot\mathbf{H}]-i\tau_2[\tfrac{1}{2}P^2-(\mathbf{S}\cdot\mathbf{P})^2-\tfrac{1}{2}e\mathbf{S}\cdot\mathbf{H}]. \tag{72b}$$

[8] Sakata and Taketani, Proc. Math. Phys. Soc. Japan **22**, 757 (1940); I. Tamm, Comptes Rendus U.S.S.R. **29**, 551 (1940); W. Heitler, Proc. Roy. Irish Academy **49**, 1 (1943).

(72) is the "Schrödinger equation" for integral spin. Here V is the external electrostatic potential; H is any external magnetic field; τ_1, τ_2, τ_3 are three Pauli spin matrices; and S_1, S_2, S_3 are the matrices describing the infinitesimal rotations in an irreducible representation of the rotation group. Thus, for spin zero the S_i are zero and ψ has two components. For spin one the S_i are 3×3 matrices and ψ has six components. The energy of a state described by a given ψ is:

$$W=\int\psi^*\tau_3\mathfrak{C}\psi d\tau, \tag{73}$$

and the charge is:

$$Q=e\int\psi^*\tau_3\psi d\tau. \tag{74}$$

One notes that $\mathfrak{C}$ is not hermitean and hence the eigenvalues of (73) are not necessarily real. Of course $\tau_3\mathfrak{C}$ is hermitean, and so the energy is real. Mathematically speaking, the eigenvalue problem is defined by the non-hermitean operator $\mathfrak{C}$ and an indefinite metric suggested by (74). This defines the scalar product between two states ψ_1 and ψ_2 as:

$$(\psi_2,\psi_1)=\int\psi_2{}^*\tau_3\psi_1 dV. \tag{75}$$

Specializing to the Coulomb field of a nucleus of charge Z and no magnetic field gives for the "Hamiltonian"

$$\mathfrak{C}=-(\alpha Z/r)+\tau_3(1+\tfrac{1}{2}P^2)-i\tau_2[\tfrac{1}{2}P^2-\tfrac{1}{2}(\mathbf{S}\cdot\mathbf{P})^2]. \tag{76}$$

Consider the scalar theory. Let

$$\psi=\begin{pmatrix}\psi_1\\ \psi_2\end{pmatrix}e^{-iEt}. \tag{77}$$

Inserting into (72) gives:

$$\begin{aligned}(E+\alpha Z/r)\psi_1&=\psi_1-\tfrac{1}{2}\Delta\psi_1+\tfrac{1}{2}\Delta\psi_2,\\ (E+\alpha Z/r)\psi_2&=-\psi_2+\tfrac{1}{2}\Delta\psi_2-\tfrac{1}{2}\Delta\psi_1.\end{aligned} \tag{78}$$

Let

$$\varphi=(i/\sqrt{2})(\psi_1-\psi_2). \tag{79}$$

Then

$$\Delta\varphi-\varphi+(E+\alpha Z/r)^2\varphi=0. \tag{80}$$

This is just the Klein-Gordon equation, as was to be expected.

Separating out the angular dependence and setting

$$\varphi=u/r, \tag{81}$$

gives the radial wave equation:

$$\frac{d^2u}{dr^2}+\left[-(1-E^2)+\frac{2E\alpha Z}{r}+\frac{\alpha^2Z^2-l(l+1)}{r^2}\right]u=0. \tag{82}$$

Before solving (82) let us consider the behavior of u for small r and the orthogonality relations. Setting

$$u\approx r^\gamma[1+a_1r+\cdots], \tag{83}$$

gives for the indicial equation of (82)

$$\gamma(\gamma-1)+\tfrac{1}{4}-m^2=0, \tag{84}$$

or

$$\gamma=\tfrac{1}{2}\pm m, \tag{85}$$

where

$$m=[(l+\tfrac{1}{2})^2-\alpha^2Z^2]^{\frac{1}{2}}. \tag{86}$$

If $\alpha^2Z^2>(l+\frac{1}{2})^2$ both solutions of (85) have essentially the same behavior near the origin. In case $\alpha Z>\frac{1}{2}$ this certainly occurs at least for S states. Let us then assume

$$m=i\lambda, \tag{87}$$

where λ is real. Then the most general u for small r is:

$$u\sim Cr^{\frac{1}{2}}\cos(\lambda\ln r+B). \tag{88}$$

Let

$$r\psi_1=v,\quad r\psi_2=w. \tag{89}$$

Consider (78) for two different energies E_1 and E_2. The equations for v and w are:

$$E_1v_1=-\frac{\alpha Z}{r}v_1-\tfrac{1}{2}v_1''+\frac{l(l+1)}{2r^2}v_1 +v_1+\tfrac{1}{2}w_1''-\frac{l(l+1)}{2r^2}w_1, \tag{90a}$$

$$E_1w_1=-\frac{\alpha Z}{r}w_1+\tfrac{1}{2}w_1''-\frac{l(l+1)}{2r^2}w_1 -w_1-\tfrac{1}{2}v_1''+\frac{l(l+1)}{2r^2}v_1, \tag{90b}$$

$$E_2v_2=-\frac{\alpha Z}{r}v_2-\tfrac{1}{2}v_2''+\frac{l(l+1)}{2r^2}v_2 +v_2+\tfrac{1}{2}w_2''-\frac{l(l+1)}{2r^2}w_2, \tag{90c}$$

$$E_2w_2=-\frac{\alpha Z}{r}w_2+\tfrac{1}{2}w_2''-\frac{l(l+1)}{2r^2}w_2 -w_2-\tfrac{1}{2}v_2''+\frac{l(l+1)}{2r^2}v_2. \tag{90d}$$

Multiplying (90a) by v_2, (90b) by w_2, (90c) by $(-v_1)$, (90d) by $(-w_1)$, adding and integrating yields:

$$\begin{aligned}(E_1-E_2)&\int_0^\infty(v_2v_1-w_2w_1)dr\\ &=\tfrac{1}{2}[(w_2'-v_2')(w_1-v_1)-(w_2-v_2)(w_1'-v_1')]_0^\infty.\end{aligned} \tag{91}$$

The integral on the left-hand side is just the scalar product (75) after integration over angular coordinates. Noting that

$$w-v=\sqrt{2}iu, \tag{92}$$

and requiring u_1 and u_2 to vanish exponentially sim-

plifies (91) to:

$$(E_1-E_2)\int_0^\infty (v_2v_1-w_2w_1)dr=(w_2'u_1-u_1'u_2)_0. \quad (93)$$

From (88) one sees that:

$$u_1\sim C_1r^{\frac{1}{2}}\cos(\lambda\ln r+B_1),$$
$$u_2\sim C_2r^{\frac{1}{2}}\cos(\lambda\ln r+B_2). \quad (94)$$

Inserting into (93):

$$(E_1-E_2)\int_0^\infty (v_2v_1-w_2w_1)dr=\lambda C_1C_2\sin(B_1-B_2). \quad (95)$$

Hence, again we see that orthogonality is obtained if all eigenfunctions are required to be of the form (88) for small r. Now B is to be considered as a fixed constant, the same for all solutions, describing the Coulomb potential.

With this condition (82) can be solved. Let

$$\rho=2(1-E^2)^{\frac{1}{2}}r. \quad (96)$$

Then:

$$\frac{d^2u}{d\rho^2}+\left[-\frac{1}{4}+\frac{k}{\rho}+\frac{\frac{1}{4}-m^2}{\rho^2}\right]u=0, \quad (97)$$

where

$$k=E\alpha Z/(1-E^2)^{\frac{1}{2}}. \quad (98)$$

Two linearly independent solutions are again $M_{k,\pm m}(\rho)$. Let

$$u=e^{i\alpha}M_{km}(\rho)+e^{-i\alpha}M_{k,-m}(\rho). \quad (99)$$

The condition for small r gives:

$$\alpha=B-\lambda\ln 2(1-E^2)^{\frac{1}{2}}. \quad (100)$$

Let

$$\sigma=arg[\Gamma(2m+1)/\Gamma(\tfrac{1}{2}+m-k)]. \quad (101)$$

The condition of exponential decrease at infinity yields:

$$\cos(\alpha+\sigma)=0, \quad (102a)$$

or

$$\alpha+\sigma=(n+\tfrac{1}{2})\pi. \quad (102b)$$

If

$$B'=B-\lambda\ln 2+arg[\Gamma(1+2i\lambda)]-\tfrac{1}{2}\pi, \quad (103)$$

the eigenvalues of the energy are given by the equation

$$\frac{B'-n\pi}{\lambda}-\frac{1}{\lambda}arg\left[\Gamma\left(\frac{1}{2}-\frac{E\alpha Z}{(1-E^2)^{\frac{1}{2}}}+i(\alpha^2Z^2-(l+\tfrac{1}{2})^2)^{\frac{1}{2}}\right)\right]=\ln(1-E^2)^{\frac{1}{2}}. \quad (104)$$

This is seen to be quite similar to Eq. (69) for the eigenvalues of the Dirac equation. The same arguments apply. Hence, for small λ (i.e., $\alpha Z\sim l+\frac{1}{2}$) the spectrum consists of a set which occurs approximately at the poles of the Γ-function. For $\alpha Z<l+\frac{1}{2}$ these poles are just the energy eigenvalues. Thus, considering S states only, as αZ passes through $\frac{1}{2}$ the spectrum changes continuously. The situation is slightly different from that of the Dirac equation for low-lying states. The lowest Klein-Gordon level tends to $mc^2/\sqrt{2}$ as $\alpha Z\to\frac{1}{2}$ from below. Therefore, no such paradoxical result as having an energy level change sign can occur.

These considerations are slightly less academic for spin zero than for spin $\frac{1}{2}$, since nuclei with charge greater than 137/2 do exist. Moreover, spin zero particles (π mesons?) may even be bound to such nuclei. However, since π mesons are quite heavy the corresponding orbits will be within or very close to the nucleus. The approximation of regarding all protons as lumped at the origin is then so crude as to make the above considerations more than questionable.

For a unit spin particle in a central Coulomb field we follow the treatment of Gunn[9] in separating out the radial and angular portions of (72). For $l=j$ and $j=0$, one obtains the radial Klein-Gordon equation appropriate to the given angular momentum. Here nothing new arises and so we skip these cases. For $l\neq j\neq 0$ the radial equations arising from (72) can be expressed in terms of four functions (F_1, F_2, G_1, G_2). Then with

$$v=(E+\alpha Z/r)/[j(j+1)]^{\frac{1}{2}}, \quad (105)$$

the radial wave equations given by Gunn[9] are (with a few minor changes in notation and units):

$$vF_1-\frac{F_2}{j(j+1)}=\frac{1}{r}\left[\frac{dG_2}{dr}+\frac{F_2}{r}\right], \quad (106a)$$

$$vG_1-G_2=-\frac{d^2G_2}{dr^2}-\frac{1}{r}\left[\frac{d}{dr}-\frac{1}{r}\right]F_2, \quad (106b)$$

$$vG_2-\frac{G_1}{j(j+1)}=\frac{G_1}{r^2}+\frac{1}{r}\left[\frac{d}{dr}+\frac{1}{r}\right]F_1, \quad (106c)$$

$$vF_2-F_1=-\left(\frac{d^2}{dr^2}-\frac{2}{r^2}\right)F_1-\frac{1}{r}\left(\frac{d}{dr}-\frac{2}{r}\right)G_1. \quad (106d)$$

Solving for F_2 and G_1 one finds:

$$F_2=(r^2vF_1-rG_2')/[1+r^2/j(j+1)], \quad (107a)$$

$$G_1=(r^2vG_2-(rF_1'+F_1))/[1+r^2/j(j+1)]. \quad (107b)$$

Let

$$G=(G_2+F_1)/\sqrt{2};\quad F=(G_2-F_1)/\sqrt{2}. \quad (108)$$

Then the resulting equations for F and G can be written as:

$$\frac{d^2G}{dr^2}+\frac{2}{r}\frac{j(j+1)}{j(j+1)+r^2}\frac{dG}{dr}+\left[j(j+1)\left(v^2-\frac{1}{r^2}\right)-1-\frac{1}{j(j+1)+r^2}+\frac{j(j+1)v'}{r}-\frac{2vj(j+1)}{j(j+1)+r^2}\right]G+\frac{F}{j(j+1)+r^2}=0, \quad (109)$$

[9] J. C. Gunn, Proc. Roy. Soc. **193**, 559 (1946).

$$\frac{d^2F}{dr^2}+\frac{2}{r}\frac{j(j+1)}{j(j+1)+r^2}\frac{dG}{dr}$$
$$+\left[j(j+1)\left(v^2-\frac{1}{r^2}\right)-1-\frac{1}{j(j+1)+r^2}\right.$$
$$\left.-\frac{j(j+1)v'}{r}+\frac{2vj(j+1)}{j(j+1)+r^1}\right]F+\frac{G}{j(j+1)+r^1}=0. \quad (110)$$

The forms (109) and (110) are particularly useful for examining the behavior near the origin, since there the two equations are effectively decoupled, the coupling term being regular. The behavior of the four linearly independent solutions of (109) and (110) can then be determined by first setting $F=0$ in (109) and finding the two solutions of (110). Then treat (110) with $G=0$ similarly. As noted by earlier authors, these equations have an essential singularity at the origin. This, of course, prohibits a power series development. However, it is possible, as in (25), to split off an exponential factor[10] and then to find a power series development. Doing this the four linearly independent solutions are, in the vicinity of the origin:

$$G=r^{-\frac{1}{2}}\exp(\pm\lambda/r^{\frac{1}{2}}); \qquad F=(\text{const.})r^{-\frac{1}{2}}r^3\exp(\pm\lambda/r^{\frac{1}{2}}), \quad (111a, b)$$

$$F=r^{-\frac{1}{2}}\exp(\pm i\lambda/r^{\frac{1}{2}}); \qquad G=(\text{const.})r^{-\frac{1}{2}}r^3\exp(\pm i\lambda/r^{\frac{1}{2}}), \quad (112a, b)$$

where now

$$\lambda=2(\alpha Z)^{\frac{1}{2}}[j(j+1)]^{\frac{1}{4}}. \quad (113)$$

Of these solutions (111a) is obviously inacceptable, since it has a horrible infinity at the origin. (111b) vanishes very strongly, and so is completely satisfactory. For (112) further investigation is necessary. Again, taking real solutions the general linear combination of (112) may be written

$$F\sim(\text{const.})r^{-\frac{1}{2}}\cos(\lambda r^{-\frac{1}{2}}+B); \quad G=0, \quad (114)$$

and then:

$$F_1\cong-r^{-\frac{1}{2}}\cos(\lambda r^{-\frac{1}{2}}+B); \quad G_2\sim r^{-\frac{1}{2}}\cos(\lambda r^{-\frac{1}{2}}+B),$$
$$F_2\sim-r^{-\frac{1}{2}}\left\{\left[-\frac{1}{4}+\frac{\alpha Z}{j(j+1)}r\right]\cos(\lambda r^{-\frac{1}{2}}+B)\right.$$
$$\left.+\frac{\lambda}{2r^{\frac{1}{2}}}\sin(\lambda r^{-\frac{1}{2}}+B)\right\},$$
$$G_1\approx r^{-\frac{1}{2}}\left\{\left[\frac{3}{4}+\frac{\alpha Z}{(j(j+1))^{\frac{1}{2}}}r\right]\cos(\lambda r^{-\frac{1}{2}}+B)\right.$$
$$\left.+\frac{\lambda}{2r^{\frac{1}{2}}}\sin(\lambda r^{-\frac{1}{2}}+B)\right\}. \quad (115)$$

[10] J. H. Bartlett, Phys. Rev. 72, 219 (1947).

Now:

$$\int\psi^*\tau_3\psi dV \sim\int_0^\infty[F_1^*F_2+F_2^*F_1+G_1^*G_2+G_2^*G_1]dr. \quad (116)$$

Inserting (115) into (116) one finds for the contribution near the origin:

$$\int\psi^*\tau_3\psi dV\sim\int r^{-\frac{1}{2}}\cos^2(\lambda r^{-\frac{1}{2}}+B)dr. \quad (117)$$

This integral certainly exists and so the charge density is integrable for these solutions. Contrary to previous statements, this means that there are too *many* rather than too few solutions of (72) which are quadratically integrable near the origin. Instead of one, there are three physically acceptable solutions of (109) and (110). The resulting set of eigenfunctions is then *over* complete. The two solutions described by (114) are, of course, to be narrowed to one by requiring orthogonality. Consider equations (106) for two different energies E_a and E_b. Multiplying these equations by various functions, adding and integrating following the previous methods and using (106), one finds on integrating out angular coordinates:

$$(E_a-E_b)\int\psi_a^*\tau_3\psi_b dV \sim\{r(F_1^bG_1^a-F_1^aG_1^b)+r(G_2^bF_2^a-G_2^aF_2^b)\}_0^\infty. \quad (118)$$

Requiring an exponential decrease at infinity and assuming

$$F^a\sim r^{-\frac{1}{2}}\cos(\lambda r^{-\frac{1}{2}}+B_a), \qquad F^b\sim r^{-\frac{1}{2}}\cos(\lambda r^{-\frac{1}{2}}+B_b), \quad (119)$$

gives:

$$(E_a-E_b)\int\psi_a^*\tau_3\psi_b dV\sim-\lambda\sin(B_a-B_b). \quad (120)$$

Once again one sees that requiring all solutions to behave like (114) with a *fixed* B gives orthogonality. With this condition the eigenfunctions of the vector meson in a Coulomb field do form a complete set, in contradiction to previous communications on the subject. Of course, the actual computation of these functions, except possibly by machine, gives rise, as pointed out by Bartlett,[10] to great difficulties.

There is, however, one possible experimental verification which would not rest on tedious calculations. The π meson may have unit spin. Then even for hydrogen the introduction of a phase constant would be necessary. It can be shown then that resonances should occur in scattering. Thus, if a beam of low energy mesons were incident on a hydrogen target one would expect maxima

and minima in the cross section as the energy of the beam varies.

With the information now at hand, it is possible to say something concerning the common conjecture that as Z increases over 137 for the Dirac particles (or over 137/2 for Klein-Gordon particles) pairs will be produced. This is, properly speaking, a many-particle process and so certainly not to be encompassed by the present single particle theory results. However, since it is found that nothing spectacular happens to the energy levels at these transition points, it is difficult to see why pairs should suddenly occur. Consider a state with certain levels filled, others empty. As Z is adiabatically increased, one would expect the particles in a given state to continue in this state as the state is slowly altered. If this happens, one sees that nothing of importance occurs at the transition points.

VII. MATHEMATICAL BASIS

In the preceding work a number of examples of singular potentials have been considered. The structures of the various problems have been rather different, and yet the same method has always worked. At each step the success seemed to be a minor miracle. Here the underlying reason that the method works and a general proof of its applicability will be given.

Two characteristics have been true of all the above problems. (1) The linearly independent solutions of the differential equations are distinguishable by a phase constant B. (2) By requiring all eigenfunctions to approach the origin with the same B, orthogonality is achieved.

In words, the general proof runs as follows: Let the potential go to infinity sufficiently rapidly (defined more precisely below) so that V is uniformly large for small r. Then the behavior of the solutions of the differential equations near the origin are determined by the potential alone; i.e., for r small all the equations approach some standard equation, say that corresponding to $E=0$. Under these conditions, Sturm's oscillation theorem shows the behavior of solutions of the standard equation to be oscillatory and hence describable by a phase constant. Requiring all eigenfunctions to have this same phase constant means that these functions are *all* to approach the same solution of the standard equation. Two solutions of the standard equation have constant Wronskian. In particular, for linearly dependent solutions, this constant is zero. Since two different eigenfunctions approach the same solution, the Wronskian of these eigenfunctions tends to zero for small r. This last is just the orthogonality condition.

For purposes of simplicity we restrict ourselves to the non-relativistic case in carrying out the proof. The generalization will then be evident and so merely sketched.

Consider the Schrödinger equation (2) in the slightly altered form:

$$d^2u/dx^2+[f(x)-\eta^2]u=0. \tag{121}$$

Let $f(x)$ go to $+\infty$ uniformly for x sufficiently small. Then for x small (121) approaches the equation:

$$d^2u_0/dx^2+[f(x)]u_0=0. \tag{122}$$

The asymptotic integration for x small is obtained by what is essentially the WKB method.

Let

$$u_0=e^{iS}. \tag{123}$$

Then

$$(S')^2-iS''=f(x). \tag{124}$$

If

$$|S''|\ll S'^2, \tag{125}$$

one has approximately:

$$(S')^2=f(x), \tag{126}$$

or

$$S=\pm\int_x^{x_0}(f(x))^{\frac{1}{2}}dx, \tag{127}$$

where x_0 is some constant. The condition of validity (125) gives:

$$f(x)\gg|\tfrac{1}{2}f^{-\frac{1}{2}}f'|, \tag{128}$$

or since f' is negative, $f(x)$ positive,

$$f(x)\gg -f'/2f^{\frac{1}{2}}. \tag{129}$$

On integration

$$f(x)\gg 1/x^2,\ x \text{ small}. \tag{130}$$

Equation (130) is our definition of "sufficiently singular." As a second approximation under the conditions (130) one finds:

$$S=\pm\int_x^{x_0}(f(x))^{\frac{1}{2}}dx+\tfrac{1}{4}i\ln f(x). \tag{131}$$

Combining the two solutions for u_0 into real solutions one finds:

$$u_0\cong f(x)^{-\frac{1}{4}}\cos\left[\int_x^{x_0}(f(x))^{\frac{1}{2}}dx+B\right] \tag{132}$$

where B is an arbitrary constant. Consider two solutions of (122), u_0^a and u_0^b, with constants B_a and B_b. Then:

$$W(u_0^a, u_0^b)=u_0^a u_0^{b\prime}-u_0^b u_0^{a\prime}=\sin(B_b-B_a). \tag{133}$$

Let us integrate (121) by assuming:

$$u=\varphi(x)u_0, \tag{134}$$

where u_0 is a solution of (122). Then (121) becomes:

$$\varphi'=\tfrac{1}{2}(\eta^2\varphi-\varphi'')u_0/u_0'. \tag{135}$$

But

$$|u_0/u_0'|\sim 1/(f(x))^{\frac{1}{2}}\ll 1 \text{ by (127)}.$$

Hence,

$$\varphi'\approx 0. \tag{136}$$

Improving the approximation by taking into account the first term on the right-hand side of (135) we find:

$$\varphi \approx \exp\left[\frac{\eta^2}{2}\int_0^x \frac{u_0}{u_{0'}}dx\right]. \tag{137}$$

Consider solutions of (121) corresponding to two different energies η^a, η^b. Then:

$$\begin{aligned} u^a &\sim \left[\exp\left(\frac{\eta_a^2}{2}\int_0^x \frac{u_0{}^a}{u_0{}^{a'}}dx\right)\right]u_0{}^a, \\ u^b &\sim \left[\exp\left(\frac{\eta_b^2}{2}\int_0^x \frac{u_0{}^b}{u_0{}^{b'}}dx\right)\right]u_0{}^b. \end{aligned} \tag{138}$$

Familiar operations on the Eqs. (121) give:

$$[(\eta^b)^2-(\eta^a)^2]\int_0^\infty u_b u_a dx = W(u_a, u_b)]_0. \tag{139}$$

But from (138):

$$W(u_a, u_b) \sim \exp\left[\frac{\eta_a^2}{2}\int_0^x \frac{u_0{}^a}{(u_0{}^a)'}dx + \frac{\eta_b^2}{2}\int_0^x \frac{u_0{}^b}{(u_0{}^b)'}dx\right]$$

$$\times\left\{W(u_0{}^a, u_0{}^b)+u_0{}^a u_0{}^b\left[\frac{u_0{}^b}{u_0{}^{b'}}-\frac{u_0{}^a}{u_0{}^{a'}}\right]\right\} \tag{140}$$

$$\to W(u_0{}^a, u_0{}^b) = \sin(B_b - B_a). \tag{141}$$

Hence, if u_a and u_b are required to approach the same solution of (122), orthogonality results.

The generalization to the more complicated relativistic equations is evident. For small r, solutions will tend to those of a standard equation whose behavior is completely determined by the singularity. In all such equations an identity exists between two solutions for different energies of the form:

$$(E_1-E_2)(\psi_1, \psi_2) = dW_G(\psi_1, \psi_2)/dr, \tag{142}$$

where (ψ_1, ψ_2) is an appropriately defined scalar product density, and W_G is a function generalizing the ordinary Wronskian which vanishes for $\psi_1=\psi_2$. Now $E_1=E_2$ for two solutions of the standard equation. Hence, $W_G=$constant for this case. Integrating (142) shows the integrated scalar product is proportional to $W_G]_0$. Since W_G, for small r, tends to that for solutions of the standard equation, it is constant sufficiently near the origin. In particular, if all eigenfunctions are required to tend to a *unique* solution of the standard equation, this constant is zero. Hence, the eigenfunctions will form an orthonormal set.

VIII. CONCLUSIONS

The above discussion gives a method for solving eigenvalue problems with a potential which tends to infinity very strongly at one end of an interval. It can be shown that the method is applicable to the $1/r^3$ tensor force problem, but with the attendant non-relativistic difficulties. However, one can prove that the relativistic equation from which the $1/r^3$ arises as an approximation gives no difficulties no matter how large the coupling constants are.

On the mathematical side the following can be said. In quantum mechanics we are interested in operators having complete orthonormal sets of eigenfunctions. Usually this requirement is taken to be hermiticity. Von Neumann[11] has shown that the condition is really that it be possible to construct a unitary operator generated by the hermitian operator. Here we have found that by formally supplementing the definition of an operator it is possible to obtain an hermitian operator with a complete set of eigenfunctions. It would be useful to have simple criteria for when this is necessary and when it is possible.

In conclusion I should like to thank Professor W. Pauli for several very instructive discussions, Professor J. Von Neumann for permission to use his unpublished results, and Professor J. R. Oppenheimer for suggestions and the kind hospitality of the Institute.

[11] W. Pauli, *Handbuch der Physik* XXIV, 1, p. 142 (1933).

Neutron Yields from Photo-Disintegration by Gamma-Rays from Lithium*

B. D. McDaniel, R. L. Walker,† and M. B. Stearns
Cornell University, Ithaca, New York
(Received July 31, 1950)

The relative neutron yield of 33 elements has been studied using the gamma-ray spectrum which arises from proton bombardment of Li. The samples which were to be irradiated were placed in a block of paraffin. The neutrons were detected using four boron trifluoride proportional counters. Absolute gamma-ray and neutron intensity measurements yielded the value (0.055±0.012) barn for the (γ,n) cross section of copper. Rough indications were also obtained concerning the relative neutron energy distribution from the samples.

I. INTRODUCTION

DURING recent months a number of experiments[1–5] have been performed to obtain information concerning the (γ,n) photo-disintegration processes. These experiments have been performed using either the radiation from a nuclear reaction process such as $Li^7(p,\gamma)Be^8$ or the bremsstrahlung spectrum from a betatron. Though activation methods have been used for the detection of the disintegration by both kinds of radiation, direct neutron detection seems to have been limited to the case of disintegrations produced by the betatron.

The experiments to be described below apply the method of neutron detection to the disintegrations produced by the gamma-rays from the Li reaction. These experiments have been briefly described earlier.[6] The gamma-ray spectrum for the Li reaction has been examined in detail by Walker and McDaniel.[7] In these experiments 750-kev protons were used to bombard a thick lithium target. Under these conditions the gamma-ray spectrum consists of two lines. One of these is located at 17.6 Mev and is presumably but a few kilovolts wide. The second component is located at about 14.8 Mev and is of the order of 2 Mev in width. The intensity of the 17.6-Mev line is about twice that of the low energy component. The measurements of neutron yield which were made in the present experiment constitute a weighted average of the cross section over this spectrum and over the isotopes present in the sample. The yields of 33 samples were measured relative to the yield of copper. For copper, a measurement of the absolute value of the cross section was made.

II. MEASUREMENT OF THE RELATIVE YIELD

The experimental arrangement which was used in the measurement of the relative neutron yield is shown in Fig. 1. A large rectangular block of paraffin was placed immediately in front of the cyclotron target. Four enriched BF_3 proportional counters, arranged in a square array, were embedded in a movable section of the paraffin. The neutron-producing sample was placed in a cavity in the paraffin located between the counters and the cyclotron target. A layer of 1 g/cm² of B_4C was placed between the sample and the counters. This absorber causes the counters to be insensitive to neutrons which are thermalized in the vicinity of the sample. Thus, variations in the slow neutron absorption cross section of the sample will not affect the slow neutron detection efficiency of the counters.

The counters were connected in pairs, front and rear, to form two counting channels. The proportional counter pulses were amplified and passed into scaling and recording circuits in two similar channels. The principal reason for the use of two counting channels was to obtain some information concerning the neutron energy spectrum of the various samples examined. It was thought that if there were radical differences between neutron spectra, this would evidence itself by a variation of the ratio of neutron counting rates in the front and rear channels.

Three lead-shielded Geiger counters were located above the cyclotron target and were used as monitors of the gamma-ray intensity.

A set of measurements on a sample consisted of consecutive observations of the counting rates in the two channels under three conditions: (a) background with no sample, (b) sample or "radiator" producing neutrons placed in the cavity, (c) standard copper radiator in cavity. All samples covered the same area, the different substances differing only in thickness. Powder samples were enclosed in thin-walled Al boxes. Their comparison measurements (a) and (c), respectively, were taken with an empty Al box, and with one containing the copper standard. In the case of heavy elements, a total of three sets of observations were taken while in the case of the light elements, five sets of observations were taken because of the lower neutron yield and consequent inaccuracy of the individual measurements. For the standard copper radiator, the ratio of the sample counting rate to the background rate was about three to one. For the samples of the heavier elements this

* This work was supported in part by a contract with the ONR.
† Now at California Institute of Technology, Pasadena, California.
[1] H. Wäffler and O. Hirzel, Helv. Phys. Acta **21**, 200 (1948).
[2] J. McElhinney (unpublished).
[3] G. Friedlander and M. L. Perlman, Phys. Rev. **74**, 442 (1948); **75**, 988 (1949).
[4] G. A. Price and D. W. Kerst, Phys. Rev. **77**, 806 (1950).
[5] L. Katz *et al.* (to be published).
[6] Walker, McDaniel, and Stearns, Phys. Rev. **79**, 242 (1950).
[7] R. L. Walker and B. D. McDaniel, Phys. Rev. **74**, 315 (1948).

ratio was frequently higher but for the lighter elements the ratio approached unity and in some cases, as will be explained below, was even less.

The calculation of the relative cross sections from the counting rates was made in the following manner. The counting rates with the sample in position were first corrected for two effects which alter the background component when the radiator is inserted. The backgrounds were then subtracted to obtain the relative number of neutrons emitted by the sample. These numbers were then corrected for the reduction, by absorption, of the gamma-ray intensity as the gamma-rays traverse the sample. The neutron yields from the samples were reduced to obtain the yield per atom. The correction for self-absorption of the gamma-rays in the radiator included a small correction for obliquity of incidence. For some of the heavy elements the self-absorption correction was as great as 30 percent.

For light elements the two effects which alter the background upon insertion of the radiator actually reduce the counting rate of the counter with radiator below that obtained with no radiator.

The first of these effects to be considered is the following. About 50 percent of the background counting rate arises from production of neutrons in the walls of the counters themselves by the incident gamma-ray flux. When the radiator is inserted, the gamma-ray flux on the counters is diminished by the absorption of the gamma-rays in the sample. This reduces the number of neutrons produced in the counter walls. In the case of light elements the neutron production may be very small and the reduction in the background may exceed the increase in the rate due to generation of neutrons in the sample. Because the cross section for neutron production decreases more rapidly with Z than does the total cross section, the effect is larger for low values of Z.

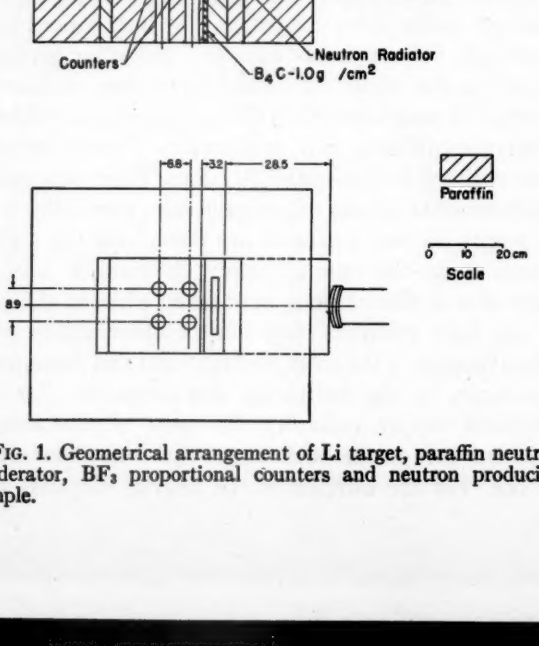

FIG. 1. Geometrical arrangement of Li target, paraffin neutron moderator, BF_3 proportional counters and neutron producing sample.

In the case of copper the correction for this effect was about seven percent of the cross section, and was as great as 100 percent for the case of calcium. The reduction of the background due to the insertion of the radiator is obtained by multiplying the fraction of the background originating in the counters by the factor $(1-T)$ where T is the gamma-ray transmission of the sample. The fraction of the background which arises in the counters was determined by a series of measurements which were made with the counters alternately bare and surrounded by an amount of brass equal to that of the counters. The calculations were made in such a manner as to take into account the change in the neutron sensitivity of the counters by the insertion of the additional brass. The transmission coefficients of the samples were calculated from the total gamma-ray cross section of the materials. These cross sections were based on the values measured by Walker[8] at 17.6 Mev. For the values of Z not directly measured by Walker, the values were determined by interpolation. The corrections to the total gamma-ray cross sections due to the presence of the 14.5-Mev line were negligible. While gamma-rays may be degraded by Compton scattering and consequently not removed from the beam, it was calculated that because of the high threshold for the (γ,n) reaction and the small fraction of high energy gamma-rays in the scattered radiation this effect could be neglected.

The second effect which contributes to a reduction in the counting rate on insertion of the absorber is the scattering of neutrons away from the counters. Some neutrons were generated in the vicinity of the target and could pass through the paraffin shielding to be detected in the counters. When a thick sample is placed in the beam, part of the neutrons are scattered away from the counters. To measure this effect a thick sample of carbon was placed in the beam. Since the gamma-ray threshold energy for neutron production in carbon exceeds 17.6 Mev, it was presumed that no neutrons were generated in the sample. When the carbon sample was inserted a reduction in the counting rate was observed. Much of the reduction was due to the effect first described but about 40 percent was due to neutron scattering. The determination of the magnitude of the scattering effect in carbon, used with the measured values for the neutron scattering cross section[9] for neutrons of about 1 Mev, permit a correction to be made for the scattering in the various samples which were used. For most samples heavier than aluminum the correction was negligible, but for the lighter elements the corrections were as great as 15 percent.

[8] R. L. Walker, Phys. Rev. **76**, 527 (1949).

[9] Goldsmith, Ibser, and Feld, *Science and Engineering of Nuclear Power, Neutron cross sections of the elements* (Addison-Wesley Press, Inc., Cambridge, 1947).

After calculation of the relative yields the results for the two channels were averaged. The results of the calculations are shown in Fig. 2. Here we have plotted as ordinate the neutron yield per atom relative to that of copper. The abscissa is Z. The smooth variation of the yield in the range of Z extending from 21 to 58 is rather striking. In this range, with the exception of Ni, no value departs from the curve shown by an amount greater than about 20 percent. Nickel is notably low, having only about one-half the value of the ordinate of the curve at this point. The yield values for Z below 20 are all low but fluctuate widely as might be expected. At high Z, Hg, Pb, and Bi seem to show a slight falling off. Uranium lies above the extrapolation of the curve, probably because of an appreciable photo-fission cross section at 17.6 Mev combined with a multiplicity of fission neutrons.

III. NEUTRON ENERGY SPECTRUM

As was mentioned above, it was hoped that one would be able to obtain some indication of the neutron energy distribution from the various samples by comparing the counting rates of the front and rear channels. After subtraction of the background it was found that the ratio of the front to rear channel counting rates increased with increasing Z by about 35 percent. This indicates a decrease in neutron energy with increasing Z. For the most part this variation was rather systematic though a few elements deviated notably from a systematic variation. Tungsten, one of these elements, seemed to have a remarkably low energy neutron distribution.

To explore this further, measurements were made of the neutron counting rate for several samples as a function of position of the counter in the paraffin behind the radiator. This position could be varied by moving the paraffin section, which contained the counters, back and forth in the outer paraffin shell. Layers of paraffin were added between the sample and the counters to keep the spaces filled with paraffin at all times. The results of the measurements are shown in Fig. 3. Here we have plotted the ratio of the corrected counting rate of the sample to that for copper. The abscissa is the distance D between the face of the cavity in the paraffin and the center of the counters. We see that the curve for tungsten falls off much faster than that of Pb. For a comparison standard the neutrons from Ra–α–Be and Po–α–Be were also examined. The counting rates for these spectra are also plotted on the curve relative to the Cu counting rate. Both of the natural sources seem to indicate the presence of appreciably higher energy neutrons than are present either in the spectrum of copper, Pb or W. It is not possible to obtain from such an experiment as this the actual neutron spectrum from the elements examined but the curves serve to indicate the gross differences between the spectra. Since the average energy of the Po–α–Be source is about 4 Mev, and the low energy component of the Ra–α–Be is probably less[10] than 1 Mev, one may guess the average energy of the neutrons from Cu to be about 1 Mev.

IV. DETERMINATION OF Cu CROSS SECTION BY MEASUREMENT OF ABSOLUTE GAMMA-RAY AND NEUTRON INTENSITY

The determination of the absolute yield of neutrons from the radiator was made by a comparison between the neutron counting rate from the radiator and that from a standard Ra–α–Be source with the counters located in their standard position. When the gamma-rays from the cyclotron target fall on the radiator, the illumination of the radiator is not uniform. Furthermore, the sensitivity of detection of the neutrons which originate from various parts of the radiator is not constant. To take these effects into account in making the calibration using the Ra–α–Be source, observations were made in the following manner. An aluminum plate,

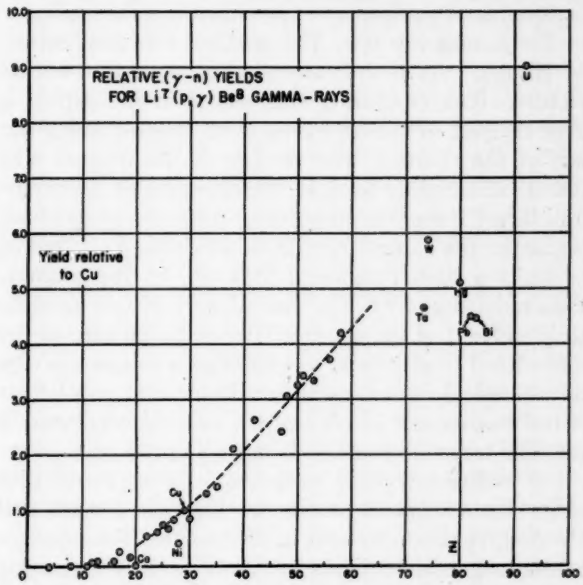

FIG. 2. Neutron yield per atom relative to that from copper.

the size of the radiator, was subdivided into 25 smaller areas. In the center of each area was drilled a hole to receive the RaBe neutron source. The plate was placed in the radiator position and the counting rate was observed for the source placed in each of the 25 source positions in the plate. The observed rates were then weighted by a factor proportional to the area represented by each location and proportional to the relative intensity of illumination of this area when irradiated by gamma-rays from the cyclotron. The intensity of illumination from the cyclotron was assumed to follow the inverse square law. The neutron detection efficiencies were found to be about one percent and one-half percent for the front and rear counter pairs, respectively.

The determination of the gamma-ray intensity was

[10] H. L. Anderson, Nuclear Science Series, Preliminary Report No. 3, National Research Council.

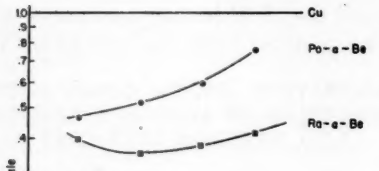

FIG. 3. Relative spatial distribution of neutron density in paraffin. Counting rate compared to that of standard Cu sample as function of distance D from center of counter to face of cavity in the paraffin which contains sample. Ratios have been multiplied by arbitrary factors and plotted on a logarithmic scale.

based upon a direct measurement of the number of Compton and pair processes produced in a thin radiator by the gamma-ray flux. This method was used earlier by Hough.[11] As is indicated in Fig. 4, a thin-walled Victoreen Geiger counter was placed in the gap of a large magnet so the field lines were directed along the axis of the counter. The air gap of the magnet was heavily shielded by lead. In the direction of the cyclotron target there was an opening in the shielding which permitted the gamma-rays from all parts of the target to strike a chosen region, 1.5×1 cm, on the counter. Thin radiators of Pb, Cu, and Al were placed immediately in front of the counter. The counting rate of the thin-walled counter was measured as a function of the thickness and material of the radiator. The gap height of the magnet was 15 cm and the pole diameter was 35 cm. The target to counter distance was 105 cm.

For sufficiently thin radiators it is expected that either the Compton process or the pair process will always give rise to a count in the counter. The presence of the magnetic field aids in this respect by increasing the probability of counting low energy electrons which are scattered through large angles. Because of the resolving time of the counters, one, and only one, count is obtained for each process. Thus the incident gamma-ray flux can be determined from a knowledge of the counting rate, the geometry and the total cross section of the material of the radiator for the gamma-ray spectrum being used. The principal function of the magnetic field is to lower the background by preventing electrons which are produced in the walls and collimator from reaching the counter. To decrease the number of electrons scattered from the walls of the chamber, the walls were covered by $\frac{1}{4}$ in. of wood. Because of the large increase in the total cross section at low energies by the Compton and photoelectric processes, it is necessary to determine that there is not a sufficient amount of degraded radiation present to cause difficulty in the measurements. To check this possibility a lead absorber was placed immediately behind the collimator. Its absorption coefficient was found to be that expected for the high energy radiation present in the spectrum. A further check on this point is the good agreement which was found between the results for the radiators of the three different elements. The background counting rate in the counter with no radiator present was quite low and was insensitive to the magnetic field strength. The value of field strength which was used was 3000 gauss.

The results of the gamma-ray intensity measurements are shown in Fig. 5. The ordinates plotted are the ratios of counting rate of the Victoreen counter to the monitor rate. Plotted on the abscissa is the grams of material contained in the radiator. It will be noticed that the increase in counting rate with radiator weight is quite linear to rather large values. From the slopes of the curves and from the gamma-ray cross-section values one can obtain the gamma-ray flux corresponding to a given monitor rate. The cross-section values which were used were taken from the measurements by Walker. A small correction was made in the case of lead for the fact that Walker's measurements[8] were taken at 17.6 Mev whereas the gamma-ray spectrum used here contained some intensity at 14.8 Mev. For copper and aluminum no correction was necessary. The results of the intensity measurements for the Pb, Cu, and Al agreed to within four percent of the average of the three measurements.

This method of measuring gamma-ray intensities was checked at an earlier time by another method which utilized the calculated efficiency of the gamma-ray pair spectrometer of Walker and McDaniel.[7] The results of the measurements by the two methods agreed to five percent. The calculated source strength was about 1×10^7 gamma-rays per second.

Price and Kerst[4] examined the angular distribution of neutrons from lead and iron and found it to be isotropic. In the present experiment it was assumed that

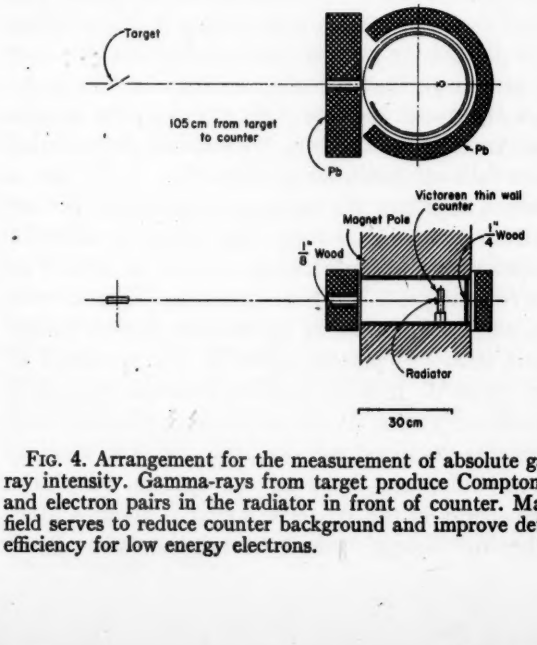

FIG. 4. Arrangement for the measurement of absolute gamma-ray intensity. Gamma-rays from target produce Compton recoil and electron pairs in the radiator in front of counter. Magnetic field serves to reduce counter background and improve detection efficiency for low energy electrons.

[11] P. V. C. Hough (unpublished).

all elements examined had an isotropic neutron distribution. Devons and Hine[12] have shown that the gamma-ray production in the Li reaction deviates slightly from isotropy for protons whose incident energy is that of the resonance energy. Though our proton energy was 750 kev, since a thick target was used, nearly all of the gamma-ray intensity arises from resonance protons. The two sets of apparatus for the neutron measurement and the gamma-ray measurement were located at slightly different angles with respect to the direction of the incident proton beam. This required a correction of three percent in the absolute cross-section measurement because of the asymmetry in gamma-ray production.

The value obtained for the Cu cross section for the (γ,n) process is 0.055 barn. This is the average of the two values arising from the neutron counting rates of the front and rear counting channels. It is also the average for both isotopes in the sample and both gamma-ray components present in the spectrum. Because of the uncertainty resulting from the difference between the neutron spectrum of the radiator and the calibrating neutrons source, it is difficult to estimate the over-all accuracy of the measurements. Our estimate of the probable error is 0.012 barn.

V. DISCUSSION

It is difficult to make a reliable comparison between the results obtained in this experiment and those of other experiments because of the widely different conditions. Wäffler and Hirzel[1] obtained their data using the Li gamma-ray spectrum but used activation methods for detecting the neutron emission process. Price and Kerst[4] measured the neutrons directly but used the broad bremsstrahlung spectrum. Friedlander and Perlman,[3] and McElhinney[2] used activation methods with a bremsstrahlung spectrum.

In order to make a comparison with other experiments our results are replotted in Fig. 6, on a logarithmic cross-section scale. Our points are indicated by the open circles. The heavy black dots indicate the values obtained by Wäffler and Hirzel while the dashed curve is that obtained by Price and Kerst using the 22-Mev bremsstrahlung spectrum. For our data and those of Wäffler and Hirzel, the absolute cross-section values are plotted. In the latter case it was necessary to average the isotopic cross sections to permit a comparison. The curve of Price and Kerst has been normalized arbitrarily to match our data at Z equal to 29. The indicated errors in our data represent the standard deviation of the average of the various runs on the individual samples. It is likely that the systematic errors are equally large or larger, in view of the high background and large corrections which are applied. The values given for Z of 20 or less are quite inaccurate but should serve as a rough measure of the cross sections.

[12] S. Devons and M. G. N. Hine, Proc. Roy. Soc. **A199**, 56–73 (1949).

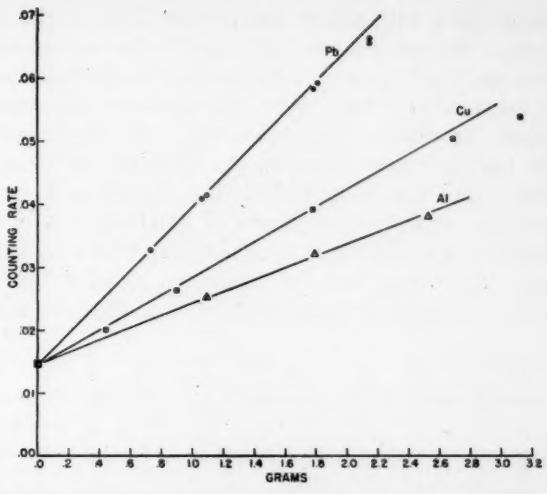

FIG. 5. Counting rate compared to monitor rate for Victoreen counter used in the measurement of absolute gamma-ray intensity. Counting rate is plotted as a function of radiator weight. Area of radiator was 1.5 cm².

Though many of the values of Wäffler and Hirzel are in fair agreement with ours, there are several values which differ widely. For Z greater than 20 the values obtained in our experiment lie rather smoothly along a curve, but the values of Wäffler and Hirzel fluctuate rather severely. This disagreement in the relative values of the cross section may perhaps be explained on the basis that the quantities measured in the two experiments are different. By necessity the activation method chooses particular isotopes of certain elements whereas the direct neutron measurement is an average over all isotopes for each of the available samples. It may be argued further that the neutron experiments give heavy weight to possible $(\gamma,2n)$ reactions. However, the measurements of Perlman and Friedlander at 50 Mev for F^{19}, P^{31}, and Cu^{63} indicate that the $(\gamma,2n)$ process is at most 10 percent of the (γ,n) cross section for the light elements. The $(\gamma,2n)$ thresholds for most of the elements examined probably exceed the 17.6-Mev gamma-ray energy. For those cases in which the $(\gamma,2n)$ reaction is possible one would expect the yield to be small because of the nearness to the threshold. One would expect that the absolute cross section measured by activation would be equal to, or smaller than, the cross section computed from the neutron yield assuming the emission of a single neutron. Of the elements measured both by Wäffler and Hirzel and by us, Cu is outstanding in that their value is 2.5 times greater than ours. While there are several other elements for which their values are notably high as compared with a smooth curve through our points, in these cases we have no measurements on elements of the same Z.

The agreement between our data and that of Price and Kerst seems to be much better. Though they also obtained data using the bremsstrahlung from 18-Mev electrons as well as those of 22 Mev, it was felt that it was better to compare our data with the 22-Mev data

rather than with either the 18-Mev data or the difference between the two. For the 18-Mev bremsstrahlung spectrum there are very few gamma-rays of energy as great as 17.6 Mev. With this spectrum one would expect the yield to depend strongly on the threshold for the reaction rather than on the cross section near 17 Mev, since the maximum in the cross-section curve probably occurs near or above 17 Mev for most of the elements. The difference spectrum is but little better in this respect and has the additional disadvantage of being very sensitive to the calibration of the gamma-ray

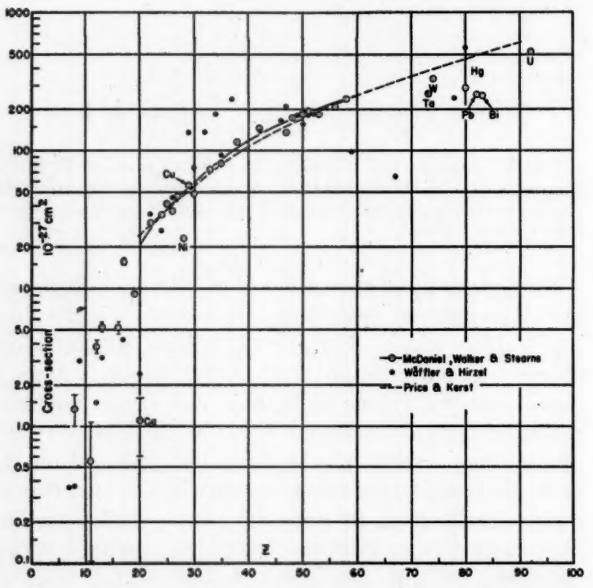

FIG. 6. Neutron yield plotted as a function of Z. The yield is plotted as (γ,n) cross section per atom. Data of Price and Kerst and McDaniel, Walker, and Stearns are plotted assuming no multiplicity of neutrons in the emission process. Errors shown on circled points are based on calculation of standard deviations. Systematic errors may be appreciably greater.

intensity in the two cases. The comparison with the 22-Mev data was not extended below $Z=20$ because the fluctuating and increasing values of the threshold for neutron production would make the comparison of little significance.

Katz and co-workers have measured the (γ,n) activation cross section of Cu^{63} and Cu^{65} using the bremsstrahlung spectrum. Assuming the shape of the spectrum they have obtained a differential cross-section curve as a function of energy. The relative values which they obtain at 17.6 Mev for Cu^{63} and Cu^{65} are in wide disagreement with those obtained by Wäffler and Hirzel. They find $\sigma^{65}/\sigma^{63}\approx 0.2$. Wäffler and Hirzel obtain the value 1.5 for the same ratio. If one takes Katz's absolute values for the differential cross section and averages over the two isotopes and over the Li spectrum one obtains the value 0.056 barn for the cross section, in agreement with our results.

By the Teller-Goldhaber[13] theory, one expects the (γ,n) cross section to show a strong peak as a function of energy. Both the Goldhaber-Teller theory and the Levinger-Bethe theory[14] predict that the mean energy of the photon absorption spectrum should decrease with increasing Z. However, neither theory indicates what one would expect for the variation of the cross section as a function of Z while using a monochromatic line at 17.6 Mev.

Other experiments[15–17] have shown the expected decrease of resonance energy with increasing Z. One feature in our results may also indicate this. It will be observed that above $Z=74$, our data indicate a decrease in the yield whereas the data of Price and Kerst indicate an increase with increasing Z. It seems possible that with increasing Z the resonance energy has fallen below the 17.6-Mev line giving rise to a decrease in the yield at that energy, whereas the yield averaged over the betatron spectrum continues to increase in about the same manner as for lighter nuclei, more-or-less independently of the location of the resonance. Because of the observed low value of the resonance energy[5,16] in Ta, one is not surprised to find that Ta also yields a low cross-section value for the Li spectrum.

It would seem to be very desirable to repeat the measurements using the high energy gamma-ray from the reaction $H^3(p,\gamma)He^4$. Such an experiment should give additional information concerning the shape of the (γ,n) cross-section curve as a function of energy and Z.

The cross sections of Ca and Ni are notable in that they deviate so far from the smooth curve which can be drawn through the other points. These deviations have also been observed in the other experiments.[3,4] Though these fluctuations may be, in a sense, accidental, one may hope that they will be explained by a correct theoretical interpretation. Measurements of the (γ,p) and $(\gamma,2n)$ cross sections would perhaps shed some light on this question.

We wish to thank Dr. Bruce Dayton for his assistance in the operation of the cyclotron. We are indebted to the Argonne National Laboratory for the calibration of the Ra–α–Be neutron source strength and to Dr. L. Katz for the communication of his results prior to publication.

[13] M. Goldhaber and E. Teller, Phys. Rev. **74**, 1046 (1948).
[14] J. S. Levinger and H. A. Bethe, Phys. Rev. **78**, 115 (1950).
[15] G. C. Baldwin and E. C. Klaiber, Phys. Rev. **73**, 1156 (1948).
[16] McElhinney, Hanson, Becker, Duffield, and Diven, Phys. Rev. **75**, 542 (1949).
[17] K. Strauch, Phys. Rev. **78**, 84 (1950); **79**, 241 (1950).

On the Origin of the Lighter Elements*

WILLIAM BAND
Department of Physics, State College of Washington, Pullman, Washington
(Received June 9, 1950)

Maria Mayer and Teller have proposed accounting for the relative abundances of the heavier elements as products of the fission of a cold polyneutron fluid. The present paper proposes to account for the lighter elements as having been formed at an earlier stage in evolution when temperatures were high enough to permit nuclear reactions, and the primordial neutron-rich nuclear fluid first separates into two phases: the condensed super-clusters or stars which eventually cool to become the Mayer-Teller polyneutrons, and an atmosphere or vapor of small clusters that become the lighter elements.

The quantum statistics of a dissociative clustering nucleon gas is worked out and yields equilibrium abundances of the small clusters or light nuclei in the vapor that agree qualitatively with the observed abundances if the temperature T of the equilibrium is assumed to be such that $kT=5$ Mev.

I. INTRODUCTION

IT is well known that the curve of relative abundances of the elements against atomic weight suffers a break at about weight 80, the lighter elements falling in abundance with increasing weight much more rapidly than do the heavier elements.[1] Maria Mayer and Teller have proposed[2] to account for the relative abundances of the heavier elements as products of the fission of a cold polyneutron fluid, or presumably of a number of such polyneutrons each having a mass of the same order of magnitude as that of a star. The present paper proposes to account for the lighter elements as forming at an earlier stage in evolution when temperatures were high enough to permit nuclear reactions, and the primordial neutron-rich fluid first separates into two phases: the condensed polyneutron super-clusters or stars in equilibrium with an atmosphere or vapor of small clusters that are later recognized as the lighter elements.

The separation can be thought of as a result of an expansion of the primordial fluid starting at a temperature above the critical. The Mayer-Teller fission of the condensed polyneutron super-clusters continues long after the temperature has fallen too low to permit further nuclear reactions among the vapor clusters whose abundances are therefore "frozen," and simply superposes on the latter, the additional distribution of the heavier elements. The question of a time-scale for these events is left entirely open, and whether an equilibrium calculation can apply to the separation into two phases of nuclear fluid must be regarded at the moment as pure speculation. The calculations of this paper tend to favor the validity of this speculation.

The statistical problem can be solved approximately without reference to the nature of nuclear forces, beyond the simple assumption that the latter are sufficient to bind nucleons into clusters and are of very short ranges compared with the inter-nucleon distance in the atmosphere. Because the cold polyneutron is undoubtedly a quantum degenerate assembly it is desirable to work with quantum statistics from the start, although it is by no means certain that the quantum degeneracy has any marked influence at the high temperatures required for nuclear reactions. In a previous paper[3] we have discussed the quantum statistics of a clustering Bose-Einstein gas in which the single unclustered particles were restricted to contain only an even number of nucleons. In that work we were interested only in a van der Waals clustering. In the present paper we have to discuss the quantum statistics of clustering nucleons and the mixture will contain both even and odd nuclei so that both Fermi-Dirac and Bose-Einstein elements exist together in the same assembly.

There is evidently a critical minimum mass below which the polyneutron cannot exist in two phases; the condensed polyneutron must be at least massive enough to hold an atmosphere at the saturated vapor pressure while at the same time the temperature must be high enough to produce nuclear reactions in the atmosphere. The kinetic energy per nucleon in the atmosphere must, namely, be of the order of several Mev, and for this to be trapped in the gravitational field of the polyneutron the latter must produce a gravitational potential at least 10^{18} erg/g. The gravitational field at the surface of a sphere of mass M and density ρ is $10.7\times10^{-8}\rho^{\frac{1}{3}}M^{\frac{2}{3}}$ erg/g. The condensed polyneutron must have a density corresponding to an inter-nucleon distance of the order 10^{-12} cm, so that $\rho\sim10^{12}$ g cm^3 and the minimum mass is of the order $M\sim3\times10^{31}$ g, roughly the same as that suggested by Mayer and Teller.

II. QUANTUM STATISTICS OF CLUSTERING NUCLEONS

The fluid assembly is treated as a mixture of perfect gases between which dissociative equilibrium exists. Each nuclear species or cluster type is regarded as a component in the mixture. Long range forces—Coulomb forces—between the clusters are neglected, and it is

* The work was supported by funds from the ONR.
[1] H. Brown, Rev. Mod. Phys. 21, 625 (1949).
[2] M. Mayer and E. Teller, Phys. Rev. 76, 1226 (1949).
[3] W. Band, Phys. Rev. 79, 871 (1950).

presumed that the temperature of the assembly is high enough to ensure frequent penetration of potential barriers so that neglect of long range forces may be justified in comparison with the energy of cluster formation. This approximation has been discussed in the previous paper.[3]

There exist only neutrons and protons in the assembly and the energy of clustering can be expressed as a sum of terms; one linear in the number of neutrons and the number of protons in the cluster, and one increasing less rapidly with the number of nucleons than linearly.

The assembly is characterized by the set of numbers $N(n, p)$ of clusters in which there are n neutrons and p protons each. It is convenient for brevity to write a single letter s to represent the ordered pair (n, p) and to write N_s for $N(n, p)$.

The total number of protons in the assembly is

$$N_\pi=\sum_n\sum_p pN(n, p)=\sum_s pN_s \tag{1}$$

and the total number of neutrons in the assembly is

$$N_\nu=\sum_n\sum_p nN(n, p)=\sum_s nN_s. \tag{2}$$

Any sub-assembly consisting only of the N_s clusters of type s will be represented by a symmetrical wave function if $n+p$ is even and by an antisymmetrical wave function if $n+p$ is odd:

$$\phi_s(\{\mathbf{p}_s\}, \{\mathbf{r}_s\})=(N_s!V^{N_s})^{-\frac{1}{2}}\sum_P(-)^{(n+p)P} \times\exp\left\{(2\pi i/h)\sum_{j=1}^{N_s}(\mathbf{p}_{sj}\cdot\mathbf{r}_{sPj})\right\}. \tag{3}$$

In this expression $\mathbf{r}_{sj}$ is the mass center position vector of the jth cluster, $\mathbf{p}_{sj}$ its momentum vector; P_j means another suffix obtained from j by a permutation P, $\sum_P$ is a sum over all such permutations, $(-)^{(n+p)P}$ is negative if $n+p$ is odd and P an odd permutation, otherwise it is positive unity; the suffix s throughout means the ordered pair (n, p). The curly brackets $\{\mathbf{r}_s\}$ indicate the whole set of vectors obtained from $\mathbf{r}_{sj}$ by including all clusters j. The wave function (3) represents only the mass center motion of the clusters; there is a factor of the form $\phi(q_{sj})$ depending only on the internal coordinates and momenta represented collectively by q_{sj} for each cluster—one such factor for each cluster in the assembly.

The assembly of N_ν and N_π nucleons, characterized by the set of cluster numbers $\{N_s\}$ is represented by wave functions

$$\phi(\{N_s\})=\prod_s\phi_s(\{\mathbf{p}_s\}, \{\mathbf{r}_s\})\prod_{j=1}^{N_s}\phi(q_{sj}). \tag{4}$$

These are the steady states of the assembly and depend on the set of numbers $\{N_s\}$, processes of dissociation are regarded as transitions between different such states. The contribution to the grand partition function from a given set of numbers $\{N_s\}$ is

$$Q(\{N_s\})=(N_\nu!N_\pi!)^{-1}h^{-3(N_\nu+N_\pi)}\int\cdots\int\phi^*(\{N_s\}) \times\exp\{-H(\{N_s\})/kT\}\phi(\{N_s\})\prod_s\prod_j d\mathbf{r}_{sj}d\mathbf{p}_{sj}dq_{sj} \tag{5}$$

where

$$H(\{N_s\})=\sum_{s=1}^{}\sum_{j=1}^{N_s}\mathbf{p}_{sj}^2/2(n+p)M+\sum_{s=1}^{}\sum_{j=1}^{N_s}U_s(q_{sj}) \tag{6}$$

is the Hamiltonian of the assembly, M being the mass of either type of nucleon. Define the mean internal energy W_s of the s-type cluster by

$$V^{N_s}\exp(-N_sW_s/kT)=(n!p!)^{N_s}h^{-3(n+p-1)N_s} \times\prod_{j=1}^{N_s}\phi^*(q_{sj})\exp(-U_s/kT)\phi(q_{sj})dq_{sj}. \tag{7}$$

The integrations over the momenta in (5) proceed in the same way as in the previous paper[3] and we finally obtain the result:

$$N_s!N_\nu!N_\pi!Q(\{N_s\})=\prod_s[2\pi(n+p)MkT/h^2]^{\frac{3}{2}N_s}(n!p!)^{N_s} \times\exp(-N_sW_s/kT)\int\cdots\int\sum_{P'}\sum_{P''}(-)^{(n+p)(P'+P'')} \times\exp\left\{-[2\pi^2(n+p)MkT/h^2]\sum_{j=1}^{N_s}(\mathbf{r}_{sP'j}-\mathbf{r}_{sP''j})^2\right\} \times\prod_s\prod_j d\mathbf{r}_{sj}. \tag{8}$$

Now if we write $P''=PP'$ then $(-)^{P'+P''}=(-)^P$ and the double sum over all the permutations can be written as $N_s!$ times the sum over P: this cancels the factor $N_s!$ from the left-hand side of (8) and the integrals over coordinate space become:

$$\int\cdots\int\sum_P(-)^{(n+p)P}\exp\left\{-[2\pi^2(n+p)MkT/h^2] \times\sum_{j=1}^{N_s}(\mathbf{r}_{sj}-\mathbf{r}_{sPj})^2\right\}\prod_s\prod_j d\mathbf{r}_{sj}. \tag{9}$$

These integrals break up into chain integrals just as in reference 3 but now we note that when P is even there is an odd number of links μ in the chain, while when P is odd the number of links μ is even. Thus the alternations of sign are properly accounted in the following:

$$N_\nu!N_\pi!Q(\{N_s\})=\prod_s(n!p!)^{N_s}\exp(-N_sW_s/kT) \times\sum_{\{m_\mu\}N_s}N_s!\prod_{\mu=1}^{N_s}(-)^{(\mu-1)(n+p)}(1/m_\mu!) \{V[2\pi(n+p)MkT/h^2]^{3/2}\mu^{-5/2}\}^{m_\mu} \tag{10}$$

where the symbol $\sum_{\{m_\mu\}N_s}$ means the sum over all sets

of numbers $\{m_\mu\}$ such that

$$\sum_{\mu=1}^{N_s} \mu m_\mu = N_s. \quad (11)$$

The number of significantly different ways of arranging the nucleons among clusters is

$$N_\nu! N_\pi! / \prod_s N_s! (n!p!)^{N_s}. \quad (12)$$

Multiplying $Q(\{N_s\})$ by this and summing over all possible sets $\{N_s\}$ we obtain the complete grand partition function:

$$Q(N_\nu, N_\pi) = \sum_{\{N_s\}} \prod_s \sum_{\{m_\mu\} N_s} \prod_{\mu=1}^{N_s} (-)^{(\mu-1)(n+p)} (1/m_\mu!) \times \{V[2\pi(n+p)MkT/h^2]^{3/2} \mu^{-5/2} \times \exp(-\mu W_s/kT)\}^{m_\mu}. \quad (13)$$

To evaluate this partition function we first observe that it can be expressed as the coefficient of $X^{N_\nu} Y^{N_\pi}$ in the following power series:

$$\exp\{\sum_s \sum_\mu (-)^{(n+p)(\mu-1)} V[2\pi(n+p)MkT/h^2]^{3/2} \mu^{-5/2} \times \exp(-\mu W_s/kT) \cdot X^{n\mu} Y^{p\mu}\}. \quad (14)$$

In confirming this we note that

$$\sum_s \sum_\mu \mu n m_\mu = \sum_s n N_s = N_\nu, \quad \sum_s \sum_\mu \mu p m_\mu = \sum_s p N_s = N_\pi, \quad (15)$$

so that the restricted summations in (13) are taken care of automatically by selecting the coefficient in (14). Going over to the complex X and Y planes in place of X and Y we therefore have

$$Q(N_\nu, N_\pi) = (1/2\pi i)^2 \oint \oint X^{-(N_\nu+1)} Y^{-(N_\pi+1)} \times \exp[V\chi(X, Y)] dX dY, \quad (16)$$

where

$$\chi(X, Y) \equiv \sum_s \sum_\mu (-)^{(n+p)(\mu-1)} [2\pi(n+p)MkT/h^2]^{3/2} \times \mu^{-5/2} e^{-\mu W_s/kT} X^n Y^p. \quad (17)$$

This is a generalization to two complex planes of the similar expression in reference 3 where only one complex plane was present. This mathematical problem has been handled[4] in any number of complex planes. Equation (16) is the analog of Eq. (4.11) of reference 4, and making use of Eqs. (7.8) and (7.9) of that work, we infer from (16) above that Lim: $N_\nu, N_\pi \to \infty$ of $(N_\nu+N_\pi)^{-1} \ln Q(N_\nu, N_\pi)$ is

$$v\chi(X_0, Y_0) - c_\nu \ln X_0 - c_\pi \ln Y_0, \quad (18)$$

where

$$v \equiv V/(N_\nu+N_\pi), \quad c_\nu \equiv N_\nu/(N_\nu+N_\pi), \quad c_\pi \equiv N_\pi/(N_\nu+N_\pi), \quad (19)$$

and X_0 and Y_0 are determined by

$$vX_0 \partial\chi(X_0, Y_0)/\partial X_0 = c_\nu, \quad vY_0 \partial\chi(X_0, Y_0)/\partial Y_0 = c_\pi. \quad (20)$$

The expression (18) is simply $(-1/kT)$ times the Helmholtz free energy A while the pressure of the assembly is $P = -\partial A/\partial v$. Thus we find

$$P/kT = \sum_s \sum_\mu (-)^{(n+p)(\mu-1)} [2\pi(n+p)MkT/h^2]^{3/2} \times \mu^{-5/2} \exp(-\mu W_s/kT) X_0^{n\mu} Y_0^{p\mu}, \quad (21)$$

where X_0 and Y_0 are determined by

$$N_\nu/V = \sum_s \sum_\mu (-)^{(n+p)(\mu-1)} n [2\pi(n+p)MkT/h^2]^{3/2} \times \mu^{-3/2} \exp(-\mu W_s/kT) X_0^{n\mu} Y_0^{p\mu} \quad (22)$$

$$N_\pi/V = \sum_s \sum_\mu (-)^{(n+p)(\mu-1)} p [2\pi(n+p)MkT/h^2]^{3/2} \times \mu^{-3/2} \exp(-\mu W_s/kT) X_0^{n\mu} Y_0^{p\mu}. \quad (23)$$

Comparing these equations with (15) we see that the mean numbers of clusters of type $s = (n, p)$ is given by

$$N(n, p)/V = \sum_\mu (-)^{(n+p)(\mu-1)} [2\pi(n+p)MkT/h^2]^{3/2} \times \mu^{-3/2} \exp(-\mu W_s/kT) X_0^{n\mu} Y_0^{p\mu}. \quad (24)$$

III. CONDENSATION PHENOMENA

In Eqs. (22), (23) and (24) write

$$X_0 = \exp(-\phi_\nu/kT), \quad Y_0 = \exp(-\phi_\pi/kT) \quad (25)$$

$$W_s = -nW_\nu - pW_\pi + S(n, p). \quad (26)$$

Here ϕ_ν and ϕ_π are simply parameters replacing X_0 and Y_0, while (26) is a crude approximation to the empirical formula for mass defects of nuclei, $-S(n, p)$ is the sum of those (usually negative) terms in the mass defect that increase more slowly than the atomic weight, the surface and Coulomb terms. In the empirical formula there is also a term of the form $(n-p)^2/(n+p)$. In the lighter elements the difference $n-p$ is comparatively small while the ratio p/n is roughly constant, so this term can be written approximately as $n-3p+4p(p/n)$. A correction to W_ν and W_π might take care of this to a first approximation. Equations (22) and (23) now become

$$N_\nu/V = (2\pi MkT/h^2)^{\frac{3}{2}} \sum_{n, p, \mu} (-)^{(n+p)(\mu-1)} \times n(n+p)^{\frac{3}{2}} \mu^{-\frac{3}{2}} e^{-\mu S(n, p)/kT} \exp\{-\mu[n(\phi_\nu - W_\nu) + p(\phi_\pi - W_\pi)]/kT\} \quad (27)$$

$$N_\pi/V = (2\pi MkT/h^2)^{\frac{3}{2}} \sum_{n, p, \mu} (-)^{(n+p)(\mu-1)} \times p(n+p)^{\frac{3}{2}} \mu^{-\frac{3}{2}} e^{-\mu S(n, p)/kT} \exp\{-\mu[n(\phi_\nu - W_\nu) + p(\phi_\pi - W_\pi)]/kT\}. \quad (28)$$

Clustering avalanches occur both where the n-series and the p-series reach their radii of convergence. These are when $\phi_\nu \to W_\nu$ and $\phi_\pi \to W_\pi$. If the assembly is neutron-rich, $N_\nu \gg N_\pi$, then it is clear from the form of these last two equations that $\phi_\nu - W_\nu$ must be smaller than $\phi_\pi - W_\pi$. This means that the limit $\phi_\nu \to W_\nu$ must be the first to occur as the temperature is decreased.

[4] K. Fuchs, Proc. Roy. Soc. A **179**, 408 (1942).

Let the temperature at which this occurs be T_ν. Then

$$N_\nu/V=(2\pi MkT_\nu/h^2)^{\frac{3}{2}}\sum_{n,\,p,\,\mu}(-)^{(n+p)(\mu-1)}n(n+p)^{\frac{3}{2}}\times\mu^{-\frac{5}{2}}e^{-\mu S(n,\,p)/kT_\nu}\exp[-\mu p(\phi_\pi-W_\pi)/kT_\nu] \quad (29)$$

$$N_\pi/V=(2\pi MkT_\nu/h^2)^{\frac{3}{2}}\sum_{n,\,p,\,\mu}(-)^{(n+p)(\mu-1)}p(n+p)^{\frac{3}{2}}\times\mu^{-\frac{5}{2}}e^{-\mu S(n,\,p)/kT_\nu}\exp[-\mu p(\phi_\pi-W_\pi)/kT_\nu]. \quad (30)$$

If now the temperature falls below T_ν, Eq. (30) can still be satisfied by choosing a smaller value of $(\phi_\pi-W_\pi)$ but this smaller value cannot be sufficiently small to continue to satisfy (29): this is because of the factor p in (30) that is replaced by n in (29). Thus neutrons must on balance condense out of the vapor into the liquid phase. This process continues until finally we reach T_π where $\phi_\pi\rightarrow W_\pi$ and

$$N_\pi/V=(2\pi MkT_\pi/h^2)^{\frac{3}{2}}\sum_{n,\,p,\,\mu}(-)^{(n+p)(\mu-1)}\times p(n+p)^{\frac{3}{2}}\mu^{-\frac{5}{2}}\exp[-\mu S(n,\,p)/kT_\pi]. \quad (31)$$

All excess neutrons have now been condensed out of the vapor until there remain only the number N_ν' given by

$$N_\nu'/V=(2\pi MkT_\pi/h^2)^{\frac{3}{2}}\sum_{n,\,p,\,\mu}(-)^{(n+p)(\mu-1)}\times n(n+p)^{\frac{3}{2}}\mu^{-\frac{5}{2}}\exp[-\mu S(n,\,p)/kT_\pi]. \quad (32)$$

However in practice $S(n, p)$ depends in first approximation only on $(n+p)$ so that the two sums (31) and (32) are to this approximation mathematically identical. Thus, going into the vapor are nearly equal numbers of neutrons and protons, $N_\nu'\doteqdot N_\pi$, all excess neutrons remaining in the liquid polyneutron phase. Any further expansion removes neutrons from the liquid phase in nearly equal numbers, and Eqs. (31) and (32) continue to represent the saturated vapor with the suffix removed from T.

In particular, the number of clusters of type (n, p) is given by

$$N(n,\,p)/V=(2\pi MkT/h^2)^{\frac{3}{2}}\textstyle\sum_\mu(-)^{(n+p)(\mu-1)}(n+p)^{\frac{3}{2}}\times\mu^{-\frac{5}{2}}\exp[-\mu S(n,\,p)/kT]. \quad (33)$$

Because of the approximations used in (26) this formula applies only approximately, the approximation being best for the lighter isotopes. Equations (31) and (32) include at least formally the existence of a critical point if it is agreed to regard $S(n, p)$ as a function of temperature which can become zero at sufficiently high T. At such a temperature both sums diverge and the density becomes infinite. This infinity arises because the model did not take into account the finite volume of the clusters; this fault can be corrected for, but we shall not attempt to do so here.

In Eq. (33) we note that when $n+p$ is even the μ-series terms are all positive, and the expression is of typical Bose-Einstein type. However, as was pointed out in reference 3 the Bose-Einstein condensation does not occur before the clustering avalanche; so long as the assembly is below the critical point the clustering avalanche induces the phase transition into the liquid phase before the Bose-Einstein transition can occur.

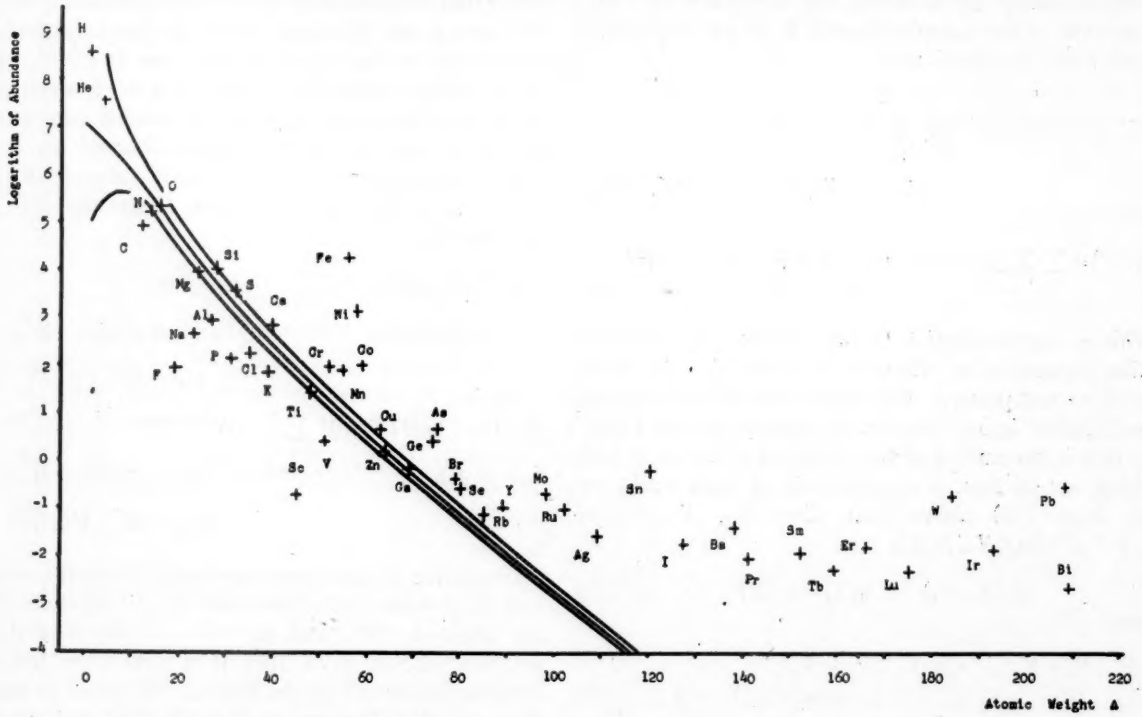

FIG. 1. Abundance of the lighter elements including a representative selection of the heavier elements, showing the theoretical curves for the lighter elements discussed in the text.

On the other hand when $n+p$ is odd, Eq. (33) gives a μ-series with alternating signs and their sums are necessarily smaller than those of even masses. At first it might be expected that this would result in greater abundance of the even mass nuclei, but it turns out that in the temperature region required to account for the general trend of nuclear abundance, the factor $\exp[-S(n, p)/kT]$ is generally so small that the μ-series reduces effectively to its first term. Finally therefore we have as a first approximation to the nuclear abundance in a vapor in equilibrium with a neutron-rich nuclear liquid:

$$N(n, p)/V=(2\pi MkT/h^2)^{\frac{3}{2}}(n+p)^{\frac{3}{2}}\epsilon^{-S(n,p)/kT}. \quad (34)$$

In other words, the relative abundance of two species of nuclei having mass numbers $(n+p)$ equal respectively to A_1 and A_2, containing Z_1 and Z_2 protons, is

$$N_1/N_2=(A_1/A_2)^{\frac{3}{2}}\exp\{-[S(A_1, Z_1) - S(A_2, Z_2)]/kT\}, \quad (35)$$

where $S(A, Z)$ is simply the non-linear repulsive term in the binding energy.

IV. ESTIMATE OF RELATIVE ABUNDANCE

The significant and perhaps surprising point about (35) is that while it looks very like a simple Boltzmann expression, *only the repulsive term in the binding energy appears in the exponent.* This is directly a consequence of the fact that the vapor is in equilibrium with the condensed polyneutron, and would of course not be true otherwise. If the picture of evolution implied in this work is to be self-consistent, Eq. (35) should yield abundances for the lighter elements of the correct general pattern with a value of kT of several Mev, which is sufficient to produce nuclear reactions in the "atmosphere."

Clearly at such temperatures the binding energies of nuclei cannot be identical with those observed under laboratory conditions, where the internal kinetic energy is negligibly greater than the zero-point energy. The surface terms must be considerably less, along with the whole binding energy. As an admittedly crude and perhaps even questionable estimate of the appropriate surface energy we shall write

$$S(n, p)=S_0(n, p)-1.5kTA^{\frac{3}{2}}. \quad (36)$$

Here S_0 is the surface term at laboratory temperatures, and the temperature term is such as to give zero S at a critical temperature about 10 Mev per k above which no phase separation could occur. This seems to be the simplest way to handle the situation without adding more unknown parameters. Using (36) it is found that the general trend of abundances of all elements of atomic weight below about 80 is given faithfully by (35) if we put $kT=5$ Mev, whereas the observed abundances of the heavier elements are progressively much greater than would be given by (35), a difference that can be understood in terms of the Mayer-Teller theory

TABLE I. Equilibrium temperature from isotope abundances.[a]

Isotope		kT in Mev	Isotope		kT in Mev
H	1:2	3.7	S	32:36	1.2
O	16:17	1.03	A	36:38	3.0
	16:18	1.2			
			K	39:41	1.8
Ne	20:21	1.29			
			Ca	40:44	2.2
	20:22	2.5			
			Cr	52:53	2.5
Mg	24:25	2.8			
	24:26	2.8	Ni	58:60	2.9
				58:64	2.2
Si	28:29	1.8			
	28:30	1.65	Cu	63:65	2.7
S	32:33	1.4	Zn	64:66	4.5
	32:34	3.5		64:70	2.6

[a] Note: the isotope abundances of Cl and Fe do not fit the formula at all.

For simplicity we refer all abundances to hydrogen, write $N/N_H=C$ and express (35) and (36) in the form

$$\log C=1.5\log A+0.434\{(S_H-S_{A,Z})/kT - 1.5(1-A^{\frac{3}{2}})\}. \quad (37)$$

The empirical values of $S(A, Z)$ lie on three curves: in Mev

$$\left.\begin{aligned} &S(A, Z)\\ &=15.1A^{\frac{3}{2}} \text{ if } A \text{ is odd}\\ &=15.1A^{\frac{3}{2}}+38.7A^{-\frac{1}{2}} \text{ if } A \text{ is even and } Z \text{ odd}\\ &=15.1A^{\frac{3}{2}}-38.7A^{-\frac{1}{2}} \text{ if both } A \text{ and } Z \text{ are even}\end{aligned}\right\}. \quad (38)$$

Figure 1 shows the three curves (37) derived from these three forms for $S(A, Z)$ together with the observed abundances given by Brown.[1] The fluctuations away from equilibrium are wider than the differences between the three curves, the worst ones being F^{19}, Sc^{45}, Fe^{56} and Ni^{58}. However the observed general tendency of the abundances of the lighter elements to decrease with increasing atomic weight is well represented, and considering that no parameter other than T has been used in making this adjustment, the agreement is as good as can be reasonably expected.

DISCUSSION

The empirical formula for the binding energy from which (38) is taken is known to be appreciably in error in a number of individual cases. One might therefore hope to improve the agreement between formula (37) and the observed abundances by taking these individual binding energy anomalies into account. Unfortunately $S(A, Z)$ is not the total binding energy, and there does not appear to be any reliable way in which blame for any individual anomaly can be apportioned between the linear and the surface terms. Nothing much better than a qualitative discussion is therefore possible until a much more complete theory of the binding energy of nuclei exists. To illustrate this situation Table I shows the result of using (37) and the observed relative abundances of various sets of isotopes

to calculate the equilibrium temperature. They are all consistently lower than the 5 Mev needed to fit the curve for the lighter elements as a whole. There are two alternative interpretations of this: (a) the less abundant isotopes were actually formed later when the temperature had dropped below the initial 5 Mev, (b) the lower temperature is fictitious, the abundances actually departing from equilibrium for some special reason. For example the abundance of O^{17} is markedly lower than would be given by (37) at 5 Mev, and this could be due to the anomalously small binding energy of the extra neutron. While from the present point of view one might equally well assert that the small binding energy is due to an anomalously large (positive) surface energy above that given by (38), this would have the effect of raising the low temperature found in Table I. Just how much of the anomaly is due to the surface energy is simply not known. The opposite anomaly, not shown in the table, occurs with the chlorine isotopes 35 and 37 where the abundance of the heavier isotope is so large that a negative temperature would be needed to fit (35). But here the binding energy of the extra neutron is anomalously high, and one may again suppose that an unknown part of this is accountable as due to anomalously small surface energy in Cl^{37}; if this anomaly is great enough to reverse the sign of the difference $S(35)-S(37)$, formula (35) would yield a reasonable value for T.

The writer is happy to thank Dr. Maria Mayer for her helpful comments on the first draft of this paper.

PHYSICAL REVIEW VOLUME 80, NUMBER 5 DECEMBER 1, 1950

Interaction of Fast Neutrons with Nitrogen*

C. H. JOHNSON AND H. H. BARSCHALL
University of Wisconsin, Madison, Wisconsin
(Received August 1, 1950)

Using neutrons from the $Li^7(p,n)Be^7$ reaction, the cross sections for the reactions $N^{14}(n,p)C^{14}$ and $N^{14}(n,\alpha)B^{11}$ were measured for neutron energies from 150 to 2100 kev. Resonances for the (n,p) reaction were found at 499, 640, 993, and 1415 kev; for the (n,α) reaction at 1415 and 1800 kev. Information was obtained about the excited state of Be^7. It was found to lie 431 ± 5 kev above the ground state, and probabilities for its formation in the $Li(p,n)$ reaction were determined.

I. INTRODUCTION

PRELIMINARY results on the variation with energy of the cross section for the disintegration of nitrogen by fast neutrons were reported previously.[1] More careful measurements of this cross section appeared to be desirable for the following reasons: (1) measurements of the cross section of the $C^{14}(p,n)N^{14}$ reaction show a discrepancy when compared with the cross section of the $N^{14}(n,p)C^{14}$ reaction on the basis of the principle of detailed balancing;[2] (2) an attempt to find the levels in N^{15} which appear in measurements of the $N^{14}(n,p)$ reaction by measuring the total cross section of nitrogen had been unsuccessful;[3] (3) information concerning the recently discovered low energy neutron group from the $Li(p,n)$ reaction[4] might be obtained from such measurements.

II. EXPERIMENTAL PROCEDURE

The procedure followed in the present experiments was very similar to that described previously. Neutrons were produced by bombarding a Li target by protons from the electrostatic generator. The protons had an energy spread of 5 kev; the Li target had a stopping power of 12 kev for 2-Mev protons.

Protons and α-particles from the disintegration of nitrogen were observed in a cylindrical ionization chamber similar to that described by Koontz and Hall.[5] The chamber was filled with nitrogen to a pressure of 10 atmospheres. 5000 volts applied to the chamber gave saturation without gas multiplication. The center of the active volume of the chamber was placed at a distance of 16 cm from the Li target in such a direction that the axis of the chamber made an angle of 30° with respect to the incident protons.

For most of the measurements ionization pulses larger than a predetermined size were counted. In order to select the proper bias for counting the desired pulses, pulse height distributions were taken at neutron energy intervals of about 100 kev by means of a differential discriminator. As a further check on the bias settings, the pulses were presented on a cathode-ray oscilloscope and photographed on moving film. Such photographic records were made at those neutron energies at which, in preliminary experiments, especially interesting features had been observed.

* Work supported by the AEC and the Wisconsin Alumni Research Foundation.

[1] H. H. Barschall and M. E. Battat, Phys. Rev. **70**, 245 (1946).

[2] Shoupp, Jennings, and Sun, Phys. Rev. **75**, 1 (1949).

[3] Bockelman, Adair, Barschall, and Sala, Phys. Rev. **75**, 336 (1949).

[4] Johnson, Laubenstein, and Richards, Phys. Rev. **77**, 413 (1950).

[5] P. G. Koontz and T. A. Hall, Rev. Sci. Inst. **18**, 643 (1947).

The neutron flux incident upon the nitrogen-filled chamber was measured by means of a "long counter",[6] the detecting efficiency of which depends very little on neutron energy. The efficiency of this counter was determined by placing a calibrated Ra—Be source at the position normally occupied by the Li target.

In Fig. 1 some typical pulse-height distribution curves are presented. Each curve shows a rapid rise at low ionization energies because of the effect of γ-rays and nitrogen recoils. Peaks in the pulse height distribution will be produced by the $N(n,p)C$ reaction and by the $N(n,\alpha)B$ reaction. Above a neutron energy of 610 kev for the main group of neutrons from the $Li^7(p,n)Be^7$ reaction, lower energy maxima in the pulse height distribution for both nitrogen reactions may be produced by neutrons from the $Li^7(p,n)Be^{7*}$ reaction, where the Be^7 nucleus is left in an excited state at about 430 kev.[7] The energies for which distributions are given in Fig. 1 were chosen to show examples of the various observed combinations of particle groups. It may be noted that the peak at the largest pulse height becomes less sharp as the neutron energy is increased. This effect arises from the fact that at the higher energies the range of the disintegration protons becomes comparable with the radius of the counter. Other factors which will contribute to a broadening of the peaks are amplifier noise, effects of the radial position of the ionization event, channel width, and neutron energy spread; however, in the present experiment it is only of importance that the peaks in the distribution curves be resolved.

In Fig. 2 the pulse heights at the various peaks in the distribution curves are plotted as a function of neutron energy. The peaks are attributed to three processes as indicated. Since the (n,p) and (n,α) pulse heights vary linearly with neutron energy, an extrapolation to zero pulse height should intercept the energy axis at the negative values of the reaction energies, and a check on the assignment of the peaks to the proper reactions may be made from the known Q-values. The intercepts are subject to considerable uncertainty as a result of the broadness of the distribution peaks and the long extrapolation; hence, these measurements are not accurate determinations of the Q-values. Intercepts (times -1) as found from Fig. 2 are 630 ± 50 kev for the (n,p) curve in agreement with the Q-value of 630 ± 6 as measured by Franzen *et al.*,[8] and -260 ± 80 kev for the (n,α) curve in agreement with the Q-value of -240 ± 80 kev determined by Stebler and Huber.[9] Since neither B^{11} nor C^{14} have any known energy levels[10] below 2 Mev and since no distribution peaks corresponding to any such levels were found, these nuclei are presumed to be left in their ground states.

It is of interest that the slope of the (n,α) curve is less than that of the (n,p) curve in Fig. 2. With the approximation that the energy is concentrated on the lighter particle, each slope is proportional to the ratio of the total ionization to the energy of the corresponding particle. According to observations by Jesse and Sadauskis[11] on ionization by α-particles in air, this ratio increases slightly with the velocity of the particle. Since the proton has a much larger velocity than the α-particle, there is a noticeable difference in slope. The difference is in qualitative agreement with the measurements of Jesse and Sadauskis. No significance is attached to the slope and intercept of the center curve in Fig. 2 since the points are not plotted at the energy of the neutrons causing the disintegrations.

By setting the bias between the several peaks formed in the pulse-height distributions, the number of disintegrations of each kind was counted at those energies at which complete distribution curves were not determined. A correction for wall effect was applied according

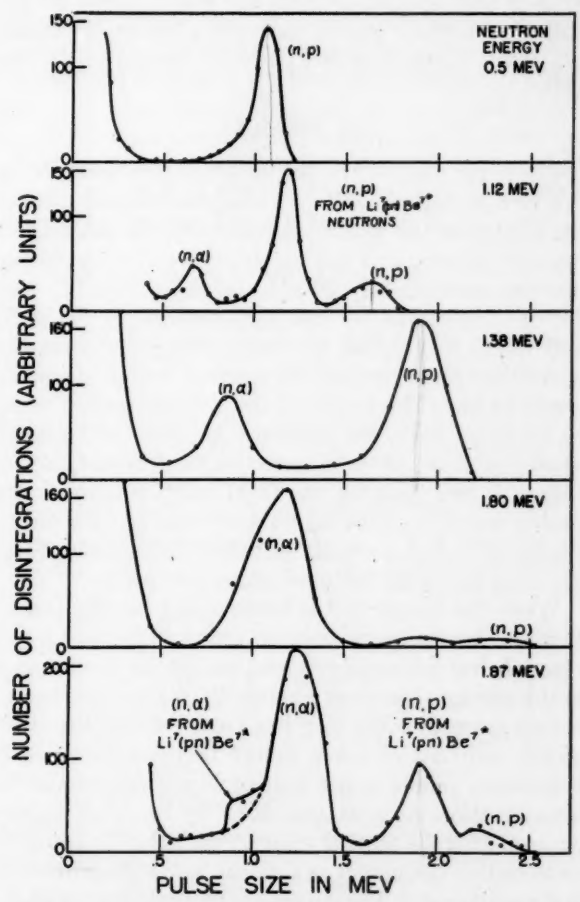

FIG. 1. Pulse-height distributions for disintegrations caused by $Li(p,n)$ neutrons entering the nitrogen-filled ionization chamber are shown for five energies of the main group of neutrons. Peaks are indicated as resulting from the $N(n,p)$ and $N(n,\alpha)$ reactions for both the main group and low energy group of neutrons.

[6] A. O. Hanson and J. L. McKibben, Phys. Rev. **72**, 673 (1947).
[7] T. Lauritsen and R. G. Thomas, Phys. Rev. **78**, 88 (1950).
[8] Franzen, Halpern, and Stephens, Phys. Rev. **77**, 641 (1950).
[9] A. Stebler and P. Huber, Helv. Phys. Acta **21**, 59 (1948).
[10] W. F. Hornyak and T. Lauritsen, Rev. Mod. Phys. **20**, 191 (1948).
[11] W. P. Jesse and J. Sadauskis, Phys. Rev. **78**, 1 (1950).

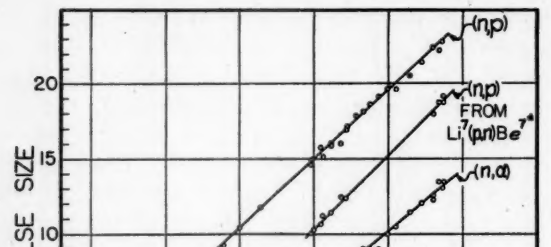

FIG. 2. Pulse heights at the various peaks in the distribution curves are plotted against the energy of the main group of Li(p,n) neutrons. The reactions causing peaks are indicated. Energy intercepts of the two curves which could be extrapolated linearly agree with the Q-values of the assigned reactions.

to the method described by Rossi and Staub.[12] Corrections were applied for both the loss of pulses by the wall effect and the gain of pulses to a low energy group as a result of counting fast particles intercepted by the wall.

III. RESULTS

The lower part of Fig. 3 shows the cross sections for the N(n,p) and the N(n,α) reactions plotted against the energy of the major neutron group in the Li(p,n) reaction. Resonances for the (n,p) reaction appear at neutron energies of 499±5, 640±7, 993±12, and 1415±15 kev; and for the (n,α) reaction at 1415±50 and 1800±15 kev. All the resonances are appreciably wider than the experimental neutron energy spread of about 15 kev. The height of the symbols used is equal to, or larger than, the statistical accuracy of the measurements. For the (n,α) reaction, the statistical accuracy is less than for the (n,p) reaction because the proton count has to be subtracted from the total count. Figure 3 includes results obtained both from direct counting and from the photographic records.

When the energy of the bombarding protons is such that the lower energy neutron group from the Li(p,n) reaction has an energy corresponding to a resonance in the nitrogen reactions whereas the main group has an energy corresponding to a low cross section, the effect of the neutrons of lower energy becomes particularly noticeable. In the upper part of Fig. 3 the number of disintegration protons produced by the low energy neutron group is plotted using as ordinate the apparent cross section calculated as if all the monitor counts were due to this group. The curves are plotted directly above the energy of the major neutron group at which data were taken, and at each resonance the actual energy of neutrons causing resonance is indicated as obtained from the corresponding resonance in the lower part of the figure.

In Table I the positions of the resonances expressed in terms of neutron energies are compared with values observed by others for the same reactions and for the inverse (p,n) and (α,n) reactions. Agreement within experimental error exists for all resonances that were prominent in every experiment. The resonance energy determined from the B(α,n) reaction[13] was found only to two significant figures and the corresponding Q-value used in Table I has an 80-kev uncertainty; hence, the resonance energy of 1700 kev is considered to agree within experimental error with the 1800-kev level. Preliminary measurements,[1] which were obtained without the large electrostatic analyzer available for the present work, show an energy shift of 50 kev compared to the values reported here; this shift is presumably caused by an error in the energy calibration of the accelerator in the earlier work.

As is shown in Table I, the small peak at 993 kev has not been observed by others, and three resonances observed in the inverse (p,n) reaction were not found in the present measurements. Of these three, one at 800 kev was reported to be doubtful and another one at 1540 kev may correspond to a small variation in cross section at 1610 kev in Fig. 3. A resonance corresponding to the one in the (n,α) reaction at 1415 kev was not observed in the B(α,n) reaction; failure to observe this small resonance might be expected since the spread in energy of the alpha-particles was about five times the observed level width.

The previously reported cross sections, which were obtained with a fission monitor, show agreement at the resonances with the present measurements prior to correction for wall effect except for the narrow 499-kev resonance. For this resonance the previously reported cross section was about 25 percent low, presumably because the neutron energy spread was comparable with the resonance width. The increased cross section reported here for this level does not remove the discrepancy mentioned in the introduction concerning the comparison with the inverse (p,n) reaction on the basis of the principle of detailed balance. Since the neutron energy spread used here was about half the width of the level, the observed cross section should be nearly the true value, whereas a value at least four times as large is required to secure agreement with the cross section reported for the inverse reaction. Part of this discrepancy might be resolved if the C(p,n) reaction has a relatively high yield of neutrons in the forward direction in the center of mass system since the cross section for the C(p,n) reaction was found by counting neutrons in the forward direction and assuming an isotropic center of mass distribution.

An exact comparison of the N(n,α) and B(α,n) cross sections on the principle of detailed balancing was not

[12] B. B. Rossi and H. H. Staub, *Ionization Chambers and Counters* (McGraw-Hill Book Company, Inc., New York), p. 236.

[13] R. L. Walker, Phys. Rev. 76, 244 (1949).

possible since the energy resolution used in the two experiments was quite different. A check was obtained by assuming that the 1800-kev resonance may be fairly well represented as a Gaussian curve having the width of the observed peak and by assuming that the energy spectrum of the α-particles used by Walker was a Gaussian distribution with a 400-kev width. Using these approximations and using the principle of detailed balancing (which indicates $\sigma_{n,\alpha}=1.8\sigma_{\alpha,n}$ for this level), one finds the experimentally observed $B(\alpha,n)$ cross section at resonance should be 28 millibarns in order to be consistent with the present measurements. This value for the cross section is in agreement with the curves reported by Walker.

The energy of the excited state in Be^7 was found from the proton bombarding energies at a resonance and at the second appearance of the resonance caused by the low energy neutron group. Systematic errors in this measurement, such as might be introduced by the finite target thickness or improper alignment of the chamber, have little effect since the calculation depends mostly on the difference in proton energies. Energy values obtained from the 499- and 640-kev resonances differ by 2 kev and average 431±5 kev for the excited state in Be^7. A determination using the 1415-kev resonance was less accurate, but the results are consistent within experimental error. Comparison with other work is given in the second column of Table II.

The intensity of the second neutron group relative to the main group was found from the ratio of the apparent cross section to the actual cross section at each resonance. In Table II the resulting intensities are shown with the corresponding proton energies and angles of observation for the present as well as other experiments.

Neutrons resulting from other Be^7 levels at 205 and 745 kev have been reported to be present to 58.5 and 32 percent of the main group when 5-Mev protons were used.[14] The present measurements give an upper limit for the intensity of the first one of these groups for the proton energies used here. In the regions of low (n,p) cross section, bias settings were low enough to detect neutrons of energies corresponding to preceding resonances so that any other neutron group could be detected just as the group already discussed. From such measurements the upper limit for the intensity of other groups corresponding to excited states in Be^7 between 100 and 680 kev was determined to be two percent of the major neutron group for proton energies from 2.53 to 3.03 Mev and three percent for proton energies from 3.3 to 3.91 Mev. For excited states between 810 to 1100 kev, a limit of five percent was determined for proton energies from 3.3 to 3.48 Mev. Measurements were not possible for the intermediate range of excited states between 680 and 810 kev because of the presence of the 1.4 Mev resonance for the main group of neutrons.

The nitrogen cross sections shown in the lower part of Fig. 3 have been corrected for the effect of the second neutron group on the monitor count using the three observed intensities reported in Table II. No correction

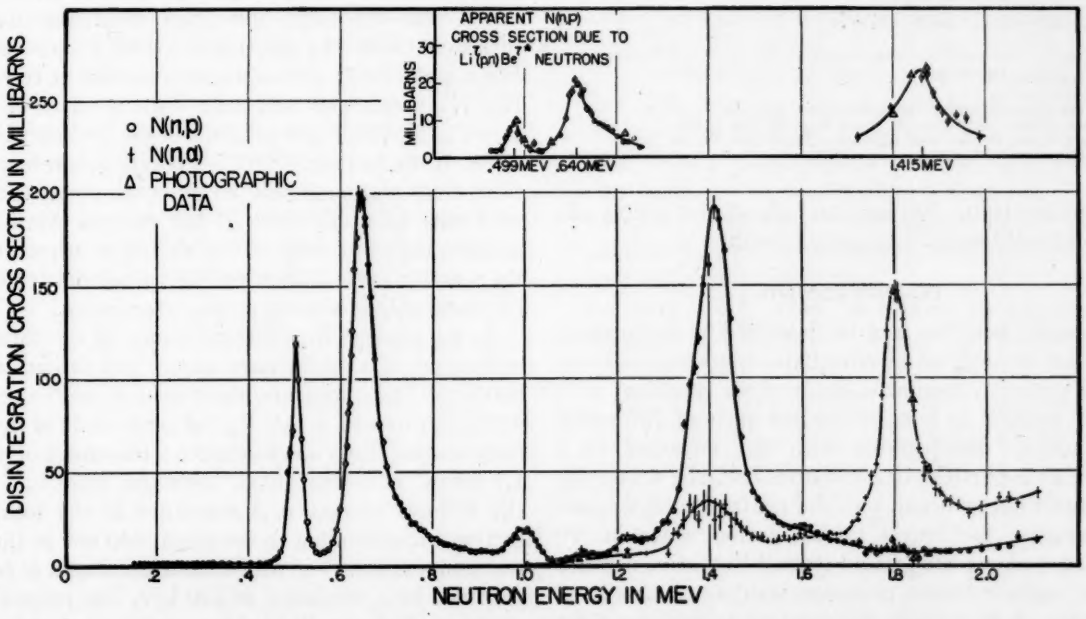

FIG. 3. In the lower part of the figure the $N(n,p)$ and $N(n,\alpha)$ cross sections are plotted against the energy of the major group of $Li(p,n)$ neutrons. On all curves triangles are used for photographic data, which were obtained by photographing the pulses presented on a cathode ray oscilloscope. The apparent cross section resulting from the low energy neutron group is plotted in the upper part of the figure directly above the energy of the major group at which data were taken, and the actual neutron energies causing resonances are indicated.

[14] J. C. Grosskreutz and K. B. Mather, Phys. Rev. 77, 580 (1950).

TABLE I. Positions of (n,p) and (n,α) resonances[a] in nitrogen expressed in terms of neutron energies in kev.

Shoupp, *et al.*[b] (n,p)[c] calculated from $C^{14}(p,n)N^{14}$	This paper (n,p)	This paper (n,α)	A. Stebler and P. Huber[d] (n,p)	A. Stebler and P. Huber[d] (n,α)	R. L. Walker[e] (n,α)[c] calculated from $B^{11}(\alpha,n)N^{14}$
470±20	499±5		480±50		
630±20	640±7		640±40		
(800±50)					
	(993±12)				
1380±20	1415±15	1415±50	1410±90	1410±90	
1540±50					
		1800±15	1770±110	1770±110	1700
1980±50					

[a] Resonances observed weakly in this work or reported as doubtful by others are indicated by parentheses.
[b] See reference 2.
[c] Q-values used for the conversion to neutron energies were $Q_{np}=-625$ kev and $Q_{n\alpha}=-260$ kev.
[d] See reference 9.
[e] See reference 13.

TABLE II. Energy of excited state in Be^7 and intensity of neutrons arising from this state in the $Li(p,n)$ reaction.

Reference	Excited state (kev)	Reaction	Proton energy (Mev)	Angle of observation	Intensity in % relative to main neutron group
This paper	431±5	$Li(p,n)$	2.75	30°	9±1.5
			2.89	30°	10.5±1
			3.66	30°	12±1
a	470±70	$Li(p,n)$	5.0	20° and 90°	52.5
b	435±15	$Li(p,n)$	3.31	0°	17±10
			3.91	0°	9±4
			3.91	60°	16±6
c	428±20	$Li(p,n)$	3.12	0°	8±2
			2.70	0°	8±2
d	428±15	$Li(p,n)$	3.49	0°	11±3
e	434±5	$B(p,\alpha)$			
f	429±5	$Be^{7*}\rightarrow Be^7+\gamma$			

[a] See reference 14.
[b] See reference 4.
[c] B. Hammermesh and V. Hummel, Phys. Rev. **78**, 73 (1950).
[d] Freier, Rosen, and Stratton, Phys. Rev. **79**, 239 (1950).
[e] Brown, Chao, Fowler, and Lauritsen, Phys. Rev. **78**, 88 (1950).
[f] See reference 7.

was applied below 900 kev, and above this energy the intensity was assumed to vary smoothly.

IV. DISCUSSION

A nuclear reaction may be described as a transition occurring through an intermediate compound nucleus. In the present experiment the neutron combines with the N^{14} nucleus to form an excited state of N^{15} which subsequently disintegrates with the emission of a proton, an α-particle, or a neutron. Inelastic scattering is assumed not to occur with the neutron energies used here because the lowest known excited state in N^{14} is 2.3 Mev above the ground state.[15] Radiative capture will be neglected since radiation widths are usually of the order of 10^{-3} times the neutron widths for light nuclei.[16]

When the incident neutron has an energy corresponding to an energy level in N^{15}, a resonance is expected in the cross section for each reaction. Isolated resonances in the (n,p) and (n,α) cross sections can be described by the single-level Breit-Wigner formula, which becomes at resonance:

$$\sigma_{np}+\sigma_{n\alpha}=\frac{2J+1}{6}\frac{4\pi}{k^2}\frac{\Gamma_n(\Gamma_p+\Gamma_\alpha)}{(\Gamma_n+\Gamma_p+\Gamma_\alpha)^2}, \quad (1)$$

where J is the spin of the compound nucleus; k is the neutron wave number; and Γ_n, Γ_p, and Γ_α are the neutron, proton, and α-particle widths. A particle-width, which is a measure of the probability for the emission of the particle from the compound nucleus, may be resolved into various contributing factors according to the relation;[16]

$$\Gamma_s=2\gamma_s^2 k_s T_{ls}, \quad (2)$$

where s refers to the particle considered; k is its wave number; T_l is the Coulomb and centrifugal barrier penetration factor for a particle with orbital angular momentum l; and γ_s^2 is called the reduced width. For a given nucleus reduced widths are not expected to differ greatly for the various particles and for levels having a given spacing; however, the effect of the wave number and penetration factor may be such that Γ_s differs appreciably between particles and between levels. This effect will cause variations in the heights and widths of resonances. A resonance observed in one process may not even be observable in another.

Any discussion of possible quantum numbers associated with the (n,p) and (n,α) resonances must be consistent with the neutron scattering cross section. For a given (n,p) and (n,α) cross section at resonance, Eq. (1) yields two solutions for the ratio of Γ_n to $\Gamma_p+\Gamma_\alpha$, of which one solution is the reciprocal of the other. If the neutron width is the larger, a resonance in total cross section should be observable and the value of J may be established. If the neutron width is the smaller, the total cross section should be approximately the reaction cross section and thus a resonance may not be observable in a transmission experiment.

At the present time measurements of the total cross section are of a preliminary nature and extend only to 900 kev.[3] These measurements indicate no resonance at 499 kev, whereas, if $\Gamma_n>\Gamma_p$, the magnitude of the (n,p) cross section leads one to expect a resonance of at least 1.7 barns. It is concluded, therefore, that $\Gamma_n<\Gamma_p$ for the 499-kev resonance. A resonance in the total cross section corresponding to the one at 640 kev in the (n,p) reaction was observed which has a maximum at 660 kev preceded by a minimum at 620 kev. The presence of a minimum indicates that the resonance is produced by s-neutrons. The difference in cross section observed between the minimum and maximum was about 1 barn. According to the Breit-Wigner formula using values of Γ_n/Γ_p obtained from the observed height of the (n,p) resonance, this difference should be 1.3 barns for $J=\frac{1}{2}$

[15] Lauritsen, Hornyak, Morrison, and Fowler, Rev. Mod. Phys. **22**, 291 (1950).
[16] E. P. Wigner, Am. J. Phys. **17**, 99 (1949).

and 2.9 barns for $J=\frac{3}{2}$. Thus, these preliminary scattering measurements are consistent only with $J=\frac{1}{2}$ for the 640-kev level.

An attempt was made to fit the observed resonance cross sections using the Breit-Wigner theory with reasonable reduced widths. In particular, it appeared to be of interest to try to account for the fact that at 499 kev no resonance scattering of neutrons was observed, and at 1800 kev no resonance in the proton emission was found. For these calculations reasonable limits for the reduced widths were taken to be in the range between 0.05 and 5×10^{-13} Mev-cm. Values thus far observed[16,17] for neutrons and protons lie well within these limits for nuclei with atomic number and level spacing comparable to that of N^{15}. It must be emphasized, however, that no strict limits can be assigned except that a reduced width cannot exceed $3\hbar^2/2ma$, where m is the mass of the particle and a is the radius of the compound nucleus.[16]

In the consideration of each resonance, particle widths were found from Eq. (1) for each possible value of J using the observed total width and the cross section at resonance, and reduced widths were found from Eq. (2) for l-values appropriate to each J. For a given J both the lowest possible even l-value and the lowest possible odd l-value are considered in order to include states of both parities; contributions to the cross section from higher l-values are negligible because of the higher centrifugal barrier. Nuclear spins of N^{14}, C^{14}, and B^{11} are 1, 0, and $\frac{3}{2}$, respectively, so that l-values considered are $J-\frac{3}{2}$ and $J-\frac{1}{2}$ for the neutron and α-particle (excepting $J=\frac{1}{2}$) and $J\pm\frac{1}{2}$ for the proton. Thus, except for $J=\frac{1}{2}$, the proton must have l-values equal to or larger than those of the neutron and α-particle. Penetration factors used in the calculation may be found explicitly for neutrons[18] and have been calculated for protons by Christy and Latter.[19] The factor for the α-particles was obtained by the WKB method using as the radius of nuclear interaction a value (5.35×10^{-13} cm) which is consistent with that assumed by Christy and Latter to obtain the proton penetration factor.

[17] C. K. Bockelman, (to be published).
[18] Feshbach, Peaslee, and Weisskopf, Phys. Rev. **71**, 145 (1947).
[19] R. F. Christy and R. Latter, Rev. Mod. Phys. **20**, 185 (1948).

TABLE III. Examples of quantum numbers for which reasonable reduced widths are found for the observed resonances in nitrogen.

Energy (kev)	$\Gamma_n/(\Gamma_p+\Gamma_\alpha)$	Quantum numbers J	l_p	l_n	l_α	Reduced widths (in 10^{-13} Mev-cm) γ_p^2	γ_n^2	γ_α^2
499	<1	1/2	0	1		0.2	0.03	
	<1	5/2	2	2		6.9	0.3	
640	>1	1/2	0	0		0.055	0.15	
	>1	1/2	1	0		0.17	0.15	
993	<1	5/2	2	2		4.8	0.052	
	>1	5/2	3	1		0.4	0.55	
1415	<1	3/2	1	1	0	0.43	0.1	1.2
	>1	3/2	1	1	0	0.1	0.4	0.28
1800	<1	5/2	3	2	1	0.8	0.16	1.9
	>1	5/2	3	1	1	0.08	0.25	0.18
	>1	5/2	3	1	2	0.08	0.25	1.0

Examples are given in Table III indicating that combinations of quantum numbers can be found which give fairly reasonable reduced widths for all resonances. No definite assignment of quantum numbers is possible from this analysis except perhaps for the 640-kev level. Both s- and p-protons are considered for this level in order to allow for both parities of C^{14} and N^{14}. For the resonances beyond the region where the total cross section has been measured, examples are given for both large and small $\Gamma_n/(\Gamma_p+\Gamma_\alpha)$. While no peak in the (n,p) cross section is shown at 1800 kev in Fig. 3, a cross section of 5 millibarns (as used for computations in Table III) is consistent with the observations. Table III indicates that the measurements beyond 900 kev may be fitted whether a resonance in scattering is observable or not.

It is of interest that the resonance shown in Fig. 3 at 640 kev does not have the symmetric character predicted by the single-level Breit-Wigner formula. The asymmetry cannot be explained as caused by a variation in wave number and barrier factors since these variations are very small. Such an asymmetry may be caused by an interference with an adjacent level, but the exact reason for it is not understood.

One of us (CHJ) wishes to express his gratitude to the Kimberly Clark Paper Company for the grant of a fellowship.

The Scattering of Gamma-Rays by Nucleons*

R. G. SACHS
University of Wisconsin, Madison, Wisconsin

AND

L. L. FOLDY
Case Institute of Technology, Cleveland, Ohio

(Received August 2, 1950)

In order to explore the possibility that information concerning nucleon structure could be obtained from the scattering of photons of energy near meson production threshold, the cross section for the process has been calculated on the basis of the symmetrical scalar and pseudoscalar meson theories. The calculation was carried out in the non-relativistic, weak coupling approximation, neglecting nucleon recoil effects. No divergence difficulties were encountered. In the scalar theory, the proton total cross section is somewhat less than the Thompson cross section (σ_0) as a consequence of intefrerence between the scattering by the nucleon and that by the meson cloud. In pseudoscalar theory the total cross section varies strongly with energy showing a resonance scattering effect with a peak value as high as 15 σ_0. The angular distribution in the scalar theory is very similar to that given by the Klein-Nishina formula: $(\frac{1}{2})(1+\cos^2\theta)$. The pseudoscalar theory gives a quite asymmetric distribution, the form of asymmetry depending strongly on energy. The results may be taken as a strong indication that observation of the process could yield, in a sensitive way, information concerning the structure of the proton.

I. INTRODUCTION

IN this period of great uncertainty concerning the nature of nucleons, it is to be hoped that new experiments will shed some light on the structure of the particles. The available empirical facts concerning their structure, aside from the indirect information provided by nuclear interactions, have to do with their static electromagnetic properties as described by magnetic moments and by the neutron-electron interaction.[1] The source of the anomalous electromagnetic properties of nucleons is generally presumed to be the relatively strong interaction of the nucleons with a charged meson field and the consequent existence of a charge cloud of virtual mesons about nucleons. Calculations[2] of the anomalous magnetic moments of nucleons and the neutron-electron interaction on the basis of this supposition have led to results of the correct order of magnitude but not to exact quantitative agreement with experiment. These essentially static electromagnetic properties of nucleons provide, however, only limited information concerning the meson charge cloud because they are integral properties of the cloud. In principle investigation of the detailed structure of the charge cloud could proceed by observation of the scattering of sufficiently energetic gamma-rays by a nucleon. This experiment, which in its physical arrangement would be much like the measurement of the Compton cross section of the electron, is actually more closely analogous to the determination of the electronic structure in an atom by the scattering of sufficiently energetic x-rays. It is the purpose of this paper to stimulate interest in such an experiment by indicating the character of the information which might be obtained. We consider the case of a measurement of the absolute cross section and the angular distribution for the scattering by protons of gamma-rays up to energies of the order of 300 Mev; i.e., up to energies twice the threshold energy for meson production.

Even if a proton did not interact with mesons it would be expected to scatter gamma-rays through the usual Compton effect. On the basis of the Klein-Nishina formula the total cross section would be estimated at about 10^{-31} cm^2. If the anomalous magnetic moment of the proton is not a result of its interaction with mesons, but is properly described in the manner proposed by Pauli[3] then an additional contribution to the scattering cross section would result. Treatments of this problem have been given by Corben, Batdorf and Thomas, and Powell.[4] The last of these has found that for 100-Mev gamma-rays this effect leads to approximately a 25 percent increase in the scattering cross section of protons over that predicted by the Klein-Nishina formula.

The more usual approach to the anomalous magnetic moment of the proton attributes it to currents flowing in the charge cloud of virtual mesons about the proton. However, such a charge cloud is not rigidly attached to the nucleon which is its source and is therefore electrically and magnetically polarizable. For electromagnetic radiation of wave-length long compared with the dimensions of the charge cloud one would therefore expect additional contributions to the scattering cross

* This work has been supported in part by the AEC and by a grant-in-aid to one of the authors (L.L.F.) from the Scientific Research Society of America.

[1] Havens, Rabi, and Rainwater, Phys. Rev. **72**, 634 (1947); E. Fermi and L. Marshall, Phys. Rev. **72**, 1139 (1947).

[2] J. M. Luttinger, Helv. Phys. Acta **21**, 483 (1948); M. Slotnick and W. Heitler, Phys. Rev. **75**, 1645 (1949); K. M. Case, Phys. Rev. **76**, 1 (1949); S. M. Dancoff and S. D. Drell, Phys. Rev. **76**, 205 (1949); S. Borowitz and W. Kohn, Phys. Rev. **76**, 818 (1949).

[3] W. Pauli, Rev. Mod. Phys. **13**, 203 (1941).

[4] S. B. Batdorf and R. Thomas, Phys. Rev. **59**, 621 (1941); J. L. Powell, Phys. Rev. **75**, 32 (1949); J. L. Powell, Phys. Rev. **74**, 1258 (1948).

section arising from the polarization of the charge cloud in exact analogy to Rayleigh scattering of light. As the wave-length of the gamma-rays decreased to where it was comparable with the dimensions of the charge cloud, that is, near the threshold for meson production, retardation effects would become important and the total cross section and angular distribution of the scattered radiation would begin to reflect the detailed structure of the meson charge cloud. The natural frequencies of the charge cloud would be expected to be in the neighborhood of $\mu_0c^2/\hbar$, where μ_0 is the meson mass; hence the polarization effects might be expected to be large at the corresponding energies and this would lead one to expect a maximum in the scattering cross section in the neighborhood of the threshold for meson production.

A further influence on the cross section which would be of interest is that due to the negative energy states of the nucleon (if such exist). It is conventional to assume that nucleons are described by the Dirac equation, in which case the negative energy states will be involved in processes produced by interaction with radiation. However, the influence of these states will be small at gamma-ray energies as much smaller than Mc^2, as are those under consideration here. It would clearly be of interest to observe the effect at energies of about Mc^2, but gamma-rays of such energy are not at present available in the required intensity. The present considerations are limited to the lower energy region for the sake of simplicity and with due regard for the fact that observations will undoubtedly be made first at the lower energies.

For electromagnetic waves of length long compared to the dimensions of the charge cloud, the polarizability effects on the scattering, in analogy with Rayleigh scattering, would be expected to yield a cross section varying as the fourth power of the gamma-ray energy E. Since the effect considered here is of second order in the electromagnetic interaction and of second order in the meson-nucleon coupling (g), the mesonic cross section for $E \ll \mu_0c^2$ is expected to be of the form

$$\sigma = C(e^2/\mu_0c^2)^2(g^2/\hbar c)^2(E/\mu_0c^2)^4$$

with C a dimensionless quantity depending on the angle of scattering and presumably of order of magnitude unity. Extrapolation of this expression to the threshold energy $E=\mu_0c^2$, would indicate a cross section due to mesons of some ten times the Klein-Nishina value. Actually the quantity C is sensitive to the meson theory employed. Also there is interference between the scattering due to polarizability and the ordinary Compton effect, and a further scattering apparently associated with the permanent magnetic moment arising from the meson cloud (which gives a contribution to the cross section varying as E^2) leading to considerable variation of the actual numerical magnitude of the cross section and of the angular distribution. These effects depend on the detailed assumptions made concerning the meson field. Some distinction between different theories is therefore possible on the basis of experimental results.

Detailed calculations have been carried out for the symmetrical scalar and pseudoscalar meson theories. These theories suffer from the fact that they lead to divergences in higher order processes[5] as well as the usual difficulty that they do not appear to give an appropriate description of nuclear interactions. Furthermore, the scalar meson theory gives rise to no anomalous moment while the pseudoscalar yields an anomalous moment of the correct order of magnitude but not actually in agreement with experimental values. Despite these limitations it would seem that the calculations could give some idea of the effects to be expected, but it must be borne in mind that the present calculations share the same deficiencies and uncertainties of all extant calculations with meson fields.

It has not proved to be necessary to employ the recently developed relativistic subtraction techniques for the present problem. The nucleons have been treated non-relativistically and recoil has been neglected. The results are free of all divergences to the order in which the calculations have been made.[6]

The approximation in which the present calculations have been made may be precisely stated as follows: The transition matrix element is expanded in a series of the form:

$$\mathfrak{M} = \frac{e^2}{\hbar c}\left\{A_1\frac{\mu_0}{M} + A_2\frac{g^2}{\hbar c} + A_3\frac{g^2}{\hbar c}\frac{\mu_0}{M} + A_4\frac{g^4}{\hbar^2c^2} + A_5\frac{\mu_0^2}{M^2} + A_6\frac{e^2}{\hbar c} + \cdots\right\}.$$

Only the first two terms, which turn out to be of the same order of magnitude, are retained in this treatment. The first represents the ordinary Compton scattering by the nucleon and the second contains the lowest order effects of the meson field. Our approximation corresponds to a non-relativistic treatment of the nucleon with neglect of nuclear recoil terms together with the weak coupling approximation in perturbation theory; also the neglect of the interaction of the nucleon with the electromagnetic field in intermediate states in which a virtual meson is present.

It will be shown that for a proton treated by the scalar theory the A_1 and A_2 terms are of the same order of magnitude but opposite in sign. The resulting cross section is about one-third of the Klein-Nishina cross section for $E \simeq \mu_0c^2$ and is a slowly varying function of energy (Fig. 1). The angular distribution differs but little from that given by the Klein-Nishina formula, i.e., $\frac{1}{2}(1+\cos^2\theta)$.

[5] K. M. Case, Phys. Rev. **75**, 1440 (1949).

[6] It is to be noted, however, that a logarithmic divergence would be introduced if recoil terms which are of order $(e^2/\mu_0c^2)^2(g^2/\hbar c)^2(\mu_0/M)$, where M is the nucleon mass, were included.

In the pseudoscalar theory the second term is small at low energies but shows a strong maximum at $E=\mu_0c^2$, the peak value being considerably larger than the A_1 term. The result is a cross section curve (Fig. 2) suggesting resonance scattering of the photon by the meson cloud. The angular distribution (Fig. 3) also shows a characteristic behavior which is very energy dependent.

All results depend on the choice of coupling constant, a choice which is bound to be ambiguous in the present state of the theory. By an appropriate adjustment of coupling constant, it might be possible to bring either theory into agreement with a measured total cross section. However, a distinction on the basis of angular distribution should still be possible.

We can conclude that observation of the process might prove to be quite informative.

II. THE INTERACTIONS

In the scalar theory four interaction terms contribute to the Hamiltonian; the nucleon-meson interaction, the nucleon-photon interaction, the first order meson-photon interaction, and the second order meson-photon interaction. Considering only the charged mesons, since they alone contribute to the scattering of photons in our approximation, the following explicit forms have been assumed for these interactions:

$$H_g=g(2\pi\hbar c/V)^{\frac{1}{2}}\sum_k k_0^{-\frac{1}{2}}[\tau_-(a_k+b_{-k}^*)\exp(i\mathbf{k}\cdot\mathbf{R}) +\tau_+(a_k^*+b_{-k})\exp(-i\mathbf{k}\cdot\mathbf{R})] \quad (1)$$

$$H_N=(e^2/Mc^2)(2\pi\hbar c/V)\sum_{\omega,u}\sum_{\omega'u'}(\omega\omega')^{-\frac{1}{2}} \times(\mathbf{u}\cdot\mathbf{u}')A_{\omega,u}A^*_{\omega',u'}\exp[i(\omega-\omega')\cdot\mathbf{R}] \quad (2)$$

$$H_e=e^2(\pi/V)\sum_{\omega u}\sum_{kk'}(k_0k_0'\omega)^{-\frac{1}{2}}\mathbf{u}\cdot(\mathbf{k}+\mathbf{k}') \times(A^*_{\omega',u'}+A_{-\omega,u})(a_{k'}^*+b_{-k'})(a_k+b_{-k}^*) \times\delta(\mathbf{k}'-\mathbf{k}+\omega) \quad (3)$$

$$H_{ee}=e^2(\pi/V)\sum_{\omega u}\sum_{\omega'u'}\sum_{kk'}(\omega\omega'k_0k_0')^{-\frac{1}{2}}(\mathbf{u}\cdot\mathbf{u}') \times(A^*_{\omega'u'}+A_{-\omega'u'})(A_{\omega u}+A^*_{-\omega u})(a_{k'}^*+b_{-k'}) \times(a_k+b_{-k}^*)\delta(\mathbf{k}-\mathbf{k}'+\omega-\omega'). \quad (4)$$

The pseudoscalar theory involves four analogous terms and a fifth expression describing the simultaneous interaction of nucleons, mesons, and photons. H_N, H_e, and H_{ee} are the same as above, and the other contributions have been taken to be:[7]

$$H_g=-ig(2\pi\hbar c/V)^{\frac{1}{2}}\sum_k(\mu^2k_0)^{-\frac{1}{2}}(\boldsymbol{\sigma}\cdot\mathbf{k})[\tau_-(a_k +b_{-k}^*)\exp(i\mathbf{k}\cdot\mathbf{R})+\tau_+(a_k^*+b_k)\exp(-i\mathbf{k}\cdot\mathbf{R})] \quad (1')$$

$$H_{eg}=eg(2\pi i/\mu V)\sum_{\omega,u}\sum_k(k_0\omega)^{-\frac{1}{2}}(\boldsymbol{\sigma}\cdot\mathbf{u})(A_{\omega,u}+A^*_{-\omega,u}) \times[(\tau_+a_k^*-\tau_-b_k^*)\exp\{-i(\mathbf{k}-\omega)\cdot\mathbf{R}\} +(\tau_+b_k-\tau_-a_k)\exp\{i(\mathbf{k}+\omega)\cdot\mathbf{R}\}]. \quad (5)$$

The notation is as follows:

g = coupling between meson and nucleon;
V = volume of box;
$\hbar\mathbf{k}$ = meson momentum;
μ = reciprocal of Compton wave-length of meson $=\mu_0c/\hbar$;
$k_0=(k^2+\mu^2)^{\frac{1}{2}}$;
τ_+, τ_- = isotopic spin operators $(\frac{1}{2})(\tau_1+i\tau_2)$ and $(\frac{1}{2})(\tau_1-i\tau_2)$ respectively, where $\tau_1\tau_2=i\tau$ and $\tau=\pm1$ for neutron and proton respectively;
a_k, a_k^* = annihilation and creation operators for positive mesons of momentum $\hbar\mathbf{k}$;
b_k, b_k^* = annihilation and creation operators for negative mesons of momentum $\hbar\mathbf{k}$;
$\mathbf{R}$ = nucleon coordinate;
M = mass of nucleon;
$\hbar\omega$ = momentum of photon;
$\mathbf{u}$ = unit polarization vector of photon;
$A_{\omega,u}, A^*_{\omega u}$ = annihilation and creation operators for photon with momentum $\hbar\omega$, polarization $\mathbf{u}$;
$\boldsymbol{\sigma}$ = spin operator for nucleon.

The value of the coupling constant has been determined on the basis of a symmetrical meson theory (although only the charged mesons appear here, the neutrals affect the value of the coupling constant) by setting the energy of the ^1S state of the deuteron equal to zero. The interaction potential between neutron and proton in this state is given for both the scalar and pseudoscalar theories by

$$\tfrac{1}{2}g^2e^{-\mu r}/r.$$

The binding energy of the ^1S state is zero if we set[8]

$$\tfrac{1}{2}(g^2/\hbar c)(M/\mu_0)=1.683. \quad (6)$$

III. METHOD OF CALCULATION

Calculation of the mesonic contribution to the matrix element has been carried out by two quite different, although equivalent, methods, a different method being used by each author. In the one treatment, fourth-order time-dependent perturbation theory was used, the interaction H_g appearing in second order and the interaction H_e appearing in second order or the (second-order) interaction H_{ee} appearing in first order. In the pseudoscalar theory the additional (second-order) interaction H_{eg} appears in first order along with a first-order contribution from H_e and another from H_g. The identification of the rather large number of transition schemes involved in this method has been facilitated by the use of diagrams similar to those introduced by Feynman. After all of the transition schemes and their corresponding energy denominators have been established, it is a straightforward matter to write down the transition amplitude.[9]

[7] If P is the nucleon momentum, these terms may be assumed to arise in order P/Mc from a pseudoscalar coupling with coupling constant gM/μ_0 or in order zero from pseudovector coupling with constant g. In both cases the (logarithmically divergent) higher order recoil terms are neglected.

[8] R. G. Sachs and M. Goeppert-Mayer, Phys. Rev. **53**, 991 (1938).

[9] The term "transition amplitude" is used here for the quantity T which appears in the transition probability $2\pi|T|^2\rho_E/\hbar$. On occasion this quantity has been called the "matrix element."

The other method, which is described in some detail in Appendix I, treats the problem in two steps. First the stationary states of the nucleon and meson field are described approximately by a wave functional which diagonalizes the Hamiltonian, including H_g, to order g^2. This set of functionals is obtained by means of ordinary stationary perturbation theory and it describes the possible stationary states of a nucleon along with its meson proper field (nucleon-meson). The second step consists in the introduction of the electromagnetic interactions H_{ee}, H_e, and H_{eg}. The transitions which these induce between the various states of the nucleon-meson are calculated by means of first and second order time dependent perturbation theory respectively. The transition amplitude is determined in the usual way from the matrix elements of H_{ee}, H_e, and H_{eg} between pairs of "nucleon-meson" states. The results of this treatment are, of course, found to be in agreement with those of the first method.

The transition amplitude produced by the interaction term H_N is calculated by means of the ordinary second-order time-dependent perturbation method.

IV. THE TRANSITION AMPLITUDE

The propagation vector of the incident quantum may be denoted by ω and that of the scattered quantum by ω'. The energies of these quanta are then $\hbar c\omega$ and $\hbar c\omega'$ respectively and they are equal in the no recoil approximation, that is $\omega=\omega'$. The transition amplitude in the scalar theory is found to be:

$$T_s=(2\pi\hbar e^2/Mc\omega V)\mathfrak{M}_s$$

with

$$\mathfrak{M}_s=(\mathbf{u}\cdot\mathbf{u}')+(g^2/\hbar c)(Mc/2\pi^2\hbar)\int\frac{d^3k}{(\mathbf{k}-\omega)_0^2(\mathbf{k}-\omega')_0^2}\times\left[(\mathbf{u}\cdot\mathbf{u}')-4\frac{(\mathbf{u}\cdot\mathbf{k})(\mathbf{u}'\cdot\mathbf{k})}{k_0^2-\omega^2}\right], \quad (7)$$

where $(\mathbf{k}-\omega)_0^2=(\mathbf{k}-\omega)^2+\mu^2$.

On the other hand, the pseudoscalar theory yields the result $\mathbf{T}_p=(2\pi\hbar e^2/Mc\omega V)\mathbf{M}_p$ with

$$\mathbf{M}_p=(\mathbf{u}\cdot\mathbf{u}')+(g^2/\hbar c)(Mc/2\pi^2\hbar\mu^2)\times\int d^3k\Big\{(\mathbf{u}\cdot\mathbf{u}')\frac{(\mathbf{k}-\omega')\cdot(\mathbf{k}-\omega)}{(\mathbf{k}-\omega)_0^2(\mathbf{k}-\omega')_0^2}$$
$$-\frac{1}{k_0^2-\omega^2}\Big[4\frac{(\mathbf{u}\cdot\mathbf{k})(\mathbf{u}'\cdot\mathbf{k})(\mathbf{k}-\omega)\cdot(\mathbf{k}-\omega')}{(\mathbf{k}-\omega)_0^2(\mathbf{k}-\omega)_0^2}$$
$$-2\frac{(\mathbf{u}'\cdot\mathbf{k})\mathbf{u}\cdot(\mathbf{k}-\omega')}{(\mathbf{k}-\omega')_0^2}-2\frac{(\mathbf{u}\cdot\mathbf{k})\mathbf{u}'\cdot(\mathbf{k}-\omega)}{(\mathbf{k}-\omega)_0^2}+(\mathbf{u}\cdot\mathbf{u}')\Big]$$
$$-\frac{i\omega}{k_0(k_0^2-\omega^2)}\Big[4\frac{(\mathbf{u}\cdot\mathbf{k})(\mathbf{u}'\cdot\mathbf{k})\sigma\cdot(\mathbf{k}-\omega')\times(\mathbf{k}-\omega)}{(\mathbf{k}-\omega)_0^2(\mathbf{k}-\omega')_0^2}$$
$$-2\frac{(\mathbf{u}'\cdot\mathbf{k})\sigma\cdot(\mathbf{k}-\omega)\times\mathbf{u}}{(\mathbf{k}-\omega')_0^2}+2\frac{(\mathbf{u}\cdot\mathbf{k})\sigma\cdot(\mathbf{k}-\omega)\times\mathbf{u}'}{(\mathbf{k}-\omega)_0^2}$$
$$+\sigma\cdot\mathbf{u}'\times\mathbf{u}\Big]+\frac{2i\omega}{k_0^2}\Big[\frac{1}{(\mathbf{k}-\omega')_0}\frac{(\mathbf{u}'\cdot\mathbf{k})(\sigma\cdot\mathbf{u}\times\mathbf{k})}{[k_0+(\mathbf{k}-\omega')_0]^2-\omega^2}$$
$$-\frac{1}{(\mathbf{k}-\omega)_0}\frac{(\mathbf{u}\cdot\mathbf{k})(\sigma\cdot\mathbf{u}'\times\mathbf{k})}{[k_0+(\mathbf{k}-\omega)_0]^2-\omega^2}\Big]$$
$$+4i\omega\frac{(\mathbf{u}'\cdot\mathbf{k})(\mathbf{u}\cdot\mathbf{k})\sigma\cdot(\mathbf{k}-\omega')\times(\mathbf{k}-\omega)}{k_0[(\mathbf{k}-\omega)_0^2-(\mathbf{k}-\omega')_0^2]}$$
$$\times\Big[\frac{1}{(\mathbf{k}-\omega)_0}\frac{1}{\omega^2-[k_0+(\mathbf{k}-\omega)_0]^2}$$
$$-\frac{1}{(\mathbf{k}-\omega')_0^2}\frac{1}{\omega^2-[k_0+(\mathbf{k}-\omega')_0]^2}\Big]\Big\}. \quad (8)$$

Here, $\mathbf{1}$ is the unit spin matrix and $\mathfrak{M}_p=(\mathbf{M}_p)_{if}$, that is, the matrix element of $\mathbf{M}_p$ between the initial and final spin states. In this sense

$$\mathbf{M}_s=\mathfrak{M}_s\mathbf{1}. \quad (9)$$

In both cases the first term represents the ordinary Thompson scattering (non-relativistic limit to the Klein-Nishina formula).

It is to be noted that $\mathbf{M}_s$ is finite while $\mathbf{M}_p$ involves integrals which would seem to diverge as $\int^\infty dk$ and $\omega\int^\infty dk/k$. The logarithmically divergent terms all arise as a consequence of the interaction term H_{eg}. Thus they are related to the production of mesons induced by the electromagnetic field. The (magnetic) polarizability of the meson cloud associated with these terms therefore depends on the frequency of the radiation so they can be expected to produce scattering quite different in its frequency dependence from Rayleigh scattering, which arises when the polarizability is independent of frequency. It turns out that the logarithmic divergences cancel and these terms lead to a cross section proportional to the square of the frequency of the gamma-radiation at low energies.

The linearly divergent integrals correspond to the more usual form of interaction with the electromagnetic field so the corresponding polarizability of meson cloud is expected to be independent of frequency. Thus the resulting cross section should be proportional to ω^4 for small ω/μ. Consequently the contribution of these integrals to $\mathbf{M}_p$ is expected to be proportional to ω^2. This implies that on expansion of the integrals in powers of ω/μ all terms of order lower than $\omega^2\int dk/k^2$ must cancel, which indicates that these divergences must drop out in any approximation, as is indeed found to be the case.

Exact evaluation of all but a few of the integrals occurring in Eqs. (7) and (8) appears to be extremely difficult as a consequence of the angular dependence of

the denominators. Recourse has therefore been taken to term by term integration of an expansion of the integrand in powers of the parameter

$$\epsilon=2\omega k/(k^2+\mu^2+\omega^2) \tag{10}$$

which determines the magnitude of the angular dependence in the denominators. Note that for all k and ω, $\epsilon<1$. For some of the terms in the pseudoscalar theory, the expansion parameter was taken to be $\frac{1}{2}(k^2+\mu^2+\omega^2)^{\frac{1}{2}}\epsilon/k_0$. This quantity is less than 1 for all values of k if $\omega<\sqrt{3}\mu$. The consequent limitation on the results is not serious since for much larger values of ω, recoil certainly cannot be neglected. Calculations were carried out up to $\omega=2\mu$.

The final expression in scalar theory for a proton is found to second order in ϵ to be

$$\mathfrak{M}_s=(\mathbf{u}\cdot\mathbf{u}')-(\pi\beta\mu/24\lambda_+)\{(\mathbf{u}\cdot\mathbf{u}')G-(2+\cos\vartheta)(\mathbf{u}\cdot\mathbf{u}')\times[(\omega^2/\lambda_+)-F]+(\mathbf{v}\cdot\mathbf{u}')(\mathbf{v}'\cdot\mathbf{u})F\} \tag{11}$$

where

$$G(\omega)=2[1-(2\mu^2\lambda_-^2/\omega^4)+2(\lambda_+\lambda_-^3/\omega^4)E(\omega)] \tag{12}$$

$$F(\omega)=\tfrac{2}{5}[1-(\lambda_-^2/\omega^2)+2(\lambda_-^4\mu^2/\omega^6)-2(\lambda_+\lambda_-^5/\omega^6)E(\omega)]$$

and

$$E(\omega)=\begin{cases}1 & \omega<\mu\\ 0 & \omega>\mu.\end{cases} \tag{13}$$

Also

$$\lambda_\pm^2=\mu^2\pm\omega^2, \tag{14}$$

$$\mathbf{v}=\boldsymbol{\omega}/\omega,\quad \mathbf{v}'=\boldsymbol{\omega}'/\omega,\quad \cos\vartheta=(\mathbf{v}\cdot\mathbf{v}'). \tag{15}$$

The coupling constant is contained in β which has the form

$$\beta=2g^2M/\pi\hbar c\mu_0. \tag{16}$$

According to Eq. (8)

$$\beta=2.14. \tag{17}$$

The corresponding result for pseudoscalar theory is

$$\mathbf{M}_p=(\mathbf{u}\cdot\mathbf{u}')+(\beta\lambda_+/\mu)\Big\{(\mathbf{u}\cdot\mathbf{u}')\Big[A_1+(2+\cos\vartheta)\times\Big(5+\frac{\omega^2}{\lambda_+^2}\cos\vartheta\Big)A_2-\cos\vartheta A_3\Big]+[(2+\cos\vartheta)(\mathbf{u}\cdot\mathbf{u}')+(\mathbf{v}\cdot\mathbf{u}')(\mathbf{v}'\cdot\mathbf{u})]\Big(\frac{\lambda_+^2}{\omega^2}-\cos\vartheta\Big)A_4\Big\}$$
$$-(4i\beta\omega/\mu)\{(\boldsymbol{\sigma}\cdot\mathbf{v}'\times\mathbf{v})(\mathbf{u}\cdot\mathbf{u}')A_5+(\boldsymbol{\sigma}\cdot\mathbf{v}'\times\mathbf{v})\times[(2+\cos\vartheta)(\mathbf{u}\cdot\mathbf{u}')+(\mathbf{v}\cdot\mathbf{u}')(\mathbf{v}'\cdot\mathbf{u})]A_6+[(\mathbf{v}\cdot\mathbf{u}')\boldsymbol{\sigma}\cdot(\mathbf{v}-\mathbf{v}')\times\mathbf{u}+(\mathbf{v}'\cdot\mathbf{u})\boldsymbol{\sigma}\cdot(\mathbf{v}-\mathbf{v}')\times\mathbf{u}']A_7+(\boldsymbol{\sigma}\cdot\mathbf{u}\times\mathbf{u}')A_8\}. \tag{18}$$

The coefficients $A_j(\omega)$ are tabulated in Appendix II.

The results for a neutron can be obtained from these by dropping the first term in Eqs. (11) and (18) and changing the sign.

Considerably simpler expressions can be obtained for the low energy region. Expansion in powers of ω/λ_+ gives to second order:

$$\mathfrak{M}_s=(\mathbf{u}\cdot\mathbf{u}')-(\pi\beta\mu\omega^2/48\lambda_+^3)\times[2(\mathbf{u}\cdot\mathbf{u}')(1-\cos\vartheta)+(\mathbf{v}\cdot\mathbf{u}')(\mathbf{v}'\cdot\mathbf{u})] \tag{19}$$

$$\mathbf{M}_p=(\mathbf{u}\cdot\mathbf{u}')\mathbf{1}+\tfrac{1}{3}\beta\{(i\mu\omega/\lambda_+^2)(\boldsymbol{\sigma}\cdot\mathbf{u}\times\mathbf{u}')-(\pi\omega^2/16\mu\lambda_+)\times[(\mathbf{u}\cdot\mathbf{u}')(10+\cos\vartheta)-(\mathbf{v}\cdot\mathbf{u}')(\mathbf{v}'\cdot\mathbf{u})]\mathbf{1}\}. \tag{20}$$

In both cases the quadratic term can be ascribed to the frequency independent polarizability of the proton. However, the spin-dependent, linear term in Eq. (20) can only be similarly described in terms of a magnetic polarizability which is inversely proportional to frequency.[10] This term arises directly from the interaction H_{sg} given by Eq. (5) by means of which the electromagnetic field induces the emission of mesons. It is not surprising that the corresponding polarizability is frequency dependent.

V. THE CROSS SECTION

The relationship between the differential cross section and the transition amplitude is:

$$d\sigma=(V/2\pi)^2(\omega/\hbar c)^2|\mathbf{T}_{if}|^2d\Omega. \tag{21}$$

Setting $\mathbf{T}=(2\pi ke^2/Mc\omega V)\mathbf{M}$, the introduction of the Thomson cross section

$$\sigma_0=(8\pi/3)(e^2/Mc^2)^2=1.93\times10^{-31}\text{ cm}^2 \tag{22}$$

yields the following expression for the differential cross section:

$$d\sigma=(3/8\pi)\sigma_0|\mathbf{M}_{if}|^2d\Omega. \tag{23}$$

This cross section describes a process for which both the initial and final states of proton spin and photon polarization are specified. The quantity of greater interest is the sum over these final states and average over the initial states. Denoting this summing and averaging process by a bar, Eq. (23) becomes

$$d\bar{\sigma}=(3/8\pi)\sigma_0\langle|\mathbf{M}_{if}|^2\rangle_{Av}d\Omega. \tag{24}$$

If the expression Eq. (11) [also see Eq. (19)] for M_s is introduced into Eq. (24) the differential cross section for a proton (scalar theory) is found to be

$$(8\pi/3\sigma_0)d\bar{\sigma}_s/d\Omega=\tfrac{1}{2}[(1-u+w\cos\vartheta)^2+v^2]+\tfrac{1}{2}\{[1-u-(2v-w)\cos\vartheta]^2-3v^2\}\cos^2\vartheta, \tag{25}$$

where

$$u=(\pi\beta\mu/24\lambda_+)(G+2F-2\omega^2/\lambda_+^2)$$
$$v=(\pi\beta\mu/24\lambda_+)F$$
$$w=\pi\beta\mu\omega^2/24\lambda_+^3 \tag{26}$$

and $F(\omega)$, $G(\omega)$ are given by Eq. (12).

[10] Although a permanent magnetic moment would lead to such a term linear in the frequency, the dependence on polarization and direction of propagation is quite different from that given by the linear term in Eq. (20).

The corresponding expression for the pseudoscalar theory is so complicated that most of the relevant material has been relegated to Appendix II in the form of coefficients B_n, C_n, and D_n:

$$\frac{8\pi}{3\sigma_0}\frac{d\bar{\sigma}_p}{d\Omega}=\tfrac{1}{2}(1+\cos^2\vartheta)+2\beta\frac{\lambda_+}{\mu}\sum_{n=0}^{4}B_n\cos^n\vartheta$$

$$+\beta^2\frac{\lambda_+^2}{\mu^2}\sum_{n=0}^{6}C_n\cos^n\vartheta+16\beta^2\frac{\omega^2}{\mu^2}\sum_{n=0}^{6}D_n\cos^n\vartheta. \quad (27)$$

The first term contains the nucleon scattering, the second is the interference term between meson and nucleon scattering, the third is the corresponding meson scattering and the fourth is due to the magnetic polarizability effect mentioned in Section IV. There is no interference term corresponding to this last contribution.

The proton total cross sections obtained from these expressions are:

$$\bar{\sigma}_s/\sigma_0=(1-u)^2+\tfrac{1}{5}(3v^2-3vw+2w^2) \quad (28)$$

for the scalar theory and, for the pseudoscalar theory,

$$\bar{\sigma}_p/\sigma_0=\left(1+\beta\frac{\lambda_+}{\mu}B\right)^2+\beta^2\frac{\lambda_+^2}{\mu^2}C+16\beta^2\frac{\omega^2}{\mu^2}D \quad (29)$$

where the functions $B(\omega)$, $C(\omega)$, $D(\omega)$ are given in Appendix II.

The low energy cross sections can be obtained from the approximate expressions for $\mathfrak{M}_s$ and $\mathbf{M}_p$ given by Eqs. (19) and (20):

$$\frac{8\pi}{3\sigma_0}\frac{d\bar{\sigma}_s}{d\Omega}=\left(1-\frac{\pi\beta}{12}\frac{\omega^2}{\lambda_+^2}\right)\cdot\tfrac{1}{2}(1+\cos^2\vartheta)+\frac{\pi\beta}{24}\frac{\omega^2}{\lambda_+^2}\cos\vartheta \quad (30)$$

$$\frac{8\pi}{3\sigma_0}\frac{d\bar{\sigma}_p}{d\Omega}=\tfrac{1}{2}(1+\cos^2\vartheta)-\frac{\pi\beta}{24}\frac{\omega^2}{\mu\lambda_+}(5+\cos\vartheta+5\cos^2\vartheta)$$

$$+\frac{\beta^2}{18}\frac{\omega^2}{\mu^2}(3-\cos^2\vartheta) \quad (31)$$

to order ω^2/λ_+^2. In the scalar theory the terms in ω^2 are both interference terms but in the pseudoscalar theory the second-order term in β is produced directly by the magnetic polarizability.

Corresponding low energy total cross sections are

$$\bar{\sigma}_s/\sigma_0=1-(\pi\beta\omega^2/12\lambda_+^2) \quad (32)$$

$$\bar{\sigma}_p/\sigma_0=1-(5\pi\beta\omega^2/12\mu\lambda_+)+(2\beta^2\omega^2/9\mu^2). \quad (33)$$

All results have been given for the proton. The neutron cross section can be obtained from Eq. (25), (27), (28), (29), (30), (31), (32), and (33) by dropping the terms independent of β and linear in β.

Numerical results are given for $\beta=2.14$ Eq. (16) in Figs. 1, 2, and 3. Figure 1 shows the total cross section for a proton as a function of energy according to the scalar theory. In addition this figure includes the results of Powell[3] for a phenomenological theory by which the anomalous magnetic moment of the proton is treated as a Pauli moment. The decrease in cross section in scalar theory results from the interference between the direct scattering from the proton and the meson scattering. The choice $\beta=2.14$ happens to result in almost equal amplitudes of meson and proton scattering. It should be remarked that by doubling the coupling constant, g, an entirely different behavior of the cross section would be expected since the meson effects are of order g^4. In this case the curve would be expected to show a marked resonance behavior in the neighborhood of $\omega=\mu$.

The total cross section for proton and neutron according to pseudoscalar theory is shown in Fig. 2. Here, with the same choice of β, the meson effects are in order of magnitude larger than the nucleon scattering. The shape of the curve suggests that the phenomenon be interpreted as resonance scattering of the photon from the meson cloud. Ahead of the resonance the proton curve shows a slight dip resulting from interference between meson and nucleon scattering. The neutron curve is, of course, free of this effect. Extrapolation of Eq. (28) to high energy leads to a cross section increasing as ω^2/μ^2. This results in the appearance of a dip at the high energy side of the resonance. In this case, halving g would result in a slowly varying cross section differing but little from the scalar curve given in Fig. 1.

The angular distribution of the scattering by a nucleon at low energies has the form $\frac{1}{2}(1+\cos^2\theta)$. Powell has shown that in the phenomenological treatment of the nucleon magnetic moment no appreciable deviation from this form is to be expected at the low energies considered here. The angular distribution in scalar theory, as given by Eq. (24) with $\beta=2.14$ does not differ significantly from this form either.

On the other hand, in pseudoscalar theory, the specific meson effects are large and they lead to considerably different angular distribution. The "electric polarizability" term, given by the C_n in Eq. (26) leads to strong forward scattering while the magnetic polariza-

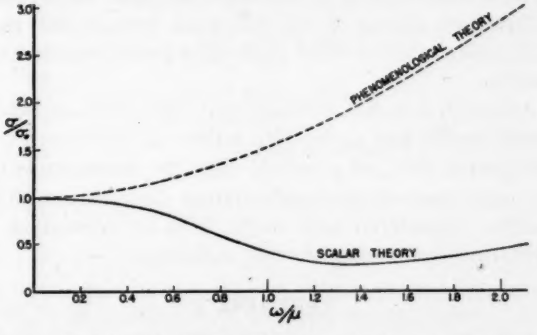

FIG. 1. Total cross section for the scattering of gamma-rays by protons according to the scalar theory (solid curve) and the phenomenological theory (dashed curve). The parameter ω/μ is the photon energy in units of the meson mass and $\sigma_0=8\pi/3\times(e^2/Mc^2)^2$.

bility associated with the D_n yields strong scattering at 90° superimposed on a large spherical term. The electric terms interfere strongly with the nucleon scattering, which has the standard form $\frac{1}{2}(1+\cos^2\theta)$. The final result is an angular distribution which is very sensitive to energy as shown in Fig. 3.

VI. CONCLUSION

The results of these calculations must be interpreted in terms of the exploratory spirit from which they originated. In view of the presently available slight knowledge of the structure of nucleons, two possible theories have been investigated in some detail to deter-

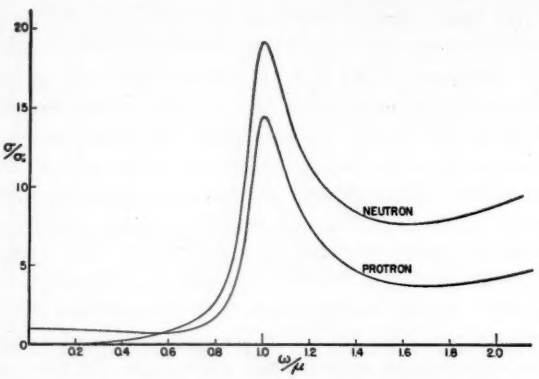

FIG. 2. Total cross section for the scattering of photons by protons and neutrons according to pseudoscalar theory.

mine the degree of sensitivity of the photon scattering cross section to the choice of theories. The results indicate that, at least in the particular cases considered, the cross section is very sensitive indeed. Both the energy dependence and the angular distribution depend distinctly on the nature of the meson theory if the present choice of coupling constant has any meaning. A considerable reduction of coupling constant would, of course, wash out these effects. On the other hand, an appreciable increase of coupling constant in scalar theory would eliminate the marked difference of the total cross section curve from pseudoscalar theory. However, a distinction between the angular distribution curves would still exist because the magnatic polarizability effect is peculiar to the pseudoscalar theory.

Although it is not unlikely that the results of experiments would not agree with either of the theories investigated, one can conclude that the measurement of the total cross section and angular distribution at the energies considered here might lead to interesting information concerning nucleon structure.

APPENDIX I

The Method of Approximate Stationary States

The method to be described consists of the determination of the wave function of nucleon plus meson field to second order in g^2 followed by the use of this wave function to determine the rate of transition induced by the electromagnetic field. The zero order wave functions are $\psi_\tau{}^0(\mathbf{K}; n, n', \cdots; \nu, \nu', \cdots)$ describing a state of a system consisting of one free nucleon with isotopic spin τ, n, $n', \cdots$ free positive mesons of momentum $\hbar\mathbf{k}, \hbar\mathbf{k}', \cdots$ and $\nu, \nu', \cdots$ free negative mesons of momentum $\hbar\mathbf{k}, \hbar\mathbf{k}', \cdots$. The total momentum of the system is $\hbar\mathbf{K}$. The convention for τ is $\tau=+1$ corresponds to a neutron, $\tau=-1$ to proton.

The interaction H_g is introduced as a perturbation and the corresponding approximate stationary wave function is a linear combination of the ψ^0. This combination can easily be expressed in operational form as a consequence of the linear dependence of H_g on meson creation and annihilation operators. We can write

$$H_g=\Sigma_k[H_a{}^+(\mathbf{k})+H_a{}^-(\mathbf{k})+H_b{}^+(\mathbf{k})+H_b{}^-(\mathbf{k})]$$

in which $H_a{}^+(\mathbf{k})$ is a creation operator and $H_a{}^-(\mathbf{k})$ an annihilation operator for positive mesons of momentum $\hbar\mathbf{k}$ and the $H_b{}^\pm(\mathbf{k})$ are corresponding operators for the negatives.

The energy values in zero order may be written $E(\mathbf{K}; n, n', \cdots; \nu, \nu', \cdots)$. If this expression is abbreviated by merely displaying those values of n and ν which are of interest, (i.e., show a change during the transition) the wave function to second order is given by

$$\begin{aligned}
&\psi_1(\mathbf{K}; n_1, n_2, \cdots; \nu_1, \nu_2, \cdots)\\
&=\Big\{1+\Sigma_k\Big[\frac{H_b{}^+(\mathbf{k})}{E(\mathbf{K},\nu)-E(\mathbf{K},\nu+1)}+\frac{H_a{}^-(\mathbf{k})}{E(\mathbf{K},n)-E(\mathbf{K},n-1)}\Big]\\
&+\Sigma_{kk'}\Big[\frac{1}{E(\mathbf{K},n')-E(\mathbf{K},n'-1)}\,\frac{H_b{}^-(\mathbf{k})H_a{}^-(\mathbf{k}')}{E(\mathbf{K},n',\nu)-E(\mathbf{K},n'-1,\nu-1)}\\
&+(1-\delta_{kk'})\Big(\frac{1}{E(\mathbf{K},n')-E(\mathbf{K},n'-1)}\,\frac{H_a{}^+(\mathbf{k})H_a{}^-(\mathbf{k}')}{E(\mathbf{K},n,n')-E(\mathbf{K},n+1,n'-1)}\\
&+\frac{1}{E(\mathbf{K},\nu)-E(\mathbf{K},\nu+1)}\,\frac{H_b{}^-(\mathbf{k}')H_b{}^+(\mathbf{k})}{E(\mathbf{K},\nu,\nu')-E(\mathbf{K},\nu+1,\nu'-1)}\Big)\\
&+\frac{1}{E(\mathbf{K},\nu')-E(\mathbf{K},\nu'+1)}\,\frac{H_a{}^+(\mathbf{k})H_b{}^+(k')}{E(\mathbf{K},n,\nu')-E(\mathbf{K},n+1,\nu'+1)}\Big]\Big\}\\
&\times\psi_1{}^0(\mathbf{K}, n_1, n_2\cdots; \nu_1, \nu_2, \cdots), \quad \text{(A1)}
\end{aligned}$$

when the nucleon under consideration is a neutron. For a proton $\psi_1{}^0$ is replaced by $\psi_{-1}{}^0$ and the a, b labels as well as the indices n, ν appearing in the brackets are interchanged. Although the labels τ, n_j, ν_j no longer have a clear-cut meaning, it is convenient to label the wave function ψ with the same numbers that appear in the ψ^0 to which it is equivalent in the zero order. Note that the function given by Eq. (A1) is not normalized. Renormalization would introduce a factor containing g^2 which does not affect the calculations concerning the scattering of radiation by mesons to order g^2 but introduces a correction to the scattering by the nucleon. However, this correction term is of order $(g^2/\hbar c)(\mu_0/M)$, i.e., of the order of recoil corrections to the meson scattering and such terms are neglected.

The particular functions of interest are those corresponding to initial and final states of a nucleon and those intermediate states which can contribute in order g^2 to transitions from the initial to the final state under the influence of the electromagnetic radiation. The initial and final states and one of the intermediate states are of the type $\psi_\tau(\mathbf{K}; 0, 0, \cdots)$ i.e., they arise from states $\psi_\tau{}^0$ with no mesons present. The four other possible intermediate states have one meson, two mesons, up to four mesons present in zero ord Since only a small number of mesons is involved, it is convenient to label the functions with the values of $\mathbf{k}$, rather than the numbers n and ν. Then the five possible intermediate states are described by

(α) $\psi_\tau(\mathbf{K})$,
(β) $\psi_{-\tau}(\mathbf{K}, \mathbf{k})$, meson of sign $(-\tau)$,
(γ) $\psi_\tau(\mathbf{K}, \mathbf{k}_1, \mathbf{k}_2)$, one positive, one negative meson,
(δ) $\psi_{-\tau}(\mathbf{K}, \mathbf{k}_1, \mathbf{k}_2, \mathbf{k}_3)$, one positive, one negative, one of sign $(-\tau)$,
(ϵ) $\psi_\tau(\mathbf{K}, \mathbf{k}_1, \mathbf{k}_2, \mathbf{k}_3, \mathbf{k}_4)$, two positive, two negative mesons.

These functions can now be obtained from Eq. (A1). Terms have

been included only if they contribute to the transition in order g^2 or lower order. For this reason the (ϵ) state has been dropped.

On introducing the electromagnetic field the initial state includes the incident photon (ω, $\mathbf{u}$) and the final state the scattered photon (ω', $\mathbf{u}'$). There are eight intermediate states: $\alpha, \beta, \gamma, \delta$ with no photon present and $\alpha', \beta', \gamma', \delta'$ with both photons present. The matrix elements of the interaction $H=H_N+H_e+H_{es}+H_{eg}$ ($H_{eg}=0$ for scalar theory) may be easily calculated from

$$H_{\mu i}=(\psi_\mu, H\psi_i) \tag{A2}$$

with $\mu=\alpha, \beta, \gamma, \delta, \alpha', \beta', \gamma', \delta'$ and i denoting the initial state of type α having total momentum $\hbar\mathbf{K}_0$ (equal to the initial nucleon momentum) and including the photon (ω, $\mathbf{u}$). Matrix elements $H_{f\mu}$ may be similarly calculated. The momentum of the nucleon in the final state is fixed by the Compton condition. Only four of the sixteen matrix elements need be calculated directly since $H_{\mu' i}$ can be obtained from $H_{\mu i}$ by substituting $(-\omega', \mathbf{u}')$ for $(\omega, \mathbf{u})$. Also $H_{f\mu}{}^*=H_{\mu f}$ which can easily be obtained from $H_{\mu i}$ by interchanging $(\omega', \mathbf{u}')$ and $(\omega, \mathbf{u})$ and substituting $\mathbf{K}_0'$ for $\mathbf{K}_0$.

In terms of these matrix elements, the transition amplitude is given by the sum over all intermediate states of the expression

$$T_\mu=H_{f\mu}H_{\mu i}/D_\mu, \tag{A3}$$

where D_μ is the appropriate energy denominator. Since momentum is conserved in the transition to the intermediate state we have

$$\mathbf{K}=\mathbf{K}_0+\omega=\mathbf{K}_0'+\omega' \tag{A4}$$

or

$$\mathbf{K}=\mathbf{K}_0-\omega'=\mathbf{K}_0'-\omega \tag{A5}$$

for the states $\alpha, \beta, \gamma, \delta$ or the states $\alpha', \beta', \gamma', \delta'$ respectively.

Equations (7) and (8) are obtained when recoil is neglected, that is, when the contribution to the D_μ of the nucleon kinetic energy is ignored.

APPENDIX II

(1) The Coefficients in Eq. (18)

We define the auxiliary functions

$$F(\omega)=(\lambda_+/\omega)\ln[(\lambda_++\omega)/\mu]$$

$$g(\omega)=\begin{cases}-(\omega/\lambda_-)\arctan(\omega/\lambda_-), & \omega<\mu\\ (i\omega/\lambda_-)\ln[(\omega-i\lambda_-)/\mu], & \omega>\mu\end{cases}$$

$$h(\omega)=(\mu/\omega)\arctan(\omega/\mu)$$

$$E(\omega)=\begin{cases}1, & \omega<\mu\\ 0, & \omega>\mu,\end{cases}$$

where $\lambda_\pm=(\mu^2\pm\omega^2)^{\frac{1}{2}}$. Then if $x=\mu^2/\omega^2$

$$A_1=-(\pi/6)[(4+\tfrac{1}{2}3x+x^3)(\omega^2/\lambda_+^2)-(2+x^2)(\lambda_-/\lambda_+)E]$$

$$A_2=(\pi/24)(\omega^2/\lambda_+^2)$$

$$A_3=\pi/6[2-x+(\lambda_-^3/\lambda_+\omega^2)E]$$

$$A_4=\pi/30[(1+\tfrac{1}{2}x-2x^2+x^3)(\omega^2/\lambda_+^2)-(\lambda_-^5/\lambda_+\omega^4)E]$$

$$A_5=(1/60)[(1+x+5x^2)-(2-6x+7x^2)f-(3+2x)(\lambda_-^4/\omega^4)g+5\ln(\lambda_+/\mu)-5xh]$$

$$A_6=(1/60)[(\tfrac{2}{3}+\tfrac{1}{6}7x-5x^2)+(1-2x+\tfrac{1}{2}x^2+6x^3)(\omega^2/\lambda_+^2)f+(\lambda_-^6/\omega^6)g]$$

$$A_7=(1/60)[\tfrac{1}{3}(\tfrac{1}{2}7+x)+(\lambda_-^6/\omega^6)g+(1-\tfrac{1}{2}5x)\ln(\lambda_+/\mu)-(\tfrac{1}{2}5-x)xh]$$

$$A_8=(1/60)[(9+\tfrac{1}{3}14x+10x^2)-3(4+8x-x^3)f+(9+20x)\ln(\lambda_+/\mu)-(3+14x-2x^3)(\lambda_-^2/\omega^2)g-11x^2h].$$

(2) The Coefficients B_n, C_n, D_n and B, C, D in Eqs. (27) and (28)

We set $y=\lambda_+^2/\omega^2$

$$B_0=\tfrac{1}{2}A_1+5A_2+yA_4 \qquad B_3=(\tfrac{1}{2}5+y^{-1})A_2-\tfrac{1}{2}A_3+(y-1)A_4$$

$$B_1=(\tfrac{1}{2}5+y^{-1})A_2-\tfrac{1}{2}A_3-A_4 \qquad B_4=\tfrac{1}{2}y^{-1}A_2-A_4.$$

$$B_2=\tfrac{1}{2}A_1+(5+\tfrac{1}{2}y^{-1})A_2+yA_4$$

$$C_0=\tfrac{1}{2}A_1{}^2+10A_1A_2+2yA_1A_4+50A_2{}^2+20yA_2A_4+\tfrac{1}{2}5y^2A_4{}^2$$

$$C_1=(5+2y^{-1})A_1A_2-A_1A_3-2A_1A_4+5(5+4y^{-1})A_2{}^2-10A_2A_3-16A_2A_4-2yA_2A_4-y(y+5)A_4{}^2$$

$$C_2=\tfrac{1}{2}A_1{}^2+(10+y^{-1})A_1A_2+2yA_1A_4+5(\tfrac{1}{2}25+2y^{-1})A_2{}^2-(5+2y^{-1})A_2A_3+20yA_2A_4+\tfrac{1}{2}A_3{}^2+2A_3A_4+\tfrac{1}{2}(y^2+4y+1)A_4{}^2$$

$$C_3=(5+2y^{-1})A_1A_2-A_1A_3+2(y-1)A_1A_4+25(1+y^{-1})A_2{}^2-(10+y^{-1})A_2A_3+4(5y-4)A_2A_4-2yA_3A_4+y(3y-1)A_4{}^2$$

$$C_4=y^{-1}A_1A_2-2A_1A_4+5(\tfrac{1}{2}5+2y^{-1})A_2{}^2-(5+2y^{-1})A_2A_3+2(5y-8)A_2A_4+\tfrac{1}{2}A_3{}^2-(y-2)A_3A_4+(2y^2-6y-1)A_4{}^2$$

$$C_5=5y^{-1}A_2{}^2-y^{-1}A_2A_3-8A_2A_4+A_3A_4-4yA_4{}^2$$

$$C_6=\tfrac{1}{2}A_4{}^2.$$

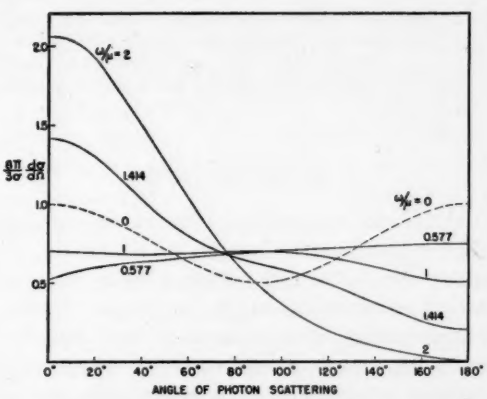

FIG. 3. Relative angular distribution of the scattering of photons by protons in pseudoscalar theory at various photon energies. The cross section units are the values of total cross section shown in Fig. 2. Note that at all energies considered the angular distribution according to either the scalar meson or phenomenological theory would be substantially the same as that given above for $\omega/\mu=0$.

Several contributions to the coefficients C_n have been dropped since they proved to be negligible over the entire energy range considered.

$$D_0=\tfrac{1}{2}A_5{}^2+2A_5A_6+\tfrac{1}{2}5A_6{}^2-2A_6A_7-A_6A_8+2A_7{}^2-2A_7A_8+\tfrac{1}{2}3A_8{}^2$$

$$D_1=2A_5A_7+A_5A_8+4A_6A_7+2A_6A_8-4A_7{}^2+2A_7A_8$$

$$D_2=-2A_5A_7-2A_6{}^2+2A_6A_7+3A_6A_8+2A_7A_8-\tfrac{1}{2}A_8{}^2$$

$$D_3=2A_5A_8-2A_5A_7-A_5A_8+4A_6{}^2-6A_6A_7-2A_6A_8+4A_7{}^2-2A_7A_8$$

$$D_4=-\tfrac{1}{2}A_5{}^2-2A_5A_6+2A_5A_7+\tfrac{1}{2}3A_6{}^2-2A_6A_8-2A_7{}^2$$

$$D_5=-2A_5A_6-4A_6{}^2+2A_6A_7$$

$$D_6=-2A_6{}^2$$

$$B=A_1+2(5+\tfrac{1}{2}y^{-1})A_2+(2y-3/10)A_4$$

$$C=\frac{2}{5}\left\{[(5+2y^{-1})A_2-A_3-(2-\tfrac{3}{2}y)A_4]^2+\frac{17}{70}(A_2-2A_4)^2+\left(\frac{15}{16}\right)^2-\frac{23}{35}\right)A_4{}^2\Big\}$$

$$D=\frac{1}{5}\left\{3A_5{}^2+12A_5A_6-2A_5A_7+\frac{97}{7}A_6{}^2-10A_6A_7-3A_6A_8+12A_7{}^2-10A_7A_8+10A_8{}^2\right\}.$$

A very small contribution to the last term and one to the next-to-last term in C has been dropped.

Penetrating Showers in Carbon*

JOHN R. GREEN†
Department of Physics, University of California, Berkeley, California
(Received July 13, 1950)

The penetrating showers generated in carbon by the cosmic radiation have been investigated by means of a cloud chamber containing both carbon and lead plates which was operated at an elevation of 12,000 ft. It is shown that the penetrating showers generated in carbon are closely the same in angular distribution and in average multiplicity of penetrating particles as the penetrating showers produced in lead, comparison values in lead being obtained from previous work with the same cloud chamber containing only lead plates. Penetrating showers produced in the carbon plates were followed not infrequently by production of secondary penetrating showers farther down in the carbon; the initiating particles of the subsequent showers are very closely aligned with the direction of the primary particles of the parent penetrating shower. The mean free path of the lightly ionizing secondary particles of the penetrating showers for subsequent production of nuclear events was found to be 237 ± 29 g/cm² carbon. The mean free path of the penetrating particles for large-angle scattering in the carbon is about four times this value. The electronic cascades produced at the same time as the penetrating component are satisfactorily explained in order of magnitude by assuming that they are produced by high energy gamma-rays which originate at the event or which may be derived from the fast decay of neutral mesons very near the original event.

I. INTRODUCTION

DURING the summer of 1949 at an elevation of 12,000 ft. above sea level in the White Mountains, California, cloud-chamber pictures were obtained of penetrating showers produced in carbon. Except for recent experiments, cloud chambers have usually been operated with plates of lead or other dense material. The present experiment was undertaken to obtain information about the production of penetrating showers and the behavior of their secondaries in carbon. A particular aspect of the showers that was to be investigated was the manner in which the electronic cascades, which have frequently been observed to accompany the production of penetrating particles in lead, arise.

II. APPARATUS

The entire apparatus was set up inside of a trailer which has a roof of $\frac{1}{4}$-in. plywood protected by $\frac{1}{16}$-in. steel. The cloud chamber, which is shown schematically in Fig. 1, had an illuminated region of $18\times21\times5$ in. that was photographed stereoscopically. In this region were ten 1-in. graphite plates (density 1.68 g/cm³, so that one graphite plate is equivalent to 0.082 radiation length) above four $\frac{1}{2}$-in. lead plates with a spacing of $\frac{1}{2}$ in. between the plates. The chamber was filled with argon gas and was saturated with alcohol vapor. There were four G-M tubes, 1-in. in diameter and 16 in. long, connected in parallel above the cloud chamber, and six similar G-M tubes connected to form five channels underneath the chamber. Two inches of lead were placed between the bottom of the chamber and the lower bank of counters to reduce the number of unnecessary expansions caused by electronic air showers. The five channels from the bottom tray of counters were fed into a discriminator that could be set to require that either two or three of the five channels should be triggered simultaneously (within about 5 μsec.) to produce an output pulse from the discriminator. The coincidence of a pulse from one or more of the four tubes on top of the chamber with a pulse from the discriminator operated the expansion and program controls. If at the same time a pulse was received from an exterior shower tray, which comprised six G-M tubes, 2 in. in diameter and 16 in. long, connected in parallel and located about five meters from the cloud chamber outside the trailer, a second coincidence unit caused a neon light on the front of the chamber to glow and so be photographed.

Inasmuch as the various events were observed in a cloud chamber containing both carbon and lead plates, care must be taken to define the terms used in naming the different types of tracks. The following classifications will be discussed.

1. Heavily ionizing particles: tracks with ionization greater than three times minimum ionization

2. Lightly ionizing particles: tracks with ionization less than three times minimum ionization. These are further divided into (a) Penetrating particles: those particles that penetrate at least one $\frac{1}{2}$-in. lead plate without cascade multiplication. (b) Non-penetrating particles: those particles that cannot be seen to penetrate any of the lead plates. This group will include (1) particles which produce secondary events in the carbon plates, (2) particles which stop in the carbon plates, (3) particles which pass outside the field of illumination before reaching the lead plates, (4) particles which cannot be followed in the lead plate section of the chamber because of the presence of electron showers, (5) particles which are ejected upward.

3. Electrons: particles identifiable as electrons because of scattering in the gas or cascade multiplication

* Assisted by the joint program of the ONR and AEC.
† Now at the University of New Mexico, Albuquerque, New Mexico.

in the lead plates. Note that in no case are these particles included in groups 1 or 2.

The events analyzed in carbon were of the following types.

1. Penetrating showers: these satisfied one or more of the requirements: (a) two or more penetrating particles, (b) one or more penetrating particles and one or more heavily ionizing particles, (c) one or more penetrating particles and three or more non-penetrating particles, (d) one or more penetrating particles making an angle of greater than 5° with the direction of the primary particle, and one or more non-penetrating particles. (The requirement of angular displacement is necessary to avoid including simple knock-on events under the minimum conditions.)

2. Stars: these satisfied one or more of the requirements: (a) one or more non-penetrating particles and one or more heavily ionizing particles, (b) two or more heavily ionizing particles, (c) four or more non-penetrating particles, (d) three non-penetrating particles, provided that at least one of them produces a secondary event

3. Abnormal scatterings: these are large-angle scatterings (greater than 5°) that are observed within the carbon plates for penetrating particles only.

In the first working of the data, the penetrating showers and stars were divided into "primary" and "secondary" classifications and these, in turn, into "accompanied" and "non-accompanied" subgroups. A secondary event was defined as one that was produced by a particle that itself visibly originated in some nuclear event occurring either in the cloud chamber or in the matter above the cloud chamber. Events not classified as secondary were called primary. This division was an attempt to separate lower energy events from higher energy events. It was found, however, that in general the properties of the two groupings were only slightly different, so that in this paper the differentiation will not be made. The same considerations apply to the accompanied events, which were coincident with the tripping of the exterior shower tray, as differentiated from the non-accompanied events, which were not.

Of about 15,000 pictures taken, 228 contained 322 events from which the data were obtained.

III. THE DATA

1. Successive Events

An estimate of the mean free path for production of secondary events can be obtained from the observed number of traversals of the carbon plates. The difficulty arises in determining which particles should be counted to obtain the total path through carbon. In finding the mean free path for secondary production in lead by this this method, the practice has been to add up the path lengths of the penetrating particles, and, as will be shown later, the nearest comparable data in this experiment are for the "lightly ionizing" particles. There are 60 secondary penetrating showers and 29 secondary stars, or a total of 89 secondary events produced by 677 penetrating and 797 non-penetrating particles. This gives a mean free path[1] of 237 ± 29 g/cm² carbon for production of secondary events in carbon by the lightly ionizing particles emitted from penetrating showers in carbon.

This value is probably too large because of the inclusion of some electrons, which were not identifiable as such, among the lightly ionizing particles. To learn whether events were being missed because of the finite probability of absorption of particles within the 1-in. plates of carbon, the events were arranged according to which third of a plate contained the origin of the event, following the method used by Brown and McKay.[2] It was found that the events were observed with close to uniform probability throughout an individual plate; therefore it is assumed that few, if any, events were lost because of absorption.

Now the value of 237 ± 29 g/cm² carbon for the mean free path for subsequent production of secondary events was obtained for all of the lightly ionizing particles, i.e., a mixture of mesons and protons. The same holds true for the corresponding values obtained in lead, such as the result of 316 ± 70 g/cm² lead found by Brown and McKay.[2] Since there is at present no way of demonstrating that the mixtures of particles used to determine the mean free path in the case of carbon and of lead are completely identical, an exact comparison of the two values cannot be made.

Recently Camerini and co-workers[3] have reported

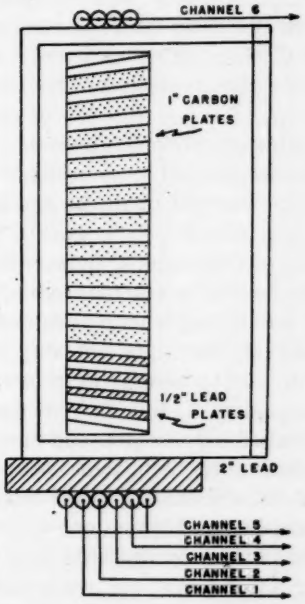

FIG. 1. Cloud chamber.

[1] Since most of the errors given in this paper are due to statistics, all errors quoted are standard errors.

[2] W. W. Brown and A. S. McKay, Phys. Rev. 77, 342 (1950).

[3] Camerini, Fowler, Lock, and Muirhead, Phil. Mag. 41, 413 (1950).

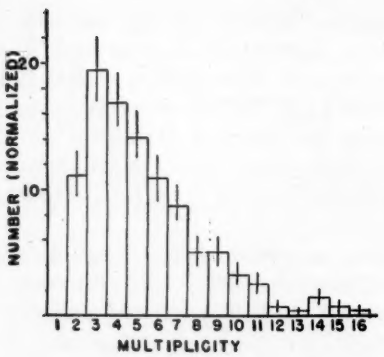

FIG. 2. Distribution of multiplicities of all ionizing particles, normalized to an area of 100 particles.

that protons and negative pi-mesons have approximately the same cross section for production of nuclear events in emulsions, and that these cross sections are very close to the geometrical area of the average emulsion nucleus. As a result of using carbon plates in this experiment, practically none of the nuclear events arising from nucleon interactions (mostly penetrating showers) have been lost in counting the secondary events; however, it is believed that almost none of any possible meson stars have been or could have been observed. Camerini remarks that the secondary stars produced by pi-mesons are quite small, and all of the stars listed by him as being produced by identifiable mesons consist only of heavily ionizing particles with no lightly ionizing "shower" particles. There is also pertinent information obtained by Perkins[4] concerning the meson stars. He found that the alpha-particles are emitted at a maximum energy of 25 Mev, with most of them below 10 Mev; the chance of seeing these in a cloud chamber is extremely small, even for carbon plates. The protons he observed to be emitted in two groups: the fast protons of energy 30 to 60 Mev, of which there are only about 0.07 per star, and the slower protons grouped in the region 5 to 10 Mev. Now protons having energies of 10, 30, and 60 Mev possess ranges in carbon of 0.03, 0.22, and 0.79 in., respectively. The bulk of the protons, those near 10 Mev, would hardly ever be able to emerge from a 1-in. carbon plate. Some of the higher energy protons would be observable; however, there are not very many of them to begin with, and those that were successful in penetrating the remainder of the carbon plate would probably be classified only as stopping mesons or protons.

Assuming, then, that the secondary events observed are due exclusively to the nucleonic secondaries of the penetrating showers, one can calculate the true mean free path, provided that it is known what fraction of the secondaries are nucleonic. If the value of this fraction be taken to be about one-quarter,[3] then the true mean free path for production of nuclear events by the nucleonic secondaries would be about 60 g/cm² carbon, and thus, the same as the geometrical cross section.

[4] D. H. Perkins, Phil. Mag. 40, 601 (1949).

2. Abnormal Scattering

From traversals of the penetrating particles and the number of scatterings greater than 5°, 10°, and 15° observed to occur in the carbon plates, it is possible to calculate values of the mean free path for abnormal scatterings. There were 14 scatterings greater than 5°, 12 greater than 10°, and 10 greater than 15° undergone by 677 penetrating particles in the carbon plates. The resulting mean free paths are 800±220, 930±280, and 1120±360 g/cm² carbon for scatterings greater than 5°, 10°, and 15°, respectively. Thus the mean free path for abnormal scattering in carbon of the penetrating particles is about four times the mean free path for production of successive events by the lightly ionizing secondary particles from penetrating showers in carbon. Little additional information concerning these rare events could be obtained in this experiment except for the fact that in none of the fourteen cases observed was there any indication that there was any electronic component associated with the abnormal scatterings.

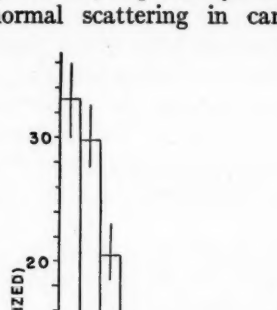

FIG. 3. Distribution of multiplicities of observed penetrating particles, normalized to an area of 100 particles.

3. Multiplicities

The average multiplicity of all ionizing particles emitted from the events in carbon is 5.32±0.13 particles per event; the largest number of ionizing particles observed to leave a single event was sixteen. The multiplicity distribution of all ionizing particles is shown in Fig. 2.

The average multiplicity of observed penetrating particles from the events in carbon is 2.33±0.09; the largest number of penetrating particles observed in a single event was ten. The multiplicity distribution of the penetrating particles is shown in Fig. 3.

Because of the geometry of the chamber and the arrangement of the carbon plates above the lead plates, it is obvious that a particle emitted from a carbon plate

near the top of the chamber has a lower probability of proceeding to the bottom of the chamber and demonstrating its possible penetrating ability in the lead plates than does a particle emitted from a carbon plate near the bottom of the chamber. It is possible to make an empirical correction for this effect to obtain a better estimate of the number of penetrating particles that would have been observed if the geometry had been most favorable. The fraction of all ionizing particles originating in a given plate that demonstrate themselves to be penetrating particles is plotted against the plate number in Fig. 4. By statistical procedures, these points are found to be best fitted by a simple straight line: Fraction$=0.210+0.038x$, where x is the plate number. Now in a cloud chamber containing only lead plates, the particles emitted from one lead plate are observed to be penetrating or otherwise in the next plate below (or, occasionally, above); therefore, if the value of this function be taken for the tenth carbon plate, and if the average multiplicity of all ionizing particles from all plates be multiplied by this fraction, the result will be the average multiplicity of penetrating particles that would have been obtained if each carbon plate had had a lead plate immediately below it. The fraction obtained from the straight line is 0.594 ± 0.047; this gives a corrected average multiplicity of penetrating particles of 3.16 ± 0.25.

This corrected value, however, is still somewhat lower than the value which should be compared to the average multiplicity of penetrating particles as observed in lead. In the first place, there are those non-penetrating particles that produce secondary events in the carbon plates; some of these would be observed to be penetrating in a lead plate cloud chamber. The same holds true for some of the non-penetrating particles that slow down and stop in the carbon before reaching the lead plates; although, at the same time, it must be considered that other particles of this subgroup would be observed as heavily ionizing particles emerging from lead plates because of the greater energy loss experienced in traversing a portion of a lead plate. Finally, there are the non-penetrating particles that are projected upward; there is no way at all by which these can be taken into account, although some of them would undoubtedly correspond to penetrating particles. Fortunately, the number of particles of this last kind is so small compared to the other kinds of particles (only 41 out of a total of 1558 ionizing particles) that the error caused by omitting them entirely is small. The corrected average multiplicity of penetrating particles including non-penetrating particles that produce secondary events and that stop in the carbon plates comes out to be 3.61 ± 0.25. Hence, the value which should be compared to the average multiplicity of penetrating particles observed in a cloud chamber containing lead plates lies between 3.16 ± 0.25 and 3.61 ± 0.25.

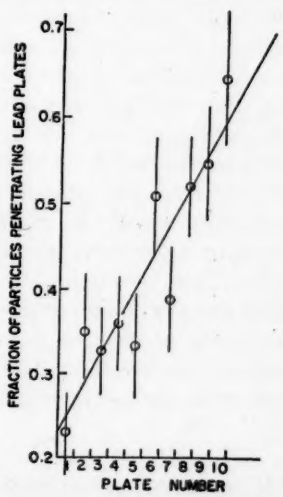

FIG. 4. Fraction of all ionizing particles emitted from a given carbon plate that demonstrate themselves to be penetrating plotted against the number of the plate.

TABLE I. Average multiplicity per event of various particles emitted from penetrating showers in carbon.

Observed penetrating particles	2.33 ± 0.09
Heavily ionizing particles	0.49 ± 0.04
Electrons	0.10 ± 0.02
Non-penetrating particles	2.40 ± 0.09
Total	5.32 ± 0.13
Corrected number of penetrating particles	3.16 ± 0.25
Penetrating particles: corrected less observed	0.83 ± 0.27
Non-penetrating particles:	
that stop or that produce successive events	0.45 ± 0.04
that are ejected upward	0.14 ± 0.02
that are lost in electron showers	0.13 ± 0.02
Total	1.55 ± 0.27
Cf. total non-penetrating particles	2.40 ± 0.09

The average multiplicity of heavily ionizing particles emitted per event is 0.49 ± 0.04; on the average, a fraction 0.091 ± 0.008 of all of the ionizing particles are heavily ionizing.

As a summary and as a check, the average multiplicity per event of each type of particle is listed in Table I. It is seen that the method used for correcting the multiplicity of penetrating particles results in 65 percent of the non-penetrating particles being accounted for. The remaining 35 percent may contain some unidentifiable electrons but most probably consists largely of penetrating particles that were not included when the corrected number of penetrating particles was obtained. It should be noted that even a lead plate cloud chamber, for geometrical reasons, cannot be completely efficient in determining the penetrating ability of all of the particles. Because of observational difficulties, the number of non-penetrating particles that are lost in electron showers may be somewhat underestimated.

4. Angular Distributions with Respect to the Vertical

The histogram in Fig. 5 represents the number of lightly ionizing particles observed per degree as a

FIG. 5. Distribution of the projected angles made by lightly ionizing secondary particles with respect to the vertical, normalized to an area of 100 particles.

FIG. 6. Distribution of the projected angles made by observed secondary penetrating particles with respect to the vertical, normalized to an area of 100 particles.

function of the projected angle with respect to the vertical, normalized to an area of 100 particles. The distribution is concentrated in a downward direction and can be represented approximately by a power law $\cos^n\theta$, with n equal to 7.

Part of the purpose of this experiment is to compare the data obtained in carbon with those in lead. Care was taken to obtain an approximately correct value of the multiplicity to be compared with the average multiplicity of penetrating particles obtained in lead experiments. It is now necessary to find the best angular distributions to compare with those obtained in lead. The histogram in Fig. 6 represents the number of observed penetrating particles per degree observed as a function of the projected angle with respect to the vertical. Comparison of this distribution with that for the lightly ionizing particles as a whole (excluding electrons) as shown in Fig. 5 reveals a very close similarity. The average angles and the root-mean-square angles for the two distributions over the range[5] 0 to 90° are given in Table II. The close correspondence of the distributions suggests that the total lightly ionizing particle distribution over the entire range 0 to 180° can be used as a close approximation for comparison with angular distributions obtained for penetrating particles in cloud chambers containing only lead plates.

The angular distribution with respect to the vertical of the primary particles that initiate the penetrating showers is represented in Fig. 7; the originating particles of secondary (i.e., successive) penetrating showers are not included in this distribution. The distribution is strongly peaked in the downward direction and up to about 20° can be approximated by a power law $\cos^n\theta$, with n between 7 and 9.

5. Angular Distributions with Respect to the Direction of the Primary Particle

The projected angle distribution of lightly ionizing particles with respect to the direction of the primary particle is represented by the histogram in Fig. 8; this is to be compared to the distribution of penetrating particles obtained in lead by Fretter[6] which is represented in Fig. 9. For more certain comparison, the data obtained by Fretter were recalculated and only those events which were obtained at high altitude were used. The values of the average projected angles and of the root-mean-square projected angles for these two distributions are given in Table III. It is seen that the two distributions are identical within the statistical errors; therefore, it is deduced that the events observed in carbon in this experiment are of the same order of energy as the events observed previously by Fretter in lead. Since this is so, it becomes possible to compare the multiplicities obtained in the two experiments as will be done in a later section.

In Fig. 10 is represented the angular distribution of those secondary particles emitted from a nuclear event that go on to produce subsequent events in the carbon plates. The angles are projected angles with respect to the direction of the primary particle which produces the parent event from which the secondary particle emerges. The distribution is very strongly peaked in the direction of the primary particle, and will be discussed in Section IV.

6. Electronic Component

One of the aspects of penetrating showers that was to be investigated in particular was that of the origin of the electronic component. The lead plates, which were previously used in cloud chambers, are so dense that the gamma-rays, if any were formed at or very close to the main event, would have an excellent chance of starting a cascade process before leaving the plate in which the event occurred. The thickness of a 1-in. carbon plate is only 0.08 radiation length as compared with 2.5 radiation lengths for a $\frac{1}{2}$-in. lead plate. This means that the propagation of cascade showers in carbon is delayed over that in lead, so that it should be possible to discover if the electron showers observed to originate with the penetrating showers arise from gamma-rays which are emitted in the act of meson creation, or if electrons are perhaps themselves emitted directly. This was done by observation of the non-ionizing links between the parent events and the points of formation of electron pairs in carbon plates. Then these data were tested to see whether they were compatible with the hypothesis of formation by gamma-rays.

In Table IV, (*i*) gives the number of the plate in which the parent penetrating shower occurred, and (*j*)

[5] Because of the geometrical arrangement in the chamber, this gives the best comparison available.

[6] W. B. Fretter, Phys. Rev. 76, 511 (1949).

gives the average distance in plates which separates the origin of the penetrating shower from the point at which an electron event occurs. The electronic events may be creation of one or more electrons which are identified in general from their cascading properties in lead, except for a few low energy electrons which are identified by their scattering in the gas between the plates. The higher energy electrons are emitted with a very high preference for the forward direction, i.e., the direction of the initiating particle. The distribution of projected angles at which the electrons are formed relative to the direction of the primary has an average of 8.3° and a root-mean-square value of 11.9°. Inasmuch as these values are smaller than the corresponding ones for the projected angular distribution of the observed penetrating particles with respect to the direction of the initiating particle, the assumption that practically all of the electrons which may have been created have successfully identified themselves regardless of where the parent event occurred or where the electrons were created seems to be not unreasonable.

It is assumed next that the average penetrating shower event, obtained by grouping together all of the events observed, will contain a certain average number of gamma-rays, which then go on to produce electrons. Hence, if the numbers in each row of Table IV be divided by the total number of events which have occurred in the corresponding plate, the values obtained will represent the number of electronic events produced per parent event for each separation from the parent event. The columns can then be averaged to give the number of electronic events occurring per plate per parent event as a function of distance in plates from the parent event. These calculations are represented in Table V. The errors quoted in Table V are obtained from the deviations of the individual points used to obtain each average from that average. The logarithm of the average number of electronic events per parent event per plate is plotted in Fig. 11 as a function of the separation of the electronic event from the parent event in plates. The points do not appear to form a very definite pattern; however, by straightforward application of the method of least squares,[7] the best straight line fitting these points can be found. This comes out to be

$$\ln(100\Delta N/\Delta x)=(1.89\pm0.41)-(0.078\pm0.73)x$$

or

$$\Delta N=(0.066\pm0.028)\exp[-(0.078\pm0.073)x]\Delta x,$$

where x is the separation in plates, $\Delta x=1$ is the interval in which ΔN electronic events occur per plate per parent event.

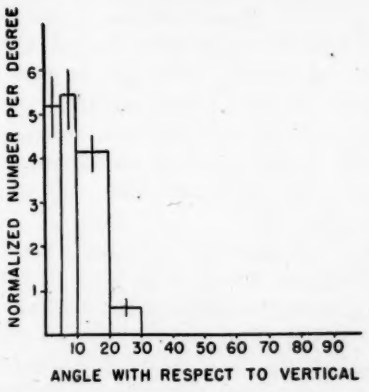

FIG. 7. Distribution of the projected angles made by particles initiating penetrating showers (except for successive ones) with respect to the vertical, normalized to an area of 100 particles.

TABLE II. Average projected angles and root-mean-square projected angles of angular distributions of penetrating and of lightly ionizing particles in the range 0 to 90° with respect to the vertical.

Type of particle	Average angle (0 to 90°)	R.m.s. angle (0 to 90°)
Lightly ionizing	18.8±0.8	25.2
Penetrating	18.3±1.1	22.5

Suppose now that from the average parent event, n_0 gamma-rays are emitted which have a mean free path L for production of electronic events; the number of gamma-rays present at a distance x is then $n=n_0e^{-x/L}$, while the number of electronic events observed will be $N=n_0(1-e^{-x/L})$. The number of electronic events taking place in a thickness Δx at x is then $\Delta N=(n_0/L)e^{-x/L}\Delta x$. Comparison of this equation with the equation of the straight line which best fits the experimental points gives $L=(13\pm12)$ plates, and $n_0=(0.85\pm0.85)$ gamma-rays per parent event. Now the mean free path for production of electrons by very high energy gamma-rays is approximately seven-ninths of a radiation length. This is equivalent to 9.5 plates of carbon. Thus it appears that all of the electronic component can be accounted for, at least in order of magnitude, by assuming that gamma-rays are responsible for creating the electron cascades. It is quite possible, of course, that the gamma-rays are derived from neutral mesons which are emitted at the same time as the charged ones and which have an extremely short half-life; this point certainly cannot be decided from these data. It is important, in any case, that there seems to be no necessity of having electrons emitted directly at the same time that the mesons are created.

In Table VI are compared the average projected angles for electronic events and for identified penetrating particles; the angles are with respect to the direction of the primary particle initiating the parent event. It is seen that the average projected angle at which electronic events occur is significantly smaller than the average projected angle for the observed penetrating particles. Since practically all of the electronic events were observed by means of the lead plates, and since classification of a particle as penetrating depended on its penetrating the lead plates,

[7] R. T. Birge, Rev. Mod. Phys. 19, 298 (1947).

the distributions in angle of the two types of events should be strictly comparable.

It must be remembered, however, that the penetrating component consists both of protons and of mesons. Since the mass of the proton is some six times that of the meson, it is to be expected that the angular distribution of the protons alone should be somewhat more widespread than that of the mesons alone. If the gamma-rays do in fact arise from neutral mesons, which will be assumed to be emitted in the same way as either positive or negative mesons in the absence of definite evidence to the contrary, then the angular distribution of the charged mesons alone would be the same as that of the electronic events, with $\bar{\theta}=8°$. Now if it be supposed that the mesons constitute a certain fraction of the observed penetrating particles, then the average projected angle of the remaining

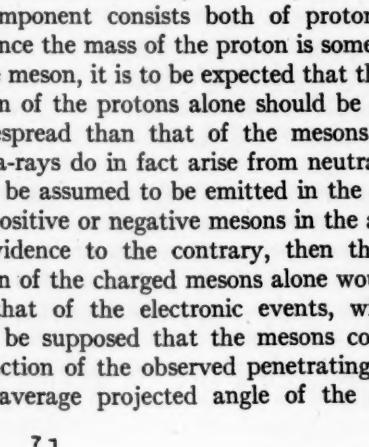

FIG. 8. Distribution of the projected angles made by lightly ionizing secondary particles with respect to the direction of the primary particle, normalized to an area of 100 particles.

particles, protons, can be readily calculated. If the mesons make up one-half of the penetrating particles, then the average projected angle for the protons alone is 16°; if the mesons are three-fourths of the penetrating particles, the average projected angle for protons alone is 24°. Hence the average projected angle for the protons would be about two to three times as large as that of the mesons; this is a reasonable ratio in view of the masses of the particles.

7. Comparison with Data Obtained in Lead

Using the same cloud chamber with sixteen $\frac{1}{2}$-in. lead plates, Fretter[6] obtained values for the multiplicity of penetrating particles produced in penetrating showers as well as the angular distribution with which they were emitted. The original data obtained by Fretter at Tioga Pass, California, elevation 3027 meters, were treated in the same way as the data obtained in this experiment for more certain comparison.

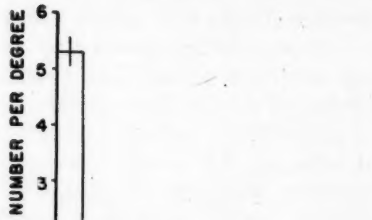

FIG. 9. Distribution of the projected angles made by penetrating secondary particles with respect to the direction of the primary particle, normalized to an area of 100 particles, from data of Fretter for events produced in lead.

Earlier in this paper it was shown that the projected angular distribution for lightly ionizing secondary particles from events in carbon could be compared, to a good degree of approximation, to the projected angular distribution of penetrating particles from events in lead. It was found that the distribution obtained by Fretter for penetrating particles was identical, within the experimental errors, with the distribution obtained in this experiment for lightly ionizing secondaries. It was therefore concluded that the events observed in the two experiments are of closely the same energy and that, therefore, other values obtained from the two experiments—in particular, the multiplicities—can be validly compared.

The value of the multiplicity found in this experiment that is to be compared to the average multiplicity of penetrating particles as observed in a cloud chamber containing only lead plates was shown previously to lie between 3.16 ± 0.25 and 3.61 ± 0.25. The average multiplicity of penetrating particles obtained by Fretter is 3.79 ± 0.14. The agreement between the two experiments is striking. A further similarity is found in the largest number of penetrating particles observed to be produced in what appears to be single events. The highest multiplicity of penetrating particles observed by Fretter was eleven. Although there is no way of correcting the number of observed penetrating particles in this experiment for a single event, a rough comparison can be made simply by using the highest multiplicity of penetrating particles that was observed, which is equal to ten particles.

The very close agreement of the data obtained in carbon with those obtained in lead implies that the penetrating showers observed in the two substances are nearly identical in regard to high energy penetrating particles for the energy range observed.

Comparison should also be made of the multiplicities of heavily ionizing particles observed in carbon with those in lead. It is difficult, however, to know just

what values should be compared. An ionizing particle loses so much more energy in traversing about $\frac{1}{2}$ in. of lead (14.4 g/cm²) than in traversing about 1 in. of carbon (4.3 g/cm²) that it is likely that many particles which would have been observed as heavily ionizing particles emerging from a carbon plate would fail to get out of a lead plate. On the other hand, particles which emerge with close to minimum ionization and stop in the carbon would, in some cases, be identified as heavily ionizing particles if the event had occurred in a lead plate. Another basis for comparison would be to consider only those cases in which at least one heavily ionizing particle is observed to emerge from the lead, assuming that if one such particle can get out of the plate, then any others will have a good possibility of doing so also. Since any events in which there were no heavily ionizing particles emitted would not be included in this selection, the multiplicities obtained in this way should be compared to those in carbon for events that also had at least one heavily ionizing particle or at least one lightly ionizing particle that stops in the carbon. The multiplicities obtained for these various methods of selection are listed in Table VII. In every case the multiplicities of heavily ionizing particles from events in lead plates are larger than the possibly comparative values in carbon plates. In addition, up to six heavily ionizing particles were seen to leave an event in lead whereas the largest number observed in carbon was only three. If these heavily ionizing particles are largely protons, then the difference may be due to the far greater probability of obtaining a number of low energy protons (and neutrons) by elastic collisions in the case of showers produced in lead. However, the uncertainty in determining any strictly comparable values for carbon and for lead would make it impossible to draw any exact conclusions regarding this.

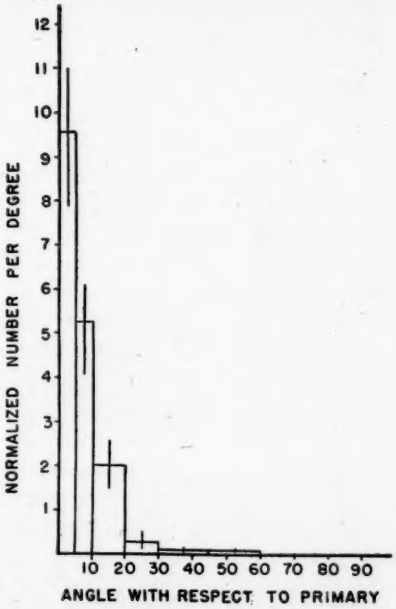

FIG. 10. Distribution of the projected angles made by those secondary particles that subsequently produce secondary penetrating showers in the carbon plates with respect to the direction of the primary particle, normalized to an area of 100 particles.

TABLE III. Average projected angle and root-mean-square projected angle for lightly ionizing secondary particles from events in carbon and for penetrating secondary particles from events in lead as obtained by Fretter.

	Average angle	R.m.s. angle
Lightly ionizing particles in carbon	20.0±1.0°	34°
Fretter's values for penetrating particles in lead	17.7±1.4°	28°

There is nothing to be gained in trying to compare the total multiplicities in the two experiments since the production of electron showers in the same lead plate that contains the origin of the penetrating shower event would render any comparisons invalid.

8. Multiplicities of Particles Produced

The average multiplicity of all ionizing particles produced in penetrating showers in carbon is about 5.3. Of this, about 0.1 is contributed by electrons, leaving a multiplicity of 5.2 ionizing particles emitted per event; these particles are assumed to be protons and charged pi-mesons, although a few unidentifiable electrons may be included (Section III.3). If the average event consists of a single nucleon-nucleon interaction, then, in general, two nucleons will be emitted from the event; but, considering only charged primaries, there is a probability of 0.5 in carbon that one of the outgoing nucleons will be a neutron, if the assumption be made that the p-p and p-n cross sections are equal. Then a multiplicity of 1.5 is due to protons (about one-fourth of the particles), leaving a multiplicity of 3.7 for charged mesons. If the ratio of neutral to charged mesons is 1:2, then there will have been a total of 5.5 mesons emitted from the average event, of which about 1.8 are neutral. If the neutral mesons are of such short half-life that they decay before emerging from the plate in which they were produced, then 3.6 gamma-rays should be produced per event. The estimated number of 0.85 ±0.85 gamma-ray per event obtained previously from the experimental data does appear to be significantly lower than the number of 3.6 just arrived at. However, the correctness of the assumptions which entered into the estimation of 3.6 gamma-rays being produced (and observed) per event is quite indeterminate, and there is no compelling reason to believe this value.

IV. COMPARISON WITH THEORY

The multiplicity of particles observed to occur in penetrating showers in carbon is easily accounted for by any of the theories of multiple production of mesons, such as those of Lewis, Oppenheimer, and Wouthuysen,[8]

[8] Lewis, Oppenheimer, and Wouthuysen, Phys. Rev. 73, 127 (1948); H. W. Lewis, Phys. Rev. 76, 566 (1949).

TABLE IV. Distribution of electronic events by plate of origin of parent penetrating shower event (i) and by separation of the electronic events from the parent events (j) in units of plates.

i	j	(0)	1	2	3	4	5	6	7	8	9	Totals
1		(3)	1	2	2	2	0	1	1	1	1	14
2		(3)	0	4	1	0	0	1	1	0		10
3		(1)	0	5	5	0	0	2	2			15
4		(0)	2	0	2	3	2	0				9
5		(0)	2	3	1	0	0					6
6		(3)	3	4	3	0						13
7		(4)	4	0	3							11
8		(6)	4	0								10
9		(1)	2									3
10		(2)										2
Totals		(23)	18	18	17	5	2	4	4	1	1	93

TABLE V. Distribution of number of electronic events per parent event by plate of origin of parent event (i) and by separation of electronic event from parent event (j).

i	j	(0)	1	2	3	4	5	6	7	8	9
1		(0.158)	0.053	0.105	0.105	0.105	0	0.053	0.053	0.053	0.053
2		(0.177)	0.0	0.236	0.059	0.0	0	0.059	0.059	0	
3		(0.035)	0	0.172	0.172	0	0	0.069	0.069		
4		(0)	0.062	0.0	0.062	0.094	0.062	0			
5		(0)	0.071	0.107	0.036	0	0				
6		(0.077)	0.077	0.103	0.077	0					
7		(0.148)	0.148	0	0.111						
8		(0.118)	0.078	0							
9		(0.024)	0.049								
10		(0.051)									
Averages		(0.079)	0.060	0.090	0.089	0.033	0.012	0.045	0.060	0.026	0.053
Errors±		(0.020)	0.014	0.029	0.016	0.019	0.012	0.013	0.004	0.018	0.053

of Heisenberg,[9] and of Leprince-Ringuet.[10] Comparison with the predictions of the plural production theory is more involved and will be discussed in greater detail.

Heitler and Jánossy[11] have applied the damped model of the theory proposed by Hamilton, Heitler, and Peng,[12] in which only one meson is produced in a single nucleon-nucleon interaction, to find the mean free path of meson-producing nucleons in nuclear matter. They find that once the primary nucleon enters a nucleus, it has a good chance of interacting with more than one of the nucleons of the nucleus. If the mean free path is small enough, it is possible to obtain any observed multiplicity of mesons from any complex nucleus without requiring that more than one meson be produced in a single interaction. The mean free path derived by Heitler and Jánossy would require, however, that the average multiplicity of mesons produced in carbon nuclei be appreciably smaller than that of mesons produced in lead. But it has been seen earlier that the penetrating showers observed in carbon are very closely the same as those in lead. This similarity, of course, could be explained by making the mean free path for interaction in nuclear matter still smaller, and by assuming that a saturation effect had already set in even for carbon, so that all of the meson-producing ability of the primary particle had been used up. In this case, then, the penetrating showers produced in carbon and in lead would be expected to be identical. However, reference to Fig. 10 will show that the particles from penetrating showers that initiate subsequent nuclear interactions are emitted with an extremely strong preference for the direction of the particle which initiated the shower from which they came. From this it can be inferred that a particle which initiates a subsequent penetrating shower is probably either the original high energy nucleon, or a nucleon resulting from a head-on collision with the primary nucleon; in addition, it will be noted that the occurrence of two generations of penetrating showers within the cloud chamber not only in carbon, but also in lead, is not an infrequent event. This would not be in accordance with an assumed saturation effect.

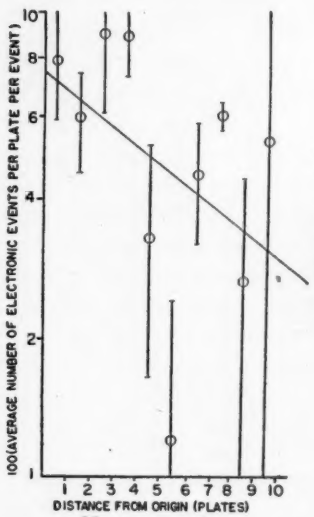

FIG. 11. Logarithm of the average number of electronic events produced per plate per parent event as a function of the separation of the electronic event from the parent event in plates.

The theories of multiple meson production have been concerned only with the single nucleon-nucleon interaction from which several mesons can arise. It is clear that if either the primary nucleon or the nucleon with which it has collided possesses sufficient energy after the collision, it will be possible to have another interaction take place within the same nucleus. Recently evidence has been obtained from very high energy stars in photographic plates that some such plural-multiple process may occur.[13] The frequency of occurrence, naturally, will depend on the mean free path for interaction with nuclear matter; at present, however, there is no reliable evidence to indicate just what the value of this mean free path should be.

In connection with this experiment, it should be

[9] W. Heisenberg, Nature **164**, 67 (1949); Zeits. f. Physik **101**, 533 (1949); **113**, 61 (1939).

[10] Peyrou, d'Espagnat, and Leprince-Ringuet, Comptes Rendus **228**, 1777 (1949).

[11] W. Heitler and L. Jánossy, Proc. Phys. Soc. **A62**, 374, 669 (1949).

[12] Hamilton, Heitler, and Peng, Phys. Rev. **64**, 78 (1943); W. Heitler, Proc. Camb. Phil. Soc. **37**, 291 (1941); W. Heitler and H. W. Peng, Proc. Camb. Phil. Soc. **38**, 296 (1942).

[13] Feld, Lebow, and Osborne, Phys. Rev. **77**, 731 (1950); Kaplon, Peters, and Bradt, Phys. Rev. **76**, 1735 (1949); Leprince-Ringuet, Bousser, Hoang-Tchang-Fong, Janeau, and Morellet, Phys. Rev. **76**, 1237 (1949), Comptes Rendus **229**, 163 (1949).

again noted that a 1-in. plate of carbon is only 4.3 g/cm², whereas a ½-in. plate of lead is 14.4 g/cm²; since even a fast singly charged particle loses about 2 Mev/g/cm², it is possible that some lower energy particles have been observed in the case of carbon that would not have been counted in the case of lead. If this be so, then the true multiplicity of penetrating showers observed in lead may be slightly greater than that of penetrating showers generated in carbon, the difference being attributed to an occasional two or even three step cascade process in the lead nucleus. Contrary to this argument is the belief that, if anything, the corrected number of penetrating particles from the events in carbon was underestimated. In any case, however, it seems unlikely that if such cascade production processes occurred in lead nuclei with an appreciable frequency, such a close correspondence would have been observed between the penetrating showers produced in carbon and those in lead.

V. SUMMARY OF CONCLUSIONS

The penetrating showers generated in carbon have been shown to be closely the same in angular distribution and in average multiplicity of penetrating particles as those produced in lead. Penetrating showers produced in the carbon plates were followed not infrequently by the production of secondary penetrating showers farther down in the carbon; the initiating particles of the subsequent showers are very closely aligned with the direction of the primary particle of the parent penetrating shower. The mean free path of the lightly ionizing secondary particles of the penetrating showers for subsequent production of nuclear events has been found to be 237±29 g/cm² carbon. This value is for a mixture of particles, some of which do not produce observable secondary events. If it be assumed that only the nucleonic component (mostly protons) contribute secondary events, with a cross section near that of the geometrical area, then it can be deduced that about one-quarter of the lightly ionizing secondary particles are nucleonic.

The electronic cascades observed to be produced at the same time as the penetrating component can be satisfactorily explained in order of magnitude by assuming that they are produced by high energy gamma-rays which originate at the event or which may be derived from the fast decay of neutral mesons very near the original event.

I wish to thank Professors W. B. Fretter and R. B. Brode for the advice and assistance that they have generously given. The assistance of Merritt L. MacKnight, Bruce J. Harris, George Plummer, and Andrew Yeiser in constructing and operating the equipment is also gratefully acknowledged. Appreciation should also be expressed for the facilities made available at the White Mountain Laboratory by the Office of Naval Research and for the interest shown by Commander Eugene Bollay. During the course of this experiment, the author was, in order, Westinghouse Fellow and Whiting Fellow in Physics at the University of California.

TABLE VI. Average projected angle and root-mean-square projected angle for electronic events and for penetrating particles with respect to primary.

Type	Average angle	R.m.s. angle
Electronic events	8.3±1.7°	12°
Penetrating particles	12.0±0.8°	17°

TABLE VII. Comparison of various average multiplicities of heavily ionizing particles from events in carbon and in lead.

In carbon:	
1. Heavily ionizing particles	
(a) From all events	0.5
(b) Only from events in which heavily ionizing particles were observed	1.3
2. Heavily ionizing particles plus lightly ionizing particles that stop in carbon	
(a) From all events	0.6
(b) Only from events in which at least one of these particles was observed	1.4
In lead:	
1. Heavily ionizing particles	
(a) From all events	1.3
(b) Only from events in which heavily ionizing particles were observed	2.0

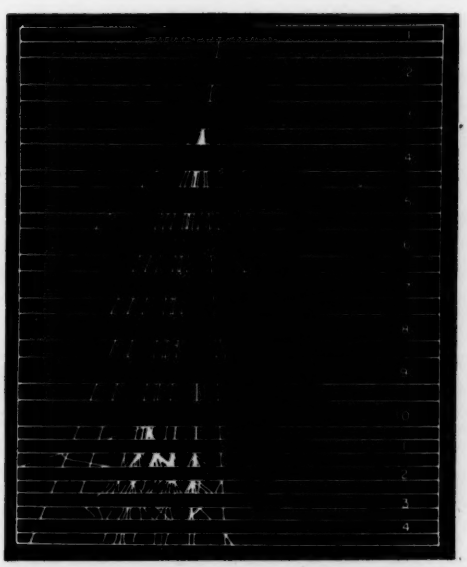

FIG. 12. This is an illustrative event, reproduced as a line drawing for greater clarity. An ionizing particle produces a penetrating shower in the third carbon plate. Of the eight ionizing particles that are emitted, four can be seen to penetrate the lead plates at the bottom; one particle goes out of the illuminated region, and two particles are lost in the electron tracks under the first lead plate. The remaining particle produces a secondary event in the tenth carbon plate. From the secondary event there emerge two penetrating particles, one heavily ionizing particle, and a fourth particle that is lost among the electrons. Creation of electron pairs that generate small cascade showers in the lead plates are seen to occur in the ninth and tenth carbon plates.

Total Cross Sections of Nuclei for 42-Mev Neutrons*

ROGER H. HILDEBRAND AND CECIL E. LEITH
Radiation Laboratory, Department of Physics, University of California, Berkeley, California
(Received July 24, 1950)

Total cross sections of 33 elements for 42-Mev neutrons have been measured using the 184-inch cyclotron as a source of neutrons and the $C^{12}(n,2n)C^{11}$ reaction as a detector. Experimental details are described and the results are compared with those measured at other energies.

I. INTRODUCTION

THE measurements of total neutron nuclear cross sections[1,2] at 90 Mev showed effects interpretable in terms of nuclear transparency,[3] whereas measurements at[4] 14 Mev and at[5] 25 Mev are interpretable in terms of an opaque nucleus.[6] The $C^{12}(n,2n)C^{11}$ reaction as a neutron detector provides a simple method for measuring cross sections at an intermediate energy. The 40-Mev neutron beam intensity from the 184-inch cyclotron operated at reduced radius is sufficient to permit accurate cross-section measurements of a large number of elements in a relatively short time with the detector 15 meters from the source.

II. GENERAL FEATURES OF THE EXPERIMENT

The 42-Mev total cross sections were obtained by good geometry attenuation measurements using essentially the same method as was used by Cook, McMillan, Sewell and Peterson[1] at 90 Mev.

The neutron beam, produced by deuteron stripping in the cyclotron target strikes an attenuator (the material being investigated) about 5 meters from the target. The incident beam activates a monitor placed just outside of the cyclotron tank and the transmitted beam activates a detector which is placed about 10 meters beyond the attenuator (Fig. 1).

The fundamental measurement in this work is the ratio, r, of detector to monitor activity. This ratio

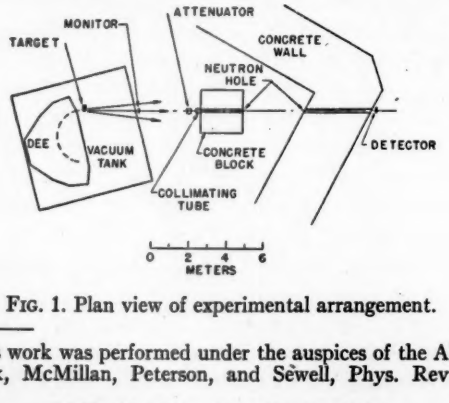

FIG. 1. Plan view of experimental arrangement.

should vary exponentially from some initial value r_0 to zero as the thickness of attenuator is varied from zero to infinity. A barely detectable background r_B persists, however, when an "infinite" attenuator consisting of 45 cm of copper is used. This amount of copper should transmit only about 10^{-4} of the incident flux which would be entirely beyond detection; hence the background must not be due to neutrons which have passed through the attenuator. Possible sources of this background are neutrons scattered by the vacuum tank wall and neutrons formed when the circulating cyclotron beam hits the dee. If, corresponding to attenuator thicknesses 0, x, and "infinity," we measure ratios of detector to monitor activity r_0, r, and r_B the transmission T of a sample of thickness x is given by

$$T=(r-r_B)/(r_0-r_B),$$

and the cross section is calculated from T using the relation,

$$\sigma=(-A/N\rho x)\ln T,$$

where $A/N\rho x$ = number of atoms per square centimeter.

III. NATURE OF SOURCE AND DETECTOR, MEAN DETECTION ENERGY

The neutron source is a 1.27 cm thick Be target bombarded by deuterons at a cyclotron radius of 55 in. where the magnetic field is 14.5 kilogauss. The neutron flux density from this target is of the order of 10^5 neutrons cm^2 $sec.^{-1}$ at the detector.

The energy distribution of the neutron beam is calculated from the deuteron stripping theory of Serber[7] taking into account the energy loss of the deuterons in the target. No experimental information exists on the energy distribution of the neutron beam at 40 Mev; however, measurements of both the angular distribution[8] and the energy distribution[9] at 90 Mev have demonstrated the validity of the stripping theory. This calculated neutron energy distribution is shown in Fig. 2 as curve A.

The neutrons were detected by measuring the activity they induced in carbon disks by the reaction $C^{12}(n,2n)C^{11}$. The manner in which the sensitivity of this detector varies with the neutron energy has not

* This work was performed under the auspices of the AEC.
[1] Cook, McMillan, Peterson, and Sewell, Phys. Rev. 75, 7 (1949).
[2] DeJuren and Knable, Phys. Rev. 77, 606 (1950).
[3] Fernbach, Serber, and Taylor, Phys. Rev. 75, 1352 (1949).
[4] Amaldi, Bocciarelli, Cacciapuoti, and Trabacchi, Nuovo Cimento 3, 203 (1946).
[5] R. Sherr, Phys. Rev. 68, 240 (1945).
[6] H. Feshbach and V. F. Weisskopf, Phys. Rev. 76, 1550 (1949).
[7] R. Serber, Phys. Rev. 72, 1008 (1947).
[8] Helmholz, McMillan, and Sewell, Phys. Rev. 72, 1003 (1947).
[9] Hadley *et al.*, Phys. Rev. 75, 351 (1949).

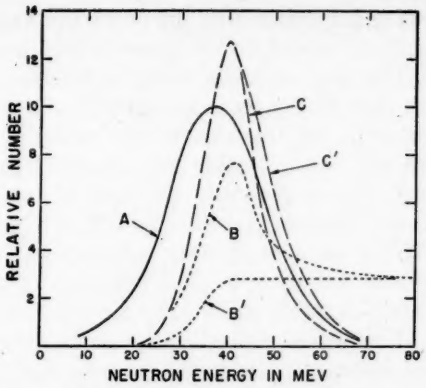

FIG. 2. Detection efficiency (see text).

been measured. The result of a theoretical calculation[10] of this function is shown in Fig. 2 as curve B. The related theoretical calculation[10] of the reaction $C^{12}(p,pn)C^{11}$ has been confirmed experimentally.[11,12] A measurement of the $C^{12}(n,2n)C^{11}$ cross sections averaged over the 40-Mev and the 90-Mev neutron energy distributions have shown them to be approximately the same.[13] Hence the peak in the theoretical curve B is probably too large with respect to the higher energy part of the curve whereas the arbitrary curve B', which has the same shape as B to the left of the peak except for a scale factor, is probably too low in the 40-Mev region. The product curves $C=A\times B\times$(constant) and $C'=A\times B'\times$(constant) show the extent to which the expected energy distribution of the detected neutrons depends on the excitation function assumed. The constants have been adjusted to make C and C' coincide to the left of the peak. The mean detection energies corresponding to C and C' are 41.3 and 43.2 Mev. Since B and B' are believed to be limiting curves the true energy distribution of detected neutrons is assumed to lie between C and C' with a mean energy of about 42 Mev.

IV. APPARATUS AND EXPERIMENTAL PROCEDURE

The detectors were carbon disks 4.3 cm in diameter and 0.32 cm thick with a density of 1.59 ± 0.02 g/cm^3. One such disk was used as a monitor of the incident beam and two were used as detectors of the transmitted beam. During bombardment the disks were placed in aluminum holders which were fixed in the positions indicated in Fig. 1. At the end of the run the (20 min.) β^+-activity was counted on mica-window Geiger-Müller counters. The counts of the two detector disks were added. All counts were made concurrently; i.e., the detector and monitor activities were counted over the same time interval eliminating the necessity of corrections for decay.

A typical determination of r_0 (see Section II) involved about 20,000 net counts from the detector disks in a period of 15 minutes. This is about 100 times the counter background and about 3 times the net count in determining r for a typical attenuator. In determining r_B a typical detector count was 500 of which 460 were counter background.

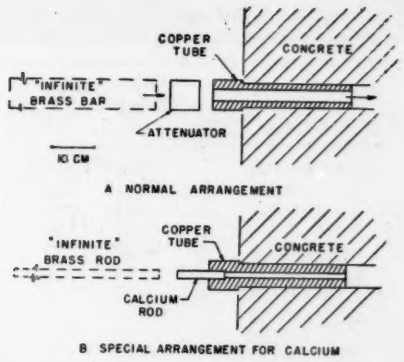

FIG. 3. Detail of collimating system and absorber.

A 2.5 cm i.d. copper collimating tube was placed just behind the attenuator as shown in Fig. 3. This was to prevent neutrons from reaching the detector unless they had passed through the attenuator. Because of the divergence of the beam, its diameter at the detector was about 7 cm hence the detectors could be placed entirely within the beam. The alignment of the apparatus was checked before each series of runs using x-ray films exposed in the beam. The equipment was adjusted so that the shadow of a small object in the attenuator position and the circular spot transmitted by the collimator were centered on the detector position.

The absence of spurious counts was demonstrated by the exponential nature of attenuation curves which were made (Fig. 4) and by the barely detectable background which was observed when the "infinite" attenuator was used.

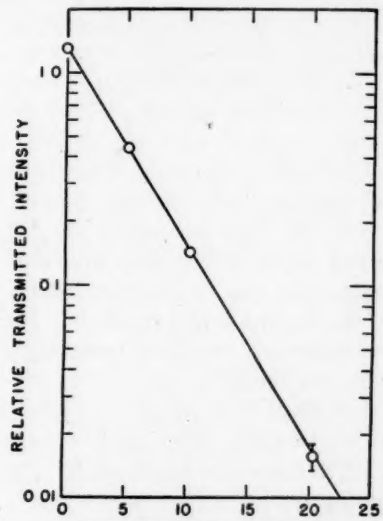

FIG. 4. Attenuation of 40-Mev neutrons in copper.

[10] W. Heckrotte and P. Wolff, Phys. Rev. 73, 264, 265 (1948).
[11] W. W. Chupp and E. M. McMillan, Phys. Rev. 72, 873 (1947).
[12] E. M. McMillan and R. D. Miller, Phys. Rev. 73, 80 (1948).
[13] R. L. Mather and H. F. York, unpublished.

TABLE I. Cross sections of elements. (The errors shown are standard deviations calculated from the counting statistics alone.)

Element	Form[a]	σ_i in barns	Z Atomic number	M Atomic weight	$M^{\frac{1}{2}}$	$R=(\sigma_i/2\pi)^{\frac{1}{2}}$ in units of 10^{-12} cm
H	d	0.203±0.007	1	1.008	1.00	0.180±0.003
D	d	0.289±0.013	1	2.015	1.26	0.214±0.005
Li	s	0.684±0.011	3	6.940	1.91	0.330±0.003
Be	s	0.853±0.010	4	9.02	2.08	0.368±0.002
B	p	0.985±0.020	5	10.82	2.21	0.396±0.004
C	d	1.089±0.011	6	12.01	2.29	0.416±0.002
N	$d(p)$	1.220±0.025	7	14.008	2.41	0.441±0.005
O	d	1.358±0.012	8	16	2.52	0.465±0.002
F	$d(p)$	1.603±0.030	9	19.000	2.67	0.505±0.005
Na	$d(p)$	1.67 ±0.06	11	22.997	2.84	0.515±0.009
Mg	s	1.723±0.024	12	24.32	2.90	0.524±0.004
Al	s	1.782±0.020	13	26.97	3.00	0.532±0.003
S	d	1.974±0.030	16	32.06	3.18	0.560±0.004
Cl	d	2.11 ±0.04	17	35.457	3.29	0.579±0.005
Ca	s	2.210±0.026	20	40.08	3.42	0.592±0.004
Fe	s	2.441±0.021	26	55.85	3.82	0.623±0.003
Ni	s	2.510±0.034	28	58.69	3.88	0.632±0.004
Cu	s	2.540±0.019	29	63.57	3.99	0.636±0.003
Zn	s	2.618±0.027	30	65.38	4.03	0.646±0.003
Br	d	2.93 ±0.06	35	79.916	4.30	0.682±0.007
Sr	$d(p)$	2.99 ±0.12	38	87.63	4.44	0.690±0.014
Mo	s	3.11 ±0.05	42	95.95	4.58	0.703±0.006
Ag	s	3.229±0.034	47	107.880	4.76	0.716±0.004
Sn	s	3.251±0.023	50	118.70	4.91	0.719±0.003
I	d	3.51 ±0.06	53	126.92	5.03	0.747±0.006
Ba	$d(p)$	3.57 ±0.12	56	137.36	5.16	0.753±0.013
Ta	s	4.20 ±0.04	73	180.88	5.66	0.817±0.004
W	s	4.31 ±0.06	74	183.92	5.69	0.828±0.006
Hg	l	4.51 ±0.06	80	200.61	5.85	0.846±0.006
Pb	s	4.44 ±0.05	82	207.21	5.92	0.840±0.005
Bi	s	4.58 ±0.06	83	209.00	5.94	0.853±0.006
Th	s	5.03 ±0.07	90	232.12	6.14	0.894±0.006
U	s	5.12 ±0.07	92	238.07	6.20	0.902±0.006

[a] d = derived from measurements listed in Table II; s = solid; l = liquid; p = powder; $d(p)$ = derived from a powdered compound.

The substances which were used in the form of solid blocks were paraffin, Li, Be, C, Mg, Al, Ca, Fe, Ni, Cu, Zn, Mo, Ag, Sn, Ta, W, Pb, Bi, Th, U. In all cases except calcium (see below) the cross section of the attenuating block was much greater than the cross section of the collimator (2.54 cm diameter) just behind them, being 5 cm×7½ cm in most cases. The thickness of the attenuating blocks was made one to two mean free paths whenever this much material was available and was never less than half of a mean free path. In many cases the "blocks" were actually stacks of thin slabs placed normal to the beam. The Be, Sn, Pb, Bi, and Th were machined from castings while all the others except Li and Ca were machined from stock. Two samples each of Be, Sn, Pb, and Th were used to reduce the chance of error due to imperfect castings. In the case of Li, blocks which had previously been pressed in a die were accurately machined under liquid vaseline. Since calcium was available only in the form of a rough cathode rod of small cross section a special collimating system had to be used. The rod was machined to a diameter of 1.75 cm and a length of 16.5 cm and used as shown in Fig. 3.

The liquids used were Hg, O, CS_2, CCl_4, CH_2Br_2, CH_2I_2, H_2O, D_2O, and pentane. The Hg was contained in a rectangular aluminum can with the same cross section as that of the solid blocks and a length of 11 cm. The liquid oxygen container was a stainless steel tank with a 13 cm×13 cm cross section and a length of 38 cm. This tank was surrounded by asbestos so that there was very little boiling and almost none in the region near the long axis of the tank through which the detected neutrons passed. The CS_2, CCl_4, CH_2Br_2, and CH_2I_2 were contained in glass tubes 3 cm in diameter and 14 cm in length. The ends of the glass tubes were ¼-in. plate glass and were made accurately parallel. The water, heavy water and pentane were contained in brass cylinders 34 cm long and 6½ cm in diameter. In each case the intensity corresponding to zero attenuator thickness was measured using the appropriate empty container.

The powdered substances used were B, melamine ($C_3N_6H_6$), S, LiF, NaCl, $SrCO_3$ and $BaCO_3$. These powders were put into 3.6 cm diameter brass tubes 20 to 30 cm long with 0.2 cm thick aluminum ends and were packed as uniformly as possible over the cross section of the tube. To minimize errors due to non-uniform packing the tubes were refilled and, of course, reweighed before each run. At least two runs were made in every case.

V. RESULTS

Cross sections of all the elements investigated are given in Table I. Those marked "d" are derived from the measurements shown in Table II by averaging all independent determinations for each element. For example, the carbon cross section in Table I is the weighted average of three independent determinations: (1) directly measured carbon; (2) the carbon disulfide-powdered sulfur difference; (3) the hydrocarbon-hydrogen difference, where the hydrogen used was that obtained from the water-liquid oxygen difference.

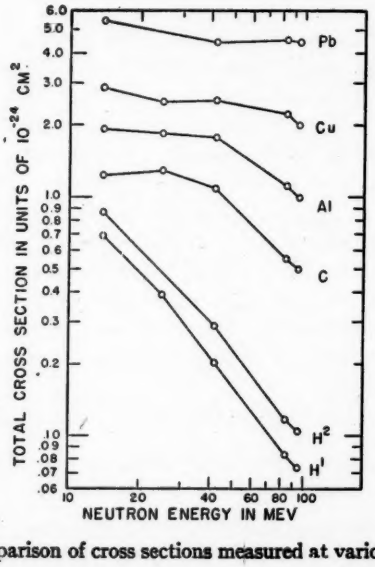

FIG. 5. Comparison of cross sections measured at various energies.

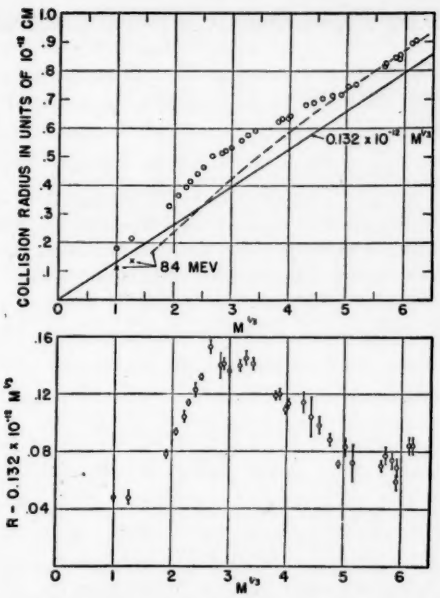

FIG. 6. Collision radii. The upper plot shows collision radii $R=(\sigma_t/2\pi)^{\frac{1}{2}}$ plotted against cube roots of atomic weights. Collision radii measured by Cook *et al.* at 84 Mev are represented by the dashed curve with radii of H and D shown separately. The points shown in the lower plot are obtained by subtracing $0.132\times10^{-12}M^{\frac{1}{3}}$ from the collision radii.

Figure 5 shows a comparison of several of the 42-Mev total cross sections given in this paper with those measured at 14 Mev,[4] 25 Mev,[5] 84 Mev,[1] and 95 Mev.[2] In the paper of Cook *et al.*[1] the energy is given as ". . . between 80 and 90 Mev." The figure 84 Mev given above is an estimate of the most probable value based on the references given in Section III. Additional measurements of hydrogen, deuterium and carbon have been made at energies below 25 Mev by several investigators.[14–16]

It is customary[1] to define a "collision radius" R by the expression

$$\sigma_t=2\pi R^2,$$

where σ_t is the measured total cross section. This definition based on the assumption of an opaque nucleus provides an estimate of the nuclear radius. Figure 6 shows collision radii plotted against the cube roots of the atomic weights. Collision radii obtained by Cook *et al.* at 84 Mev are represented by the dashed curve with radii of H^1 and H^2 shown separately. The points shown in the lower plot are obtained by subtracting $0.132\times10^{-12}M^{\frac{1}{3}}$ cm from the collision radii. This plot makes it possible to show the statistical errors associated with the points and shows the deviation of the points from a linear dependence on $M^{\frac{1}{3}}$.

TABLE II. Directly measured cross sections not listed in Table I. (The errors shown are standard deviations calculated from the counting statistics alone.)

Substance[b]	Form[a]	σ_t in barns
$CH_{2.08}$(paraffin)	s	1.510±0.031
$CH_{2.4}$(pentane)	l	1.568±0.018
H_2O	l	1.774±0.020
D_2O	l	1.935±0.023
N_2CH_2(melamine)	p	3.936±0.046
LiF	p	2.287±0.028
NaCl	p	3.777±0.045
C	s	1.092±0.011
S	p	1.985±0.036
CS_2	l	4.989±0.105
CCl_4	l	9.516±0.148
CH_2Br_2	l	7.361±0.106
$SrCO_3$	p	8.150±0.118
CH_2I_2	l	8.523±0.109
$BaCO_3$	p	8.731±0.109
O	l	1.353±0.014

[a] s=solid; l=liquid; p=powder.
[b] The cross sections refer to the formulas given, e.g., the "paraffin" cross section is that for one atom of C+2.08 atoms of H.

An analysis of the consistency of individual measurements has been made for two groups of data: first, a group of 65 measurements involving solid and liquid attenuators; and second, a group of 23 measurements involving powdered attenuators. The first group showed a spread just consistent with the errors due to counting statistics (given in the tables). The second group showed random errors eight percent greater than those expected from counting statistics alone. The larger spread in the powder measurements is assumed to be due to the difficulty in obtaining uniform packing of the powder tubes. This apparent random error raises the question of possible non-random packing errors hence the powder measurements are probably less reliable than the others.

The authors wish to thank Professor E. O. Lawrence and Dr. B. J. Moyer for their interest in this work. We also wish to thank Mr. James Vale and the cyclotron operating crew for their assistance.

[14] W. Sleator, Jr., Phys. Rev. **72**, 207 (1947).
[15] E. O. Salant and N. F. Ramsey, Phys. Rev. **57**, 1075 (1940).
[16] Ageno, Amaldi, Bocchiarelli, and Trabacchi, Phys. Rev. **71**, 20 (1947).

Changes in Conductivity of Germanium Induced by Alpha-Particle Bombardment

W. H. Brattain and G. L. Pearson
Bell Telephone Laboratories, Murray Hill, New Jersey
(Received August 7, 1950)

The bombardment of *n*-type germanium by alpha-particles from polonium first removes the conducting electrons at the rate of 78 per alpha-particle. After the electrons are gone conducting holes are introduced at the initial rate of 8.6 per alpha-particle. Some of these holes disappear with time at room temperature after bombardment is stopped, leaving only two conducting holes per alpha-particle. This change takes place only to the depth of penetration of the particles, namely 1.9×10^{-3} cm. The distribution of holes with depth is not uniform. The concentration rises from an initial value to a maximum at 1.4×10^{-3} cm depth and then falls to zero. The maximum is about 2.5 times the initial value and the integral under the curve is, of course, two holes per alpha-particle.

I. INTRODUCTION

THE extensive changes undergone by solid materials exposed to radiations of various types have been treated theoretically by Seitz.[1] Lark-Horovitz and his associates[2] have altered the conductivity of germanium by bombardment with nucleons. The mechanism involved was the production of defects or increased *p*-type conductivity as a result of the germanium atoms being displaced from their normal lattice positions by the incident nucleons. This paper[3] reports quantitative measurements on the change in conductance of an *n*-type germanium sample during bombardment with alpha-particles from polonium as well as relaxation changes in conductance immediately after stopping the bombardment. An analysis of these data yields values for the rate of change of conduction during the course of the experiment.

A thin slab of material was bombarded on one side and its conductance normal to the direction of bombardment was measured as a function of time. The conductance first decreased linearly, passed through a minimum, and then increased at a diminishing rate as long as the bombardment was continued. The germanium converted from *n*-type to *p*-type at the minimum conductance point. After the bombardment was stopped the conductance decreased with time in an asymtotic manner, reaching a final value somewhat larger than the value before bombardment.

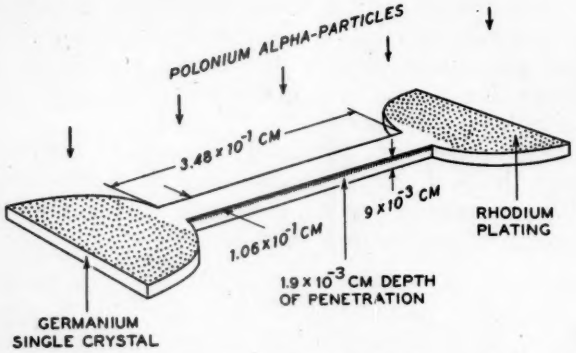

FIG. 1. Germanium single crystal for alpha-particle bombardment experiments.

The interpretation of this experiment is, of course, that the bombardment first removed the conducting electrons through the production of acceptors or traps and after conversion to *p*-type continuously increased the concentration of acceptors and thus conducting holes. Some of the germanium atoms, after being displaced from their normal lattice positions by alpha-particles, diffused back at room temperature while the remainder were fixed in their new positions. From an analysis of the data we obtain the following quantitative results: (1) at first when the bombarded layer is *n*-type, electrons are removed from the conduction band at the rate of 78 electrons per alpha-particle, (2) after conversion to *p*-type conducting holes are introduced at the rate of 8.6 per alpha-particle, and (3) 6.6 of these conducting holes decay with a half-life of 13 hours at room temperature and the remaining 2.0 holes are permanent at this temperature.

After the bombardment and the decay, the distribution in depth of the bombardment produced holes was determined by removing the outer material, a small amount at a time, and measuring the resultant conductance change. It was found that the density of holes is greater near the end of the alpha-particle range than close to the surface, the ratio being 2.5. This is to be expected since it is similar to that found for alpha-particle ionization as a function of range in gases. The total range of polonium alpha-particles in germanium was measured as 1.9×10^{-3} cm.

II. REMOVAL OF CONDUCTION ELECTRONS IN *n*-TYPE GERMANIUM

The general conditions of the experiment are shown in Fig. 1. The sample was made from a single crystal[4] of high purity *n*-type germanium having a conductivity of 0.125 $(\text{ohm cm})^{-1}$. It was in the shape of a thin rectangular plate with the dimensions shown. Ohmic

[1] F. Seitz, Discussions Faraday Soc. No. 5, 271 (1949).
[2] W. E. Johnson and K. Lark-Horovitz, Phys. Rev. 76, 442 (1949).
[3] A preliminary account of this work was presented by the authors at the American Physical Society Meeting in Oak Ridge (March, 1950), Phys. Rev. 78, 646 (1950).
[4] G. K. Teal and J. B. Little, Phys. Rev. 78, 647 (1950).

contact was made to the enlarged ends of the sample with rhodium electroplating.

The alpha-particle source was a square polonium capsule 0.41 cm on a side. The germanium was placed 2 cm away from the source so that the alpha-particles entered the sample at no greater than 12° from the normal. The energy of the particles was 5.3 Mev and the experiment was performed in an evacuated chamber to prevent any reduction in speed of the particles before striking the germanium. The polonium source as calibrated by A. J. Ahearn on April 22, 1949 emitted 1.82×10^{10} alpha-particles per unit solid angle per hour. The actual experiment was performed between March 21 and March 28, 1949, at which time the activity was calculated to be 2.1×10^{10} alpha-particles per solid angle per hour for a polonium half-life of 140 days. This corresponds to 1.9×10^{8} alpha-particles per hour striking the effective portion of the germanium sample.

Figure 2 is a plot of the conductance Y in mhos ($Y=1/R$) *vs.* the time of bombardment for the first eight hours of the experiment. It can be seen that the conductance first decreased linearly at a rate of 7.2×10^{-5} mho per hour, reached a minimum after about three hours and then increased slowly thereafter. A test with a thermoelectric junction showed that the sample changed from *n*-type to *p*-type shortly after the minimum in conductance was reached.

A theoretical calculation by Bardeen[5] indicates that 5.3-Mev alpha-particles penetrate germanium to a mean depth of 1.9×10^{-3} cm. A major portion of the sample, as shown in Fig. 1, was therefore not effected and merely contributed a constant conductance in parallel with the bombarded layer. Since parallel conductances are additive in this geometry and since we are primarily interested in conductance changes this contribution was easily handled in the analysis.

The relation between conductance change dY and the change in the total number of conduction electrons

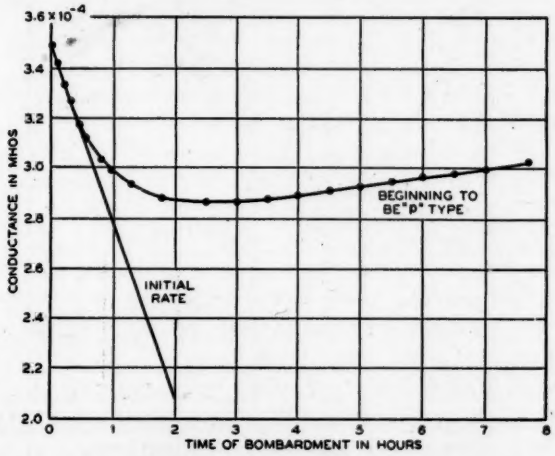

FIG. 2. Conductance *vs.* time characteristic for initial eight hours of bombardment.

[5] These calculations were based on the data of M. S. Livingston and H. A. Bethe, Rev. Mod. Phys. 9, 245 (1937).

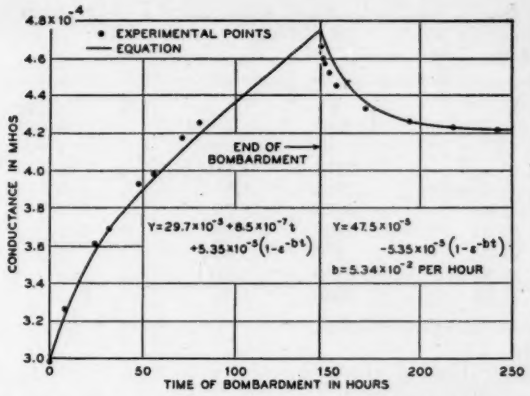

FIG. 3. Conductance *vs.* time characteristic for final 150 hours of bombardment and 100 additional hours of relaxation.

dN_e is

$$dN_e=l^2dY/e\mu_e=2.07\times10^{14}dY, \tag{1}$$

where l is the length of the sample, e the electronic charge (1.59×10^{-19} coulomb), and μ_e the drift mobility of electrons in germanium[6] which has the value 3600 cm²/volts sec. The similar relation for conduction holes dN_h is

$$dN_h=l^2dY/e\mu_h=4.45\times10^{14}dY, \tag{2}$$

where μ_h the drift mobility of holes[6] is 1700 cm²/volt sec.

The initial rate of conductance decrease as shown in Fig. 2 is $dY/dt=7.2\times10^{-5}$ mho per hour. The rate of arrival of alpha-particles as determined by the source calibrated is $dN_\alpha/dt=1.9\times10^{8}$ per hour. Substituting these values in Eq. (1) we find that

$$dN_e/dN_\alpha=78 \text{ electrons per alpha-particle.}$$

Thus in the initial stage of the bombardment each alpha-particle impact removed, on the average, 78 conduction electrons from the *n*-type germanium sample.

This part of the experiment yields data from which the approximate depth of penetration of the alpha-particles can be calculated. The conductance Y is given by

$$Y=\sigma wd/l, \tag{3}$$

where σ is the electrical conductivity and l, w, and d are the sample length, width, and thickness, respectively.

$$\Delta Y=wd\Delta\sigma/l, \tag{4}$$

has the value 6.3×10^{-5} mho as determined from the initial value and the minimum value of Fig. 2. $\Delta\sigma$ is the difference between the initial conductivity (0.125 mho/cm) and that of intrinsic germanium at 296°K (0.014 mho/cm) or 0.11 mho/cm. If the effect of the bombardment is non-uniform the left-hand side of Eq. (4) will be less than the right so that

$$d\geqq l\Delta Y/w\Delta\sigma. \tag{5}$$

[6] Pearson, Haynes, and Shockley, Phys. Rev. 78, 295 (1950).

TABLE I. Resistance R and conductance Y of the bombarded germanium sample after etching layers of thickness x from its surface.

x (cm)	R (ohms)	Y (mhos)	Y (corrected) (mhos)
0	2411	4.15×10^{-4}	4.15×10^{-4}
3.50×10^{-4}	2502	3.99	3.99
7.00	2673	3.75	3.79
10.50	2897	3.45	3.52
14.00	3270	3.06	3.13
17.50	3740	2.67	2.76
21.00	3940	2.54	2.65

Substitution of the numerical values in this equation gives $d \geqq 1.83\times10^{-3}$ cm, which is consistent with Bardeen's calculated value of 1.9×10^{-3} cm. In another experiment on a similarly bombarded sample the thickness of the converted p-type layer was found to be 2.0×10^{-3} cm by testing with a thermoelectric junction.

The final calculation to be made from the data of Fig. 2 is the average rate of formation of traps plus acceptors near the filled band up to the time at which p-type conductivity definitely appears which we take as four hours. The total number of conduction electrons at the start of the experiment can be determined from the conductivity relation,

$$\sigma = ne\mu_e, \tag{6}$$

where n is the number of conduction electrons per cm³. Substitution of the numerical values gives $n=2.17\times10^{14}$ and $N_e = n\times\text{volume} = 1.5\times10^{10}$ conduction electrons so that

$$dN_{(T+A)}/dN_a = (1.5\times10^{10})/(4\times1.9\times10^{8}) = 19.$$

III. PRODUCTION AND RELAXATION OF CONDUCTION HOLES IN p-TYPE GERMANIUM

After the data shown in Fig. 2 were obtained the alpha-particle bombardment was interrupted for 16 hours. During this period the conductance of the sample decreased from 3.02×10^{-4} to 2.97×10^{-4} mho. A second experiment was then performed in which the conductance of the sample was measured as a function of time during additional bombardment of the p-type layer for 150 hours after which bombardment was stopped and the conductance followed for a relaxation period of 100 hours. These data are plotted as experimental points in Fig. 3. We see that during bombardment the conductance Y increases rapidly at first and then at a slower rate. Finally, after the bombardment is stopped, the conductance decreases asymptotically with time and approaches a final value of 4.2×10^{-4} mho which is somewhat larger than the original value before bombardment.

It was found that these results could be explained if it were assumed that two processes were going on: One a production of holes proportional to time of bombardment, or number of alpha-particles, and another process in which the mechanism of hole production was proportional to the number of alpha-particles plus the additional assumption that this mechanism of hole production was decaying with time at a rate proportional to the number of holes present. Expressed in terms of conductance, one then has the two equations.

$$dY_1/dt = A \tag{7}$$

$$dY_2/dt = K - bY. \tag{8}$$

Integrating these two equations and adding the conductances we get:

$$Y = Y_1 + Y_2 = Y_0 + At + (K/b)(1-\epsilon^{-bt}) \tag{9}$$

for the equation of the curve during bombardment in Fig. 3. An easy way to determine the constants for Eq. (9) is to differentiate this equation and note that

$$(dY/dt) - A = K\epsilon^{-bt}. \tag{10}$$

The circles in Fig. 4 show the experimental data treated in this manner, indicating that the assumptions are reasonably well justified.

The critical test is whether the decay, after the bombardment is stopped, follows the equation:

$$Y = Y_0' + (K/b)\epsilon^{-bt}, \tag{11}$$

or

$$dY/dt = -K\epsilon^{-bt} \tag{12}$$

with, of course, the same values of K and b as determined for Eq. (10). The solid points in Fig. 4 show the experimental data obtained during the relaxation period treated according to Eq. (12) and it is seen that the results before and after bombardment do agree reasonably well. Using the constants determined from Fig. 4, namely $b=5.34\times10^{-2}$, $K=2.8\times10^{-6}$, and $A=8.5\times10^{-7}$ and also $Y_0=2.97\times10^{-4}$, the solid curve in Fig. 3 has been drawn using Eq. (9) during bombardment and

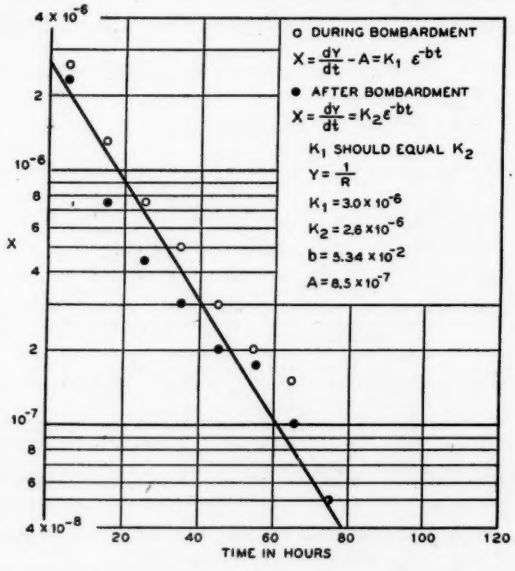

FIG. 4. The time rate of change of conductance during and after bombardment.

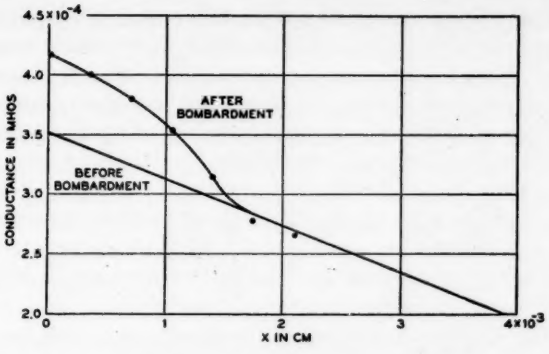

FIG. 5. Conductance of sample as successive layers are etched from the bombarded surface.

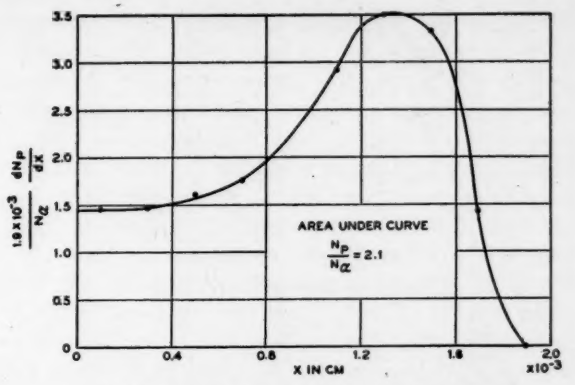

FIG. 6. Holes per alpha-particle per length of range as a function of the depth x.

Eq. (11) after bombardment. The solid curve does not fit the experimental points perfectly, but the agreement is quite good. It is known from other experiments that the fractional part that decays will increase with temperature and since room temperature during the experiment did fluctuate from about 22°C during the night to 26°C during the day, the agreement is probably as good as can be expected. From the above rate of decay one can calculate that the 16-hour wait before the start of this experiment was fortunately long enough for the sample to be reasonably near equilibrium at the start, otherwise the results would have been more complicated due to the previous bombardment.

From these values of A and K one gets the figures 2.0 holes per alpha-particle for that part which does not decay at room temperature, and 6.6 holes per alpha-particle for the part that decays at room temperature. From the value of b one gets 5.34×10^{-2} per hour per hole for the rate of this decay which corresponds to a half-life of 13 hours. Note that these rates say nothing about the number of acceptors themselves, but give only the rates for the net number of added and/or subtracted carriers or holes.

IV. HOLE CONCENTRATION *VS.* DEPTH

The next experiment was to measure the conductivity of the specimen as a function of thickness and determine the distribution of carriers in the sample as a function of depth after the bombardment and subsequent decay.[7] This was done by etching away successive layers starting from the bombarded side. The numerical results are given in Table I. It was necessary to correct for the reduction in width as both sides as well as the top face were exposed to the etchant. These corrected values of Y *vs.* x are plotted in Fig. 5. In this figure the solid straight line represents what the results of such an experiment would have been before bombardment. The experimental data approach the straight line when the amount removed approaches the penetration depth of the alpha-particles. Of course, the conductivity from $x=0$ to $x=1.9\times10^{-3}$ is now p-type where it was n-type before bombardment. By differentiating the smooth curve drawn through the experimental points and converting from changes in conductivity to changes in number of holes per total number of alpha-particles, one gets the curve in Fig. 6, giving the number of holes per alpha-particle per length of range as a function of depth x. The integral under this curve gives the total number of holes per alpha-particle as 2.1, which agrees reasonably well with the previous value of 2.0 for the part that does not decay. A uniform distribution of holes would have given a curve in Fig. 6 constant and equal to 2 up to 1.9×10^{-3} cm where it would drop to zero. A distribution such as that found here is to be expected, however, since it is of the same general shape as that for alpha-particle ionization in gases.

V. DISCUSSION

The experimental results described here are in qualitative agreement with the earlier study of Lark-Horovitz.[2] In addition our analysis of these data yield accurate quantitative values for a number of important parameters. One of these is the factor 78 for the number of conduction electrons removed by each impinging alpha-particle during the initial part of the experiment when the sample was n-type. This is in good agreement with the theoretical analysis of Seitz[1] which predicts 59 displaced germanium atoms for each impinging alpha-particle, suggesting that each displaced atom removes one conduction electron either by creating an acceptor level or a trap. Seitz's calculations were for 5.0-Mev alpha-particles whereas our polonium source emitted 5.3-Mev particles.

Our quantitative results suggest the following conclusions. At the start electrons are removed at the rate of 78 per alpha-particle. This process can be due to creation of either electron traps or acceptors most anywhere in the energy gap between the filled band and the conduction band. Such traps or acceptors would lower the Fermi level, thus draining out the electrons. In fact, this initial result might be expressed in terms

[7] This experiment was suggested by W. Shockley who predicted the distribution found here.

of the rate of lowering of the Fermi level. When this level has reached the halfway point, the conduction process is intrinsic. Now, however, before appreciable hole conductivity can occur, the Fermi level must be lowered still further to very near the top of the filled band. When this happens all the electrons must be in traps or acceptors near the top of the filled band. From the time at which hole conductivity shows up, about four hours in Fig. 2, one concludes that the rate of formation of this last group of levels is at least 19 per alpha-particle. This is twice the initial value for hole production. One can explain the latter fact several ways. Each alpha-particle produces 19 acceptor levels but they are so far above the filled band that only half of them are ionized to give holes at room temperature could be one explanation. The other possible explanations would involve a combination of electrons traps and acceptors near the top of the filled band or a combination of acceptors and hole traps or some combination of all three. The important point is that the p-type conductivity due to alpha-particle bombardment is not the simple case of the formation of acceptor levels each producing a conduction hole at room temperature.

The authors are indebted to J. Bardeen for assistance with the theory, to G. K. Teal for the preparation of the single crystal germanium sample, and to P. W. Foy and E. G. Dreher who prepared the sample and took many of the data. This research was carried out under the direction of W. Shockley, who made many suggestions during the course of the work.

PHYSICAL REVIEW VOLUME 80, NUMBER 5 DECEMBER 1, 1950

The High Energy Neutrons from the Disintegration of C^{13} by Deuterons*

J. E. RICHARDSON**
The Rice Institute, Houston, Texas
(Received August 3, 1950)

An excitation curve for the 5-Mev neutrons resulting from C^{13} bombarded by deuterons has been obtained for neutrons emitted at $0°\pm28°$ to the direction of the deuteron beam. The curve covers deuteron energies from 200 kev to 2.1 Mev. Resonances in the yield were observed at deuteron energies of 0.6, 0.9, 1.55, and 1.80 Mev with half-widths of 0.1, 0.4, 0.1, and 0.5 Mev respectively. These correspond to excited states in the intermediate N^{15} nucleus of 16.7, 16.9, 17.47, and 17.69 Mev.

I. INTRODUCTION

TWO groups of neutrons from the disintegration of carbon by deuterons were observed by Bonner and Brubaker[1] in 1936 and were attributed to the reaction:

$$C^{13}+H^2\rightarrow(N^{15*})\rightarrow N^{14}+n^1+Q_1. \quad (1)$$

By means of cloud-chamber measurements, they observed Q-values of 1.2 and 5.2 ± 0.4 Mev respectively for the two groups.

As natural carbon contains 99 percent C^{12} and only one percent of the C^{13} isotope, one would expect the relative intensity of neutrons from C^{13} to be very weak when a natural carbon target is bombarded by deuterons. Using such a target and a methane-filled cloud chamber, they observed the relative intensities of the 5.2- and 1.2-Mev groups from C^{13} and the -0.281 ± 0.003-Mev group[2] from C^{12} to be 1, 3, and 300 respectively.

In order to explain the 5-Mev gamma-rays from the disintegration of carbon by deuterons, Bennett, Bonner, Hudspeth, Richards, and Watt[3] looked for a third group of neutrons from reaction (1). They obtained a target which was enriched to 23 percent of C^{13} and found a low-energy group of neutrons with a Q-value of 0.4 ± 0.05 Mev.

A weak group of 50-cm protons from carbon was observed by Bower and Burcham,[4] and independently by Pollard.[5] These protons result from the reaction:

$$C^{13}+H^2\rightarrow(N^{15*})\rightarrow C^{14}+H^1+Q_2. \quad (2)$$

Bennett and Bonner[3] bombarded a target containing 23 percent of C^{13} with 1.00-Mev deuterons and found the Q value of this group of protons to be 6.09 ± 0.2 Mev. Using a target enriched to two percent C^{13}, they obtained an excitation curve for these protons with the counter placed at 90° to the direction of the deuteron beam. The curve showed a maximum at a deuteron energy of 1.55 Mev which may be interpreted as a resonance in the yield. This would indicate an excited state in the intermediate N^{15} nucleus at 17.47 Mev.

This group of workers also studied the 5-Mev gamma-rays and obtained an excitation curve for

* Supported by the joint ONR–AEC program and by a grant from the Research Corporation.
** Now at The Alabama Polytechnic Institute, Auburn, Alabama.
[1] T. W. Bonner and W. M. Brubaker, Phys. Rev. **50**, 308 (1936).
[2] Bonner, Evans, and Hill, Phys. Rev. **75**, 1398 (1949).
[3] Bennett, Bonner, Hudspeth, Richards, and Watt, Phys. Rev. **59**, 781 (1941).
[4] J. C. Bower and W. E. Burcham, Proc. Roy. Soc. **A173**, 379 (1939).
[5] E. Pollard, Phys. Rev. **56**, 1168 (1939).

deuteron energies from 450 kev to 1.9 Mev. A two percent C^{13} target was used which was 30-kev thick. Coincident Geiger-counter measurements were taken with an arrangement such that gamma-rays of energies below 3 Mev would not produce a coincident count. The excitation curve was rising steadily up to a deuteron energy of 1.55 Mev. At that point a resonance was observed where the curve remained flat and started rising again at 1.75 Mev.

Humphries and Watson[6] bombarded enriched C^{13} targets with 3.82 Mev deuterons and observed two groups of protons with Q values of 0.58 and 5.82 Mev, respectively. Thus the 5-Mev gamma-rays can be explained by either of the above reactions.

The object of the present experiment was to study the high energy group of neutrons from reaction (1) using a carbon target containing 48 percent C^{13}. It was thought to be practicable to detect this group of neutrons by use of a counter filled with 20 atmospheres of helium and five percent argon, if the discriminator was biased to record only large pulses.

II. APPARATUS

The Rice Institute pressure Van de Graaff generator was used to accelerate the deuterons. The magnetic analyzer,[7] used with an electron gun stabilizer,[8] gave an energy spread of the order of one kev when the bombarding energy was one Mev. The magnetic analyzer, calibrated by gamma-ray resonances in $F^{19}+p$ and $C^{12}+d$, allowed absolute energies to be known to better than 5 kev.

The targets were prepared from enriched methyl iodide which was purchased from the Eastman Kodak Company of Rochester, New York. A complete description of the method used in preparing the targets will be published elsewhere. It consists essentially by cracking carbon from the methyl iodide vapor onto nickel disks. The targets are estimated to be about 20-kev thick for 1.4-Mev deuterons and contain 52 percent C^{12} and 48 percent of the C^{13} isotope. This thickness corresponds to 60 micrograms of carbon per cm^2.

The counter used for deuteron energies above 350 kev was a cylindrical proportional counter with a 5-mil tungsten wire. The inner diameter of the counter was 2 inches and the sensitive length of the counter was also 2 inches. It was filled with 19 atmospheres of helium and one atmosphere of argon and was operated at 4000 volts with 5000 volt regulated power supply. Pulses from the counter were amplified by a linear amplifier and were recorded by a scale of 64. Calculations and experimental determinations show the counter to have an efficiency of the order of 0.3 percent for 5-Mev neutrons.

A "long counter" filled with enriched boron trifluoride was used as the neutron detector for deuteron energies between 200 kev and 450 kev. The counter was constructed after that built by Hanson and McKibben.[9] The pulses from this counter were amplified and detected by the same equipment as was used with the helium counter. Its efficiency, as determined by a standard Po-Be source, was 0.1 percent.

III. EXPERIMENTAL RESULTS

The enriched C^{13} targets were bombarded with homogeneous beams of deuterons of energies ranging from 200 kev to 2.09 Mev. The helium counter was placed at $0°(\pm 28°)$ to the direction of the deuteron beam. The sensitive volume of the counter subtended a solid angle of 0.98 steradians to the target.

Helium nuclei recoiling from neutrons entering the counter were counted if the neutron energy was greater than 3 Mev. This value was determined by the bias setting of a discriminator unit which was a part of the scale of 64. Only the high energy group of neutrons from reaction (1) should be counted. The maximum range in the counter of the highest energy neutrons detected was slightly greater than one-tenth of the counter diameter. Thus there should be little trouble from wall effects.

For data taken between 200- and 450-kev bombarding deuteron energy, the "long counter" was placed as close to the target as was possible and subtended a solid angle of 2π-steradians to the target. As this counter would count low energy as well as high energy neutrons, cans containing water saturated with borax were used to form a wall between the counter and the magnetic analyzer. This served to minimize background counts.

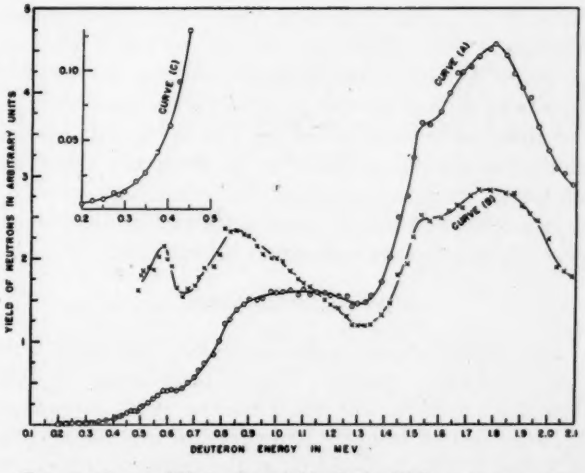

FIG. 1. Curve (A) is the yield of the high energy neutrons observed at $0°\pm 28°$ from the reaction $C^{13}(d,n)N^{14}$. Curve (B) is curve (A) divided by the penetrability of the deuterons times the square of their wave-lengths. Curve (C) is an enlargement of curve (A) in the region of low deuteron energies.

[6] R. F. Humphries and W. W. Watson, Phys. Rev. **60**, 542 (1941).
[7] Bennett, Bonner, Mandeville, and Watt, Phys. Rev. **70**, 882 (1946).
[8] S. J. Bame, Jr. and L. M. Baggett, Rev. Sci. Inst. **20**, 839 (1949).
[9] A. O. Hanson and J. L. McKibben, Phys. Rev. **72**, 673 (1947).

TABLE I. Data concerning the resonances. Total cross sections were computed assuming spherical symmetry.

	E_0 (Mev) Curve (A)	E_0 (Mev) Curve (B)	Γ (Mev)	σ (barns) for $Q=5.2$ Mev
(1)	0.58	0.58	0.1	6.6×10^{-3}
(2)	0.90	0.85	0.4	2.4×10^{-2}
(3)	1.55	1.55	0.1	6.3×10^{-3}
(4)	1.80	1.78	0.5	8.0×10^{-2}

For deuteron energies above 500 kev, over 3000 single neutron counts were taken for each point of the curve. For points below 500 kev, about 1500 neutron counts were taken. The background was determined by means of a target chamber containing two targets. One was the enriched C^{13} target and the other was a silver blank. The positions of the two were controlled externally by a small magnet so that either could be moved into the path of the deuteron beam.

The background with the helium counter was found to be less than 10 percent of the total number of counts for deuteron energies above 600 kev and became increasingly smaller as the deuteron energy increased. For points taken with the "long counter," the background remained at about 40 percent over the small range of deuteron energies covered. An equal number of counts were taken with the silver blank in the path of the deuteron beam as with the C^{13} target.

A small Geiger-counter shielded by 1.85 cm of lead was used to count the gamma-rays. All gamma-rays from the C^{12} and the C^{13} reactions were counted as no precautions were taken to count only gamma-radiation of a single energy. The excitation curve was consistent with the results of Bennett and Bonner.

The excitation curve for the high energy neutrons from reaction (1) is shown as curve (A) of Fig. 1. An enlargement of the low energy region is also given as curve (C). Curve (A) indicates several pronounced resonances. Since the cross section for disintegration, as given by the Breit-Wigner formula, is strongly influenced by the barrier penetration of the deuteron, the observed cross sections have been divided by the product of the penetrability of the deuterons times the square of their wave-length. The resulting curve (B) should show the true resonance shapes if the interference between neighboring resonances is negligible.

IV. CONCLUSIONS

The excitation curve for the 5-Mev neutrons from the $C^{13}(d,n)N^{14}$ reaction shows resonances at four deuteron energies. The deuteron energy at resonance, E_0, as estimated from the two curves of Fig. (1), is given in Table I. The half-widths of the resonances and the cross sections at these energies, calculated from the experimental arrangement, are also given. Because of uncertainties in absolute neutron intensities, the cross sections are not very precise and may be in error by as much as 50 percent.

Curves (A) and (B) show that there is a very small shift of the peaks in the resonance curves because of changing deuteron penetrability for resonances with widths of this order of magnitude. The resonances correspond to excited states in the intermediate N^{15} nucleus of 16.7, 16.9, 17.47, and 17.69 Mev.

Since the 5-Mev gamma-rays, the 50-cm protons and the 5-Mev neutrons all show a resonance at 1.55 Mev, there are three competing processes at this energy. The resonances at 0.9 Mev and 1.8 Mev were not observed for the long range protons. This is difficult to understand since the neutrons and protons have comparable amounts of energy and it is possible for the compound nucleus, in a particular state, to break up either way and conserve angular momentum and parity. It is possible that the long range protons observed at 0°, instead of 90°, would show similar resonances. It would be very puzzling if reactions (1) and (2) were not competitive.

Data taken with the "long counter" showed the yield of neutrons to have a very slow rise between 200 and 300 kev, and then to start rising more rapidly for deuteron energies above 300 kev. When corrected for penetrability and energy, the curve shows a steep rise as the energy decreases in the neighborhood of 200 kev. As this counter has a flat response over a wide range of energies, neutrons from other sources could be counted. The yield of neutrons from reaction (1) is very low in the energy region between 200 and 300 kev, and although this is below the threshold for C^{12} neutrons, those from the deuteron on deuterium reaction may have caused a large percentage of the counts. Between 200 and 300 kev, curve (A) is rising only 50 percent faster than does the deuterium plus deuteron yield over this energy range.[10] For deuteron energies greater than 300 kev, curve (A) rises much more rapidly than does the $D(d,n)He^3$ reaction.[11] Thus it seems to be likely that most of the neutrons counted below 300 kev were due to deuterium contamination, although the possibility of another resonance in this region cannot be ruled out.

The author wishes to thank Professor T. W. Bonner, Dr. G. C. Phillips and Professor J. R. Risser for help and advice during the course of this work.

[10] R. B. Roberts, Phys. Rev. 51, 810 (1937).
[11] Bennett, Mandeville, and Richards, Phys. Rev. 69, 418 (1946).

The Total Scattering Cross Section of Neutrons by Hydrogen and Carbon*

E. E. Lampi, G. D. Freier, and J. H. Williams
University of Minnesota, Minneapolis, Minnesota
(Received August 14, 1950)

The total cross sections of hydrogen and carbon for neutrons has been determined by measuring the transmission of polythene and graphite scatterers for neutrons with energies 0.798, 1.078, 1.340, 1.578, 4.92, and 4.97 Mev. The correction for the finite geometry of the experiment was made by measuring the cross section as a function of the scatterer area and extrapolating to zero area. The cross sections are considered to be reliable to approximately ±2 percent.

I. INTRODUCTION

THE scattering of neutrons by protons is of prime importance in the study of the interaction between these fundamental particles. The total cross section has been measured by a number of investigators, but the data have not been accurate enough for an evaluation of the constants for the potential functions which describe the nuclear scattering.

The work of Bailey *et al.*[1] as analyzed by Bohm and Richman[2] showed that the interaction between the neutron and proton could not be represented by a square well potential of radius e^2/mc^2 and depth determined by the binding energy of the deuteron for the triplet interaction and the thermal cross section for the singlet interaction.

In terms of Schwinger's shape independent approximation analysis[3,4] the values of the singlet scattering length, triplet scattering length, and triplet effective range have been fairly accurately determined. A determination of the total scattering cross section in the 0.5- to 5-Mev energy range would then give the singlet effective range. An accuracy of ±1 percent in the measurement of the total cross section is necessary in order to obtain an evaluation of the singlet range to $\pm 0.5\times 10^{-13}$ cm without allowance for the error in the triplet effective range. A comparable accuracy is also necessary in the measurement of the neutron energy.

II. EXPERIMENTAL METHOD

The total cross section, σ_t, of a scatterer can be defined in terms of the transmission for neutrons by the expression

$$T=\exp(-nx\sigma_t) \tag{1}$$

where T is the transmission and nx is the number of atoms per sq. cm of the scattering sample. The transmission is given by

$$T=(N_1-N_B)/(N_0-N_B), \tag{2}$$

where N_1 is the number of neutrons transmitted by the scatterer. N_0 is the number of neutrons counted with no scatterer and N_B is the background count determined with a 3 inch by 8 inch paraffin cylinder between the source and detector. Because the radiative capture cross section is small, we assume that the measured cross section is the elastic scattering cross section.

The geometry of the source, scatterer, and detector is shown in Fig. 1. The measured transmission will be greater than the true value since the detector subtends a finite solid angle at the scatterer. Consider the source to be of strength Q per unit solid angle. The number of neutrons with no scatterer is given by

$$Q\omega_{qd}\epsilon_1, \tag{3}$$

where ω_{qd} is the solid angle subtended by the detector at the source, and ϵ_1 is the efficiency of the detector. With a scatterer in position the number of neutrons detected will be

$$T_0Q\omega_{qd}\epsilon_1+\frac{(1-T_0)Q\omega_{qs}\omega_{sd}\epsilon_2}{4\pi}, \tag{4}$$

where T_0 is the true transmission of the scatterer, ϵ_2 is the efficiency of the detector to neutrons which have been scattered through a small angle but still reach the detector, ω_{sd} is the solid angle subtended by the detector at the scatterer measured in the center-of-mass system of coordinates, and ω_{qs} is the solid angle subtended by the scatterer at the source. The measured transmission, T, is then given by

$$T=T_0\left[1+\frac{1-T_0}{T_0}\left(\frac{\omega_{qs}\omega_{sd}\epsilon_2}{4\pi\omega_{qd}\epsilon_1}\right)\right]. \tag{5}$$

The correction term could be evaluated with some assumption of the angular distribution of the scattered neutrons and a determination of the dependence on energy of the sensitivity of the neutron detector. A

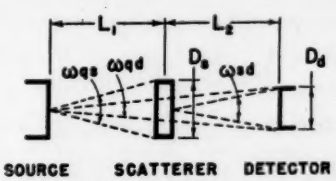

FIG. 1. Geometry of source, scatterer, and detector.

* This research was done under the partial support of the ONR.
[1] Bailey, Bennett, Bergstralh, Nucholls, Richards and Williams, Phys. Rev. **70**, 583 (1946).
[2] D. Bohm and C. Richman, Phys. Rev. **71**, 567 (1947).
[3] J. M. Blatt and J. D. Jackson, Phys. Rev. **76**, 18 (1949).
[4] H. A. Bethe, Phys. Rev. **76**, 38 (1949).

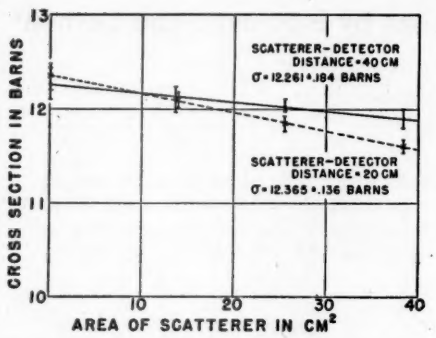

FIG. 2. Cross section of polythene at 0.807 Mev as a function of scatterer area. Dashed curve is for 20 cm and full curve for 40 cm scatterer-detector distance.

simple expression of the measured cross section, σ_t, can be obtained by substituting Eq. (5) into (1). If the correction is considered to be small compared to unity in the expansion of the logarithm, the cross section is given by

$$\sigma_t=\sigma_{t0}-\frac{1}{nx}\left[\left(\frac{1-T_0}{T_0}\right)\frac{\omega_{sd}\epsilon_2 A_s}{4\pi\omega_{qd}\epsilon_1 L_1^2}\right], \tag{6}$$

where A_s is the area of the scatterer, and L_1 is the distance from the scatterer to the source. This equation shows that the measured cross section is a linear function of the area of the scatterer. In order to determine the true cross section for a given E_n, we have measured the cross section for three areas of scatterer and extrapolated a straight line to zero area by least squares.

The scatterers were disks of polythene, C_6H_{12}, and carbon graphite. The polythene was obtained from E. I. duPont deNemours and Company. They reported that the hydrogen-carbon ratio was 2.00 as closely as could be measured and that there were only traces of impurities present. The carbon graphite was obtained from the National Carbon Company.

The number of atoms per cm³ was determined from the density, the atomic weights as given in the Segrè chart of nuclear properties, and the value of Avogadro's number, taken to be 6.0251×10^{23}. The consistency for a large number of scatterers showed that number of atoms per cm³ could be measured to 0.1 percent.

III. MEASUREMENT OF NEUTRON ENERGY

The source of 0.798- to 1.578-Mev neutrons was the reaction

$$Li^7+H^1\rightarrow Be^7+n+Q. \tag{7}$$

The neutron source for 5-Mev determination was the reaction

$$D^2+D^2\rightarrow He^3+n+Q. \tag{8}$$

The University of Minnesota Van de Graaff generator provided monoenergetic protons and deuterons up to 3.6 Mev. The voltage of the generator was measured and controlled by means of an electrostatic analyzer described by Hanson.[5] The threshold of reaction (7) was used as a reference for the calibration of the generator energy scale. We have taken it to be the value, 1.882 Mev, given by Herb *et al.*[6] The linearity of our analyzer was checked by measuring the value of the $Li^7(p,n)Be^7$ threshold for molecular ions. Within the accuracy of our experiments this was twice the value determined for atomic ions.

The lithium was evaporated on a thin tantalum cap of a rotating target. The lithium target thickness was measured by the method described by Taschek and Hemmindinger.[7]

The source for neutrons from the *D-D* reaction was similar to the gas target described by Hanson, Taschek, and Williams[8] with a 0.0001-inch thick nickel foil separating the deuterium gas from the vacuum.

IV. DETECTION OF NEUTRONS

The neutrons were detected by counting recoil protons from a paraffin radiator inside the front face of an argon filled ionization chamber. The chamber was 5 cm in diameter and 9 cm long. It was filled with a 97 percent argon and a 3 percent methane mixture at 1-atmos. pressure. The ionization pulse was collected on a concentric cylinder 2.5 cm in diameter. The amplifiers were similar to the Los Alamos type 100. The pulses were counted with scaling circuits described by Higginbotham, Gallagher, and Sands.[9]

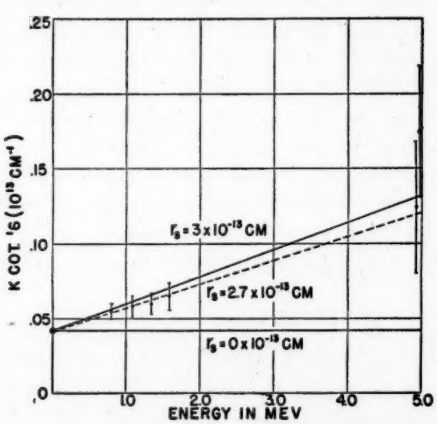

FIG. 3. The function $K\cot^1\delta=-(1/a_s)+\frac{1}{2}r_sK^2$ plotted against incident neutron energy in the laboratory system of coordinates. The singlet scattering contribution to the measured total scattering cross section is calculated on the assumption that the triplet scattering length is 5.39×10^{-13} cm and the triplet effective range is 1.73×10^{-13} cm. The value of a_s, the singlet scattering length, is taken as -23.68×10^{-13} cm. The slopes of the straight lines correspond to values of the effective singlet range of 3×10^{-13}, 2.7×10^{-13} and 0×10^{-13} cm.

[5] A. O. Hanson and D. L. Benedict, Phys. Rev. **65**, 33 (1944).
[6] Herb, Snowden, and Sala, Phys. Rev. **75**, 246 (1949).
[7] R. Taschek and A. Hemmindinger, Phys. Rev. **74**, 373 (1948).
[8] Hanson, Taschek, and Williams, Rev. Mod. Phys. **21**, 635 (1949).
[9] Higginbotham, Gallagher, and Sands, Rev. Sci. Inst. **18**, 706 (1947).

TABLE I. Total cross sections of hydrogen and carbon.

Run	Neutron energy	Carbon cross section	Hydrogen cross section	Average carbon cross section	Average hydrogen cross section
1	0.798±0.008 Mev	2.85±0.04 barns	4.81±0.16 barns		
2	0.807±0.008	2.78±0.13	4.74±0.11		
3	0.807±0.008	2.82±0.07	4.77±0.08		
	0.798±0.008			2.82±0.07 barns	4.79±0.11 barns
4	1.078±0.010	2.56±0.05	4.10±0.06		
5	1.078±0.010		4.06±0.06		
6	1.078±0.010		4.06±0.11		
7	1.078±0.010	2.55±0.06	4.13±0.08		
	1.078±0.010			2.55±0.05	4.09±0.08
8	1.340±0.011	2.24±0.04	3.66±0.06		
9	1.340±0.011	2.27±0.05	3.65±0.06		
	1.340±0.011			2.26±0.04	3.66±0.06
10	1.578±0.013	1.99±0.04	3.38±0.08		
11	1.578±0.013	2.03±0.04	3.35±0.08		
12	1.578±0.013	1.94±0.04	3.23±0.06		
	1.578±0.013			1.99±0.04	3.32±0.07
13	4.92 ±0.14	1.36±0.04	1.64±0.04	1.36±0.04	1.64±0.04
14	4.97 ±0.14	1.34±0.03	1.56±0.04	1.34±0.03	1.56±0.04

V. PROCEDURE

The scatterers were supported on fine wires halfway between the source and the detector. The detector was placed 40 cm from the target at zero degrees to the direction of the proton beam. The neutrons were monitored with a paraffin-covered, boron trifluoride-filled, proportional counter placed about 200 cm from the source.

At the beginning of each day's run all the scatterers were aligned with respect to the detector. The analyzer zero setting was adjusted, and then the analyzer voltage was set to give the desired proton or deuteron energy. The following sequence of runs was taken for a determination of the hydrogen cross section: a background run, a run with no scatterer, a run with each of three polythene scatterers of different diameter, another run with no scatterer, and a run with each of two carbon scatterers of different diameter. From these data a polythene and a carbon cross section was calculated for each size of scatterer. The mean values were extrapolated to zero area of scatterer to obtain the true polythene and carbon cross section. The value $\sigma_{t0}(H)$ was obtained from the above results by taking

$$\sigma_{t0}(H)=\tfrac{1}{2}[\sigma_{t0}(\text{polythene})-\sigma_{t0}(c)]. \quad (9)$$

Since the lithium target collected a carbon deposit during bombardment, the carbon thickness was measured by determining the shift in the threshold voltage for reaction (7) immediately after the target was made and then after completion of the data for one energy. One-half of the average energy loss in the Li target was subtracted from the nominal energy of the incident proton beam.

The geometry correction was checked by increasing the distance from the source to the scatter from 20 cm to 40 cm. The cross section of polythene as a function of scatterer areas at a neutron energy of 0.807 Mev is shown in Fig. 2.

The data taken with the deuterium gas target required a correction for the neutrons emitted by the slit surfaces and other parts of the target assembly that were bombarded by the deuteron beam. In order to evaluate this effect the deuterium target was filled with hydrogen gas to one atmosphere pressure, and runs were taken with the paraffin cylinder, with the 2.25-inch diameter polythene scatterer, with the 2.75-inch carbon scatterer, and with no scatterer. These counts were normalized and subtracted from the counts obtained with deuterium gas in the target. This background was approximately 9 percent of the counts with deuterium as a target.

When several determinations of σ_{t0} were made with the same proton energy, the neutron energies would not, in general, be exactly equal because of different lithium target thickness or different electrostatic analyzer calibration. For purposes of comparison, the values of total cross section were interpolated to one value of neutron energy by assuming that the cross section varied as $E^{-\frac{1}{2}}$. In most cases this correction was $\frac{1}{2}$ percent or less.

Since this work was done, several investigators[10–12] have found a second group of neutrons in reaction (7) arising from an excited state of the Be^7 nucleus 430 kev above the ground state. The intensity of the second group is approximately 10 percent of the main group in our energy range. Our proton recoil ionization chamber detector had a threshold of approximately 0.5 Mev so that the low energy group was biased out at neutron energies of less than 1 Mev. At energies greater than 1 Mev our data have been corrected for the presence of this low energy group. The correction was approximately 1 percent for these higher energies. There is some uncertainty in these corrections because we lacked exact

[10] J. C. Grosskreutz and K. B. Mather, Phys. Rev. 77, 580 (1950).
[11] Johnson, Laubenstein, and Richards, Phys. Rev. 77, 413 (1950).
[12] Freier, Rosen, and Stratton, Phys. Rev. 79, 239 (1950).

knowledge of the energy dependence of the sensitivity of our detector.

VI. RESULTS

Values of σ_{t0}, the total cross section for a neutron energy E_n, are given in Table I. The statistical uncertainty in σ_{t0} was calculated from the extrapolation formula and the reproducibility of the cross section for each scatterer during the run. The probable errors assigned to the cross section include the uncertainty in the background count and the uncertainty in the correction for the low energy group of neutrons.

The data have been analyzed by Schwinger's shape independent method described by Blatt and Jackson[3] and by Bethe.[4] To calculate the triplet scattering cross section, we have used Hughes'[13] value of -3.75×10^{-13} cm as the coherent scattering amplitude, 20.36 barns[14] as the zero energy neutron proton scattering cross section, and 2.23 Mev as the binding energy[15] of the deuteron. In terms of this shape independent approximation the effective range and scattering length are 1.73×10^{-13} cm and 5.39×10^{-13} cm, respectively for the triplet interaction. The value of the singlet scattering length is -23.68×10^{-13} cm. The singlet scattering cross section was obtained by subtracting the triplet contribution from the total cross section. The values of the phase shift function, $K\cot^1\delta$ for the singlet interaction were calculated from the singlet scattering cross section and are shown as a function of neutron energy in Fig. 3. The singlet effective range for the neutron proton interaction appears to be approximately equal to the proton-proton effective range[4] of 2.7×10^{-13} cm. One can then infer, to within the accuracy of the above experiments, the charge independence of nuclear forces in the energy range up to 5 Mev.

We wish to express our thanks to Mr. M. Fulk for assistance in taking the data.

This research was assisted by the University of Minnesota Technical Research Fund subscribed to by General Mills, Inc., Minneapolis Star Journal and Tribune Company, Minnesota Mining and Manufacturing Company, and Northern States Power Company.

[13] Hughes, Burgy, and Ringo, Phys. Rev. **77**, 291 (1950).
[14] Melkonian, Rainwater, and Havens, Phys. Rev. **75**, 1295 (1949).
[15] R. E. Bell and L. G. Elliot, Phys. Rev. **74**, 1552 (1948).

PHYSICAL REVIEW VOLUME 80, NUMBER 5 DECEMBER 1, 1950

Pressure Measurement in Superflow

R. BOWERS, B. S. CHANDRASEKHAR, AND K. MENDELSSOHN
Clarendon Laboratory, Oxford University, England

(Received July 24, 1950)

The pressure of flowing liquid HeII has been measured in the capillary link as well as on its ends. Flow under gravitational and thermal potential has been studied in narrow slits and tubes packed with fine powder. On the basis of ordinary pressure measurement the results are not consistent and it is concluded that the definition of "pressure" in superflow requires additional parameters.

I. INTRODUCTION

THE experiments on liquid HeII have disclosed the existence of a peculiar type of flow which has not been observed in any other fluid. The main characteristic of this "superflow" seems to be the disappearance of viscous dissipation of energy. Linked with this is often the phenomenon of pressure independent flow which is completely free of friction. However, the first condition is evidently the more general one since, as the present work shows, there exist cases in which superflow is accompanied by a loss in kinetic energy. The situation is unfortunately complicated by the fact that liquid HeII in bulk seems to exhibit superflow and ordinary viscous flow side by side and that it is usually difficult to separate the two components of the transport mechanism. In first approximation the flow phenomena can be interpreted by means of a semi-empirical "two-fluid model"[1] which treats the liquid as an interpenetrating mixture of a normal and an anomalous component, the relative concentration of which varies with temperature. The question as to whether or not there exists any theoretical justification for such a concept must be left open, but it is already clear that in spite of the general success of the two-fluid model it cannot be applied in this simple form to some of the observed facts. In particular, most of the results on capillary flow near the lambda-point[2,3] cannot be represented as a simple superposition of viscous and frictionless flow.

A simplification of the flow phenomena can be achieved experimentally by decreasing the diameter of the flow channel and thereby suppressing the viscous component. Pure frictionless flow is observed in film transfer[4] and these results are closely approximated by

[1] L. Tisza, Nature **141**, 913 (1938).

[2] J. F. Allen and A. D. Misener, Proc. Roy. Soc. A **172**, 467 (1939).
[3] R. Bowers and K. Mendelssohn, Proc. Roy. Soc. A (to be published).
[4] J. G. Daunt and K. Mendelssohn, Proc. Roy. Soc. A **170**, 423 (1939).

the flow in very narrow capillaries.[2] In all of these experiments the flow rate was found to be independent of the length of the flow channel and of the pressure difference at its ends, but flow through a tube closely packed with fine powder[2] was clearly pressure dependent. This discrepancy shows that the "pressure" in superflow may not be a straightforward concept and requires further elucidation. Pressure measurements were therefore carried out on these two types of superflow.

II. METHOD

In the conventional type of flow experiment two volumes of liquid A and B are connected by a capillary link C (Fig. 1) and the mass of liquid transported per unit time through C is determined in relation to the pressure difference $p_A - p_B$. The flow experiments on HeII have so far been carried out in the same manner but it is clear that in the case of pressure independent flow determinations of the pressure at the ends of the capillary link are insufficient. We have therefore also measured[5] the intermediate pressure p_I at a point I in the capillary link between A and B. Care was taken in all experiments to make the dimensions of the apparatus so that p_I was not falsified by the Bernoulli force.

The experiment was varied in two different ways. The flow was studied on:

(a) narrow slits or channels; and
(b) channels tightly packed with fine powder.

The pressure under which the flow took place was produced by:

(1) gravitational potential; and
(2) thermal potential.

Two types of slit were used, one in the form of a conical joint and the other between two optically flat glass plates (Fig. 2a, b). In each case the slit was divided into two lengths by means of a groove to which a narrow side tube was connected. The pressure at the ends of C was then given by the height of the helium levels in the experimental vessel and the bath while the intermediate pressure was indicated by the level in the side tube. The present paper deals only with the narrowest slits produced in this way which were of the order of 1 to 5×10^{-4} cm. The general arrangement for the experiments with

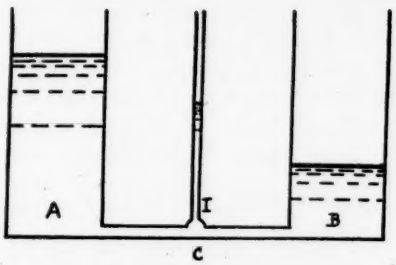

FIG. 1. Scheme of measurements.

[5] R. Bowers and K. Mendelssohn, Proc. Phys. Soc. A 63, 178 (1950).

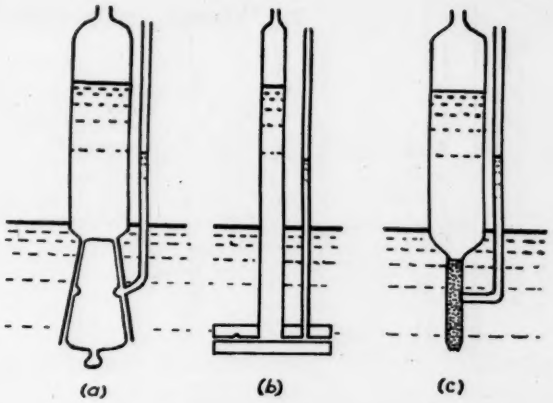

FIG. 2. Experimental arrangements.

packed channels (Fig. 2c) was similar, except that the slits were replaced by glass or metal tubes into which jewellers rouge was pressed tightly. While the results on slits differed from those on packed channels those in each of the two groups were completely consistent in themselves.

The experiments were carried out in a combined liquefier-cryostat[6] in which the helium is free from contamination[7] and the heat influx is reduced to a minimum. The light used in the observations was supplied by a 12-watt bulb at one meter distance from the cryostat and passed through screens of copper sulfate solution in water, liquid air and liquid hydrogen. Under these conditions the total evaporation from the helium cryostat was 2 cc of liquid per hour. All measurements described here were carried out at ~1.3°K where the rate of superflow is practically independent of temperature.

III. RESULTS

Under equilibrium conditions the levels in the helium vessel and in the bath adjusted themselves to equal height while the position of the side level was ~1.5 mm higher owing to surface tension forces. In the experiments under gravitational potential the vessel was partly lifted out of the bath and the change with time of its level and that in the side tube were noted. In the case of slits (Fig. 3, 1a) the drop in the vessel was almost linear, showing that the flow was, in first approximation, pressure independent. The side level fell rapidly immediately on lifting and adjusted itself to the height of the bath level. The side level also took up the position of the bath level when the direction of the flow was reversed. Thus, as was expected[8] in the case of pressure independent flow, the total pressure drop was concentrated at the narrowest part of the slit. In the present case the ratio of resistances to ordinary laminar flow between the two parts of the slit was ~1:4, but in similar experiments on narrow channels ratios of ~1:2

[6] J. G. Daunt and K. Mendelssohn, J. Sci. Inst. 25, 318 (1948).
[7] R. Bowers and K. Mendelssohn, Nature 163, 870 (1949).
[8] K. Mendelssohn, Proc. Phys. Soc. London 57, 371 (1946).

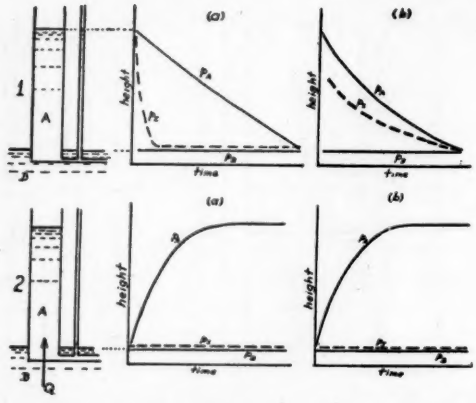

FIG. 3. Pressure distribution: (1) under gravity, (2) under thermal potential, (a) in slits, (b) in tubes packed with powder.

were used and even under these conditions the whole of the pressure drop occurred in the slightly more constricted channel.

The flow through powder (Fig. 3, 1b) is completely different, the rate depending on $(p_A-p_B)^{\frac{1}{2}}$ which indicates turbulence. The dissipation of kinetic energy is clearly not an end effect but takes place over the length of the powder tube as is shown by the position of the side level taking up an intermediate position. Comparison experiments above the lambda-point showed that the flow of HeI is more than 500 times smaller, which means that the dissipation cannot simply be caused by the viscosity of the "normal" component of liquid HeII. Estimates[9] of the viscosity of this component vary at ~1.3°K between 0.8 and 0.1 of that of HeI but a factor 0.002 seems to be quite inadmissable. The type of transport in the packed tubes therefore is evidently pressure dependent but non-viscous and might be described as turbulent superflow. Thus this observation also seems to contradict the two-fluid model in its simple form.

For the observations on flow under thermal potential heating coils were inserted into the helium vessels and the small apertures at the top were sealed off. In this case the results on slits and packed tubes were identical (Fig. 3, 2a and b). On application of a steady heating current the level in the helium vessels was found to rise and ultimately to reach a constant thermo-mechanical pressure.[10] In *all* cases the side level remained constant at the height of the bath.

IV. CONCLUSIONS

The four experiments illustrated in Fig. 3 present a curious inconsistency. They show that in superflow the intermediate pressure p_I is not determined unambiguously by the pressures p_A and p_B at the ends of the tube. In the cases 1a, 2a, and 2b for any given value of p_A-p_B, p_I is equal p_B but in 1b, $p_A>p_I>p_B$. The inconsistency remains even when a distinction is made between hydrostatic and thermo-mechanical pressure. On the basis of such a distinction one can argue that the flow in 2a and b takes place under zero hydrostatic pressure. However, then we are faced with the difference between cases 1a and 1b together with the fact (from 2b) that the powder tube can carry flow under zero hydrostatic pressure. Taking the discrepancy between cases 1b and 2b we must conclude that for a given flow velocity a pressure gradient may or may not exist along the tube. It thus appears that, in contradistinction to ordinary flow, the intermediate pressure is not simply a function of the end pressures but requires for its determination one or more additional parameters.

[9] F. London, Phys. Soc. Camb. Conf. Rep. **2**, 1 (1947).

[10] J. F. Allen and J. Reekie, Proc. Camb. Phil. Soc. **35**, 114 (1939); L. Meyer and J. H. Mellink, Physica **13**, 180 (1947).

Anomalous Heat Flow in Superconductors

K. MENDELSSOHN AND J. L. OLSEN
Clarendon Laboratory, Oxford University, England
(Received July 24, 1950)

Measurements of heat flow in the superconductive and in the normal state have been carried out on pure lead and lead containing a small quantity of bismuth. The heat conduction has been measured in its dependence on magnetic field and temperature. The alloy shows a smaller heat conduction in the intermediate state than in either the superconductive or the normal state. This anomalous behavior is taken to indicate the existence in superconductors of a type of heat transport similar to that observed in liquid HeII.

I. INTRODUCTION

RECENT measurements on the heat transport in superconductors[1] have revealed the existence of two competing processes responsible for the variation of heat flow with temperature. One is the progressive passage of electrons into the superconductive state as the temperature is lowered. Since the "superconductive electrons" have zero entropy[2] they cannot take part in the ordinary heat conduction process and the heat flow through the metal is consequently decreased. This mechanism, in which at any given temperature below the transition point the heat conductivity of the superconductive metal is smaller than in the normal state (which can be re-established by a magnetic field), is dominant in pure metals.[1,3] In certain alloys on the other hand the superconductive state conducts heat better than does the normal one. Intermediate cases in which the curves for the normal and the superconductive heat flow intersect at some temperature below the transition point have been observed in columbium[1] and in pure lead to which controlled quantities of bismuth had been added.[4] Thus a second type of heat transport which opposes the reduction in heat flow mentioned above clearly exists, but its cause is not so certain. We have tentatively put forward the explanation[1,5] of a circulation current of electrons within the metal which somewhat resembles the heat transport in liquid HeII. One can think of a flow of superconductive electrons towards the warm end of the specimen which is compensated electrically by the return flow of normal electrons. Since in the pure superconductive metal the magnetic induction must be zero, this return current is prohibited. In a superconductive alloy, on the other hand, where as is well known the induction is different from zero "normal" return currents are possible. Their formation will even be facilitated because there are indications that the electrical conductivity of the normal enclosures in the metal is exceptionally high. An alternative explanation for the high heat conductivity in certain superconductors has been suggested by Hulm[6] who considers that the lattice conduction may be increased when the metal becomes superconducting. Recent experiments on controlled impurities[4] however show that such a mechanism, though it may well exist, would be inadequate to account for the observed heat flows. In most researches the heat conductivity has been measured as it depends on the temperature but further information can be gained when these observations are supplemented by measurements of the heat conduction in its dependence on the magnetic field.[7] Such measurements have now been carried out on pure lead and lead with a small quantity of bismuth.

II. METHOD

The specimens used were cylindrical rods along which a temperature gradient of $\sim 0.1°$ per cm or less was established. At two places along the specimen, about 2 cm apart, gas thermometers were attached without the use of solder and the temperature measured differentially. The lead specimen was prepared from Johnson Matthey H.S. lead (laboratory number 1932) with an impurity content of less than 0.002 percent. The alloy specimen was prepared from the same metal to which a small quantity (~ 0.02 percent) of very pure bismuth from the same source had been added. A homogeneous magnetic field could be established in the direction of the specimen or normal to it. Heat was supplied electrically to one end of the specimen while the other end was firmly attached to the helium container of an expansion liquefier. By carefully regulating the escape of helium gas this apparatus could be used as a thermostat between the temperatures of liquid hydrogen and liquid helium.[8] Below the boiling point of helium the device was thermostated through the vapor pressure of the liquid.

III. RESULTS

Figure 1 gives the change of the heat conduction of the pure lead specimen with a longitudinal magnetic field. The mean temperatures for the two experiments were 4.6°K and 2.7°K. The values of magnetic field at

[1] K. Mendelssohn and J. L. Olsen, Proc. Phys. Soc. London A 63, 2 (1950).
[2] J. G. Daunt and K. Mendelssohn, Proc. Roy. Soc. A 185, 225 (1946).
[3] W. J. de Haas and A. Rademakers, Physica 7, 992 (1940).
[4] K. Mendelssohn and J. L. Olsen, Proc. Phys. Soc. A63, 1182 (1950).
[5] K. Mendelssohn, Royal Coll. Sci. J. 16, 105 (1946).
[6] J. K. Hulm, M.I.T. Conf. Very Low Temp., (1949), p. 90.
[7] K. Mendelssohn and R. B. Pontius, Phil. Mag. 24, 777 (1937).
[8] D. K. C. MacDonald and K. Mendelssohn, Proc. Roy. Soc. A 202, 103 (1950).

which the change occurs are in fair agreement with the threshold values Hc for the electrical resistance.[9] As this value is reached and the specimen changes from the superconductive into the normal state the heat conductivity rises suddenly; a similar change in the reverse direction is observed on reducing the field. There is a very small amount of hysteresis between the two curves; this is slightly more pronounced at the lower temperature. However, as on the return curve the field is again reduced to zero the value of the heat conductivity is sensibly the same as before superconductivity was destroyed. Observations in transverse magnetic fields yield similar results except that the transition was, of course, gradual between $\frac{1}{2}Hc$ and Hc.

The addition of a very small quantity of bismuth (~0.02 percent) affects the absolute value of the heat conduction but the character of the transition at a relatively high temperature is hardly influenced. Figure 2 gives the longitudinal and the transverse transitions of this specimen a little above 5°K. The change in heat conduction again agrees well with that of electrical resistance and the hysteresis is still small. After superconductivity was destroyed and the field reduced to zero the conductivity is now actually slightly higher than originally.

The situation changes completely, however, as the temperature is lowered. Figure 3 shows the longitudinal and transverse transition curves for the same specimen at ~2.9°K. As the field is increased and superconductivity is destroyed there is again a sharp increase in the longitudinal case; however, on decreasing the field the heat conductivity now falls well below the original value and at zero field the heat flow through the specimen in the superconductive state is 22 percent lower than at first. An even more striking behavior is exhibited on the destruction of superconductivity by a transverse field. The heat conduction remains constant until a field of about $\frac{1}{2}Hc$ is reached and then begins to fall to a minimum value well below the heat flow in either the superconductive or the normal state. On further increasing the field the heat conductivity rises again until the normal value is reached at Hc. On returning the specimen into the superconductive state by reducing the field a monotonic fall of the heat conduction similar to that of the longitudinal case takes place.

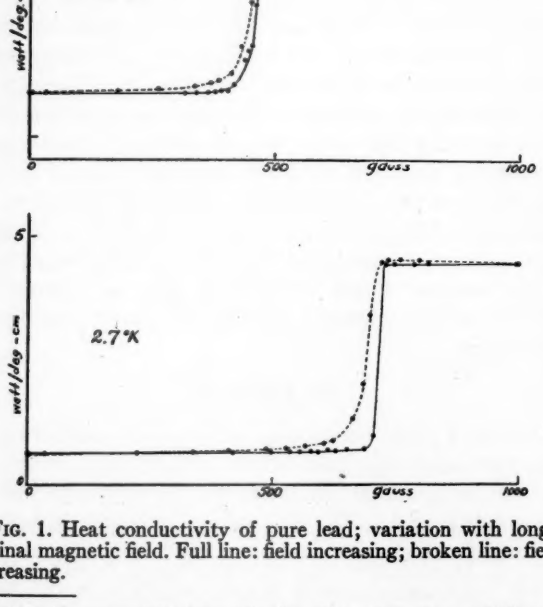

FIG. 1. Heat conductivity of pure lead; variation with longitudinal magnetic field. Full line: field increasing; broken line: field decreasing.

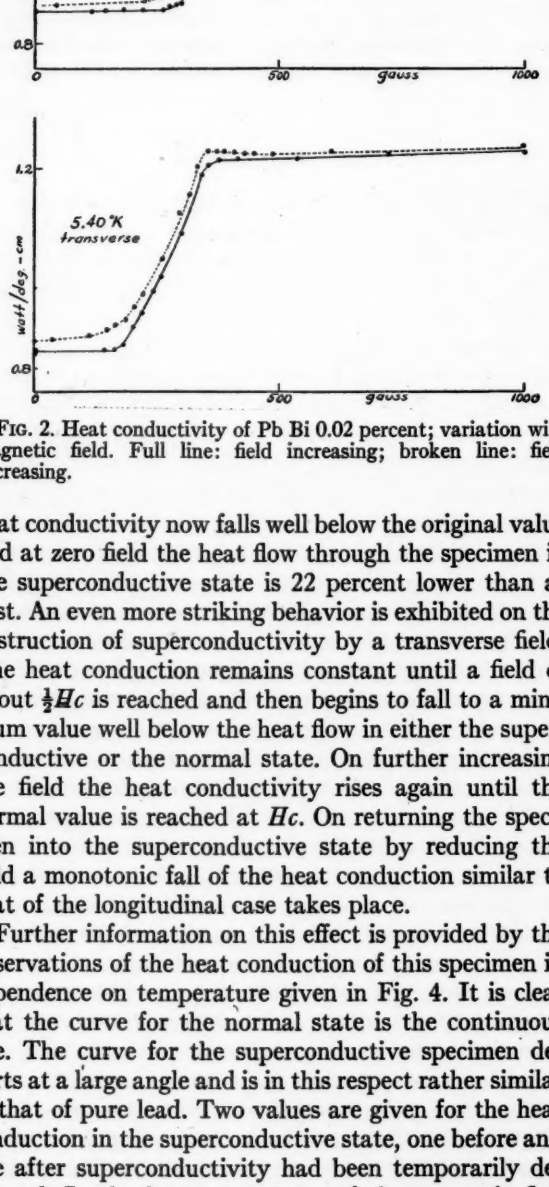

FIG. 2. Heat conductivity of Pb Bi 0.02 percent; variation with magnetic field. Full line: field increasing; broken line: field decreasing.

Further information on this effect is provided by the observations of the heat conduction of this specimen in dependence on temperature given in Fig. 4. It is clear that the curve for the normal state is the continuous one. The curve for the superconductive specimen departs at a large angle and is in this respect rather similar to that of pure lead. Two values are given for the heat conduction in the superconductive state, one before and one after superconductivity had been temporarily destroyed. In the latter case some of the magnetic flux was evidently "frozen in." As can be seen, the values with and without the frozen in field coincide at the higher temperatures but below ~4°K the heat flow with frozen in field is consistently smaller, decreasing to about two-thirds of the value of that without frozen in field at the lowest temperature.

IV. CONCLUSIONS

It is known from our other experiments[1,4] that as the bismuth content is increased the heat conduction in the

[9] J. G. Daunt and K. Mendelssohn, Proc. Roy. Soc. A 160, 127 (1937).

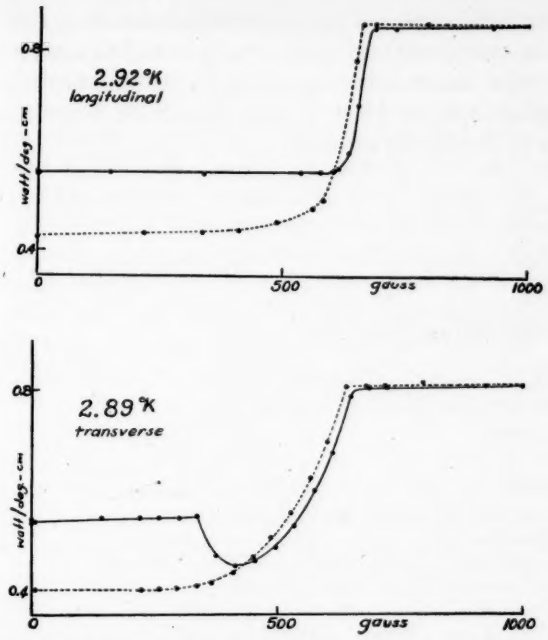

FIG. 3. Heat conductivity of Pb Bi 0.02 percent; variation with magnetic field at ~2.9°K. Full line: field increasing; broken line: field decreasing.

superconductive state grows steadily in comparison with the normal heat conductivity until eventually their relation is completely reversed. It is therefore significant that the superconductive curve without frozen in field shown in Fig. 4 indicates higher heat flows than the curve with frozen in flux. Moreover, the shape of the curve definitely gives the impression that the frozen in values represent a true continuation of the original curve from which the values without frozen in flux branch off. We are clearly encountering here the first sign of the new heat transmission process in the superconductive state and the conclusion is reached that this transmission of heat is inhibited by the magnetic flux frozen into the specimen. The interesting point is that when the alloy specimen at 2.9°K is partly in the superconductive and partly in the normal state, the heat conduction is *smaller* than in either of these states. This shows that the observed heat flow cannot be simply due to a mixture of superconductive and normal materials each having its specific heat conductivity. At the higher temperature and in pure lead on the other hand this is evidently the case.

While thus any explanation simply based on different heat conductions in the two states must fail to account for our results, they seem to offer an unexpected confirmation of our model. We assume that as with falling temperature the alloy character of the specimen increases,[9] and with it the deviation from zero induction grows, a circulation of electrons along the specimen will be established. The superconductive electrons take up their *total* entropy which is returned by the flow in the opposite of normal electrons. For this reason the circulation flow is a powerful means of heat transport and as it develops can outstrip the negative effect of electrons being lost into the superconducting state. The present results seem to show that at higher temperatures or in a pure metal no anomalous effects occur because no circulation flow exists. Circulation flow can take place in the alloy specimen at low temperatures but it will be broken up by the formation of normal enclosures in the specimen. In this respect the transverse transition in Fig. 3 is of particular significance. When at $\frac{1}{2}Hc$ the threshold value on the surface of the cylindrical specimen is exceeded the rod passes into the intermediate state. At the establishment of this state normal laminae perpendicular to the axis of the specimen are formed[10] which gradually increase at the expense of the superconductive material as the field is increased. Although therefore at the beginning of the transition the actual amount of normal material within the specimen is small the circulation process will be inhibited very soon and the total heat flow will fall instead of rising. Only when enough normal material is present will the original value of the conductivity be reached again and the actual value for the normal state will ultimately be attained. No such intermediate decrease is observed in the longitudinal destruction where no transverse laminae are formed. On the other hand, as the field is decreased to zero and the frozen in lines of force curl up like those in a permanent bar magnet the circulation flow is evidently again inhibited.

It would thus appear that the heat flow given by the experiments with the frozen in field is nearer to the true value of the heat conduction in the superconductive material than that before magnetic penetration. This fact must be borne in mind when analyzing the heat conduction of a superconductor. Apart from its theoretical interest the anomalous heat conduction has some bearing on the practice of cryogenic technique. It has

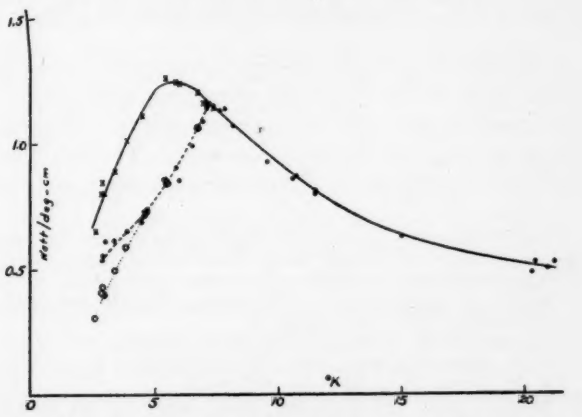

FIG. 4. Heat conductivity of Pb Bi 0.02 percent; variation with temperature. Small circles: zero field; crosses: field $>Hc$; large circles: field frozen in.

[10] It can easily be shown that laminae in any other direction to the cylinder axis are unstable.

been suggested by us[1] (and independently by Daunt and Heer[11]) to make use of the change of heat conduction in superconductors for make and break thermal contacts at very low temperatures. The present results show that in order to get a great difference of heat flow in the two states very pure metals should be used. On the other hand, it now seems to be possible to design thermal switches which *break* a contact on magnetization by employing an alloy.

[11] C. V. Heer and J. G. Daunt, Phys. Rev. **76**, 854 (1949).

PHYSICAL REVIEW VOLUME 80, NUMBER 5 DECEMBER 1, 1950

The Disintegration of Praseodymium 142

ERLING N. JENSEN, L. JACKSON LASLETT, AND D. J. ZAFFARANO
*Institute for Atomic Research and Department of Physics, Iowa State College, Ames, Iowa**

(Received July 26, 1950)

The radiations from Pr^{142} have been examined with a thin lens spectrometer. One gamma-ray was found having an energy of 1.57_6 Mev. The beta-spectrum is complex, the two groups observed having maximum kinetic energies of 2.15_4 Mev and 0.63_6 Mev. It is suggested that the high energy beta-group gives a transition to the ground state of Nd^{142} and that the gamma-ray follows the low energy beta-transition. The half-life was found to be 19.1 hr. The electron distribution produced by bremsstrahlung, due to the absorption of the beta-rays, was observed.

I. INTRODUCTION

THE characteristic radiations of Pr^{142} were investigated by Amaldi[1] and others, but in more detail recently by absorption and coincidence methods by Bothe,[2] Mandeville,[3] and Jurney.[4] Data obtained with spectrometers have been reported by DeWire *et al.*,[5] Peacock *et al.*,[6] Cork *et al.*,[7] and Rae.[8]

The radiations found by these authors are shown in Table I.

The coincidence work of Mandeville and Jurney has established that the 1.6-Mev gamma-ray probably follows the soft beta-transition, while the higher energy beta results from a disintegration to the ground state of Nd^{142}. Delayed coincidence work by DeBenedetti and and McGowan[9] showed that there are no metastable states in Nd^{142} with half-lives in the range 10^{-6} to 10^{-3} sec.

DeWire *et al.*[5] remark that the higher energy beta-ray arises from a first-forbidden transition, according to Konopinski's notation,[10] and a characteristic "forbidden shape" is suggested by their Kurie plot. The fact that Nd^{142} is a "magic number" nucleus in neutrons, and the somewhat conflicting evidence for the decay scheme of Pr^{142} led the authors to the present study.

Two 100-mg samples of spectrographically pure (contaminants less than 0.1 percent) Pr_6O_{11} (empirical formula) made available through the courtesy of Dr. F. H. Spedding and Mr. T. A. Butler of this laboratory were bombarded in the Oak Ridge pile and then examined with a thin-lens spectrometer[11] modified to incorporate ring focusing.[12]

II. HALF-LIFE

The half-life of Pr^{142} was determined by following the activity of a sample of $PrCl_3$ with a Lauritsen electroscope for more than four half-lives. A value of 19.1 hr. was obtained. This is in good agreement with the values reported by Bothe[2] (19.2 hr.) and DeWire, Pool, and Kurbatov[5] (19.3 hr.).

III. SECONDARY ELECTRON SPECTRUM

The spectrometer was calibrated by means of the F conversion line of ThB (1385 $H\rho$). All the data reported in this paper were obtained with a spectrometer resolution of 2.1 percent (half-width) and a Geiger counter window of Formvar with a cut-off at 15 kev. The data have not been corrected for window absorption.

Since praseodymium has a single isotope,[13] namely Pr^{141}, it is assumed that only the radiations of Pr^{142} were observed in this investigation.

To obtain the secondary electron spectrum, the Pr^{142} was placed in a Lucite holder and covered with a copper cap, of surface density 1.4 g/cm^2, in order to absorb the

* Contribution No. 112 from the Institute for Atomic Research and Department of Physics, Iowa State College, Ames, Iowa. Work was performed in the Ames Laboratory of the AEC.

[1] Amaldi, D'Agostino, Fermi, Pontecorvo, Rasetti, and Segrè, Proc. Roy. Soc. 149A, 522 (1935).
[2] W. Bothe, Zeits. f. Naturforsch. **1a**, 173 (1946).
[3] C. E. Mandeville, Phys. Rev. **75**, 1287 (1949).
[4] E. T. Jurney, Phys. Rev. **76**, 290 (1949).
[5] DeWire, Pool, and Kurbatov, Phys. Rev. **61**, 544 (1942); Phys. Rev. **61**, 564 (1942).
[6] Peacock, Jones, and Overman, PPR Mon N-432 (1947).
[7] Cork, Schreffler, and Fowler, Phys. Rev. **74**, 1657 (1948).
[8] E. R. Rae, Proc. Phys. Soc. (London), **63A**, 292 (1950).
[9] S. DeBenedetti and F. K. McGowan, Phys. Rev. **74**, 728 (1948).
[10] E. J. Konopinski, Rev. Mod. Phys. **15**, 209 (1943).
[11] Jensen, Laslett, and Pratt, Phys. Rev. **75**, 458 (1949).
[12] Pratt, Boley, and Nichols, Phys. Rev. **79**, 208 (1950); Keller, Koenigsberg, and Paskin, Phys. Rev. **76**, 454 (1949).
[13] Inghram, Hess, and Hayden, Phys. Rev. **74**, 98 (1948).

beta-particles. On the copper cap was fastened a uranium foil having a surface density of 42 mg/cm². This source was placed in the spectrometer about 19 hours after the sample was removed from the Oak Ridge pile. The spectrum obtained is shown in Fig. 1. The insert in Fig. 1 shows the arrangement of the source of Pr^{142}, Lucite holder, copper cap, and uranium foil.

The *K* and *L* photo-electron lines of a single gamma-ray were observed. The mean value of the weighted gamma-ray energies, as determined from the *K* and *L* lines, was found to be 1.57_6 Mev. In calculating the gamma-ray energy a correction was made for the surface density of the uranium foil.[11] A search was made for low energy gamma-rays, using an Ag foil as a radiator, but none was found.

The broad distribution of electrons, exhibiting a maximum intensity at 1800 gauss-cm (Fig. 1), resembles the Compton distribution of a single gamma-ray but is not accompanied by the photoelectric conversion lines which would be expected to be associated with such a distribution. A search for weak photo-electron lines was made with a second sample of Pr^{142}, but none was found. The broad electron distribution, which shows the same decay constant as the remainder of the spectrum, is, accordingly, attributed to secondary electrons produced by bremsstrahlung arising from the passage of the beta-rays through the source-material and into the copper cap. An approximate calculation was made of the Compton electron distribution which would arise in a thick radiator from the bremsstrahlung expected[14] to originate in copper traversed by electrons possessing an energy distribution similar to those of the Pr^{142} beta-rays. The computed distribution resembled closely, in magnitude and in shape throughout the region of major interest, the extended distribution observed.

As a check of the foregoing interpretation for the prominent broad electron distribution observed, a source of $Sr^{90}-Y^{90}$ was placed in the spectrometer and covered with the same copper cap and uranium radiator

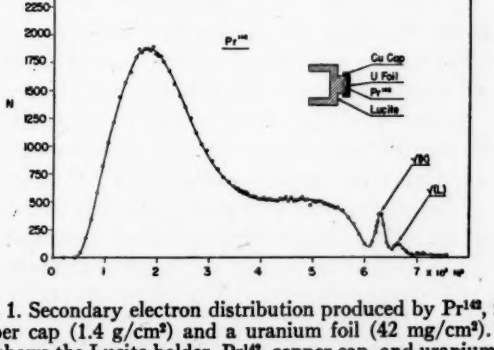

FIG. 1. Secondary electron distribution produced by Pr^{142}, from a copper cap (1.4 g/cm²) and a uranium foil (42 mg/cm²). The insert shows the Lucite holder, Pr^{142}, copper cap, and uranium foil. N is the observed counting rate. This diagram shows the electron distributions produced by bremsstrahlung, Compton scattering and the photoelectric effect.

[14] W. Heitler, *The Quantum Theory of Radiation* (Oxford Univeristy Press, New York, 1944), Ed. 2, p. 161.

TABLE I. Radiations from Pr^{142} reported by previous investigators.

Authors	β (Mev)	γ (Mev)
Mandeville	2.22, 0.215	1.74, 0.17
Jurney	2.52, 0.350	1.53
Cork *et al.*		0.62, 0.49, 0.33, 0.13 (from internal conversion lines)
DeWire *et al.*	2.14	1.9
Peacock *et al.*	2.23	~1.65, ~1.3
Rae	2.23, 0.66	1.59, 0.14 (I.C.).

used in the work with Pr^{142}. The strontium-yttrium source, which is gamma-free and emits beta-particles with a maximum energy[15] (2.23 Mev) close to that for Pr^{142}, was found to give under these conditions a secondary electron distribution (Fig. 2) of the type which we have attributed to bremsstrahlung in the case of Pr^{142}. The spectrum shown in Fig. 1 is thus regarded as a *composite* of the photoelectrons and Compton electrons arising from a single gamma-ray plus the electrons produced by bremsstrahlung. The contribution of bremsstrahlung to the secondary electron spectrum is especially prominent in the case of Pr^{142}, since there are about 25 beta-particles per gamma-ray (see Section V).

IV. BETA-RAY SPECTRUM

The beta-ray source was prepared by dissolving a portion of the irradiated Pr_6O_{11} in dilute HCl. A drop of the solution was deposited on a Formvar-polystyrene film, of surface density about 40 μg/cm², and allowed to evaporate to dryness. The average surface density of the source was about 1.1 mg/cm². The source was grounded by means of the technique described by Langer.[16] The beta-spectrum obtained is shown by the solid line in Fig. 3. The beta-spectrum determined with an earlier source revealed no internal conversion lines between the counter window cut-off and about 1100 gauss-cm. If the internal conversion lines reported by Cork *et al.*[7] actually exist, we estimate that the height of the lines is less than five percent of the counting rate at the corresponding positions of the beta-spectrum.

The allowed Kurie plot did not yield a straight line, but gave a curve characteristic of a first-forbidden transition (Gamow-Teller selection rules), with a spin change of two units and a parity change. The allowed Kurie plot is shown in Fig. 4. The modified Kurie plot with the approximate correction factor $a=(W_0-W)^2+W^2-1$, which has been considered appropriate for a spin change of two units with a parity change,[10] is shown by the crosses in Fig. 5. This curve indicates the presence of two beta-groups. The maximum kinetic energy of the high energy group is 2.15 Mev. On subtracting the high energy group, estimated in this way, from the total distribution, the maximum kinetic energy of the low energy group, as determined from the Kurie plot, was about 1.1 Mev. The difference between these

[15] E. N. Jensen and L. J. Laslett, Phys. Rev. **75**, 1949 (1949).
[16] L. M. Langer, Rev. Sci. Inst. **20**, 216 (1949).

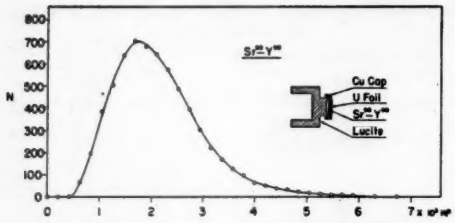

FIG. 2. Secondary electron distribution produced by a pure beta-source of $Sr^{90}-Y^{90}$, from a copper cap (1.4 g/cm²) and a uranium foil (42 mg/cm²). The electron distribution is produced by the bremsstrahlung formed in the copper cap due to the absorption of the beta-rays from $Sr^{90}-Y^{90}$.

two beta-energies is *not* in good agreement with the gamma-ray energy of 1.57_6 Mev.

The work of Marshak[17] and Greuling[18] suggests that a more precise form for the correction factor would be $a=(W_0-W)^2+\Lambda(W^2-1)$, where the coefficient Λ is not strictly independent of the electron momentum and differs appreciably from unity when Z is large. A graph showing Λ as a function of electron momentum for $Z=40$ and $Z=60$, which is appropriate for Pr, has been published recently.[19] In the case of Pr^{142} the coefficient Λ makes an appreciable difference in the modified Kurie plot, as is shown by the circles in Fig. 5. This plot gives a maximum kinetic energy of 2.15_4 Mev. An additional indication of the improvement obtained by including the coefficient Λ is given by the r.m.s. weighted relative differences between the straight line modified Kurie plots and the individual observed counting rates. Including all points with W greater than 2.3 mc², these values are 2.5 percent with $\Lambda=1$ and 0.8 percent with Λ as given by Fig. 1 of reference 19.

In subtracting the high energy beta-group and making a Kurie plot of the low energy beta-group, the data were not sufficiently accurate to determine whether or not this beta-group is of the allowed form. The allowed Kurie plot of this low energy group is shown in Fig. 5. The maximum kinetic energy is 0.63_6 Mev. This energy is in fairly good agreement with the maximum energy of the high energy beta-group and the energy of the

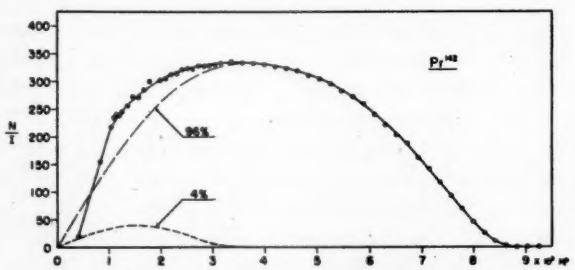

FIG. 3. Beta-spectra of Pr^{142}. The solid curve is the observed spectrum while the dashed curves represent the two beta-groups, calculated from the respective Kurie plots. N is the observed counting rate and I is the current in the spectrometer coil.

[17] R. E. Marshak, Phys. Rev. **61**, 431 (1942).
[18] E. Greuling, Phys. Rev. **61**, 568 (1942).
[19] Laslett, Jensen, and Paskin, Phys. Rev. **79**, 412 (1950).

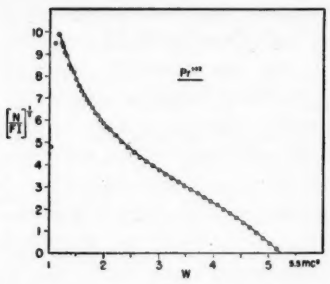

FIG. 4. The allowed Kurie plot of the beta-spectrum of Pr^{142}.

gamma-ray. The agreement is much better if a modified Kurie plot is made using the correction factor, a. This gives a maximum kinetic energy of 0.58_1 Mev. However, for reasons discussed in Section V, it is believed that the low energy beta-group is probably a first-forbidden transition, but is *not* of the type in which the correction factor is appropriate.

There are two primary sources of error in the low energy beta-group. One is the low intensity of the group together with the additional error introduced by subtraction of the high energy group. The second error involves a small apparent loss of the source while in the spectrometer. The mean half-life determined from points taken at different times at 20 different current values was found to be 18.4 hr. This is appreciably lower than that reported in Section II. It is believed that the vacuum in the spectrometer is sufficient to remove some of the water of hydration of the $PrCl_3$, which in turn may result in the removal of a small amount of the $PrCl_3$. This would explain the smaller half-life obtained from the spectrometer data. The importance of this effect was minimized by repeated traversals of the spectrum, which led to consistency in the data when a correction was applied for the observed half-life.

The deviations from the straight line of the points below $W=1.55$ mc² is thought to be due to the fairly large surface density of the source.

V. DISCUSSION

A consistent decay scheme for Pr^{142} is shown in Fig. 6. Since Nd^{142} is an even-even nucleus, it is reasonable to assume that the ground state has a spin of zero and even parity. The high energy beta-group is first forbidden with a spin change of two units and a parity change. Hence the ground state of Pr^{142} is assigned a spin of two units with odd parity. This is in complete agreement with the predictions of the nuclear shell model[20] in regard to parity, and to spin in accordance with rule nine proposed by Nordheim[21] for the case of beta-decay for odd-odd nuclei.

Although the Kurie plot with the correction factor gave a suitable straight line and a maximum energy for the soft beta in excellent agreement with the difference

[20] M. G. Mayer, Phys. Rev. **78**, 16 (1950).
[21] L. W. Nordheim, Phys. Rev. **78**, 294 (1950).

between the high energy beta-group and the gamma-ray, it appears to be very unlikely that the transition is one with a spin change of two units and a parity change. This would demand a spin of zero or four units with even parity for the 1.57-Mev level. A gamma-ray transition between two states with $I=0$ is strictly forbidden. A gamma-ray transition of 1.57 Mev with a spin change of four units and no change of parity would require a

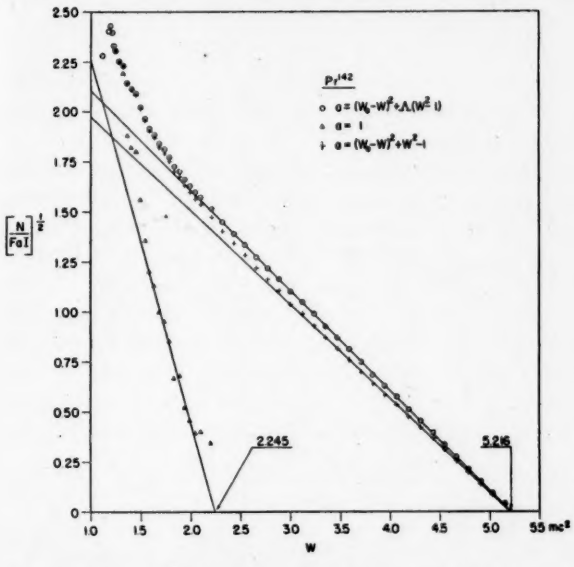

FIG. 5. The modified Kurie plots of Pr^{142}. The low energy group was obtained by the usual subtraction.

metastable state with a half-life[22] of 3.2×10^{-6} sec. DeBenedetti and McGowan[9] report a negative result of a search for a metastable state of Nd^{142} in the range 10^{-6} to 10^{-3} sec. The *ft* value of the low energy group is 9×10^{6}, which is classed empirically as first forbidden.[10] According to selection rules this demands a change in parity, hence the 1.57 Mev level is assigned an even

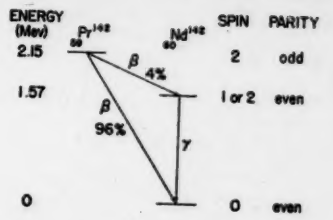

FIG. 6. Decay scheme of Pr^{142}.

parity. The gamma-ray transition then involves no change in parity. The possible spin assignments of the 1.57-Mev level are 1 or 2 units. For a spin of 1 unit the gamma-radiation is either magnetic dipole or a mixture of magnetic dipole and electric quadrupole. For a spin of 2 units the gamma-radiation is electric quadrupole. This gives a spin change of one or zero units for the low energy beta-transition.

The high energy beta-group has an *ft* value of 0.6×10^{8}, which is in agreement with the values of *ft* given by Nordheim[21] in rule number six for this type of transition. The (W_0^2-1) *ft* value for this group is 0.2×10^{10} which also is in good agreement with the values given by Shull and Feenberg[23] for several other nuclei undergoing beta-transitions of a similar character, in which the spin change is two units with a parity change.

Assuming that the high energy group is first forbidden with a spin change of two units and a parity change, and the low energy group to be represented by an "allowed" Kurie plot the percentage transitions associated with these groups are 96 and 4, respectively. These two beta-groups are shown by the dashed curves in Fig. 3.

The authors wish to express their appreciation to Mr. W. J. Heiman of the radiochemistry section of this laboratory for preparing the sources, Mr. E. R. Rathbun, Jr. for construction of the Geiger counter and Mr. A. Paskin for helpful discussions on the theoretical aspects of the problems.

[22] E. Segrè and A. C. Helmholz, Rev. Mod. Phys. **21**, 271 (1949).

[23] F. B. Shull and E. Feenberg, Phys. Rev. **75**, 1768 (1949).

Internal Conversion in the L_I-Shell

H. GELLMAN, B. A. GRIFFITH, AND J. P. STANLEY
Computation Centre, McLennan Laboratory, University of Toronto, Toronto, Canada
(Received April 3, 1950)

Analytical expressions obtained by Goertzel and Rose for the internal conversion of γ-radiation have been simplified from a computational viewpoint for the L-shell. Complex expressions involving gamma-functions and hypergeometric functions are simplified and reduced, in several cases, to algebraic expressions. Numerical calculations have been carried out for the L_I-shell, for electric dipole, electric quadrupole and magnetic dipole radiation.

I. INTRODUCTION

THE theoretical evaluation of the internal conversion of γ-radiation in an atomic system is a well known problem and has been treated by a number of writers. In particular, the case in which the atomic nucleus is assumed to radiate the field of an electric dipole has been treated exhaustively in a paper by Hulme.[1] Hulme employs Dirac's relativistic equations and derives formulas for the conversion coefficients corresponding to the electrons of the K and L_I-shells. Goertzel and Rose[2] have generalized Hulme's treatment to obtain results for radiation from multipoles of arbitrary order. Except that screening effects have been neglected, these formulas are exact and enable us to calculate numerical values of the internal conversion coefficient if the atomic number Z and the energy of γ-radiation are assigned.

The expressions for the internal conversion coefficients are extremely complex and the task of calculating numerical values for the various conversion coefficients from such expressions is a formidable one. Recently, considerable importance has been attached to more exact calculation of these coefficients and a paper by Stanley[3] contains the results of work done in an attempt to provide a table of K-shell values in the electric dipole case. A more extensive table has recently been prepared by Rose and his co-workers[4] containing K-shell internal conversion coefficients for electric and magnetic multipole radiation up to poles of order 2^5.

As a preliminary to the calculations reported by Stanley[3] the formula given by Hulme[1] was simplified. The present paper contains corresponding simplifications of the formulas obtained by Goertzel and Rose. These are summarized in Section II. A brief account of the method used and the resulting modified expressions are given in Section V; Section IV is devoted to a summary of Goertzel and Rose's formula for the internal conversion coefficient in the L_I-shell, for the case of electric dipole radiation. The calculations based on the simplified formulas for the L_I-shell are tabulated in Section III.

It should be noted that the calculations given here do not take account of screening effects. The purpose of our work was to obtain "unscreened" coefficients as a basis for comparison with "screened" calculations, whereby screening effects could be evaluated. Consequently no attempt at completeness has been made. In particular, it should be emphasized that no calculations were made for the L_{II} and L_{III}-shells.

II. SUMMARY OF SIMPLIFIED FORMULAS

Relations and formulas are presented in their approximate order of calculation.

(A) L_I-Shell

(a) *All Multipoles*

$\alpha=1/137.03$, $k=\gamma$-ray energy, $Z=$atomic number

[Relativistic units are used throughout. That is, $m=c=\hbar=1$, $e^2=\alpha$. Units of energy, momentum and length are mc^2, mc and $\hbar/mc$, respectively.]

$$\gamma=+(1-(\alpha Z)^2)^{\frac{1}{2}},$$

$E=[\frac{1}{2}(1+\gamma)]^{\frac{1}{2}}=$initial state energy inclusive of rest energy,

$W=k+E=$final state energy inclusive of rest energy,

$p=+(W^2-1)^{\frac{1}{2}}=$final state momentum,

$$\theta=\alpha ZW/p,$$

$$2\zeta=\frac{p}{2kE(W-p)}[2E(p-k)+i(\alpha Z)],$$

$$1/2\zeta=(1/4Ep)[2E(p-k)-i(\alpha Z)]$$

$$|N|^2=\frac{p^{-2\gamma-1}e^{\pi\theta}(\alpha Z)^{2\gamma+1}|\Gamma(\gamma-i\theta)|^2}{4\pi k\cdot\Gamma(2\gamma+1)\cdot(1+\gamma)|(-2\zeta)^{-(\gamma-i\theta)}|^2}\times\frac{(1+E)}{(2E-1)(2E)^{2\gamma+2}}$$

$$\lambda=((W-1)/k)^{\frac{1}{2}},\quad \mu=((W+1)/k)^{\frac{1}{2}}.$$

[1] H. R. Hulme, Proc. Roy. Soc. (London), **A138**, 643 (1932).
[2] G. Goertzel and M. E. Rose, 1947 (unpublished).
[3] J. P. Stanley, Can. J. Research, **A27**, 17 (1949).
[4] Rose, Goertzel, Spinrad, Harr, and Strong, Phys. Rev. **76**, 184 (1949). These authors have distributed privately an extensive table of their results.

(b) *Electric Dipole Case*

$$\gamma'=(4-(\alpha Z)^2)^{\frac{1}{2}},$$

$$F_1=F(\gamma'+i\theta,\ i\theta-\gamma';\ 1-\gamma+i\theta;\ 1/2\zeta),$$

$$F_2=F(\gamma+\gamma',\ \gamma-\gamma';\ 1+\gamma-i\theta;\ 1/2\zeta),$$

$$F_3=F(1+\gamma'+i\theta,\ 1-\gamma'+i\theta;\ 2-\gamma+i\theta;\ 1/2\zeta),$$

$$F_4=F(\gamma+\gamma',\ \gamma-\gamma';\ \gamma-i\theta;\ 1/2\zeta),$$

$$w=\frac{\Gamma(i\theta-\gamma)\cdot\Gamma(1+\gamma'-i\theta)\cdot\Gamma(\gamma+\gamma')}{\Gamma(\gamma'-\gamma+1)\cdot\Gamma(\gamma'+i\theta)\cdot\Gamma(\gamma-i\theta)}\cdot(-2\zeta)^{-(\gamma-i\theta)}$$

$$\Lambda=\frac{1}{2k}\{(\alpha Z)(k+2)(2E-3)+i[6(k+1)(E-1)-(k+2)(1+\gamma)(2E-3)]\},$$

$$\mathrm{M}=\frac{1}{2k}\left\{-\frac{\alpha Z}{E}[E(k+2)(2E-3)+3]+i(2E-1)[(k+2)(1+\gamma-2E)-6k]\right\},$$

$$P_1=(\Lambda\lambda+\mathrm{M}\mu)\cdot F_1-(\Lambda\lambda-\mathrm{M}\mu)\left[\left(\frac{1}{2\zeta}\right)\left(\frac{2+i\alpha Z/p}{1-\gamma+i\theta}\right)\right]\cdot F_3,$$

$$P_2=(\Lambda\lambda+\mathrm{M}\mu)\cdot F_2-(\Lambda\lambda-\mathrm{M}\mu)\left[\frac{-\gamma+i\theta}{2-i\alpha Z/p}\right]\cdot F_4,$$

$$|P|^2=|P_1+wP_2|^2,$$

$$|Q|^2=16E^2\frac{(1-k)^2}{k^3}(W-\gamma)\left|\left(1-\frac{1}{2\zeta}\right)^{-(\gamma+i\theta)}\right|^2,$$

β = internal conversion coefficient

$$=\tfrac{1}{3}\pi\alpha k|N|^2\cdot[2|P|^2+|Q|^2].$$

(c) *Magnetic Dipole Case*

γ', F_1, F_2, F_3, F_4, w as in the electric dipole case,

$$F_1'=F(\gamma+i\theta,\ i\theta-\gamma;\ 1-\gamma+i\theta;\ 1/2\zeta),$$

$$F_3'=F(1+\gamma+i\theta,\ 1-\gamma+i\theta;\ 2-\gamma+i\theta;\ 1/2\zeta),$$

$$w'=\frac{\Gamma(2\gamma)\cdot\Gamma(1+\gamma-i\theta)\cdot\Gamma(i\theta-\gamma)}{\Gamma(\gamma+i\theta)\cdot\Gamma(\gamma-i\theta)}\cdot(-2\zeta)^{-(\gamma-i\theta)},$$

$$\Lambda=-(2E-1)(E^2+E+1)+i(\tfrac{1}{2}\alpha Z)\left(\frac{1}{kE}-2E-1\right),$$

$$\mathrm{M}=\left[(2E^3+E^2-E-1)+\frac{1}{k}(1-E)\right]+i(\tfrac{1}{2}\alpha Z)(2E+1),$$

$$\Lambda'=-\frac{2E}{2\gamma-1}(E^2-1)(4E^2-4E+3)-i(\alpha ZE)\left(4E^2-4E+3+\frac{4}{k}\right)\frac{1}{2\gamma-1}$$

$$\mathrm{M}'=\frac{2E^2}{2\gamma-1}\left(4E^3-4E^2-5E+\frac{4E}{k}-\frac{4}{k}+4\right)+i(\alpha ZE)(4E^2-4E+3)\frac{1}{2\gamma-1}$$

$$P_1=(\Lambda\lambda+\mathrm{M}\mu)F_1+(\Lambda\lambda-\mathrm{M}\mu)\left[\left(\frac{1}{2\zeta}\right)\cdot\frac{2-i(\alpha Z/p)}{1-\gamma+i\theta}\right]\cdot F_3,$$

$$P_2=(\Lambda\lambda+\mathrm{M}\mu)F_2-(\Lambda\lambda-\mathrm{M}\mu)\left[\frac{\gamma-i\theta}{2+i\alpha Z/p}\right]\cdot F_4,$$

$$Q_1=(\Lambda'\lambda+\mathrm{M}'\mu)F_1'-(\Lambda'\lambda-\mathrm{M}'\mu)\left[\left(\frac{1}{2\zeta}\right)\cdot\frac{1+(\alpha Z/p)}{1-\gamma+i\theta}\right]\cdot F_3',$$

$$Q_2=(\Lambda'\lambda+\mathrm{M}'\mu)+\left(\frac{1+i(\alpha Z/p)}{\gamma'+i\theta}\right)(\Lambda'\lambda-\mathrm{M}'\mu),$$

$$|P|^2=|P_1+wP_2|^2,\quad |Q|^2=|Q_1+w'Q_2|^2,$$

β = internal conversion coefficient

$$=(\pi\alpha k/3)|N|^2\cdot[2|P|^2+4|Q|^2].$$

(d) *Electric Quadrupole Case*

$$\gamma_1'=[9-(\alpha Z)^2]^{\frac{1}{2}},\quad \gamma_2'=[4-(\alpha Z)^2]^{\frac{1}{2}},$$

F_1 to F_4 are defined as the F_1 to F_4 of the electric dipole case with $\gamma'=\gamma_1'$,

F_1' to F_4' are defined as the F_1 to F_4 of the electric dipole case with $\gamma'=\gamma_2'$,

$w_1=w$ of the electric dipole case with $\gamma'=\gamma_1'$,

$w_2=w$ of the electric dipole case with $\gamma'=\gamma_2'$,

$$\lambda_1=2kE[-4(k+3)E^5+8(k+3)E^4-(k+9)E^3+(4k+15)E^2+2(7k+6)E-12(k+1)],$$

$$\mu_1=2E[4k(k+3)E^5-8k(k+3)E^4-k(3k-21)E^3-(4k^2+3k+6)E^2+(-19k^2+3k+18)E+12(k^2-1)],$$

$$\lambda_2=(\alpha Z)[-4k(k+3)E^4+8k(k+3)E^3+k(7k-9)E^2+(4k^2+27k+6)E-12(k+1)],$$

TABLE I. Internal conversion coefficients as functions of gamma-ray energy. (Observed L_I-electrons/observed photons of energy k.)

Atomic number Z	Gamma-ray energy k (mc^2 units)	Electric dipole	Electric quadrupole	Magnetic dipole
92	0.09273	0.2372	9.199	43.98
	0.2927	0.02097	0.1548	1.896
	0.6427	0.003916	0.01694	0.2079
84	0.0833	0.2910	5.300	27.85
	0.2333	0.03011	0.1103	1.381
	0.5333	0.004569	0.01546	0.1313
49	0.0283	2.202	5.787	19.22
	0.2083	0.01520	0.1026	0.05396
	0.4083	0.002440	0.01176	0.007751

$$\mu_2=(\alpha Zk)[4(k+3)E^4-8(k+3)E^3+(33-7k)E^2-(4k+39)E+30],$$

$$\Lambda=\frac{1}{k^2E(4E^2+5)}(\lambda_1+i\lambda_2),$$

$$\mathrm{M}=\frac{1}{k^2E(4E^2+5)}(\mu_1+i\mu_2),$$

$$\lambda_1'=2E[E^6(48k^2-96k)+E^5(24k^2-48k)+E^4(-78k^2+48k)+E^3(-3k^2+60k)+E^2(57k^2-24k)+E(-21k^2+24k)],$$

$$\mu_1'=2E[E^6(-48k^2+96k)+E^5(-24k^2+48k)+E^4(126k^2-192k)+E^3(3k^2-24k+12)+E^2(-87k^2+129k-36)+E(21k^2-45k+24)],$$

$$\lambda_2'=(\alpha Z)[E^5(48k^2-96k)+E^4(24k^2-48k)+E^3(-54k^2+48k)+E^2(-3k^2+96k-12)+E(-21k+24)],$$

$$\mu_2'=(\alpha Z)[E^5(-48k^2+96k)+E^4(-24k^2+48k)+E^3(54k^2-96k)+E^2(3k^2-12k)],$$

$$\Lambda'=\frac{1}{2k^2E^2(8E^2-5)}(\lambda_1'+i\lambda_2'),$$

$$\mathrm{M}'=\frac{1}{2k^2E^2(8E^2-5)}(\mu_1'+i\mu_2'),$$

$$P_1=(\Lambda\lambda+\mathrm{M}\mu)F_1-(\Lambda\lambda-\mathrm{M}\mu)\left[\left(\frac{1}{2\zeta}\right)\left(\frac{3+i\alpha Z/p}{1-\gamma+i\theta}\right)\right]\cdot F_3,$$

$$P_2=(\Lambda\lambda+\mathrm{M}\mu)F_2-(\Lambda\lambda-\mathrm{M}\mu)\left[\frac{-\gamma+i\theta}{3-i\alpha Z/p}\right]\cdot F_4,$$

$$Q_1=(\Lambda'\lambda+\mathrm{M}'\mu)F_1'+(\Lambda'\lambda-\mathrm{M}'\mu)\left[\left(\frac{1}{2\zeta}\right)\left(\frac{2-i\alpha Z/p}{1-\gamma+i\theta}\right)\right]\cdot F_3',$$

$$Q_2=(\Lambda'\lambda+\mathrm{M}'\mu)F_2'+(\Lambda'\lambda-\mathrm{M}'\mu)\left[\frac{-\gamma+i\theta}{2+i\alpha Z/p}\right]\cdot F_4'.$$

$$|P|^2=|P_1+w_1P_2|^2,\quad |Q|^2=|Q_1+w_2Q_2|^2,$$

β = internal conversion coefficient

$$=\frac{4}{15}\pi\alpha k|N|^2\left[3|P|^2+\frac{1}{2}|Q|^2\right],$$

(B) L_{II}-Shell, Electric Dipole Case

α, k, W, E, γ, θ, p, Z, ζ, λ, μ are the same as those defined for the L_I-shell,

$|N|^2$ is the same as in the L_I-shell except that the factor $(2E-1)(2E)^{2\gamma+2}$ is replaced by $(2E+1)(2E)^{2\gamma+2}$,

$\gamma'=[4-(\alpha Z)^2]^{\frac{1}{2}}$, w, F_1, F_2, F_3, F_4 as in the L_I-shell, electric dipole case,

$$\Lambda=\frac{\alpha Z}{2kE(E+1)}[E^2(2-k)(2E+3)+E(5k+2)+3k]+i((E-1)/k)[E(k-2)(2E+3)-3],$$

$$\mathrm{M}=\frac{\alpha Z}{2kE(E+1)}[E^2(k-2)(2E+3)-3(E+1)(k-1)]-i((E-1)/k)\cdot E\cdot(k-2)(2E+3),$$

$$P_1=(\Lambda\lambda+\mathrm{M}\mu)F_1+(\Lambda\lambda-\mathrm{M}\mu)\left[\left(\frac{1}{2\zeta}\right)\left(\frac{2-i\alpha Z/p}{1-\gamma+i\theta}\right)\right]\cdot F_3,$$

$$P_2=(\Lambda\lambda+\mathrm{M}\mu)F_2-(\Lambda\lambda-\mathrm{M}\mu)\left[\frac{\gamma-i\theta}{2+i\alpha Z/p}\right]\cdot F_4,$$

$$|P|^2=|P_1+wP_2|^2,$$

$$|Q|^2=\frac{4(k+1)^2}{k^3}\cdot\frac{(\alpha Z)^2}{(1+E)^2}\cdot(W+\gamma)\left|\left(1-\frac{1}{2\zeta}\right)^{-(\gamma+i\theta)}\right|^2,$$

β = internal conversion coefficient

$$=\frac{\pi\alpha k}{3}|N|^2[2|P|^2+|Q|^2].$$

(C) L_{III}-Shell, Electric Dipole Case

α, k, W, θ, p, Z, λ, μ as in the L_I-shell, electric dipole case,

$\gamma=[4-(\alpha Z)^2]^{\frac{1}{2}}$, $E=\gamma/2$,

$$\zeta=\frac{ip}{(\alpha Z/2)-ik+ip},\quad \frac{1}{\zeta}=\frac{1}{2p}[2(p-k)-i\alpha Z],$$

$$|N|^2=\frac{(2p)^{-2\gamma-1}e^{\pi\theta}(\alpha Z)^{2\gamma+1}|\Gamma(\gamma-i\theta)|^2}{8\pi k\Gamma(2\gamma+1)\cdot(\gamma+2)|(-2\zeta)^{-(\gamma-i\theta)}|^2},$$

$$\gamma_1'=[9-(\alpha Z)^2]^{\frac{1}{2}},$$

$$\gamma_2'=[4-(\alpha Z)^2]^{\frac{1}{2}}=\gamma,$$

$$\gamma_3'=[1-(\alpha Z)^2]^{\frac{1}{2}},$$

F_1 to F_4 defined as in the L_I-shell, electric dipole case with new ζ, γ and with $\gamma'=\gamma_1'$,

F_1' to F_4' defined as F_1 to F_4 above, with new ζ, γ, and with $\gamma'=\gamma_3'$,

w_1 defined as w in L_I-shell, electric dipole case, with new γ and $\gamma'=\gamma_1'$,

w_2 defined as w in L_I-shell, electric dipole case, with new γ and $\gamma'=\gamma_3'$,

$$\Lambda_1=i\left[(3-\gamma)+\frac{1}{2k}(\gamma+2)\right],$$

$$\mathrm{M}_1=\frac{\alpha Z}{2k}(1-2k)-5i,$$

$$P_1=(\Lambda_1\lambda+\mathrm{M}_1\mu)F_1-(\Lambda_1\lambda-\mathrm{M}_1\mu)\left[\frac{1}{2\zeta}\left(\frac{3+i\alpha Z/p}{1-\gamma+i\theta}\right)\right]\cdot F_2,$$

$$P_2=(\Lambda_1\lambda+\mathrm{M}_1\mu)F_2+(\Lambda_1\lambda-\mathrm{M}_1\mu)\left[\frac{\gamma-i\theta}{3-i\alpha Z/p}\right]\cdot F_4,$$

$$|P|^2=|P_1+w_1P_2|^2,$$

$$|Q|^2=\frac{16(\gamma+2)}{k^2}(2k-1)^2\left|\left(1-\frac{1}{2\zeta}\right)^{-(\gamma+i\theta)}\right|^2,$$

$$\Lambda_2=\frac{\alpha Z}{2k(2-\gamma)}[6k+i(\alpha Z)(2k-1)],$$

$$\mathrm{M}_2=-\frac{\alpha Z}{2k(2-\gamma)}[2k(\gamma+1)+(2-\gamma)],$$

$$R_1=(\Lambda_2\lambda+\mathrm{M}_2\mu)F_1'-(\Lambda_2\lambda-\mathrm{M}_2\mu)\left[\left(\frac{1}{2\zeta}\right)\left(\frac{1+\alpha Z/p}{1-\gamma+i\theta}\right)\right]\cdot F_3',$$

$$R_2=(\Lambda_2\lambda+\mathrm{M}_2\mu)F_2'+(\Lambda_2\lambda-\mathrm{M}_2\mu)\left[\frac{\gamma-i\theta}{1-\alpha Z/p}\right]\cdot F_4',$$

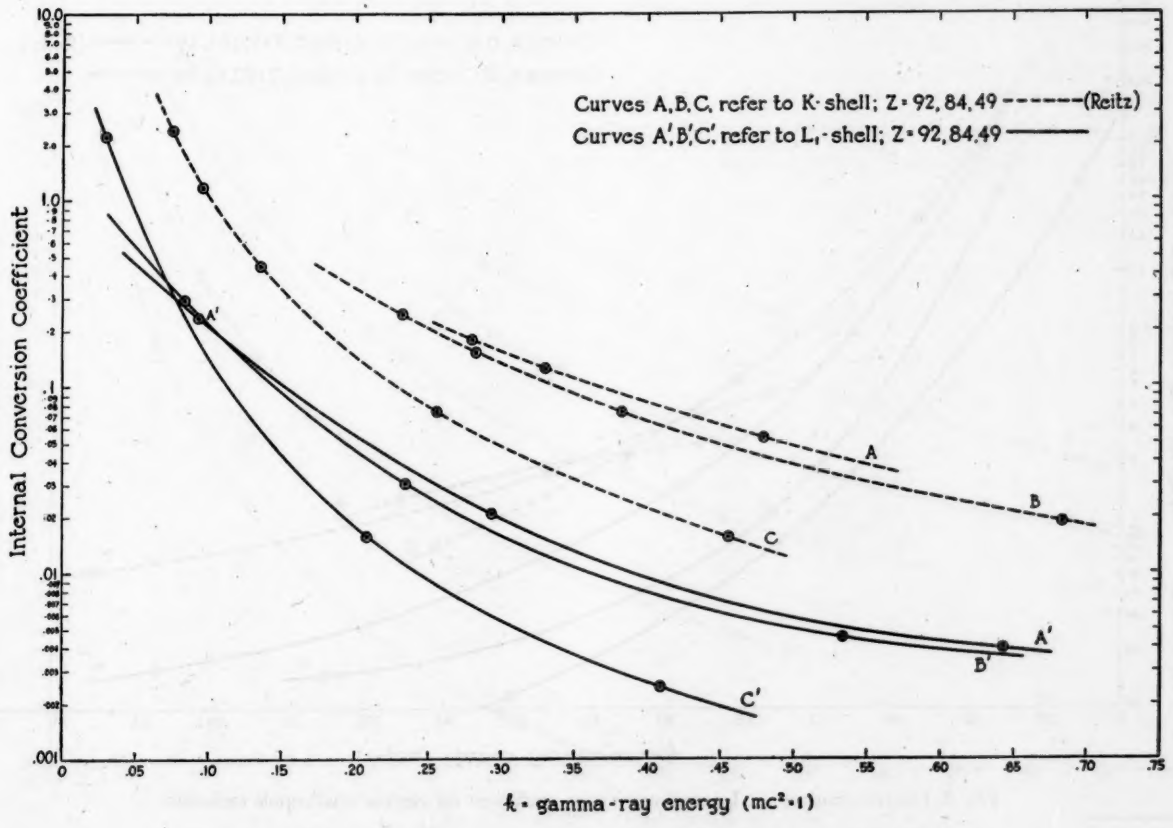
Curves A, B, C, refer to K-shell; Z = 92, 84, 49 ------(Reitz)
Curves A', B', C', refer to L1-shell; Z = 92, 84, 49 ———
Internal Conversion Coefficient
k = gamma-ray energy (mc²=1)
A
B
C
A'
B'
C'

FIG. 1. Electric dipole. Internal conversion coefficient for electric dipole radiation.

$|R|^2=|R_1+w_2R_2|^2$,

β=internal conversion coefficient

$$=\frac{\pi\alpha k}{3}|N|^2\cdot\left[\frac{18}{5}|P|^2+\frac{2}{5}|Q|^2+2|R|^2\right].$$

III. THE NUMERICAL CALCULATIONS OF THE COEFFICIENTS FOR THE L_I-SHELL

For each of atomic numbers 92, 84 and 49, the formulas for the L_I-shell given in Section II were used to calculate the internal conversion coefficients corresponding to certain γ-ray energies. These γ-ray energies cover the range used by Reitz[5] in calculating internal conversion coefficients for the K-shell. Reitz has taken account of screening in his calculations. Our results are given in Table I and plotted in Figs. 1, 2 and 3 together with those obtained by Reitz for the K-shell. Comparison of the two sets of curves leads us to suspect errors in the curves A, B of Fig. 2 obtained by Reitz.

All of the numerical calculations were carried out with the use of Marchant and Friden desk calculators except in the case of the ninety (90) hypergeometric functions which were evaluated on I.B.M. punched card machines.

IV. CONVERSION IN THE L_I-SHELL: ELECTRIC DIPOLE CASE

Summary of Goertzel and Rose Formula

β=internal conversion coefficient$=\frac{1}{3}\pi\alpha kS$, (1)

α=fine structure constant$=1/137.03$,
$k=\gamma$-ray energy,

$S=2|P_{1,\frac{1}{2}}|^2+|Q_{1,\frac{1}{2}}|^2$, (2)

$P_{1,\frac{1}{2}}=(R_1+R_2+2R_4)_{1,\frac{1}{2}}$,
$Q_{1,\frac{1}{2}}=(R_1+R_2-3R_3-R_4)_{1,\frac{1}{2}}$. (3)

Definition of $P_{1,\frac{1}{2}}$

$$(R_1+R_2+2R_4)_{1,\frac{1}{2}}=N_{\frac{1}{2}}\cdot D\{\mathcal{J}_1(\gamma+\gamma')(-ib_1C_1+d_1C_2)$$
$$+\varphi_{\frac{1}{2}+}\mathcal{J}_1^*(\gamma+\gamma')(ib_1C_1+d_1C_2)$$
$$+\mathcal{J}_1(\gamma+\gamma'+1)(-ib_2C_1+d_2C_2)+$$
$$\varphi_{\frac{1}{2}+}\mathcal{J}_1^*(\gamma+\gamma'+1)(ib_2C_1+d_2C_2)-2b_1C_4\mathcal{J}_0(\gamma+\gamma')$$
$$-2b_1C_4\varphi_{\frac{1}{2}+}\mathcal{J}_0^*(\gamma+\gamma')-2b_2C_4\mathcal{J}_0(\gamma+\gamma'+1)$$
$$-2b_2C_4\varphi_{\frac{1}{2}+}\mathcal{J}_0^*(\gamma+\gamma'+1)\}, \quad (4)$$

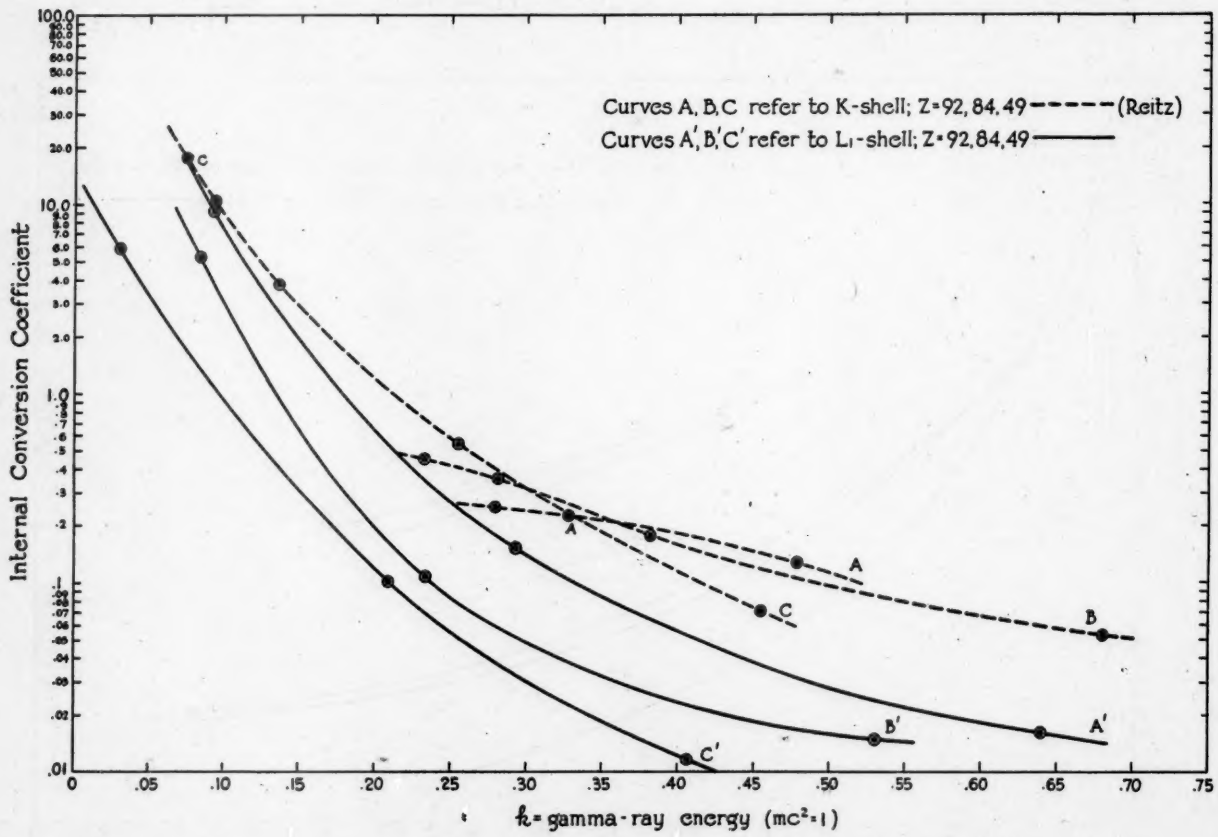

FIG. 2. Electric quadrupole. Internal conversion coefficient for electric quadrupole radiation.

[5] J. R. Reitz, Phys. Rev. 77, 10 (1950).

$$N_{\frac{1}{2}}=\frac{e^{\pi\theta/2}\cdot(p/2)^{\gamma'}}{2(\pi p)^{\frac{1}{2}}|\Gamma(\gamma'+i\theta)|},\quad \theta=\frac{\alpha ZW}{p},\quad p=[W^2-1]^{\frac{1}{2}}, \tag{5}$$

Z=atomic number, $W=E+k$, $E=\left[\frac{1+\gamma}{2}\right]^{\frac{1}{2}}$,

$\gamma=[1-\alpha^2Z^2]^{\frac{1}{2}}$, $\gamma'=[4-\alpha^2Z^2]^{\frac{1}{2}}$,

$$D=\left[\frac{2\gamma+1}{\Gamma(2\gamma+1)}\right]^{\frac{1}{2}}\cdot\frac{(2\alpha Z)^{\gamma+\frac{1}{2}}}{2\cdot(2E)^{\gamma+1}(2E+1)^{\frac{1}{2}}}, \tag{6}$$

$$b_1=2(E+1),\ b_2=-\frac{\alpha Z}{E}\cdot\frac{2E+1}{2\gamma+1},\ d_1=2E,\ d_2=b_2, \tag{7}$$

$$C_1=[(W-1)(1-E)]^{\frac{1}{2}}=k^{\frac{1}{2}}\lambda\cdot(1-E)^{\frac{1}{2}},$$

$$(W-1)^{\frac{1}{2}}=k^{\frac{1}{2}}\lambda, \tag{8}$$

$$C_2=[(W+1)(1+E)]^{\frac{1}{2}}=k^{\frac{1}{2}}\mu(1+E)^{\frac{1}{2}},\ (W+1)^{\frac{1}{2}}=k^{\frac{1}{2}}\mu,$$

$$C_3=[(W-1)(1+E)]^{\frac{1}{2}}=k^{\frac{1}{2}}\lambda(1+E)^{\frac{1}{2}},$$

$$C_4=[(W+1)(1-E)]^{\frac{1}{2}}=k^{\frac{1}{2}}\mu(1-E)^{\frac{1}{2}},$$

$$p=(W^2-1)^{\frac{1}{2}}=k\lambda\mu,$$

$$\varphi_{\frac{1}{2}+}=\frac{\gamma'+i\theta}{2+(i\theta/W)}\ \text{and has unit modulus,} \tag{9}$$

$$\mathcal{J}_1(\gamma+\gamma')=A\left\{\Gamma(\gamma+\gamma')F(\gamma+\gamma')-\frac{p}{k\zeta}\Gamma(\gamma+\gamma'-1)F(\gamma+\gamma'-1)\right\}, \tag{10}$$

$$\mathcal{J}_1^*(\gamma+\gamma')=\bar{A}\left\{\Gamma(\gamma+\gamma')\bar{F}(\gamma+\gamma')+\frac{p}{k\bar{\zeta}}\Gamma(\gamma+\gamma'-1)\bar{F}(\gamma+\gamma'-1)\right\}$$

$$\mathcal{J}_1(\gamma+\gamma'+1)=\frac{\zeta}{ip}\cdot A\left\{\Gamma(\gamma+\gamma'+1)F(\gamma+\gamma'+1)-\frac{p}{k\zeta}\Gamma(\gamma+\gamma')F(\gamma+\gamma')\right\}$$

$$\mathcal{J}_1^*(\gamma+\gamma'+1)=\frac{-\zeta}{ip}\bar{A}\left\{\Gamma(\gamma+\gamma'+1)\bar{F}(\gamma+\gamma'+1)+\frac{p}{k\bar{\zeta}}\Gamma(\gamma+\gamma')\bar{F}(\gamma+\gamma')\right\},$$

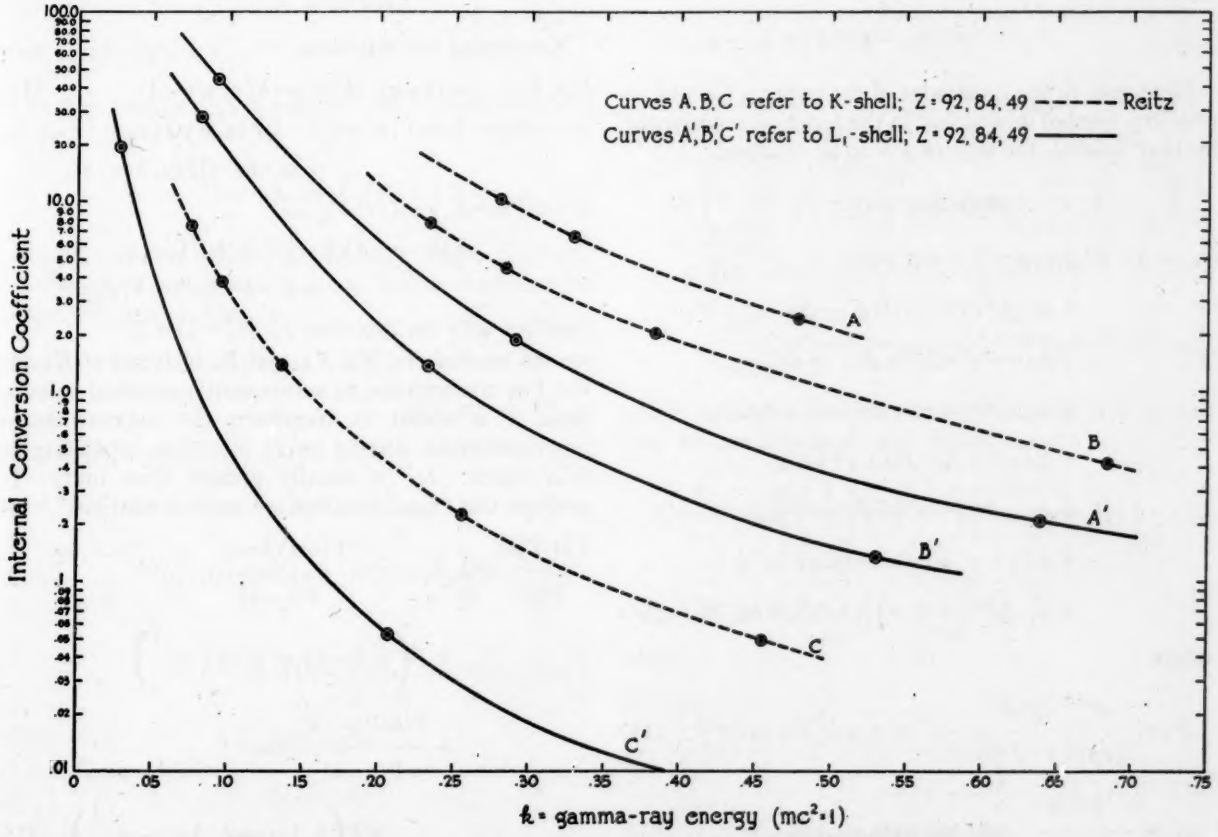
Curves A, B, C refer to K-shell; Z = 92, 84, 49 ----- Reitz
Curves A', B', C' refer to L1-shell; Z = 92, 84, 49 ———
Internal Conversion Coefficient
k = gamma-ray energy (mc²=1)
A
B
A'
B'
C
C'

FIG. 3. Magnetic dipole. Internal conversion coefficient for magnetic dipole radiation.

$$\mathcal{J}_0(\gamma+\gamma')=iA\Gamma(\gamma+\gamma')F(\gamma+\gamma'),$$

$$\mathcal{J}_0^*(\gamma+\gamma')=i\bar{A}\Gamma(\gamma+\gamma')\bar{F}(\gamma+\gamma'),$$

$$\mathcal{J}_0(\gamma+\gamma'+1)=\frac{\zeta}{p}A\Gamma(\gamma+\gamma'+1)F(\gamma+\gamma'+1),$$

$$\mathcal{J}_0^*(\gamma+\gamma'+1)=-\frac{\zeta}{p}\bar{A}\Gamma(\gamma+\gamma'+1)\bar{F}(\gamma+\gamma'+1),$$

$$A=\frac{-2^{2\gamma'}}{k}\cdot\left(\frac{\zeta}{ip}\right)^{\gamma+\gamma'}\frac{\Gamma(\gamma'-i\theta)\cdot\Gamma(1+\gamma'+i\theta)}{\Gamma(1+2\gamma')}$$
$$=A(k,p), \quad (11)$$

$$\bar{A}=A(k,-p)=\frac{-2^{2\gamma'}}{k}\left(\frac{-\bar{\zeta}}{ip}\right)\cdot\frac{\Gamma(\gamma'+i\theta)\Gamma(1+\gamma'-i\theta)}{\Gamma(1+2\gamma')}$$

since $\theta=\alpha ZW/p$,

$$\zeta=\frac{ip}{a-ik+ip}, \quad \bar{\zeta}=\frac{-ip}{a-ik-ip}, \quad a=\alpha Z/2E,$$

$$F(\nu)=F(\nu,\gamma'+i\theta+1;1+2\gamma';2\zeta)$$
$$=F(k,p)=F(k,\lambda,\mu), \quad (12)$$

$$\bar{F}(\nu)=F(\nu,\gamma'-i\theta+1;1+2\gamma';2\bar{\zeta})$$
$$=F(k,-p)=F(k,\lambda,-\mu).$$

Here, and in the remainder of the paper a bar placed over any symbol means that in the function represented by that symbol, the sign of μ is to be changed.

Definition of $Q_{1,\frac{1}{2}}$

$$\begin{aligned}Q_{1,\frac{1}{2}}=N_{\frac{1}{2}}\cdot D\{&\mathcal{J}_1(\gamma+\gamma')(-ib_1C_1+d_1C_2)\\&+\varphi_{\frac{1}{2}-}\mathcal{J}_1^*(\gamma+\gamma')(ib_1C_1+d_1C_2)\\&+\mathcal{J}_1(\gamma+\gamma'+1)(-ib_2C_1+d_2C_2)\\&+\varphi_{\frac{1}{2}-}\mathcal{J}_1^*(\gamma+\gamma'+1)(ib_2C_1+d_2C_2)\\&+\mathcal{J}_0(\gamma+\gamma')(-3id_1C_3+b_1C_4)\\&+\varphi_{\frac{1}{2}-}\mathcal{J}_0^*(\gamma+\gamma')(3id_1C_3+b_1C_4)\\&+\mathcal{J}_0(\gamma+\gamma'+1)(-3id_2C_3+b_2C_4)\\&+\varphi_{\frac{1}{2}-}\mathcal{J}_0^*(\gamma+\gamma'+1)(3id_2C_3+b_2C_4)\}, \quad (13)\end{aligned}$$

where

$$N_{\frac{1}{2}}=\frac{e^{\pi\theta/2}\cdot(p/2)^{\gamma'}}{2(\pi p)^{\frac{1}{2}}|\Gamma(\gamma'+i\theta)|}; \quad \gamma'=\gamma=[1-(\alpha Z)^2]^{\frac{1}{2}}, \quad (14)$$

$$\varphi_{\frac{1}{2}-}=\frac{\gamma+i\theta}{(i\alpha Z/p)-1}$$ and has unit modulus.

V. MODIFICATION OF GOERTZEL AND ROSE FORMULA

We begin by writing

$$\begin{aligned}\bar{F}(\gamma+\gamma') &= K_1, \quad F(\gamma+\gamma') &= K_2,\\ \bar{F}(\gamma+\gamma'-1)&=K_3, \quad F(\gamma+\gamma'-1)&=K_4,\\ \bar{F}(\gamma+\gamma'+1)&=K_5, \quad F(\gamma+\gamma'+1)&=K_6.\end{aligned} \quad (15)$$

We then have

$$\begin{aligned}P_{1,\frac{1}{2}}=N_{\frac{1}{2}}\cdot D\Big\{&K_1\Gamma(\gamma+\gamma')\bar{A}\cdot\varphi_{\frac{1}{2}+}\cdot\Big[ib_1C_1+d_1C_2\\&+\frac{i}{k}(ib_2C_1+d_2C_2)-2ib_1C_4\Big]+K_2\Gamma(\gamma+\gamma')\\&\times A\Big[-ib_1C_1+d_1C_2+\frac{i}{k}(-ib_2C_1+d_2C_2)-2ib_1C_4\Big]\\&+K_3\Gamma(\gamma+\gamma'-1)\varphi_{\frac{1}{2}+}\bar{A}\left(\frac{p}{k\bar{\zeta}}\right)[ib_1C_1+d_1C_2]\\&+K_4\Gamma(\gamma+\gamma'-1)A\left(\frac{-p}{k\zeta}\right)[-ib_1C_1+d_1C_2]\\&+K_5\Gamma(\gamma+\gamma'+1)\bar{A}\cdot\varphi_{\frac{1}{2}+}(-\bar{\zeta}/ip)\\&\times[ib_2C_1+d_2C_2-2ib_2C_4]+K_6\Gamma(\gamma+\gamma'+1)\\&\times A\left(\frac{\zeta}{ip}\right)[-ib_2C_1+d_2C_2-2ib_2C_4]\Big\}. \quad (16)\end{aligned}$$

Now, using the relations,

$$F(a,b;c;z)=(1-z)^{-a}F(a,c-b;c;z/z-1) \quad (17)$$

$$(c-a)F(a-1,b;c;z)=b(1-z)F(a,b+1;c;z)+(c-b-a)F(a,b;c;z),$$

$$(c-a)F(a-1,b+1;c;z)=(b-a+1)(1-z)F(a,b+1;c;z)+(c-b-1)F(a,b;c;z),$$

together with the fact that $2\bar{\zeta}/(2\bar{\zeta}-1)=2\zeta$, we can express K_3, K_4, K_5, and K_6 in terms of K_1 and K_2. For convenience in subsequent numerical calculations it is useful to transform the hypergeometric functions which depend on 2ζ into ones depending on $1/2\zeta$, since $|2\zeta|$ is usually greater than unity. To perform this transformation we use the relation

$$\begin{aligned}\frac{\Gamma(a)\Gamma(b)}{\Gamma(c)}F(a,b;c;z)=&\frac{\Gamma(a)\Gamma(b-a)}{\Gamma(c-a)}(-z)^{-a}\\&\times F\left(a,1-c+a;1-b+a;\frac{1}{z}\right)\\&+\frac{\Gamma(b)\Gamma(a-b)}{\Gamma(c-b)}(-z)^{-b}\\&\times F\left(b,1-c+b;1-a+b;\frac{1}{z}\right), \quad (18)\end{aligned}$$

and find the following relations to hold

$$K_1=(1-2\bar{\zeta})^{-(\gamma+\gamma')}(-2\zeta)^{-(\gamma'+i\theta)}\cdot vI_1,$$
$$K_2=-(\varphi_{\frac{1}{2}+})\left(\frac{\gamma'-i\theta}{\gamma'+i\theta}\right)(-2\zeta)^{-(\gamma'+i\theta)}\cdot vI_2, \tag{19}$$

where

$$v=\frac{\Gamma(\gamma-i\theta)\Gamma(1+2\gamma')}{\Gamma(1+\gamma'-i\theta)\Gamma(\gamma+\gamma')},$$

$$I_1=F_1+wF_2,$$

$$I_2=\left(-\frac{1}{\varphi_{\frac{1}{2}+}}\right)\left[\left(\frac{\gamma'+i\theta}{1-\gamma+i\theta}\right)\left(\frac{1}{2\zeta}\right)F_3+\left(\frac{-\gamma+i\theta}{\gamma'-i\theta}\right)wF_4\right],$$

$$w=\frac{\Gamma(i\theta-\gamma)\Gamma(1+\gamma'-i\theta)\Gamma(\gamma+\gamma')}{\Gamma(\gamma'-\gamma+1)\Gamma(\gamma'+i\theta)\Gamma(\gamma-i\theta)}(-2\zeta)^{-(\gamma-i\theta)},$$

$$F_1=F(\gamma'+i\theta, i\theta-\gamma^1; 1-\gamma+i\theta; 1/2\zeta), \tag{20}$$

$$F_2=F(\gamma'+\gamma, \gamma-\gamma'; 1+\gamma-i\theta; 1/2\zeta),$$

$$F_3=F(1+\gamma'+i\theta, 1-\gamma'+i\theta; 2-\gamma+i\theta; 1/2\zeta),$$

$$F_4=F(\gamma+\gamma', \gamma-\gamma'; \gamma-i\theta; 1/2\zeta),$$

with $|\arg(-2\zeta)|<\pi$.

If we now rewrite $P_{1,\frac{1}{2}}$ in terms of the I_k defined above, we find

$$P_{1,\frac{1}{2}}=\sum_{k=1}^{6}M_kL_kI_k, \tag{21}$$

where I_3 to I_6 are defined in a manner similar to I_1 and I_2; the values of the M's given below render these quantities unique. Also

$$M_1=N_{\frac{1}{2}}\cdot D(\varphi_{\frac{1}{2}+})\Gamma(\gamma+\gamma')\bar{A}(1-2\bar{\zeta})^{-(\gamma+\gamma')}\times(-2\zeta)^{-(\gamma'+i\theta)}\cdot v,$$

$M_2=-M_1$, $M_3=iM_1$, $M_4=-iM_1$,

$M_5=2EM_1/\alpha Z$, $M_6=-2EM_1/\alpha Z$, and

$$L_1=\frac{ik^{\frac{1}{2}}(1+E)^{\frac{1}{2}}}{E(2E-1)}\left\{\left[\alpha Z(2E-1)(\lambda-2\mu)-\frac{w}{k}\mu\right]+i(1+\gamma)\left[\frac{E-1}{kE}\lambda-(2E-1)\mu\right]\right\}$$
$$=i\xi J_1, \text{ say, where } \xi=\frac{k^{\frac{1}{2}}(1+E)^{\frac{1}{2}}}{E(2E-1)},$$

$$L_2=-i\xi\bar{J}_1=-i\xi J_2, \text{ say,}$$

$$L_3=\xi(2E-1)[(1+\gamma)\mu+i\alpha Z\lambda]=\xi J_3,$$

$$L_4=-\xi\bar{J}_3=-\xi J_4,$$

$$L_5=i\xi\frac{\alpha Z}{2E}\left[-\frac{\alpha Z}{E+1}(\lambda-2\mu)+i(2E)\mu\right]=i\xi\frac{\alpha Z}{2E}J_5,$$

$$L_6=-i\xi\frac{\alpha Z}{2E}\bar{J}_5=-i\xi\frac{\alpha Z}{2E}J_6.$$

We can therefore write

$$P_{1,\frac{1}{2}}=N\sum_{k=1}^{6}J_kI_k=N\cdot P, \text{ say,} \tag{22}$$

where

$$|N|^2=|M_1\xi|^2=\frac{p^{-2\gamma-1}e^{\pi\theta}(\alpha Z)^{2\gamma+1}|\Gamma(\gamma-i\theta)|^2}{4\pi k\Gamma(2\gamma+1)(1+\gamma)|(-2\zeta)^{-(\gamma-i\theta)}|^2}\times\frac{1+E}{(2E-1)(2E)^{2\gamma+2}}$$

P itself can be expressed in the form $P=P_1+wP_2$, where P_1, P_2 are complex expressions which can however be readily deduced. In particular:

$$P_1=F_1\left\{J_1+\frac{ip}{k(1+\gamma)}\left(\frac{1}{2\zeta}\right)\left[(1-\gamma-i\theta)J_3+(\gamma'+i\theta)\left(\frac{-1}{\varphi_{\frac{1}{2}+}}\right)J_4\right]-\frac{i\alpha Z}{4Ep}\left[(\gamma-i\theta)(2\zeta)J_5-(\gamma'+i\theta)\left(-\frac{1}{\varphi_{\frac{1}{2}+}}\right)(2\bar{\zeta})J_6\right]\right\}+F_3\left(\frac{1}{2\zeta}\right)\times\left(-\frac{1}{\varphi_{\frac{1}{2}+}}\right)\left(\frac{\gamma'+i\theta}{1-\gamma+i\theta}\right)\left\{J_2+\frac{ip}{k(1+\gamma)}\left(-\frac{1}{2\bar{\zeta}}\right)\times[(\gamma'-i\theta)(-\varphi_{\frac{1}{2}+})J_3+(1-\gamma+i\theta)J_4]-\frac{i\alpha Z}{4Ep}[(\gamma'-i\theta)(-\varphi_{\frac{1}{2}+})(2\zeta)J_5-(\gamma+i\theta)(2\bar{\zeta})J_6]\right\},$$

and a similar expression exists for P_2. In fact we find that we can express P_1 and P_2 in the form:

$$P_1=BF_1+\bar{B}\left[\left(\frac{1}{2\zeta}\right)\left(-\frac{1}{\varphi_{\frac{1}{2}+}}\right)\left(\frac{\gamma'+i\theta}{1-\gamma+i\theta}\right)F_3\right], \tag{23}$$

$$P_2=BF_2+\bar{B}\left[\left(\frac{-1}{\varphi_{\frac{1}{2}+}}\right)\left(\frac{-\gamma+i\theta}{\gamma'-i\theta}\right)F_4\right],$$

where

$$B=J_1+g+h,$$

$$g=(ip/k(1+\gamma))(1/2\zeta)[(1-\gamma-i\theta)J_3+(\gamma'+i\theta)(-1/\varphi_{\frac{1}{2}+})J_4], \tag{24}$$

$$h=-(i\alpha Z/4Ep)[(\gamma-i\theta)(2\zeta)J_5+(\gamma'+i\theta)(-1/\varphi_{\frac{1}{2}+})(2\bar{\zeta})J_6].$$

After considerable algebra we deduce the following simplified expression for B:

$$B=\frac{1}{2k}\left\{\left[\alpha Z(k+2)(2E-3)(\lambda-\mu)-\frac{3\alpha Z}{E}\mu\right]\right.$$
$$+i[6(k+1)(E-1)\lambda-(k+2)(1+\gamma)(2E-3)\lambda$$
$$\left.+(2E-1)(k+2)(1+\gamma-2E)\mu-6k(2E-1)\mu]\right\}. \quad (25)$$

In an exactly parallel manner, we obtain

$$Q_{1,\frac{1}{2}}=Q_1+w'Q_2=\sum_{k=1}^{6}M_k'L_k'I_k', \quad (26)$$

where

$I_k'=I_k$ with γ' replaced by γ,
$w'=w$ with γ' replaced by γ,
$M_k'=M_k$ with γ' replaced by γ,
$\varphi_{\frac{1}{2}+}$ is replaced by $\varphi_{\frac{1}{2}-}$.

As before we can write:

$$Q_1=B'G_1+\bar{B}'[(1/2\zeta)(-1/\varphi_{\frac{1}{2}-})\times(\gamma+i\theta)G_3/(1-\gamma+i\theta)], \quad (27)$$
$$Q_2=B'G_2+\bar{B}'[(1/\varphi_{\frac{1}{2}-})G_4],$$

where

$G_1=F(\gamma+i\theta, i\theta-\gamma; 1-\gamma+i\theta; 1/2\zeta)$,
$G_2=F(2\gamma, 0; 1+\gamma-i\theta; 1/2\zeta)\equiv 1$,
$G_3=F(1+\gamma+i\theta, 1-\gamma+i\theta; 2-\gamma+i\theta; 1/2\zeta)$,
$G_4=F(2\gamma, 0; \gamma-i\theta; 1/2\zeta)\equiv 1$,

and we find

$$B'=\left(\frac{1-k}{k}\right)2E\{(\alpha Z)(\lambda-\mu)+i[(1+\gamma)\lambda+(1-\gamma)\mu]\} \quad (28)$$

$B'(\gamma+i\theta)-\bar{B}'\left(1-\frac{i\alpha Z}{p}\right)=0$; therefore $Q_2\equiv 0$,

also

$$|B'|^2=|\bar{B}'|^2 \quad \text{since} \quad |\varphi_{\frac{1}{2}-}|^2=1,$$

so that

$$|Q_{1,\frac{1}{2}}|^2=|Q_1|^2=\frac{16E^2}{k^3}(k-1)^2(W-\gamma)\left|G_1+\frac{1}{2\zeta}\left(\frac{\gamma+i\theta}{1-\gamma+i\theta}\right)G_3\right|^2.$$

If we now use the relation,

$$(az/c)F(a+1, b+1; c+1; z)=F(a, b+1; c; z)-F(a, b; c; z),$$

we find

$$G_1+\left(\frac{1}{2\zeta}\right)\left(\frac{\gamma'+i\theta}{1-\gamma+i\theta}\right)G_3=\left(1-\frac{1}{2\zeta}\right)^{-(\gamma+i\theta)}$$

and

$$|Q_{1,\frac{1}{2}}|^2=\frac{16E^2}{k^3}(k-1)^2(W-\gamma)\left|\left(1-\frac{1}{2\zeta}\right)^{-(\gamma+i\theta)}\right|^2. \quad (29)$$

VI. SUMMARY

We have thus obtained the following simplified formula for the coefficient of internal conversion of the L_I-shell for the electric dipole case:

$\beta=$ internal conversion coefficient $=(\pi\alpha k/3)|N|^2\cdot[2|P|^2+|Q|^2]$,

where

where $|N|^2$ is as defined in IIA and

$$|P|^2=|P_1+wP_2|^2,$$

$$|Q|^2=16E^2\frac{(1-k)^2}{k^3}(W-\gamma)\left|\left(1-\frac{1}{2\zeta}\right)^{-(\gamma+i\theta)}\right|^2,$$

$$P_1=(\Lambda\lambda+\mathrm{M}\mu)F_1-(\Lambda\lambda-\mathrm{M}\mu)\left[\left(\frac{1}{2\zeta}\right)\left(\frac{2+i\alpha Z/p}{1-\gamma+i\theta}\right)\right]\cdot F_3,$$

$$P_2=(\Lambda\lambda+\mathrm{M}\mu)F_2-(\Lambda\lambda-\mathrm{M}\mu)\left(\frac{-\gamma+i\theta}{2-i\alpha Z/p}\right)\cdot F_4,$$

$$\Lambda=\frac{1}{2k}\{(\alpha Z)(k+2)(2E-3)+i[6(k+1)(E-1)-(k+2)(1+\gamma)(2E-3)]\},$$

$$\mathrm{M}=\frac{1}{2k}\left\{-\frac{\alpha Z}{E}[E(k+2)(2E-3)+3]+i(2E-1)[(k+2)(1+\gamma-2E)-6k]\right\}.$$

The Goertzel and Rose formula is not stated in its simplest terms and the above modification has put the expressions in a form more suitable for numerical calculations. In particular, we note that the expression for $|Q|^2$ no longer contains either gamma-functions or hypergeometric functions. Corresponding simplifications have been obtained for the L_I-shell in the case of electric quadrupole and magnetic dipole radiation, and for the L_{II}, L_{III}-shells in the case of electric dipole radiation. These are summarized in Section II.

The authors wish to thank Dr. M. E. Rose and Dr. G. Goertzel for permitting them to refer to their unpublished results. They would also like to thank Dr. L. G. Elliott, Mr. Harold Coish, and Dr. W. H. Watson, of the staff of the National Research Council of Canada, who suggested the problem. This project was carried out under a grant from the National Research Council of Canada.

Experimental Verification of Space Charge and Transit Time Reduction of Noise in Electron Beams

C. C. CUTLER AND C. F. QUATE
Bell Telephone Laboratories, Murray Hill, New Jersey
(Received June 8, 1950)

This paper describes a simple experiment which indicates some significant properties of the noise currents in a long electron stream, and verifies the applicability of the theory as worked out by Rack, Peterson, and Pierce to the noise properties of klystrons and traveling-wave tubes. An appendix shows that the observations are reasonably consistent with the theory.

I. INTRODUCTION

THERE has been considerable skepticism as to the validity of conclusions concerning space charge and transit time effects on signal and noise in microwave tubes as worked out by Rack,[1] Peterson,[2] and Pierce.[3] Great significance has been put on the possible applicability of the theory, however, because it predicts a noise performance far different from that which more naive assumptions give.

It is the purpose of this paper to report a simple and direct experiment which gives an excellent verification of the basic assumptions of Peterson's theory. The measurements agree very closely with the predicted noise amplitude, and the distance along the beam between successive points of noise cancellation. The position of the first noise minimum differs somewhat from that predicted but agreement is remarkably close considering the assumptions involved. It is indicated that the practical limit on the noise cancellation at noise minima is due to partition current.

II. THEORETICAL BACKGROUND

An exact theoretical analysis of the noise properties of space charge limited electron flow in a vacuum is not available. In 1938, however, Rack[1] suggested that noise calculations might be made by using the Llewellyn-Peterson[4] equations, and assuming that at the potential minimum there is an electron flow having a single valued velocity, but a velocity fluctuation with a mean square value equal to that for a Maxwellian velocity distribution. With this assumption Rack calculated the noise properties of a diode for various transit angles. Peterson[2] applied these ideas to the over-all noise performance of a microwave tetrode and predicted a cancellation, which would give a great improvement of the noise figure of a tetrode under certain conditions of space charge and transit angles. Recently Pierce[3] used the same procedure in calculating the noise figure of a traveling-wave tube.

In short, the theory assumes the noise in the entire stream to arise from a velocity variation at the space charge induced potential minimum near the cathode. The subsequent dynamics of the electron flow in the accelerating region cause the stream at the anode to have correlated velocity and density fluctuations. In the following drift regions noise phenomena may be visualized in terms of two space charge waves excited by these fluctuations. These waves propagate and interfere, giving actual cancellation of the noise current at certain points.

It is important to remember that in this theory the electron velocity over the beam cross section is assumed to be single valued, and that the actual multivalued velocity distribution is taken into account only through the velocity fluctuation assigned at the potential minimum. The approximation involved is certainly questionable, especially at high frequencies. Thus, for example, application of the equations to the operation of diodes and triodes at microwave frequencies predicts reasonably the observed mutual conductance but fails to predict the observed input load impedance or the rectification properties. It is not obvious therefore that Pierce's calculations should predict correctly the noise performance of a traveling-wave tube. Because of the importance of having a working theory and the doubt as to the validity of this particular one, a simple experiment was devised to check the conclusions as applied to electron beams having large transit angles.

III. EXPERIMENTAL APPARATUS

The experiment consisted in measuring the noise power coupled from an electron stream into a resonant

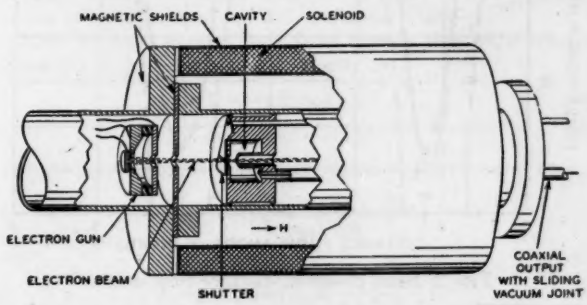

FIG. 1. Apparatus used for measuring noise current in an electron beam.

[1] A. J. Rack, Bell Sys. Tech. J. **17**, 592, (1938).
[2] L. C. Peterson, Proc. I.R.E. **35**, 1264 (1947).
[3] J. R. Pierce, manuscript for forthcoming book entitled *Traveling Wave Tubes* (D. Van Nostrand Company, Inc., New York, 1950).
[4] F. B. Llewellyn and L. C. Peterson, Proc. I.R.E. **32**, No. 3, 144 (1944).

cavity as a function of the length of the stream. This was done by mounting a cavity resonant at 4200 Mc in a cylinder as indicated in Fig. 1 so that it could be moved parallel to the beam from an electron gun. A Pierce gun was used having a perveance of 0.08×10^{-6} amp./volt[4] and designed to produce a beam converging to a minimum diameter of 0.050 in. at a distance of 0.392 in. in front of the accelerating electrode. The cathode current density was 40 ma per square cm obtained from a thoria cathode surface on a molybdenum disk.

To obtain parallel electron flow as described by Brillouin[5] and Samuel[6] the beam was made to enter a longitudinal magnetic field abruptly at the point of minimum beam diameter. The cavity was mounted so that it could be moved along the electron beam for a distance of approximately four inches. A shutter with holes of various diameters was attached to the cavity so that the beam diameter could be measured and its cross section determined.

IV. MEASUREMENTS

Peterson's theory indicates that the noise current in the electron beam should go through a minimum at a given distance from the anode. This theory is applied to cover the immediate case including space charge and cylindrical beams in the appendix to this paper where it is indicated that the noise current should vary periodically with beam length.

The primary results of this experiment are shown in Fig. 2, where the measured noise power is plotted as a function of distance from the gun anode. The measured points show a good correlation with the theoretical curve worked out in the appendix showing that the noise does give the predicted minima and varies periodically.

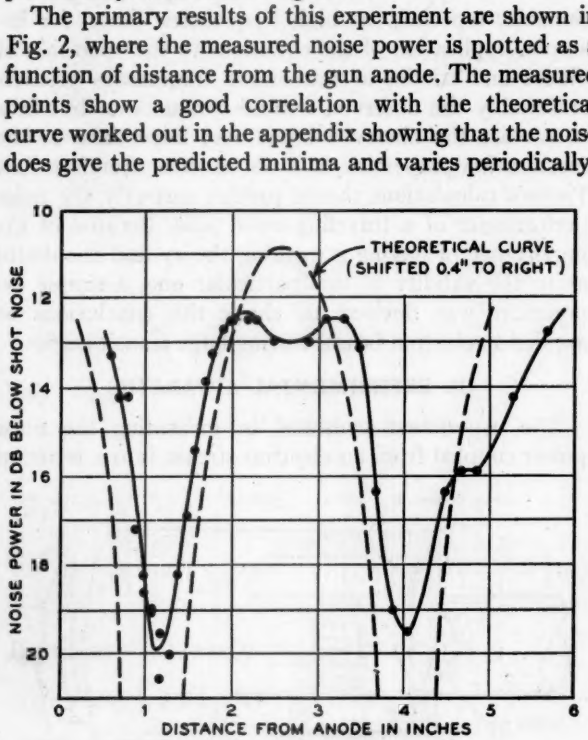

FIG. 2. Noise power *vs.* distance from anode.

[5] L. Brillouin, Phys. Rev. 67, 260 (1945).
[6] A. L. Samuel, Proc. I.R.E. 37, 1252 (1949).

Also, the variation of the minimum position with voltage and gun transit angle corresponds to theoretical prediction. The position of the noise minimum differs by 0.4 in. from that predicted, which is attributed to the use of the infinite plane diode solution instead of a cylindrical beam solution in the cathode-anode region. The absolute value of the noise level was obtained by comparing it with temperature limited shot noise in the beam. The comparison was made by reducing the cathode temperature and plotting noise power as a function of collector current as illustrated in Fig. 3. The asymptotic slope at low currents shows the shot noise power to be proportional to beam current as expected. At larger currents, space charge reduction appears and the noise power passes through a minimum. The greatest total reduction of noise power obtained was 20 db below shot noise at a distance corresponding to the first minimum of Fig. 2. The predicted noise level at the maximum is also closely verified as may be seen from Fig. 4.

The chief difficulty in making a measurement of noise *vs.* beam length is that of getting sufficient beam uniformity. If the beam cross section varies with its length, there is a corresponding variation of cavity coupling and intercepted current. Figure 5 shows measurements of the beam cross section corresponding to the noise measurements of Fig. 1 and it can be seen that there is no correspondence between the changes in beam diameter and the gross character of the noise curve, but that the small variations in noise from the theory correspond to the beam variations. Furthermore, altering the strength of the magnetic field directly affects the small ripples on Fig. 2 but has only minor effects on the gross character of the curve.

The increase of noise power near the maximum beam current as shown in Fig. 3 indicates that another source of noise is present. This source of noise which limits the depth of a null in Fig. 2 might be attributed to par-

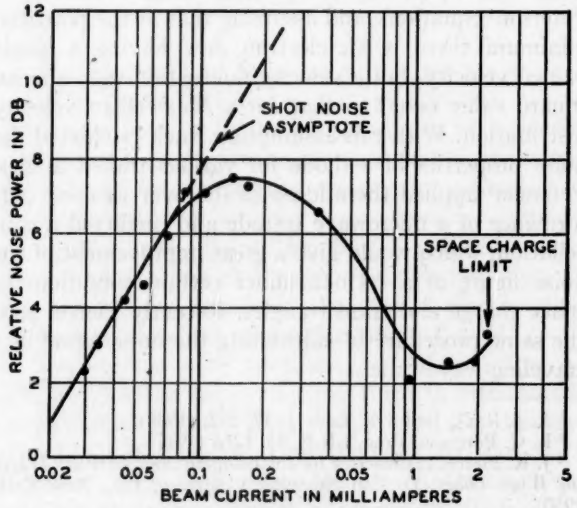

FIG. 3. Noise power *vs.* beam current for temperature limited emission.

tition noise currents created by the beam striking electrodes other than the collector, to residual temperature limited emission, or to multivalued electron velocity at the cathode. For small partition currents there should be contributed[7] to the beam an amount of shot noise equal to the shot noise contained in a temperature limited current equal to the partition current. In the case described the partition current was approximately one percent of the total current, which would cause partition noise 20 db below the full shot noise value. That this remaining noise is largely partition noise is also indicated in Fig. 6 for which the data were obtained by moving the shutter to intercept a small fraction of beam current, thus controlling the partition current. This curve shows a direct correlation between noise power and partition current even down to the smallest currents measured. That the noise power varies with the partition current at less than the first power is probably due to the fact that the additional partition currents were abstracted from one side of the beam instead of randomly throughout the beam cross section.

V. CONCLUSIONS

The most significant conclusions from these measurements are:

(1). The single valued velocity stream assumption is definitely valid for gross effects at a frequency of 4200 Mc.

(2). A high degree of correlation in the current flow of an electron beam can be obtained.

(3). Noise currents in an electron stream originate principally as a velocity fluctuation at the cathode.

(4) The most probable noise figure limitation in microwave tubes is partition noise.

The authors are indebted to Mr. C. F. Chapman for his valuable cooperation in this experiment.

APPENDIX

In analyzing the noise behavior of a space charge limited electron beam we follow the attack which Pierce uses for the traveling wave tube.[8] As mentioned in the text we begin with the mean square fluctuation of velocity at the potential minimum and apply the Llewellyn-Peterson equations[4] for the plane diode to determine the resulting noise current and velocity at the anode. The plane diode equations are used as they are the only solutions available for the accelerating region. However, solutions are available for a cylindrical beam in a constant potential drift region such as exists beyond the anode.

We follow the notation of Pierce.[8]

Pierce has obtained for the noise current and velocity fluctuations at the anode.[8]

$$v_b = -v_a \exp(j\theta_1) \tag{1}$$

$$q_b = -j(I_0/u_0)\theta_1 v_a \exp(j\theta_1). \tag{2}$$

$\langle v_a^2 \rangle_{kT}$ is the mean square fluctuation of velocity at the potential minimum which is evaluated in reference 1 to give

$$\langle v_a^2 \rangle_{kT} = (4-\pi)\eta(kT_c/I_0)B.$$

[7] J. R. Pierce, Bell Sys. Tech. J. 27, No. 1, 158 (1948).
[8] J. R. Pierce, Proc. I.R.E. 36, 993 (1948).

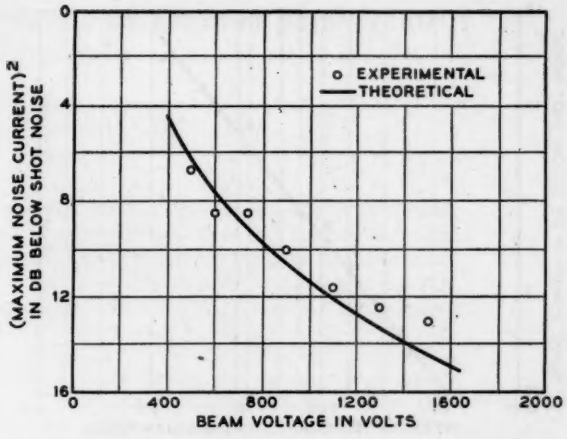

FIG. 4. Relation between beam voltage and noise current.

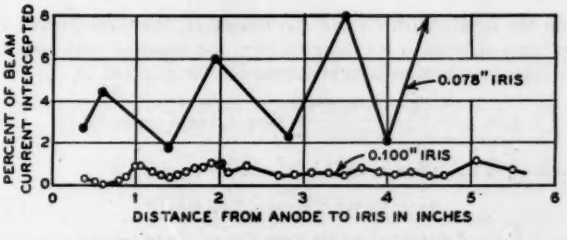

FIG. 5. Beam current interception *vs.* distance.

θ_1 = d.c. transit angle from cathode to anode which is assumed to be greater than 3π; $\eta = e/m$, the ratio of the electron charge to the electron mass; u_0 = d.c. electron velocity; I_0 = d.c. beam current; k = Boltzmann's constant; T_c = temperature of the cathode in degrees Kelvin; B = band width of the receiving system.

We may now use q_b and v_b as the input boundary conditions to the drift region and evaluate the noise current in the beam as a function of the beam length. The drift region through which the cylindrical beam travels is capable of propagating two unattenuated space charge waves. One wave travels faster than the average electron speed, u_0, and the second wave travels slower than the electron speed. Pierce[8] describes the waves in terms of the electric field, a.c. velocity, and current associated with each wave. Thus, we have associated with the fast wave a field E_I given by

$$E_I = E_{I_0} \exp(j^{\omega t - j\beta z + \delta I z}) \tag{3}$$

and with the slow wave a field E_{II} given by

$$E_{II} = E_{II_0} \exp(j^{\omega t - j\beta z + \delta II z}), \tag{4}$$

where

$$\delta_I = -\delta_{II} = j\beta(4QC^3)^{\frac{1}{3}} \tag{5}$$

and $\beta = \omega/u_0$.

$(4QC^3)^{\frac{1}{3}}$ is a term which describes the space charge properties of the cylindrical beam and will be discussed later.

Also, for each wave we have from Pierce's theory the relation between the fields, current and velocity as

$$v_I = -\eta E_I/u_0\delta_I \tag{6}$$

$$q_I = j(\beta I_0 E_I/2V_0\delta_I^2). \tag{7}$$

Therefore at the input to the drift region we have

$$v_b = v_I + v_{II} = -\frac{\eta}{u_0}\left(\frac{E_{I_0}}{\delta_I} + \frac{E_{II_0}}{\delta_{II}}\right) \tag{8}$$

and

$$q_b = q_I + q_{II} = j\frac{\beta I_0}{2V_0}\left(\frac{E_{I_0}}{\delta_I^2} + \frac{E_{II_0}}{\delta_{II}^2}\right). \tag{9}$$

From (8) and (9) we can evaluate E_{I_0} and E_{II_0} and from (3) and (4) determine E_I and E_{II} as a function of z, the axial distance

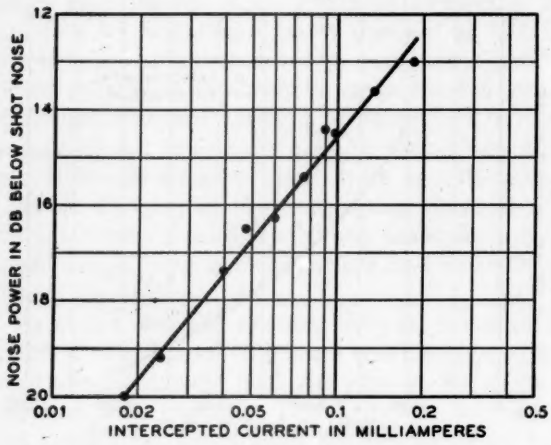

FIG. 6. Noise power *vs.* intercepted current.

from the input. With E_I and E_{II} known q_n, the noise current in the beam at point z, is evaluated from the equation analogous to (9). This process results in an expression for q_n given by

$$q_n=-j\frac{I_0}{u_0}\frac{[1+(\theta_1{}^2 4QC^3)]^{\frac{1}{2}}}{(4QC^3)^{\frac{1}{2}}}\sin\alpha\cdot v_a\cdot\exp[-j(\theta_1+\theta_2)], \quad (10)$$

where q_n is the noise current in the beam at point z

$$\alpha=-\theta_2(4QC^3)^{\frac{1}{2}}+\tan^{-1}[\theta_1(4QC^3)^{\frac{1}{2}}] \quad (11)$$

and θ_2 is the d.c. transit angle from the anode to point z along the beam.

Equation (10) contains the information which is pertinent to this experiment. The factors of interest are the distance of the first minimum from the anode, $X_{\min}$, the distance between minima, ΔX, and the noise current in the stream at the position of maximum current.

For the position of the first current null we have

$$\sin\alpha=0$$

or

$$\theta=[1/(4QC^3)^{\frac{1}{2}}]\tan^{-1}[\theta_1(4QC^3)^{\frac{1}{2}}]$$
$$=\omega T=(2\pi/\lambda_g)X_{\min} \quad (12)$$

thus

$$X_{\min}=[\lambda_g/2\pi(4QC^3)^{\frac{1}{2}}]\tan^{-1}[\theta_1(4QC^3)^{\frac{1}{2}}] \quad (13)$$

where

$$\lambda_g=\lambda_0 u_0/c.$$

The distance between current minima is given by

$$\Delta\theta_2=\pi/(4QC^3)^{\frac{1}{2}} \quad (14)$$

and

$$\Delta X=\lambda_g/2(4QC^3)^{\frac{1}{2}}. \quad (15)$$

At the position of current maximum the mean square noise current is given by

$$\langle q_n{}^2\rangle_{Av}=(I_0{}^2/u_0{}^2)(1+\theta_1{}^2 4QC^3)\langle v_a{}^2\rangle_{Av}/4QC^3.$$

From the shot noise formula we have

$$\langle q_{sn}{}^2\rangle_{Av}=2eI_0B.$$

Therefore with the use of the equation for $\langle v_a{}^2\rangle_{Av}$ we can write

$$\frac{\langle q_n{}^2\rangle_{Av}}{\langle q_{sn}{}^2\rangle_{Av}}=0.035\frac{(1+\theta_1{}^2 4QC^3)}{(4QC^3)V_0}. \quad (16)$$

It is now necessary to evaluate $4QC^3$ and this is done with the use of Pierce's theory for the beams in traveling-wave tubes. In Appendix IV of reference 3, Pierce works out the value of $4QC^3$ for a hollow cylindrical beam of radius a_1. If the surrounding cylinder is far removed from the beam $4QC^3$ is given by

$$4QC^3=60(c/u_0)I_0(\gamma a_1)K_0(\gamma a_1)(I_0/2V_0). \quad (17)$$

$I_0(\gamma a_1)$ and $K_0(\gamma a_1)$ are the modified Bessel Functions and $\gamma\cong\omega/u_0$.

It is interesting to note that for $\gamma a_1>1.8$ the product $I_0(\gamma a_1)K_0(\gamma a_1)$ can be approximated by $1/2\gamma a_1$ and thus

$$4QC^3\cong 60(c/u_0)(1/2\gamma a_1)(I_0/2V_0)$$

and since

$$\gamma a_1=2\pi c a_1/\lambda_0 u_0$$

we can write

$$4QC^3\cong 60\lambda_0 I_0/8\pi a_1 V_0. \quad (18)$$

Equation (18) applies to a hollow cylindrical beam with γa_1 greater than 1.8 inside of a conducting cylinder of a diameter much larger than the beam diameter. To evaluate $4QC^3$ for a solid beam we use Fletcher's results[9] wherein he determines the radius and beam current of a hollow beam which is equivalent to the solid beam.

To proceed with the computation we have for the experiment

$$a_1=0.025'';$$
$$V_0=900\text{ v};$$
$$I_0=2.1\times10^{-3}\text{ amp.};$$
$$\gamma a_1=0.94\text{ for solid beam.}$$

The equivalent hollow beam has a radius of $0.782a_1$ and a current of $0.96I_0$.

We then have

$$(4QC^3)^{\frac{1}{2}}=2.8\times10^{-2}$$

and since $\theta_1=32$ radians at 900 v for the gun which was used we have at the first minimum

$$\theta_2=26\text{ radians}\quad\text{or}\quad X_{\min}=0.7''$$

which compares with a measured value of 1.1". It is felt that this discrepancy arises from the use of the infinite plane equations in the accelerating region.

For the period we have

$$\Delta\theta=110\text{ radians or }17.6\text{ cycles,}$$

which gives

$$\Delta X=2.95'',$$

as compared to 2.91" as measured.

For the values of the ratio of max. noise power to shot noise power we calculate

$$\langle q_n{}^2\rangle_{Av}/\langle q_{sn}{}^2\rangle_{Av}=1/11.5\text{ or }10.6\text{ db below shot noise}$$

as compared with approximately 12.5 db as measured.

[9] R. C. Fletcher, Proc. I.R.E. 38, 413 (1950).

Equilibrium Currents Induced in Zincblende by Electron Bombardment of Negative Electrode

MERRIL F. DISTAD
*Naval Research Laboratory, Washington, D. C.**
(Received May 8, 1950)

The current induced in zincblende crystals when the negative electrode is bombarded by 5- to 900-volt electrons has been measured. The electrodes were evaporated copper films 0.02 or 0.05 micron thick. The experimentally observed ratio of the equilibrium bombardment-induced crystal current to the bombarding current (a) had values ranging from about 10^{-5} to 10^{-9}, (b) was independent of the magnitude of the bombarding current, (c) was proportional to the bombarding voltage raised to the nth power where n ranged from 2.0 to 2.6 for bombarding voltages up to 600 volts, (d) did not show a dependence on the crystal temperature, and (e) increased as the potential difference between the crystal electrodes was increased. A space charge in the crystal, apparently very near the bombarded electrode, had a major effect on the time variation of the bombardment-induced current and on the magnitude of its equilibrium value. The primary result of bombardment seems to be the emission of electrons into the crystal from the electrode. It does not appear to be necessary to assume that internal secondaries were a major source of conduction electrons.

I. INTRODUCTION

IT has been shown by Wilson[1] that the electrons in a metal electrode on an insulating crystal ordinarily do not have sufficient energy to pass into the lowest unoccupied ("conduction") band of the crystal. If, however, the negative electrode is exposed to electron bombardment, some of the electrons in the metal may be excited to a sufficiently high energy so that they may pass into the crystal, where they can act as conduction electrons. Experimental observations of such bombardment-induced currents will be presented.[2]

Zincblende, which has energy bands[3] typical of insulating crystals, was chosen as a suitable insulating material. It is well known that zincblende crystals become conducting when exposed to ultraviolet illumination,[4] when exposed to 15-kilovolt electron or positive ion beams,[5] and when exposed to alpha-ray bombardment.[6] These results show that electrons excited to a normally unoccupied band can move through the zincblende lattice under the influence of an electric field; consequently, one would expect that this would also be true for the extra electrons which come into the crystal from the bombarded electrode.

Very thin copper electrodes were evaporated onto opposite faces of a zincblende crystal and, as is shown in Fig. 1, a small spot near the center of the negative electrode on the crystal surface was bombarded by a beam of 5- to 900-volt electrons. The resulting increase in the current through the crystal was measured. Bombardment was continued, sometimes for over an hour, until the bombardment-induced current reached a steady value.

Most of the experimental results will be expressed in terms of the ratio of the bombardment-induced crystal current to the bombarding current. This ratio, which will be designated by δ and called the "bombardment yield," is essentially the probability that a bombarding electron will cause an electron to pass through the crystal to the positive electrode. One may think of this as the product of four probabilities: P_1, the probability that a bombarding electron or its secondaries will pass through the bombarded electrode to the metal-crystal interface; P_2, the probability that these electrons will pass from the metal into the crystal; P_3, the probability that, for each electron coming into the crystal, a conduction electron will leave the space-charge layer near the bombarded electrode; and P_4, the probability that, for each electron leaving the space-charge layer, an electron will pass through the crystal into the positive electrode. When the bombarding voltage is large, one may need to multiply P_3 by a suitable factor to take into account the liberation of additional conduction electrons within the crystal.

Since P_2 depends on the electric field near the bombarded electrode, it is to be expected that space-charge changes in the crystal could have a marked effect on the bombardment yield. If an equilibrium bombardment-induced crystal current exists, the probabilities P_3 and P_4 must approach unity as a limit for equilibrium conditions. Consequently the equilibrium yield is, at least for small bombarding voltages, essentially equal to the product of probabilities P_1 and P_2, and is primarily a measure of the probability of electron emission into the crystal from the bombarded electrode.

* The experimental work covered in this paper was completed while the author was in the Physics Department of the University of Minnesota.

[1] A. H. Wilson, Proc. Roy. Soc. A133, 458 (1931); A134, 277 (1931); A136, 487 (1932).

[2] M. Distad, Phys. Rev. 55, 1146 (1939), paper No. 176.

[3] D. A. Wright, Proc. Phy. Soc. London 60, 13 (1948); F. Seitz, J. Chem. Phys. 6, 454 (1938); Y. Uehara, Bull. Chem. Soc. Japan 14, 542 (1939).

[4] B. Gudden, R. Pohl and others. Summarized by A. L. Hughes and L. A. DuBridge, *Photoelectric Phenomena* (McGraw-Hill Book Company, Inc., New York, 1932), Chapter 8; and by F. C. Nix, Rev. Mod. Phys. 4, 723 (1932).

[5] H. Lenz, Ann. d. Physik 77, 449 (1925); 82, 775 (1927); Physik. Zeits. 26, 365 (1925); B. Gudden and R. Pohl, Physik. Zeits. 26, 481 (1925).

[6] A. J. Ahearn, Phys. Rev. 73, 524 (1948).

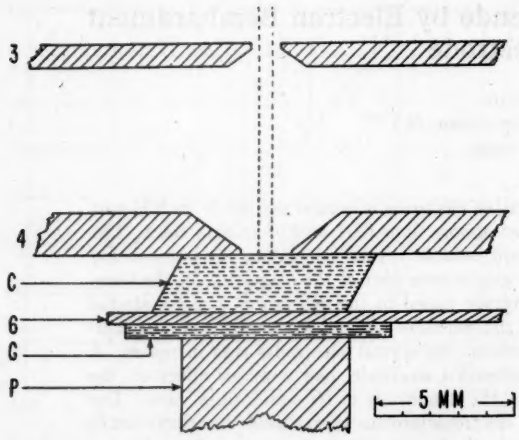

FIG. 1. Details of the crystal mounting. The electron beam, indicated by the vertical dashed lines, passes through the openings in electrodes 3 and 4 and strikes the thin evaporated copper film on the upper surface of the crystal (*C*). This conducting film is in contact with electrode 4 and completely covers the opening in it. Electrode 6 is in contact with the evaporated copper film on the lower face of the crystal (*C*) and is held in place by spring pressure acting on the plunger (*P*) and the glass plate (*G*).

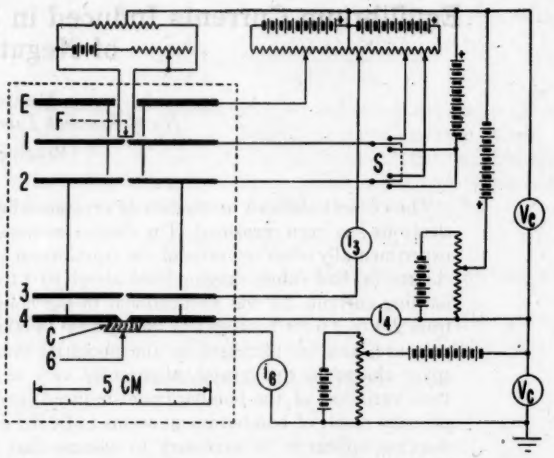

FIG. 2. The electron gun and associated electrical circuit. The electron gun, which is drawn to scale, consists of the tungsten filament *F* and electrodes *E*, 1, 2, 3, and 4 which are circular copper disks with attached spun copper shields. See Fig. 1 for details of the crystal mounting.

II. EXPERIMENTAL EQUIPMENT AND PROCEDURE

Natural yellowish-brown zincblende crystals[7] of Japanese origin were split into irregularly shaped plates to furnish the two transparent and only slightly colored samples which were used for the experimental work. The dimensions of crystal *A* were approximately 4×5 ×1.6 mm and those of crystal *B* were 4×4×1.2 mm, the large faces being natural cleavage faces without visible flaws in the central area where the electron beam would strike. The face which was to be exposed to electron bombardment was covered by a semi-transparent layer of evaporated copper whose thickness, as determined from its electrical properties,[8] was about 0.02 micron for crystal *A* and 0.05 micron for crystal *B*. An opaque layer of copper was evaporated onto the opposite face of each crystal.

The essential features of the electron-gun assembly are shown in Fig. 2. Electrons emitted from the tungsten filament (*F*) passed through the holes in the center of electrodes 1 to 4 and bombarded the thin copper film on the upper surface of the crystal (*C*) which was either crystal *A* or *B*. External Helmholtz coils furnished a magnetic field of 100 gauss directed along the axis of the tube. This collimated the electron beam. The diameter of the beam when it struck the crystal face was about 0.5 mm, the diameter of the opening in electrode 1, and appeared to be almost independent of the magnitude of the bombarding current. The bombarded area was only two percent of the total area of the evaporated electrode on the upper crystal face and about fifteen percent of the crystal surface area exposed to illumination from the filament. The crystal (*C*), electrode 6, and the lead to electrode 6 were enclosed in a metal shield (not shown on Fig. 2) which prevented stray electrons from reaching electrode 6.

The electron-gun assembly was enclosed in a Pyrex tube and a high vacuum was maintained in this tube. Unless specifically stated otherwise, a mixture of dry ice and acetone was placed around the Pyrex tube to cool the crystal to a temperature near that of dry ice. Heat from the filament warmed up the electron-gun assembly and the crystal temperature increased slowly for several hours after the filament was turned on. After completing the runs on crystal *A* and before crystal *B* was put in the electron-gun assembly, additional radiating sleeves (not shown in Fig. 2) were attached to each electrode disk to give better thermal contact with the Pyrex tube. While the maximum rise in the crystal temperature was probably of the order of 15°C for crystal *A*, it was apparently less than 5°C for crystal *B*.

The electrical circuit is shown in Fig. 2. Switch *S* was used to turn the electron beam off by applying a 45-volt retarding potential to electrodes 1 and 2. The potential of electrode 3 was kept at 0 to 3 volts positive with respect to the filament, thus maintaining electrode 3 at a relatively large negative potential with respect to electrode 4 so that most of the reflected and secondary electrons from the crystal electrode would return to electrode 4. A shunted Compton electrometer was used to measure the crystal currents for the early runs which will be designated as group *K* on Fig. 5. A vacuum-tube electrometer,[9] using a Western Electric D-96475 tube with input shunts ranging from 10^9 to 10^{11} ohms, was used for the remainder of the readings.

[7] A. J. Ahearn (see reference 6) found that a crystal from this lot was satisfactory as a crystal counter. He found, by spectrochemical analysis, that this crystal had 0.01 to 0.3 percent mercury impurity and less than 0.03 percent each of cadmium, copper, iron, and lead.

[8] A. Riede, Ann. d. Physik 45, 881 (1914).

[9] M. Distad and J. H. Williams, Rev. Sci. Inst. 5, 289 (1934).

The measured crystal currents ranged from 10^{-10} ampere to less than 10^{-14} amp.

The following voltages and currents were measured:

V_e = Electron bombarding voltage, the potential difference between electrode 4 and the midpoint of the filament (F) plus a small contact potential correction.

i_e = Electron bombarding current falling on the crystal electrode, essentially the same as i_4 on Fig. 2 except for minor corrections for the crystal current and secondary electrons collected on electrode 3.

V_c = Crystal voltage, the potential difference between electrodes 6 and 4 (considered positive when electrode 6 is positive with respect to electrode 4). The voltage V_c was +450 volts except where specifically stated otherwise.

i_6 = General expression for the current through the crystal to electrode 6 (considered positive when electrons flow from electrode 4 through the crystal to electrode 6). Currents i_b, (i_B+i_b), and (i_F+i_b) are special cases of i_6.

i_b = Background current through the crystal when the filament current is on and the electron beam is off.

i_B = Bombardment-induced current through the crystal. The total current through the crystal during electron bombardment is the sum of the two currents i_B and i_b.

i_F = Equilibrium or final value of the bombardment-induced crystal current i_B.

$\delta = i_B/i_e$, the bombardment yield.

$\delta_F = i_F/i_e$, the equilibrium or final bombardment yield.

The filament current, the crystal voltage (V_c), the bombarding voltage (V_e), and the voltage on electrode 3 were kept constant during and after each electron bombardment run. The voltages on electrodes 1 and 2 were adjusted when necessary to keep the bombarding current (i_e) constant during a run and, through switch S, to turn the electron beam on and off. The input to the vacuum-tube electrometer was short-circuited when the electron beam was turned either on or off, and the first reading of the crystal current was taken not earlier than twenty seconds after the change had been made. The large time-constant of the vacuum-tube electrometer made earlier readings impractical.

The example given in Fig. 3 shows the observed crystal current for a set of runs for which the bombarding voltage was small. Starting with a relatively small dark current, the crystal current abruptly increased

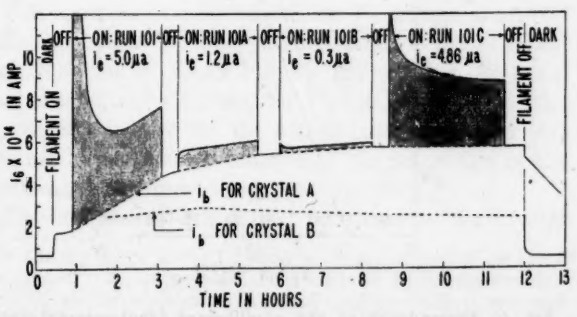

FIG. 3. The observed crystal current (i_6) for a set of runs on crystal A. The bombarding voltage (V_e) was 45 volts and the crystal voltage (V_c) was +450 volts for all runs, but the bombarding current (i_e) was different for each run as is indicated on the figure. The shaded areas represent the bombardment-induced current. "OFF" and "ON" refer to the electron beam.

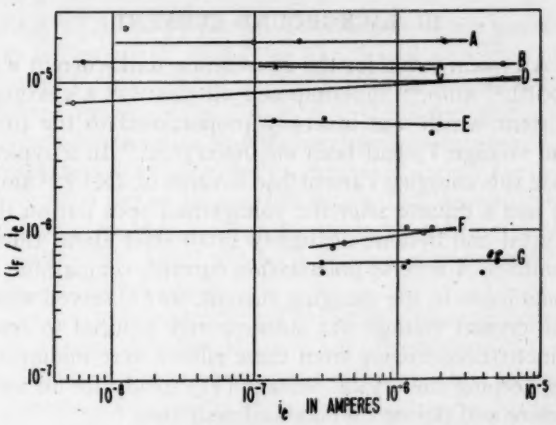

FIG. 4. Dependence of the equilibrium bombardment yield (i_F/i_e) on the bombarding current (i_e). The bombarding voltage (V_e) was 450 volts for groups A and D, 600 for B, 900 for C, 270 for E, 150 for F, and 45 for G. The actual (i_F/i_e) values for group G were a hundred times smaller than those plotted. The crystal voltage (V_c) was +450 volts for all runs.

when the filament current was turned on at 0.4 hour. This increase represents the photo-conduction current produced by illumination from the filament. When the electron beam was turned on at 0.9 hour, the crystal current jumped to about 2.4×10^{-12} amp., which is off the graph. The crystal current decreased rapidly, reaching a minimum at 2.0 hours, and then increased slowly until the electron beam was turned off at 3.1 hours. The bombardment-induced current (i_B) at any given time is represented on this figure by a vertical line from the top to the bottom of the shaded area. The current i_B was essentially constant for the last half hour, and the equilibrium current i_F is represented by the right-hand edge of the shaded area. Although the crystal current was still increasing at the end of the first run, this increase was caused by the increase in the background current (i_b) as indicated by the upper dashed line. The slow rise in i_b was a consequence of the slow increase in crystal temperature produced by heat from the filament. The lower dotted line shows that the rise in i_b was much smaller for crystal B because the temperature rise was much smaller. One can see that the bombardment-induced current reached an equilibrium value more rapidly for the second and later runs shown on Fig. 3.

If the bombarding voltage (V_e) was less than 30 volts, it was necessary to continue bombardment for over three hours before the bombardment-induced current reached a steady value; but less than an hour was sufficient if V_e was greater than 150 volts. When the bombarding voltage was large, the background current (i_b) was usually negligibly small compared to the equilibrium bombardment-induced current (i_F). The current i_F was as much as two thousand times larger than i_b.

III. BACKGROUND CURRENT

A typical value for the equilibrium dark-current was 6×10^{-15} amp.[9a] Superimposed on this was a charging current which was inversely proportional to the time the voltage V_c had been on the crystal.[10] In a typical case this charging current had a value of 2×10^{-13} amp. at half a minute after the voltage had been put on the crystal and became negligibly small after about thirty minutes. A reverse polarization current, comparable in magnitude to the charging current, was observed when the crystal voltage was subsequently reduced to zero. Fluctuations arising from these effects were minimized by keeping the crystal voltage (V_c) steady for an hour before and during all bombardment runs.

The background current (i_b) was both a dark current and a photo-conduction[4] current resulting from the illumination from the filament. The current i_b was approximately proportional to the crystal voltage (V_c), had almost the same magnitude for positive and negative V_c, and was zero when V_c was zero. It was markedly dependent on the crystal temperature and on the illumination from the filament.

Electron bombardment had no apparent effect on either the time variation or the magnitude of the background current (i_b) when the equilibrium bombardment-induced current (i_F) was less than twenty times larger than i_b. When i_F was more than fifty times larger than i_b, a small temporary increase in i_b was usually observed just after the electron beam was turned off. For example, in an extreme case where i_F was 1700 times larger than i_b, the crystal current was 6×10^{-14} amp. at two minutes after the electron beam had been turned off, and within ten minutes the background current had returned to its normal value of 4×10^{-14} amp. In all cases the magnitude of the temporary increase in the background current was very small in comparison to the magnitude of the bombardment-induced current.

The useful life of the crystals was abruptly terminated by the onset of dielectric breakdown.[11] At first there were only occasional surges in the crystal current and normal bombardment-induced currents were observed during the quiet intervals. Within a few days the fluctuations became so large and so frequent that it was impossible to obtain accurate readings. Crystal *A* was used for over three months, but crystal *B* showed signs of breakdown after only three weeks. The maximum externally applied fields, when the crystal voltage (V_c) was 450 volts, were 2800 volt/cm for crystal *A* and 3750 volt/cm for crystal *B*. These are below the limits set by Lenz[5] for avoiding rapid breakdown, namely

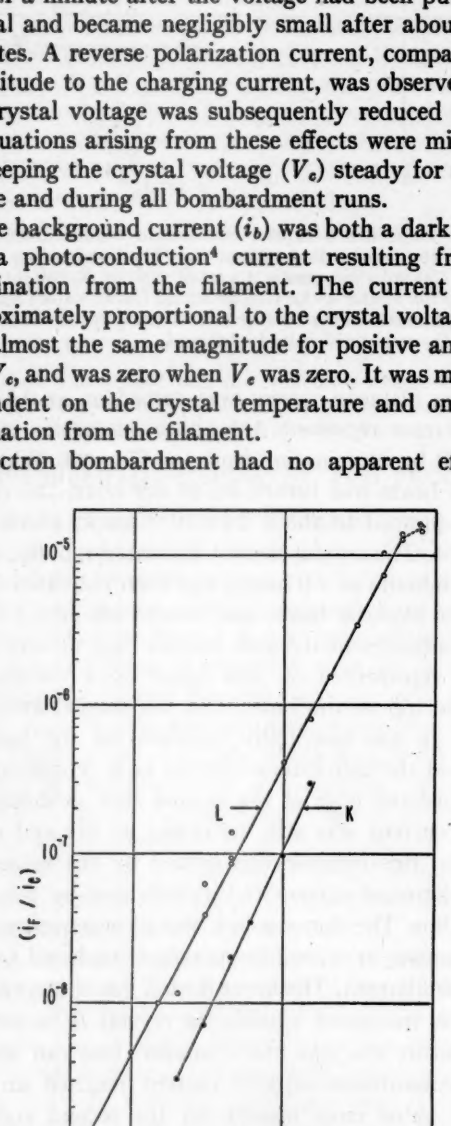

FIG. 5. Dependence of the equilibrium bombardment yield (i_F/i_e) on the bombarding voltage (V_c) for runs using crystal *A*. The crystal voltage (V_c) was +150 volts for group *K* and +450 volts for group *L*.

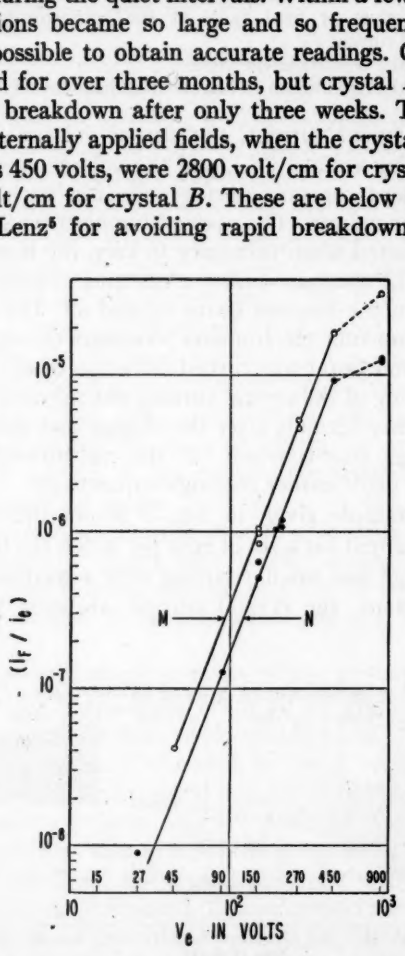

FIG. 6. Dependence of the equilibrium bombardment yield (i_F/i_e) on the bombarding voltage (V_c) for runs using crystal *B*. Group *M* gives the results for the earlier runs and group *N* those for the later runs. The crystal voltage (V_c) was +450 volts for both groups.

[9a] This included leakage currents across the sides of the crystal. The measured background and total crystal currents also included the very small surface leakage current. It had no effect, however, on the observed bombardment-induced crystal current because this was the difference between the total and the background currents.

[10] See also Paper No. 182, M. Distad, Phys. Rev. 55, 1147 1939).

[11] B. Gudden and R. Pohl, Zeits. f. Physik 6, 248 (1921).

5 kv/cm at room temperature and 20 kv/cm at liquid air temperature.

IV. EQUILIBRIUM BOMBARDMENT YIELD

The observed values for the *equilibrium* bombardment yield were relatively reproducible in spite of variations in the background current, in the previous bombardment history, and in the time variation of the bombardment-induced current. Once equilibrium had been reached, the yield was observed to have a steady value for hours of continuous bombardment.

The dependence of the equilibrium yield ($\delta_F = i_F/i_e$) on the bombarding current (i_e) is shown in Fig. 4, the bombarding voltage (V_e) being kept constant for each group. Groups A to D show that as much as a thousandfold change in i_e had only a relatively small effect on the observed δ_F for large V_c. The four points on the plotted line for group G, which are the most reliable readings in this group, give the results for the runs shown on Fig. 3 and lead to the same conclusion for small V_c. On the whole, the data on Fig. 4 show that the equilibrium bombardment-induced current was proportional to the bombarding current to within the experimental errors.

The dependence of the equilibrium yield (δ_F) on the bombarding voltage (V_e) is shown by Figs. 5 and 6 for the runs on crystals A and B respectively. In each case most of the observed values fell on a straight line on the log-log graph to within the experimental error for V_e up to 600 volts. This indicates that

$$\delta_F = (i_F/i_e) = KV_e^n, \qquad (1)$$

where n is the slope of the lines in Figs. 5 and 6 and K is a constant which is dependent on the crystal voltage (V_c) and on the thickness of the bombarded electrode.[11a] The measured values of n are 2.2 for group K, 2.0 for group L, and 2.6 for groups M and N. It is to be noted that the results agree with the simple relation given by Eq. (1) for as much as a ten-thousandfold change in δ_F. Group L includes data for V_e as small as 5 volts and a detectable bombardment-induced current was observed when V_e was 3 volts.

The experimental δ_F values for V_e greater than 600 volts fall below the line passing through the observations for smaller V_e on Figs. 5 and 6. This deviation from the behavior for smaller V_e was greater than the experimental error for these particular runs and was not due to progressive changes in the properties of the bombarded electrode.

The equilibrium yield (δ_F) increased as the crystal voltage (V_c) was increased. Comparison of the plotted lines for groups K and L on Fig. 5 indicates that increasing V_c from +150 to +450 volts increased δ_F by a factor ranging from 3.4 to 5.6, the larger increase being associated with smaller bombarding voltages. No similar data were obtained on crystal B except for one observation (when V_e was 100 volts) that showed only a sixfold increase in δ_F when V_c was increased from +50 to +450 volts. There was no indication of a saturation of δ_F with increasing V_c.

The available experimental evidence, although somewhat meager, does not indicate any dependence of the equilibrium bombardment yield (δ_F) on the crystal temperature. Changes in crystal temperature which increased the background current by a factor of two or more had no marked effect on δ_F. This was checked for bombarding voltages (V_e) ranging from 45 to 900 volts. In addition, two temperature runs were made, for which V_e was 10 volts and the crystal voltage (V_c) was +150 volts, going from the temperature of dry ice to room temperature. Although the background current increased by a factor of 38, the observed δ_F did not change by more than ten percent, which was less than the estimated experimental error for these particular runs. A later run with V_e equal to 45 volts and V_c equal to +450 volts indicated similar results, but in

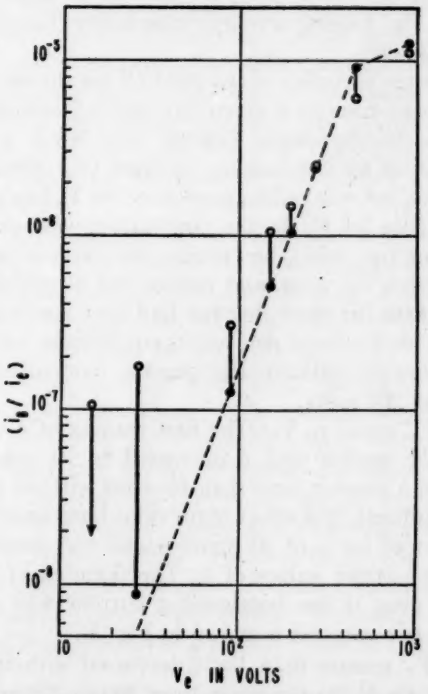

FIG. 7. Total change in the observed bombardment yield (i_B/i_e) as a function of the bombarding voltage (V_e) for typical runs on crystal B without previous bombardment. The open circles are the "first readings" which were taken from a half to four minutes after the electron beam was turned on. The solid dots represent final or equilibrium values. The crystal voltage (V_c) was +450 volts for all runs. The run for V_e equal to 15 volts was stopped before equilibrium was attained.

[11a] The difference in yield values for groups M and N on Fig. 6 was caused by an increase in the thickness of the bombarded electrode by matter evaporated from the filament when it was accidentally operated for a short time at a higher than normal temperature. Within each group, however, checks were made to determine that progressive changes in the crystal electrode did not have a major effect on the yield values. For example, except for group K, the same bombarding voltage was used for the first and last readings in each group and in each case the yield values agreed to within ten percent.

this case the onset of dielectric breakdown made accurate measurements impossible.

V. TIME VARIATION OF THE BOMBARDMENT YIELD

The bombardment yield (δ) varied with the bombardment time and, except for some of the earlier runs on crystal A, asymptotically approached its equilibrium value without any intermediate maxima or minima. The direction and magnitude of the change in δ were a function of the bombarding voltage (V_e) and of the previous bombardment history. Omitting a detailed discussion of the time variation, our attention will be confined to those aspects which indicate the general nature of the space-charge changes and their influence on the equilibrium crystal currents.

We will first consider the behavior, as shown in Fig. 7, for typical runs on crystal B when it had not been previously bombarded for at least twelve hours. These show that the bombardment yield (a) *increased* to its equilibrium value for V_e greater than 270 volts, (b) showed practically no time variation when V_e was about 270 volts, and (c) decreased to its equilibrium value for V_e less than 270 volts.

It is to be noted that for V_e less than 270 volts the ratio of the "first" to the final yield values[12] was larger for smaller bombarding voltages, and that the ratio had values as large as twenty. Even larger values were observed on crystal A, the "first" yield value for run 101 on Fig. 3 being seventy times larger than the equilibrium value.

The time variation of the yield (δ) for the second and subsequent runs on a given day was influenced by the previous bombardment history. The effect was relatively small for bombarding voltages (V_e) greater than 300 volts, but was quite pronounced for V_e less than 200 volts. If we let V_e' be the bombarding voltage for the preceding run, and t_0 be the time the electron beam was off between the runs, and confine our attention to the cases where the preceding run had been continued long enough for δ to have reached its equilibrium value, then the following indicate the general tendencies for V_e less than 200 volts:

(a) V_e' equal to V_e: The first reading of δ was considerably smaller and δ decreased to its equilibrium value in a shorter time than for runs without previous bombardment. The effect of previous bombardment was pronounced for t_0 of 30 minutes and was present even for much larger values of t_0. The same effect was observed even if the bombarding current was different for the two runs (as is shown in Fig. 3).

(b) V_e' greater than V_e: δ decreased with time and, at least for V_e' in the range from 200 to 270 volts, previous bombardment had only a slight effect on the time variation of δ if V_e was considerably smaller than V_e'.

(c) V_e' less than V_e: δ *increased* to its equilibrium value if the beam had not been off too long. For example, this was observed when V_e' was 90 volts, V_e was 150 volts, and t_0 was 20 minutes.

VI. DISCUSSION OF SPACE-CHARGE EFFECTS

The time variation of the yield appeared to be caused by a bombardment-induced space charge in the crystal which, by changing the field near the bombarded electrode, changed the probability of electron emission from the electrode into the crystal.[12a] We will consider this space charge to be superimposed on any space charges which may have existed in the crystal before the start of bombardment. The results shown on Fig. 7 indicate that the polarity of the bombardment-induced space charge was a function of the bombarding voltage (V_e), being positive for large V_e (i.e., over 270 volts for crystal B) and negative for small V_e.

The equilibrium yield was found to be independent of the magnitude of the bombarding current. This indicates that the equilibrium density of the bombardment-induced space charge was probably also independent of the magnitude of the bombarding current. The time-variation characteristics discussed in the preceding section indicate that the equilibrium density of the negative space charge, which is associated with small bombarding voltages (V_e), apparently increased in magnitude as V_e was decreased.[12b] A similar consistent trend was not observed for the positive space charge associated with large V_e, a larger space-charge effect being observed when V_e was 450 volts than when V_e was either 270 or 900 volts. Since the equilibrium yield did not show a dependence on the crystal temperature, it appears, as a first approximation, that the equilibrium density of the space charge was not dependent on the crystal temperature.

The dependence of the time-variation characteristics on the previous bombardment history shows that the negative bombardment-induced space charge persisted for tens of minutes after the cessation of electron bombardment. This space charge apparently was very close to the bombarded electrode because it had practically no effect on the background current, but

[12] The actual *initial* values of δ, which were not measured, probably were very different from the "first" readings plotted on Fig. 7. It may be true for zincblende, as K. G. McKay, Phys. Rev. 74, 1606 (1948), found for diamond, that large changes in the bombardment-induced current take place during the first few microseconds of bombardment.

[12a] The runs discussed in the preceding section gave results which were qualitatively consistent and quantitatively reproducible to a degree that made it seem unlikely that changes in the transmissivity of the bombarded electrode were the primary cause of the time variation for these runs. Some of the earlier runs on crystal A did have an erratic behavior which was ascribed to variations in the properties of the bombarded electrode, but the time variation for these runs has not been considered in this paper.

[12b] This is suggested by the observation that the ratio of the "first" to final yield values, as shown on Fig. 7, had larger values for smaller V_e when V_e was less than 270 volts. It is more definitely shown by the experimental observation that the yield *increased* with time when V_e was larger than the bombarding voltage for the preceding run (V_e'), and decreased if V_e was smaller than V_e'.

had a very pronounced effect on the bombardment yield.[12c]

One can think of the bombardment-induced space charge as being composed of both a negative space charge consisting of trapped electrons and a positive space charge formed by the ionizing action of the electrons coming into the crystal. It is quite possible that the equilibrium density of the negative space charge is relatively independent of the bombarding voltage (V_e), while the equilibrium density of the positive space charge probably increases as V_e is increased. Thus the negative space charge would predominate for small V_e, the magnitude of the net space charge would decrease as V_e was increased, and the positive space charge could predominate for large V_e. The effect of thermal or photoelectric action on the rate of liberation of electrons from traps and on the neutralization of the positive space charge was apparently so small that it did not have a major effect on the equilibrium magnitude of the bombardment-induced space charge.

VII. DISCUSSION OF RESULTS

The maximum externally applied fields, 3750 volt/cm for crystal B, were such that it was unlikely[13] that electrons would travel 1.2 mm (or 1.6 mm) through the crystal without being temporarily trapped at some imperfection or flaw. One might expect that this would build up a negative space charge distributed throughout the body of the crystal and that the resulting space charge would cause a decrease in the background current after the cessation of bombardment, but no such effect was observed.[13a] Apparently either the density of available traps was small or, as seems more probable, the rate of liberation of electrons from these traps by thermal or photoelectric action of the illumination from the filament was large. It seems, at least under semi-equilibrium conditions, that an electron has a relatively high probability of eventually passing through the crystal once it gets past the space-charge layer near the bombarded electrode.

It is quite possible, however, that the presence of inhomogeneities is the explanation for the apparent absence of a negative space charge in the body of the crystal. Ahearn and Wannier[14] have suggested that the current through the crystal may be carried principally along conducting channels. Using this concept, one may assume that the electrons coming into the crystal as a consequence of bombardment would pass through the lattice until they reached one or more of the conducting channels, and that they would then pass along these channels to the positive electrode. Bombardment-induced changes in the space charge—even if they extended for some distance into the crystal—would have only a relatively small effect on the background current if the bombardment-induced current was carried by only a relatively small fraction of the total number of conducting channels. Although inhomogeneities undoubtedly existed, the available information is insufficient to determine the extent to which they affected the space-charge formation in the crystal and the conduction processes through the crystal.

The effect of surface irregularities makes it difficult to determine the probability of electron transmission through the bombarded electrode. The bombardment yield values for the "first readings" on Fig. 7 for a 0.05-micron copper electrode are about an order of magnitude smaller than the transmissivities observed by Becker[15] for electrons passing through 0.04-micron nickel foils when he did not include transmitted secondaries with energies less than four electron volts. The dependence on bombarding voltage is, to a crude approximation, similar in the two cases. This indicates, if one assumes that nickel and copper have similar transmission properties, that the bombardment yield is probably of the same order of magnitude as the crudely estimated transmissivity of the bombarded electrode.[16]

The large bombardment yields observed by McKay[12] in diamond, and by others[17] in other substances, yields which were considerably greater than unity, were ascribed to the production of a large number of internal secondaries by each bombarding electron. The currents observed by Lenz[5] when he exposed a zincblende crystal to electron beams, with bombarding voltages ranging from 5 kv to 15 kv, also appear to have been caused principally by the liberation of conduction electrons and holes within the crystal. In the experiments described in this paper, some of the electrons entering the crystal probably had sufficient energy to produce internal secondaries. If these secondary electrons were free to move through the crystal, the bombardment yield could be considerably greater than the probability

[12c] Only two percent of the total electrode area was exposed to electron bombardment. If the space charge were very close to the bombarded electrode and covered an area equal to that of the bombarded spot, its effect on the bombardment-induced electron emission into the crystal could be large and, at the same time, its effect on the total background current after the cessation of bombardment could be small.

[13] B. Gudden and R. Pohl, Zeits. f. Physik. 17, 331 (1923), found that a field of about 10 kv/cm was required to saturate the primary photoconduction current through a typical zincblende crystal which was 1.3 mm thick.

[13a] Instead of a decrease, the passage of very large bombardment-induced crystal currents produced a small temporary increase in the background current after the cessation of bombardment. This seems to indicate that there was a small temporary increase in the density of electrons trapped in the body of the crystal, and that the observed increase in the background current was caused by the subsequent liberation of the trapped electrons by thermal or photoelectric action.

[14] Informal discussion. See G. H. Wannier, Phys. Rev. 76, 438 (1949) and D. D. Pant, Proc. Ind. Acad. Sci. 19A, 329 (1944).

[15] A. Becker, Ann. d. Physik 84, 779 (1927); 2, 249 (1929).

[16] The observed bombardment yields are, however, very much smaller than one would estimate from the results of H. Katz, Physik. Zeits. 38, 981 (1937) and Ann. d. Physik 33, 160 (1938), on 0.1-micron silver foils.

[17] E. S. Rittner, Phys. Rev. 73, 1212 (1948); L. Pensak, Phys. Rev. 75, 472 (1949); F. Ansbacher and W. Ehrenberg, Nature 164, 144 (1949).

of electron transmission through the bombarded electrode and into the crystal.[17a] The degree to which internal secondaries contributed conduction electrons to the crystal current is uncertain because the transmission probabilities are not known with sufficient accuracy, but the observed yields were so small that it does not appear necessary to assume that internal secondaries were a major source of the electrons making up the bombardment-induced crystal current.[18]

We have seen that certain factors, such as crystal temperature and illumination from the filament, which had a pronounced effect on the dark conductivity and on the photoconductivity of the crystal, seemed to have little or no effect on the bombardment yield. This emphasizes the observation that the magnitude of the yield was primarily determined by factors, such as space charge and bombarding voltage, which affected the probability of electron emission from the bombarded electrode into the crystal. It has also been observed,[19] but not discussed in this paper, that there was no detectable bombardment-induced current for large negative crystal voltages (bombardment of positive electrode) when the bombarding voltage was 150 volts or less. It appears that the "conductivity" of the crystal was not the major limiting factor, but that the bombardment yield was primarily a measure of the probability of electron emission into the crystal.

VIII. SUMMARY

Equilibrium bombardment-induced crystal currents were observed when the negative electrode on a zinc-blende crystal was exposed to bombardment by 5- to 900-volt electrons. The crystal temperature was near that of dry ice for most of the runs. The equilibrium yield, which was the ratio of the bombardment-induced crystal current to the bombarding current, (a) had values ranging from about 10^{-5} to 10^{-9}, (b) was independent of the magnitude of the bombarding current, (c) was proportional to the bombarding voltage raised to the nth power where n ranged from 2.0 to 2.6 for voltages up to 600 volts, (d) did not show a dependence on the crystal temperature, and (e) increased as the crystal voltage was increased. The yield did not depend on the magnitude of the background current. Only large bombardment-induced currents had an effect on the background current.

The time variation of the yield indicated that a bombardment-induced space charge, apparently very close to the bombarded electrode, had a marked effect on the yield. This space charge was positive for large bombarding voltages (i.e., over 270 volts for crystal *B*), and negative for small voltages. The equilibrium density of the space charge was independent of the magnitude of the bombarding current and of the crystal temperature, but depended on the bombarding voltage. The equilibrium magnitude of the negative space charge was greater for smaller bombarding voltages.

The primary result of bombardment seems to be the emission of electrons into the crystal from the electrode. Once these electrons get past the space charge near the surface, they apparently have a high probability of passing through the crystal into the positive electrode under equilibrium conditions. It does not appear to be necessary to assume that internal secondaries were a major source of conduction electrons.

The writer wishes to express his appreciation to Professor J. T. Tate who in 1934 first suggested the possibilities in an investigation of this type, to Professor J. W. Buchta who was the faculty adviser for the later part of the work at the University of Minnesota, and to Professor E. L. Hill who also generously gave his time to discuss the results.

[17a] The rate of positive space-charge formation was so small, particularly after a few minutes of bombardment, that the resulting secondaries probably were only a small part of the total bombardment-induced crystal current.

[18] N. Bloembergen, Physica 11, 343 (1945), who bombarded a silver chloride crystal with short pulses of 10- to 500-volt electrons and was unable to detect a bombardment-induced crystal current, concluded that the yield was less than 0.05 percent of what one might expect from crystal-counter experiments with high energy electrons. In this particular case it also appears that internal secondaries were not an effective source of conduction electrons when the bombarding voltage was small.

[19] M. F. Distad, *Summaries of Ph.D. Theses* (University of Minnesota, Minneapolis, Minnesota), Vol. II (1943), p. 191.

Periodic Deviations in the Schottky Effect for Tantalum*

R. J. MUNICK,† W. B. LABERGE,‡ AND E. A. COOMES
University of Notre Dame, Notre Dame, Indiana
(Received July 17, 1950)

Periodic deviations from the Schottky law in the thermionic emission from patchy surfaces of tantalum and thorium on tantalum have been measured for fields up to 3×10^5 volts cm^{-1}, and at temperatures of 1200 and 1500°K. The work function of the clean tantalum as determined by Richardson plots was 4.03 ±0.04 ev, and was changed by approximately 1/2 volt by thorium deposition. A method was found for separating the periodic deviations from the patch effects.

For clean tantalum the phase and amplitude of the deviations are in approximate agreement with the theory when the tunnel effect is neglected. The temperature variation was found to be in accordance with theory.

The thorium on tantalum caused the amplitudes of the deviations to decrease and the phase to shift toward lower fields. The decrease of amplitude seems to rule out the existence of a potential peak at a composite emitter surface of this type.

I. INTRODUCTION

PERIODIC deviations in the Schottky effect[1] have been reported for thermionic emission from tungsten[2–5] and from tantalum.[3] Mott-Smith[6] suggested that these deviations might be a quantum-mechanical effect. Upon this suggestion Guth and Mullin[7,8] derived expressions which describe the observed phenomenon as a function of the electric field, the temperature, and certain electronic properties of the emitter. It was also implied[7,8] that a patchy emitting surface might influence the observed deviations.

The present investigation was undertaken to study the effects of patches, temperature, and change of work function, and thereby to determine the applicability of the phenomenon to research upon the surface physics of solids. Thermionic emission from patchy surfaces of tantalum was measured at 1500 and 1200°K with collecting fields up to 3×10^5 volts cm^{-1}. The work function was altered by evaporating thin films of thorium from a thoriated tungsten filament upon the tantalum, and corresponding changes were observed in the periodic deviations.

II. PREVIOUS RESULTS

The Schottky law[1] for a uniform metal surface can be written as

$$I=I_0\exp[e(eE)^{\frac{1}{2}}/kT], \qquad (1)$$

where I is the emission current for the collecting field E, I_0 the zero field current, and T the absolute temperature of the emitter. From this equation it follows that the common logarithm of I plotted against the square root of E should be the straight line

$$\log I-\log I_0-C_0\xi/T=0, \qquad (2)$$

where the constant C_0 is 1.914 deg. K (cm volts^{-1})$^{\frac{1}{2}}$, and $E^{\frac{1}{2}}$ is designated by the symbol ξ.

Experiments on tungsten[2–5] and tantalum[3] have indicated that the right side of Eq. (2) is not zero, but instead is an oscillating function of the field. Typical periodic deviations obtained experimentally by Turnbull and Phipps[4] are shown by the open circles in Fig. 1, where the amplitude F_2 is plotted against ξ. The amplitude and period increase with the applied field. A more complete examination of published data indicates that the amplitudes may increase with decrease in temperature without affecting the phase,[2–4] and that the deviations for tantalum appear to be the same as those for tungsten.[3]

The derivation of Eq. (1) is based on the assumption that all electrons within the metal moving toward the surface barrier have a transmission coefficient which is independent of the field. Since a humped potential barrier is formed outside the metal surface, quantum

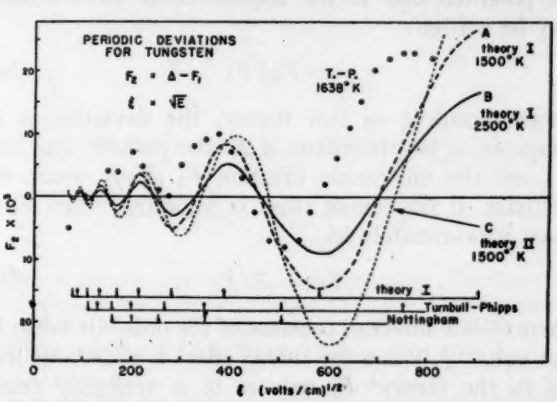

FIG. 1. Periodic deviations in the Schottky effect for tungsten. The theoretical curves are calculated for $W_0=10.3$ electron volts. Theory I neglects the tunnel effect which is included in Theory II. The arrows indicate positions of maxima and minima.

* This research was sponsored by the U. S. Navy Bureau of Ships.
† Now at the National Argonne Laboratory, Chicago, Illinois.
‡ Now at the U. S. Naval Ordnance Test Station, Inyokern, California.

[1] W. Schottky, Physik. Zeits. 15, 872 (1914).
[2] R. L. E. Seifert and T. E. Phipps, Phys. Rev. 53, 493 (1938).
[3] R. L. E. Seifert and T. E. Phipps, Phys. Rev. 56, 652 (1939).
[4] D. Turnbull and T. E. Phipps, Phys. Rev. 56, 663 (1939).
[5] W. B. Nottingham, Phys. Rev. 57, 935 (1940).
[6] H. M. Mott-Smith, Phys. Rev. 56, 668 (1939).
[7] E. Guth and C. J. Mullin, Phys. Rev. 59, 575 (1941).
[8] E. Guth and C. J. Mullin, Phys. Rev. 61, 339 (1942).

TABLE I. Values of the constants for the Guth-Mullin theory (see Eq. (5)). Units for the field and temperature are volts cm^{-1} and deg. K respectively. W_a was taken as 9.27 electron volts for tantalum and 10.3 electron volts for tunsten. It was assumed $W_a = W_i + \varphi e$, where W_i is the chemical potential and φe the work function.

$C's$	General	Tantalum	Tungsten
$C_1 \times 10^3$	-1.58	-1.58	-1.58
$C_2 \times 10^3$	$-9.29 W_a^{\frac{1}{2}}$	-28.2	-29.8
C_3	358	358	358
C_4	$-\frac{7.38}{W_a^{\frac{1}{2}}}+\frac{W_a^{\frac{1}{2}}}{14.8}-0.5$	-2.7	-2.5
C_5	$-\frac{7.38}{W_a^{\frac{1}{2}}}+\frac{W_a^{\frac{1}{2}}}{14.8}+0.3$	-1.9	-1.7

mechanics predicts the reflection[9] of some of the electrons with kinetic energies sufficient to escape in classical mechanics. Interference among the reflected electron waves leads to maxima and minima in the transmission coefficient as the height and thickness of the barrier vary with change of field. The quantum-mechanical probability that some electrons may tunnel through the barrier also contributes to the transmission coefficient. When allowance is made for the variation of transmission coefficient with field the Schottky law becomes

$$I = I_0[\bar{D}(E)/\bar{D}(0)] \exp[e(eE)^{\frac{1}{2}}/kT], \quad (3)$$

where $\bar{D}(E)$ is the mean transmission coefficient for field E, obtained by averaging over the energy distribution of the emitted electrons and $\bar{D}(0)$ is the mean transmission coefficient for zero field. Then Eq. (2) becomes

$$\log I - \log I_0 - C_0\xi/T = \log\bar{D}(E) - \log\bar{D}(0) = \Delta, \quad (4)$$

where Δ represents deviations from the Schottky law. Guth and Mullin[7,8] computed Δ in Eq. (4) for the Maxwellian distribution of electrons transmitted through a barrier composed of an image potential combined with the potential due to the applied field. Their results may be written

$$\Delta = F_1 + F_2 \quad (5a)$$

where according to this theory, the deviation Δ is composed of two functions of E: the periodic function F_2, and the monotonic function F_1 about which F_2 oscillates. If the tunnel effect is neglected,[7] then F_1 is given approximately by

$$F_1 = C_1\xi^{\frac{1}{2}}/T \quad (5b)$$

where C_1 is a universal constant of the order 10^{-3} deg. K $(\text{cm volts}^{-1})^{\frac{1}{2}}$. When the tunnel effect is added, according to the theory[8] F_1 reduces to a negligibly small quantity.

The complete expression for the periodic term F_2 is

$$F_2 = \frac{C_2\xi^{\frac{1}{2}}}{T}\left[\frac{1}{f_1}\cos\left(\frac{C_3}{\xi^{\frac{1}{2}}}+C_4\right)+\frac{1'}{f_2}\cos\left(\frac{C_3}{\xi^{\frac{1}{2}}}+C_5\right)\right], \quad (5c)$$

where the second cosine term results from taking into account the tunnel effect and reduces to zero if this effect is neglected. The slowly varying functions f_1 and f_2 in formula (5c) are

$$f_1 = [(15.1+0.158\xi^{\frac{1}{2}}/T)^2+88.9]^{\frac{1}{2}}, \quad (5d)$$

$$f_2 = [(30.2-0.158\xi^{\frac{1}{2}}/T)^2+88.9]^{\frac{1}{2}}, \quad (5e)$$

if the field is in volts cm^{-1} and the temperature in deg. K. To a good approximation C_1, C_2, C_3, C_4, and C_5 are constants for a given emitter, whose computation as well as that of the functions f_1 and f_2 involve only natural physical constants. Computed values are listed in Table I.

The function $F_2 = \Delta - F_1$ should represent the experimentally observed periodic deviations from the Schottky line. Computed curves for F_2 in the case of tungsten are displayed with the experimental data in Fig. 1. Curves A and B have been computed for tungsten at 1500 and 2500°K respectively, neglecting the tunnel effect. Curve C includes the tunnel effect at 1500°K.

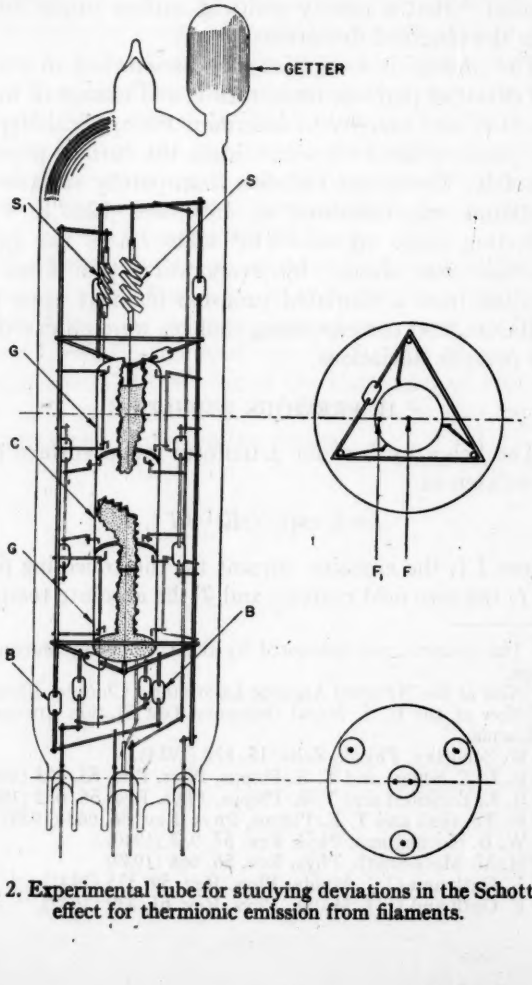

FIG. 2. Experimental tube for studying deviations in the Schottky effect for thermionic emission from filaments.

[9] S. Dushman, *The Elements of Quantum Mechanics* (John Wiley and Sons, Inc., New York, 1938), Chapter 3.

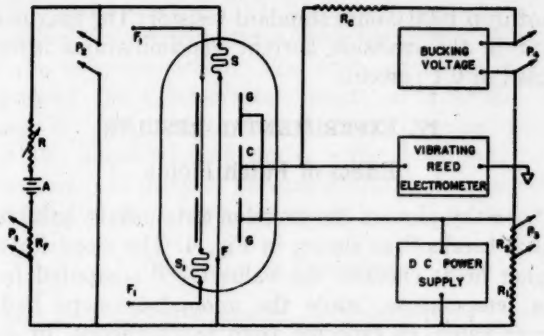

FIG. 3. Circuit diagram. The vibrating reed electrometer is used as the null indicator.

General features agree, but at higher fields a large phase difference occurs between computed and experimental curves. This is particularly apparent when positions of the extrema, indicated by the arrows in Fig. 1, are compared; the data of Turnbull and Phipps[4] are consistent with those of Nottingham,[5] but both are at variance with the theory when fields reach the order of 10^5 volts cm^{-1}, even when the tunnel effect is neglected.

III. EXPERIMENTAL METHOD

Tube Construction

The present study of Schottky deviations was made on fine-grained unpolished filaments of tantalum.[10] Figure 2 shows the construction of the experimental tube. The 0.001-inch tantalum filament F is held taut along the axis of the coaxial collector-guard-ring-system CGG by the molybdenum spring S. The diameter of F was determined within 0.2 percent by weighing measured lengths and using the value of 16.60 g cm^{-3} for the density.[11] The collector and guard rings were tantalum cylinders 2 cm in diameter and 3 cm long. The source of thorium was the thoriated tungsten filament[12] F_1 held taut by spring S_1 and located near the collector to minimize distortion of the field at the cathode F. Mechanical precision was attained by mounting the tube elements on the beaded framework, upon which centering and aligning were done independently of the glass envelope. The 7052 glass beads BB were able to withstand a cathode to anode potential difference of 15 kv and maintain a leakage conductance of less than 10^{-15} mhos. Essentially standard procedure[13] was followed in the preparation of parts for vacuum and in pumping the tube and outgassing the parts during evacuation. The tube was sealed off at a pressure

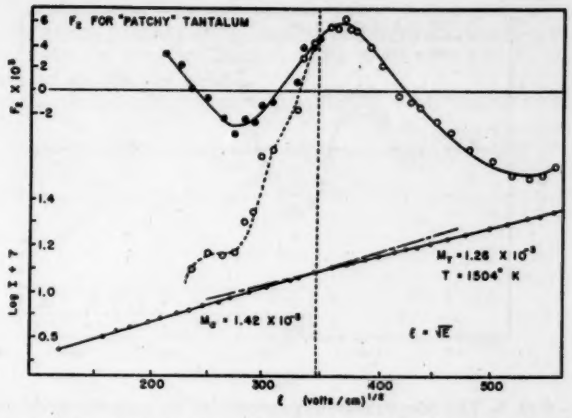

FIG. 4. Periodic deviations about a patch break. The slope of the normal Schottky region is M_T; the slope of the anomalous region is M_a.

of 2×10^{-8} mm of Hg, measured by a conventional type ionization gauge, after barium getter[14] was flashed in the end bulb illustrated in the drawing. The tantalum filament was cleaned and stabilized by 10-minute periods of flashing at 2350°K. After the source filament F_1 was flashed initially at 2900°K for one hour for outgassing and for reducing the thoria, it was maintained at 2500°K for the evaporation of thorium. At this temperature it required about 20 hours to deposit a fraction of a monatomic layer of thorium sufficient to reduce the work function of clean tantalum by approximately one-half volt. During evaporation periods the receiver filament F was held at 1500°K to encourage migration over its surface.[15] Even at this temperature it required about one-half hour after F_1 was turned off to complete the migration process and obtain an equilibrium state of the emitter system.

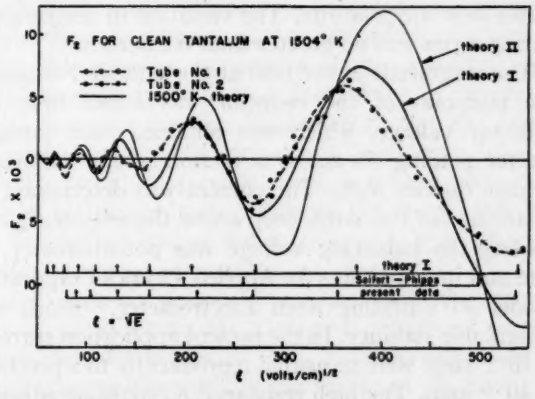

FIG. 5. Periodic deviations for clean tantalum. The theoretical curves are calculated for W_a=9.3 electron volts. Theory I neglects the tunnel effect which is included in theory II. The arrows indicate positions of maxima and minima.

[10] Experiments now in progress on highly polished 0.005-inch tantalum wires have revealed no differences in the deviations for polished or unpolished filaments.

[11] L. Malter and D. B. Langmuir, Phys. Rev. 55, 743 (1939).

[12] The thoriated tungsten wire was furnished by the Cleveland Wire Works of the General Electric Company through the courtesy of Mr. W. M. Rossington.

[13] W. B. Nottingham, J. App. Phys. 8, 762 (1937).

[14] The getter was KIC type 61018F, furnished by the Kemet Laboratories of Cleveland, Ohio, through the courtesy of Mr. Milo Wells.

[15] C. J. Gallagher, Phys. Rev. 65, 46 (1944).

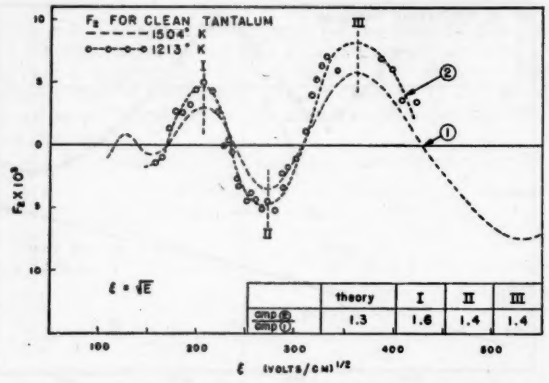

FIG. 6. The temperature dependence of the periodic deviations for clean tantalum. Curve (1) for 1504 deg. K is transferred from Fig. 5. Both curves (1) and (2) are drawn as the best fit to experimental data. The theoretical ratio of the amplitudes is computed from the inverse temperature relation (see Eq. (5)).

Electrical Measurements

The measuring circuit is represented by the block diagram in Fig. 3. The temperature of the filament F was obtained from the Malter-Langmuir[11] tables of the $V'A'^4$ function; the voltage across the filament was measured by the potentiometer P_2, and the heating current was determined from the voltage across the standard 1-ohm resistor R_F measured by the potentiometer P_1. While the absolute value of the temperature is not accurate[11] to better than 10°K, constancy of temperature was checked during the taking of emission data by monitoring the filament heating current and voltage. The filament current was supplied by a bank of five lead storage batteries connected in series and operated on the part of their discharge characteristic over which the voltage was constant. The batteries were inspected daily and the specific gravity kept between 1.200 and 1.250, in order to keep the current stable over any one run. The variation in temperature during a run was no greater than 0.2 percent.

The magnitude of the field at the cathode F opposite the midpoint of the collector was found from the collector voltage, which was obtained from potentiometer reading P_3 across a section of the calibrated voltage divider R_2R_1. The current was determined by balancing out the ohmic drop across the resistor R_c, and reading the balancing voltage was potentiometer P_4. The null indicator was an Applied Physics Corporation Model 30 Vibrating Reed Electrometer,[16] which had remarkable stability. In the present application currents of 10^{-11} amp. were measured reproducibly to a precision of 10^{-14} amp. The high resistance R_c could be adjusted to 0.1008, 1.185, 12.10, 120.0, or 1580 megohms by switching. The high resistance components were S. S. White resistors mounted on Teflon standoff insulators of shunt resistance greater than 10^{15} ohms; these components were checked periodically against a Leeds and Northrup 1000.0-ohm standard resistor. The maximum error in the emission current determinations is estimated at 0.1 percent.

[16] Palevsky, Swank, and Grenchik, Rev. Sci. Inst. 18, 298 (1947).

IV. EXPERIMENTAL RESULTS

Effect of Patch Fields

Schottky plots of the emission data usually exhibited patch breaks,[17] as shown in Fig. 4. The slope for the higher fields checked the value C_0/T computed from the temperature, while the anomalous slope had a larger value, as expected from patch theory. In each field region the slope M and the intercept $\log I_0$ were determined graphically and the periodic deviations computed as the quantity $F_2=\log I-\log I_0-M\xi$; the slope and the intercept in a given region of constant slope must be used to compute the experimental values of F_2 in that region. This is illustrated in Fig. 4, where the open circles are the deviations computed using M_T alone. In this case there is a drifting of points below the break, which does not occur if the slope and intercept appropriate to the region are employed. When the anomalous slope M_a is used for the lower fields, the computed deviations represented by the closed circles in Fig. 4 are obtained.

Clean Tantalum

The value of 4.03 ± 0.04 ev obtained for the thermionic work function of tantalum by means of Richardson plots was taken as evidence for an uncontaminated surface.[18] Experimental curves of F_2 for clean tantalum are shown in Fig. 5 and Fig. 6. Figure 5 shows a comparison of experimental and theoretical curves for 1500°K. The open and closed circles in Fig. 5 represent data from two different experimental tubes, corrected for the patch effect by the method described in the preceding section. The arrows indicate positions of the extrema according to Seifert and Phipps,[3] the theory,[7] and the present results.

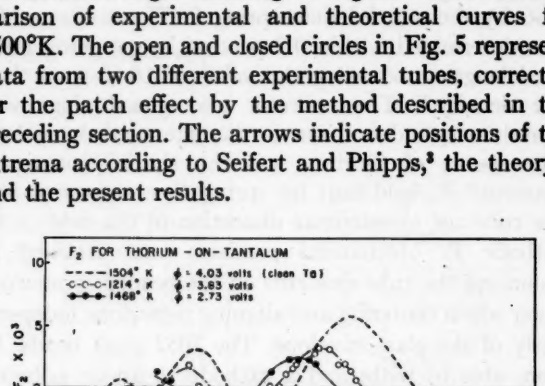

FIG. 7. Periodic deviations in the Schottky effect for thin films of thorium on tantalum. The values of work function were determined experimentally by Richardson plots. The amplitudes decrease and the extrema shift to lower values of applied field with decrease in work function.

[17] C. Herring and M. H. Nichols, Rev. Mod. Phys. 21, 185 (1949), Chapter 2.

[18] Dushman, Rowe, Ewald, and Kidner, Phys. Rev. 25, 338 (1925).

In Fig. 6 the experimental curve for 1504°K is drawn as the reference curve. The open circles in Fig. 6 represent the experimental results at 1213°K. The phase is unaffected by the decrease in temperature, but the amplitudes of the periodic deviations have increased. The ratios of the amplitudes at three extrema are listed in the table in the figure.

Thorium on Tantalum

In Fig. 7 the experimental F_2 deviations for thorium on tantalum are compared with those for clean tantalum. As the work function of the filament was decreased from 4.03 to 3.83 to 2.73 ev, not only did the amplitudes decrease in each instance, but the extrema of the deviations also shifted to lower values of applied field.

V. DISCUSSION

The mean positions for the maxima and minima in F_2 for clean tantalum are listed in Table II for the present experiment. Over the range of fields studied these data for the phase of the deviations are in fair agreement with theory if the tunnel effect is neglected. The experimental amplitudes are always less than theoretical (Fig. 5), this discrepancy increasing at the higher fields.

The two important aspects of lowering the emitter temperature are encountered when the deviations observed at 1213°K for a clean tantalum filament are compared with the 1504°K data taken on the same filament. First, the amplitudes as shown in Fig. 6 increase inversely with temperature, in substantial accordance with the theory. This may be brought out by comparing the ratios of the amplitudes at the three principal extrema, which has been done in the table in the figure. Secondly, it may be observed that experiment reveals no change in phase as the temperature is changed, which is also implied by the theory whether or not the tunnel effect is included.

The principal effects experienced when the work function of the tantalum surface was lowered by thin films of thorium were two: (a) the amplitudes of the periodic deviations decreased, and (b) the positions of the extrema shifted to lower values of field. These results are displayed in Fig. 7. Herring[19] has pointed out that the existence of a peak in the potential barrier near the surface of a composite emitter, which has sometimes been surmised, should become noticeable through an *increase* in the amplitudes of the periodic deviations. The *decrease* in amplitudes exhibited by the present data does not substantiate the existence of such a barrier modification for thorium on tantalum, within a range of work functions from 4.03 to 2.73 ev.

The shift of extrema to lower fields and the decrease in amplitudes when thorium is deposited on clean tantalum may be accounted for in part by a decrease in W_a with decrease in work function. This can be seen qualitatively from an examination of Eq. (5), where W_a occurs in such a manner in both the amplitude factor C_2 and in the phase factors C_4 and C_5 that a decrease in W_a implies a simultaneous decrease in amplitudes and a shift in extrema to lower values of ξ.

TABLE II. Positions of the maxima and minima in the periodic deviations for clean tantalum in terms of $E^{\frac{1}{2}}$ (volt cm^{-1})$^{\frac{1}{2}}$. The maxima are given in italics.

Observed by Seifert and Phipps[a]	Observed by Munick, LaBerge, and Coomes	Computed from the Guth-Mullin theory[b] neglecting tunnel effect
	80	78
	90	*92*
	104	110
110	*132*	*132*
160	164	164
200	*206*	*208*
260	267	273
355	*364*	*374*

[a] See reference 3.
[b] See reference 7.

VI. CONCLUSIONS

The results of this experiment tend to establish the following points. (a) The temperature variations for periodic deviations are as theory predicts, namely an inverse variation of the amplitude with no shift in phase. (b) The deposition of a thin film of thorium on a clean tantalum surface does not produce a potential peak, since the addition of the thorium decreases rather than increases the amplitudes of the deviations. The data seem to indicate that the theory in its present state accounts for the fundamental physical factors involved in periodic deviations from the Schottky effect; probably a revision in the basic theoretical model to include such details as the atomic structure of the surface and of the interior of the metal would lead to more exact quantitative agreement.

The authors gratefully acknowledge the help of Dr. C. Herring and Mr. George E. Moore of the Bell Telephone Laboratories. Dr. Herring offered many helpful suggestions during the course of the work, and together with Mr. Moore read and criticized the manuscript. Thanks are expressed to Mr. H. W. Weinhart of the Bell Telephone Laboratories for his assistance with the filament structures. We also wish to thank Mr. Ernest Parsons and Mr. Fay Gifford of our own group for their technical assistance in carrying out the experiment and in preparing the manuscript.

[19] C. Herring and M. H. Nichols, Rev. Mod. Phys. 21, 185 (1949), Chapter 4.

Magnetoresistance of Bismuth at 3000 Megacycles

C. W. HEAPS
Rice Institute, Houston, Texas
(Received July 17, 1950)

The magnetoresistance of bismuth for frequencies of 3.5 Mc has been found to be of the same magnitude as for steady direct currents. On the other hand, for long infra-red waves (8μ) the magnetoresistance is zero. Using a resonating bismuth cavity and a slotted wave-guide measurements of the standing wave ratio have indicated that magnetoresistance at 3000 Mc is not more than half as big as for direct currents. This small value of magnetoresistance is possibly due to the fact that the skin depth is of the same order of magnitude as the mean free path of electrons in the metal.

I. INTRODUCTION

THE effect of a magnetic field on the resistance of bismuth for electric currents of high frequency has been investigated at 3.5 Mc by Blunt[1] and found to be of the same magnitude as for direct currents. For frequencies in the infra-red no magnetoresistance is to be observed[2] for wave-lengths of 8μ. It appears, therefore, that somewhere in the region between wave-lengths of 85 meters and 8μ the magnetoresistance of bismuth drops to zero. In order to investigate this phenomenon more precisely some experiments have been performed at wave-lengths of 9.2 cm using a klystron oscillator and a resonating cavity made of bismuth.

II. APPARATUS

Power was fed from the klystron through a flexible coaxial line and a slotted coaxial wave guide into a bismuth cavity which was loop coupled to the end of the slotted section. This cavity was of the cylindrical re-entrant type, of diameter 2.1 cm and length 2.3 cm. A central coaxial rod of length 1.8 cm and diameter 0.57 cm extended from the top of the cavity to within 0.5 cm of the bottom. Tuning for resonance was effected by a screw through the bottom. All parts were of cast and machined bismuth.

In operation much of the incident energy was reflected from the cavity and the standing wave in the slotted section was investigated in the usual way with a probe, crystal rectifier, and sensitive galvanometer. Large attenuation was inserted between the klystron and the slotted section in order to cut down the power to the microwatt region where the crystal rectifier gives readings accurately proportional to the power. This attenuation also served to insulate the klystron from the effects of the reflected energy.

The bismuth cavity was placed between the poles of an electromagnet with pole faces 5.1 cm in diameter and 4.1 cm apart. A field of 6900 oersteds was used in most of the experiments. The cavity was excited in the fundamental TEM mode and thus the predominant current direction was transverse to the magnetic field.

The experimental procedure consisted in adjusting the probe carefully to a point of minimum or maximum power in the slotted section, observing the deflection of the galvanometer, then throwing on the magnetic field and observing the change of galvanometer deflection. These observations sufficed for a calculation of the fractional change of electrical resistance produced in the bismuth by the magnetic field. This fractional change was found to decrease in a regular way with the magnetic field.

The wave-length, measured with a TFS-5 coaxial wave meter, was 9.2 cm.

III. THEORY

Let P_i be the power incident upon the bismuth cavity, P_a the power absorbed in the cavity, and P_r the total reflected power. Then $P_a=P_i-P_r$. Some of the power is reflected at the cavity window. This reflection will not be affected by the magnetic field. When the field is applied the absorbed power will be increased dP_a if the resistance of the bismuth is increased, so that the reflected energy will be changed by dP_r. The incident power is unchanged and thus

$$dP_a=-dP_r.$$

The power loss in a metal cavity[3] is proportional to ρ/δ, where ρ is the resistivity of the wall material, and the skin depth $\delta=[\rho/(\pi f\mu)]^{\frac{1}{2}}$. Here f=frequency of the current, μ=magnetic permeability of the metal. Hence P_a is proportional to $\rho^{\frac{1}{2}}$ and we get $dP_a/P_a=d\rho/(2\rho)$. Substitution of the equivalent values of dP_a and P_a gives

$$d\rho/\rho=-2dP_r/(P_i-P_r).$$

Let A and B be, respectively, the amplitudes of the incident and reflected waves, so that $P_i=KA^2$, $P_r=KB^2$, where K is a constant. We then have

$$d\rho/\rho=-4BdB/(A^2-B^2).$$

Let the power at a node of the standing wave be P_n,

[1] R. F. Blunt, Phys. Rev. 73, 654 (1948).
[2] C. W. Heaps, Phys. Rev. 27, 764 (1926); McLennan, Allin, and Burton, Phil. Mag. 14, 508 (1932); E. Englert and K. Schuster, Zeits. f. Physik 79, 194 (1932).
[3] M. I. T. Radar School, *Principles of Radar* (McGraw-Hill Book Company, Inc., New York, 1946), p. 10-57.

and at a loop or antinode, P_a. Then

$$P_n=K(A-B)^2, \qquad P_a=K(A+B)^2,$$
$$dP_n/P_n=-2dB/(A-B), \quad dP_a/P_a=2dB/(A+B).$$

The probe current at any point in the slotted section is proportional to the power at that point, so the quantities $\Delta_1=dP_n/P_n$ and $\Delta_2=dP_a/P_a$ are determined by observing galvanometer deflections. When Δ_1 and Δ_2 are expressed in terms of the amplitudes and added together we get

$$d\rho/\rho=\Delta_1+\Delta_2.$$

The reflected amplitude B is not greatly different from A so that Δ_2 is much smaller than Δ_1. dB is always a negative quantity so that Δ_1 is positive and Δ_2 negative.

IV. RESULTS

Table I gives representative results, including the largest and smallest values obtained.

The machined surface for the set of data beginning December 3 was several weeks old. Each of the remaining sets for different surfaces began within about an hour after the surface was prepared.

The values of $d\rho/\rho$ from Table I are distributed over a considerable range. It is probable that lack of stabilization of the oscillator is responsible for some of this fluctuation. However, it seems to be possible to draw certain general conclusions. First, the magnetoresistance observed at this frequency is smaller than that found with steady, direct currents. A small bar of this polycrystalline bismuth when tested in this same transverse field was found to have a direct current value of $d\rho/\rho=0.25$. Second, the character of the surface appears to have a significant effect on the magnitude of $d\rho/\rho$. A freshly machined surface gave the largest value, a surface freshly etched with nitric acid and then carefully washed, the smallest.

It is to be expected that roughness of the surface[4] would affect the magnitude of $d\rho/\rho$ because the direction of current flow would be altered by scratches or projections on the surface. The average direction of the current with respect to the magnetic field would thus be altered and so the magnitude of the magnetoresistance would be changed.

Another important factor would be the chemical purity of the surface. If a film of oxide or other bismuth compound formed on the surface and a substantial fraction of the current flowed in this film the magnetoresistance would not be characteristic of pure bismuth.

TABLE I. Fractional resistance change of bismuth under different conditions for a magnetic field of 6900 oersteds.

Date	Surface	Δ_1	Δ_2	$d\rho/\rho$
Dec. 3	Machined	0.084	−0.013	0.071
Dec. 5	Machined	0.088	−0.013	0.075
Dec. 6	Machined	0.093	−0.028	0.065
Dec. 6	Etched	0.036	−0.018	0.018
Dec. 6	Etched	0.057	−0.011	0.046
Dec. 8	Machined	0.13	−0.006	0.12
Dec. 9	Machined	0.11	−0.000	0.11
Dec. 27	Machined	0.038	−0.013	0.025
Dec. 28	Machined	0.064	−0.018	0.046
Dec. 28	Polished	0.067	−0.000	0.067

In case the skin depth approaches a magnitude comparable to the mean free path of the conduction electrons an effect on magnetoresistance may be expected. Statistical theories[5] explain magnetoresistance as being due to the fact that the conducting electrons possess different values of L/v, where L is the free path and v the velocity of agitation. When the skin thickness is less than the mean free path those electrons moving normal to the surface make a smaller contribution to the current during a free path than those moving parallel to the surface. Their effective mean free path is changed. Hence the fluctuation of L/v among the electrons is different when the skin effect is important, so the magnetoresistance is different.

The skin depth in bismuth for the frequency used in these experiments is about 1×10^{-3} cm. It has been suggested that the mean free path of electrons in bismuth is abnormally large. Eucken and Förster[6] have deduced from experiments on very fine wires of bismuth a value $L=1.08\times10^{-3}$ cm at 273°K. If this estimate is accepted the skin depth and the mean free path are of the same order of magnitude and it is therefore not surprising that the magnetoresistance is considerably smaller than for direct currents.

Mott and Jones[7] have stated that it is not necessary to assume an abnormally large mean free path for bismuth. They believe that the experiments of Eucken and Förster should have some other explanation.

The results of this experiment, if we assume the high frequency resistance of a freshly machined bismuth surface to behave like that of bulk material, seem to favor the idea of an abnormally long free path for electrons in bismuth.

[4] It is interesting to note in this connection that A. B. Pippard, Proc. Roy. Soc. A191, 385 (1947), has found the skin resistivity of a drawn copper wire to be nearly equal to that of the bulk material. Polishing the wire resulted in deterioration of the surface and an increase of skin resistivity.

[5] A. Sommerfeld and N. H. Frank, Rev. Mod. Phys. 3, 1 (1931).
[6] A. Eucken and F. Förster, Göttingen Nachrichten 1, 43 (1934).
[7] N. F. Mott and H. Jones, *Properties of Metals and Alloys* (Oxford University Press, London, 1936), p. 303.

Magnetic Moments and Eddy Currents in Spheres of Superconducting Tin*

JAMES J. FRITZ, OSCAR D. GONZALEZ, AND HERRICK L. JOHNSTON
Cryogenic Laboratory and Department of Chemistry, Ohio State University, Columbus, Ohio
(Received July 7, 1950)

Experiments have been carried out to measure the "frozen in" magnetic moments produced in superconducting spheres of tin, through demagnetization from fields sufficient to completely or partially destroy their superconductivity. Moments were determined by measuring periods of a torsion pendulum made from the spheres. Both solid tin spheres and spheres filled with nonsuperconducting material were examined.

Small permanent moments, fixed in magnitude and direction, and probably associated with traces of impurity, were observed for the solid spheres while considerably larger fixed moments were observed for the hollow spheres. The observed permanent moments, which amounted to one to three percent of the induced moments calculated for the critical field depended to a slight extent on the magnitude of the fields used to produce them and were also dependent on the size and geometry of the spheres and on the temperature.

Entry of the spheres into the intermediate state was evidenced by a sudden gain in the total magnetic moment when the measuring field attained a value which was close to 2/3 of the critical field, H_c. This gain was best observed by measurements of this coefficient for eddy current damping. We interpret this effect as due to the formation of regions of normal metal in the intermediate state. We also interpret the permanent moments, which can only be changed by bringing the specimens into fields in excess of $2/3\ H_c$, as due to isolated regions of normal metal. The amounts of normal metal, in either the superconducting or the intermediate regions, can be evaluated either from measurements of magnetic moment or from measurements of coefficients of eddy current damping. Results obtained by the two methods are in agreement.

The results can be explained in terms of Landau's theory of the intermediate state that postulates the presence of threads or plates of normal metal. Our results indicate that these regions of normal metal must have diameters or thicknesses which are quite small compared to their lengths and that the magnetic moments which they represent can be trapped in a particular direction for a considerable length of time.

I. INTRODUCTION

THIS investigation was undertaken to determine the nature and magnitude of the magnetic moments that can be induced in spherical specimens of superconductive material upon transition from their normal to their superconductive state. In most bodies there are obvious geometrical constraints to hinder the free movement of magnetic moments (or persistent currents) about the surface of a specimen, but in case of a sphere it is possible that the moment might move without hindrance. Tuyn[1] investigated the rotation of the magnetic moment of a lead sphere within a magnetic field produced by a persistent current in a ring surrounding the sphere and found that the moment remained fixed with respect to the sphere. Since the magnitude and nature of the magnetic field was not known for his experiments, uncertainties were introduced as to the state of the spherical specimens. A variation of the Tuyn method was used by Daunt and Desirant in preliminary work in this Laboratory, but their experiments were not carried far enough to give quantitative results.

The present investigation is an extension of the work begun by Daunt and Desirant, with considerable modification of their apparatus and method, and is concerned with the magnitude and nature of the magnetic moments induced in specimens of superconducting material on transition from the normal to the superconducting state. In particular, it was of interest to know whether the magnetic moment, once induced, was constrained to stay in its original position with respect to the specimen. The results of our investigation have already been reported briefly.[2] Experiments very similar to our own were reported at the same time by Condon and Maxwell.[3]

II. APPARATUS AND EXPERIMENTAL PROCEDURE

Five specimens of pure (melting point) tin and one specimen containing 0.2 percent copper were investigated. Two of the samples were solid, and four contained spherical cores of material that would not become superconducting under the experimental conditions. Table I presents the dimensions of the specimens.

A diagram of the apparatus is shown in Fig. 1. The tin sphere (H) was fastened by cellulose tape to a cylindrical Lucite mounting (G), which was secured to the rigid part of the suspension system by a small set screw (F). The rigid portion of the system consisted of three parts: a 20-cm length of 1.5-mm Bakelite rod (C_2), a 57-cm length of thin-walled nickel-silver tube (E), and a 9-cm length of 1.5-mm brass rod (C_1). The rod (C_1) carried a mirror (D) and was connected through a clamp (K) to the torsion head (A). The wire (B) was approximately 4.5 cm long and usually was of 0.15-mm stainless steel. The entire apparatus was located inside a liquid helium dewar vessel (N), which in turn was contained in a dewar vessel (not shown) filled with liquid nitrogen to protect the inner dewar from room temperature radiation. The material under investigation was viewed through parallel unsilvered slits in the dewar flasks.

Magnetic fields were provided by multilayer Helm-

* This work was supported, in part, by a sub-contract with the Curtiss-Wright Corporation as part of a contract with the Army Air Force.

[1] Tuyn, Comm. Phys. Lab. Univ. Leyden No. 198 (1929).

[2] Fritz, Gonzalez, and Johnston, Phys. Rev. 76, 580–581 (1949).

[3] Condon and Maxwell, Phys. Rev. 76, 578 (1949).

holtz coils, shown schematically at M. The suspension system was rotated by means of the torsion head (A), and its motion observed with a lamp and scale located 110 cm from the mirror (D). A window, not shown in the diagram, permitted passage of light through the head (J).

A "frozen in" magnetic moment was induced in the specimen, at temperatures below 3.7°K, by applying an appropriate magnetic field for about 60 seconds. Oscillations of the system were then set up, and their period was observed in various magnetic fields. Magnetic moments were calculated from these data by the relationship, valid for small oscillations,

$$1/\tau^2=(n+MH)/4\pi^2I, \qquad (1)$$

where n is the torsion constant of the suspension, M the magnetic moment, H the magnetic field, and τ the period. The constant n was evaluated from the intercept of the straight line obtained when $(1/\tau^2)$ was plotted against H, for fields below $\frac{2}{3}H_c$. For these fields, M is constant.

Equation (1) neglects damping. The observed damping of the oscillations during our experiments had, in all cases, a negligible effect upon the period. Its magnitude could be expressed in terms of a damping coefficient b as

$$d=d_0e^{-bt/2I}, \qquad (2)$$

where d_0 and d are the initial and final amplitudes of oscillation, I the moment of inertia of the system, and t the elapsed time.

Separate damping experiments were carried out.

III. "FROZEN IN" MAGNETIC MOMENT

The observed "frozen in" magnetic moments depended upon the size of the fields used to produce them, upon the size and geometry of the spheres, and upon the temperature. They were generally independent of the field used to measure them, unless the measuring field exceeded that required to cause entry of the specimen into the intermediate state, as discussed later in this paper.

The fact that the moments were independent of small measuring fields showed that the effect could not be due to the sort of shielding currents described by Condon and Maxwell.[3] For such currents the observed torque should vary as the square of H and the apparent magnetic moment should be proportional to H, whereas, in our experiments, the torque was proportional to H. For very small effects, such as those reported by Condon and Maxwell, the difference between the two cases is slight enough to cause uncertainty, but in our experiments the total moments were large enough to have shown clearly the linear dependence on H, had it existed.

Specimens cooled from above the transition temperature in zero field showed no magnetic moment; subsequent application and removal of magnetic fields of less than two-thirds of the critical field likewise did not induce such an effect. However, "frozen in" magnetic moments always appeared when the field exceeded $\frac{2}{3}H_c$. In general, the "frozen in" moment produced when the field was just over $\frac{2}{3}H_c$ was not much below the maximum moment reached at critical field, although there was a small increase up to H_c. Fields above H_c produced no additional moment. The ratios of minimum to maximum moment observed at a given temperature were 0.95 for solid sphere II, 0.70 for hollow sphere II, and 0.75 for hollow sphere III.

TABLE I. Dimensions of tin spheres used in investigation.

Designation of specimen	Outside diameter of tin cm	Inside diameter of tin cm	Nature of core	Weight of tin gm	Moment of inertia gm-cm²
Solid sphere I[a]	1.99 ±0.01	—	—	30.0	11.92
Solid sphere II	2.795±0.003	—	—	83.3	65.0
Hollow sphere I	2.30 ±0.02	1.60	Aluminum	31.9	22.3
Hollow sphere II[b]	2.895±0.005	1.59	Aluminum	75.1	73.1
Hollow sphere III	2.926±0.003	1.19	Glass and air	87.8	79.7
Hollow sphere IV	2.162±0.003	1.19	Glass and air	31.0	16.5

[a] Solid sphere I was machined from the ingot as received. The other specimens were first vacuum cast and then machined to size.
[b] Hollow sphere II contained 0.2 percent copper.

Table II shows the influence of temperature on the "frozen in" moments produced in hollow sphere IV, upon applying and removing fields greater than H_c. The accuracy of the determinations is estimated to be two to five percent.

The dependence on size and geometry of the sphere is shown in Table III, where for simplicity only the value at the lowest temperature for each specimen is presented.

The "frozen in" moments for solid spheres I and II correspond to one and three percent, respectively, of the induced moments present at the critical field[4] and are of the same order of magnitude as those previously determined for tin and lead by other methods.[5] The moments observed with hollow spheres were proportionately larger, due apparently to failure of the hollow spheres to be completely superconductive. This failure was observed experimentally by Shalnikov[6] and analyzed theoretically by Koch.[7]

The "frozen in" moments observed did not change with time nor were they altered by cooling the specimen, provided the field was not raised by a sufficient amount to put the specimen again into the intermediate state.

[4] de Haas and Engelkes, Comm. Phys. Lab. Univ. Leyden No. 247d (1937).
[5] Nakhutin, J. Phys. (USSR) **6**, 114 (1942). Shoenberg, Proc. Roy. Soc. **A155**, 712 (1936). Mendelssohn, Daunt, and Pontius, VII Congres du Froid (1936).
[6] Shalnikov, J. Phys. (USSR) **6**, 53 (1942).
[7] Koch, Zeits. f. Physik **121**, 488–494 (1943).

TABLE II. Maximum "frozen in" magnetic moments observed with hollow sphere IV.

Temperature °K	Magnetic moment ergs-gauss^{-1}	Temperature °K	Magnetic moment ergs-gauss^{-1}
1.15	6.4	2.62	3.31
1.41	6.0	2.95	2.82
1.70	5.6	3.16	2.28
1.98	5.0	3.39	1.70
2.38	3.6	3.56	1.40

IV. INTERMEDIATE STATE

Entry into the intermediate state was evidenced by a sudden gain of magnetic moment as the magnetic field was increased above a definite value for each temperature. This is illustrated in Fig. 2, for hollow sphere II, whose "frozen in" moment of 75.5 erg-gauss was obtained initially by quickly dropping the field from 254 gauss. This gain in moment can be ascribed to the beginning of penetration of the bulk of the specimen by the external magnetic field. The field at which this penetration occurred depended mainly on temperature and was increased slightly by the presence of magnetic moment on the specimen, due apparently to a shielding action of the moment.

Table IV gives the magnetic field, as a function of temperature, at which penetration occurred for hollow sphere IV; the measured values have been extrapolated where necessary to zero magnetic moment. These values are in approximate agreement with those (two-thirds of the critical field) predictable from the critical field measurements of de Haas and Engelkes,[4] except at the highest temperature. Measurements on the other specimens agreed within 1 or 2 gauss with those reported in Table IV. This is illustrated in Fig. 3.

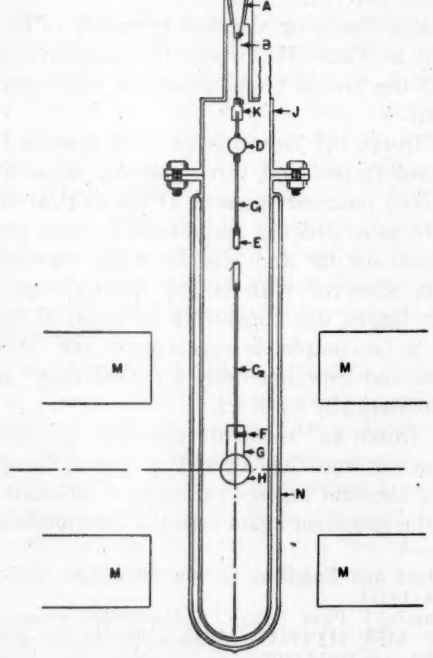

FIG. 1. Apparatus for measurement of magnetic moments and damping.

TABLE III. Dependence of maximum "frozen in" magnetic moment on the size and geometry of the spheres.

Designation	Temperature °K	Magnetic moment ergs-gauss^{-1}	Volume of tin cm
Solid sphere I	1.37	1.00	4.12
Solid sphere II	1.15	9.9	11.42
Hollow sphere I	1.23	4.9	4.38
Hollow sphere II[a]	1.27	89.2	10.30
Hollow sphere III	1.15	15.7	12.05
Hollow sphere IV	1.15	6.4	4.26

[a] Hollow sphere II shows the effect of impurity. This sphere contained less tin than hollow sphere III, but showed a much higher moment, apparently due to the small percentage of copper present.

Increasing the magnetic field beyond the level required for entry into the intermediate state caused a continued rapid increase in the magnetic moment, as evidenced in Fig. 2, and in the damping, up to fields at which the latter became too strong for observation of the period of oscillation. Table V gives typical results for two specimens.

The increase of observed magnetic moment would seem to be in contradiction with the generally accepted belief that the intermediate state corresponds to the growth of normal areas in the body, since the induction in an ordinary diamagnetic material should be free to follow the direction of the external magnetic field. However, our results can be explained readily if one accepts a model of the type of penetration similar to that proposed by Landau[8] and others, the gross features of which have been demonstrated experimentally by Meshkovskii.[9] In a model of this type the normal regions are viewed as fine threads, or thin plates, imbedded in the superconducting material. As the field is increased, these regions grow in size and number until the body becomes entirely normal. At the instant when normal regions are set up, the direction of induction within them will correspond to that of the applied magnetic field. If the body is then rotated the lines of force at the surface can follow the direction of the applied field without hindrance, but those within the threads or plates can realign themselves only by an actual rotation of the threads as a whole. If the time allowed for this process is too short, or if the forces hindering redistribution of the regions are too great, the induced moment within will be "trapped" in its original direction. The same reasoning can be applied to the reverse transition and also to the transition from intermediate to normal condition.

The conditions brought out in the previous paragraph appear to be fulfilled in the spheres investigated, wherein the period of oscillation was generally less than two seconds. The marked increase of magnetic moment upon entry into the intermediate state was matched by a corresponding hysteresis in the reverse transition to

[8] L. Landau, J. Phys. (USSR) 7, 99 (1943).
[9] Meshkovskii, J. Exp. Theor. Phys. (USSR) 19, 54 (1949).

the superconducting state, and relaxation effects were noted in both transitions. Table VI shows the hysteresis observed for two cycles of magnetization from zero into the intermediate state and back; the measurements were made in the order presented. Results obtained with solid sphere II are plotted in Fig. 4, which is similar to curves obtained by other workers for the magnetic induction in the transition to the normal state.[10]

The magnetic moments given in Table VI are the constant values attained when equilibrium has been established a few minutes after a given change in field. The time required to reach equilibrium for hollow sphere III varied from about three minutes after the change from 151.5 to 154.5 gauss to 10 or 12 minutes after reverse transitions from 61 to 46 gauss and from 46 to 25.5 gauss. In a few cases, slow changes were observed even after 10 minutes, and the final value had to be determined by extrapolation. These time effects are quite similar to those reported by de Haas and Engelkes,[4] by Guinau,[11] and by Mendelssohn and Pontius.[12]

The persistence of "excess" magnetic moment in the reverse transition and the existence of long relaxation times make it likely that induced moment can be "trapped" in a particular direction, as suggested above. The possibility that the effect might be due to some abnormality, such as a ferromagnetic impurity, in the normal material was eliminated when measurements made at 4.2°K, where the specimens were entirely normal, showed no magnetic moment.

V. DAMPING MEASUREMENTS

There were two major sources of damping in the oscillating system:

(1) Small, ordinary fluid damping due to viscous drag of the surrounding gas or liquid.

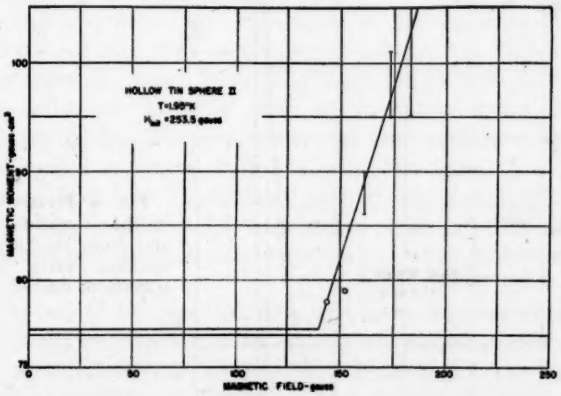

FIG. 2. Observed magnetic moment *vs.* applied magnetic field.

[10] Burton *et al.*, *Phenomena at the Temperatures of Liquid Helium* (Reinhold Publishing Corporation, New York, 1940), p. 105 ff.

[11] de Haas, Engelkes, and Guinau, Comm. Phys. Lab. Univ. Leyden No. 247e (1937).

[12] Mendelssohn and Pontius, Physica 3, 327 (1936).

TABLE IV. Magnetic field at entry into intermediate state for hollow sphere IV.

Temperature °K	Magnetic field gauss	Temperature °K	Magnetic field gauss
1.15	192	2.63	102
1.41	185	2.94	74
1.70	166	3.14	57
1.98	148	3.39	34.5
2.39	117	3.56	18

TABLE V. Magnetic moment in the intermediate state.

Specimen	Temperature °K	Magnetic field gauss	Magnetic moment ergs-gauss^{-1}
Solid sphere I	1.37	0 to 190	1.0
		193	4.7
		194	7.7
		246	21.9
Hollow sphere III	2.20	0 to 130	8.35
		131	8.49
		136.5	18.1
		141.5	37.1
Hollow sphere III	1.90	0 to 150	11.9
		151.5	11.9
		154.5	13.6
		159.7	29.9

(2) Eddy current damping due to the presence of non-superconducting metal in the suspension or in the tin spheres.

The fluid damping was independent of magnetic field and could be evaluated separately by setting it equal to the total damping in zero field, when eddy current damping was absent.

Eddy current damping, on the other hand, depended on the magnetic field. It increased slowly with the field at low fields until the tin sphere was in the intermediate state, and then rose sharply with further increase in the field. The damping was so great for tin in the normal state that it could only be measured for small fields. This effect was checked many times in measurements at 4.2°K, which is above the tin transition point. Eddy current damping was evaluated by subtracting fluid damping from the total damping.

Extraneous influence of the suspension system on eddy current damping was minimized by fabricating the suspension from non-magnetic materials, except for the thin nickel-silver tube that constituted the upper portion of the suspension. This tube was well outside of the Helmholtz magnet. The fact that the total damping proved to be independent of the field in all runs for which the tin spheres possessed no magnetic moment constituted good evidence that we were successful in eliminating the influence of the suspension system on eddy current damping, to within the limits of our experimental error. There was no eddy current damping when the magnetic moments of the tin spheres were zero, even with fields present, but eddy current damping was always present when the spheres possessed a magnetic moment.

Eddy current damping in the normal and intermediate states can be understood readily in terms of

TABLE VI. Hysteresis in transition from intermediate to superconducting state.

Solid sphere II 2.64°K		Hollow sphere III 1.89°K	
Magnetic field gauss	Magnetic moment ergs-gauss^{-1}	Magnetic field gauss	Magnetic moment ergs-gauss^{-1}
0 to 100	0	0 to 140	11.9
102.0	1.6	151.5	12.0
109.0	73.0	154.5	13.6
107.0	63.5	160.0	29.4
103.5	29.0	166.0	90
101.5	20.6	157.0	80
96.0	12.7	147.0	72
89.0	8.4	137.0	74
75.0	4.9	127.0	66
45.0	3.9	100.0	58
20.0	3.8	80.5	54
0	3.6	61.0	44
101	3.6	46.0	29
0	3.6	25.5	19
		11.0	16
		0	12
		102	12

ordinary phenomena, since normal metal must be present under these conditions. The damping which occurred for supposedly superconducting specimens must also arise from the presence of normal regions, and is probably due to the presence of a magnetic moment. Examination of the measurements provides some information as to the mechanism of their production. At a given temperature, eddy current damping increased with increasing magnetic moment, whereas, at constant magnetic moment, it decreased with decreasing temperature. Finally, damping was about proportional to the ratio (M/H_c) at constant temperature and constant field.

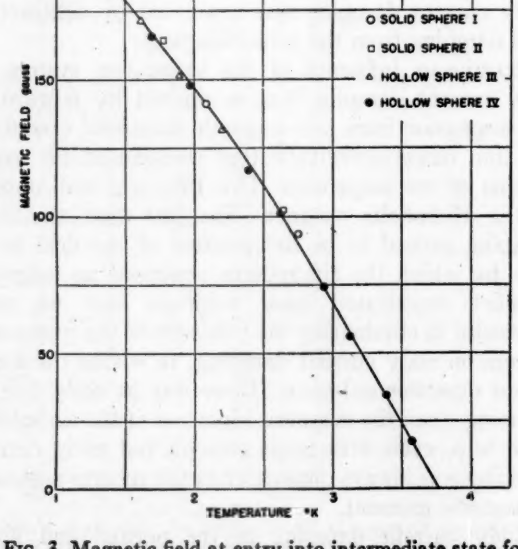

FIG. 3. Magnetic field at entry into intermediate state for spheres of tin.

The experimental results suggest that both the observed magnetic moments and the damping effects are a measure of the amount of normal metal in the superconductor. If this is true, a quantitative correlation of the two effects should be possible. The damping coefficient due to eddy currents should vary as H^2, where H is applied field, when a body of normal metal rotates in a fixed magnetic field; this expectation was realized, approximately, in the measurements of damping at 4.2°K. In addition, if the effect of changes in geometry is not serious, the amount of damping should be proportional to the amount of normal material present. In terms of these hypotheses, the size of the normal portion would be proportional to the ratio M/H_c, where M is the magnetic moment and H_c the critical field for the destruction of superconductivity; it is immaterial whether the normal metal persists in bulk or is disposed into very fine structure in an intermediate state. The damping coefficient should thus be represented by

$$(b-b_0)=kH^2M/H_c, \tag{3}$$

where b is the observed total damping coefficient, b_0 the contribution due to fluid damping, and k a constant involving the geometry of the arrangement. This equation should hold for both the "superconducting" and intermediate conditions, provided the relative distribution of the regions of normal metal does not change greatly, and should be independent of the temperature.

Table VII gives the results observed for several specimens. As the last column indicates, except for three or four entries the data are in reasonably good agreement with Eq. (3).

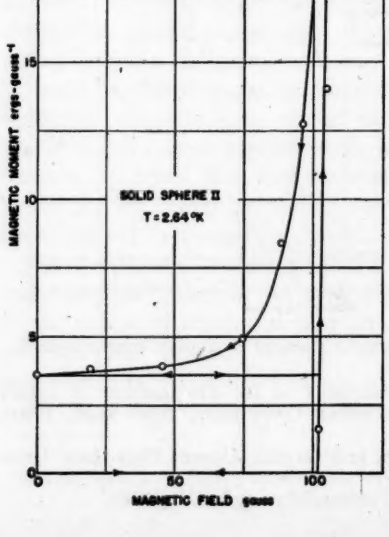

FIG. 4. Hysteresis in the transition to and from the intermediate state for spheres of tin.

The results for solid sphere II at 1.80° and 1.15°K and those for hollow sphere III at 2.2°K gives values for k which are constant at each temperature to within the probable limits of error. The 2.63° values show considerable scattering in the neighborhood of 100-gauss fields, which may be due to improper time correlation of the eddy currents with the magnetic moments since the two were measured at separate times. Although the correlation supports Eq. (3) in general, the decrease of k with decrease in temperature is contrary to prediction and indicates that the actual phenomena are more complex than assumed. The temperature dependence may be due to some change in the distribution of normal metal with temperature, which would change the geometry even though the total volume of normal region remained constant.

It is evident that the production of magnetic moment is the primary phenomenon at fields insufficient to produce the intermediate state throughout the body of the superconductor. When moment is induced, there must be produced at the same time normal, or intermediate, regions in the superconductor which can cause eddy current damping. Small applied fields must not appreciably alter the distribution of such regions, since for an alteration of this type the observed magnetic moment would vary with the measuring field, just as in the intermediate state. However, our experimental magnetic moments generally remained constant to within the estimated limits of error.

VI. CONCLUSIONS

Demagnetization of a superconducting material from fields sufficient to completely or partially destroy its superconductivity produces a "frozen in" magnetic moment fixed in magnitude and direction with respect to the body. This moment can be changed in size and in direction only by the application of fields sufficient to destroy its superconductivity.

The magnitude and character of the moments observed are such that they cannot be due to the "shielding currents" which have been suggested to explain the distortion of magnetic fields by superconductors. In all probability these currents are free to follow the total field resulting from the magnetic moment and the applied field. However, the experiments present no additional evidence as to whether such currents are macroscopic or, as in paramagnetic materials, molecular in nature.

As would be expected, the specimens bearing magnetic moment (either fixed or induced) contain regions of material in the intermediate state which can be measured by the damping they produce on the oscillations of the specimen in a steady magnetic field. The damping observed with several specimens indicated that the amount of normal metal, regardless of its distribution, is proportional to the size of the magnetic moment and to the threshold field.

TABLE VII. Eddy-current damping in spherical superconductors.

Specimen	Temp. °K	Crit. field[a] H_c gauss	Applied mag. field H gauss	Obs. mag. moment M ergs-gauss^{-1}	Coef. of eddy cur. damping $(b-b_0)$ erg-sec.	H^2	$\frac{k}{H_c(b-b_0)/MH^2}$ sec.
Solid sphere II	2.63	167	100.4	1.0	7.4	10,080	0.12
			61.6	3.6	0.17	3,800	0.0021
			86.2	3.6	0.52	7,430	0.0032
			100.9	3.6	0.82	10,180	0.0037
			105.5	14.0	21.4	11,130	0.023[c]
Solid sphere II	1.80	228	42.6	3.7	0.05	1,815	0.0020
			71.7	3.7	0.18	5,140	0.0020
			100.4	3.7	0.23	10,080	0.0014
			130.8	3.7	0.35	17,100	0.0013
			140.9	3.7	0.39	19,850	0.0012
			162.2	3.7	0.58	26,310	0.0014
			48.7	7.5	0.11	2,372	0.0014
			125.7	7.5	0.92	15,800	0.0018
Solid sphere II	1.15	272	101.4	9.9	0.18	10,280	0.0005
			147	9.9	0.49	21,600	0.0006
			189	9.9	0.89	35,720	0.00066
Hollow sphere III	2.21	190	71	7.8	2.47	5,040	0.012
			111.5	7.8	7.4	12,430	0.014
			134.4	16.6	22.0	18,060	0.014[c]
	2.20	190	50.7	8.4	0.05	2,570	0.001
			101.4	8.4	1.30	10,280	0.003
			121.6	8.4	9.8	14,970	0.015
			131.3	8.4	13.1	17,240	0.017
			136.4	18.1	28.3	18,605	0.016[c]
			141.5	37	48.3	20,020	0.012[c]
			147	50[b]	64.2	21,610	0.011[c]

[a] See reference 6.
[b] Estimated.
[c] Points for the intermediate region.

The production of "frozen in" moment with solid spherical specimens was probably due to imperfections or impurities and was comparatively small. The chief factor in producing moment with hollow spheres was apparently the geometry of the specimens. In the latter cases, the specimens would remain partially in the intermediate state after demagnetization regardless of the perfection of the sample.

Magnetic fields sufficient to put the mass of the body into the intermediate state produced marked increases in the fixed magnetic moment as observed with the torsion pendulum. This result indicated that magnetic induction could be "trapped" in a particular direction for considerable periods of time and afforded additional confirmation of the view that regions of normal metal in the intermediate state have diameters quite small in comparison with their lengths.

Hysteresis and relaxation effects in the transition from the superconducting to the intermediate state have been examined in detail.

We wish to thank Mr. L. E. Davis and Mr. D. E. Williams for assistance in the measurements, and Mr. R. E. Probst for aid in the entire program.

Letters to the Editor

PUBLICATION of brief reports of important discoveries in physics may be secured by addressing them to this department. The closing date for this department is five weeks prior to the date of issue. No proof will be sent to the authors. The Board of Editors does not hold itself responsible for the opinions expressed by the correspondents. Communications should not exceed 600 words in length.

Production of a π^+ Meson Beam Using the Deflected Proton Beam of the 184-Inch Synchro-Cyclotron*

C. RICHMAN, M. SKINNER,† J. MERRITT, AND B. YOUTZ
Radiation Laboratory and Department of Physics, University of California, Berkeley, California
October 13, 1950

SOME progress has been made toward the production of an approximately monochromatic meson beam with the 340-Mev protons from the Berkeley 184-inch synchro-cyclotron.

Owing to the large peak at about 70 Mev in the spectrum of π^+ mesons produced at 0° by protons on protons,[1] hydrogen is peculiarly suited for use in a meson production target. Many more mesons are produced per *nucleon* in an 8- or 10-Mev interval from hydrogen than from any other material that has been studied.[2]

A convenient target, rich in hydrogen and easy to handle, is polyethylene $(CH_2)_n$. Because of the hydrogen, the production from CH_2 for a thin target is strongly peaked[3] at about 69 Mev. (See curve I, Fig. 1.) A 5-cm thick piece of CH_2 was used as a meson production target. One would expect that such a thick target would broaden the peak considerably. This, however, is not the case. With a 5-cm CH_2 target, a 69-Mev meson created at the front of the target by a 340-Mev proton loses 15 Mev in the target and emerges with 54 Mev, whereas at the back of the target the protons have an energy of 323 Mev and produce mesons with a peak energy of 54 Mev.

The experimental arrangement was designed with a meson scattering experiment in mind. For this purpose it was desirable to use the external proton beam of the 184-inch cyclotron. This beam emerges from a 2-inch diameter collimator and has at present a maximum intensity of about 6×10^{-10} amp.

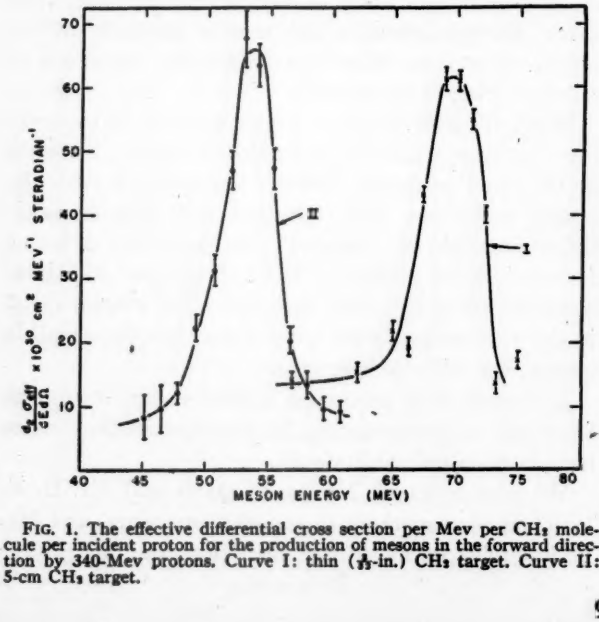

FIG. 1. The effective differential cross section per Mev per CH_2 molecule per incident proton for the production of mesons in the forward direction by 340-Mev protons. Curve I: thin ($\frac{1}{32}$-in.) CH_2 target. Curve II: 5-cm CH_2 target.

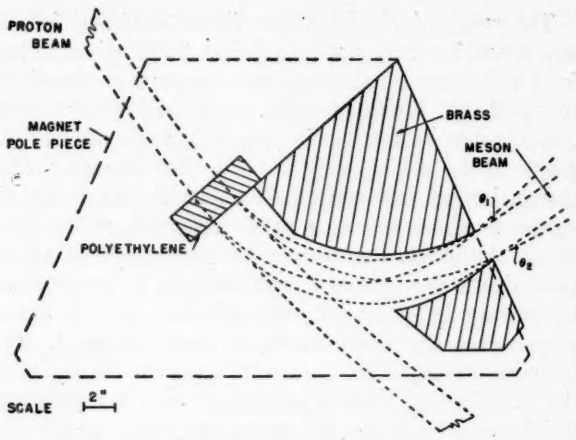

FIG. 2. Arrangement of the apparatus in the magnetic field.

Since the mesons come off from the CH_2 target predominantly in the forward direction, they must be separated from the proton beam. This is achieved with a magnetic field of 14,300 gauss across a gap of 3.4 inches, which gives a 54-Mev meson and a 340-Mev proton radii of curvature of 12.4 inches and 80 inches, respectively.

In order to collimate the meson beam, and also to eliminate all particles other than mesons in the desired energy interval, a channel for the mesons was cut in the brass shielding (Fig. 2). The channel accepts mesons with energies between 48 and 60 Mev. A 54-Mev meson produced at 0° in the center of the target is turned through 85° before emerging from the center of the channel. The exit area of the channel is 2 inches wide by 2.5 inches high, subtending a solid angle of about 2.2×10^{-2} steradian at the CH_2 target. With this arrangement the meson beam collimation was such that $\theta_1\simeq\theta_2\simeq9°$.

The meson energy spectrum was measured by means of nuclear emulsions embedded in absorbers.[2] Curve II of Fig. 1 shows the spectrum of the mesons leaving the 5-cm CH_2 target in the forward direction. To obtain this curve, the meson density in the emulsions was corrected for (a) the loss of about 9 percent of the mesons due to decay in flight and (b) the loss of about 16 percent of the mesons due to nuclear scattering and absorption in the aluminum absorber holding the emulsions, assuming nuclear area for the total nuclear cross section. The errors indicated are probable errors due to the statistics.

The peak of the spectrum occurs at 53.5 Mev, and the half-width of the peak is 5 Mev. Comparison of the thin and thick target spectra shows that a thick target does not indeed spread the peak.

Integrating curve II of Fig. 1 over the 12-Mev meson energy interval from 48 to 60 Mev, one obtains 4.0×10^{-28} cm² per steradian per CH_2 molecule per incident proton. This is the effective differential cross section for the production of mesons from a thick CH_2 target. The thin target spectrum integrated from 62 to 74 Mev gives 4.4×10^{-28} cm² per steradian. Apparently, the excitation does not fall off rapidly over the proton energy interval from 340 to 323 Mev.

With a proton beam of 5×10^{-10} amp. there are about 5000 mesons per second with energies between 48 and 60 Mev issuing from the channel.

It is a pleasure to acknowledge the encouragement we have received from Professor R. L. Thornton. We would also like to think Mr. J. Vale and the cyclotron crew for making the bombardments.

* This work was performed under the auspices of the AEC.
† AEC Postdoctoral Fellow.
[1] Cartwright, Richman, Whitehead, and Wilcox, Phys. Rev. 78, 823 (1950). V. Z. Peterson, Phys. Rev. 79, 407 (1950).
[2] C. Richman and H. A. Wilcox, Phys. Rev. 78, 496 (1950). M. Weissbluth, Ph.D. thesis, University of California (1950) (UCRL-568).
[3] Cartwright, Richman, Whitehead, and Wilcox (to be published).

A Geometrical Model for the Unified Theory of Physical Fields*

J. I. HORVÁTH
Department of Theoretical Physics, University of Debrecen, Debrecen, Hungary
July 20, 1950

IT is possible to give a unified field theory based on the generalized geometry introduced by Finsler.[1] Finsler's geometry, as is well known,[2] is a generalization of Riemann's and can be regarded as a manifold of line elements in the space of which the metric is defined by

$$ds = L(x^i, \dot{x}^i)dt \tag{1}$$

where x^i represents a point of the n-dimensional space and $\dot{x}^i$ will be in our case the derivative of x^i with respect to the arc length of the curve $x^i = x^i(t)$. The space has a general covariant formalism, which also is a direct generalization of Riemann's. As a consequence of (1), the metrical ground tensor, being a symmetric covariant tensor of the second order is

$$g_{ik} = g_{ik}(x^i, \dot{x}^i) = \tfrac{1}{2}\partial^2(L^2)/\partial\dot{x}^i\partial\dot{x}^k \tag{2}$$

and the parallel displacement of a covariant vector ξ_i is defined by

$$d\xi_i = C_i{}^r{}_s\,\xi_r d\dot{x}^s + \Gamma_i{}^r{}_s\,\xi_r dx^s \tag{3}$$

where the coefficients of the affine connection $C_i{}^r{}_s$ and $\Gamma_i{}^r{}_s$ are deducible from $L(x^i, \dot{x}^i)$ as follows

$$\begin{aligned}
&C_i{}^k{}_j = g^{kr}C_{irj},\\
&C_{ikj} = \frac{1}{2}\frac{\partial g_{ik}}{\partial \dot{x}^j} = \frac{1}{4}\frac{\partial^3(L^2)}{\partial\dot{x}^i\partial\dot{x}^k\partial\dot{x}^j},\\
&\Gamma_i{}^k{}_j = g^{kr}\Gamma_{irj},\\
&\Gamma_{ijk} = \frac{1}{2}\left\{\frac{\partial g_{ij}}{\partial x^k} + \frac{\partial g_{jk}}{\partial x^i} - \frac{\partial g_{ik}}{\partial x^j}\right\} + C_{ikr}\frac{\partial G^r}{\partial \dot{x}^j} - C_{jkr}\frac{\partial G^r}{\partial \dot{x}^i},\\
&G^r = G_i g^{ir},\\
&G_i = \frac{1}{4}\left\{\frac{\partial^3(L^2)}{\partial\dot{x}^i\partial x^r}\dot{x}^r - \frac{\partial(L^2)}{\partial x^i}\right\},\\
&\Gamma^*{}_i{}^r{}_k = \Gamma_i{}^r{}_k - C_i{}^r{}_s\,\Gamma_k{}^s{}_h\,\dot{x}^h.
\end{aligned} \tag{4}$$

The space is characterized by its curvature and torsion. It is usual to introduce the totally symmetric covariant tensor of the third order

$$A_{ikh} = L(x^i, \dot{x}^i)\cdot C_{ikh} \tag{5}$$

which determines the deviation of Finsler's space from Riemann's, which arises from the original space by discarding the dependence of the g_{ik} on the $\dot{x}^i$ (this is equivalent to $A_{ikh} \equiv 0$). The curvature and torsion are given by the tensors

$$\begin{aligned}
R^k{}_{ihj} = {}&\frac{\partial\Gamma^*{}_i{}^k{}_h}{\partial x^j} - \frac{\partial\Gamma^*{}_i{}^k{}_h}{\partial\dot{x}^s}\frac{\partial G^s}{\partial\dot{x}^j} - \left\{\frac{\partial\Gamma^*{}_i{}^k{}_j}{\partial x^h} - \frac{\partial\Gamma^*{}_i{}^k{}_j}{\partial\dot{x}^s}\frac{\partial G^s}{\partial\dot{x}^h}\right\}_i\\
&+\Gamma^*{}_i{}^s{}_h\cdot\Gamma^*{}_s{}^k{}_j - \Gamma^*{}_i{}^s{}_j\cdot\Gamma^*{}_s{}^k{}_h,
\end{aligned} \tag{6}$$

$$P_{ijkh} = \Gamma^*{}_j{}^r{}_k\cdot A_{ihr} - \Gamma^*{}_i{}^r{}_k\cdot A_{jhr} - L\cdot\frac{\partial C_{ijh}}{\partial x^k} + L\cdot\frac{\partial\Gamma_{ijk}}{\partial\dot{x}^h},$$

$$S_{ijkh} = A_j{}^r{}_k\cdot A_{ihr} - A_j{}^r{}_h\cdot A_{ikr}.$$

We now suppose that, in accordance with Einstein's original idea, the curvature of the space is determined by the distribution of the matter localized in the space and the deviation from Riemann's geometry; as an example, the torsion of the space originates from the electromagnetic, or generally from the meson field.

To realize this assumption we give the connection between the structure of the Finsler space and the electromagnetic (meson) field. We characterize the field by its symmetrized stress-energy tensory S_{ik}, and from this we deduce the following total symmetric covariant tensor of the third order

$$A_{ikh} = -\tfrac{1}{2}\cdot\{S_{ik|h} + S_{hi|k} + S_{hk|i}\} \tag{7}$$

(where $S_{ik|h}$ is the covariant derivative of S_{ik}) which we shall regard as the torsion tensor of Finsler's geometry.

Assumption (7) has also a physical meaning ,and it is easy to see that it can be considered as a generalization of the Lorentz force. To justify this remark we deduce from (7), by contraction of the indices k and h, the following covariant vector

$$A_i = A_i{}^k{}_k = g^{kr}\cdot A_{irk} = -\partial S_i{}^k/\partial x^k, \tag{8}$$

which is just the density of the Lorentz force of the field.

Mathematically (7) gives in the case of the four-dimensional space-time continuum 20 independent partial differential equations for the determination of the dependence of L (or g_{ik}) on the $\dot{x}^i$.

For the determination of the dependence on the x^i we have also Einstein's original equations

$$R_{ik} - \tfrac{1}{2}g_{ik}R = \kappa T_{ik} \tag{9}$$

but now R_{ik} and R are deduced from (6) by the well-known method. T_{ik} is as usual the energy-momentum tensor of the matter. Equation (9) gives also the further 10 partial differential equations for the determination of the dependence of the g_{ik} on the x^i.

Finally, we must pay attention to the fact that the proposed connection between the field theories and the geometrical basis is not only a formal one. We have mentioned that Finsler's space can be regarded as a manifold of line elements defined along curves of the space. If we regard such a curve as the world-line of a particle (electron, nucleon, etc.) by which the field is originated, the line elements have also a direct physical meaning since the unit vector

$$l^i = \dot{x}^i/L \tag{10}$$

deduced from $\dot{x}^i$, can be regarded as the velocity of the particle along the world-line. It is well known that the field of such a moving particle has a strong inhomogeneity. Now this inhomogeneity is faithfully expressed by Finsler's geometry. In cases in which the inhomogeneity would be dissolved (e.g., the static case) every component of A_{ikh} vanishes, as can be verified by elementary calculations, taking account of some of the methods of Finsler's geometry and the usual relations of homogeneous functions. Thus we are not led by our method away from the Riemann space. This theory is also interesting especially in the non-static case, which will be discussed in detail in the near future.

* Extract of the author's habilitation lecture.

[1] P. Finsler, Über Kurven und Flächen in allgemeinen Räumen, Diss., Göttingen, 1918.
[2] E. Cartan, Les espaces de Finsler, Act. scient. et ind. 79 (Hermann et Cie, Paris, 1934); O. Varga, Monat. f. Math. und Phys. Leipzig und Wien 50, 165 (1941); Comm. Math. Helv. 19, 367 (1947).

The Diamagnetic Correction for Protons in Water and Mineral Oil

H. A. THOMAS
National Bureau of Standards, Washington, D. C.
October 16, 1950

THE proton nuclear resonance shifts between H_2 gas and water, mineral oil, and the standard sample used in the determination of the proton gyromagnetic ratio[1] have been measured as previously suggested.[1,2] The shifts were measured in a large electromagnet having a 4½-inch gap with pole faces 24 inches across and regulated[3] by means of nuclear resonance. The spatial field variation over a region somewhat larger than that occupied by the sample was of the order of 10 p.p.m. and produced a line width for the distilled water sample of 0.043 gauss.

The three samples were contained in identical spherical Pyrex glass vessels, 1.4-cm i.d. and 2.0-cm o.d. The hydrogen sample was tank hydrogen at a pressure of 40 atmospheres. The distilled water sample was free of dissolved oxygen and the oil sample was Petrolatum U.S.P.-Light.

The resonance shifts between samples were measured relative to a fixed sample and resonance detector probe by means of calibrated Helmholtz coils. Because it is known that slight unpredictable changes in field distribution with time might occur, a

means was provided for rapidly interchanging and accurately positioning the samples in another resonance detector located close to the reference resonance probe.

The tuned r-f coil of the measuring probe was coupled through a high impedance to a low noise 24-Mc crystal oscillator also supplying the reference probe. The r-f voltage across this coil was detected by a high vacuum diode and the resulting audio output fed into a 30 cycle-sec. lock-in amplifier. The diode method of detection was used to eliminate the effect of the dispersion component of the signal, so that the true center of resonance could be obtained. Even with the H_2 gas, which gives a weak signal, the signal-to-noise ratio was sufficient to obtain a consistency of measurement that resulted in an average deviation of 1 part in four million over 10 determinations of the H_2 gas$\rightarrow H_2O$ shift. This average deviation was somewhat greater than in the determination of the other shifts measured.

It is assumed that the time average of the field seen by a particular molecule in the sample is that which would be computed if it were in a spherical cavity surrounded by a diamagnetic medium of volume susceptibility χ. Hence the time average value of the local field is decreased by the fraction $4\pi\chi/3$. But, since the sample itself is spherical and is located in a medium of zero susceptibility, an increase in the field of $4\pi\chi/3$ is produced which causes the net correction to the local field to be zero, at least in the first order of χ.

The actual shifts from H_2 gas for oil and water are respectively: $\Delta H/H=+1.6\times10^{-6}$; and $\Delta H/H=-0.6\times10^{-6}$. Combining these shifts with the diamagnetic correction for H_2 gas calculated[2] by Ramsey, the diamagnetic corrections for mineral oil and water are, respectively, $\delta_{oil}=28.4\times10^{-6}$, and $\delta H_2O=26.2\times10^{-6}$.

The comparison of the standard sample used in the determination of the proton gyromagnetic ratio with the H_2 gas indicates that a diamagnetic correction of 28.1×10^{-6} should be made on the uncorrected value of γ reported[1] earlier. This makes the present corrected value $\gamma=(2.67530_5\pm0.00006)\times10^4$ sec.$^{-1}$ gauss^{-1} and the previously reported[1] value $e/m=(1.75891_2\pm0.00005)\times10^7$ e.m.u. gram^{-1}.

The valuable discussions and interest of R. D. Huntoon, U. Fano, E. M. Purcell, H. Sommer, and R. Driscoll are gratefully acknowledged; and in particular I wish to thank H. Sommer for his assistance in making some of the measurements.

[1] Thomas, Driscoll, and Hipple, Phys. Rev. 78, 787 (1950).
[2] N. F. Ramsey, Phys. Rev. 78, 699 (1950).
[3] H. A. Thomas, Phys. Rev. 78, 339 (1950).

Spectrum of the Boron Monosulfide (BS) Molecule

P. B. ZEEMAN*
Merensky Institute for Physics, University of Stellenbosch, South Africa
October 16, 1950

THE spectrum of the boron monoxide (BO) molecule has been analyzed by Mulliken[1] and Jenkins and McKellar,[2] but the analogous spectrum of boron monosulfide has not yet been described. Recently, however, the writer has observed three extensive band systems in an electric discharge through boron trisulfide and has attributed these bands to the BS molecule.

The apparatus consisted of a vacuum system of Pyrex glass, and a quartz discharge tube of the end-on type. Through this tube helium or argon was circulated at low pressure by means of a mercury diffusion pump. A quartz tube, having a glass stopper at one end, contained amorphous boron in a silica boat, and projected horizontally from the one end of the capillary of the discharge tube. A reservoir containing vacuum distilled sulfur protruded vertically downwards from the center of this tube. By means of a cylindrical electrical heater, the amorphous boron could be heated to the desired temperature, while the amount of sulfur vapor entering the system could be controlled separately. The sulfur vapor was carried over the heated boron by the circulating helium or argon gas.

At about 700°C, boron trisulfide (B_2S_3) was formed, and this substance was carried into the capillary of the discharge tube. When this reaction started, the brilliant S_2 spectrum, excited in the capillary at the early stages of the heating process, disappeared and was superseded by a very intense spectrum resembling a "daylight" fluorescent lamp.

The following three strong band systems were observed in the discharge:

(a) An extensive system of open bands in the visible, red, and infra-red regions of the spectrum, degraded to the red. This system will be referred to as the α-system of BS.

(b) A strong system, consisting mainly of two band groups, each with several heads. This system which is degraded to the violet, has a very close fine structure.

(c) A system of double double-headed bands in the ultraviolet region, degraded to the red. This system also has a close fine structure and will be referred to as the γ-system of BS.

The bands of the α- and γ-systems have been arranged in Deslandres Tables. The band heads were measured on plates taken on a large Hilger spectrograph and in the first order of a 21-foot concave grating in a Paschen mounting.

The bands of the α-system originate from a $^2\Pi\rightarrow{}^2\Sigma$ transition, and the rotational analysis showed that the Π-state is inverted. This is analogous to the α-system of BO. These band heads are given by the following equations:

$$^2\Pi_{3/2}\rightarrow{}^2\Sigma:\ \nu_{\text{head}}=\begin{matrix}15663.0\\15668.4\end{matrix}\Big\}+[749.37v'-4.77v'^2]-[1173.93v''-6.37v''^2],$$

$$^2\Pi_{1/2}\rightarrow{}^2\Sigma:\ \nu_{\text{head}}=\begin{matrix}15996.7\\16002.1\end{matrix}\Big\}+[749.37v'-4.77v'^2]-[1173.93v''-6.37v''^2].$$

The ultraviolet bands originate from a $^2\Pi\rightarrow{}^2\Sigma$ transition, with a normal splitting of the Π-state. These band heads are given by the following equations:

$$^2\Pi_{1/2}\rightarrow{}^2\Sigma:\ \nu_{\text{head}}=\begin{matrix}38785\\38796\end{matrix}\Big\}+[884.7v'-6.60v'^2]-[1173.3v''-6.40v''^2],$$

$$^2\Pi_{3/2}\rightarrow{}^2\Sigma:\ \nu_{\text{head}}=\begin{matrix}38899\\38912\end{matrix}\Big\}+[884.7v'-6.60v'^2]-[1173.3v''-6.40v''^2].$$

The $^2\Pi_{3/2}\rightarrow{}^2\Sigma$ components of the (2,1), (3,0), (4,0), and (5,0) bands of the α-system have been analyzed from plates taken in the third order of the grating. The following constants were obtained:

$$B_e''=0.7949_0\ \text{cm}^{-1},\quad \alpha_e''=0.0060_5\ \text{cm}^{-1}.$$
$$B'_{e,eff}{}^{(1)}=0.6213_1,\quad \alpha'_{e,eff}{}^{(1)}=0.0058_8\ \text{cm}^{-1}.$$

Preliminary analyses of the (0,0) and (0,1) bands of the γ-system have been made from plates taken in the sixth order of the grating. The following tentative values were obtained:

$$B_e''=0.793\ \text{cm}^{-1},\quad \alpha_e''=0.006\ \text{cm}^{-1}.$$
$$B_0'=0.702\ \text{cm}^{-1}.$$

The vibrational and rotational analyses prove that the α- and γ-systems have the same lower state ($^2\Sigma$).

The bands of the blue-green system have not yet been interpreted.

A paper giving further details of these band systems is being prepared at present and will be published in the course of time.

The writer wishes to express his thanks to the South African Council for Scientific and Industrial Research for a grant in aid of the work done. The writer also wishes to thank Dr. G. Herzberg for suggesting the subject of the research.

* Now at the Spectroscopy Section of the Canadian National Research Council, Ottawa, Canada.
[1] R. S. Mulliken, Phys. Rev. 25, 259 (1925).
[2] F. A. Jenkins and A. McKellar, Phys. Rev. 42, 464 (1932).

The Slow Neutron Resonant Scattering of Gold*

J. TITTMAN, C. SHEER, J. RAINWATER, AND W. W. HAVENS, JR.
Pupin Physics Laboratories, Columbia University, New York, New York
October 5, 1950

ALTHOUGH much information has been accumulated concerning slow neutron resonances, relatively little experimental evidence is available concerning the detailed energy dependence of the scattering cross section near a resonance.

Using the apparatus described previously,[1] in conjunction with the Columbia slow neutron velocity spectrometer,[2] the 4.87-ev Au resonance[3] has been investigated with results in excellent agreement with theory, and the level parameters have been evaluated.

TABLE I. Level widths and neutron cross sections in gold.

	Γ_{NO}	Γ	σ_{P2}	σ_{P1}
$J_1=1$	(0.0211 ± 0.002)	(0.172 ± 0.010)	(10.6 ± 0.6)	(13.3 ± 1.3)
$J_1=2$	(0.0163 ± 0.0015)	(0.133 ± 0.010)	(17.6 ± 0.9)	(8.0 ± 1.4)

If a sample is thick enough to give very small transmission and if the ratio of the scattering to total cross sections, (σ_s/σ_t), is less than about 0.5, in which case the diffusion length is less than the sample thickness, then the ratio of the sample counting rate to that of a reference thick graphite sample, (N_x/N_C), is independent of sample thickness and depends only on the ratio (σ_s/σ_t). A calibration curve for (N_x/N_C) *vs.* (σ_s/σ_t) was obtained, for our geometry, using thick B_2O_3 and Ni_2B standards. The scattering and $1/v$ terms for the standards were determined by transmission measurements to give $(\sigma_s/\sigma_t)_{B_2O_3}=(1+10.4E^{-\frac{1}{2}})^{-1}$ and $(\sigma_s/\sigma_t)_{Ni_2B}=(1+3.31E^{-\frac{1}{2}})^{-1}$.

Using this calibration, the ratio (σ_s/σ_t) was measured for a thick gold sample in the vicinity of the resonance, and compared with theoretical curves based on the Breit-Wigner one-level formulas of the form[4]

$$[\sigma_c=\sigma_{co}\Gamma^2(E_0/E)^{\frac{1}{2}}]/[4(E-E_0)^2+\Gamma^2] \quad (1)$$

$$\sigma_s=(G_2\sigma_{P2})+4\pi G_1\{R_1^2+[\lambda_0^2\Gamma_{NO}^2+4\lambda_0\Gamma_{NO}R_1(E-E_0)]/[4(E-E_0)^2+\Gamma^2]\} \quad (2)$$

$$\sigma_{co}=4\pi\lambda_0^2G_1\Gamma_{NO}\Gamma_Y/\Gamma^2. \quad (3)$$

Gold has one stable isotope of spin $\frac{3}{2}$, so $J_1=1$ or 2 and $G_1=\frac{3}{8}$ or $\frac{5}{8}$ for the "resonant spin state," and $G_2=\frac{1}{4}$ or $\frac{3}{4}$ for the "non-resonant spin state." The first term on the right in Eq. (2) is the constant (potential) scattering of the "non-resonant spin state." The second term gives the potential, resonance, and interference terms in the scattering for the "resonant spin state." The symbols have their usual significance.

The value $\sigma_{co}\Gamma^2=(638\pm17)$ barn-ev[2] in Eq. (1) was determined by a least squares fit to σ_t (from transmission measurements) in the thermal energy region. With $\sigma_{co}\Gamma^2$ fixed, only Γ_{NO}/Γ, $(G_2\sigma_{P2})$, R_1, and J_1 remain as undetermined parameters. Near 2 to 3 ev the scattering is nearly zero for the resonant spin state, so (σ_s/σ_t) determines $(G_2\sigma_{P2})=(6.6\pm0.33)$ barns. For a given choice of $\sigma_{co}\Gamma^2$ and the *total potential* scattering, almost identical curves for (σ_s/σ_t) result for $J_1=1$ and $J_1=2$, when suitable related choices are made for (Γ_{NO}/Γ) in the two cases, so further evidence is needed to determine J_1. When J_1, $\sigma_{co}\Gamma^2$, and $G_2\sigma_{P2}$ are given, (σ_s/σ_t) is mainly sensitive to (Γ_{NO}/Γ) near resonance, and to R_1 far from resonance on either side. Thus, both of these parameters can be evaluated by comparison with experiment to give Table I.

The values of σ_{P2} and other results[5] indicate strongly that $J_1=1$. A detailed report of this work will be published shortly.

* We express appreciation to the AEC for support of this work.
[1] Tittman, Sheer, Rainwater, and Havens, Phys. Rev. 77, 748 (1950).
[2] J. Rainwater and W. W. Havens, Jr., Phys. Rev. 70, 136 (1946); Rainwater, Havens, Wu, and Dunning, Phys. Rev. 71, 65 (1947).
[3] Energy value by J. Rainwater and W. W. Havens, Jr., unpublished.
[4] H. A. Bethe, Rev. Mod. Phys. 9, 69 (1937).
[5] J. Tittman and T. Sheer, unpublished Au resonance transmission data; Groendijk, Thesis, Groningen (1949); O. Frisch, Kgl. Danske Videnskab. Selskab. Mat.-fys. Medd. 14, No. 12 (1937).

Screening of Electronic Interactions in a Metal

DAVID BOHM AND DAVID PINES*
Palmer Physical Laboratory, Princeton University, Princeton, New Jersey
October 16, 1950

IN recent publications,[1,2] Landsberg and Wohlfarth have shown that the assumption of a screened Coulomb interaction between electrons in a metal eliminates certain difficulties arising from the treatment of the effects of the exchange energy according to the free particle approximation. With the free particle approximation, the exchange contribution to the Coulomb interaction energy of two electrons of wave vectors $\mathbf{k}_1$ and $\mathbf{k}_2$ is $W_{1,2}=-2\pi e^2/L^3|\mathbf{k}_1-\mathbf{k}_2|^2$, where $\mathbf{k}=\mathbf{p}/\hbar$ and $\mathbf{p}$ is the electronic momentum. For a given electron, the total energy of interaction with all the other electrons is

$$W_i=\sum_{j\neq i}W_{i,j}=-\frac{e^2k_0}{2\pi}\left(2+\frac{k_0^2-k^2}{k_0k}\ln\left|\frac{k+k_0}{k-k_0}\right|\right),$$

where k_0 is the absolute value of the wave vector of an electron at the top of the Fermi distribution, and all of the levels are assumed to be occupied up to k_0. Since the *E versus k* curve for a given electron becomes very steep as k approaches k_0, at low temperatures the density-in-energy of electron levels is correspondingly reduced. Bardeen[3] has shown that for this reason the specific heat of the electron gas should vary as $-\ln T/T$, in contrast to the linear dependence on T obtained when the exchange energy is ignored. Experiments indicate that a linear dependence is correct and therefore that calculations based on perturbation theory overestimate the effects of exchange energy. This overestimate is found also to lead to incorrect predictions at low temperatures for conductivity and diamagnetism, and for the soft x-ray spectrum. In fact, Landsberg proposed the screened Coulomb interaction on a purely empirical basis in order to obtain agreement with experiment for the width of the tail of the soft x-ray emission spectrum of sodium.

Simple mathematical analysis makes clear the fact that the increased steepness of the *E versus k* curve originates in the long range of the Coulomb interaction, which, as we have seen, leads to a very large exchange energy for electrons of nearly equal momenta. If, with Landsberg, one assumes the Coulomb force to be screened, then one will no longer obtain so large a modification of the *E versus k* curve. Wohlfarth showed that a linear dependence of the specific heat on temperature is regained, and that agreement with experiment is obtained with a potential $V=(e^2/r_{ij})\times\exp(-r_{ij}/\lambda)$ when the screening radius λ is chosen to be of the order of 10^{-8} cm, the value introduced by Landsberg.

We have been led independently to the concept of an effective screened Coulomb force as a result of a systematic classical and quantum-mechanical investigation of the interaction of charges in an electron gas of high density. We have treated this problem with the aid of certain canonical transformations, which make possible a solution which is much more accurate than the perturbation theory solutions on which previous calculations have been based.[4] Our results show that the Hamiltonian for a system containing a high density of electrons can be split into two parts

in a natural way. The first part corresponds to organized oscillations of the medium as a whole. These are the so-called plasma oscillations, which resemble sound waves and represent the long-range correlations brought about by the Coulomb force. At low temperatures, these oscillations are so weakly excited that they make a negligible contribution to the specific heat. The remainder of the Hamiltonian then reduces to a screened Coulomb interaction, since the long-range part of the interaction has been effectively included in the oscillations of the medium as a whole. The screening radius is found to be $\lambda \cong v_0/\omega_p = (\hbar k_0/m)(m/4\pi n_0 e^2)^{\frac{1}{2}}$ where v_0 is the velocity of an electron at the top of the Fermi distribution, $\omega_p = (4\pi n_0 e^2/m)^{\frac{1}{2}}$ is the "plasma frequency," and n_0 is the electron density. For sodium, $k_0 \cong 0.9 \times 10^8$ cm, and $\lambda \cong 10^{-8}$ cm, in agreement with the screening radius adopted empirically by Landsberg and Wohlfarth.

A more detailed report of this work is being prepared for publication.

* Now at Randal Morgan Laboratory of Physics, University of Pennsylvania, Philadelphia, Pennsylvania.
[1] P. T. Landsberg, Proc. Phys. Soc. London A **162**, 49 (1949).
[2] E. P. Wohlfarth, Phil. Mag. **41**, 534 (1950).
[3] J. Bardeen, Phys. Rev. **50**, 1098 (1936).
[4] D. Pines and D. Bohm, Phys. Rev. **79**, 232 (1950).

Neutron Yield from $Be^9(\gamma,n)Be^8$ Reaction*

G. J. Hine† and F. E. Senftle‡
Departments of Electrical Engineering and Metallurgy, Massachusetts Institute of Technology, Cambridge, Massachusetts
October 16, 1950

ALTHOUGH the $Be^9(\gamma,n)Be^8$ reaction is one of the most commonly employed neutron sources, only a small amount of information is available concerning the obtainable neutron flux under various conditions. In the experiments reported here, the thickness of the beryllium target necessary to yield the maximum slow neutron flux was determined.

With a 200-gram powdered beryllium target and a Van de Graaff generator as an x-ray source, Wiedenbeck[1] compared the neutron yield directly with that of a Ra-Be source. He obtained a yield equivalent to 10^3 curies of radium with an electron accelerator potential of 3.2 Mev and a beam current of 100 μamp.

The present measurements have also been made with a Van de Graaff accelerator, but at a potential of 2.5 Mev and a 100 μamp. electron current. The beryllium target consisted of solid square pieces of beryllium (9×9 cm) of various thicknesses. These were placed about 3 mm from the x-ray exit window. Directly beneath the last beryllium block a stack of large thin paraffin plates (35 cm in diameter) were mounted. Copper and indium foils were placed (with and without cadmium covers) at different depths between the paraffin plates, and on the axis of the x-ray beam. Their induced activity was taken as a measure of the slow neutron flux. The highest activity was observed with about 2 cm of paraffin between the beryllium target and the detector foil. When the beryllium target was also surrounded by paraffin, the slow neutron flux at points below the target increased only slightly.

Under the above conditions and with a 4 cm thick beryllium target, the slow neutron flux was observed to reach a maximum density of about 10^7 neutrons/cm^2/sec., while at thicknesses of 2 and 7 cm, the flux is only 85 percent of the maximum value. The neutron production increases in proportion to the amount of beryllium penetrated by the x-rays. Therefore, the activity of the foils decreased as the thickness of the beryllium target was reduced below 4 cm. However, with a beryllium target more than 4 cm thick, the activity of the foils also decreased because of the effect of the inverse square law. With increasing target thickness fewer neutrons reach the detector foils beneath it, regardless of the fact that the total neutron production increases. A reduction of the target dimensions from 9×9 to 5×5 cm reduces the flux by a factor of three. As a result of the predominantly forward direction of the x-ray beam, an increase in target diameter beyond 9 cm had little effect on the neutron flux.

Measurements with a BF_3 counter placed five feet from the beryllium target in a plane perpendicular to the x-ray beam showed an increase of the neutron flux with target thickness up to 15 cm. At greater thicknesses, a steady value of the neutron flux was obtained. Although neutrons from any point of the target have about equal probability of reaching the counter, the attenuation and divergence of the x-ray beam limits the increase of the total neutron emission with increasing amount of target material.

* This work was supported in part by the AEC.
† Special Research Fellow of the National Cancer Institute, Bethesda, Maryland.
‡ Research Associate, Department of Metallurgy, Massachusetts Institute of Technology.
[1] M. L. Wiedenbeck, Phys. Rev. **69**, 235 (1946).

Half-Life of Cu^{66}

A. G. W. Cameron and L. Katz
Department of Physics, University of Saskatchewan, Saskatoon, Saskatchewan, Canada
October 9, 1950

IN 1949 Silver[1] reported precision measurements of the decay periods of a number of isotopes using a differential ionization chamber with a vibrating reed condenser electrometer and feedback amplifier. The half-life of Cu^{66} was found to be 4.34 ± 0.03 minutes. We were unable to reconcile this value with an activity obtained in copper which had been exposed to photo-neutrons, and we have therefore made a careful measurement of this half-life.

Lead bricks were piled in front of the "22"-Mev betatron to absorb the gamma-ray beam and to provide a source of photo-neutrons. An electrolytically pure copper disk was placed at the center of a block of paraffin beside the lead bricks. After the lead had been irradiated for 11 minutes, the copper disk was counted with an end-window β-counter connected through scalers to a time-stamping machine. The decay curve shown in Fig. 1 is that

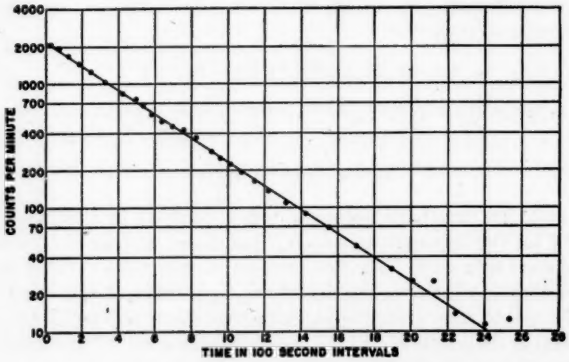

FIG. 1. Decay of Cu^{66}. The background of 34 counts/min. and a long-lived activity of 7 counts/min. have been subtracted.

obtained after subtraction of background of 34 counts/min. and a long-lived activity of 7 counts/min. (presumably 12.9 hour Cu^{64}).

A similar irradiation was made with a copper disk surrounded by cadmium. The initial activity of this disk was only 50 percent above background. This established that the activity of Fig. 1 resulted from the capture of slow neutrons by copper, and hence must arise from the reaction $Cu^{65}(n,\gamma)Cu^{66}$.

We therefore find the half-life of Cu^{66} to be 5.18 ± 0.10 minutes. This is in good agreement with the old value of 5 minutes measured by Amaldi *et al.*[2]

[1] L. M. Silver, Phys. Rev. **76**, 589 (1949).
[2] Amaldi, D'Agostino, Fermi, Pontecorvo, Rasetti, and Segrè, Proc. Roy. Soc. **A149**, 522 (1935).

Stars Induced by 350- to 400-Mev Protons*

G. Bernardini, E. T. Booth, and S. J. Lindenbaum
Columbia University, New York, New York
October 17, 1950

ILFORD G5 plates with emulsions 400 microns thick were exposed to the 385-Mev proton beam of the Nevis cyclotron. The exposures were made inside the vacuum chamber at maximum orbit radius. Very brief exposures with the ion source off, yielded about 2×10^5 proton tracks per cm² in the emulsion, and the average length of each track was greater than 10 mm. These tracks were parallel, on the average, to $\pm1°$.

Four hundred and four stars induced by the protons in the emulsion have been analyzed. The star prongs are classified as "gray" for grain densities less than three times minimum, "sparse black" for grain densities between three and six times minimum, and "black" for grain densities greater than six times minimum. These ranges correspond approximately to proton energies greater than 100 Mev, between 30 Mev and 100 Mev, and less than 30 Mev, respectively. In Fig. 1 is shown the distribution of the number of stars with various numbers of black plus sparse black prongs. In Fig. 2 is plotted the percentage of stars with at least one outgoing gray prong. The incoming proton tracks were observed in all cases but have not been counted in any of the prong statistics.

For 219 of the stars, the distribution of black, sparse black, and gray prongs are summarized in Table I.

The mean free path for the production of stars with one or more black prongs by 350- to 400-Mev protons has been determined by measuring by sampling, the total track length in the emulsion scanned, and dividing by the number (404) of stars found. In this way, a mean free path of 56 ± 9 cm was found. This corresponds to a nuclear cross section for the production of stars in G5 emulsion of 45 ± 6 percent of geometric, indicating considerable nuclear transparency.

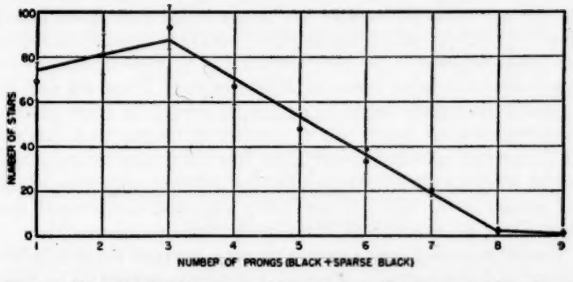

FIG. 1. The distribution curve for number of stars as a function of number of prongs (black+sparse black) with grain densities greater than three times minimum.

The angular distribution of prongs in the different energy ranges was determined for one hundred stars. The gray and sparse black prongs were peaked markedly in the forward direction with respect to the primary proton. The mean angle for these prongs was about 30°. The black prong angular distribution can be interpreted as consisting of $\frac{2}{3}$ isotropic prongs and $\frac{1}{3}$ projected in the forward 90°.

The Wouthuysen[1]-Goldberger[2] model for the interaction of nucleons with the nucleus predicts considerable transparency and the immediate ejection of sharply projected fast nucleons and some slower less collimated knockons before the evaporation process. All of these features are in agreement with our results.

TABLE I. Properties of 219 stars as a function of the number of black (grain density greater than 6 minimum) prongs.

No. of black prongs	0	1	2	3	4	5	6	7	8	9
No. of stars	6	47	47	48	34	23	10	3	0	1
No. of stars with gray prongs	5	30	20	20	10	5	3	0	0	0
No. of stars with a gray or sparse black prong	6	35	31	32	20	13	3	0	0	0

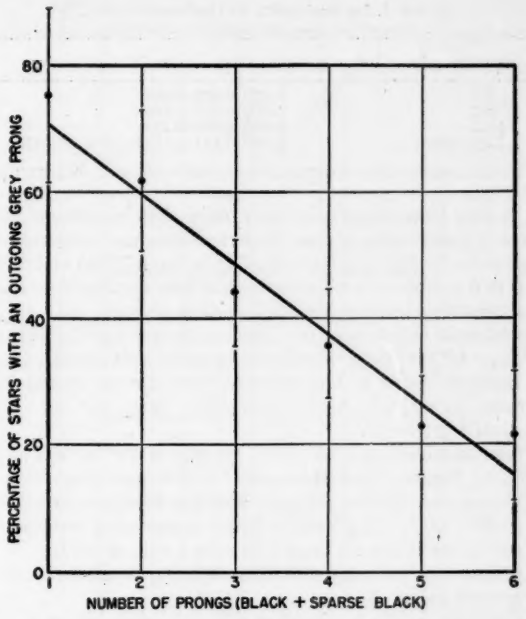

FIG. 2. The percentage of stars with an outgoing gray prong as a function of the number of prongs (black+sparse black) with grain densities greater than three times minimum.

Figure 2 shows that as the number of black prongs increases, the percentage of stars with gray prongs decreases, gray prongs were not observed in stars having more than six black prongs. This is interpreted to mean that for the 7-, 8-, or 9-prong stars most of the primary proton energy was absorbed by the nucleus. In these cases, the average energy associated with a black prong is 50 Mev, in approximate agreement with values measured in stars produced by cosmic rays.[3]

Reference to Table I shows that for stars between 2 and 5 (inclusive) black prongs, the percentage of stars which have a gray or sparse black prong is approximately constant and equal to 60 percent. Furthermore, less than 7 percent of all stars have two or more outgoing gray or sparse black prongs. Allowing for the fast neutrons which are not visible, the inference is that in nearly all stars there is at least one outgoing fast nucleon.

The authors wish to thank Miss E. Wimmer for assisting with the analysis of the plates.

* This project was supported jointly by the ONR and AEC.
[1] S. A. Wouthuysen, Phys. Rev. **75**, 1329 (1949).
[2] M. L. Goldberger, Phys. Rev. **74**, 1269 (1948).
[3] Brown, Camerini, Fowler, Heitler, King, and Powell, Phil. Mag. **40**, 862 (1949); Bernardini, Cortini, and Manfredini, Phys. Rev. **79**, 952 (1950).

The Nuclear Spin of $_{43}Tc^{99}$

Karl G. Kessler and William F. Meggers
National Bureau of Standards, Washington, D. C.
October 16, 1950

THE emission spectrum of Tc^{99} has been investigated in this laboratory,[1] the wave-lengths of the principal lines have been reported[2-4] and an analysis of the spectrum has now been prepared.[5]

A 2.1-mg portion of the Tc^{99} sample was used in making a series of interference spectrograms with a liquid-nitrogen-cooled beryllium hollow cathode discharge tube filled with helium gas at about 1 mm pressure. Fabry-Perot interferometers having 3.75

TABLE I. Interval ratios for the line 4238.19A.

Theory spin	Ratio
7/2	1.000:0.800:0.600
9/2	1.000:0.833:0.667
11/2	1.000:0.857:0.714
Experiment	1.000:0.831±0.011:0.654±0.011

and 5 mm invar separators were used with aluminum-coated quartz interferometer plates. Hyperfine structure patterns were observed in the 30 strongest lines of Tc between 2900A and 5000A.

Up to 8 components were resolved in lines attributed to transitions involving levels with $J \geq 7/2$, thus showing that $I \geq 7/2$. Interval-ratio calculations for the 4-component line 4238.19A($4d^5\,5s^2\,{}^6S_{5/2}-4d^5\,5s\,({}^7S)\,5p\,{}^6P_{3/2}{}^\circ$) are compared with measured interval ratios in Table I. Theoretically, the intervals should be in a ratio $(I+J):(I+J-1):(I+J-2)$, that is, for $J=\frac{3}{2}$, $(I+\frac{3}{2}):(I+\frac{1}{2}):(I-\frac{1}{2})$.

These data indicate clearly that the spin of Tc^{99} is $9\hbar/2$ as predicted by Feenberg and Hammack,[6] and in agreement with the model proposed by Mrs. Mayer.[7] The line 4031.63A ($4d^6\,({}^5D)\,5s\,{}^6D_{9/2}-4d^6\,({}^5D)\,5p\,{}^6D_{9/2}{}^\circ$) shows only 6 components resolved, but the end of the pattern is consistent with a spin of $9\hbar/2$.

The magnetic moment of Tc^{99} is now being determined and will be reported soon.

[1] Loaned by the AEC.
[2] W. F. Meggers and B. F. Scribner, J. Opt. Soc. Am. 39, 1059 (1949).
[3] W. F. Meggers and B. F. Scribner, Oak Ridge Spectroscopy Symposium Abstracts, March 25, 1949.
[4] W. F. Meggers and B. F. Scribner, J. Research Nat. Bur. Stand. (to be published).
[5] W. F. Meggers, J. Research Nat. Bur. Stand. (in preparation).
[6] E. Feenberg and K. C. Hammack, Phys. Rev. 75, 1877 (1949).
[7] M. G. Mayer, Phys. Rev. 78, 22 (1950).

Erratum: Nuclear Isomerism and Shell Structure

[Phys. Rev. 79, 1021 (1950)]

R. D. HILL
Physics Department, University of Illinois, Urbana, Illinois
October 6, 1950

SEVERAL points in Fig. 1 were incorrectly located. This figure should be replaced by the accompanying plot.

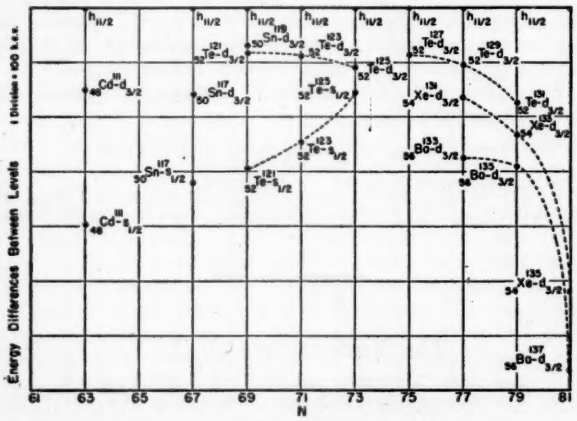

FIG. 1. Plot of level positions against odd neutron numbers for the even-odd isomers of the fifth nuclear shell. Only isomers exhibiting internally converted gamma-ray transitions are shown.

Subsequent to the communication of the letter, another isomer, Xe^{133m}, has been investigated.[1] This new point, $_{54}Xe^{133}-d_{3/2}$, falls accurately on the $Xe-d_{3/2}$ curve and further emphasizes the consistent level trends particularly in this region.

[1] I. Bergström and S. Thulin, Phys. Rev. 79, 538 (1950).

On the π-Meson Absorption and Emission Mechanisms in Nuclei

P. CÜER
Université de Strasbourg, Strasbourg, France
October 10, 1950

TWO groups of Berkeley experimenters[1] have recently reported preliminary results on the pp-interaction producing π^+ mesons which may indicate a high probability to find the resulting proton and neutron in a bound state. In this connection we would like to recall some considerations we made in 1948 which might be still of interest and which stress more precisely a possible analogy between the number of particles involved in the π^- absorption and production processes in nuclei.

After a preliminary analysis of σ-stars we concluded[2] that the most probable process of the primary act of π^- absorption in a nucleus was not a radiative one but the emission of a high energy neutron, the momentum being balanced by a recoil aggregate (nucleon, H^2, H^3, He^4 or more, depending on their instantaneous presence in the absorption spot). These primary particles could afterwards heat the residual nucleus and give rise to an evaporation process. The hypothesis was worked out by Heidmann and Leprince-Ringuet[3] and was found to be in accordance with experimental results, however with poor statistics. Further experimental data by Perkins[4] indicated a considerable probability of ejection of pairs of nucleons. Later studies agreed that emitted particles could be divided in two main groups, an analysis[5] showed that a peculiar scheme in which a neutron and a recoil triton were produced was close to the truth as for the relative number of high energy protons of σ-stars found in β-sensitive emulsions.

An extensive analysis performed recently by the Bristol group[6] gives strong support to the hypothesis of fast neutrons in the primary act for light elements. In the heavy component, as the authors find a ratio of fast protons lower than that predicted by Tamor[7] in the nucleon-nucleon model, mainly in light elements, they conclude that the process is not likely. The argument may be not so serious as appears at first sight because we have found[8] that fast particles of $|e|$ charge ($E>25$ Mev) are ejected in Berkeley plates exposed to 80-Mev neutrons in only 10 percent of the stars, this ratio being lower for light elements. These are also the approximate figures found in σ-stars. However, in these plates a phenomenological study of the number of prongs as a function of the known incident energy (free from the uncertainty arising in the classification of stars) indicates a higher excitation energy for σ-stars ($\sim$70 Mev for the heavy emulsion component) than do 80-Mev neutrons ($\sim$50 Mev for the same component).

As the ratio (3 prong/4 prongs) is very sensitive in the 100-Mev region and lies between 80- and 150-Mev neutrons, it is likely that recoils of $M>1$ are sometimes involved. It seems then that the Bristol excitation value for evaporation stars in BrAg (100 Mev) is overestimated, Fujimito's model which they use does not appear to fit with current evaporation calculations.[9]

Protons of $\sim$100 Mev as occasionally found suggest cases in which the effective recoil is at least a Be^8 clustering balancing the moment of a neutron of about 125 Mev. Deuterons, tritons, and even α-particles with energies well above the mean temperature have also been detected.

It has commonly been assumed hitherto that mesons arise in nuclei by nucleon-nucleon collisions, the threshold energy of production being lowered by the internal dynamics of the systems.[10] For such threshold calculations Barkas[11] has given an ingenious method similar to that used in nuclear physics. Such an analogy between nuclear dynamics and meson production seems, however, to be somewhat strained. In an ordinary nuclear reaction, as the whole nucleus contributes to the excitation which is given up to the products much later, we are entitled to consider only the initial and final states.

In a meson production at threshold incident energy the residual nucleus, if any, is generally heated after the π-emission by the reacting particles at rest in the c.m. system. It appears then that some definite hypothesis must be made for the primary event, as

the available energy in the c.m. system for meson creation will depend on the masses of the interacting particles and not on the final state of the more or less excited nucleus.

We propose to introduce for this primary stage a clustering process similar to this used in the absorption process: the incident nucleon would interact with a nucleon, H^2, H^3, He^4···depending on either their probability of existence or the possibility that a minimum volume of the nucleus would be involved in large transfers of energy. Without taking account of the internal dynamics which would decrease the figures, thresholds would be obtained with heavy clusters. For effective π-production if we start with He^4 as a safe limit, we get values a little higher than Barkas'. Nuclei showing α-structure like C^{12} would give low thresholds. The excitation curve below the pure nucleon-nucleon threshold would give the relative proportions of clusters in $\sim 10^{-22}$ sec. Extensive statistics of stars emitting π-mesons in light elements at known incident energies would give evidence on this mechanism. With 260-Mev neutrons, the cross section is too low to draw conclusions from our Berkeley plates.

Association at high energies could explain too the high probability of (n,d) and (n,T) reactions with or without π-emission.[12]

Finally, we recall[13] that neutron-hydrogen experiments with defined neutron beams, similar to those performed with protons, would give definitive evidence on the di-neutron.

We wish to take this opportunity of thanking warmly Drs. Bradner and Gardner, and Professor Lattes who very kindly have given to our group the possibility of studying some high energy events.

[1] Cartwright, Richman, Whitehead, and Wilcox, Phys. Rev. 78, 823 (1950). V. Z. Peterson, Phys. Rev. 79, 407 (1950).
[2] P. Cüer and M. Morand, Comptes Rendus 226, 649 (1948).
[3] J. Heidemann and L. Leprince-Ringuet, Comptes Rendus 226, 1719 (1948).
[4] D. H. Perkins, Phil. Mag. 40, 601 (1949).
[5] W. Cheston and L. Goldfarb, Phys. Rev. 78, 683 (1950).
[6] Menon, Muirhead, and Rochat, Phil. Mag. 41, 583 (1950).
[7] S. Tamor, Phys. Rev. 77, 412 (1950).
[8] P. Cüer, and L. Van Rossum, C. R. congrès de Côme (1949).
[9] W. Horning and L. Baumhoff, Phys. Rev. 75, 378 (1949).
[10] W. G. MacMillan and E. Teller, Phys. Rev. 72, 1 (1947).
[11] W. H. Barkas, Phys. Rev. 75, 1109 (1949).
[12] Cüer, Morand, and Van Rossum, Comptes Rendus 228, 481 (1949).
[13] Morand, Cüer, and Moucharafyeh, Comptes Rendus 226, 1974 (1948).

Noise Temperature of a D.C. Gas Discharge Plasma

SHOJI KOJIMA AND KAZUO TAKAYAMA
Tokyo University of Education, Tokyo, Japan
September 29, 1950

IN a discharge tube, noise is generated from the cathode fall and the plasma. To pick up the noise of the plasma, a floating probe was inserted near the anode. The fluctuation of the voltage between the probe and the anode was observed by a narrow band amplifier of 14 Mc/sec. The discharge tubes used, of which the diameter is 3 cm and length 7.8 cm, were filled with argon at a pressure of 1 to 3 mm Hg, whereas the tubes filled at higher pressures frequently showed some oscillations.

The noisiness of the plasma is expressed by the noise temperature T_n, which is defined by the formula

$$\langle e^2 \rangle_{Av} = 4kT_nR,$$

where $\langle e^2 \rangle_{Av}$ is the mean square voltage fluctuation per cycle and R is the resistance between the probe and the anode. The mean square voltage was determined by comparison with the shot noise of a diode with the aid of a square law detector. The resistances were deduced from the characteristic curves of the probe.

The measurements were performed at various electron temperatures, varying the applied voltage of the discharge tubes. The electron temperature was more easily determined by the double-probe[1] than the single-probe method. The relations between the electron temperature T_e and the noise temperature T_n were studied with tubes A and B. The results are shown in Fig. 1. This shows that the noise temperature agrees with the electron temperature as far as orders of magnitude are concerned and that they are in a proportional relation.

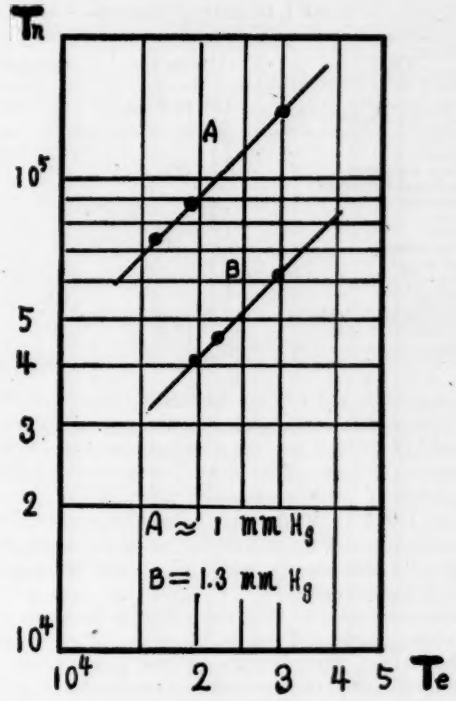

FIG. 1. Relation between the noise temperature T_n and the electron temperature T_e.

The noise of the plasma, as discussed by Parzen and Goldstein,[2] consists of the thermal noise, which depends on the electron temperature, and of the current noise, which depends on the d.c. current. The latter shows a frequency dependence, but the former does not. A preliminary experiment[3] with an amplifier of 600 kc/sec. indicated that the noise temperature at this frequency is nearly equal to that at 14 Mc. Therefore, the observed noise is mainly thermal noise. This explains the approximate agreement between the noise temperature and the electron temperature.

[1] E. O. Johnson and L. Malter, Phys. Rev. 76, 1411 (1949).
[2] P. Parzen and L. Goldstein, Phys. Rev. 79, 190 (1950).
[3] Kojima, Takayama, and Shimanuchi (to be published.)

Fluorescent Decay of Scintillation Crystals

S. H. LIEBSON, M. E. BISHOP, AND J. O. ELLIOT
Electricity Division, Naval Research Laboratory, Washington, D. C.
October 16, 1950

IN order to clarify recent observations of the behavior of organic fluors which scintillate under gamma-ray bombardment, measurements have been made of the decay time of fluorescence under ultraviolet excitation. The technique employed is similar to one suggested by Tumerman[1] and involves a measurement of the phase shift between incident modulated ultraviolet light and the resultant modulated fluorescence of a fluor whose mean lifetime for excited states is τ. The decay of excited states is assumed to be of the form $e^{-t/\tau}$. The exciting ultraviolet light is modulated by passage through a quartz crystal oscillating at about 5 Mc/sec., the resultant light being modulated at about 10 Mc/sec. It is easily shown that the phase shift is related to the mean lifetime of the fluor by the relation $\tan\phi = 2\pi f\tau$, where ϕ

TABLE I. Decay times of fluors.

Fluor	Uv decay	Gamma-decay
anthracene	1.7×10^{-8} sec.	3.0×10^{-8} sec.
anthracene (−195°C)	0.8	1.3
carbazole	0.7	1.3
chrysene	2.2	2.6
diphenyl acetylene	0.25	0.4
1,4 diphenyl butadiene	0.2	0.6
fluoranthene	4.6	...
fluorene	0.88	...
perylene	1.2	...
phenanthrene	0.52	...
quaterphenyl	0.38	0.7
stilbene	0.31	0.8
terphenyl	1.1	0.6
½% anthracene in benzene	0.20 ± 0.05	...
½% terphenyl in toluene	0.25 ± 0.05	0.2

is the phase shift and f is the modulating frequency. Measurements of phase shift can be made which correspond to time decays of the order of 2×10^{-10} sec., the principal source of error for these measurements being amplifier noise. The ultraviolet source was a 10 kw carbon arc with transmission filters to limit the spectral range from 2500A to 3500A. Table I shows the results of measurements made at room temperature on some fluors together with measurements obtained by means of a pulse technique under gamma-ray bombardment.[2]

The times measured by the pulse technique have been corrected for the decay introduced by the photo-multiplier, estimated at 4×10^{-9} sec. from measurements on dark noise pulses. The accuracy of both sets of measurements was estimated to be about 10 percent. Measurements by the shorted-line technique are in substantial agreement with those of recent investigators.[3-5]

Measurements using modulated ultraviolet light were checked with measurements made by Gaviola,[6] corrected according to Tumerman.[1] For a solution of rhodamine B in water and glycerine, values of 2.5×10^{-9} sec. and 5.2×10^{-9} sec., respectively, were obtained, in agreement within experimental error with Gaviola's results. A grid-controlled x-ray tube operated at 80 kv was modulated at 10 Mc/sec. and used in place of a light source. Measurements on the decay times for stilbene, anthracene, terphenyl, diphenyl acetylene, and a ½ percent solution of terphenyl in toluene yielded results in good agreement with the ultraviolet excitation decay times. Oscillator strengths based on measurements of absorption spectra for stilbene and 1,4-diphenyl butadiene[7] were calculated as 3.5×10^{-9} sec. and 3.3×10^{-9} sec., respectively, indicating a reasonable if not fortuitous agreement with measurements on ultraviolet decays.

The discrepancies between ultraviolet and gamma-ray excitation cannot be easily resolved. A measurement on a crystal of 0.05 percent anthracene in napthalene at the anthracene wavelengths gave a mean lifetime in good agreement with the ultraviolet measurements on pure anthracene, indicating that the migration of energy within the crystal does not contribute appreciably to the measured decay time. The temperature dependence of the anthracene fluorescence was again demonstrated under ultraviolet excitation. Of equal interest were the results on a liquid solution of anthracene in benzene which gave a decay time of $2\pm0.5\times10^{-9}$ sec., and measurements on terphenyl in toluene which were in agreement with gamma-ray measurements. The measurements under x-ray bombardment were undertaken to obtain correlation with gamma-ray measurements, the agreement with ultraviolet excitation being unexpected.

We would like to express our thanks to Professor L. Zechmeister of the California Institute of Technology for the preparation of 1,4-diphenyl butadiene.

[1] L. A. Tumerman, J. Phys. U.S.S.R. 4, 151 (1941).
[2] Elliot, Liebson, Myers, and Ravilious, Rev. Sci. Inst. 21, 631 (1950).
[3] G. G. Kelley and M. Goodrich, Phys. Rev. 77, 138 (1950).
[4] R. F. Post and N. S. Shiren, Phys. Rev. 78, 80 (1950).
[5] Elliot, Liebson, and Ravilious, Phys. Rev. 79, 393 (1950).
[6] E. Gaviola, Zeits. f. Physik 42, 862 (1927).
[7] R. S. Mulliken and C. A. Rieke, Rep. Prog. Phys. 8, 231 (1941).

The Thermal Neutron Absorption Cross Section of Silicon*

C. W. TITTLE
North Texas State College, Denton, Texas
AND
HENRY FAUL
U. S. Geological Survey, Washington, D. C.
July 24, 1950

THE thermal neutron absorption cross section of silicon has been determined experimentally by the method of Frisch, von Halban, and Koch.[1] A Ra-α-Be neutron source was placed in a mixture of pure silica sand and water, large enough to be effectively infinite; and the thermal neutron distribution was measured with indium foils. Counting was done with mica window Geiger-Mueller counters. Correction for the indium resonance was made by determining the activation of the foils when shielded by 0.10 cm of Cd. To correct for the absorption of indium resonance neutrons by Cd, this measured activity was multiplied by the factor 1.13, determined for indium foils of the thickness used (58 mg/cm²). Sufficient data were taken to make the space integrals of the thermal neutron density good to 2 percent in the case of the sand-water mixture, 2 percent in one experiment in which the comparison mixture was a heterogeneous lattice consisting of graphite rods and water, and 1 percent in another experiment in which the comparison medium was water. Correction for the depression of the thermal neutron density by the indium foils was made by use of Bothe's formulas.[2]

In these experiments the silicon cross section was compared with the hydrogen cross section for absorption. Correction for other nuclei was made by assuming σ_a(oxygen)$=0.0016$ barn and σ_a(carbon)$=0.0045$ barn.[3] Impurities were negligible.

From the experiment in which sand-water was compared with carbon-water,

$$\sigma_a(\mathrm{H})/\sigma_a(\mathrm{Si})=2.3\pm20 \text{ percent.}$$

From the one in which sand-water and water were compared,

$$\sigma_a(\mathrm{H})/\sigma_a(\mathrm{Si})=2.0\pm15 \text{ percent.}$$

Errors shown are estimated probable errors based on reasonable values of uncertainties in the corrections, concentrations, and space integrals. The weighted average of the two determinations is

$$\sigma_a(\mathrm{H})/\sigma_a(\mathrm{Si})=2.1\pm12 \text{ percent.}$$

If σ_a(H) is taken to be 0.313 ± 0.013 barn[3] at the standard neutron speed of 2.2×10^5 cm/sec.,

$$\sigma_a(\mathrm{Si})=0.15\pm0.02 \text{ barn.}$$

The calculations have neglected the possibility of resonance absorption in Si. An experiment to search for resonance absorption showed that the resonance escape probability $p=1.01$, i.e., 1.00 within the experimental uncertainty of about 2 percent.

* The experimental work reported here was done at the Massachusetts Institute of Technology, Cambridge, Massachusetts, in connection with the Nuclear Shielding Project, which is supported by a joint program of the ONR and the BuShips.
[1] Frisch, v. Halban, and Koch, Kgl. Danske Videnskab. Selskab, Mat.-fys. Medd. 15 (10), 1 (1938). See also W. J. Whitehouse and G. A. R. Graham, Can. J. Research 25A, 261 (1947).
[2] C. W. Tittle, Phys. Rev. 80, 758 (1950).
[3] M. Ross and J. S. Story, Physical Society *Reports on Progress in Physics* 12, 291-304 (1948-49).

The Gamma-Ray Spectrum of Ba^{131}

E. L. ZIMMERMAN, E. B. DALE, D. G. THOMAS, AND J. D. KURBATOV
Department of Physics, Ohio State University, Columbus, Ohio
July 10, 1950

THE Ba^{131} photo-electron spectrum from a lead radiator has been investigated below 700 kev. A thin lens spectrometer adjusted for two percent resolution was used. The spectrometer calibration constant was 598.9 gauss-cm/amp. This was determined by measuring the K and L photo-electron peaks of the

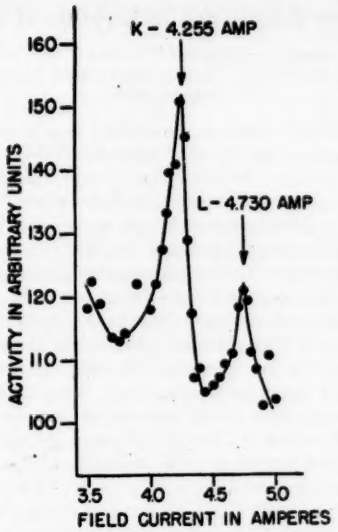

FIG. 1. Ba^{131} —496.5-kev peaks.

364.18-kev gamma-ray in I^{131}. The energy of this gamma-ray is known[1] accurately and lies in the region of gamma-ray energies of Ba^{131}. The calibration was repeated with gamma-rays of Co^{60} and found to be within 0.05 percent of that of I^{131}.

Activated barium nitrate was obtained from the Oak Ridge National Laboratory. The sample was purified and the cesium removed chemically. Since the material had a low specific activity a large volume of sample (about one cubic centimeter) was used. The total activity after decay of Ba^{133} at the beginning of observations was about 0.5 millicurie. The spectrum was found to complex. The peaks occurring at current settings 4.255 ± 0.01 and 4.370 ± 0.02 amp. were much stronger and better defined than any of the others. These are shown in Fig. 1. The separation and relative intensity of the two peaks indicate that they are the K and L peaks of a single gamma-ray.

Values for the gamma-ray energy calculated from the K and L photo-electron peaks are 496.5 ± 1 kev and 496.5 ± 2 kev.

The high background due to the large sample caused considerable uncertainty in the analysis of the other peaks. There was a substantial increase in the counting rate corresponding to photo-electron energies in the range from 95 to 130 kev. The distribution was too broad to be due to either the K or the L photo-electrons from a single gamma-ray energy. The shape of the distribution indicated the superposition of photo-electrons from at least three gamma-ray energies.

A grant in aid from the Ohio State University Development fund for construction of a thin lens spectrometer made this work possible and is gratefully acknowledged by the authors.

[1] Lind, Brown, Klein, Muller, and Dumond, Phys. Rev. 76, 1633 (1949).

On the Radioactivity of Potassium

M. CECCARELLI, G. QUARENI, AND A. ROSTAGNI
Istituto di Fisica dell' Universita di Padova, Italy
October 13, 1950

IT is known that K^{40} decays into Ca^{40} through β^- emission; v. Weizsacker[1] suggested that it may also decay into A^{40} through β^+ emission or K-capture. β^+ radioactivity was excluded by an experiment due to Bothe[2] and K-capture was apparently demonstrated first by Thompson and Rowlands, and then by Bleuler and Gabriel,[3] who gave for the ratio λ_K/λ_- the figure 1.9 ± 0.4. Doubts on the reliability of this result and of the value $\lambda_-=1.0\times10^{-9}$ yr.$^{-1}$ given by the same authors were raised in different places.[4] Direct search[5] for A^{40} in old potassium ore showed quantities which are far inferior to those expected on the basis of the value given by Bleuler and Gabriel and suggests for λ_K/λ_- a maximum possible value of 0.1.

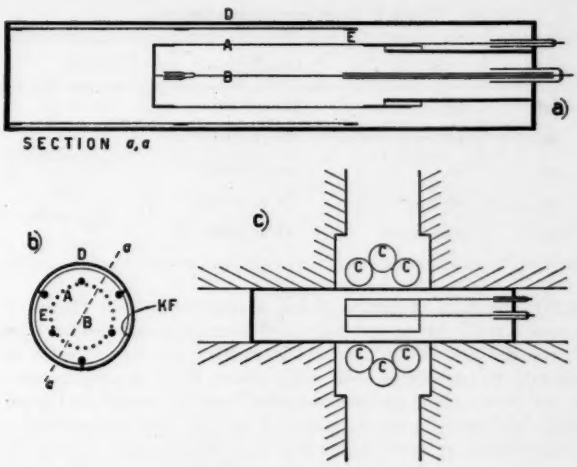

FIG. 1. Experimental arrangement.

We made first an investigation[6] on β- and γ-radiation from K^{40} with an experimental arrangement which was derived from those of Occhialini, Bocciarelli, Libby, and Lee.[7] Then, as we describe below, we tackled the problem of the K-capture with other equipment, similar to that used by Bleuler and Gabriel, but with an essential improvement, in the addition of a magnetic field which eliminates the background due to β-rays (which outnumber by far the x-rays looked for) and an anticoincidence system which substantially reduces the background due to cosmic rays.

The experimental arrangement is shown in Fig. 1, *a* and *b*. A and B are respectively the cathode and the anode of a Geiger-Müller counter, 58 mm in diameter, the effective length of which is 140 mm; the cathode consists of a parallel system of brass wires 0.3 mm thick at a distance of 4 mm from each other. The counter is coaxial with the tube D, 95 mm in diameter and 500 mm long. On the internal surface of D and facing the counter is deposited a layer of KF, 2.5 mg/cm^2 thick and 140 mm long. The movable frame E is covered half (140 mm) with an aluminum foil 0.03 mm thick, and half with a net of wires 0.1 mm in diameter. The frame can be moved by inclining the tube in order to insert either the foil (which is supposed to absorb completely the soft x-rays from A^{40}) or the net between the KF layer and the counter. Both electrodes of the counter are insulated, and the cathode A is maintained at a potential about 300 volts negative with respect to the tube D. This is necessary to restrict the sensitive volume of the counter to the space inside A, by preventing the entry of electrons generated outside. The counter is located between the pole pieces of an electromagnet, taking advantage of a hole along its axis (Fig. 1*c*). The field, parallel to the axis of the cylinder and uniform in the region used in the experiment, is regulated so as to prevent β-rays from penetrating to the inside of the counter. Actually the pulse frequency decreases by increasing the field up to 6000 gauss and then remains constant. In our experiment we used a field of 10,000 gauss. Calculation shows then that β-particles from the KF layer cannot come nearer than 5 mm to the cathode of the counter. Residual pulses are therefore due either to more energetic, or to field-insensitive rays, mainly cosmic, γ- or possibly x-rays. The six counters C, in parallel with each other, are in anticoincidence with the counter AB.

After some trials with various gas mixtures, a filling with 400 mm Hg argon and 10 mm Hg ethyl alcohol proved the most satisfactory. The calculated efficiency of this filling for the argon x-rays is about 0.48. Taking into account the average absorption in the KF layer (0.50) and in the gas between this layer and the cathode

TABLE I. Experimental counting rate.

Field	Shield	Counts/min.	Diff.
off	off	393	297
on	off	96.19±0.16	0.07±0.23
on	on	96.12±0.16	
on	off (-coinc.)	34.16±0.06	0.15±0.08
on	on (-coinc.)	34.01±0.06	

(0.21), the final efficiency of our arrangement with respect to x-rays is 0.19. As we are interested directly in the ratio x-rays/β-rays and not in the absolute intensities, we do not need apparently to consider a solid angle effect, both measurements of x- and β-rays being performed under identical geometrical conditions. We must, however, take into account the back-scattering of β-particles, an effect which had been neglected by Bleuler and Gabriel[3] and was first brought into consideration by Graf.[4] That implies in our experimental conditions, according to Graf's result, a correction factor on β-intensity of the order of 0.5.

Table I represents the results obtained in a total time of 123 hours.

We assume the difference of the first and second lines of Table I to represent the intensity of β-rays. This has been confirmed by a control experiment with the *KF* layer off. This intensity must be corrected for the back-scattering effect; using the correction factor 0.5 we obtain $I_\beta=0.5\times297=148$. The numbers in the fourth and fifth lines are obtained from those in the second and third by subtracting the coincidences of counter *AB* with counters *C* (cosmic rays background). The differences between the second and third or between the fourth and fifth lines give as upper limits (considering statistical errors) for the x-rays intensity 0.30 and 0.23, respectively, the second figure (corresponding to a reduced background) being the more reliable. For the ratio x-rays/β-rays, taking into account the counting efficiency and the Auger coefficient, we obtain

$$\frac{\lambda_K}{\lambda_-}\leq\frac{0.23}{148\times0.19\times0.12}=0.07$$

as an approximate upper limit.

For unavoidable reasons we could not protract our experiment long enough to obtain a substantial reduction in the statistical error and to be able to give a more explicit value of λ_K. When the experiment had been completed the paper by Sawyer and Wiedenbeck[8] appeared, where a ratio $\lambda_K/\lambda_-=0.13\pm0.04$ is given, in substantial agreement with our upper limit. The same conclusion, that λ_K/λ_- is at most of the order of 0.1, has also been obtained at the same time by Haxel, Heintze, and Houtermans, by a third different experiment.[9]

All of these experiments agree among themselves and with Suess' and Aldrich and Nier's geochemical determinations,[5] indicating for λ_K/λ_- a value at least 20 times smaller than Bleuler and Gabriel's value. We think that an actual quantitative determination of this ratio could best be performed by our method, more direct than the others attempted, using a layer of *KF* enriched with K^{40} by a factor of 10 or more. Further details of our experiment will be found in a paper to appear shortly in the *Nuovo Cimento*.

[1] C. F. v. Weizsacker, Physik. Zeits. **38**, 263 (1937).
[2] W. Bothe and A. Flammersfeld, Naturwiss. **29**, 194 (1941).
[3] F. C. Thompson and S. Rowlands, Nature **152**, 103 (1943); E. Bleuler and M. Gabriel, Helv. Phys. Acta **20**, 67 (1947).
[4] F. Birch, Phys. Rev. **72**, 1128 (1947); T. Graf, Phys. Rev. **74**, 831 (1948).
[5] H. E. Suess, Phys. Rev. **73**, 1209 (1948); L. T. Aldrich and A. O. Nier, Phys. Rev. **74**, 876 (1948).
[6] Ceccarelli, Merlin, and Rostagni, Nuovo Cimento **6**, 151 (1949).
[7] G. Occhialini, Lincei Rend. **14**, 103 (1931); D. Bocciarelli, Nature **128**, 374 (1931); W. F. Libby and D. D. Lee, Phys. Rev. **55**, 245 (1939).
[8] G. A. Sawyer and M. L. Wiedenbeck, Phys. Rev. **79**, 490 (1950).
[9] Private communication from Professor F. G. Houtermans.

Microwave Resonance Absorption of $NiOFe_2O_3$

TOSIHIKO OKAMURA, YOSIHARU TORIZUKA, AND YŪZŌ KOJIMA
Research Institute for Scientific Measurement, Sendai, Japan
July 24, 1950

MICROWAVE resonance absorption in a semiconductor was first reported by Hewitt,[1] using MnO ZnO $2Fe_2O_3$. In the ferromagnetic ferrites, $NiOFe_2O_3$ has an especially high resistivity of 10^6 ohm-cm, when the heat treatment is suitable.[2] Since the absorption in a semiconductor is not so affected by the surface condition of specimen, it should be possible to measure the resonance field accurately. The measurements of resonance absorption were made in the range of 7.5-cm and 3.2-cm wave-length.

In Fig. 1, curve (A) shows the results of a measurement at 4051 Mc of the curve of high frequency loss *versus* the static magnetic field applied to the disk specimen (16 mm diam., 0.5 mm thick). The curve has a rather broad maximum, but after repeated measurements we were able to fix a maximum resonance field of 450 to 470 oersteds; when M_∞ for the specimen is known, the *g*-value can be calculated according to Kittel's formula[3] $\omega_0=\gamma(BH)^{\frac{1}{2}}$. By means of the isthmus method, a value of M_∞ of 307 gauss was obtained at 8000 oersted. This is in good agreement with the result obtained by Gorter.[4] The *g*-value was thus found to be 2.05±0.07 with 307 gauss for M_∞.

As the r-f skin depth in the specimen is large, owing to its high resistivity, it is possible to measure the absorption by using a spherical specimen. As Kittel has shown, the resonance formula will be $\omega_0=\gamma H$ when the specimen is a sphere, and does not involve the observed value of M_∞ explicitly. The curve observed by using the spherical specimen (10 mm diam.) is shown by curve (*B*), and we obtained a *g*-value of 2.02±0.10. This result is in good agreement with the case of the disk, with 307 gauss for M_∞.

Furthermore, the absorption was also observed with the disk specimen (4.5 mm diam., 0.5 mm thick) at 3.2-cm wave-length, 9317 Mc in frequency. The result is shown in curve (*C*). The maximum absorption was observed at 1810 oersted and a minimum absorption was also observed, the *g*-value was determined as 2.26±0.02 considering a demagnetizing factor of $Ny-Nz=0.775$ which was calculated from the dimension of the specimen. Curve (*D*) is a resonance curve of a spherical specimen (2.2 mm diam.) and the *g*-value obtained was 2.26±0.02. Beljers and Ploder[5] have reported the *g*-value of $NiOFe_2O_3$ as 2.23 (3 mm diam.) and 2.36 (2 mm diam.). We could not observe such a size effect by using spherical specimens of 2.2 mm and 3 mm in diameter. However, we can point out that it is difficult to observe the resonance

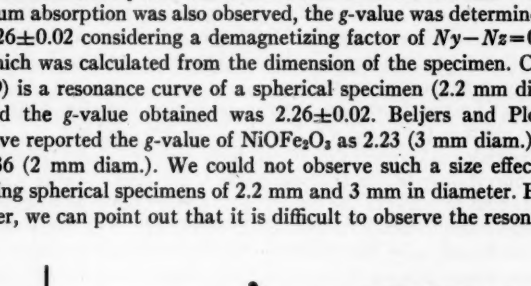

FIG. 1. Resonance curves of $NiOFe_2O_3$ at the wave-length of 7.5 cm and 3.2 cm.

TABLE I. g-Value of $NiOFe_2O_3$.

Form of specimen	Wave-length 7.5 cm	3.2 cm
Disk	2.05±0.07	2.26±0.02
Sphere	2.02±0.10	2.26±0.02

field accurately when the 3-mm sphere was used, owing to the marked drop of the Q-value of a resonance cavity.

The g-value of $NiOFe_2O_3$ obtained is shown in Table I.

It was ascertained experimentally that the wave-length becomes shorter as the g-value becomes greater. Kittel[6] has discussed such a frequency dependence on the g-value for some metals, but the phenomenon should be studied further using a semiconductor, which has a deeper skin-depth.

[1] W. H. Hewitt, Jr., Phys. Rev. 73, 1118 (1948).
[2] Recently published in Sci. Rep. RITU.
[3] C. Kittel, Phys. Rev. 73, 155 (1948).
[4] E. W. Gorter, Nature 165, 789 (1950).
[5] H. G. Beljers and D. Polder, Nature 165, 800 (1950).
[6] C. Kittel, Phys. Rev. 76, 743 (1949).

Microwave Spectroscopic Evidence for Internal Rotation in Methyl Silane

DAVID R. LIDE* AND DONALD K. COLES
Westinghouse Research Laboratories, East Pittsburgh, Pennsylvania
October 18, 1950

WHILE thermodynamic evidence for the existence of internal rotation in molecules is conclusive, there are some questions as to the nature of the hindering potential barrier. This has recently been emphasized by Blade and Kimball,[1] who introduced a shape parameter into an assumed potential barrier, and found that the best modern thermodynamic data were inadequate for distinguishing between widely different barrier shapes and heights. Raman and infra-red spectroscopic studies have also proved somewhat inconclusive—partly because of the limited resolution obtainable in the visible and infra-red regions of the spectrum. Fortunately, microwave absorption lines associated with different stages of torsional vibration can be resolved easily. By careful intensity measurements of these absorption lines, it seems possible to determine the energy levels and therefrom the barrier height and shape rather accurately.

Probably the lightest symmetric-top molecule which is capable of internal rotation and of absorbing in the microwave region is H_3C-SIH_3 (methyl silane). We find that the $J=0\rightarrow1$ transition of this molecule has the interesting appearance shown in Fig. 1a. Here the more highly excited levels of torsional oscillation are seen to be split into two components, in agreement with the theory of internal rotation.[2] The spectrum of the deuterated compound (Fig. 1b) has a similar appearance, except for the relative intensities of the two components of a doublet. The statistical weight associated with each of these components, which depends on the nuclear spin of the two sets of equivalent nuclei, can be found by calculating the weight for each end of the molecule separately, as if it were rotating with perfect freedom, and then multiplying the two weights together to get that for the state of hindered rotation.

In the notation of reference 2, the two components of the normalized statistical weight g_I are 3/4 and 3/8 for CH_3SiH_3, giving a total of 9/8, while for CH_3SiD_3 the component weights are 11/18 and 8/18, giving a total of 19/18. For molecules with large nuclear spins of the equivalent nuclei, the component weight factors g_I would be 1/3 and 2/3 respectively.

In order to study the splitting for molecules with over-all axial rotation, we examined the spectrum corresponding to the transition $J=1\rightarrow2$, $K=1\rightarrow1$. In agreement with the prediction of Koehler and Dennison for this case,[3] these torsional vibrational levels appeared to be split into *three* components.

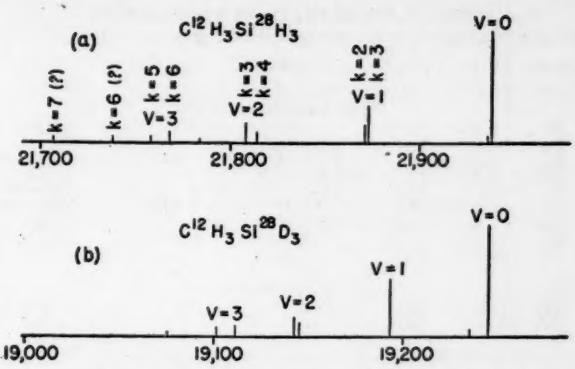

FIG. 1. The $J=0\rightarrow1$ transitions in methyl silane.

The rotational constants B_0 for different isotopic species of methyl silane are found to be:

$CH_3Si^{28}H_3$—10,968.96 Mc	$CH_3Si^{28}D_3$—9622.78 Mc
$CH_3Si^{29}H_3$—10,885.54 Mc	$CH_3Si^{29}D_3$—9572 Mc
$CH_3Si^{30}H_3$—10,806.53 Mc	$CH_3Si^{30}D_3$—9525 Mc.

Stark effect measurements show that this molecule has a dipole moment of 0.73 Debye.

Intensity measurements were attempted on absorption lines corresponding to different stages of torsional vibration and internal rotation. We used sinusoidal Stark effect modulation at 85 kc, two stages of 85 kc amplification, and then a calibrated r-f attenuator. Comparing two lines with the same statistical weight, the intensity ratio provided a measure of the corresponding energy level spacing, at the rate of 15.6 cm^{-1} per decibel of attenuation (temperature of dry ice). Preliminary values of the energy level spacings above the ground level are:

Level	$V=1$	$V=2$	$V=3, k=5$	$V=3, k=6$
Energy (cm^{-1})	183	313	415	465

These values are consistent with Blade and Kimball's two-parabola potential, where $V_0/V_{cos}=1$, $V_0=460\pm80$ cm^{-1}. With improvements to eliminate standing waves in the absorption cell, we believe that the barrier shape and height can be determined within 20 cm^{-1}.

* Present address: Department of Chemistry, Harvard University, Cambridge, Massachusetts.
[1] E. Blade and G. E. Kimball, J. Chem. Phys. 18, 630 (1950).
[2] D. K. Coles, *Advances in Electronics*, Vol. II (Academic Press, New York, 1950), p. 335.
[3] J. S. Koehler and D. M. Dennison, Phys. Rev. 57, 1006 (1940).

An Empirical Correlation Among Superconductors

J. G. DAUNT
The Mendenhall Laboratory, Ohio State University, Columbus, Ohio
October 6, 1950

THE recent experimental results of Maxwell[1] and of Reynolds, Serin, Wright, and Nesbitt[2] on the change in the superconducting transition temperatures of Hg and Sn with change in isotopic mass has served to re-emphasize the important role of the lattice in determining electronic superconductivity, a feature of the phenomenon which was also evident from the marked observable effects of mechanical stress on the transition temperatures.[3] Moreover, these experiments on isotopic changes, being such that one clearly evident parameter is varied, afford an elegant check on theory, such as has been carried out for example recently by Bardeen[4] and Froehlich.[5]

On the other hand, the electronic character of the phenomenon also shows certain regularities among the superconducting pure metals and in view of the increased recent theoretical attention

TABLE I. Tabulated data for the superconductors.*

Element	T_c(°K)	V(cc)	($\gamma\times10^4$)**	($\gamma\times10^4$)***	Θ(°K)
			"Soft" Superconductors		
Pb	7.22	18.2	7.1[a,b]	—	90[j]
Hg	4.15	13.4	3.75[a]—4.5[c]	—	96[j]
Sn	3.71	16.2	3.45[a]—3.95[b]	4.0[d]	185—260[j]
In	3.38	15.8	3.5[b] —3.6[c]	—	110
Tl	2.4	17.3	2.8[b] —3.4[c]	—	90—100[j]
Al	1.15	10.1	2.59[c]	3.48[f]	390—420[j]
Ga	1.12	11.75	0.8[g] —1.5[g]	—	240
Zn	0.95	9.15	1.36[c]	1.25[h]—1.5[i]	290[i]—320[j]
Cd	0.54	13.0	0.75[g]	—	170[j]
			"Hard" Superconductors		
Th	1.3	20.5	7.1[k]		170[j]
Ta	4.4	10.9	14.1[l]		240[j]

* T_c is the transition temperature, V is the atomic volume, γ is the normal electronic specific heat coefficient, and Θ is the Debye temperature.
** γ is given in units of cal./mole-deg.^{2}. The values in this column for the soft superconductors are obtained from magnetic measurements of the threshold curves.
*** γ is given in units of cal./mole-deg.^{2}. The values in this column for the soft superconductors are obtained from calorimetric measurements.
[a] J. G. Daunt and K. Mendelssohn, Proc. Roy. Soc. **A160**, 127 (1937).
[b] Daunt, Horseman, and Mendelssohn, Phil. Mag. **27**, 754 (1939).
[c] A. D. Misener, Proc. Roy. Soc. **A174**, 262 (1940).
[d] W. H. Keesom and P. H. Van Laer, Physica **5**, 193 (1938).
[e] J. G. Daunt and C. V. Heer, Phys. Rev. **76**, 1324 (1949).
[f] J. A. Kok and W. H. Keesom, Physica **4**, 835 (1937).
[g] Results to be reported subsequently.
[h] W. H. Keesom and J. N. van den Ende, Proc. Amst. Akad. Sci. **35**, 143 (1932).
[i] A. A. Silvidi and J. G. Daunt, Phys. Rev. **77**, 125 (1950).
[j] Burton, Grayson-Smith, and Wilhelm, *Phenomena at the Temperature of Liquid Helium* (Reinhold Publishing Corporation, New York, 1940), p. 347.
[k] Calculated from Eq. (2) using Schoenberg's data, reference 7.
[l] From calorimetric data of Keesom and Desirant, reference 8.

paid to the problem of superconductivity it is thought worth while to point out one empirical correlation which concerns the electronic structure.

Recent measurements[6] of the magnetic properties of pure Ga and Cd in the superconducting state below 1°K have completed all the data necessary for the calculation of the electronic specific heat of the normal state ($C_{el}=\gamma T$) for *all* the known "soft" superconductors. In Table I, the Sommerfeld γ-values have been tabulated together with other pertinent data for the superconductors. It is to be noticed that the γ-values increase approximately linearly with increasing transition temperature, T_c, such that

$$\gamma = AT_c \qquad (1)$$

where $A\approx1\times10^{-4}$ cal./mole-degree^3. Al, however, appears to be exceptional, but in view of its high Debye temperature as compared with the other soft superconductors, it may not be strictly permissible to class it in the same grouping.

No similar complete data can be tabulated for the hard superconductors since with the possible exceptions of thorium measured magnetically by Schoenberg[7] and of Ta measured calorimetrically by Keesom and Desirant,[8] either their observed magnetic threshold curves do *not* represent a reversible equilibrium boundary between the normal and superconductive states thus allowing no reliable derivation of γ or no calorimetric observations at low temperatures have been made. The pertinent data for Th and Ta are included in Table I, the γ-value for Th being calculated from Schoenberg's data[7] using the equation that can be derived for γ from Gorter and Casimir's thermodynamical theory[9] assuming a parabolic magnetic threshold curve, namely

$$\gamma=(V/8\pi)(dH_c/dT)^2_{T=T_c}. \qquad (2)$$

From Table I it can be deduced that if the γ-values of Ta and Th satisfied an equation of type (1), it would be with a value of the constant A more than three times larger than that for the soft superconductors. More data here would be of value; for example, calorimetric measurements of γ for such readily obtainable metals as Nb, V, and Ti would be of interest.

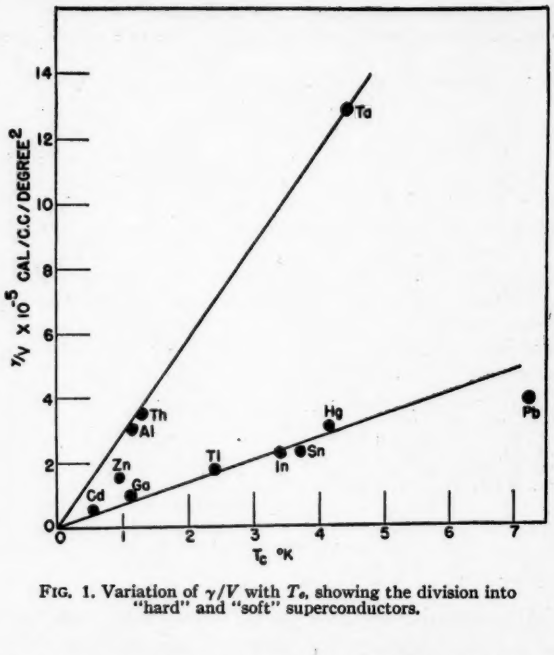

FIG. 1. Variation of γ/V with T_c, showing the division into "hard" and "soft" superconductors.

As a first approximation it would be expected that the interaction energy between the electrons responsible for the condensation into the superconductive state would increase with increasing number density of electrons and hence on the Sommerfeld theory[10] with the quotient γ/V where V is the atomic volume. It seemed to be of interest, therefore, to examine the empirical relationship between kT_c and γ/V. A plot of the experimentally observed values of γ/V against T_c is given in Fig. 1, for the elements listed in Table I, the γ-values being taken as the mean of those listed in the above tables. It will be seen that with exception of Zn the elements fall along two approximately straight lines, one for the soft superconductors and another for the hard superconductors (which group appears to include Al). The difference between the groups is not surprising in view of the known differences in their electronic band structures.

[1] E. Maxwell, Phys. Rev. **78**, 477 (1950); **79**, 399 (1950).
[2] Reynolds, Serin, Wright, and Nesbitt, Phys. Rev. **78**, 487 (1950).
[3] G. J. Sizoo and H. K. Onnes, Leiden Communications, Nos. 133 and 180b; N. Alekseyevsky, J. Phys. U.S.S.R. **9**, 147 (1945); B. Lasarew and A. Galkin, J. Phys. U.S.S.R. **8**, 376 (1944).
[4] J. Bardeen, Phys. Rev. **79**, 167 (1950).
[5] H. Froehlich, Phys. Rev. **79**, 845 (1950).
[6] J. G. Daunt, to be reported later.
[7] D. Schoenberg, Proc. Camb. Phil. Soc. **36**, 84 (1940).
[8] W. H. Keesom and M. C. Desirant, Physica **8**, 273 (1941).
[9] C. J. Gorter and H. G. B. Casimir, Physica **1**, 305 (1934).
[10] A. Sommerfeld, Zeits. f. Physik **47**, 1 (1928).

On the Cohesive Energy of Metallic Lithium

R. A. SILVERMAN AND W. KOHN*
Harvard University, Cambridge, Massachusetts
October 13, 1950

ON the basis of the Wigner-Seitz atomic sphere approximation, Bardeen[1] has evaluated the first two terms of a series expansion for the energy $E(k)$ of an electron with wave number k moving in the lattice of metallic Li. He found that $E(k)=E_0+E_2k^2+E_4k^4+\cdots$, where $E_0=-0.6635$ and[2] $E_2=0.6539$ for the experimentally determined lattice constant[3] of 3.4492A. Bardeen's calculations were based on the Li ion-core potential published by

TABLE I. Cohesive energy of metallic lithium by various methods of calculation.

Method used	Cohesive energy (kcal./mole)
Experimental	39.0
Power series to order k^2	35.2
Variable coefficients using (4)	34.6
Power series to order k^4	34.9
Variable coefficients using (5)	34.8

Seitz[4] which, as a result of an error, differed somewhat from the potential which Seitz had actually used. Bardeen has forwarded to us the correct potential and with it we have repeated his calculation with the results $E_0=-0.6832$, $E_2=0.7270$. These values differ only slightly from those calculated by Seitz[4] who used a perturbation method (-0.682 and 0.744). With our values of E_0 and E_2 and the expression $(0.284/r_s)-[0.58/(r_s+5.1)]$ (r_s=radius of Wigner-Seitz sphere) usually assumed as the correction resulting from correlations between electrons, one finds the value of 35.2 kcal./mole for the cohesive energy of metallic Li, as compared with the experimental value[5] of 39.0 kcal./mole. (The theoretical values of Seitz and Bardeen were 33.7 and 33.9 kcal./mole respectively.)

On the basis of order of magnitude estimates it was thought that a considerable part of the discrepancy between theory and experiment might be due to the fourth-order term in the series expansion of $E(k)$. We therefore evaluated E_4 by an extension of Bardeen's method. This required the calculation of the lattice wave function to order k^2.

$$\psi_k=[u_0+ikP_1\phi_1+k^2(\phi_0+P_2\phi_2)]\exp i(\mathbf{k}\cdot\mathbf{r}) \tag{1}$$

where u_0 is the normalized s-solution of the Schroedinger equation for energy E_0, ϕ_1 is rv of Bardeen's paper,[1] P_1 and P_2 are the Legendre polynomials of degree 1 and 2 respectively, while ϕ_0 and ϕ_2 are given by the following expressions:[6]

$$\phi_0=\tfrac{1}{3}r^2v_1-\tfrac{1}{3}r^2u_0+E_2(du_0/dE)_{E=E_0} \tag{2}$$

$$\phi_2=\tfrac{2}{3}r^2v_1-\tfrac{1}{3}r^2u_0+c_Df_D. \tag{3}$$

Here rv_1 is the radial part of the p-solution as defined by Bardeen and f_D the radial part of the d-solution (again for energy E_0); c_D is chosen in such a way that ϕ_2 satisfies the boundary condition $\varphi_2'(r_s)=0$.

By expanding in power series the expectation value of the Hamiltonian computed with the function (1), one obtains the energy $E(k)$ correct to order k^4. In this way we found $E_4=0.0175$, an unexpectedly small value which does not appreciably change the second-order result for the cohesive energy. (Table I.)

To extract the optimum result from our wave functions we have also computed $E(k)$ using the modified functions

$$\psi_k^{(1)}=[c_1u_0+ic_2P_1\phi_1]\exp i(\mathbf{k}\cdot\mathbf{r}) \tag{4}$$

and

$$\psi_k^{(2)}=[c_1u_0+ic_2P_1\phi_1+c_3(\phi_0+P_2\phi_2)]\exp i(\mathbf{k}\cdot\mathbf{r}) \tag{5}$$

and adjusting the coefficients c_i to make the expectation value of the Hamiltonian an extremum. Table I summarizes our results.

One notes that none of these refinements of Bardeen's work appreciably improves the agreement with experiment.

It should be mentioned in this connection that the atomic sphere approximation on which the above calculations were based cannot be expected to be reliable near the top of an energy band. One of us (W. Kohn) is therefore investigating the cohesive energy by means of a variation iteration procedure based on the integral equation

$$\psi_k(\mathbf{r})=\int G(\mathbf{r},\mathbf{r}')V(\mathbf{r}')\psi_k(\mathbf{r}')d\mathbf{r}',$$

where G is the Green's function appropriate to a periodic lattice and V is the lattice potential. This method takes into account the actual shape of the atomic polyhedron and should give a better description of the upper part of the energy band.

* Now at Carnegie Institute of Technology, Pittsburgh, Pennsylvania.
[1] J. Bardeen, J. Chem. Phys. 6, 367 (1938).
[2] Atomic units are used throughout.
[3] Perlitz and Aruja, Phil. Mag. 30, 55 (1940).
[4] F. Seitz, Phys. Rev. 47, 400 (1935).
[5] Bichowsky and Rossini, *Thermochemistry of Chemical Substances*, (Rheinhold Publishing Corporation, New York, 1936).
[6] Equations (1) and (2) agree with the expressions derived in Appendix III of Herring and Hill, Phys. Rev. 58, 132 (1940).

Remarks on the Nuclear Resonance Shift in Metallic Lithium

W. KOHN
Carnegie Institute of Technology, Pittsburgh, Pennsylvania
N. BLOEMBERGEN*
Harvard University, Cambridge, Massachusetts
October 13, 1950

RECENTLY Knight[1] has found that the nuclear resonance frequency for an atom in the metallic state exceeds the frequency of the same atom in a non-metallic compound in the same external field. Townes, Herring, and Knight[2] have subsequently proposed a simple theory for this effect. They find that for lithium the fractional frequency shift (for a given external magnetic field) is given by

$$\Delta f/f=155\chi_p\cdot P_F/P_A; \tag{1}$$

here χ_p is the spin contribution to the paramagnetic susceptibility of metallic lithium per unit mass, and $P_F=|\psi_F(0)|^2_{Av}$, $P_A=|\psi_s(0)|^2$ are the mean probability densities at the nucleus of an electron on the Fermi surface of metallic lithium and of the S-electron in the lithium atom respectively.

Using the experimental results[1] $\Delta f/f=3.6\times10^{-4}$ and[2,3] $\chi_p=3.0\times10^{-6}$ one is led to the experimental value,

$$P_F/P_A=0.77 \tag{2}$$

for the ratio occurring in (1). Townes *et al.*[2] estimated on theoretical grounds that this ratio had a value near 0.8, but they did not actually calculate P_F since the then available wave functions were based on an incorrect ion potential.

The correct ion-core potential, calculated by Seitz, has been kindly supplied to us by Bardeen. For atomic lithium it gives $P_A=0.22$. This value is also checked within a few percent by the measured hyperfine structure separation of the ground state of lithium.[4]

For metallic lithium we have used the wave function (5) of the preceding letter[5] which was calculated by means of an extension of the Wigner-Seitz-Bardeen theory. It gives $P_F=0.30$.

Thus, according to theory,

$$P_F/P_A=1.4. \tag{3}$$

The agreement between theory and experiment is seen to be much worse than was anticipated by Townes *et al.* If one assumes that the difficult measurement of χ_p, which enters into (2), can be relied on, the large discrepancy between theory and experiment is probably due to the theoretical value of P_F. This would indicate that the Wigner-Seitz-Bardeen method is not suitable for a description of the electrons on the Fermi surface of metallic lithium.[5]

* Society of Fellows.
[1] W. D. Knight, Phys. Rev. 76, 1259 (1950).
[2] Townes, Herring, and Knight, Phys. Rev. 77, 852 (1950).
[3] S. R. Rao and K. Sarithrin, Proc. Ind. Acad. Sci. 16, 207 (1942).
[4] M. Fox and I. Rabi, Phys. Rev. 48, 746 (1935).
[5] R. A. Silverman and W. Kohn, Phys. Rev., preceding letter.

The Nature of Wide-Angle Sprays. I†

R. RONALD RAU
Palmer Physical Laboratory, Princeton University, Princeton, New Jersey
October 9, 1950

OPPENHEIMER and Ney[1] have reported the occurrence of wide-angle sprays of minimum ionization particles produced in ¼-in. Pb plates in a cloud chamber sent to balloon altitudes. Rau and Harris[2] have confirmed these cloud-chamber observations of sprays in 1 cm Pb plates.

In order to study in detail the origin of these events and the identity of the spray particles, we have modified the system of thick absorbers used previously. A schematic diagram of the new absorber system is shown in Fig. 1. The Pb foils were 0.92 mm thick and the bottom plate was $\frac{3}{16}$-in. Al for one flight and ¼-in. Pb for a second flight. The cloud chamber was expanded at 1-min. intervals. Plastic balloons manufactured by the General Mills Company carried the equipment aloft to a mean pressure altitude of 16 g/cm². Approximately 3.5 g/cm² of solid material was immediately above the cloud chamber. The balloons were launched at 55°N geomagnetic latitude. We have analyzed thoroughly 487 photographs from these two flights for spray events. This represents about 80 sec. sensitive time.

We have designated as sprays those events which have at least 6 tracks of minimum ionization particles and which have an angular spread of 30° or more. Thirty-five events were found in the upper ¼-in. Pb plate, 23 with 6 to 9 tracks, and 12 with 10 to 25 tracks. Two events were found in the foils. Thirteen events were initiated by ionizing radiation, 14 by non-ionizing radiation and 10 events were so situated in the cloud chamber as to make identification of the initiating radiation impossible. The rate of occurrence of sprays in the upper Pb plate checks with the rate previously obtained.[2] Each track in an event was followed until it stopped in an absorber or left the active volume of the cloud chamber. Range and scattering measurements were made whenever possible. From this data we are able to draw the following conclusions concerning sprays having between 6 and 25 tracks: (1) the spray particles are predominantly electrons; (2) sprays of this size are mainly electromagnetic cascades.

Evidence that the spray particles are electrons resulted from three observations. (a) The tracks of particles which ended in the thin foils did not appreciably increase their ionization above minimum. (b) The multiple scattering of spray particles showing minimum ionization tracks are consistent with the electronic mass. (c) The tracks of spray particles were directly compared with electron tracks in typical electromagnetic cascades and found to be similar in all respects.

We have obtained evidence for the second conclusion by analyzing all electromagnetic phenomena in 167 photographs and comparing them with sprays. It is clear from this direct comparison that sprays of the category defined above are mainly electromagnetic cascades having the property of wide angular divergence. One unusual event strongly suggests the correctness of this interpretation. A cascade event is started in the top Pb plate by one electron and one or more photons. The cascade develops nearly vertically down through the foils, most of the electrons being absorbed before reaching the bottom Pb plate. However, in the bottom Pb plate a spray of 8 particles is seen which is time and space related to the cascade. It is presumably initiated by a photon or photons associated with the cascade. The wide angular spread results from low energy electrons (1 to 10 Mev) which have undergone large multiple scattering in the Pb. Additional evidence comes from the fact that the four foils have 0.6 times the mass of the Pb plate and hence, if the sprays were caused by a single interaction rather than a cascade, one would expect about 20 sprays in the foils rather than two.

Presumably not all of the sprays are pure electromagnetic cascades. One 12-particle spray originating in the upper ¼-in. Pb plate had three particles which penetrated 4 Pb foils, the ¼-in. Al plate, and the ¼-in. lower Pb plate without scattering or multiplication. This event was started by an ionizing particle and may have been a mixed shower rather than a pure electromagnetic cascade.

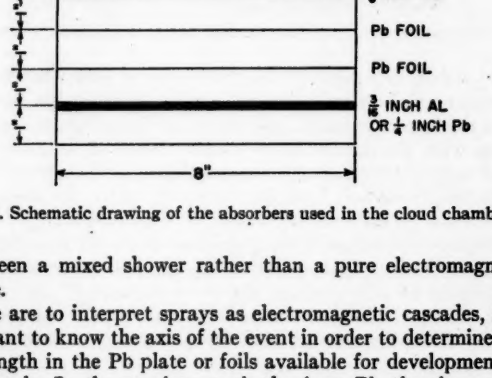

FIG. 1. Schematic drawing of the absorbers used in the cloud chamber.

If we are to interpret sprays as electromagnetic cascades, it is important to know the axis of the event in order to determine the path length in the Pb plate or foils available for development of the cascade. In the previous work the 1-cm Pb absorbers were 2 in. apart. Thus if electrons and photons initiated a shower in the Pb plate at 45° or less to the horizontal, the core of the shower would probably be missed since it would most likely leave the chamber before penetrating the next lower Pb plate. In the present investigation with Pb foils separated by 1 in., low angle cascades are likely to penetrate a foil and the core can usually be identified. The core provides a good means of locating the general momentum direction of the shower and also the initiation radiation. Without the shower core as a guide the initiating radiation is not easy to locate, owing to the large background of random tracks in the cloud chamber.

One-third of the sprays have their axes inclined at 45° or less to the horizontal. Of the 11 events having ≥ 10 particles, 8 are in this category while three are at angles greater than 45° to the horizontal. One event had approximately 25 particles and originated in a thin foil. Particles appeared both above and below the foil and traversed the cloud chamber from front to rear. This event appears to have arisen from a very nearly horizontal particle or particles. A large number of small cascades (3 to 5 particles) in the thin foils and Pb plate are observed which have axes at low angles to the horizontal. From these facts we believe it is possible to present a plausible argument that most and perhaps all sprays, even those larger than 25 particles, can be explained reasonably as either pure electromagnetic cascades or mixed showers. Further arguments will be presented in the following letter.

† Assisted by the joint program of the ONR and the AEC.
[1] F. Oppenheimer and E. P. Ney, Phys. Rev. 76, 1418 (1949).
[2] R. R. Rau and G. G. Harris, Phys. Rev. 79, 915 (1950).

The Nature of Wide-Angle Sprays. II†

R. RONALD RAU AND A. S. WIGHTMAN
Palmer Physical Laboratory, Princeton University, Princeton, New Jersey
October 9, 1950

IN the preceding letter new experimental evidence is presented concerning the wide-angle sprays of minimum ionization particles which have been observed at balloon altitudes in cloud chambers.[1,2] Evidence is presented there for the interpretation of these sprays as being mainly electromagnetic cascades. A few sprays originate in mixed showers in the Pb. Of the remainder some appear to be initiated by ionizing and non-ionizing particles, presumably electrons and photons incident on the Pb.

At the time of the original work on sprays,[1] there were several objections to this interpretation.

(1) The large number of particles produced in relatively small thicknesses of Pb (approximately two radiation units) was apparently incompatible with shower theory.

(2) Events related to the spray apparently should have been produced in other Pb plates by the photons associated with the spray.

(3) There was little evidence for the required photon and electron flux at high altitudes.

The first two points are explained qualitatively by the assumption that the core of the event is at a rather small (>45°) angle to the horizontal. The experimental evidence indicates that especially for the larger events this is true. Such an assumption means that the cascade develops through a considerably longer path of Pb than the thickness of the plate. For example, for a photon of 1 to 10 Bev incident on a 1-cm thick Pb plate at 20°–30° to the horizontal, one could expect on the average 10 to 100 electrons at the shower maximum.[3] One can perhaps expect an even larger number of low energy electrons than is predicted by shower theory. For example, if a core is inclined at 25° to the horizontal and is 1 mm from the lower surface of the Pb, its remaining path length in the plate is 3 mm. More low energy electrons will then be scattered out of the Pb than if the core were normal to the Pb surfaces. Furthermore, the photons tend to remain near the core of the cascade and they will be unable to produce related events since it is most likely that the core of the shower will not strike another Pb plate. It is also possible that some large events may result from at least two photons traveling together. If a spray is due to a mixed shower started in the Pb by a high energy primary then it is possible that several photons contribute to the multiplicity of electrons observed. It seems to us that the above explanations are probably sufficient to invalidate the first two objections, provided that a suitable source of photons and electrons exist.

It is clear from the recent experiments of Bjorklund *et al.*[4] that an appreciable number of photons are produced in nucleon-nucleus collisions as a result of the production of π^0-mesons and their subsequent decay. Furthermore, Carlson *et al.*[5] have determined the energy and angular distribution of photons at 70,000 feet. Extrapolating these results we have estimated the γ-ray flux expected in the cloud chamber at 90,000 feet.

We assume: (1) The absolute vertical nucleon flux at 55°N geomagnetic latitude and under 15 g/cm² of air to be that reported by Winckler *et al.*,[6] namely 0.22 primaries per sec. per cm² per steradian; (2) that the cross section for star production in both Pb and air is geometrical.[7] We can make a check on these assumptions by counting the number of stars produced in the 0.92 mm Pb foils and using the sensitive time of the cloud chamber, 0.15 second. The number of stars which result from these assumptions is about twice that counted. Only stars of 2 or more particles were counted. We find the number of π-mesons produced per second in air or Pb by extrapolating to energies larger than 1 Bev the number spectrum for charged mesons as found by Camerini *et al.*[7] The π^0-meson spectrum is determined from the fact that π^0-mesons are produced with the same spectrum but half the total number.[8] The γ-ray spectrum can then be easily calculated. From these calculations we find that approximately one γ-ray per sec. is generated having an energy greater than 1 Bev in a ¼-in. thick Pb plate having 200 cm² area. In estimating the photon flux which passes through a plate in the cloud chamber due to the generation of π^0-mesons in the air, we take the source function proportional to the density of the air. In order to get a lower limit we neglect the multiplying effect of the cascades in the air and the contributions due to photons at angles lower than 15° to the horizontal. This angular cut-off is due to the experimental arrangement. Under these limitations we find 10 γ-rays per sec. with energy larger than 1 Bev which traverse a Pb plate in the cloud chamber.

These theoretical estimates must be compared to the 1.5 electromagnetic events per sec. observed in the cloud chamber. A small fraction ($\approx 1/20$) appear to be associated with mixed showers. These numbers are based on a small number of photographs. The theoretical estimates appear to indicate more than a sufficient number of γ-rays to produce the observed events. The fact that about half of the sprays are produced by ionizing radiation is reasonable since some of the γ-rays produced in the air will be converted to electrons.

A number of factors in the theoretical estimate: electromagnetic cascades in air, nucleonic cascades, use of the vertical flux at all zenith angles, uncertainties in the π^0-meson spectrum, could effect the agreement with experiment. However, in view of the fact that a detailed examination of the experimental data has not been completed, we feel that further refinements in the above estimates are premature.

In summary, we have presented in the preceding letter experimental evidence that the smaller sprays (<25 particles) are electromagnetic cascades. In this letter we argue that recent work on π^0-mesons provides experimental evidence for a source of γ-rays adequate to account for the observed electromagnetic cascades.

† Assisted by the joint program of the ONR and AEC.

[1] F. Oppenheimer and E. P. Ney, Phys. Rev. 76, 1418 (1949).
[2] R. R. Rau and G. G. Harris, Phys. Rev. 79, 915 (1950).
[3] W. Heisenberg, *Cosmic Radiation* (Dover Publications, New York, 1946).
[4] Bjorklund, Crandall, Moyer, and York, Phys. Rev. 77, 213 (1950).
[5] Carlson, Hooper, and King, Phil. Mag. 41, 701 (1950).
[6] Winckler, Stix, Dwight, and Sabin, Phys. Rev. 79, 656 (1950).
[7] Camerini, Fowler, Lock, and Muirhead, Phil. Mag. 41, 413 (1950).

On the Half-Life of Actinium*

J. M. Hollander and R. F. Leininger
Radiation Laboratory, University of California, Berkeley, California
October 6, 1950

THE half-life of Ac^{227} has not been established with certainty. The most widely quoted[1] values are 21.7 years[2] and 13.5 years.[3] In the interest of resolving this discrepancy, we have followed the decay of a sample of actinium using the differential ionization chamber employed by Segrè, Wiegand, and Leininger in the course of their studies[4,5] of the influence of chemical binding on the decay constant of Be^7.

The sample of actinium used in these measurements was produced and separated in 1947 from pile irradiated radium at the Argonne National Laboratory. Because of its age, the actinium can safely be assumed to be in secular equilibrium with the daughter products in its decay chain. A second sample, kindly furnished us by F. Hagemann in January, 1950, has also been observed. This sample, however, has not yet reached equilibrium and will be followed further. At present, therefore, the results obtained with the older sample alone should be considered as preliminary.

Determination of long periods by the differential technique rests upon the fact that during the course of the measurement $\lambda t \ll 1$ and that the decay is essentially linear. By expansion of the exponential in the first-order decay law $N(t)=N(0)e^{-\lambda t}$ and retention of only the linear term, one has

$$N(t)=N(0)-\lambda N(0)t$$

or in terms of activities,

$$A(0)-A(t)=A(0)\lambda t.$$

One uses a sample of actinium of strength $A_x(t)$ balanced in activity as closely as possible with a Bureau of Standards radium source of strength $A_r(t)$ such that $A_x(0)=A_r(0)$. Because of the constancy of the radium standard, $A_r(t)=A_r(0)=A_x(0)$. Thus, $A_r(t)-A_x(t)=A_x(0)\lambda t$. Defining the quantity $A_r(t)-A_x(t)$ as $\delta(t)$, the unbalance of the samples at time t, one has

$$\lambda=\delta(t)/A_x(0)\cdot t.$$

One must therefore measure $\delta(t)$ as a function of time. Provided

that $A_x(0)$ can be determined with comparable relative precision, the decay constant of the actinium can be found.

Differential measurement enjoys several advantages over separate measurement of standard and unknown: measuring the samples at the same time and interchanging them minimizes systematic errors; the readings on the difference of the two activities are always small and with ionization chambers are much more convenient to take than readings on the activities; it is practical to use considerably stronger samples than for single readings.

The differential chamber has been amply described by Segrè and Wiegand.[4]

Our measuring procedure was as follows. The actinium sample is placed in chamber 1 and the radium standard in chamber 2; the rate of drift of the galvanometer is then

$$p=A_x(t)S_1-A_r(t)S_2,$$

where S_1 and S_2 are the sensitivities of chambers 1 and 2, respectively, and are very nearly equal. When the samples are interchanged, the rate of drift becomes

$$q=A_r(t)S_1-A_x(t)S_2,$$

from which

$$p-q=[A_x(t)-A_r(t)](S_1+S_2)$$
$$\cong -2\delta(t)\cdot S$$
$$\delta(t)\cong -(p-q)/2S.$$

The initial rate of drift due to the actinium sample alone, $a(0)$, is then measured. Since $a(0)=A_x(0)\cdot S$,

$$A_x(0)=a(0)/S.$$

But we had from the decay law that

$$t_{\frac{1}{2}}=0.693A_x(0)\cdot t/\delta(t).$$

Substituting from above for $\delta(t)$ and $A_x(0)$, we obtain

$$t_{\frac{1}{2}}=-0.693\cdot a(0)/(p-q/2t).$$

We have measured $(p-q)$ over a period of about 100 days and have found $(p-q)/t$ to be -0.05916 ± 0.00020 (mm/sec.)/day. Also, the initial activity of the actinium sample, corrected for decay, was $a(0)=343.7\pm2.9$ mm/sec.

From these data, the half-life of actinium is calculated to be 22.0 ± 0.3 years, comparing favorably with the value offered by Curie and Bouissières.

We wish to thank Professors E. Segrè and I. Perlman for their helpful suggestions during the course of this experiment.

* This work was performed under the auspices of the AEC.

[1] G. T. Seaborg and I. Perlman, Rev. Mod. Phys. 20, 585 (1948).
[2] I. Curie and G. Bouissières, Cahiers phys., No. 26, 1 (1944).
[3] St. Meyer, *et al.*, Rev. Mod. Phys. 3, 427 (1931).
[4] E. Segrè and C. Wiegand, Phys. Rev. 75, 39 (1949).
[5] Leininger, Segrè, and Wiegand, Phys. Rev. 76, 897 (1949).

Large Angle Scattering of π^--Mesons*

H. Bradner and B. Rankin
Radiation Laboratory, University of California, Berkeley, California
October 5, 1950

AN investigation is being made of the mean free path for large angle scattering and nuclear interaction of π^--mesons in G-5 emulsion. Mesons entering the edge of a plate with approximately 38-Mev energy are identified by measurement of grain density *versus* small angle scattering. These mesons are then followed for several millimeters until they leave the 600 μ-thick emulsion or reach an energy of 30 Mev. In a scan of 568 cm of meson track the scatters tabulated in Table I have been observed. There were also five cases in which an energetic meson produced a star, and two cases in which a meson ended abruptly with no visible star or scatter.

The average nuclear area for the elements in a G-5 emulsion is equivalent to a mean free path of 23 cm. Within the limits of the poor statistics it appears that the cross section for large angle scattering and star production of 20–38 Mev π^--mesons in emulsion are each roughly equal to one-half of the nuclear area. The disappearance of mesons in flight may be evidence for charge exchange scattering on a proton, although we cannot rule out the possibility that there was a star in which only a neutron was emitted, or a large angle scatter in which we were unable to follow the outgoing meson.

TABLE I. Observed scattering for 20–40 Mev π^--mesons in emulsion.

Scattering angle			Meson energy (Mev)	
Horizontal projection	Actual	No. events	By position in plate	By grain count (±5 Mev)
5°– 9.9°	1@46°	96	1@36.0	40
10°–19.9°		29		
20°–29.9°	1@30.5	2	1@35.0	35
29°	36.6	1	34.5	40
30°	35	1	26.5	40
40°	48	1	37.0	40
47°	76	1	36.0	25
108°	105	1	28.5	30
119°	112	1	32.0	25
143°	123	1	37.0	<20*
158°	154	1	26.0	30
171°	155	1	36.0	25
178°	160	1	34.5	40

* Definitely inelastic scattering.

Scatters less than 30° for 30 Mev π-mesons can certainly not be considered as "nuclear," since either Coulomb scatter or decay in flight could result in nearly that angle. Grain density *versus* scattering measurements cannot distinguish with certainty between a π-scatter and a π-μ-decay in our energy region. The mean free path for decay in flight is approximately 230 cm. A frequency plot of scatters between 5° and 30° is in agreement with single Coulomb scattering.

Dr. G. Bernardini of Columbia University has kindly communicated to us the prepublication results on a very similar experiment being performed on the Columbia cyclotron. The two experiments show a difference in relative numbers of stars *versus* scatters which seems to be outside of statistics. We believe that this is probably due to a difference in scanning techniques. Bernardini scans an area of plate looking for stars and scatters whereas we follow individual tracks to determine what happens to them.

We wish to express our appreciation to O. Piccioni who originally suggested the experiment, and to L. W. Alvarez for helpful discussion. Edith Goodwin has done much of the plate scanning.

* This work was performed under the auspices of the AEC.

The Branching Ratio of K^{40} Radioactive Decay

Mark G. Inghram, Harrison Brown, Clair Patterson, and David C. Hess
Institute for Nuclear Studies and Argonne National Laboratory, Chicago, Illinois
October 5, 1950

THE ratio of K-capture to beta-emission for the naturally occurring radioactive isotope K^{40} has been determined using the mass spectrometric isotopic dilution method.[1] In this method the amounts of the daughter isotopes A^{40} and Ca^{40} in a geologically old potassium sample are determined by addition of a known quantity of a tracer isotope of the element in question, and determining the element content of the ore from the resulting change in the isotopic composition of the tracer material. Previous measurements of the branching ratio have used counting techniques or age data to get the beta-decay rate, and counting techniques or argon extraction data to get the K-capture.[2–7]

The sample used in this investigation was a 1×10^8-year old KCl sample from the Stassfurt sylvite deposits. The sample was divided into four aliquots. Two were used for the A^{40} content and two for the Ca^{40} content. The agreement between the various runs

TABLE I. Measured isotopic ratios of argon.

Sample	A^{40}/A^{36}	A^{38}/A^{36}
Tracer	1.172 ±0.001	0.02242 ±0.00002
4.90 cm/cc. tracer +197.8 g sylvite	2.633 ±0.002	0.02239 ±0.00002

indicate that the composition of the sample was constant within the errors of the experiment.

The argon content was determined by placing 197.8 g of sylvite in a quartz furnace and evacuating at room temperature for 12 hours. At this point 4.90 cc of tracer argon with an A^{40}/A^{36} ratio of 1.172 was added to the volume and heating started. The temperature was held at 1050°C for one hour. At this temperature the KCl was refluxing vigorously. The gas over the molten sylvite was finally mixed by sorption and desorption from charcoal three times. The gases were then purified in a greaseless system. The purification train consisted of a CuO_2 furnace at 400°C, a KOH trap, an $Mg(ClO_4)_2$ dryer and finally a calcium furnace. The gas was treated in the system to constant volume. The excess A^{40} in this sample was then determined by the increase at the A^{40} position as measured on a mass spectrometer. The results are shown in Table I. Within the limits of error of the A^{38}/A^{36} ratio shown in Table I there is no atmospheric argon in the sylvite. In order to check this more accurately the second aliquot of sylvite was run through the procedure without the addition of tracer material. The argon obtained was 99.0±0.5 percent radiogenic. The chemical purity of the tracer argon was determined by dilution of a known volume of the tracer material with a known volume of Linde spectroscopic argon, and measurement of the mixture ratio on the mass spectrometer. Combining the factors the A^{40} content of this particular sylvite sample is 0.360±0.007 p.p.m. by weight.

To measure the Ca^{40} content two samples containing 10.770 and 8.849 g, respectively, of sylvite were used. To each was added a weighed quantity of the separated isotope Ca^{48}, the purity of which was checked by dilution against normal CP calcium. The complete sample was then brought into solution to insure mixing. The first stage of chemical purification was fractional crystallization. After the KCl had been depleted by a factor of 10 the Ca was precipitated with oxalate[8,9] and washed two times to reduce the potassium. It was then reprecipitated with oxalate and rewashed twice. The diluted Ca^{48} was then compared with the tracer Ca^{48} to determine the Ca^{40} content and the normal calcium content of the sylvite. The results are shown in Table II. From the change in the Ca^{44} peak the "normal" calcium impurity in the KCl was determined. The excess Ca^{40} over this impurity was 2.82±0.02 p.p.m. in the first case and 2.87±0.03 p.p.m. in the second.

Combining the above individually determined radiogenic A^{40} and Ca^{40} contents gives the ratio of *K*-capture to beta as 0.1263 ±0.0027. Due to systematic errors we do not believe this result to be of the precision accuracy given, but it is believed the result is good to ±4 percent. This error does not include errors due to possible loss of A^{40} or Ca^{40} from the sample during geologic times. It can, however, be considered as a lower limit since any alteration would affect the A^{40} content more strongly than the Ca^{40}. The agreement of this value for the branching ratio with the most recent counting value of 0.136 determined by Sawyer and Wiedenbeck[7] indicates that leakage in this sample was not serious. It should be noted that this branching ratio is sufficient to account for the A^{40} in the atmosphere.

TABLE II. Measured isotopic ratios of calcium.

Sample	40/48	44/48
Ca^{48} spike	0.585 ±0.001	0.02042 ±0.00005
91.5γ Ca^{48} +8.849 g sylvite Ca	1.040 ±0.002	0.02316 ±0.00007
91.5γ Ca^{48} +10.770 g sylvite Ca	1.157 ±0.003	0.02396 ±0.00007

We wish to thank Professor W. W. Watson of Yale for supplying the A^{36} tracer used in this experiment. The Ca^{48} tracer was supplied from the Y-12 Plant of Oak Ridge on allocation from the Isotopes Division of the AEC.

[1] J. H. Reynolds, Phys. Rev. **79**, 789 (1950).
[2] E. Bleuler and M. Gabriel, Helv. Phys. Acta **20**, 67 (1947).
[3] L. B. Borst and J. J. Floyd, Phys. Rev. **74**, 989 (1948).
[4] L. H. Ahrens and R. D. Evans, Phys. Rev. **74**, 279 (1948).
[5] H. E. Suess, Phys. Rev. **73**, 1209 (1948).
[6] L. T. Aldrich and A. O. Nier, Phys. Rev. **74**, 876 (1948).
[7] G. A. Sawyer and M. L. Wiedenbeck, Phys. Rev. **79**, 490 (1950).
[8] G. H. Ellis, Anal. Chem. **10**, 112 (1938).
[9] P. L. Kirk and E. G. Moberg, Anal. Chem. **5**, 95 (1933).

The Precision Determination of Some Half-Lives*

JAMES W. COBBLE AND R. W. ATTEBERRY
Chemistry Division, Oak Ridge National Laboratory, Oak Ridge, Tennessee
October 5, 1950

THE decay periods of several radioactive nuclides have been measured at this Laboratory using sources which were bombarded in the Oak Ridge National Laboratory pile and subsequently purified by ion-exchange column techniques using both cation and the new strong base anion exchangers. The activity was followed by a 4π-geometry ionization chamber filled to 40 atmos. with argon. This chamber was connected through a "vibrating reed" electrometer to a recording potentiometer which continuously records the *instantaneous* value of the activity as a function of time. The instrument had been previously calibrated to determine the effects of ion-recombination, scale drift, etc. Such a procedure is of great advantage with the shorter periods, and the arrangement is capable of a very high precision.

Results for four nuclides are given in Table I.

TABLE I. Half-lives of nuclides.

Isotope	$T_{\frac{1}{2}}$ (this research)	$T_{\frac{1}{2}}$ (previously recorded values)
Na^{24}	15.10±0.04 hr.[a]	14.8±0.1;[b] 15.04±0.06[c]
Cl^{38}	37.29±0.04 min.	37.0±0.3;[b] 38.5 ±0.5[d]
Br^{82}	35.87±0.05 hr.	33.9±0.3;[e] 36.0 ±0.1[f]
Tc^{96}	4.20±0.04 days[g]	4.2±0.1;[h] 4.25±0.05[i]

[a] Errors estimated from reproducibility in duplicate determinations.
[b] S. N. Van Voorhis, Phys. Rev. **49**, 889 (1936).
[c] A. K. Solomon, Phys. Rev. **79**, 403 (1950).
[d] N. Hole and K. Siegbahn, Arkiv Mat., Astron. Fys., **33A**, 9 (1946).
[e] A. H. Snell, Phys. Rev. **52**, 1007 (1937).
[f] E. Berne, Phys. Rev. **77**, 568 (1950).
[g] Sample prepared from a Mo(*d*, *n*) reaction; the larger error in this isotope is due to uncertainties in the subtraction of the longer-lived Tc^{95}.
[h] J. E. Edwards and M. L. Pool, Phys. Rev. **69**, 253 (1946).
[i] G. E. Boyd, private communication.

In the case of Na^{24} and Br^{82}, this work confirms the longer periods recently reported (references c and f of Table I).

* This document is based on work performed for the AEC at Oak Ridge National Laboratory.

The Virial Theorem and the Variation Principle

IRVIN ISENBERG
Institute for the Study of Metals, University of Chicago, Chicago, Illinois
October 9, 1950

IT has been called to the author's attention that the theorem proven in a Letter to the Editor,[1] under the above title, was originally proven by V. Fock.[2] The author regrets not being familiar with this work prior to publication of the letter.

[1] I. Isenberg, Phys. Rev. **79**, 737 (1950).
[2] V. Fock, Zeits. f. Physik **63**, 855 (1930).

Note on the Inertia and Damping Constant of Ferromagnetic Domain Boundaries

C. KITTEL*
Bell Telephone Laboratories, Murray Hill, New Jersey
October 5, 1950

THE Bloch wall is the transition layer separating adjacent ferromagnetic domains. In the presence of a magnetic field a free wall moves as if endowed with mass and as if retarded by damping forces. The effective mass of a moving Bloch wall was calculated by Döring,[1] and recently Becker[2] has given a simplified treatment leading to the same result. The associated damping effect in substances in which eddy current losses may be neglected was calculated by Landau and Lifschitz.[3] Both the inertial and damping effects have been observed experimentally,[4] and they play important roles in magnetization processes in the ferrites at high frequencies.

The present letter generalizes the Döring equation in order to include the case where the intrinsic relaxation frequency of the substance is high; we then apply the device introduced by Becker to the Landau-Lifschitz problem, thereby greatly simplifying the calculation and giving insight into the physical mechanism of the wall damping, and extend the calculation to cubic crystals.

Becker noticed that the rotational motion of the local magnetization which accompanies the uniform motion of a Bloch wall (with velocity v in the z-direction normal to the wall) may be described as caused by an effective field $H_e(z)$ such that the resulting precessional velocity $d\varphi(z)/dt$ is equal to the rotational velocity required by the motion. We have

$$d\varphi/dt=-v(d\varphi/dz)=\gamma^*H_e, \tag{1}$$

with

$$(\gamma^*)^2=\gamma^2+(\lambda^2/M_s^2), \tag{2}$$

where $\gamma=ge/2mc$, and the relaxation frequency λ is defined by Eq. (5) below; the relaxation frequency may be estimated from the line width in a microwave resonance experiment. Döring and Becker write γ instead of γ^* in Eq. (1), and in this sense our equation is more general. The kinetic energy of the wall is given by the field energy, so that, per unit area,

$$\delta\sigma=\sigma-\sigma_0=(1/8\pi)\int H_e^2dz=(v^2/8\pi\gamma^{*2})\int_{-\infty}^{\infty}(d\varphi/dz)^2dz, \tag{3}$$

σ_0 being the surface energy of the wall at rest. Now $\int(d\varphi/dz)^2dz$ occurs in the elementary theory of the Bloch wall[5] and is in fact equal to $\sigma_0/2A$, A being the usual exchange factor.[5] The generalization of the Döring result follows dierctly:

$$\delta\sigma=\sigma_0v^2/16\pi\gamma^{*2}A. \tag{4}$$

In calculating the damping effects we start from the equation of motion for the magnetization:

$$d\mathbf{M}/dt=\gamma\mathbf{M}\times\mathbf{H}-\lambda[(\mathbf{H}\cdot\mathbf{M})\mathbf{M}/M^2-\mathbf{H}], \tag{5}$$

where λ is the relaxation frequency. The power dissipation per unit volume is $\mathbf{H}\cdot(d\mathbf{M}/dt)\cong\lambda H_e^2$, so that the power per unit area which must be supplied to keep the spins in uniform motion is

$$\int_{-\infty}^{\infty}\mathbf{H}\cdot(d\mathbf{M}/dt)dz=\lambda\int_{-\infty}^{\infty}H_e^2dz=8\pi\lambda(\delta\sigma)=v^2\lambda\sigma_0/2\gamma^{*2}A. \tag{6}$$

The power supplied by the constant external field H_0 which drives the wall along is $2H_0M_sv$ per unit area; we equate this to the dissipation, and find the result

$$v=4(\gamma^2M_s^2+\lambda^2)AH_0/\lambda M_s\sigma_0. \tag{7}$$

Now for a wall parallel to the axis of a uniaxial crystal $\sigma_0=4(AK_1')^{\frac{1}{2}}=4A\Delta$, where $\Delta=(A/K_1')^{\frac{1}{2}}$ is the usual wall thickness parameter, so that in this case $v_{\text{uniaxial}}=(\gamma^2M_s^2+\lambda^2)\Delta H_0/\lambda M_s$, which is exactly the Landau-Lifschitz result. Our Eq. (7) applies however to plane walls in general. For a 180° wall in an (001) plane of a cubic crystal, $\sigma_0=2(AK_1)^{\frac{1}{2}}$, so that $v_{(001)}=2(\gamma^2M_s^2+\lambda^2)\Delta H_0/\lambda M_s$, where $\Delta=(A/K_1)^{\frac{1}{2}}$.

It should be noted that any result involving λ is in general no better than Eq. (5) defining λ in a phenomenological way; the applicability of this equation is by no means assured by existing microwave resonance results.

I wish to thank Dr. J. K. Galt and Dr. Conyers Herring for a helpful conversation.

* Present address: Department of Physics, University of California, Berkeley, California.

[1] W. Döring, Z. Naturforsch. 3, 373 (1948).
[2] R. Becker, Proceedings of the Grenoble Conference, July, 1950.
[3] L. Landau and E. Lifschitz, Physik. Z. Sowjetunion 8, 153–169 (1935).
[4] G. T. Rado, R. W. Wright, and W. H. Emerson, Phys. Rev., to be published; a discussion of other evidence is given by C. Kittel, Proceedings of the Grenoble Conference, July, 1950.
[5] See, for example, C. Kittel, Rev. Mod. Phys. 21, 541 (1949); ibid., pp. 560–565.

Radiative Capture of Neutrons in Deuterium

B. B. KINSEY AND G. A. BARTHOLOMEW
Division of Atomic Energy, National Research Council of Canada
Chalk River, Ontario, Canada
October 9, 1950

IN a study of the γ-rays produced in the reacting vessel of the heavy water pile at this laboratory we have found only two strong peaks in the coincidence spectrum of our pair spectrometer. These peaks are superposed on a continuous unresolved background. One of these, corresponding to a γ-ray with an energy of 7.72 Mev, is due to the capture of neutrons in aluminum. The other peak is shown by the full line (A) in Fig. 1, where the coincidence counting rate is plotted against the energy. It is produced by a γ-ray with an energy of 6.244±0.008 Mev. This γ-ray is attributed to the capture of neutrons by deuterium for, as shown below, its energy is very close to the expected binding energy of the triton and its intensity has the value expected. The continuous background is due to uranium and to the other constituents of the pile. The only materials which are likely to produce a strong peak superposed on this background are those which, like Cu, Al, etc., emit very intense homogeneous γ-rays. We have found very few such elements and none of these emit a γ-ray at 6.24 Mev.

We have made a rough estimate of the relative peak coincidence counting rates of the 6.2 and 7.7 Mev-γ-rays to be expected if the former is due to capture in deuterium. In this calculation we have taken into account the geometry of the pile and measurements of the distribution of neutron flux near the periphery of the reactor. No excited states are known in H^3 and we assume therefore that

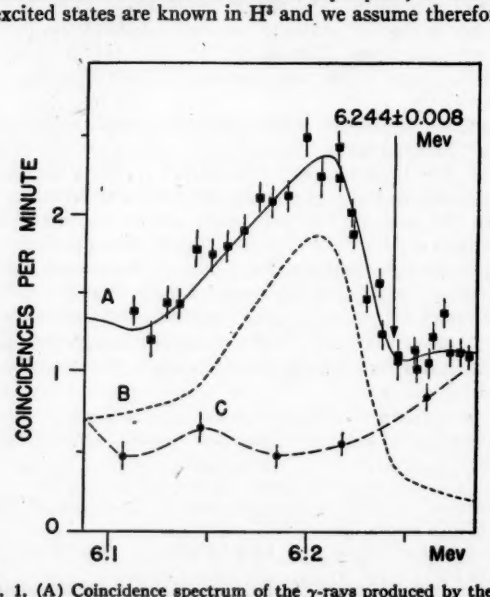

FIG. 1. (A) Coincidence spectrum of the γ-rays produced by the heavy water pile near 6.2 Mev. (B) Pile radiation with aluminum spectrum subtracted. (C) Contribution to the spectrum due to pure aluminum.

one γ-ray only is produced per capture. Neglecting the capture cross section of oxygen we assume further that the cross section of deuterium is one-half of that obtained by Sargent and his collaborators[1] for the D_2O molecule (0.92 mb). For the cross section of aluminum we use the value 220 mb. From our measurements of the capture γ-ray spectrum of aluminum[2] we find that the 7.72-Mev γ-ray is radiated in 40 percent of the captures in that element. With these figures we find that the peak coincidence counting rate of the deuterium γ-ray should be about 0.07 of that of the 7.72 Mev aluminum γ-ray. The ratio observed was 0.08. The agreement is good but it may be accidental for such a calculation is difficult to make with precision. The error might amount to 30 percent.

In our method of measurement the energy of the γ-ray is determined from the end point of the coincidence peak. Near 6.2 Mev it seemed possible that the shape of the peak produced by that γ-ray was modified and the position of its end point was shifted by the presence of γ-rays produced by aluminum in the pile. To examine this possibility we have studied the spectrum produced by pure aluminum using the same resolving power. A part of this spectrum is shown by curve C in Fig. 1. The ordinates of this curve have been adjusted so that the peak coincidence counting rate for the 7.72-Mev aluminum γ-ray is equal to that produced by the aluminum in the pile. The difference between the two curves, given as curve B in Fig. 1, represents the contribution to the pile spectrum produced by neutron capture in deuterium and other constituents. It is clear that this subtraction does not shift the end point of the 6.2-Mev peak.

The binding energy of the triton, obtained by adding the recoil energy of that nucleus to the γ-ray energy, is 6.251 ± 0.008 Mev. This result is in good agreement with the binding energy obtained from disintegration data. According to Tollestrup, Fowler, and Lauritsen[3] the best value of the Q of the reaction $D^2(d,p)T^3$ is 4.032 ± 0.022 Mev. Adding to this the binding energy of the deuteron,[4] 2.230 ± 0.007 Mev the binding energy of the triton is 6.262 ± 0.023 Mev.

[1] Sargent, Booker, Cavanagh, Hereward, and Niemi, Can. J. Research A25, 134 (1947).
[2] The details of this spectrum will be published shortly.
[3] Tollestrup, Fowler, and Lauritsen, Phys. Rev. 78, 372 (1950).
[4] R. E. Bell and L. G. Elliott, Phys. Rev. 79, 282 (1950).

Pressure Dependence of Resistance of Germanium*

JULIUS H. TAYLOR†
Randal Morgan Laboratory of Physics, University of Pennsylvania, Philadelphia, Pennsylvania
September 22, 1950

AN intrinsic semiconductor may exhibit a relatively large change in electrical resistivity with hydrostatic pressure due to the change in band structure which accompanies a compression of the lattice; the concomitant changes in Debye temperature and electron mass produce relatively small effects upon the resistivity. In germanium the application of hydrostatic pressure increases the forbidden band width, decreases the number of free holes and electrons and hence increases the resistivity.

The equations connecting the change in resistivity $\Delta\rho$ with the change in energy gap ΔE_G may be derived in the following way. It is known that the product of the electron concentration n_e and hole concentration n_h remains constant for fixed temperature and pressure as the concentration of impurity atoms is varied:

$$n_e n_h = C^2. \tag{1}$$

If one considers the dependence on gap width and temperature,

$$n_e n_h = C' \exp(-E_G/kT),$$
$$C' = 4(2\pi mkT/h^2)^3(m_e m_h/m^2)^{\frac{3}{2}}, \tag{2}$$

where m_e and m_h are the masses of electrons and holes respectively, and the other symbols have their usual meaning. The resistivity is given in terms of the mobilities μ_e and μ_h by

$$1/\rho = e(n_e\mu_e + n_h\mu_h). \tag{3}$$

If one assumes that only E_G changes with hydrostatic pressure and that the number of impurity atoms which are ionized is constant, then at constant temperature

$$(\Delta\rho/\rho) = (\mu_e+\mu_h)n_e n_h \Delta E_G/(n_e+n_h)(n_e\mu_e+n_h\mu_h)kT. \tag{4}$$

This equation is very simple for the case of an intrinsic semiconductor (for which $n_e = n_h = C$):

$$(\Delta\rho/\rho)_{\text{pure}} = \Delta E_G/2kT; \tag{5}$$

but, as it is often necessary to make pressure measurements at temperatures below the intrinsic range owing to the impurity content of the material, the general form of Eq. (4) must be retained. However, it may be expressed in terms of more convenient parameters by letting $c=\mu_e/\mu_h$ and $x=C/n_e$, so that

$$(\Delta\rho/\rho) = x^2(c+1)\Delta E_G/(x^2+c)(x^2+1)kT. \tag{6}$$

The value of c is assumed to be 1.5 and x is determined from resistivity measurements which may be easily extended well into the intrinsic temperature range if the material is reasonably pure. Thus, at any given temperature at which $\Delta\rho/\rho$ is observed the ratio

$$\rho_{\text{pure}}/\rho = (c+x^2)/[x(c+1)] \tag{7}$$

may be used to calculate the corresponding value of x and hence to obtain $(\Delta\rho/\rho)_{\text{pure}}$ from Eqs. (5) and (6). Here, ρ_{pure} refers to the resistivity value obtained by extrapolation from high (intrinsic) temperature measurements to the temperature at which the pressure measurements are made. If the samples are inhomogeneous with regard to distribution of impurity atoms, the correction factor of Eq. (6) is too large. Consequently, observations requiring large correction factors have been weighted lightly in obtaining the average. The values $(\Delta\rho/\rho)_{\text{pure}}$ computed from observations taken at different temperatures have been reduced by an inverse temperature factor to values at 300°K for purposes of intercomparison; this reduction is based on Eq. (4) and the further assumption that $\Delta E_G/\Delta P$ is independent of pressure and temperature.

TABLE I. Summary of experimental data and calculation.

Sample	T °K	$(\Delta\rho/\rho)$ $\times10^6$ (per atmos.)	$\rho_{\text{pure}}/\rho_{\text{obs}}$	Correction factor	$(\Delta\rho/\rho)_{\text{pure}}$ $\times10^6$ (per atmos.)	$(\Delta\rho/\rho)_{300°K}$ $\times10^6$ (per atmos.)	Weight used in average
A	475*	2.1	2.5	5.3	11.1	18.0	1
B	297	1.5	3.4	9.6	14.4	14.3	0
	352	5.5	1.25	1.44	7.9	9.3	2
	373	7.0	1.1	1.18	8.2	10.2	3
	413	6.9	1	1.00	6.9	9.5	5
	428	7.0	1	1.00	7.00	10.0	5
C	299	1.7	6.0				
	352	4.1	1.6	2.22	9.1	10.8	2
	413	7.7	1	1.00	7.7	10.6	5
	428	7.3	1	1.00	7.3	10.4	5
D	361*	1.6	2.4	4.8	7.7	9.3	1
	413	5.5	1.15	1.25	6.9	9.5	2
	428	6.2	1.05	1.1	6.8	9.7	3
					Weighted average	10.2	

* Measurements taken at peak of resistivity.

The experimental observations were taken on germanium samples of high purity enclosed in a steel tube which was submerged in a boiling liquid to keep the temperature constant to about 0.01°C. Pressures up to 4500 lb/in.^{2} were applied to the sample through silicone oil which completely filled the tube; glass wool inside the tube and an auxiliary heater at the top of the tube were used to prevent circulation of the oil. The results of the measurements and calculations are shown in Table I. A weighted

average $(\Delta\rho/\rho)_{\text{pure}}=10.2\pm0.4\times10^{-6}$/atmos. was obtained for the pressure coefficient of resistance of germanium at 300°K. Assuming a compressibility 1.4×10^{-6}/atmos. and a coefficient of linear expansion 8×10^{-6}/°C leads to a value $\Delta E_G/\Delta T=-0.87\times10^{-4}$ ev/°C.

This result is, with one exception, in excellent agreement with calculations from other experiments. Shockley and Bardeen[1] found for this constant the value -0.9×10^{-4} ev/°C using data on the mobilities of holes and electrons; their result is proportional to $m_e^{5/4}$. Johnson and Fan[2] have estimated from data on the temperature dependence of the Hall effect a value -1.1×10^{-4} ev/°C. Correction of this result by subtraction of the contribution of the lattice vibrations computed by Fan[3] leads to the value -1.0×10^{-4} ev/°C for the contribution of the volume effect alone. Only the latter value is comparable to the results of the pressure measurements; the uncorrected result of Johnson and Fan, which depends on $(m_e m_h)^{5/4}$, includes both the volume effect and the change in lattice vibrations which accompany a change in temperature. Fan,[4] using data from optical absorption measurements found the quite different value -4.0×10^{-4} ev/°C.

* This work was supported by the BuShips. A more extended account will be found in Technical Report No. 22, copies of which can be obtained by addressing P. H. Miller, Jr., Randall Morgan Laboratory.
† Now at Morgan State University, Baltimore, Maryland.
[1] W. Shockley and J. Bardeen, Phys. Rev. 77, 407 (1950).
[2] V. A. Johnson and H. Y. Fan, Phys. Rev. 79, 899 (1950).
[3] H. Y. Fan, *Proceedings of Conference on Properties of Semiconducting Materials* (Butterworth's Scientific Publications, Ltd., London, 1951).
[4] H. Y. Fan, Phys. Rev. 78, 808 (1950).

Penetrating Showers of Cosmic Rays

ANDRÉ G. VOISIN*
Division of Physics, National Research Council of Canada, Ottawa, Canada
October 9, 1950

AN experiment has been carried out at sea level in which the relative penetration of local penetrating showers was investigated as a function of their lateral spread. Figure 1 shows the experimental arrangement of the counters and lead absorbers. The figure is drawn to scale except that the upper absorber P_1 was 35 cm thick. The counters M were connected in fivefold coincidence. The analyzer counters A_1, A_2, B_1, B_2, C_1, C_2, each connected in coincidence with the fivefold coincidence M, indicated the lateral spread of the showers of which the range was measured by coincidence with K and L. This arrangement of coincidences reduces the error due to secondaries from a single meson to 6 percent or less. To discharge one of the analyzer counters in coincidence with M, a single meson would have to produce at least three successive knock-on electrons. The group of counters S allowed the discrimination between local showers and Auger showers.

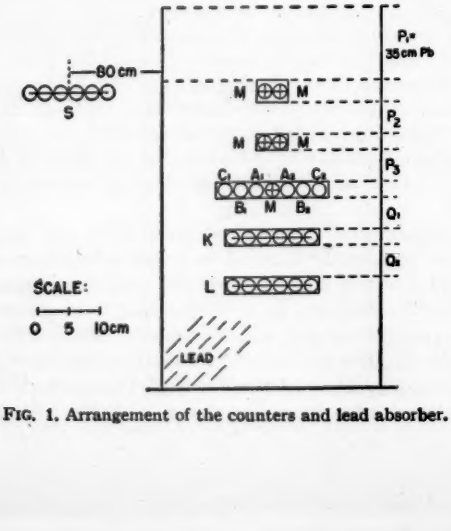

FIG. 1. Arrangement of the counters and lead absorber.

TABLE I. The lateral spread gives the separation in number of counters between the most remote particles of the showers.

Lateral spread	2	3	4	5	6	7
Showers per hour						
stopped in Q_1=5 cm Pb	0.022	0.026	0.022	0	0	0
stopped in Q_2=5 cm Pb	0.017	0.017	0.013	0.013	0.009	0
penetrating Q_1+Q_2	0.043	0.061	0.077	0.048	0.030	0.069
Total rate (per hour)	0.082 ±0.018	0.104 ±0.021	0.112 ±0.022	0.061 ±0.016	0.039 ±0.013	0.069 ±0.017
Stopped in (Q_1+Q_2) / Total rate ×100	48%	41%	31%	21%	23%	0

The results indicate that *the most penetrating showers are the most divergent*. It can be seen from Table I that nearly 50 percent of the narrower showers are stopped in the absorber $Q_1+Q_2=10$ cm Pb, whereas most of the larger showers include particles which can penetrate these absorbers. This unexpected result, however, is not inconsistent with the theoretical calculations of Peyrou, d'Espagnat, and Leprince-Ringuet.[1] Figure 2 also shows that the relative range of the showers is increasing with their divergence.

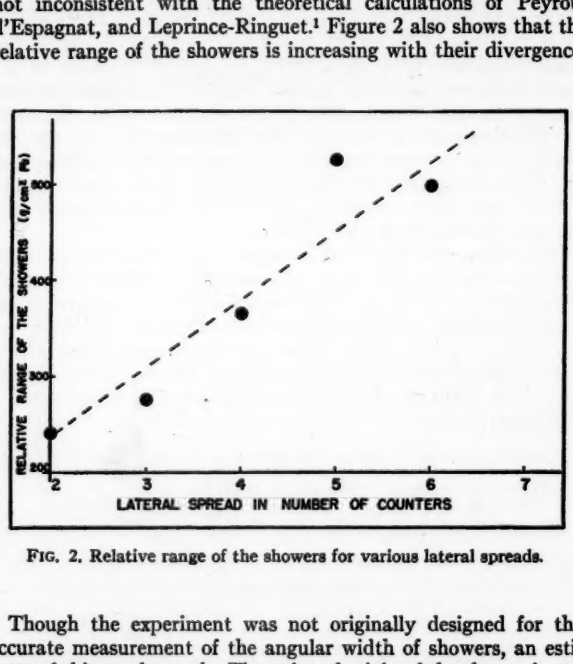

FIG. 2. Relative range of the showers for various lateral spreads.

Though the experiment was not originally designed for the accurate measurement of the angular width of showers, an estimate of this can be made. The point of origin of the shower is not indicated by the counter arrangement, but assuming this to be within 5 cm from the top of the upper absorber, P_1 (this distance corresponds to a cross section of the same order as the geometrical cross section of the nucleus[2]) the measurements indicate that the average angular spread is represented by a cone having a half angle of 15°. Walker[3] has shown that the directional distribution of primary particles producing penetrating showers varies rapidly with zenith angle. It is assumed, therefore, that most of the showers defined by the fivefold coincidence M are produced by primaries in a vertical direction and the angular spread may be referred to the direction of the primary.

The number of analyzer counters $A_1, \cdots, C_2$ discharged per shower gives a lower limit of the multiplicity. It is found that the multiplicity averages at least 3.7 penetrating particles per shower.

A more extensive account of these experiments is being prepared for publication.

The author would like to thank the National Research Council of Canada for the use of the laboratory facilities and Dr. A. Rogozinski and Dr. D. C. Rose for their assistance and suggestions.

* Attaché de recherches au Centre National de la Recherche Scientifique, Paris. Holder of a National Research Council postdoctorate fellowship.
[1] B. d'Espagnat and Ch. Peyrou, Comptes Rendus 228, 674 (1949); Peyrou, d'Espagnat, and Leprince-Ringuet, Comptes Rendus 228, 1777 (1949).
[2] L. Jánossy and Broadbent, Nature 155, 142 (1945).
[3] W. D. Walker, Phys. Rev. 77, 686 (1950).

High Energy Neutron Scattering by Nuclei*

SIMON PASTERNACK AND HARTLAND S. SNYDER
Brookhaven National Laboratory, Long Island, New York
October 9, 1950

THE so-called transparent model[1] of a nucleus seems to be a useful model in treating the scattering of 90-Mev neutrons by nuclei, since the nuclear radii fitted from experiment by this model agree well with an $A^{\frac{1}{3}}$ law.[2] However, the calculated differential scattering cross sections deviate somewhat from the experimental observations,[3] the latter being 10 to 20 percent higher at low scattering angles.

The differential scattering calculations for the transparent model were made by assuming the nucleus to be representable by a square well with potential 30.8 Mev, plus absorption, leading in the classical (W.K.B.) approximation to a sphere with a complex constant index of refraction. The angular distribution amplitude was found to be

$$f(\theta)=k\int_0^R\{1-\exp[(-K+2ik_1)(R^2-\rho^2)^{\frac{1}{2}}]\}J_0(k\rho\sin\theta)\rho d\rho,$$

where k is the neutron wave number, K is the absorption coefficient, and k_1/k the real part of the index of refraction. This integral was evaluated by converting it to a sum of approximately kR terms.

The integral for $f(\theta)$ can be evaluated by means of a series representation due to Van de Hulst,[4] viz.,

$$f(\theta)=kR^2\left\{\frac{J_1(z)}{z}-\frac{\rho}{w^3}e^{iw}(1-iw)+\frac{J_0(z)}{\rho^2}-\frac{1\cdot3zJ_1(z)}{\rho^4}+\frac{1\cdot3\cdot5z^2J_2(z)}{\rho^6}-\cdots\right\},$$

where

$$\rho=(2k_1+iK)R;\quad z=kR\sin\theta;\quad w=(\rho^2+z^2)^{\frac{1}{2}}.$$

This series for $f(\theta)$ is particularly useful for large mass nuclei and for high energies, for which kR (the approximate number of terms in the summation method) is large. Van de Hulst derived this formula by a double series expansion of $f(\theta)$ in powers of z and ρ. A simpler proof can be obtained by writing

$$f(\theta)=kR^2\left\{[J_1(z)/z]+i(\partial/\partial\rho)\int_0^{\frac{1}{2}\pi}e^{i\rho\cos\gamma}J_0(z\sin\gamma)\sin\gamma d\gamma\right\}.$$

If we define

$$I_n=\int_0^{\frac{1}{2}\pi}J_n(z\sin\gamma)e^{i\rho\cos\gamma}\sin\gamma d\gamma/(z\sin\gamma)^n,$$

then integration by parts yields

$$I_n=(e^{i\rho}/2^n n!i\rho)-[J_n(z)/z^n i\rho]+2z^2\partial I_{n+1}/\partial\rho^2.$$

Repeated integrations by parts yield the series for $f(\theta)$.

Since the complex constant index of refraction is equivalent to the assumption of a square well with a complex constant potential, it was considered desirable to check the validity of the classical approximation by making an exact partial wave analysis for the complex square well, using the corresponding values of the parameters. This was done for aluminum, the results being shown in Fig. 1. The circles represent the experimental points of Bratenahl, *et al.*, the dotted line the values of $\sigma(\theta)$ calculated using the classical approximation, and the solid line the values of $\sigma(\theta)$ calculated by means of the exact partial wave analysis. It is seen that the apparent deviations from experiment are at least partly due to the calculational method rather than to the use of the complex square well model.

The calculated scattering and absorption cross sections differ somewhat from those obtained with the classical approximation. The scattering cross section becomes 0.83 instead of 0.75 barn, and the absorption cross section is 0.45 instead of 0.36 barn. To make a closer comparison of the calculated differential scattering cross section with the experimental results, it would be necessary first to adjust the complex potential parameters to fit the experimentally determined scattering and absorption cross sections.

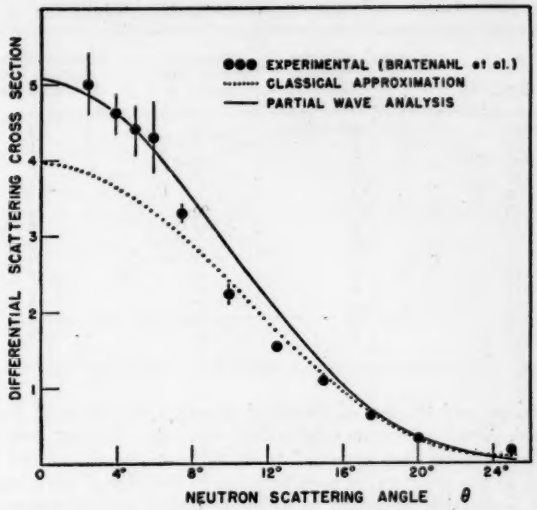

FIG. 1. Comparison of experimental differential scattering cross sections with those calculated from transparent model theory, in units of barns per steradian.

The phase shifts calculated by the exact partial wave analysis deviate considerably from those obtained by the W.K.B. method.[2] The latter gives, for aluminum,

$$\delta_l=(1.35+0.452i)\{1-(l+\tfrac{1}{2})^2/73.1\}^{\frac{1}{2}}\quad l\leqq8$$
$$=0\quad l>8.$$

The former method yields the following phase shifts for aluminum (for $l=0, 1, 2, \cdots$): $1.29+0.38i$, $1.44+0.56i$, $1.20+0.40i$, $1.36+0.40i$, $1.12+0.49i$, $1.01+0.29i$, $1.11+0.32i$, $0.85+0.47i$, $0.27+0.19i$, $0.065+0.025i$, $0.012+0.005i$, $0.002+0.001i$, etc.

We would like to express our appreciation to Richard J. Weiss for some helpful discussion, and to William Donoghue, Theresa Danielson, and Dale Meyer for performing the numerical work.

* Research carried out under contract with AEC.
[1] R. Serber, Phys. Rev. 72, 1114 (1947).
[2] Fernbach, Serber, and Taylor, Phys. Rev. 75, 1352 (1949).
[3] Bratenahl, Fernbach, Hildebrand, Leith, and Moyer, Phys. Rev. 77, 597 (1950).
[4] H. C. Van de Hulst, Recherches Astronomiques de l'Observatoire d'Utrecht XI, Part 1 (1946).

Penetrating Showers from Lithium*

W. B. FRETTER†
Department of Physics, University of California, Berkeley, California
October 6, 1950

THE analysis of penetrating showers originating in heavy elements is complicated by the possibility that more than one collision may occur inside a single nucleus. Thus, it is difficult to determine whether a number of mesons can be created in a single nucleon-nucleon collision from the data obtained on penetrating showers in lead, gold, aluminum, or even carbon. Hydrogen would be ideal as a generator, but the obvious experimental difficulties have led us to try lithium first.

A block of sodium-free lithium 6 inches thick, 5 inches wide, and 16 inches long was placed over a cloud chamber previously used in penetrating shower investigations.[1] Lead plates in the chamber served to analyze the showers produced in the lithium.

Fourteen showers appeared to have originated in the lithium block and have been analyzed. Origin in the lithium was determined by tracing the paths of the particles observed in the upper section of the chamber to see whether they came from a common point. This was done on a large print of the photograph in question and by re-projecting the stereoscopic pictures through the original camera.

The lithium was encased in a tin-coated steel can of $\frac{1}{32}$-inch

TABLE I. Multiplicity of penetrating showers from lithium.

Event no.	Charged particles traceable to point of origin	Identified penetrating particles	Electron showers starting from first lead plate
37250	10	3	>3
37260	2	2	1
37370	2	2	3
37737	2	2	0
38287	10	5	>2
38340	13	10	6
38459	4	4	2
39514	12	7	4
40173	2	2	0
40514	5	4	0
40971	6	6	0
41596	4	3	2
41804	7	5	3
42586	7	5	>2

thickness and the top of the cloud chamber was made of ¼-inch Dural. About 15 events originating above the chamber were rejected because they appeared to come from the aluminum, the steel, or the counters, or were too close to the edge of the lithium. Any event that appeared to originate within one centimeter of the edge of the lithium was rejected.

The results of the analysis are given in Table I. In the large events the total number of charged particles traceable to the point of origin may be underestimated by one or two, but probably not more than this. Penetrating particles were identified by their passage through two ¼-inch lead plates without interaction. In several cases the number of penetrating particles given is probably much lower than the true value because of the difficulty in analyzing the complicated events after the electron showers started in the first lead plate.

The size of the showers observed is certainly influenced by the counter and cloud-chamber arrangement. The chamber was tripped when one and only one of the five one-inch counters above the lithium discharged in coincidence with two 2-inch counters below the chamber covered by ¼ inch of lead and separated by one inch of lead. There was a total of 5¼ inches of lead in the chamber. The apparatus was located at Berkeley and the counting rate for lithium showers was about three per month. The largest shower observed (event No. 38340) was not an exceptionally high-energy event, judging from the lack of high energy electronic radiation that usually orginates in high energy nuclear events.

The maximum number of nucleon-nucleon interactions that can occur within a single nucleus of lithium is seven. If a single charged meson is produced in each interaction,[2] one can imagine on the most extreme assumptions of the plural production theory that 4 negative mesons, 3 positive mesons, and 5 protons could emerge, a total of 12 charged particles. No provision is made in this for neutral mesons. In event No. 38340 the above extremely unlikely event could not explain the number of charged particles observed, even omitting the electron showers presumably caused by the decay of neutral mesons into gamma-rays.

Several of the other showers have multiplicities of charged particles which are too large to be explained by a single interaction under the plural theory. If multiple interactions occur fairly frequently in an element as light as lithium, they must be extremely common in lead; and one might expect that in lead an incoming nucleon would nearly always dissipate all of its energy in one nucleus. Observations of successive events in cloud chambers[1] and with counters[3] contradict this idea.

If mesons are produced multiply, even with very small multiplicities of perhaps 2 to 5 per collision, the large lithium showers would be easily explained. Successive events within the same nucleus very likely occur, but it seems necessary to allow at least a small multiplicity to explain the lithium showers.

* Assisted by the joint program of the ONR and AEC.
† Reported at the Mexico City Meeting of the American Physical Society, June 22, 1950.
[1] W. B. Fretter, Phys. Rev. 76, 511 (1949).
[2] W. Heitler and L. Jánossy, Proc. Phys. Soc. London 62, 669 (1949).
[3] Cocconi, Tongiorgi, and Widcoff, Phys. Rev. 79, 768 (1950).

Two Comments on the Limits of Validity of the P. R. Weiss Theory of Ferromagnetism

P. W. ANDERSON
Bell Telephone Laboratories, Murray Hill, New Jersey
October 6, 1950

I SHOULD like to make two comments on the P. R. Weiss theory of ferromagnetism.[1] I should emphasize that these comments are literally indications of the limits of validity of this theory, and do not detract much from the main (and very considerable) achievements of the Weiss method, which has recently found gratifying confirmation in the work of Zehler.[2]

The first comment is a very simple one. In spite of the fact that until now the criteria of the Bloch spin-wave[3] and Weiss theories have agreed in giving ferromagnetism in precisely the same lattice structures and no others, a cursory glance tells one that these criteria are in principle very different. The Bloch criterion is merely that the lattice be three-dimensional; the Weiss criterion, however, is that the nearest neighbors of a given atom have certain topological—not spatial—relations to each other and to the central atom. That is, it involves counting the number of nearest neighbors, finding the nearest neighbor relationships among these, and similar purely topological considerations, which without explicit proof or disproof do not seem to have anything to do with the dimensionality of the lattice. For instance, if no nearest neighbors are nearest neighbors of each other, all that is required in the Weiss theory is that there be six or more nearest neighbors. A counter-example which shows the non-equivalence of the two criteria is the diamond lattice with nearest-neighbor spin interaction. In this lattice each atom has only four nearest neighbors, so it would not be ferromagnetic according to Weiss, although it would be ferromagnetic according to Bloch, since it is three-dimensional. Since the Bloch theory is rigorous in its low-temperature domain of applicability, this seems to indicate that the Weiss theory criterion is not always correct.

The second comment shall be stated primarily in the form of results. It is found that at sufficiently low temperatures, for all lattices, ferromagnetism is no longer present in the Weiss theory; and thus at some low temperature there must be an "anti-Curie point" below which ferromagnetism vanishes. This is true in the Weiss theory in spite of the fact that it is not true for the non-quantum-mechanical Ising model of Peierls and Bethe[4] upon which it is based, and indeed the effect can be traced to a specifically quantum-mechanical cause.

In either case at very low temperatures, only the very lowest state of the Bethe "cluster" of an atom and its neighbors is appreciably populated. However, this state is aligned completely, and thus the moment m_0 of the central atom is rigorously equal to that (m_1) of a boundary atom; and to find the result of the consistency condition $m_0=m_1$, we must appeal to higher order effects.[5] In the Ising case[4] the only such effect is thermal excitation of the next higher level, which leads easily to $m_0>m_1$ at very low ordering fields H_1, but to $m_1>m_0$ at high fields. Thus, $m_1=m_0$ is certainly satisfied for a finite intermediate field H_1, at low temperatures.

In the quantum-mechanical problem, however, there is a new effect, of exponentially [$\exp(J/kT)$] greater magnitude than thermal excitation at low enough temperatures: the second-order perturbation of the cluster levels due to the ordering field H_1. It is easily shown that this effect has the wrong sign at low fields H_1, giving $m_1>m_0$; and thus, since $m_1>m_0$ always at high fields, we have no crossing point $m_1(H_1)=m_0(H_1)$ and no ordering field or ferromagnetism. Actual computations have been carried out using the formulas (30, 36, and 37) of reference 1, and it is found that an anti-Curie point (for the simple cubic lattice) can be located at $kT=0.269J$. (J is the exchange integral.) This is at a temperature one-seventh of that of Weiss' computed "true" Curie point T_c; however, it is clear from other computations made that Weiss' method fails completely at temperatures lower than $\frac{1}{2}T_c$.

The reason for this failure is clear. The small dimensions of the cluster exclude the low energy spin-wave states, which are all-important in ferromagnetic behavior at low temperatures. If it were possible to increase the cluster size, these states would come in in increasing numbers and the "anti-Curie point" would move to lower and lower temperatures.

It is not possible to draw many conclusions from this work as to the validity of Weiss' method at or near the Curie point. It does seem that the differences between quantum and Ising ferromagnetism are not entirely summed up in the concept of spin waves. We may also conclude that the Weiss method is probably a somewhat worse approximation to the true statistical problem than the Bethe method is to its corresponding Ising model problem.

[1] P. R. Weiss, Phys. Rev. 74, 1492 (1948).
[2] V. Zehler, Zeits. f. Naturforsch. 5a, 344 (1950).
[3] F. Bloch, Zeits. f. Physik 61, 206 (1930).
[4] H. A. Bethe, Proc. Roy. Soc. A150, 552 (1935).
[5] We borrow all notation from reference 1.

Two-Fluid Theory of Liquid Helium II below 1°K

S. NAKAJIMA AND M. SHIMIZU
Physical Institute, Nagoya University, Nagoya, Japan
October 6, 1950

RECENTLY, Usui[1] has developed the general formalism of the two-fluid theory of liquid He II, avoiding ingeniously the use of the Tisza's relation, $\rho_n/\rho=s/s_\lambda$, the role of which has been critically discussed by us[2] in connection with the second-sound velocity[3] below 1°K. We are now applying the general formalism to the construction of the two-fluid theory below 1°K. New results obtained are as follows.

Usui has assumed that the two fluid components are always in local equilibrium, the normal fluid concentration, $x=\rho_n/\rho$, being a function of the pressure and temperature determined by the condition of minimum Gibbs free energy. Thus, we may use the total density, ρ, and the concentration, x, as the independent thermodynamic variables. The entropy per unit mass, s, is regarded as the function of ρ and x. Usui has shown that the entropy flow is given by

$$\rho s\mathbf{V}_1+(\partial s/\partial x)_\rho\rho_n(\mathbf{V}_n-\mathbf{V}_1), \tag{1}$$

where $\mathbf{V}_1$ is the velocity of the center of gravity. He has obtained the generalized expressions for the fountain pressure and the second-sound velocity, respectively, as follows:

$$x(\partial s/\partial x)_\rho \operatorname{grad}T \tag{2}$$

and

$$C_2^2=x(1-x)(\partial s/\partial x)_\rho(\partial T/\partial x)_\rho. \tag{3}$$

The latter expression is not identical with that used by Landau,[4] as we predicted in our previous report.[2] C_2 calculated on the basis of Landau's model by means of Eq. (3) is shown by curve II in Fig. 1.

Now, following Tisza's idea,[5] we extend the two fluid theory to include the phonon entropy:

$$s=s_\lambda x+s_{ph}. \tag{4}$$

The entropy flow, Eq. (1), then takes the form

$$(s_\lambda+(\partial s_{ph}/\partial x)_\rho)\rho_n\mathbf{V}_n+(s_{ph}-x(\partial s_{ph}/\partial x)_\rho)\rho\mathbf{V}_1. \tag{5}$$

Even in the limiting case of the extremely narrow capillary ($\mathbf{V}_n\to 0$), the phonon entropy is transferred by the superfluid flow. Accordingly the experimental evidence proved by Kapitza[6] and, therefore, H. London's expression for the fountain pressure should be invalid below 1°K, as we have suggested previously.[2]

In order to calculate C_2 by means of Eqs. (3) and (4), one needs the expressions for x, s_λ, and s_{ph}. x would be determined by the analysis of the viscosity measurement and the proportionality relation between the fountain pressure and heat current.[7] The available data, however, are lacking at present. If we assume that

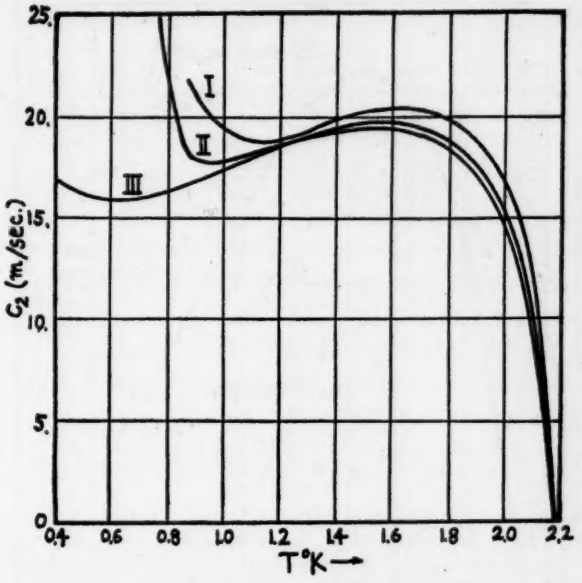

FIG. 1. Second-sound velocity *vs.* temperature. I: observed curve (M.H.); II: Landau's model; III: generalized model of Tisza.

$x=(T/T_\lambda)^r$, the second-sound velocity has a non-zero or infinite value as $T\to 0$, only when $r\geqq 4$. The preliminary result of the calculation is shown by curve III in Fig. 1, where we have used the following values: $s_\lambda=0.397$ cal./g-deg., $r=6$, and $s_{ph}=0.75\times 10^{-3}T^3$ cal./g-deg. The calculated C_2 has a minimum and increases as the temperature decreases. C_2 increases too rapidly in Landau's model and too slowly in Tisza's model in comparison with the experimental results.

At any rate, we may say that one should not decide on the superiority of Landau's theory from the analysis of the second-sound velocity alone. In our opinion, the generalized model of Tisza, Eq. (4), has the advantage that it can be connected easily with Bose-Einstein statistics by the idea of B-E liquid. The detailed discussion will appear in the forthcoming paper.

One of us has enjoyed stimulating discussions with Associate Professor T. Usui at the University of Tokyo.

[1] T. Usui, unpublished paper.
[2] S. Nakajima and M. Shimizu, Prog. Theor. Phys., to be published.
[3] J. R. Pellam and R. B. Scott, Phys. Rev. 76, 869 (1949); R. D. Maurer and M. A. Herlin, Phys. Rev. 76, 948 (1949).
[4] L. Landau, J. Phys. U.S.S.R. 5, 71 (1941).
[5] L. Tisza, Phys. Rev. 72, 838 (1947).
[6] P. Kapitza, Phys. Rev. 60, 354 (1941).
[7] C. J. Gorter and J. H. Mellink, Physica 15, 285 (1949); Nakajima, Tomita, and Usui, Phys. Rev. 78, 768 (1950).

A 1.7×10^{-9}-Sec. Isomeric State in $_{68}Er^{166}$

F. K. MCGOWAN
Oak Ridge National Laboratory, Oak Ridge, Tennessee*
October 6, 1950

THE half-life of the 80-kev transition in Er^{166} has been measured as $(1.7\pm0.2)\times10^{-9}$ sec. with a delayed coincidence scintillation spectrometer.

The β-spectrum of Ho^{165} (27 hr.) is known to consist of two components of 1.84- and 0.55-Mev maximum energy and intensities 89 and 11 percent, respectively.[1] Siegbahn and Slätis showed that the 80-kev transition follows the higher energy component of the β-spectrum and that the L shell conversion coefficient is ~ 0.4.

The delayed coincidence scintillation spectrometer is similar to that described previously.[2] In addition, a second differential

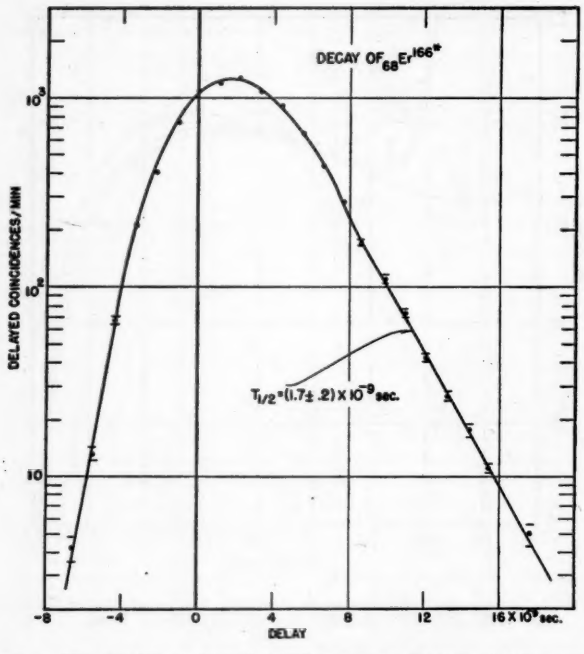

FIG. 1. The number of delayed coincidences as a function of delay time.

pulse-height analyzer has been added to the apparatus. In this way only significant events from each channel are selected. Figure 1 shows the number of coincidences as a function of delay time obtained with a source of Ho^{166}. This delayed coincidence resolution curve was recorded by exciting one channel of the delayed coincidence apparatus by 600- to 900-kev nuclear beta-rays and the other channel by the L, M, or N internal conversion electrons of the 80-kev transition. With a source of Au^{198} a resolution curve (not shown) for prompt events was obtained between 600- to 900-kev beta-rays and 60- to 90-kev Compton recoil electrons from the 411-kev γ-radiation. This measurement showed that for delay $T \geq 8\times10^{-9}$ sec. the half-life of Er^{166*} can be determined from the slope of the curve of Fig. 1. However, for half-lives less than 10^{-9} sec. it would be necessary to analyze the data by the methods of Newton[3] and Bay.[4]

The energy and half-life of this isomeric state suggests that the transition is probably electric quadrupole or a combination of electric quadrupole and magnetic dipole radiation.

It is interesting to note the distinct similarity of the short-lived isomeric states of $_{70}Yb^{170}$ (1.6×10^{-9} sec.)[5] and $_{68}Er^{166}$. They occur in neighboring nuclei with an even number of protons and neutrons. The energies of the isomeric transitions are 83 and 80 kev, respectively; and the half-lives are the same within the experimental error.

* This document is based on work performed for the Atomic Energy Project at Oak Ridge National Laboratory.

[1] K. Siegbahn and H. Slätis, Arkiv Fysik 1, 559 (1950).
[2] F. K. McGowan, Phys. Rev. 79, 404 (1950).
[3] T. D. Newton, Phys. Rev. 78, 490 (1950).
[4] Z. Bay, Phys. Rev. 77, 419 (1950).
[5] R. E. Bell and R. L. Graham, Phys. Rev. 78, 490 (1950).

Nuclear Interaction of π^--Mesons*

G. BERNARDINI, E. T. BOOTH, L. LEDERMAN, AND J. TINLOT†
Columbia University, New York, New York
October 2, 1950

A PRELIMINARY report is here presented on the nuclear interactions of 30 to 50 Mev π^--mesons in nuclear emulsions. The interactions observed to date are of three types, (1) production of a nuclear star, (2) nuclear scattering, and (3) disappearance in flight, with no visible secondary particle. The mean free path for interaction of all of these types combined is very nearly equal to the geometrical mean free path in the emulsion.

TABLE I. Star prong distribution.

Number of prongs	Number of stars
1	2
2	15
3	4
4	1

The π^--mesons were produced in the Nevis cyclotron by bombarding an internal carbon target with 385-Mev protons. Mesons having about 95-Mev energy were deflected by the magnetic field of the cyclotron and collimated by a 2×10-in. hole in the six-foot thick concrete shielding. Ilford G-5 400μ-plates were exposed in the direct meson beam, and after a copper absorber 2 cm thick. Only the data obtained from the plates after the absorber, at which point the mesons had energies of 30 to 50 Mev, will be discussed. The spread is caused mostly by the energy loss in the glass and emulsion. It should be noted that an appreciable portion of the mesons were μ^--mesons, resulting from $\pi^- - \mu^-$-decay in flight.

A total of 27 interactions of π^--mesons in a scanned area of 20.2 cm² of emulsion were found. Of these, 22 were stars. Table I gives the frequency *vs.* star prong distribution. Nineteen of the stars had only "black" prongs, and the average length of the prongs ending in the emulsion was about 200μ. In these cases, therefore, a large part of the energy of the incident meson must be carried off by neutral particles. In the case of the three other stars (one of which is reproduced in Fig. 1), the visible prongs had energies sufficient to account for most of the meson energy. Three cases were found of scattering (Fig. 2) through an angle of more than 30°, which were thought to be caused by nuclear interaction. One of these scatterings is evidently inelastic. Two clear cases of disappearance in flight were observed. In the latter cases, the particles appeared to stop without increase of ionization or scattering, in a fully sensitive region of the emulsion. To insure correct identification, nuclear interactions of particles with track lengths of less than 500μ, or of particles incident at an angle of more than 15° from the beam direction, were not considered.

The uncorrected total length of meson track ($\pi^- + \mu^-$) was found to be 1130 cm, with an uncertainty of about 5 percent. This figure was obtained by sampling various regions of the scanned area, rejecting only tracks incident at large angles from the beam direction, and tracks whose relative ionization was appreciably different from that expected for mesons of 30- to 50-Mev energy.

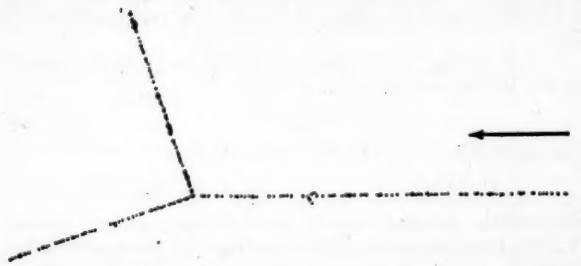

FIG. 1. Two-proton star produced by meson. The length of the incoming meson track is 4800 microns. The energies of the two protons are about 120 and 50 Mev, respectively. The three tracks are not in the same plane. Observed by Elizabeth Wimmer.

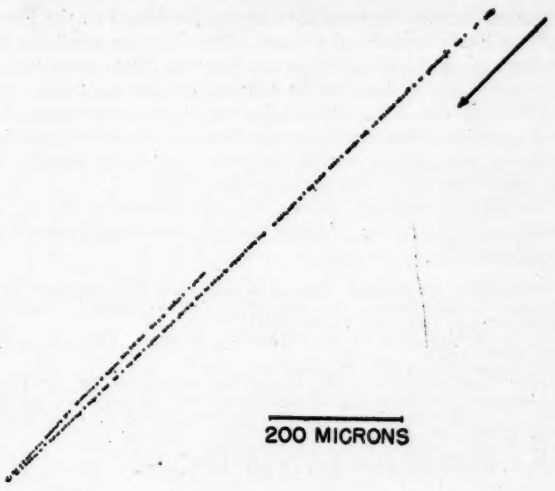

FIG. 2. Large angle meson scattering. The length of the incoming meson track is 8000 microns. The angle of scattering is 177 degrees. Observed by Leon Lederman.

In order to compute the relative numbers of π^-- and μ^--mesons, the ratio of σ- to ρ-mesons[1,2] stopping in another group of plates placed after an additional absorber was determined. After making a small correction for the nuclear absorption of π^--mesons in this last absorber, a total of 900 cm of π^--track was obtained in the 30- to 50-Mev energy range. This length was further reduced to 780 cm by the correction for the condition on the minimum length of tracks. In this way a mean free path of 29 cm of emulsion was obtained. The geometric mean free path is 25 cm.

A similar study is in progress to determine the interaction in emulsions of the directly incident mesons (energy about 95 Mev). Up to the present, 13 stars, 3 inelastic scatterings, and one elastic scattering have been observed. Further reports on both experiments will be made when better statistics are available.

The authors wish to thank Dr. Hugh Bradner, Berkeley, California, for privately communicating to us his results on an experiment of a similar nature. They also wish to thank Mr. S. Lindenbaum for assisting with the computations of the meson orbits, and Messrs. R. Durbin, W. Goodell, and H. Loar for performing counter experiments for locating the meson beam.

* Assisted by the joint program of the ONR and AEC.
† Now at the University of Rochester, Rochester, New York.
[1] C. Franzinetti, Phil. Mag. 41, 86 (1950).
[2] Menon, Muirhead, and Rochat, Phil. Mag. 41, 583 (1950).

Secondary Electron Emission and Atomic Shell Structure*

E. J. STERNGLASS
U. S. Naval Ordnance Laboratory, White Oak, Silver Spring, Maryland
August 21, 1950

A SIMPLE correlation has been found between the maximum value of the true secondary electron yield (Δ_m) and the atomic shell structure of the elements. The values of Δ_m, defined as the number of low energy ($\lesssim$50 ev) electrons leaving the surface per incident primary electron, were obtained by subtracting the fraction of high energy back-scattered electrons (η) from the maximum total yield coefficient δ_m reported in the literature.

Table I lists the data used in this investigation. The data obtained by Bruining and DeBoer and Warnecke have been used wherever possible in view of the careful experimental techniques used by these workers, which insured a maximum degree of freedom from surface impurities and uncertainties due to multiple scattering between target and collector. For the remaining elements, the results of other authors were used whose measurements on "standard" materials such as Ni, Cu, and Au agreed to better than 10 percent with the values found by Bruining and DeBoer and Warnecke. The values of δ_m listed in Table I agree to better than 5 percent with those given by McKay,[1] except in the cases of Pt, K, Be, and Fe, where they differ by about 10 percent because the work of different authors was chosen for reasons mentioned above.

TABLE I. Values of maximum total yield δ_m.

Element	δ_m	±%	Element	δ_m	±%	Element	δ_m	±%
Ni*	1.24;[a] 1.28[b,†,d]	5	Zr	1.10[a]	5	K	0.78[e]	10
Cu*	1.28;[a] 1.29;[b] 1.40;[c,†,f]	5	Ag	1.53[a]	5	Rb	0.90[e]	10
Au*	1.58;[b] 1.50;[c] 1.56;[c] 1.44[g]	5	Cs	0.76[a]	5	Co	1.16[d]	5
Li	0.47[a]	5	Ba	0.83[a]	5	Cd	1.13[e]	10
Be	0.51[a]	5	Cb	1.17[b]	5	Fe	1.11[f]	10
Mg	0.93[a]	5	Mo	1.25[b]	5	Pt	1.79[g]	10
Al	0.97[a]	5	Ta	1.28[b]	5	Si‡	1.1[h]	>10
Ti	0.92[a]	5	W	1.36[b]	5	Ge‡	1.2[h]	>10

* Standard values for comparison.
† Data do not extend as far as the maximum yield.
‡ Tentative, pending more detailed investigations.
[a] H. Bruining and J. H. DeBoer, Physica 5, 17, 901, 913 (1938).
[b] R. Warnecke, J. de phys. et rad. 7, 270 (1936).
[c] A. V. Afanasjewa and P. V. Timofeev, J. Tech. Phys. U.S.S.R. 4, 953 (1937).
[d] L. R. G. Treloar and D. H. Landon, Proc. Phys. Soc. London 50, 625 (1938).
[e] R. Suhrmann and W. Kundt, Zeits. f. Physik 121, 118 (1943).
[f] H. E. Farnsworth, Phys. Rev. 27, 243 (1926).
[g] P. L. Copeland, Phys. Rev. 40, 122 (1932); 48, 96 (1935).
[h] L. R. Koller and J. S. Burgess, Phys. Rev. 70, 571 (1946).

Experimental values of η from nine elements ranging from $Z=6$ to $Z=79$ at primary energies from 2 to 16 kv have recently been obtained by Palluel.[2] His results indicate that η is very nearly independent of the energy for all except the heaviest elements, where back-scattering appears to increase somewhat with increasing primary energy. Using these data, as well as those of Schonland[3] at higher energies, the following empirical equations for η as a function of Z were found to hold:

$$\eta=0.01Z \quad (\pm 5 \text{ percent}) \quad \text{for } Z<30;$$
$$\eta=0.18+0.004Z (\pm 10 \text{ percent}) \quad \text{for } Z>30.$$

The values of Δ_m obtained for 24 elements are plotted against Z in Fig. 1.

It is seen that a surprisingly regular pattern emerges when elements of neighboring atomic numbers are grouped together (heavy

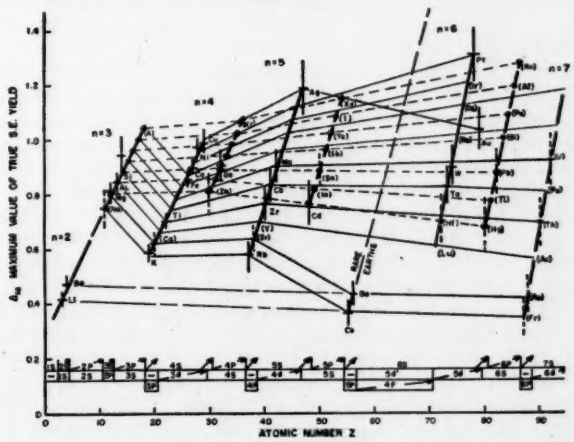

FIG. 1. Plot of the maximum value of the true yield *versus* the atomic number. Solid vertical bars—experimental points; dotted vertical bars—sample predicted values.

slanting lines), and when elements of similar outer shell configuration are connected (light horizontal lines). Δ_m increases steadily as long as successive shells are filled without leaving an inner shell vacant. Whenever a new shell is begun outside of one that is subsequently filled, as for $Z=19$, 37, 55, and 87, Δ_m drops discontinuously. Likewise, when an inner shell is completed and a new sub-shell is begun, as for $Z=30$, 48, 71, and 80, Δ_m drops to a lower value, thereby giving rise to two parallel sets of lines for complete and incomplete inner shell structures. Δ_m varies as the number of outer shell electrons, so that it appears to be a true atomic property much like the x-ray emission characteristics of the elements.

The regularity of the plot is such that it is possible to complete it as indicated in Fig. 1 for values of Z where no data are at present available.[4] This makes it possible to predict the values of Δ_m to better than 10 percent for nearly all metals in the atomic table. The basic pattern as it appears in Fig. 1 is not materially affected by relatively large errors in η or δ_m, and it is even apparent when δ_m is plotted against Z.

Present theories of secondary emission are based on the Fermi gas[5,6] or Bloch model[7,8] of a metal. These theories predict a dependence of the yield on the lattice spacing, Fermi energy level, and work-function, but not on the atomic shell structure. The simple correlation of Δ_m with position in the periodic system would seem to indicate that a satisfactory theory of secondary emission must take into account atomic electrons more firmly bound than the valence or conduction electrons of a metal.

The author wishes to express his appreciation to Dr. L. P. Smith and Dr. L. R. Maxwell for their encouragement and helpful criticism.

* Preliminary results were reported at the April 1949 meeting of the American Physical Society (see Phys. Rev. **76**, 189 (1949)). A detailed account is being prepared for publication.

[1] K. G. McKay, *Advances in Electronics* (Academic Press, Inc., New York, 1948), Vol. I.
[2] P. Palluel, Comptes Rendus **224**, 1492 (1947).
[3] B. F. J. Schonland, Proc. Roy. Soc. A **104**, 235 (1923); **108**, 187 (1925).
[4] The special position of Au will be discussed in detail in the full account.
[5] A. E. Kadyschewitch, J. Exptl. Theoret. Phys. (U.S.S.R.) **2**, 115 (1940).
[6] E. M. Baroody, Phys. Rev. **78**, 780 (1950).
[7] H. Fröhlich, Ann. d. Physik **13**, 229 (1932).
[8] D. E. Wooldridge, Phys. Rev. **56**, 562 (1939).

Proceedings of the American Physical Society

Minutes of the 1950 Autumn Meeting of the New York State Section at Potsdam

THE 1950 Fall Meeting of the New York State Section of the American Physical Society was held on September 29–30, 1950, in the Department of Physics of Clarkson College of Technology. Ninety people attended the meeting. Provisions were made for inspection of the New Building. The Dinner Address on Friday evening, Scientific Adventures, was given by Vincent J. Schaefer, General Electric Company. Abstracts of four contributed papers are appended. The following invited papers were presented:

(W. R. FREDRICKSON, presiding)

Rotation-Vibration Spectra of Methane. JOHN S. BURGESS, *St. Lawrence University.*

Electron Diffraction Line Broadening in Thin Nickel Films. EBER K. HALTEMAN, *Clarkson College of Technology.*

(C. K. BOSWORTH, presiding)

Physics Principles Illustrated in Astronomy. S. L. BOOTHROYD, Professor Emeritus, *Cornell University.*

Application of Physics to Geology. R. O. BLOOMER, *St. Lawrence University.*

Modern Physics in Modern Medicine. HERTA R. LENG, *Rensselaer Polytechnic Institute.*

Symposium on the Undergraduate Education of Physicists for Industry.

(W. R. FREDRICKSON, presiding)

Industry's Views as to Type of Physics Education Desirable. GLENN W. GIDDINGS, *General Electric Company.*

Education Offered by Curriculum Leading to B.S. in Physics. HAROLD E. WAY, *Union College.*

Education Offered by an Engineering Physics Curriculum. LLOYD P. SMITH, *Cornell University.*

C. LUTHER ANDREWS, *Secretary*
New York State College for Teachers
Albany, New York

Contributed Papers

Application of the Theory of Reaction Rates to Studies of Dye Diffusion in a Gel System. R. B. PONTIUS, *Eastman Kodak Company.*—In the study of diffusion in a condensed system it is necessary to consider the intermolecular forces. The magnitudes of these forces can be obtained from diffusion measurements because the diffusion coefficient can be assumed proportional to the specific reaction rate. The activation energy for the diffusion process is given by the Arrhenius rate equation. A method of measuring diffusion of dyes in gelatin suggested by E. E. Jelley consists in dyeing thin-coated gelatin layers under controlled conditions, arresting the dye at the position reached by diffusion in the dye bath by freezing the sample in an alcohol-dry ice mixture, and dehydrating at −2°C in a stream of cold dry nitrogen. The dry samples are sectioned and the penetration of the dye into the sample measured under the microscope. The activation energy can be obtained from measurements made at several temperatures if the diffusion coefficients are normalized by taking into account the swelling of the gelatin to different amounts at different temperatures. Results are given for two simple acid dyes. It is possible to utilize the Eyring[1] theory of reaction rates to estimate the entropy changes associated with the diffusion.

[1] Glasstone, Laidler, and Eyring, *The Theory of Rate Processes* (McGraw-Hill Book Company, Inc., New York, 1941), p. 524.

Recent Developments in Electric Servo Power Drive Systems. F. M. BAILEY, *General Electric Company.*—The application of ignitrons to high performance servo mechanisms has simplified the control loop, and improved both the frequency response and phase shift characteristics of power drives with capacities greater than sixty horsepower. A performance comparison of ignitron-thyratron controllers with amplidyne positioning systems is presented.

Verification of Bragg's Law by the Use of Microwaves. ROLAND A. ALLEN, *Siena College.*—The importance of the use of microwave optics to provide a better understanding of the phenomena of polarization, diffraction, and interference cannot be overemphasized. Microwaves too can be employed to observe the Bragg diffraction by a model crystal made up of metal disks. When a beam of 10- to 12-cm microwaves is incident at the correct grazing angle to the model crystal, a microwave intensity meter rotated about the incident beam reference point will indicate the points of constructive interference. Using Bragg's Law, $n\lambda = 2d \sin\theta$, and inserting the measured values of λ and d, the angles at which constructive interference should appear can be determined for the order n. The observed angles as indicated by the intensity meter are within one or two degrees of the calculated value.

Optical Dichroism from Adsorbed Dyes and its Correlation with Orientation of the Substrate. D. R. MOREY, *Eastman Kodak Company,* AND E. V. MARTIN, *Tennessee Eastman Corporation.*—A method is described for making quantitative measurements of dichroism, applicable to cellulose acetate film base or continuous filament yarn. The method is predicated upon the choice of a dye which is itself intrinsically dichroic in its optical absorption, and which is adsorbed in the polymeric substrate in preferential directions corresponding to regions of anisotropy in the chain polymer matrix. Yarn samples of increasing orientation were prepared by suitable hot drafting processes, and were then examined for mechanical properties and for orientation as obtained from x-ray fiber diagrams. The correlations between these properties and optical dichroism is found from experiment to be good. The conditions of adsorption, such as the state of dispersion of the dye and the degree of swelling of the polymer during the dyeing process, also affect the observed dichroism.